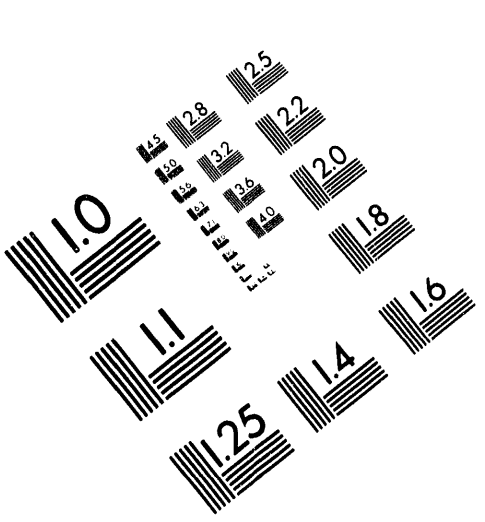
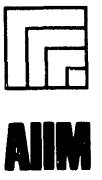
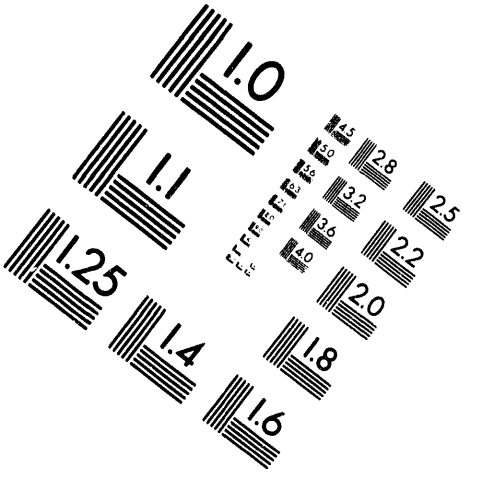
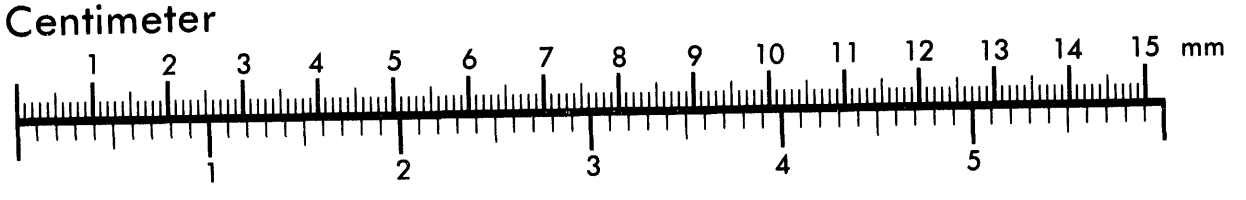


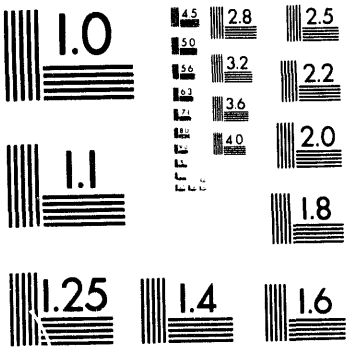


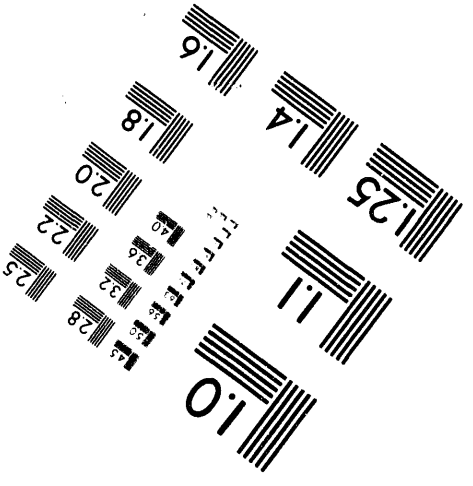
AIIM

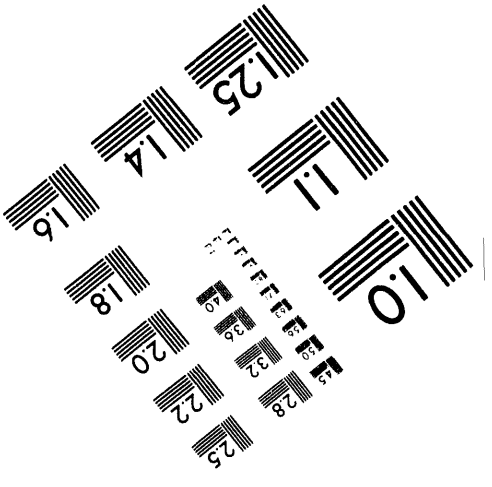
Association for Information and Image Management
1100 Wayne Avenue, Suite 1100
Silver Spring, Maryland 20910
301/587-8202











MANUFACTURED TO AIIM STANDARDS
BY APPLIED IMAGE, INC.

1 of 6

ORNL/TM-12817

Fourth Conference

on

Radiation Protection and Dosimetry

Program, Abstracts, and Proceedings

Edited by: W. H. Casson, M. Thein, and J. S. Bogard

Sheraton Plaza Hotel
Orlando, Florida

October 23-27, 1994

Date Published: October 1994

Prepared by Oak Ridge National Laboratory, Oak Ridge, Tennessee 37831
Managed by Martin Marietta Energy Systems, Inc., for the U.S. Department of Energy
under Contract No. DE-AC05-840R21400

MASTER

DISTRIBUTION OF THIS DOCUMENT IS UNLIMITED

DEDICATION

The Fourth Conference on Radiation Protection and Dosimetry is dedicated to Bonnie S. Reesor, who retired from employment with Oak Ridge National Laboratory in September 1994, after 34 years of loyal service. Bonnie has been instrumental in the success of the series of Conferences on Radiation Protection and Dosimetry sponsored by ORNL, having served as the Conference Coordinator for each. The Conference Committee expresses its heartfelt gratitude to Bonnie for her capable support and guidance, and we extend our fondest wishes for fulfillment and happiness in her retirement.

FOURTH CONFERENCE ON RADIATION PROTECTION AND DOSIMETRY

October 23-27, 1994

CONFERENCE CHAIRMAN

James S. Bogard
Oak Ridge National Laboratory
Oak Ridge, Tennessee

CONFERENCE COORDINATOR
Bonnie S. Reesor/Thelma G. Patton
Oak Ridge National Laboratory
Oak Ridge, Tennessee

SECRETARY/TREASURER
Barbara B. Clark/Beverly D. Stewart
Oak Ridge National Laboratory
Oak Ridge, Tennessee

PUBLICATIONS
Myint Thein/Karen H. Galloway
Oak Ridge National Laboratory
Oak Ridge, Tennessee

TECHNICAL EXHIBITS
John R. Frazier
Auxier and Associates
Knoxville, Tennessee

PUBLICITY
Mark A. Buckner
Oak Ridge National Laboratory
Oak Ridge, Tennessee

TECHNICAL PROGRAM
William H. Casson, Sr.
Los Alamos National Laboratory
Los Alamos, New Mexico

HONORARY CHAIRMAN
C. S. Sims
Oak Ridge National Laboratory
Oak Ridge, Tennessee

FOURTH CONFERENCE ON RADIATION PROTECTION AND DOSIMETRY

October 23-27, 1994

TECHNICAL PROGRAM COMMITTEE

R. Douglas Carlson
U.S. Department of Energy
Idaho Falls, Idaho

Chris G. Soares
NIST
Gaithersburg, Maryland

Keith F. Eckerman
Oak Ridge National Laboratory
Oak Ridge, Tennessee

Richard E. Swaja
Oak Ridge National Laboratory
Oak Ridge, Tennessee

C. Glenn Hudson
Consultant
Chattanooga, Tennessee

Richard J. Vetter
Mayo Clinic
Rochester, Minnesota

John W. Poston
Texas A&M University
College Station, Texas

Myint Thein
Oak Ridge National Laboratory
Oak Ridge, Tennessee

FOREWARD

Radiation protection and dosimetry disciplines are evolving through a period in which increasing regulatory requirements for programmatic rigor often conflict with reduced budgets and demands for increased efficiency. This conflict is compounded by the loss of many health physicists and scientists whose experiences reach back to the seminal years of World War II and who are now choosing to retire from employment. Part of the answer in this complicated environment is found in the increasing dependence on standards developed from the experience of the past half century. Some of these standards relate to the ways in which a radiation protection program can be designed and implemented in order to address conditions found in the workplace. Other standards are implemented technologically through the development of automated methods of performing complicated or time-consuming tasks with a high degree of repeatability. Standard practices and technological advances find generalized use and acceptance by radiation protection professionals only after their availability and suitability are communicated within the professional community. Communication is a key to innovation and progress.

This Conference is the fourth in a series of conferences organized by staff members of Oak Ridge National Laboratory in an effort to improve communication in the field of radiation protection and dosimetry. Scientists, regulators, managers, professionals, technologists, and vendors from the United States and countries around the world have taken advantage of this opportunity to meet with their contemporaries and peers in order to exchange information and ideas. The program includes over 100 papers in 9 sessions, plus an additional session for works in progress. Papers are presented in external dosimetry, internal dosimetry, radiation protection programs and assessments, developments in instrumentation and materials, environmental and medical applications, and on topics related to standards, accreditation, and calibration.

The primary objective of this Conference is communication. There will be a full schedule of formal presentations, but adequate lunch and coffee breaks will allow visits to the vendor area and an opportunity to visit also with colleagues and friends. Refreshments will be served at the back of the vendor area; be sure to take advantage of the opportunity to see the latest in commercially available equipment for your radiation protection and dosimetry needs. Members of our Technical Program Committee, all recognized experts in various areas of radiation protection and dosimetry, are available throughout the meeting for consultation and discussions. Take advantage also of the opportunity to discuss ideas and issues with the many attendees from other countries who have traveled to the Conference in order to share their experiences.

We hope all the attendees enjoy their visit to Orlando, and that they will take the opportunity to enjoy some of the area attractions. We also hope you enjoy the Conference and find it useful. Both of us are available throughout the Conference and will be glad to answer questions or consider suggestions for improvement.

James S. Bogard
General Chairman
Oak Ridge National Laboratory

William H. Casson, Sr.
Technical Program Chairman
Los Alamos National Laboratory

TABLE OF CONTENTS

Technical Program xiii

Session I. Programs and Assessments 1

Session II. TLD Materials and Dosimeter Design 81

Session III. External Dosimetry 117

Session IV. Instrumentation 225

Session V. Internal Dosimetry 299

Session VI. Environmental 367

Session VII. Calibration, Standards, and Accreditation 423

Session VIII. Medical, Accident, and High-Level Dosimetry 501

Session IX. TLD Systems 549

FOURTH CONFERENCE ON RADIATION PROTECTION AND DOSIMETRY

October 23-27, 1994

Technical Program

All technical sessions will be held in the Grand Ballroom of the Sheraton Plaza Hotel. Presentations will last about 15 minutes, refreshment breaks will be 15-20 minutes, and about an hour will be available for lunch.

Monday, October 24

8:00 a.m. Registration

8:30 a.m. Welcome and Introduction to the Conference
General Chairman: Jim Bogard (ORNL)
Technical Program Chairman: William Casson (LANL)

Welcome Address
Honorary Chairman: *Steve Sims (ORNL)*

9:00 a.m. Session I - Programs and Assessments
Chairman: R. Douglas Carlson (DOE-Idaho)

PERSONAL MONITORING IN THE UNITED KINGDOM
T.O. Marshall (NRPB-UK)

STATUS OF RADIOPROTECTION AT BRAZILIAN UNIVERSITIES
K.C.S. Caballero, J.C. Borges (COPPE-EE, Brazil)

ASSESSMENT OF RADIATION DOSES AT THE INSTITUTO DE PESQUISAS ENERGÉTICAS E NUCLEARES
M.P. Sanches(LAS), A. Sahyun (HPS) and G.M.A.A. Sordi (HPS) (IPEN-CNEN/SP, BRAZIL)

OCCUPATIONAL DOSE RECONSTRUCTION IN THE NUCLEAR INDUSTRY: A KNOWLEDGE MANAGEMENT APPROACH
B. Le Blanc (Univ de Bordeaux), H. Dagorn, D. Bard (Institut de Protection et de Sûreté Nucléaire)

THE CENTRAL INDEX OF DOSE INFORMATION: DOSE DISTRIBUTIONS IN THE UNITED KINGDOM OVER THE PERIOD 1986-1991
W.J. Iles (NRPB, UK), M.K. Williams (Health & Safety Executive, UK), T.O. Marshall (NRPB, UK)

10:20 a.m. Coffee Break

10:35 a.m. Session I (con't)

CANCER MORTALITY EXPERIENCE IN THE WORKERS OF THE FRENCH NUCLEAR INDUSTRY: SOME QUESTIONS OF DOSE RECONSTRUCTION FROM AN EPIDEMIOLOGICAL PERSPECTIVE
D. Bard, Ph. Hubert and H.Dagorn (Institut de Protection et de Sûreté Nucléaire, France)

GENERAL APPROACH AND PRELIMINARY RESULTS ON GAMMA - FIELD RECONSTRUCTION FOR THE TECHA RIVER
D. Burmistrov, V. Valchuk (Urals Research Center for Radiation Medicine, Russia)

THE NATIONAL DOSE REGISTRATION AND INFORMATION SYSTEM: DOSE DISTRIBUTIONS IN THE NETHERLANDS OVER THE PERIOD 1989-1993
J.W.E. van Dijk and H.W. Julius (TNO Radiological Service, The Netherlands), M.A. van de Bogaerde (Ministry of Social Affairs and Employment, The Netherlands)

RADIOLOGICAL SAFETY ASSESSMENT OF GAS MANTLE INDUSTRIES IN INDIA
Geetha Sadagopan and G. Venkataraman (BARC, India)

MONTE CARLO TECHNIQUE APPLICATIONS IN THE FIELD OF RADIATION DOSIMETRY AT THE ENEA RADIATION PROTECTION INSTITUTE: A REVIEW
G.F. Gualdrini, L. Casalini, B. Morelli (ENEA, Italy)

THE IMPLEMENTATION OF NEW RADIATION QUANTITIES IN NUCLEAR POWER PLANTS IN TAIWAN
C.J. Tung, H. Niu (National Tsing Hua University), T.J. Chen (Radiation Protection Association), T.L. Chou, W.W. Yeh and R.Y. Liao (Taiwan Power Company)

12:05 p.m. Lunch Break

1:00 p.m. Session I (con't)

OCCUPATIONAL RADIATION EXPOSURES TO RAILROAD WORKERS FROM SHIPMENTS OF RADIOACTIVE MATERIALS
D.E. Fields, and W.D. Cottrell (ORNL)

FIELD EXPERIENCE WITH REMOTE MONITORING
Arthur E. Desrosiers (Bartlett Services, Inc.)

IMPLEMENTATION OF A SELF-DIRECTED WORK TEAM IN A TLD PROCESSING CENTER
A.A. Arnwine, R.S. Bogard, N.A. Teasley , D.E. Somers, and M.L. Souleyrette (MMES)

EXPERIENCE WITH REIRS FOR THE REVISED 10 CFR 20
Derek A. Hagemeyer, (SAIC)

A FEW EXPERIENCES AND LESSONS LEARNED IN INSTALLING RADIOLOGICAL ACCESS CONTROL SYSTEMS
Robert Gunn Benson, Aaron Clemmons, and Peter Clemmons(Pro-Tem, Inc.)

SYSTEM INTEGRATION FOR RADIATION RECORDS
Brian J. Lawson, Linda Farrell, Clifford Meacham, Jane Tapio (KAPL)

2:30 p.m. Coffee Break

2:50 p.m. Session II - TLD Materials and Dosimeter Design
Chairman: Christopher Soares (NIST)

A NEW COMBINATION BETA/GAMMA/NEUTRON WHOLE-BODY DOSIMETER
J.M. Hoffman, M.W. Mallett, H.H. Hsu, T. E. Buhl, D.G. Vasilik (LANL) , R.A. Tawil, (Harshaw/Bicron Corporation)

DESIGN, MODELING, AND IMPROVEMENTS TO THE LOS ALAMOS NATIONAL LABORATORY TLD BASED NEUTRON DOSIMETER
W. H. Casson, T.E. Buhl, R.T. Devine, J. M. Hoffman, H. H. Hsu, M.W. Mallett, and D.G. Vasilik, (LANL)

TLD SYSTEM ENDOVA-20 FOR INDIVIDUAL MONITORING ACCORDING TO THE ICRU RECOMMENDATIONS
Jan Loez and Georg Holzapfol (ENDOS, FRG)

A COMPARISON OF HYPERSENSITIVE TL MATERIALS IN CARD CONFIGURATIONS
K. J. Velbeck, Y. Tan, and R. A. Tawil (Harshaw/Bicron)

USING THE HIGH TEMPERATURE THERMOLUMINESCENCE PEAK OF ZrO_2 FOR THE PRECISION DOSIMETRY OF UV RADIATION
Ching-shen Su (National Tsing Hua University, Taiwan)

ULTRAVIOLET AND LASER RADIATION DOSIMETRY USING PHOTOSTIMULATED THERMOLUMINESCENCE IN CaSO4:Dy
Ademar J. Potiens Jr., and Leticia L. Campos (IPEN, Brazil)

A PRECISION BROAD-RANGE DOSIMETER-SPECTROMETER BASED ON CERIUM DOPED YTTRIUM ALUMINUM PERVOSKITE (YAP)
W. Peter Trower, Andrei A.Fyodorov, and Mark Mattson (Virginia Tech)

UV RADIATION IMAGE SENSOR UTILIZING PHOTOSTIMULATED LUMINESCENCE
A. Kalninsh, I. Plavina (Latvian Academy of Sciences), A.I. Popov, and A. Tale (University of Latvia)

OPTIMIZATION OF A NEW TLD ANNEALING PROCEDURE
René Michel, Fred N. Eichner, JosephC. McDonald (PNL), and Patrick J. Papin (San Diego State University)

4:55 p.m. Opening of Vendors Exhibits

Tuesday, October 25

8:30 p.m. Announcements

8:35 p.m. Session III - External Dosimetry
Chairman: Steve Sims (ORNL)

ESTIMATES OF BIAS AND UNCERTAINTY IN RECORDED EXTERNAL RADIATION DOSE
J.J. Fix, E. S. Gilbert, and W. V. Baumgartner (PNL)

EXPOSURE REDUCTIONS ENCOURAGED BY THE DETERMINATION OF THE EFFECTIVE DOSE EQUIVALENT FOR NON-UNIFORM EXTERNAL EXPOSURES
M.D. Matheny, C.G. Brown and S.G.Dyer (Westinghouse Savannah River Company)

DEVELOPMENT OF NEW METHODOLOGY FOR DOSE CALCULATION IN PHOTOGRAPHIC DOSIMETRY
Teresinha F.L. Daltro, and Letícia L. Campos, (IPEN, Brazil)

ENERGY DEPENDENCE OF PEN DOSEMETERS FOR X-RAYS (20-60 kV)
Eliane C. Oliveira, , Marcos Xavier, and Linda V.E. Caldas, (IPEN, BRAZIL

ELECTRONIC PERSONNEL DOSIMETER USE IN LOW ENERGY PHOTON AND BETA ENVIRONMENTS FOR LOW EXPOSURE DOSE TRACKING AND CONTROL
T. E. Goff, C. F. Wu (WIPP) and T. R. Ohlhaber (Siemens Dosimetry Services)

NEW PHOSPHATE GLASS DOSIMETER SYSTEMS FOR ROUTINE PERSONAL MONITORING
B. Burgkhardt, E. Piesch, and S. Ugi (Karlsruhe Nuclear Research Centre, Germany) T. Ishikawa, I. Ikegami, T. Omori, (Toshiba Glass, Japan)

10:10 a.m. Coffee Break

10:30 a.m. Session III (con't)

PERSONAL MONITORING AT ACCELERATORS USING CR-39
N. Anthony Greenhouse (LBL)

SITE SPECIFIC CALIBRATION OF THE HANFORD PERSONNEL NEUTRON DOSIMETER
A.W. Endres, L.W. Brackenbush, W.V. Baumgartner, B.A. Rathbone (PNL)

FIELD EVALUATION OF BUBBLE DOSIMETERS AT LOS ALAMOS NATIONAL LABORATORY
L. L. Romero, J. M. Hoffman, and R. T. Devine (LANL)

PERSONAL NEUTRON DOSIMETRY -- CONVERSION FACTORS, CALIBRATION AND DOSIMETER PERFORMANCE
Wolfgang G. Alberts, Marlies Luszik-Bhadra and Bernd R.L. Siebert (PTB,Germany)

ANGULAR VARIATION OF THE PERSONAL DOSE EQUIVALENT, Hp(0.07), FOR BETA RADIATION AND NEARLY MONOENERGETIC ELECTRON BEAMS
T.A. da Silva and C. G. Soares (NIST)

A TABULATION OF ABSORBED DOSE PER UNIT FLUENCE CONVERSION COEFFICIENTS FOR SLAB PHANTOMS OF THREE TISSUE EQUIVALENT MATERIALS FOR ELECTRON ENERGIES FROM 70 keV TO 10 MeV
G.F. Gualdrini, F. Padoani, U. de Maio (ENEA, Italy)

CONVERSION COEFFICIENTS FOR INDIVIDUAL MONITORING CALCULATED WITH INTEGRATED TIGER SERIES, ITS3, MONTE CARLO CODE
Robert T. Devine and Hsiao-Hua Hsu (LANL)

AGE DEPENDENCE OF ORGAN DOSE FROM EXTERNAL PHOTON SOURCES COMPUTED USING A MATHEMATICAL PHANTOM
Richard C. Ward, Mohammad T. Hussain, Jeffrey C. Ryman, Mark Cristy and Keith F. Eckerman (ORNL)

SKIN DOSE DETERMINATION USING SURVEY METERS AND VARSKIN MOD 2
René Michel, John J. Fix, and Joseph C. McDonald (PNL)

RESPONSE OF PANASONIC UD-802 AND UD-809 PERSONNEL DOSIMETERS TO FAST (PuBe) NEUTRONS
Becky S. Sobel and Kenneth A. Hardy (USAF)

12:30 Lunch Break

1:30 Session IV - Instrumentation
Chairman: John Frazier (Auxier and Assoc.)

A NEW NEUTRON DOSE EQUIVALENT RATE METER WITH IMPROVED NEUTRON ENERGY RESPONSE IN TERMS OF H*(10)
B. Burgkhardt, D. Fieg, E. Piesch (Karlsruhe Nuclear Research Centre, Germany), A. Klett, R. Maushart (EG&G Berthold, Germany)

RESPONSE CHARACTERISTICS OF AN EXTRAPOLATION CHAMBER MADE AT IPEN TO X RADIATION
Simone K. Dias, and Linda V.E. Caldas, (IPEN, Brazil)

MINIMUM DETECTABLE ACTIVITY OF PORTABLE CONTAMINATION SURVEY INSTRUMENTS
M.L. Johnson (PNL)

A FILTER TECHNIQUE FOR OPTIMIZING THE PHOTON ENERGY RESPONSE OF A SILICON PIN DIODE
Richard H. Olsher (LANL) Yosef Eisen (Soreq Nuclear Research Center, Israel)

ROUTINE CALIBRATION OF RADIATION PROTECTION MONITORING INSTRUMENTS: A FIVE YEARS PROGRESS REPORT
Maria P.P. Albuquerque and Linda V.E. Caldas, (IPEN, Brazil)

2:50 p.m. Coffee Break

3:10 p.m. Session IV (con't)

DEVELOPMENT OF A CALORIMETRIC SYSTEM FOR ELECTRON BEAM DOSIMETRY IN RADIATION PROCESSING
Homero E.B. Pérez, and Letícia L. Campos, (Instituto de Pesquisas Energéticas e Nucleares - CNEN/SP, Brazil)

USE OF PHOTOTRANSISTOR AS A RADIATION MONITOR
S.D. Dhole and V.N. Bhoraskar (Univ of Poona, India)

PHOTOSTIMULATED LUMINESCENCE IN KBr-IN INDUCED BY EXCITATION WITH UV RADIATION
I. Plavina (Latvian Academy of Sciences, Latvia) and A.I. Popov (University of Latvia, Latvia)

POWDERED KBr-In AS AN EFFECTIVE X-RAY STORAGE MATERIAL WITH A WIDE DYNAMIC RANGE
A. Kalninsh, I. Plavina, A. Tale (Latvian Academy of Sciences, Latvia) and A.I. Popov (University of Latvia, Latvia)

THE DEVELOPMENT OF A PASSIVE FIBER OPTIC SENSOR SYSTEM FOR REMOTE MONITORING IN LOW ENERGY GAMMA ENVIRONMENTS

M.A. Buckner, M.L. Bauer, D.E. Holcomb and M.L. Simpson (ORNL)

HOW HAND-HELD COMPUTERS ASSIST FACILITIES WITH FIELD INSTRUMENT SOURCE AND CALIBRATION CHECKING TO MEET THE INTENT OF 10 CFR 20 AND 10 CFR 835 REGULATIONS
W. Henry Bailey (NFS Radiation Protection Systems, Inc.)

PENCIL-CHAMBER MEASUREMENTS OF BACKSCATTER FROM ELONGATED FIELDS OF LOW-ENERGY X-RAYS
H.P. Maharaj (Department of Health, Canada)

RADIATION IMAGE SENSOR UTILIZING PHOTOSTIMULATED LUMINESCENCE
A. Kalninsh , I. Plavina (Latvian Academy of Sciences, Latvia), A.I.Popov and A. Tale (University of Latvia, Latvia)

DOSIMETRY OF MIXED RADIATION USING RECOMBINATION CHAMBER
Mieczyslaw Zielczynski and Natalia Golnik (Institute of Atomic Energy, Poland)

EVALUATION OF THE LONG TERM PERFORMANCE OF ELECTRONIC DOSIMETERS IN THE USA
Joseph Leon (MGP Instruments)

MICRODOSIMETRY MEASUREMENTS WITH THE REM-III ON THE SPACE SHUTTLE
Kenneth A. Hardy (USAF), M.J. Golightly (NASA), W. Atwell (Rockwell International), and W. Quam (EG&G Energy Measurements)

5:55 p.m. End of Session

Wednesday, October 26

8:30 a.m. Announcements

8:35 a.m. Session V - Internal Dosimetry
Chairman: Richard Vetter (Mayo Clinic)

DIFFERING INTERNAL DOSE CALCULATIONS FOR THE REVISED 10 CFR 20
Tony A. Rhea, (SAIC)

THE DEPARTMENT OF ENERGY'S LABORATORY ACCREDITATION PROGRAM FOR INTERNAL DOSIMETRY
T. L. Taylor and G. E. Grothaus (U.S. DOE-Idaho)

"IN VIVO" MEASUREMENTS PERFORMED WITHIN AN INTERNATIONAL INTERCOMPARISON PROGRAM FOR WHOLE BODY COUNTERS USING A "FOUR YEARS OLD" PHANTOM
T. Navarro Bravo, M.A. Lopez Ponte (CIEHAT- IMA, Spain)

RESULTS OF SUBSTITUTING THE NaI BY A Ge DETECTOR IN A SIMPLE SHADOW SHIELD WHOLE BODY COUNTER
Peter Sahre and Thomas Schönmuth (Nuclear Engineering and Analytics Inc., Germany), Klaus Thieme (Amersham Buchler Ltd & Co, Germany)

DOSE CONTRIBUTION FROM ORGANICALLY BOUND TRITIUM AFTER AN ACUTE TRITIATED WATER INTAKE
A. Trivedi, D. Galerui and R.B. Richardson (AECL , Canada)

NEW METHOD OF Sr-90 DETERMINATION IN LIQUID SAMPLES BY LIQUID SCINTILLATION COUNTING
A. Alvarez, N. Navarro, S. Salvador (CIEMAT, Spain)

DETERMINATION OF TRANSURANIC DAC EQUIVALENT FROM Ce-144
C. D. Stretch and E.A. O'Connor (Union Electric)

PROPOSAL OF A BIOASSAY PROGRAM FOR WORKERS OF THE THORIUM NITRATE PURIFICATION FACILITY AT THE IPEN-CNEN/SP
Janete C.G. Gaburo, Enocles E.M. Oliveira, Gian M.A.A. Sordi (Instituto de Pesquisas Energéticas e Nucleares, Brazil), Joyce L. Lipsztein (Instituto de Radioproteção e Dosimetria , Brazil)

DOSE DEPENDENT QUALITATIVE ANALYSIS OF THE EFFECTS OF TRITIATED WATER (HTO) ON THE DEVELOPING MOUSE CEREBELLUM FROM 15th DAY POST-COITUM
Narendra Jain (Govt. College,India) and A.L. Bhatia (University of Rajasthan, India)

10:55 a.m. Coffee Break

11:15 a.m. Session VI - Environmental
Chairman: Richard E. Swaja (ORNL)

EXTERNAL EXPOSURE TO ARBITRARY DISTRIBUTIONS OF RADIONUCLIDES IN SOIL
Jeffrey C. Ryman and Keith F. Eckerman (ORNL)

EVALUATION OF NEW AND CONVENTIONAL THERMOLUMINESCENT DOSIMETER PHOSPHORS FOR USE IN ROUTINE ENVIRONMENTAL MONITORING PROGRAMS USING AUTOMATED TLD READERS
B. A. Rathbone, A. W. Endres, E. J. Antonio (PNL)

HARSHAW/BICRON 8807 ENVIRONMENTAL DOSEMETER - IMPLEMENTATION ISSUES
Brian J. Lawson, Mark Moleski, Robert Karandy, Charles R. Phillips, Robert Champagne, and Richard J. Winslow (KAPL)

12:05 p.m. Lunch Break

1:00 p.m. Session VI (con't)

METHODOLOGY FOR PERFORMING SURVEYS FOR FIXED CONTAMINATION
J. S. Durham (PNL) and D. L. Gardner (Westinghouse Hanford Company)

CALIBRATION OF SURFACE CONTAMINATION MONITORS AT IPEN/SÄO PAULO
Linda V.E. Caldas, and Marcos Xavier (CNEN/SP, Brazil)

AUTOMATED RADIOACTIVE CONTROL SYSTEM OF THE MOSCOW MESON FACTORY'S RELEASES

S.V. Serezhnikov and V.E. Stepanov (Russian Academy of Sciences, Russia.)

RADIUM EQUIVALENT ACTIVITY OF BUILDING MATERIALS AND GAMMA RAY DOSE RATES IN ORDINARY HOUSES OF SÃO PAULO, BRAZIL
M.P. Campos and B.R.S. Pecequilo (Instituto de Pesquisas Energéticas e Nucleares, Brasil)

MICROCLIMATIC EFFECTS ON OUTDOOR RADON AND ITS PROGENY IN A LONG-TERN STUDY
M. Schütz, G. Keller, R.J.A. Kappel (Univ of Saarland, Germany)

INTERCALIBRATION OF VARIOUS TYPES OF PASSIVE RADON DOSIMETERS EMPLOYING PARTICLE TRACK DETECTORS
A.A. Qureshi, K. Jamil, Daiss Al-Ahmady, Fazal-ur-Rehman and H.A. Khan (PINSTECH, Pakistan)

2:30 p.m. Coffee Break

2:50 p.m. Session VII - Calibration, Standards, and Accreditation
Chairman: John Poston (Texas A&M)

STATUS OF THE REVISION OF ANSI N13.27, "PERFORMANCE SPECIFICATIONS FOR POCKET-SIZED ALARMING DOSIMETERS/ RATEMETERS"
J.S. Bogard (ORNL)

THE DOE LABORATORY ACCREDITATION PROGRAM PERFORMANCE TESTING LABORATORY AUTOMATED CALIBRATION VERIFICATION PROGRAM
Rick Cummings and Rich Kershisnik (U.S. DOE-Idaho), Randy Holloway (EG&G Idaho, Inc.)

THE DOE LABORATORY ACCREDITATION PROGRAM 8 YEARS LATER
Rick Cummings, Rich Kershisnik, Tansy Taylor and Gary Grothaus (U.S. DOE-Idaho), Robert M. Loesch (U.S. DOE, Washington D.C.)

RECENT CHANGES IN ACCREDITATION PHILOSOPHY
R.M. Loesch (U.S.DOE Washington, DC)

NEUTRON FIELD CHARACTERIZATION FOR A CALIBRATION LABORATORY
A.J.P. Ghilardi (Universidade de Sao Paulo, Brasil), E.B. Lee (Univ of Tennessee), W.H. Casson (LANL), J.S. Bogard (ORNL)

NEUTRON CALIBRATION FACILITIES
Gordon K. Riel (NSWC)

CALIBRATION OF REFERENCE NEUTRON FIELDS FOR DOSIMETER AND CRITICALITY ALARM VALIDATION AND INTERCOMPARISON
Michael B. Stanka and Richard C. Harrison (Aberdeen Proving Ground)

ESTABLISHING A ^{252}Cf SOURCE FOR NEUTRON IRRADIATIONS OF PERSONNEL DOSIMETRY AT THE IDAHO NATIONAL ENGINEERING LABORATORY (INEL)
Orval R. Perry and Paul E. Ruther (EG&G Idaho, Inc.)

COMPARISON OF NIST AND ISO FILTERED BREMSSTRAHLUNG CALIBRATION BEAMS
C.G. Soares and M. Ehrlich, (NIST)

OPTIMAL FILTERS FOR ISO K-FLUORESCENCE REFERENCE RADIATIONS
Jing Chen (GSF, Germany) and Hsiao-Hua Hsu (LANL)

ESTABLISHING A URANIUM SLAB SOURCE FOR BETA IRRADITIONS OF PERSONNEL DOSIMETRY AT THE IDAHO NATIONAL ENGINEERING LABORATORY (INEL)
Laird C. Bean, Orval R. Perry, and Paul E. Ruhter (EG&G Idaho, Inc.)

CALIBRATION STANDARDS USING NUCLIDES INCORPORATED INTO POLYMERIC MEMBRANES
Gary E. Strathearn, Karl Amlauer, Aman Khan, and Ana R. Ramirez (Isotope Products Laboratories)

TRACEABILITY OF A PANORAMIC GAMMA IRRADIATOR USING DIFFERENT TLD SYSTEMS AS TRANSFER INSTRUMENTS
J.C. Saez-Vergara and A.M. Romero (CIEMAT, Spain)

6:10 p.m. End of Session

Thursday, October 27

8:30 a.m. Announcements

8:35 a.m. Session VIII - Medical, Accident, and High Level Dosimetry
Chairman: Keith Eckerman (ORNL)

THE IMPORTANCE OF RADIOPROTECTION CONTROLS IN NUCLEAR MEDICINE
A Sahyun, M.P. Sanches and G.M.A.A. Sordi (IPEN-CNEN/SP, Brazil)

RADIATION PROTECTION IN HOSPITALS
Richard J. Vetter (Mayo Clinic/Foundation)

OCCUPATIONAL HEALTH EXPERIENCE IN THE PRODUCTION AND DISTRIBUTION OF RADIONUCLIDES USED IN MEDICINE
Janete C. Gaburo, Matias P. Sanches, and Gian M.A.A. Sordi, (CNEN/SP, Brazil)

VERIFICATION OF RADIONUCLIDE CALIBRATORS USED IN THE NUCLEAR MEDICINE LABORATORIES IN THE CZECH AND SLOVAK REPUBLICS
J. Suran, P. Jasanovsky, and P. Dryak

CALIBRATION OF CLINICAL DOSEMETERS IN THE IAEA WATER PHANTOM
Linda V.E. Caldas and Maria P.P. Albuquerque (CNEN/SP, Brazil)

CUTANEOUS MITOCHONDRIAL PROTECTION BY TOPICAL TREATMENT OF HERBAL ANTIOXIDANTS FOLLOWING 60 CO-GAMMA IRRADIATION
Faramarz Ashoori, Rei Takahashi, Jain Zhou, Taketoshi Sugiyama (Kyoto University School of Medicine, Japan), and Ikuo Nishigaki (Institute of Applied Biochemistry, Japan)

10:10 a.m. Coffee Break

10:30 a.m. Session VIII (con't)

DOSIMETRY OF ELECTRON AND GAMMA RADIATION WITH DL-ALANINE
Zelia M. Costa and Leticia L. Campos (CNEN/SP, Brazil)

SENSITIVITY IMPROVEMENT OF FRICKE DOSIMETER FOR 14 MeV NEUTRONS
N. Nagesh, G.R. Pansare and V.N. Bhoraskar (Univ of Poona, India)

THE LOS ALAMOS NATIONAL LABORATORY NUCLEAR ACCIDENT DOSIMETER: OVERVIEW AND RECENT DEVELOPMENTS
T.E. Buhl, W.H. Casson, J.M. Hoffman, D.L. Upp, L.L. Romero, and D.G. Vasilik (LANL)

A ROUTINE CHEMICAL DOSIMETRIC SYSTEM USING THE MODIFIED CERIC SULPHATE DOSIMETER
Lucy K. Yamanaka and Linda V.E. Caldas (CNEN/SP, Brazil)

A STUDY OF IRRADIATION-INDUCED DAMAGE IN α-QUARTZ
I.Kh. Abdukadyrova

HERMETIC INPUTS OF POWER AND CONTROL CABLES FOR ATOM ENERGETICS
M. Muminov, M. Mukhamedzhanov, Kh. Nurmatov, Yu. Skripnikov (Institute of Nuclear Physics, Uzbekistan), N. Kostyukov, N. Minakov (Engineering Technologic Center, Russia)

IONIZING RADIATION DOSIMETRY BASED ON OPTICAL PARAMETERS WIDTH MEASUREMENTS OF OXIDES
I.Kh. Abdukadyrova

12:15 p.m. Lunch Break

1:15 p.m. Works in Progress Session

2:15 p.m. Session IX - TLD Systems
Chairman: C. Glenn Hudson

ANGULAR DEPENDENCE OF DOSE EQUIVALENT RESPONSE OF AN ALBEDO NEUTRON DOSIMETER

B. A. Torres (Georgetown University), E. Boswell and R. B. Schwartz (NIST)

COMPARISON OF RESPONSES OF THERMOLUMINESCENT DOSEMETERS IRRADIATED BY SOFT X-RAYS AT VERY LOW AND VERY HIGH DOSE RATE LEVELS
M. Pietriková-Fárníková, J. Krása, L. Juha (Academy of Sciences of the Czech Republic)

ESTABLISHING A MINIMUM REPORTING LEVEL (GAMMA) FOR THE PERSONNEL DOSIMETRY DEVICE WORN AT THE IDAHO NATIONAL ENGINEERING LABORATORY (INEL)
Orval R. Perry, Brian L. Andersen, and Paul E. Ruther (EG&G Idaho, Inc.)

A NEW EXTREMITY SYSTEM AND PERFORMANCE AT INEL
O.R. Perry (EG&G Idaho, Inc.), R.A. Tawil, K.J. Velbeck, J.E. Rotunda (Harshaw/Bicron Radiation Measurements Products)

3:10 p.m. Coffee Break

3:30 p.m. Session IX (con't)

IMPROVED BETA SENSITIVITY UNDER FIELD CONDITIONS FOR THE PANASONIC UD-807 EXTREMITY DOSIMETER
J. Robert Flood (TVA)

TIME-DEPENDENT, LOW-DOSE REPORTING LIMIT FOR DOSIMETERS THAT ARE TAKEN HOME AT THE END OF THE WORKDAY
Edward Sonder (ORNL)

MODIFICATION OF DOSE ALGORITHM FOR TELEDYNE 9150 TLD SYSTEM AND PERFORMANCE TEST OF THE ALGORITHM VIA INTERCOMPARISON STUDIES
Jang-Lyul Kim and Si-Young Chang (KAERI, Korea)

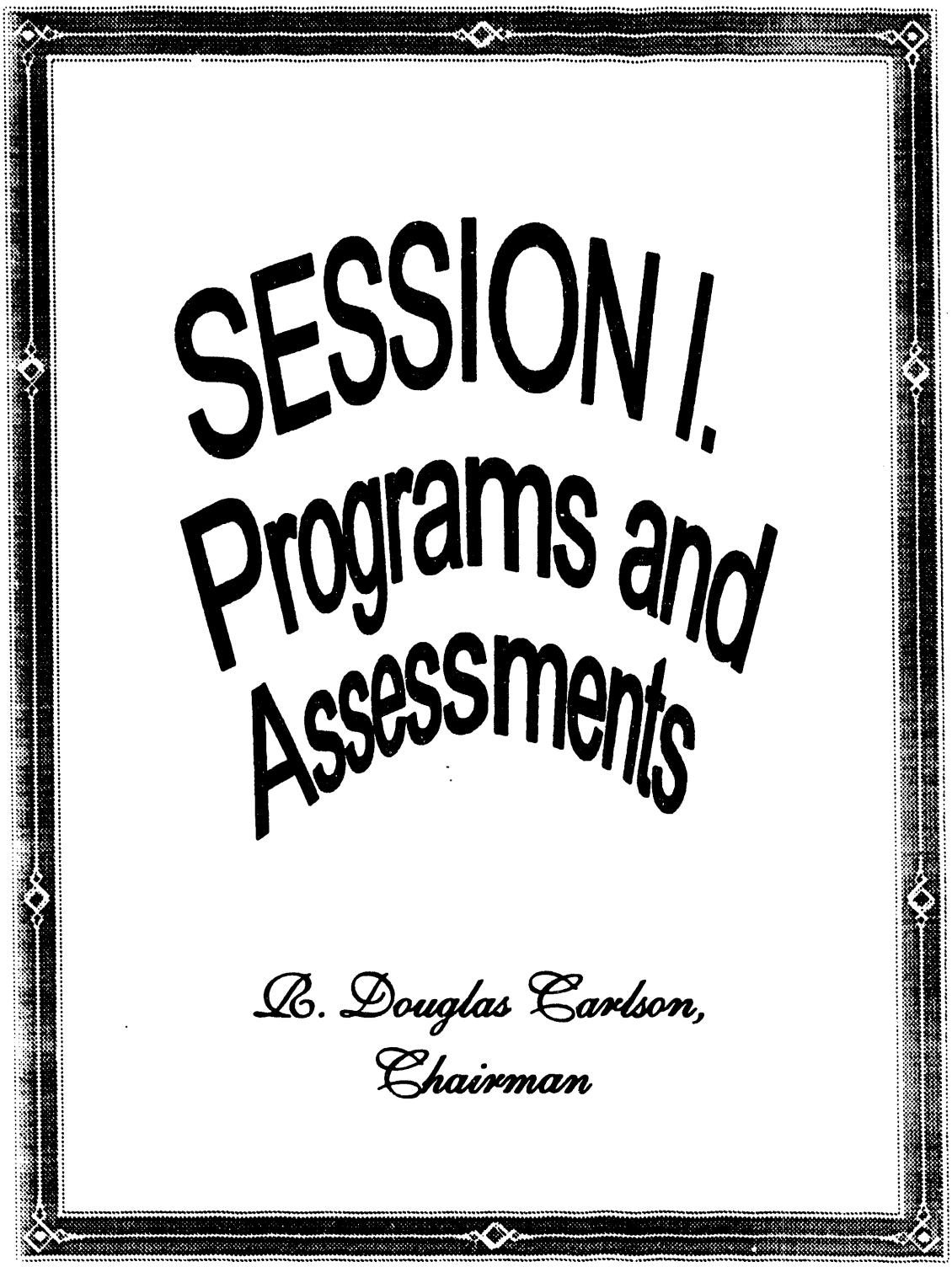
A TLD DOSE ALGORITHM FOR MIXED FIELDS AT A NUCLEAR WEAPONS FACILITY
Neil Stanford (Stanford Dosimetry), Christopher N. Passmore, Mark Prather, Jerome B. Martin (Battelle Pantex)

A NEW APPROACH TO TLD DOSE ALGORITHMS
Marko Moscovitch (Georgetown University), D.J. Rotunda (Harshaw/Bicron)

AUTOMATIC SCREENING OF ABNORMAL LiF:Mg,Ti GLOW CURVES FOR USE IN ROUTINE DOSIMETRY
Y.Tan, J.E.Rotunda, K.J. Velbeck, and R.A. Tawil (Harshaw/Bicron)

SELFDOSE MEASUREMENTS IN ROUTINE PERSONAL AND ENVIRONMENTAL TLD SYSTEMS
J.C. Saez-Vergara, A.M. Romero, A. Delgado (CIEMAT , Spain)

5:30 p.m. Closing Remarks


SESSION I.
Programs and
Assessments
R. Douglas Carlson,
Chairman

PERSONAL MONITORING IN THE UNITED KINGDOM

T.O. Marshall
National Radiological Protection Board, Chilton, Didcot, Oxon, OX11 0RQ, UK

ABSTRACT

This paper is intended to provide some insight into the status of personal monitoring in the United Kingdom for external radiation.

Personal dosimetry services for classified workers must operate within the legislative framework of the Ionising Radiations Regulations, stemming from the Directive of the Council of the European Economic Community. The Regulations are, in the main, the work of the Health and Safety Executive (HSE) who also approve dosimetry services for the monitoring of classified workers. The basis of approval and performance tests dosimetry services are obliged to pass are discussed.

There is a relatively larger number of services in operation in the UK: an indication of the number and their size is given. Until recently these services measured a variety of radiation quantities but from 1st January 1994 they were required to measure the ICRU operational quantity Personal Dose Equivalent at depths of 10 and 0.07 mm. The design and performance of dosemeters used in the UK to measure these quantities for neutrons and photons are discussed paying particular attention to progress made on the introduction of an approved service based on an electronic dosemeter.

There is also a large number of services in UK approved for co-ordination and dose record keeping. In addition the HSE operates a central index of dose information (CIDI) to which the approved dosimetry services send annual summaries of dose information collected throughout the year. Each year HSE publishes a summary of statistics from the data it receives and recently it published an analysis of data collected over the period 1986-1991 in which important trends could be seen. These data are discussed in more detail in another paper presented at the Conference.

Increasing attention is being paid by UK personal monitoring services to quality assurance since some customers insist on delving into this aspect in considerable depth. Quality control and assurance procedures followed at the NRPB are discussed.

1. Introduction

This article is intended to provide some insight into the status of personal monitoring in the United Kingdom for external radiation. The topics covered are, the legislative position, the number of monitoring services in the UK, the radiation quantities measured, the types of dosemeters used, dose record keeping services including the Central Index of Dose Information concluding with a section on quality assurance.

2. The Legislative Position

To understand the development of regulations concerning the use of ionising radiations in UK one must remember that the UK is a Member State of the European Community (EEC). The basis of national regulations within EEC is the Council Directive of 15th July 1980[1] and Council Directive of 3rd September 1984[2]. These documents which are based on recommendations of the ICRP were produced by the Commission of the European Communities (CEC) after taking advice from a number of expert groups.

The major responsibility for the implementation of the Directive in the UK falls to the Health and Safety Executive (HSE) although some responsibility falls to the Ministry of Transport, the Department of Trade and Industry, the Department of Energy and Her Majesty's Inspectorate of Pollution.

The current Directive and hence the UK Ionising Radiations Regulations (1985)[3] are based on ICRP recommendations given in Publication 26 (1977)[4]. However, following the issue of Publication 60 (1990)[5] a new Directive is in preparation and new UK regulations will follow within a period of about 5 years.

The current legislation requires employers of workers likely to receive doses in excess of three tenths of the dose limits to have these persons monitored by a dosimetry service approved by HSE and the results recorded by a service also approved by HSE. The dose record keeping service is also required to supply annual summaries of these doses to the Central Index of Dose Information (CIDI).

The HSE have published several documents giving guidance to services seeking approval. A general document is entitled "HSE Statement of the Approval of Dosimetry Services" September 1992. More detailed guidance is given in a three part document entitled "Requirements for the approval of dosimetry services under the Ionising Radiations Regulations 1985": Part 1 - External Radiations; Part 2 - Internal Radiations; and Part 3 - Co-ordination and record keeping.

These publications are available from the Secretary of the HSE Dosimetry Services Panel.

An application for approval should include: a description of the scope of the service, a laboratory statement giving the required details on the service, a copy of the authorised dosimetric performance test, and the appropriate fee - approximately £500 per service.

The approval does not apply to the dosemeter but to the service as a whole and HSE will make enquiries into the service's organisation, resources, personnel and methods. An inspector will also visit the service to carry out an inspection. Guidance on these more general requirements is given in another HSE document "General Guidance for Laboratories Providing Personal Dosimetry Services" 1991.

Once approval has been granted the service is obliged to undergo performance tests at yearly intervals. HSE inspectors will also visit the service regularly and a reassessment will be carried out at intervals of 3, 5 or 7 years depending upon the nature of the service.

HSE retains the right to revoke the approval of a dosimetry service which no longer meets the requirements laid down.

3. UK Approved Dosimetry Services

There are approximately 150,000 persons monitored within the UK of which about 60,000 are classified workers who require dose record keeping. These are monitored by a large number of services approaching 40 in all. Six major organisations are involved each operating a number of laboratories. The organisations, and the number of laboratories they operate are given in Table 1.

Table 1: UK Personal Monitoring Services

Organisation	Laboratories
National Radiological Protection Board	3
Health Authorities	12
Nuclear Electric	10
AEA Technology	3
Ministry of Defence	2
British Nuclear Fuels	3
Others	7
TOTAL	39

About 85% of the personal monitoring workload in the UK concerns whole body monitoring for X-, beta- and γ-radiation. About 5% concerns whole body monitoring for neutron radiations and the remaining 10% concerns monitoring of the extremities. A very small workload concerns monitoring the exposure of non-coal miners to radon gas.

4. Radiation Quantities

Until several years ago a mixture of radiation quantities was measured by dosimetry services in the UK. Thermoluminescent dosemeters were designed to measure the dose equivalent at depths of 0.07 mm and at a specified depth in the range 4 mm to 10 mm in the wearers body. Photographic film dosemeters were designed to measure the dose equivalent at or near the surface of the body. Neutron dosemeters were designed to measure the maximum of the dose equivalent distribution in a 30 cm diameter x 60 cm tissue equivalent cylindrical phantom. Skin dosemeters attempted to measure the dose equivalent at a depth of 0.07 mm and extremity dosemeters at a depth of 0.5 mm. This was a very untidy approach to dosimetry and resulted in some conceptual difficulties in that doses of different radiation types measured with different types of dosemeter were strictly not additive.

Recently there has been a move towards the use of the ICRU operational quantities first defined in ICRU Report 39[6] (1985) and elaborated upon in Reports 43[7] (1988) and 47[8] (1992). The personal dose equivalents $H_p(10)$ and $H_p(0.07)$ are defined in Report 47 as the dose equivalents at depths of 10 mm and 0.07 mm respectively beneath a specified point on the body and are meant to provide a reasonable approximation of the effective dose equivalent and of the dose equivalent to the most heavily exposed single organ and to skin. Calculations and experimental work have shown that by and large these quantities do achieve the above objectives and personal monitoring services approved by the HSE are now required to measure them. This was the case from 1st January 1994.

The ICRU quantities have a number of important advantages as follows:

a) their use is fully supported by ICRP and ICRU,
b) they represent a unified system of dose measurement,
c) results of all measurements irrespective of the type and energy of the radiation are additive, and
d) it is not difficult to design dosemeters to measure the new quantities.

Some aspects of the implementation of these quantities still have to be resolved concerning the choice of shape and material of phantoms for dosemeter calibration and type testing. Initially ICRU recommended (Report 39)[6] the use of a tissue equivalent 30 cm diameter sphere. In a later report (Report 47)[8] ICRU recommended a 30 cm x 30 cm x 15 cm slab as being a more convenient shape and indicated that perspex would be a suitable material. However, a committee of the International Standards Organisation on dosemeter calibration is moving towards a thin perspex walled slab filled with water. It is hoped that for reasons of harmonisation and consistency in the field of dosimetry that a phantom will be decided upon very soon which is universally accepted and used throughout the world.

5. Dosemeters

Although a large number of personal dosimetry services operate in the UK the types of dosemeter used are relatively few in number.

Approximately 60% of all X-, beta- and γ-ray measurements are made with the NRPB/AERE film dosemeter[9], about 30% are made with the NRPB thermoluminescent[10] dosemeter and the remainder are carried out with either Panasonic or NE Technology thermoluminescent dosemeters. Some measurements are made with the Landauer film dosemeter, the dosemeters being processed in their US laboratory at Glenwood.

The British photographic film dosemeter was designed about 30 years ago as a joint venture by the Radiological Protection Service (later amalgamated into NRPB) and the United Kingdom Atomic Energy Authority (UKAEA). The film used is the Eastman Kodak Type 2 which is a double emulsion film, the fast emulsion being used for low dose evaluation and the slow emulsion for large doses. The fast emulsion is removed whenever it is necessary to use the slow emulsion.

To overcome the energy dependence of the film response it is worn in a holder which contains a number of plastic and metallic filters as follows:

- unfiltered area
- 50 mg cm^{-2} plastic filter
- 300 mg cm^{-2} plastic
- 1 mm duralumin
- 0.7 mm tin plus 0.3 mm lead

The unfiltered area together with both plastic filtered areas are used for beta-ray dosimetry; the dosemeter is suitable for beta-ray fields with energies (E_{max}) greater than 0.5 MeV.

X- and γ-ray doses are evaluated using the metallic and 300 mg cm^{-2} plastic filtered areas. This is done by means of two algorithms one to evaluate H_p10) and the other for $H_p(0.07)$. The algorithms are given in report NRPB-R236[9].

The variation in dosemeter response with photon energy and angle of incidence for the quantities $H_p(10)$ and $H_p(0.07)$ is shown in Figure 1[9]. The values at each energy are the mean values for angles of incidence of 0°, 30° and 60°.

The NRPB thermoluminescent[10] dosemeter is the most commonly used thermoluminescent dosemeter in the UK. It is a two element dosemeter incorporating two ^{7}LiF in teflon disks, one positioned beneath a plastic/aluminium filter to measure $H_p(10)$ and the other which is unfiltered to measure $H_p(0.07)$. The ^{7}LiF in teflon disks are tissue equivalent so that with the correct calibration these measure the required quantities without the use of an algorithm. The variation in response with photon energy and angle of incidence of the radiation is shown in Figure 2[11] for both $H_p(10)$ and $H_p(0.07)$. The values at each energy are the means for angles of incidence of 0°, 20°, 40° and 60°.

Over the past decade work has proceeded on the development of an electronic personal dosemeter for the measurement of photon and beta-ray doses in terms of $H_p(10)$ and $H_p(0.07)$. The development has been carried out by NRPB and a commercial organisation with appropriate electronic design and manufacturing experience, Siemens Plessey Controls Ltd[12]. The dosemeter is capable of displaying dose or dose rates and is much more sensitive than passive dosemeters. It can register dose equivalents as low as 1 μSv and dose equivalent rates as low as 1 μSv h^{-1}. Visual and audible alarms are provided which can be set at prescribed levels by authorised persons. There are two dose stores having different security levels. The dose store used for legal dose record keeping purposes can be read by the wearer but can only be reset by an Approved Dosimetry Service. The other dose store meant for daily dose control can be reset by the Operational Health Physicist. This dosemeter has been successfully type tested, has undergone wearer trials and a successful submission for approval has been made to HSE. NRPB will now operate an EPD service for its own staff. This is expected to be extended to outside customers after about 1 year's operational experience. The EPD is shown in Figure 3 and its energy response is shown in Figure 4 for $H_p(10)$ and $H_p(0.07)$ for normal incidence.

Extremity monitoring is carried out in UK exclusively with thermoluminescence detectors. Some are in the form of ring dosemeters but the NRPB uses detectors in tape form. These dosemeters and their coverings are sufficiently thin to measure the dose at a depth of 0.07 mm even from low energy beta-ray emitters such as ^{147}Pm (mean energy 60 keV). They are in some cases fixed to the finger using an adhesive tape or sometimes worn in a finger stall.

Three types of dosemeter are in use in the UK for personal neutron monitoring. In the late 1950s the nuclear track emulsion was introduced. This consisted of a fine grained emulsion capable of recording the tracks of recoil protons. These tracks could be observed and counted using a high magnification (X1000) microscope. It was always recognised that this dosemeter had serious disadvantages but it has proved difficult to find a replacement. The energy response is poor with a threshold in the region 0.75 to 1 MeV and the dose range is limited ie., about 0.2 to 50 mSv. The tracks are tedious to count and they fade with a half life of about 14 days unless the emulsion is desiccated and sealed in a nitrogen atmosphere in moisture proof packets before use. Nevertheless the dosemeter is still in use for fast neutrons such as those from $^{241}Am/Be$ sources used in soil moisture/density meters and those produced by the D-T and D-D reactions in neutron generators.

In the early 1970's Albedo neutron dosemeters were developed. These use thermoluminescence detectors to measure gamma radiation and thermal neutrons reflected from the body of the wearer following moderation of the incident neutrons in his body. These devices measure neutrons with energies less than 10 keV reasonably accurately but above this energy the response falls rapidly to practically zero. Thus a correction has to be applied to allow for that part of the neutron spectrum the dosemeter is unable to measure. This correction is usually large and site specific and determined for each area by using a crude spectrometer. This type of device is still in use in circumstances where a substantial part of the spectrum is made up of low energy neutrons such as in shielded areas around nuclear reactors.

However both the above techniques are now giving way to the track etch method usually using a plastic, poly-allyl diglycol carbonate (PADC), sometimes referred to by its trade name CR-39. Recoil protons leave damage tracks in this plastic which can be made visible to the naked eye and easily counted with a

X40 magnification by etching with sodium hydroxide. In some systems a simple chemical etch is applied, in others, to extend the energy range to as low a value as possible, an electro chemical etch is used.

This type of dosemeter although expensive has a number of advantages. It is insensitive to gamma radiation and the tracks do not fade. The energy response is far superior to that of either the nuclear emulsion or Albedo dosemeters. The energy response is shown in Figure 5 for the electro-chemically etched NRPB dosemeter for rotationally isotropic fields.

6. Record Keeping

There is a large number of services in UK approved for co-ordination and dose record keeping. One of the larger ones is operated by the NRPB and is described here.

This service has been approved by the Health and Safety Executive under the Ionising Radiations Regulations 1985 to enable an employer to meet his statutory obligation to delegate to NRPB the statutory responsibility for maintaining the dose records of his classified workers.

The service was initially based primarily on the standard thermoluminescent dosemeter, since the automated processing and computer control of this type of dosemeter allows record keeping to be carried out accurately and economically with the minimum of 'form filling', but it has now been linked also to the photographic film, neutron film and radon dosemeters in a similar manner. Entry of doses from other NRPB services are made manually.

Individual dose records contain the worker's name and national insurance number and employer's reference number. The database can be queried so as to group data for all employees of an employer. The record comprises each individual dose assessment and summarised dose history.

There is very little administrative work involved for the customer once the worker's name and national insurance number and previous dose history have been registered with the service; all information is safeguarded.

Dose reports are issued whenever a dose is added to the record and in addition a dose summary is issued routinely by the computer following each calendar quarter. Details of the reports supplied are given below.

The basis of the dosemeter issue and record keeping is a suit of programs under the acronym ARKID (Approved Record Keeping and Issue of Dosemeters) using ORACLE and operating in a DEC VAX computer.

ARKID contains details of employers and their requirements for dosemeters. It also contains the dose records for all workers for whom records are currently being maintained together with details of their age, sex and employment address. The data is reorganised annually and individual dose assessments are maintained for the current year and the previous two to three years. Earlier data is archived at the annual reorganisation.

A record is maintained of national insurance numbers for persons who do not have active records on ARKID but where data is archived. Details are maintained of all dosemeters issued by ARKID under computer control. These include the thermoluminescent dosemeters, film dosemeters, neutron dosemeters and radon dosemeters. For the re-usable TLD, a record of previous users, individual dose assessments and total cumulative dose is recorded, together with details of any damage or contamination.

The dose information from the automated processing equipment is fed to the DEC VAX computer by direct link. All other information is entered via visual display units. This will include information about

employers and workers together with dose information provided by other ADSs. Dosemeter issue requirements are received by direct link from the NRPB Finance Computer.

Reports supplied to employers for employees registered with the dose record keeping service are as follows:-

i) **Registration Report**

This report is supplied to the employer after a worker is registered. The registration report certifies that the worker's record is being kept by NRPB on behalf of his employer. In addition, the report summarises any known radiation dose prior to NRPB undertaking the current record keeping.

ii) **Information Report**

This report is supplied should an up-to-date summary of a dose record be required.

iii) **Quarterly Dose Report**

This is issued during the sixth week after the end of each calendar quarter and summarises the dose records of each registered person. Dose summaries are included for the last completed quarter and previous quarters in the year. The report for the fourth quarter of the year acts as an annual dose summary. The annual dose summary of all classified persons is sent by NRPB to the Central Index of Dose Information (CIDI) of the Health and Safety Executive.

iv) **Termination Record**

When a classified person leaves his employment a Termination Record is sent by NRPB to CIDI. A copy is supplied to the employer to give to the worker as required by the Ionising Radiations Regulations 1985. Where records have been kept for a person who is not a classified worker, a termination record is provided for the worker but not sent to CIDI.

v) **Closing Report**

This report is a summary of the dose record and is supplied to the employer whenever dose record keeping is terminated for an employee.

vi) **Dose Notification Report**

The Dose Notification Report (DNR) is issued whenever a dose is added to a person's dose record. This may be from a dosemeter undergoing automated processing or by a manual entry of a dose provided by another ADS. Where a dosemeter has been laundered or otherwise damaged, the report states that no dose assessment was possible and requests an estimated dose to be provided.

vii) **Warning Reports**

If a worker's accumulated dose exceeds 60% of any limit a warning message is included on the DNR. Should a limit be exceeded a letter is sent to the employer stating the action required under the Ionising Radiations Regulations 1985.

7. <u>The Central Index of Dose Information (CIDI)</u>

CIDI is the Health and Safety Executive's national database of occupational exposure to ionising radiation operated on an agency basis by NRPB. It receives information on annual radiation doses recorded

for classified persons in the UK, and on termination of employment. This is provided by approved dosimetry services to satisfy the requirements of the Ionising Radiations Regulations 1985. The data provided for CIDI are treated as confidential in respect of individual persons and employers. The computer files are protected under various safeguards and the database is registered by the Health and Safety Executive under the Data Protection Act 1984. CIDI is the subject of a separate report to be presented at the Conference.

8. Quality Assurance

The basis of Quality Assurance (QA) in personal monitoring in the UK is the scheme of approval operated by the HSE. However, some services are moving towards the spirit of more formal schemes specified by standards organisations such as ISO. The NRPB, for example has stated its commitment to a QA programme and the personal monitoring services are producing a QA manual and all the associated documentation and procedures in accordance with ISO QA standard 9000.

Currently type tests of all the NRPB dosemeters are carried out periodically and whenever any modification is introduced. In addition regular traceability determinations are made for all services to link their measurements to primary radiation standards held at the National Physical Laboratory. NRPB has also introduced a novel idea first introduced by the Radiological Protection Services of TNO in the Netherlands. The overall performance of each service is assessed from the users' point of view via the issue of dosemeters to a dummy customer. These tests are part of a thorough quality assurance programme. This quality assurance programme, which includes detailed quality control procedures, has been developed to cover all personal monitoring services, and all aspects from acceptance of dosimetric materials through to the dummy customer. It includes full documentation, established routine quality control procedures, and testing and commissioning of new equipment as well as an annual audit.

9. Summary

An attempt has been made to provide an overview of personal monitoring in the UK. This activity has always been recognised as an important part of radiological protection and a great deal of effort has been devoted, over the years, in UK, to the development of personal dosemeters and personal dosimetry systems as well as running high quality services.

10. References

1. Council Directive of 15th July 1980 amending the Directives laying down the basic safety standards for the health protection of the general public and workers against the dangers of ionising radiation. Official Journal of the European Communities 23 (1980) L246.

2. Council Directive of 3rd September 1984 amending Directive 80/836/Euratom as regards the basic safety standards for the health protection of the general public and workers against the dangers of ionising radiation. Official Journal of the European Communities 27 (1984) L265.

3. The Ionising Radiations Regulations 1985. London, Her Majesty's Stationary Office SI (1985) 1333.

4. International Commission on Radiological Protection. Recommendations of the International Commission on Radiological Protection. ICRP Publication 26, Ann. ICRP, 1, No.3 (Pergamon Press, Oxford) (1977).

5. International Commission on Radiological Protection. 1990 Recommendations of the ICRP. ICRP Publication 60, Ann. ICRP 21(1).

6. International Commission on Radiation Units and Measurements. Determination of dose equivalents resulting from external radiation sources. ICRU Report 39, Bethesda, MD (1985).

7. International Commission on Radiation Units and Measurements. Determination of dose equivalents from external radiation sources - part 2. ICRU Report 43, Bethesda, MD (1988).

8. International Commission on Radiation Units and Measurements. Determination of dose equivalents from external radiation sources - part 3. ICRU Report 47, Bethesda, MD (1992).

9. Iles, W.J., Milton, M.I.L., Bartlett, D.T., Burgess, P.H. and Hill, C.E. Type testing of the NRPB/AERE film badge dosemeter in terms of the new ICRU secondary quantities. Part 1 - Photons over the energy range 10 keV - 1250 keV. NRPB-R236 (1990).

10. Bartlett, D.T., Hessey, J.D., Burgess, P.H., Hill, C.E., McClure, D.R., Steele, J.D. and Watson, P. A modified design of photon personal dosemeter to measure the ICRU personal monitoring quantity $H_p(10)$. Rad. Prot. Dosim. 48(2), pp209-211 (1993).

11. Marshall, T.O., Bartlett, D.T., Burgess, P.H., Cranston, C.S., Higginbottom, D.J. and Sutton, K.W. The development of an electronic dosemeter. Occupational Radiation Protection, BNES, London (1991).

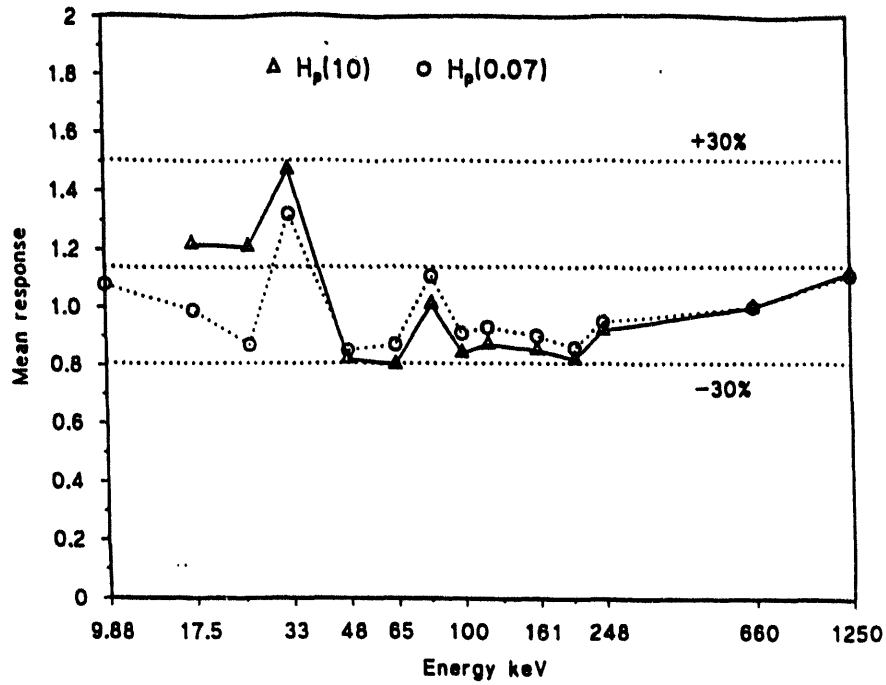


Figure 1: Energy Response of NRPB/AERE Film Dosemeter

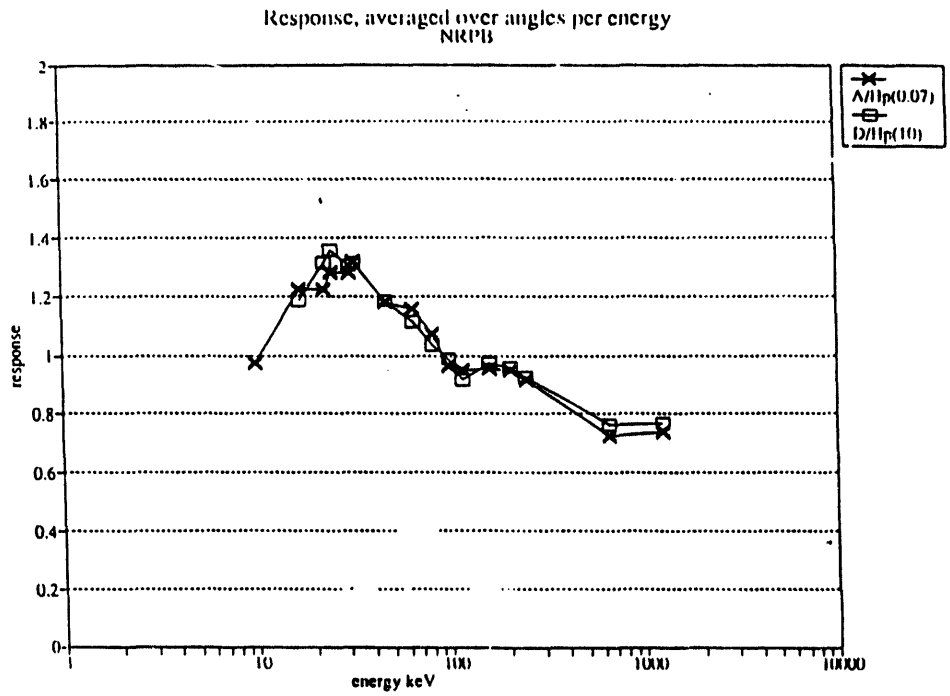


Figure 2: Energy Response of NRPB Thermoluminescent Dosemeter

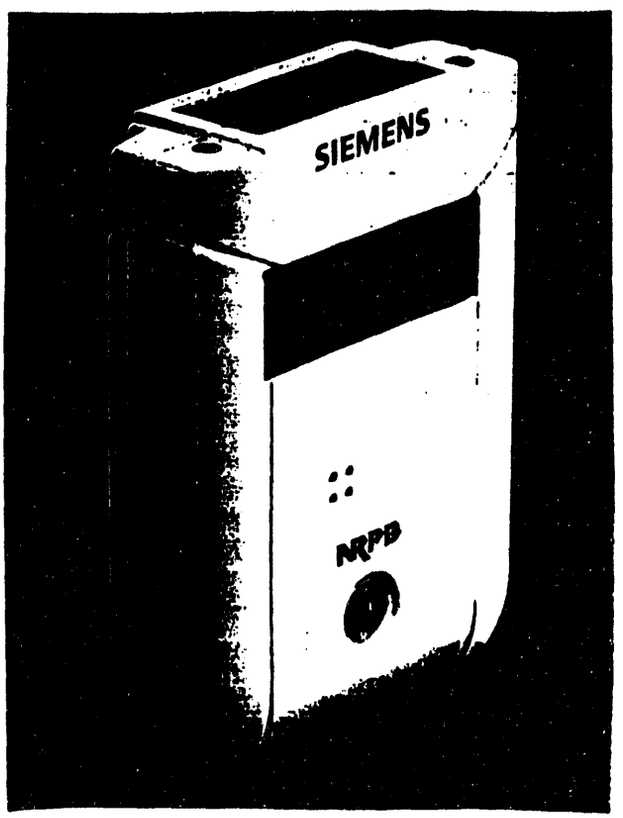


Figure 3: The Electronic Personal Dosemeter

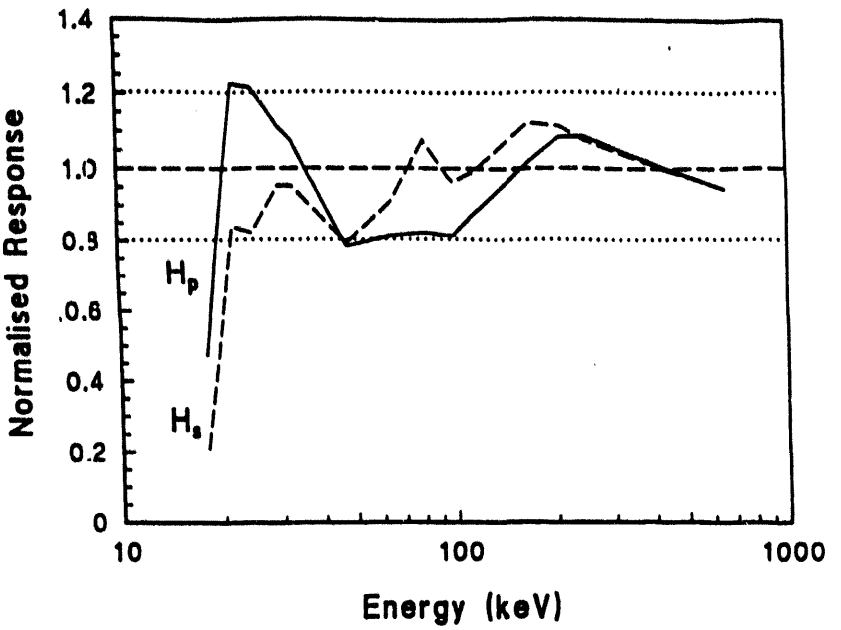


Figure 4: Energy Response of the Electronic Personal Dosemeter

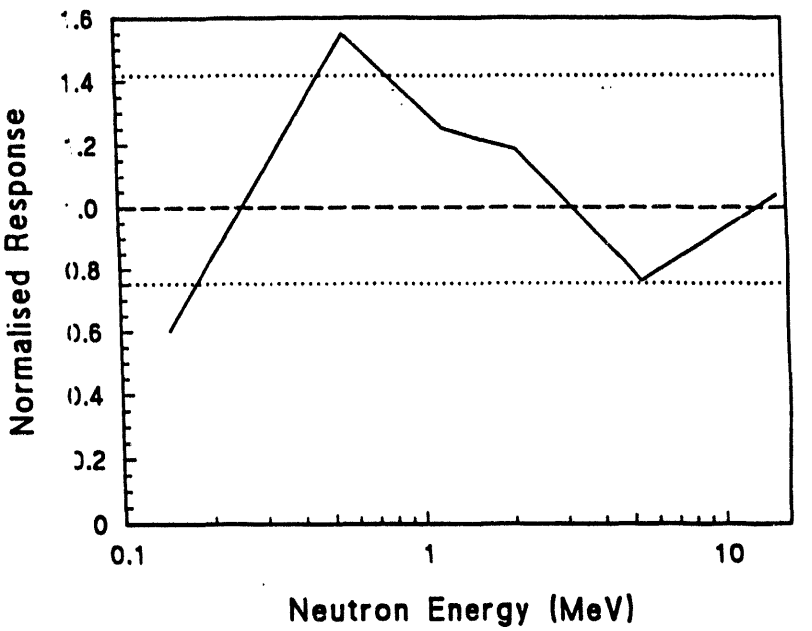


Figure 5: Energy Response of the PADC Neutron Dosemeter

STATUS OF RADIOPROTECTION AT BRAZILIAN UNIVERSITIES

K.C.S. Caballero and J.C. Borges
EE/COPPE UFRJ C.P. 68509
21945-970 - Rio de Janeiro - RJ - Brazil

I — INTRODUCTION

Since the Brazilian Nuclear Energy Commission - CNEN - didn't know the whole reality of radiation control at academic institutions, we decided, in 1991, to undertake a research effort in order to elucidate how such activities were indeed conducted.

A questionnaire covering technical, administrative and legal subjects, was sent to 91 institutions (36% answered back), propiating substantial data, that showed an equilibrium among institutions which have and have not radioprotection plans/services/supervisers. Based on the tree analysis technique proposed by AIEA, a Reference Radioprotection Program was elaborated to help people envolved with ionizing radiations to improve safety of their activities and workrooms.

II — DATA SURVEY

Based on the experience of the UFRJ Radioprotection Control Service - SECRAD (1,2), a questionnaire, covering eight topics related to activities with radioations was elaborated and sent, by mail, to 91 institutions (universities and isolated faculties). These topics were:

a) identification and classification of radioactive installations;

b) existence and structure of a radioprotection office/team;

c) existence of a radioprotection plan/program;

d) concession of legal (labourite) rights;

e) description of installations and radiation sources;

f) management of radioactive wastes;

g) individual and environmental monitoring;

h) training of personnel for routine and emergency situations.

Information from answered questionnaires was evaluated searching for qualitative and quantitative diagnosis. The southeast region of the country concentrated 75% of global answers, making of its profile a national outlook. Nevertheless, particular information was also picked up from questionnaires and taken into account.

Analysis of available data showed that:

a) there is a wide range of activities envolving radiations, which can be grouped in teaching, research and medical assistance (in universitary hospitals), the last one being predominant;

b) half of the institutions have neither a radioprotection superviser nor a radioprotection office, despite CNEN's exigence for both. In addition, there are institutions where: there is only a supervisor (not an office) or an office (not a supervisor), or, both exist but are not officialy recognized by CNEN. Therefore, only 30% satisfy CNEN's exigency, although 56% have some radioprotection plan or program, generally ~~established~~ sometime in the past and not reviewed ever since;

c) majority of people envolved in activities with ionizing radiation don't know regulations and safe procedures for their work, but know well their legal rights, since 85% receive some additional of salary due to "exposure to radiation";

d) although people exposed to radiation in federal institutions should, as a legal right, work 24 hours/week, only 43% are actually in this situation, perhaps because those envolved in teaching and research don't worry or care too much about time charging of their journey-work. Another legal right - 20 days vacations each 6 months — is observed by 70% of people in federal institutions but, in private institutions, only 8% (mainly "radiology technicians") have the right to and enjoy such a privilege;

e) in 40% of the institutions, exists some kind of Special Commission to decide who should usufruct these legal rights;

f) 70% of workers exposed to radiation received some training for routine work but only 30% know what to do in an emergency situation;

g) although 70% of the institutions seems to practice some kind of signalling/warning for their sources/installations, only 30% declare to match CNEN's exigencies concerning this topic;

h) 40% of the institutions produce some solid or liquid radioactive waste; half of the liquid is launched in the sewerage system; 2/3 of the solid are stored, temporarily, and 1/3 is sent to some of CNEN's repositories;

i) 30% of people exposed to radiation don't use any kind of personal dosimeter, for two reasons: economical and legal (CNEN prescribes the exigence of personal dosimeter only for those receiving more than 15 mSv/year);

j) 1/3 of the radioactive installations have never been monitored, and doses for workers are estimated theoretically;

k) 1/3 of the institutions have no radiological or medical registry of people exposed to radiation, one of CNEN's exigencies;

l) in institutions with a radioprotection office and, therefore, activities control, 10% of people working with radiation reported some kind of annomalous exposure.

III — CONCLUSIONS

To resume, we can say that:

1 - CNEN's Basic Norm is not well know (3), the same applying for specific ones (4,5,6,7,8);

2 - Academic institutions don't care too much about employing experts in radioprotection to supervise their specific problems, generally handled by people not technically trained or recognized by CNEN;

3 - Institutions in the southeast region, as well as their personnel, present a better radioprotection panorama than those in other regions of the country;

4 - Even in institutions were a central radioprotection office exists, sectional services acts independently,because of the weak hierarchy of the academic world;

5 - CNEN, untill now,have not been rigorous with academic institutions, and don't know what is going on in some of them, which even don't answer CNEN's requerements for information;

6 - Personnel monitoring is undertaken by private enterprises, one of CNEN's institutes or the institution itself, but many of them have no monitoring at all;

7 - Some incoherences also appear in data collected, as institutions where nobody is in charge of radioprotection activities but all CNEN's exigences are fullfilled, or where a special commission exists only to decide about concession of privileges stablished by legislation, ignoring radioprotection problems.

Although some brazilian universities work with radiation for more than 40 years, only after Chernobyl and Goiânia accidents,radioprotection became a "serious" affair and, even today, almost ignored at some institutions. One of the reason for this situation is that CNEN has no specific norm for teaching and research, as it has for industrial, medical and fuel cycle activities. Therefore, academic people exposed to radiations only worry about AIEA recommendations (9,10,11)or CNEN's Basic Norm (3).

Anyway, analysis of collected data was used to support some suggestions to CNEN and academic institutions, the principal one being a Reference Radioprotection Program, elaborated to help people concerned not only with implantation or optimization of radioprotection at their institution, but also any teaching or research activity.

IV — THE REFERENCE RADIOPROTECTION PROGRAM - "PRADIO 93"

The main objective of PRADIO-93 was to present in a didactic structure,basic information necessary/sufficient for the establishment of a radioprotection plan/program in brazilian institutions dedicated to research/teaching. Requisites to be fullfilled are those estipulated by basic (3) and specific (4,5,6,7,8) norms of CNEN.

The text tries to transmit to those envolved in any activity with ionizing radiations:

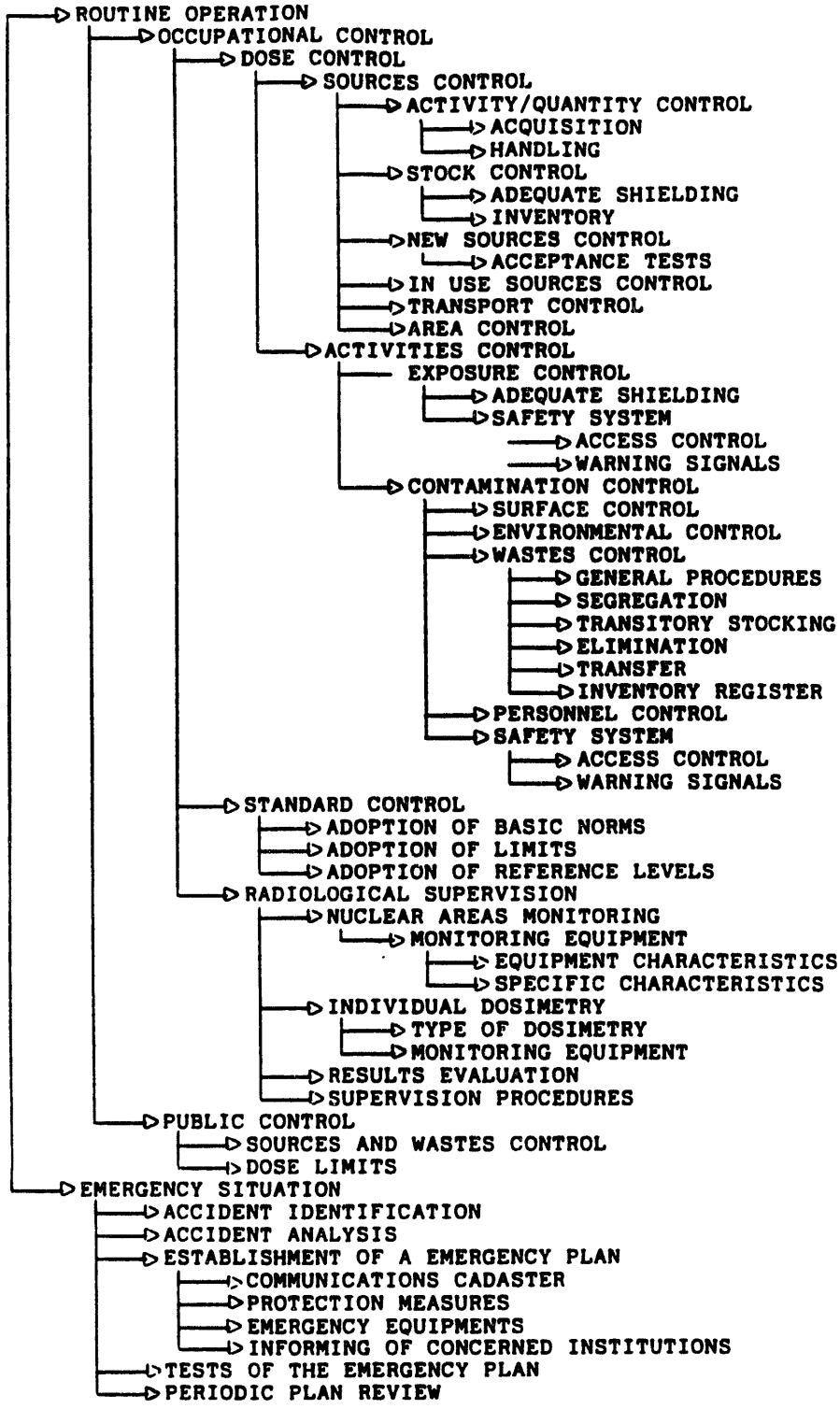
a) enough conscientiousness of detriment associated with exposure/dose;

b) scientific procedures and equipments adequate for a safety work in each specific activity.

Since data collected from questionnaires indicated that CNEN's norms are almost unknown, the structure of Pradio-93 (see diagram)took into account the "tree analysis technique" proposed by IAEA to mount a didactic route describing safe ways to deal with radiations.

To help diffusion/utilization of PRADIO-93, a software for IBM-PC type computers, using CEL, was elaborated and distributed to potential concerned public.

We can assume that such a reference program as really a national need, because, once distribution was stanted, invoices for it proliferated.



STRUCTURE OF PRADIO-93

V — REFERENCES

1 - BORGES, J.C., **Análise das Atividades com Radiações na UFRJ**, Anais do 3º Congresso Geral de Energia Nuclear, p. 75, (1990).

2 - COTAR-X/UFRJ, **Manual de Instrução**, Rio de Janeiro, (1988).

3 - Comissão Nacional de Energia Nuclear, **Diretrizes Básicas de Radioproteção**, CNEN - NE-3.01, Rio de Janeiro, (1988).

4 - Comissão Nacional de Energia Nuclear, **Serviço de Radioproteção**, CNEN - NE-3.02, Rio de Janeiro, (1988).

5 - Comissão Nacional de Energia Nuclear, **Certificação de Qualificação de Supervisores de Radioproteção**, CNEN - NE-3.03, Rio de Janeiro, (1988).

6 - Comissão Nacional de Energia Nuclear, **Transporte de Materiais Radioativos**, CNEN - NE-5.01, Rio de Janeiro, (1988).

7 - Comissão Nacional de Energia Nuclear, **Licenciamento de Instalações Radiativas**, CNEN - NE-6.02, Rio de Janeiro, (1984).

8 - Comissão Nacional de Energia Nuclear, **Gerencia de Rejeitos Radioativos**, CNEN - NE-6.05, Rio de Janeiro, (1985).

9 - International Atomic Energy Agency, **Recommendations for the Safe Use and Regulation of Radiation Sources in Medicine, Industry, Research and Teaching**, Safety Series nº 102, Vienna, (1990).

10 - International Atomic Energy Agency, **Basic Safety Standards for Radiation Protection**, Safety Series nº 09, Vienna, (1982).

11 - International Atomic Energy Agency, **Operational Radiation Protection - A Guide to Optimization**, Safety Series nº 101, Vienna, (1988).

ASSESSMENT OF RADIATION DOSES AT THE INSTITUTO DE PESQUISAS ENERGÉTICAS E NUCLEARES

Sanches M.P.(LAS), Sahyun A.(HPS) & Sordi G.M.A.A.(HPS)
Instituto de Pesquisas Energéticas e Nucleares - IPEN-CNEN/SP
Travessa R, 400 - 05508-900 - São Paulo, SP, BRAZIL

External monitoring for air dose measurement using thermoluminescence $CaSO_4$:Dy dosimeters put in fixed points was done inside the IPEN-CNEN/SP area. This measure was done with the objective to understand the influence of nuclear and radioactive facilities inside the IPEN-CNEN/SP workplaces into the environment.

The adopted method involves the use of TLD'S, which measure dose rather than dose rate. TLD's are placed in the field, at the point where the dose is to be measured, for a period of 3 months, and then read out at the same time as reference dosimeters treated similarly in the same general site, but not exposed to radiation. The badge used consist of a small double layer containing three TL discs of $CaSO_4$:DY, inside an outer holder normally used in routine personal dosimetry. Using this badge, in the laboratory it is possible to measure doses as low as 1 μGy, with an error of approximately 0.2 μGy, but in field measurements the limit of detection is probably an order of magnitude higher.

This study was carried out to evaluate the radiation level for electromagnetic radiation in different places at IPEN-CNEN/SP. The reference values obtained for background level was 77 nGy/h. The observed results at the previously established points was up to 15 times the background level. From the results of this evaluation we could get a gross estimation of plant influence and specific influence of some types of sources.

This analysis opens a window to make in the near future, more accurate studies to evaluate the contribution of each installation to background dose variation and what is its contribution to collective dose of IPEN-CNEN/SP population, inside the facilities, as well in those people that suffer contributions from each facility.

OCCUPATIONAL DOSE RECONSTRUCTION IN THE NUCLEAR INDUSTRY: A KNOWLEDGE MANAGEMENT APPROACH

B. Le Blanc (Université de Bordeaux 2 - F.33076 BORDEAUX),
H. Dagorn, D. Bard (Institut de Protection et de Sûreté Nucléaire - DPHD/SEGR - F.92265 FONTENAY AUX ROSES)

The nuclear industry has undergone a tremendous development since its beginnings in the early '50s. Scientific knowledge on health effects, dosimetry and optimization techniques has been accumulated. As a result, many practices in radioprotection have evolved. Furthermore, this has been accompanied by a burgeoning of new structures, both scientific and administrative.

The need for reconstructing dosimetric histories in the nuclear industry has been addressed for a long time, both for epidemiological research and liability purposes. The French Atomic Energy Commission (C.E.A.) has benefitted over the years from a few individuals who have been in charge of dosimetry management issues since the beginning. These have been able to disentangle the various aspects of professional histories (i.e. changes in registration practices, dosimetric methods, and administrative organization, leading to a huge body of heterogeneous information) both at an individual and epidemiological level. Unfortunately, these individuals are about to retire, and a considerable amount of valuable information and expertise is at risk.

Implementation techniques for Expert Systems were derived in order to save the above information in a transparent, formalized manner. We first described the static knowledge, using an object database representation for the basic vocabulary, and a derived-SADT method for representation of activities. We then used cognitive engineering methods for the expression of cognitive tasks. Finally, we used these entities to rebuild the dosimetry management process for the C.E.A.

The developed tool has been tested and shown to constitute a useful guide for a search of information relating to an individual (e.g. finding what was the cumulative dose of an individual for a given time period), as well as to epidemiologic purposes. More generally, it allows one to interpret heterogeneous information in terms of dose reconstruction.

THE CENTRAL INDEX OF DOSE INFORMATION: DOSE DISTRIBUTIONS IN THE UNITED KINGDOM OVER THE PERIOD 1986-1991

M.K. Williams
Health and Safety Executive, Baynards House, 1 Chepstow Place, Westbourne Grove, London, W2 4TF, UK

W.J. Iles
National Radiological Protection Board, Chilton, Didcot, Oxon, OX11 0RQ, UK

T.O. Marshall
National Radiological Protection Board, Chilton, Didcot, Oxon, OX11 0RQ, UK

ABSTRACT

The Central Index of Dose Information (CIDI) is the Health and Safety Executive's (HSE) national database of occupational exposure to radiation. It is operated for the regulatory authority on an agency basis by the National Radiological Protection Board (NRPB).

This paper describes the functions and method of operation of CIDI, the types and method of data transfer between CIDI and the approved dosimetry services and the summarised annual data to be published relating to the CIDI.

One of the functions of CIDI is to provide statistics to guide policy making on a national basis. To facilitate this, dose information for individuals on CIDI is associated with particular occupational categories. Last October HSE published an analysis of the dose information received by CIDI for the years 1986-1991. This analysis revealed a number of important facts and trends which will be discussed. For all classified persons, for example, the mean doses are low, ie., 1.5 mSv in 1991 about 50% of the 1986 figure. There was a sustained downward trend in both mean and collective dose over the whole period, the reduction in collective dose over the period was more than 50%. There was a dramatic reduction (more than 10-fold) over the 6 year period in the proportions of classified persons who had a reported annual dose in excess of 15 mSv (the principal investigation level). 147 persons were reported as having received more than 15 mSv in 1991 compared with more than 1900 classified persons for 1986. Data on a number of work categories will be presented.

1. Introduction

The Central Index of Dose Information (CIDI) is the Health and Safety Executive's (HSE) national database of occupational exposure to radiation. It is operated for the HSE on an agency basis by the National Radiological Protection Board (NRPB). The Health and Safety Executive (HSE) is the regulatory authority for health and safety legislation in Great Britain.

In Great Britain, the Ionising Radiations Regulations 1985 (IRR 85)[1], require that doses received by employees designated as classified (Category A) persons must be assessed and recorded by a dosimetry service approved by HSE. In addition, these approved dosimetry services (ADS) are required to provide HSE with annual summaries of recorded doses for each classified person. Separate information is also required whenever a classified person changes employer or terminates employment for some other reason (a termination record). CIDI was established on 1st January 1987 to receive this information.

At present there are about 40 dosimetry services approved in Great Britain for the purpose of keeping dose records. For any one year approximately 60000 dose records are held on the database. All the data provided to CIDI are protected by various safeguards, and treated as confidential with respect to individual persons and employers. The database is registered under the Data Protection Act 1984[2] (Registration No. C0607047).

The functions and general operation of CIDI are described in the Report of the Working Party on the Central Index of Dose Information[3], in the associated Reference Manual[4] and in a paper by Iles and Williams[5]. The specification of the dose data required for CIDI purposes before 1991 was given in Guidance on the Approval of Dosimetry Services under the Ionising Regulations 1987[6]. In 1991 the specification was modified slightly to require additional information[7].

CIDI has a number of functions as listed below:

- to provide the new ADS with summarised information of an individual's dose history as a classified person (where available?), and the dose for the current year so far when an individual changes employment, so that the new employer may be aware of any special need to restrict that person's future exposure;
- to enable additional data to be transmitted from the previous ADS to the next, when a classified worker changes employer;
- to provide an index to show which ADS is currently responsible for dose-record keeping in respect of any classified person;
- to conduct an annual audit of the numbers of classified persons for whom doses are reported each year to ensure that the total is consistent with the figure for the previous year, allowing for new registrations and terminations of employment;
- to provide statistics to guide policy making on a national basis.

This paper deals in some detail with the last of these functions.

2. Dose Data for CIDI

The following shows the types of dose information sent to CIDI each year by ADS. Precise details of the types of dose data and personal data supplied are contained in The Reference Manual for Data Transfer to CIDI[4]. Not all the data are obligatory.

2.1 Current year dose data

(a) Sum of effective dose equivalent from external radiation and committed effective dose equivalent from internal emitters.

(b) Neutron component of (a), where assessed.

(c) Notional component of (a), where this exceeds 10% of the total.

(d) Sum of dose equivalent from external radiation and committed dose equivalent from internal emitters to organs and tissues (if separately assessed), where doses exceed 10% of the proportion of the annual dose limit for the period in question. The categories of organs and tissues used for the purpose of CIDI are indicated in reference 4.

(e) A flag if (a) above includes a component from long-lived or other internal emitters.

2.2 Cumulative (lifetime) dose data (to the extent that this is available)

(a) Effective dose equivalent from external radiation (including (b) below).

(b) Notional component of (a), where this exceeds 10% of the total.

2.3 Additional note

In 1992, a modification was introduced to the original requirements for information provided in termination reports when a person changes employer or terminates employment so as to include separate dose summaries for each of the previous four years (excluding any year before January 1, 1988). This information is supplied by CIDI to the new ADS. The purpose of this additional information is to assist employers to identify new employees who may be approaching 75 mSv in 5 years, which is the level at which an investigation should be carried out into the past and likely future exposure of that person in accordance with the fourth part to the Approved Code of Practice supporting IRR 85[8].

3. Personal Data for CIDI

The personal data sent to CIDI includes:

- sex and date of birth,
- national insurance number (the unique identifier),
- CIDI code number of the ADS supplying the dose information,
- occupational classification of the employee,
- CIDI code number of the individual's employer,
- date of commencement/termination of classified work in this employment.

In exceptional circumstances where the national insurance number for an individual is unavailable, then a surrogate number is issued by CIDI to the ADS.

The occupational category classification for the purpose of CIDI is given in reference[5]. For the purpose of the 1986-1991 report the HSE have grouped the work categories as shown in Table 1.

Table 1 Occupational groupings for the 1986-1991 report

Occupational grouping	CIDI occupational category
All classified persons	All occupational categories
Nuclear power	{Nuclear reactor operations {Nuclear reactor maintenance
Nuclear fuel fabrication/reprocessing	{Nuclear fuel fabrication {Nuclear fuel reprocessing
General industrial	{Application + servicing activities of {machines producing ionising radiation
	{Application and manipulation of {radioactive substances
	{Industrial research/teaching
Industrial radiology	{Industrial radiography using permanent {installations
	{Industrial radiography on site or works {of engineering construction
Non-coal mining underground	{Mining minerals other than coal - {underground workers
Medical	{Medical application-doctors {Medical application-nurses {Medical application-radiography {Medical application-physics {Medical application-other {Dental work
Transport	{Transport of radioactive sources

3.1 Publication of CIDI data

Although the individual data on the database are treated as confidential, annual summaries of statistics are published by HSE for each year's data; summaries have already been published for 1986, 1987, 1988, 1989, 1990, 1991 and 1992. Also, further analyses of the data will be published periodically to assist in the identification of any trends in reported doses; the first such report covering the years 1986-1991 has been published[9] by HSE.

The tabulated data presented in each annual statistical summary are divided into three parts: Part A - Whole body doses, Part B - Dose variation with age and sex, and Part C - Doses to specific organs and ussues. A common feature of the tabular presentation is that all doses are related to occupational category. The majority of the tables present the data distributed within dose intervals, together with the total number of classified persons, collective dose, and mean dose for each occupational category. There is also a table that gives the distribution of workers, by age and sex, that exceeded 15 mSv for the year. However, it is the data for the period 1986-1991, the first six years of CIDI operation, that will be presented and discussed here.

4. Reported Doses of Zero

The 1986-1991 report[9] shows that most classified persons receive an annual dose much less than 15 mSv per year (88% of reported doses were less than 5 mSv even in 1986). Therefore, it is likely that employers are designating far more employees as classified persons than is strictly required by IRR 85, probably for dose control purposes and reassurance. Nevertheless, this additional information is useful, particularly in the nuclear sector, in giving a fuller picture of changes in recorded doses over the period. Employers in some other sectors, most notably the medical sector, tend not to classify staff unless they are likely to exceed three-tenths of a relevant dose limit. It is important to recognise these differences in practice between sectors.

In any year during the period, between 20-30% of the persons for whom annual dose summaries were submitted had a reported dose of zero. The effect of including these individuals in any analyses of reported dose is to lower the mean dose for the group being considered, which might be misleading. Therefore, for the purposes of the 1986-1991 report, HSE have included only those persons with a non-zero reported dose in the Figures. The report shows that the total number of classified persons with a non-zero dose fell over the period 1986-1991 from 46 206 to 40 222.

5. Notional Doses

CIDI data used for statistical purposes such as the HSE report are adjusted to remove 'notional doses'. Notional doses are entered into a dose record for a period when no dose assessment could be made, for example when a dosemeter has been damaged, and it is not possible to estimate the dose received from available information. The proportion of notional doses in dose summaries reported for 1986 (about 13%) was significantly higher than for 1991 (about 5%).

Notional doses are used in these circumstances as a precautionary measure to try to ensure that dose limits are not exceeded. They are calculated on the basis of the proportion of the relevant dose limit for the period concerned. However, they are rarely representative of the likely dose received by the employee. For that reason a dose estimate for the relevant period has been substituted for each notional dose by the CIDI statistics programmes when compiling the data used for the report. Each substitute dose estimate is based on the doses assessed for that person during the rest of the year concerned. This is a well established convention in the graphical presentation of dose data and it gives a more realistic value for the purposes of analysis.

The substitution of notional doses is only applied to the data when they are undergoing statistical analysis. The annual dose summaries reported by Approved Dosimetry Services and kept on CIDI remain unchanged.

6. Analysis of CIDI Data (from the HSE 1986-1991 Report[9])

6.1 All classified persons (Figure 1) (Figure 3 in Ref.9)

Figure 1A shows a definite and sustained downwards trend in both mean and collective dose for classified persons over the whole period, even taking account of uncertainties in dose assessment. The reduction in collective dose over the period was more than 50%, which cannot be explained by a reduction in work activity: over the same period the number of classified persons with non-zero doses fell by only 13%.

Figure 1B shows that there was a dramatic reduction (more than 10-fold) over the six year period in the proportion of classified persons who had a reported annual dose in excess of 15 mSv (the principal investigation level).

These figures show clearly that the most highly exposed groups of workers now form a much smaller proportion of the total number of classified persons with a non-zero reported dose.

6.2 Nuclear power (Figure 2) (Figure 4 in Ref.9)

A similar downwards trend in mean and collective dose can be seen for the nuclear power group. Figure 2A shows that collective dose decreased by about 50% over the period; mean dose also fell by about the same order to 1.6 mSv.

Figure 2B shows a strong downwards trend in the proportion of persons in the nuclear power group with a reported dose in excess of 15 mSv (down to around 1% of the 1986 figure). The sharpest drop occurred between 1990 and 1991, but there was a plateau between 1988 and 1989. In 1991 only nine persons had reported doses in excess of 15 mSv (two had reported doses above 20 mSv). The proportion of those who had a reported dose above 5 mSv was reasonably constant between 1987 and 1990.

Data for nuclear fuel fabrication/reprocessing showed trends very similar to those of nuclear power.

6.3 General industrial activities (Figure 3) (Figure 6 in Ref.9)

This group covers a wide range of activities but excludes industrial radiography, which is considered separately. Figure 4A shows reductions in collective dose and mean dose (around 60% and 40% respectively) similar to those seen in Figure 1A. However, there was a 30% reduction in the number of persons in this occupational group between 1986 and 1991. In 1991 the mean dose for those with a non-zero reported dose was 0.9 mSv.

Figure 3B shows a considerable reduction between 1986 and 1991 in the proportion of classified persons who had a reported dose in excess of 15 mSv; but the proportion did not alter between 1990 and 1991 and the number who had reported doses above 20 mSv rose slightly to 11. The proportion with reported doses above 5 mSv increased by about 15% between 1987 and 1989, which may suggest some dose sharing.

6.4 Industrial radiography (Figure 4) (Figure 7 in Ref.9)

Figure 4A presents collective dose and mean dose for this group in each year of the period. Collective dose fell by about 40% over the six years but it was lowest in 1988 (about 20% lower than in 1991). Also, the number of classified persons in the group who had a non-zero reported dose fell by more than 30% between 1986 and 1991, although the number increased between 1989 and 1990. The mean dose of those for whom a non-zero dose was reported showed no real downward trend from 1986-1991: it was only 5% lower by the end of the period.

Figure 4B shows doses for the most exposed industrial radiographers as a proportion of all classified persons in that occupational group with a reported non-zero dose; for most of the dose categories shown, the percentage increased from 1988 to 1991. For example, the proportion of those who had a recorded dose above 5 mSv rose by over 30% and the proportion with a reported dose in excess of 15 mSv more than doubled to 50 persons.

6.5 Non-coal miners underground (Figure 5) (Figure 8 in Ref.9)

Non-coal mining exposes miners to the naturally-occurring radioactive gas radon-222 and its short-lived radioactive daughters. Figure 5A shows that the collective dose for this group has reduced significantly over the period but the mean dose (for those with a non-zero reported dose) reached a low in 1988 at 10.1 mSv and rose steadily to 15.1 mSv in 1991. Significantly, during this period of three years the group contracted to such an extent that under 40% of the classified persons employed in 1988 remained. For 1991, this

represents less than 1% of the total of classified persons for whom non-zero doses were reported to CIDI. By 1991 the mean dose was back to within 20% of the 1986 figure.

A similar pattern is seen in Figure 5B which shows the doses reported for the most exposed miners in this group. The proportion of those with a non-zero dose above 5 mSv, 10 mSv, 15 mSv or 20 mSv was at its lowest in 1988 and increased over the remaining years of the period. For example, the percentage with a dose exceeding 15 mSv was 18% in 1988 and about 50% in 1991. Forty miners (30%) had reported doses above 20 mSv in 1991.

6.6 Medical and dental

The data for this group are probably less comprehensive than those for other occupational groups. The number of classified persons in this occupational group fell significantly and some classified persons were assigned the wrong occupational category in the earlier years of the period. The number of persons with a non-zero dose fell by 60% over the six years to just over 400. The fall in collective dose follows the same trend: in 1991, collective dose was 60% lower than in 1986.

The mean dose for this occupational grouping was around 1 mSv over the period: in 1991 it was 0.9 mSv. Perhaps the absence of a clear trend is not surprising when the mean dose is already low.

Over the whole period 1986-1991, only 10 persons had reported doses in excess of 15 mSv (and 34 persons had doses above 10 mSv) in any one year. Therefore, there is no figure showing the breakdown by dose band. This shows the proportion of those with a reported dose above 5 mSv a year decreased by about a half between 1986 and 1991.

6.7 Transport

Persons in this occupational category made up less than 1% of the total each year; some may have been mistakenly assigned to the sector mainly associated with the business of the employer, for example fuel reprocessing or medical. After a small increase in collective and mean (non-zero) dose in 1987 there was a clear downwards trend in reported doses. Collective dose fell by more than 60% and mean dose by just under 50% over the six years. In 1991 the mean dose was 1.2 mSv.

Only 20 classified persons associated with the transport of radioactive sources had doses in excess of 15 mSv in any one year of the period (none since 1989). Therefore, there is no figure showing the breakdown by dose band. Between 1986 and 1991 the proportion of classified drivers with a reported dose above 5 mSv fell by more than 60%.

6.8 HSE Conclusions

In general, the analysis of dose data reported to HSE's CIDI over the period 1986-1991 demonstrates that the framework provided by IRR 85 for the restriction of occupational exposure to ionising radiations, in conjunction with other pressures on employers, has led to a sustained reduction in doses. Inevitably, the decline in economic activity in some sectors towards the end of the period may have enhanced the general reduction in doses, but the information in this report has been presented in such a way as to minimise the effect of that factor.

The impact of IRR 85 has been particularly noticeable for individuals liable to receive 15 mSv in a year. Above this level of recorded dose the employer must carry out an investigation to find out whether enough is being done to restrict exposure. There was more than a 10-fold reduction in the number of persons for whom these investigations were required between 1986 and 1991.

In general, based on the information reported to CIDI, there has been a clear downwards trend in dose at all levels above 5 mSv, and a marked decrease in mean dose and collective dose. There is still room for improvement, most obviously for industrial radiography and non-coal mining; and HSE has work in hand to focus more effort on these sectors. The challenge for the future is to maintain the general downwards pressure on exposure to ionising radiations, where it is still reasonably practicable to make further improvements, while ensuring that dose reductions are not achieved at the expense of either delaying safety critical work or increased dose sharing.

Acknowledgements

The authors have used extensively data and text from reference number 9. This has been reproduced with the permission of the Controller of Her Majesty's Stationery Office.

7. References

1. The Ionising Radiations Regulations 1985 SI 1985/1333.

2. Data Protection Act 1984. Her Majesty's Stationary Office, London (1984).

3. Kendall, G.M., Greenslade, E. and Young, T.O. Report of the Working Party on the Central Index of Dose Information. Chilton, NRPB-M92 (1983).

4. Greenslade, E., Kendall, G.M., Iles, W.J., Gardner, P.H. and Young, T.O. Reference manual for data transfer to the Central Index of Dose Information. NRPB-M176 (1989).

5. Iles, W.J. and Williams, M.K. The Central Index of Dose Information in the United Kingdom. Kerntechnik 58(4) (1993).

6. HSC Protection of persons against ionising radiation arising from any work activity: Approved Code of Practice, Parts 1 and 2 COP 16 ISBN 0 7176 0508 6.

7. HSC Exposure to Radon: Approved Code of Practice Part 3 COP 23 ISBN 0 11 883978 0.

8. HSC Dose limitation - restriction of exposure: Additional guidance on regulation 6 of the Ionising Radiations Regulations 1985 Approved Code of Practice Part 4 L7. ISBN 0 11 885605 7.

9. Health & Safety Executive. Occupational exposure to ionising radiation 1986-1991. Analysis of doses reported to the Health and Safety Executive's Central Index of Dose Information (1993). IBSN 0 7176 0657 0.

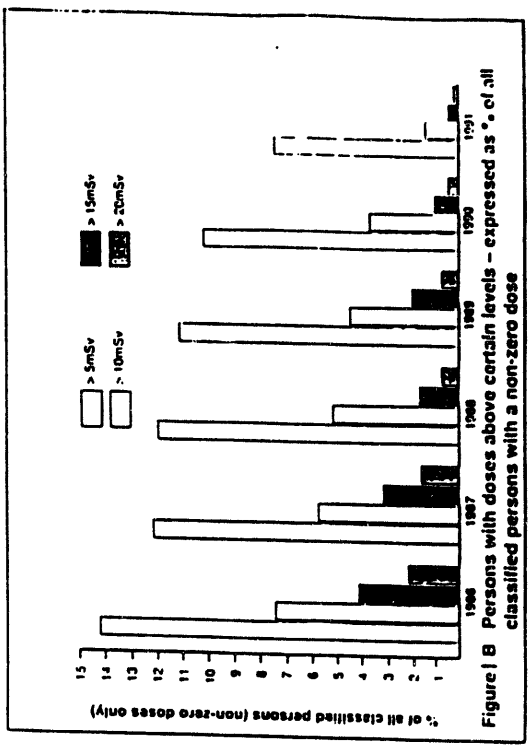


Figure 1 B Persons with doses above certain levels – expressed as % of all classified persons with a non-zero dose

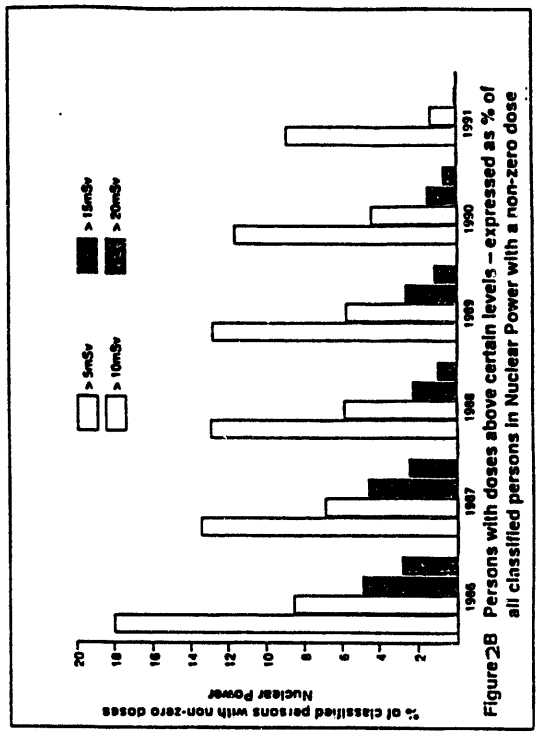


Figure 2B Persons with doses above certain levels – expressed as % of all classified persons in Nuclear Power with a non-zero dose

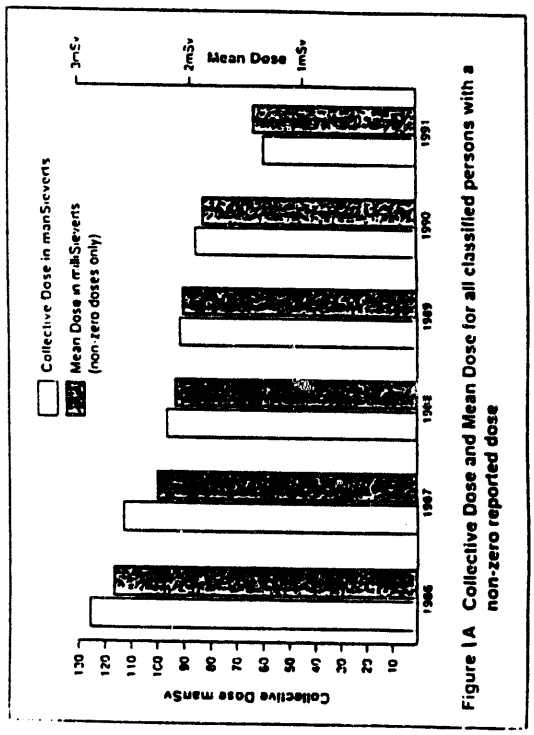


Figure 1A Collective Dose and Mean Dose for all classified persons with a non-zero reported dose

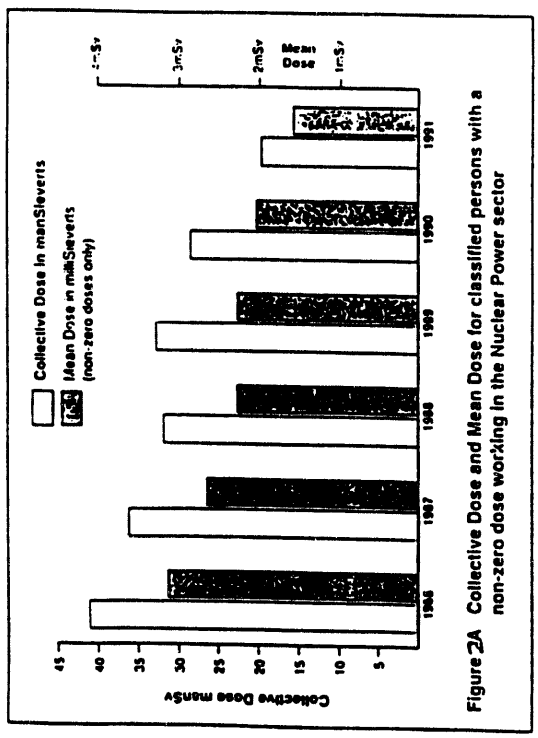
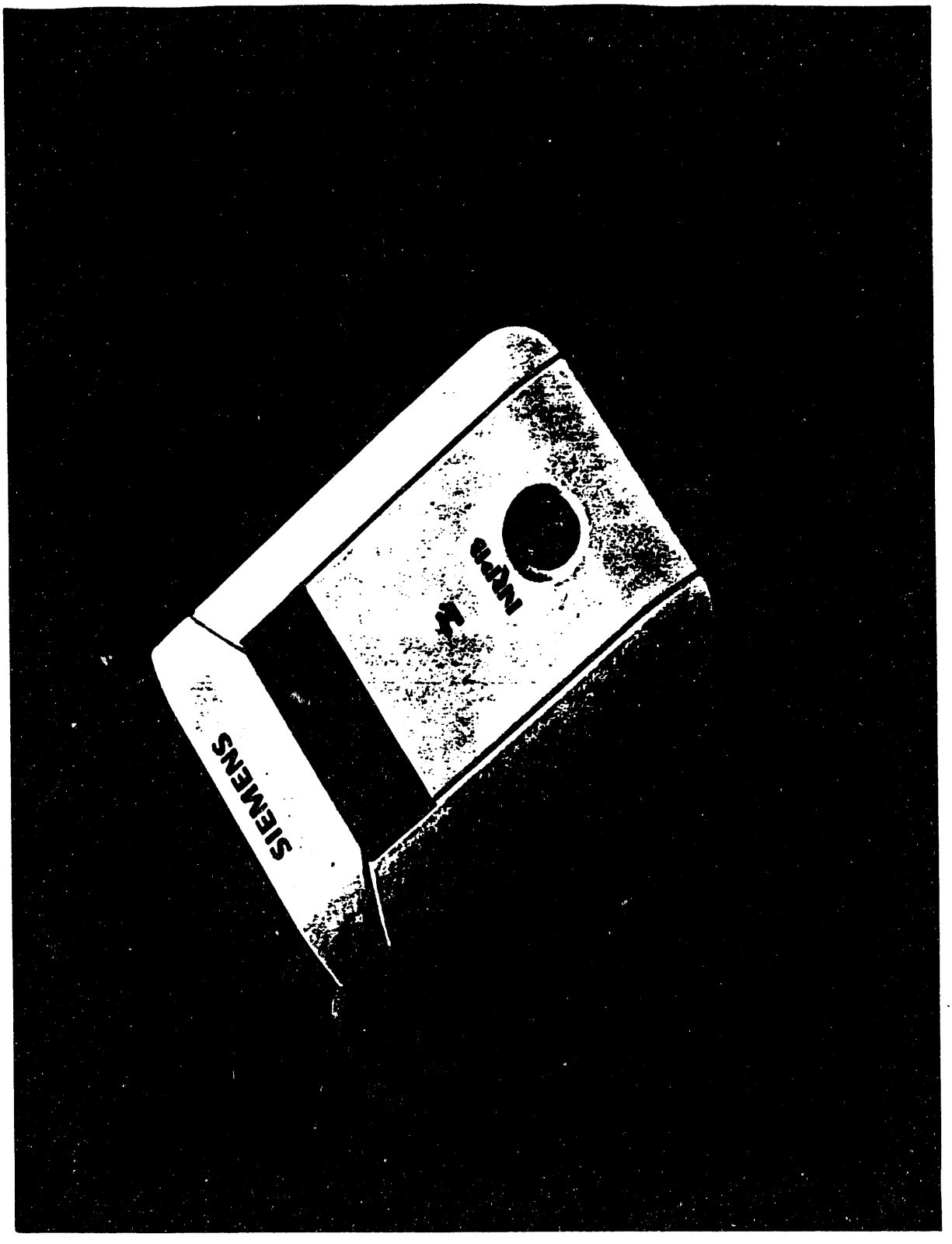


Figure 2A Collective Dose and Mean Dose for classified persons with a non-zero dose working in the Nuclear Power sector


SIEMENS
MOPTIC

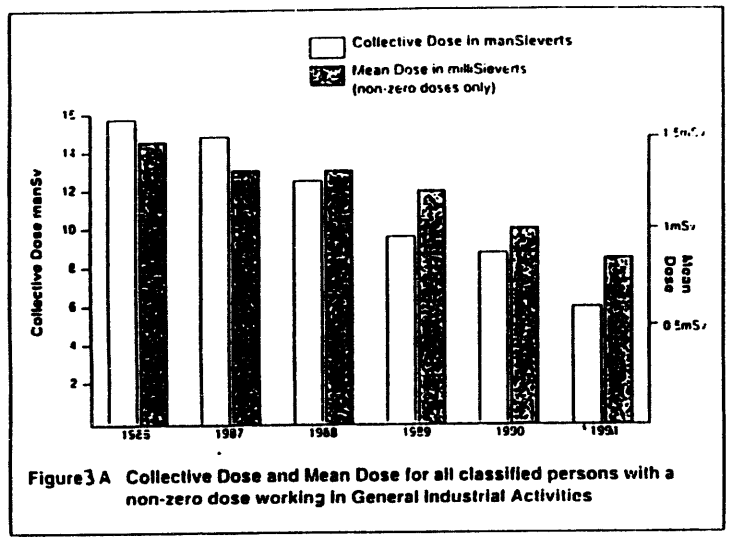


Figure 3 A Collective Dose and Mean Dose for all classified persons with a non-zero dose working in General Industrial Activities

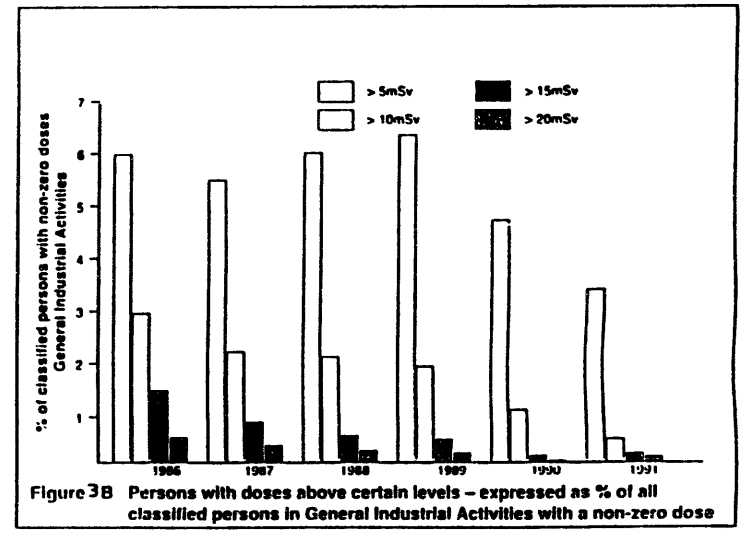


Figure 3 B Persons with doses above certain levels – expressed as % of all classified persons in General Industrial Activities with a non-zero dose

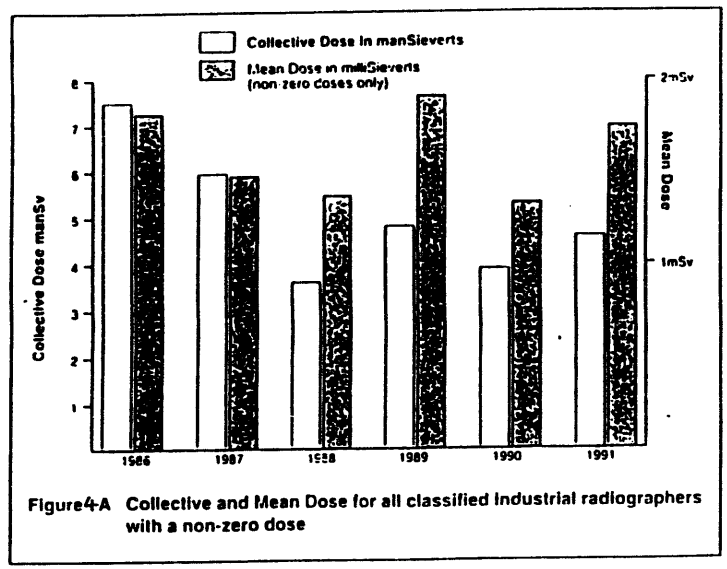


Figure 4 A Collective and Mean Dose for all classified industrial radiographers with a non-zero dose

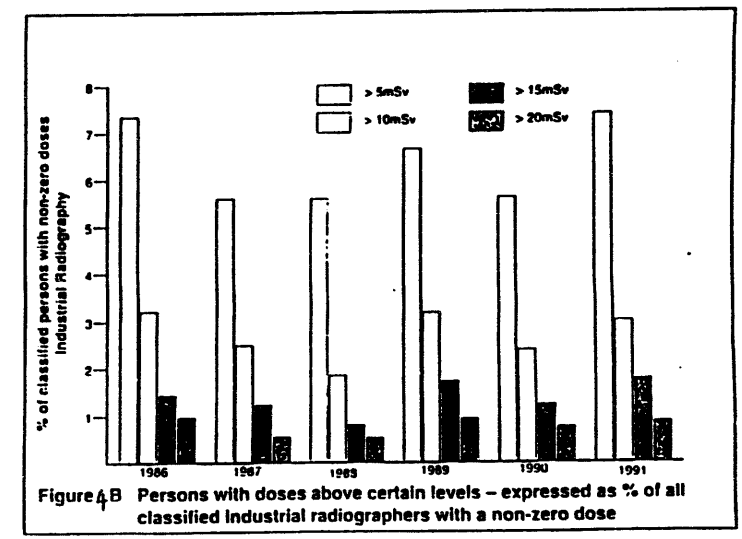


Figure 4 B Persons with doses above certain levels – expressed as % of all classified industrial radiographers with a non-zero dose

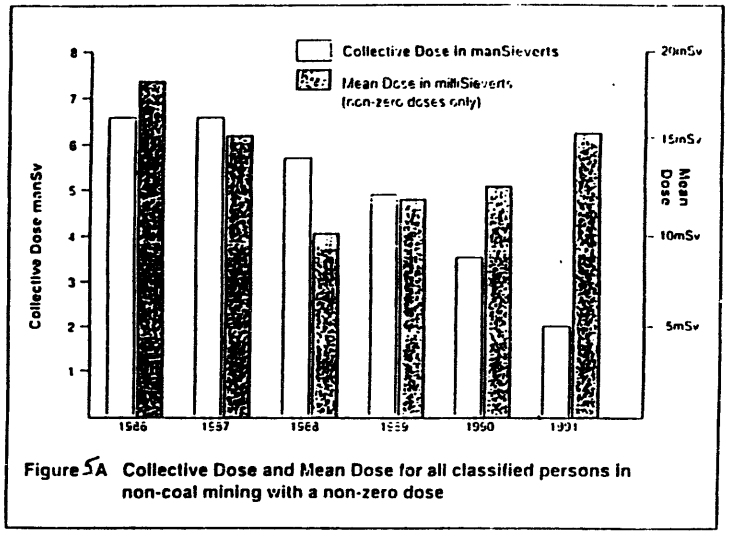


Figure 5A Collective Dose and Mean Dose for all classified persons in non-coal mining with a non-zero dose

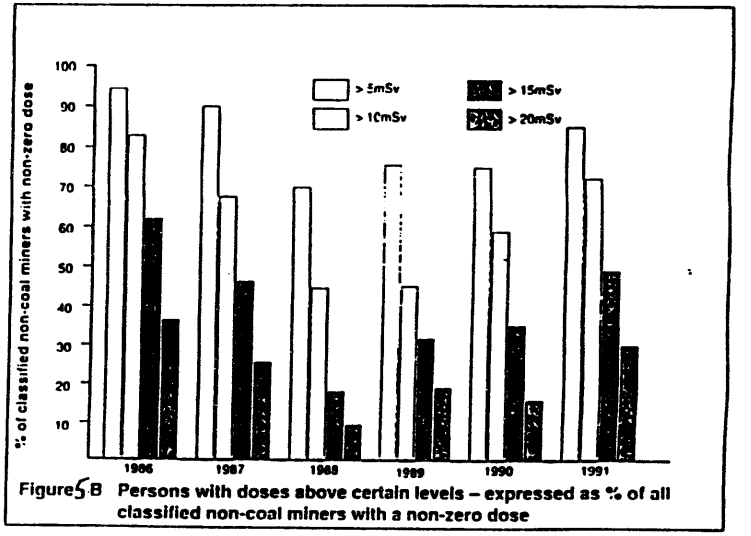


Figure 5B Persons with doses above certain levels – expressed as % of all classified non-coal miners with a non-zero dose

CANCER MORTALITY EXPERIENCE IN THE WORKERS OF THE FRENCH NUCLEAR INDUSTRY: SOME QUESTIONS OF DOSE RECONSTRUCTION FROM AN EPIDEMIOLOGICAL PERSPECTIVE

D. Bard, Ph. Hubert and H. Dagorn (Institut de Protection et de Sûreté Nucléaire, Department of Risk Assessment and Risk Management, Laboratory of Epidemiology and Health Detriment Analysis, BP 6, F-92265 Fontenay-aux-Roses Cedex, France)

The International Agency for Research on Cancer has initiated an International Study on Cancer Risk among Radiation Workers in the Nuclear Industry, in which our group participates with respect to the French Atomic Commission (CEA) workforce. The aim of this epidemiological study is to examine cancer risk in subjects with protracted exposure to lowdose ionizing radiation. In this regard, associating a study subject with a reliable, accurate and precise cumulative dosimetry estimate is of paramount importance. However, estimates of historical exposures have been influenced by variations in populations surveyed, in frequency of devices readings and registration practices (e.g. methods for handling undetectable levels). Also, the types of monitoring devices and their lower limits of detection

This paper presents these changes within the various plants or installations of the CEA, from 1950 to 1990. The implications for epidemiological endpoints analyses are discussed.

GENERAL APPROACH AND PRELIMINARY RESULTS ON GAMMA - FIELD RECONSTRUCTION FOR THE TECHA RIVER.

D. Burmistrov, V. Valchuk (Urals Research Center for Radiation Medicine)

From 1949 to 1956 radioactive wastes of nuclear plant "Mayak" were being dumped into the Techa river. About 28,000 people were exposed to elevated doses. A vast amount of long-term observation data for the exposed population was accumulated in our center. Yet, the dose estimations used now are not adequately substantiated for risks assessment and do not take into account of all the measurements that were made in the '50s.

The suggested dose reassessment is based on data put recently at our disposal by "Mayak". They include average rates and relative radionuclide composition of the releases; total activities of river water, bottom sediments and flood plain soils, and measured dose-rates at various space-time points; topography and meteorological data.

The necessary part of the project is to reconstruct the gamma-fields at the banks of the river over the period of massive releases. The suggested approach to the problem consists of elaborations on mathematical models for the available measurements, introducing the goal function, which represents the proximity of the model predictions to the whole set of measurements, and determination of the best fit parameters of the models by minimization of the goal function. To simulate radionuclide transport a compartment model is applied. There are two types of compartments included in the model, describing the river itself, and ponds, bogs or floods. The number of the compartments is about 30. The river is divided into 7 zones with different hydrology characteristics. The compartment interactions are described in terms of volumetric flow rate and the effective diffusion rate. The model is in good agreement with the measurements.

Air dose-rates in the geometry of the river system are calculated by the method of "influence functions". Analytical representation of these functions is similar to expression of dose-rate of unscattered radiation from a point source, but some of its terms are considered as free parameters, which are approximated using Monte Carlo calculations. The goal function is initially considered as a weighted sum of the squares of the deviations of the model predictions from measured data. To find the global minimum of the goal function a random search is applied. The results of extreme value sampling theory are applied for narrowing down the area of the random search in parameter space.

The next step will consist of the creation of a model of measurement uncertainties, sensitivity analysis and identifications of model parameters.

THE NATIONAL DOSE REGISTRATION AND INFORMATION SYSTEM: DOSE DISTRIBUTIONS IN THE NETHERLANDS OVER THE PERIOD 1989-1993

J.W.E. van Dijk & H.W. Julius (TNO Radiological Service, P.O. Box 9034, 6800 ES Arnhem, The Netherlands)
M.A. van de Bogaerde (Ministry of Social Affairs and Employment, The Hague, The Netherlands)

In 1988 the Ministry of Social Affairs and Employment commissioned TNO Radiological Service to set up a National Dose Registration and Information System (NDRIS). The government had three reasons in view to build NDRIS:

1. To improve radiation protection by supervising the occupational doses of radiation workers by using one central database system.
2. To improve the reliability of long term storage of dose data.
3. To improve the possibilities for statistical analysis of occupational doses to guide policy making.

Each approved dosimetry service (ADS) in the country sends its dose information to NDRIS on a monthly basis. In its turn NDRIS sends back for each worker monitored by that ADS, the integrated dose as measured by any ADS. This creates the possibility for each ADS to report to the workers their total annual dose irrespectively whether they work for more than one employer or are monitored by more than one ADS, either simultaneously or successively in the course of the year.

European legislation requires that the occupational dose should be controlled in this way. The availability of the centralized database replaces the need of a radiation passbook for national use. The passbook that is needed by radiation workers during interstate travelling can be produced using data from NDRIS.

Analysis of the data available shows a slight tendency towards a decrease of the average annual dose per worker from 0.62 mSv to 0.45 mSv. With regard to the fraction of workers who receive a dose in excess of 5 mSv, there is also a tendency towards a decrease from 15 to 10 percent.

Data will be presented on dose distributions of workers in different categories of work. Before the official introduction of NDRIS, dose data of 80% of the radiation work force has already been stored in such a way that these could be transferred to NDRIS. Results of these data, covering the decade since 1983 will be presented. Finally, all dose data of the Dutch nuclear power industry have been transferred to NDRIS. So NDRIS covers the two decades since 1973 for the nuclear power industry.

Making an estimation of the consequences of the reduction of the annual dose limit from 50 to 20 mSv is another application of the data in NDRIS. NDRIS can be used for quality control e.g. by analyzing comparable data from different ADS's.

RADIOLOGICAL SAFETY ASSESSMENT OF GAS MANTLE INDUSTRIES IN INDIA

Geetha Sadagopan and G.Venkataraman
Radiation Protection Services Division
Bhabha Atomic Research Centre
Trombay, Bombay- 400 085.INDIA.

Introduction

Thorium, a radioactive element of actinide family was discovered by Berzelius in 1828 and named by him in honour of the Scandinavian God 'Thor'. Following its discovery the earliest known use of thorium was in the making of gas mantles. The other use as an X ray contrast medium 'Thorotrast' has since long been discontinued, where as even today its use in gas mantles is continued. Gas lights have been used as a source of light since 1800's. In India, although electric bulbs have replaced most of the gas lights, even today in villages and in urban areas where there is no continuous power supply and in outdoor lightings gas lamps are used. The mantle which is used in these lamps is called the Welsbach mantle and is a netted hose that is impregnated with thorium nitrate and other metals. The function of a gas mantle is to produce a bright light during operation of the lighting device (gas or kerosene lamp) in which the mantle is placed. When placed in a lighting device and heated to 1300 - 1800 degree Celcius thorium in the mantle incandesces and gives off bright light. In India presently there are about 70 manufacturing units handling 150 metric tons of thorium nitrate annually. There are about four hundred persons involved in manufacturing 200 million mantles per year. Thorium is chosen because of its property of incandescence, however since it is radioactive, radiation safety of the workplace, handling personnel and safe environmental condition for members of public have to be mintained.

Methods and Measurements

Stationary air sampling in the workplace was done using a Staplex high volume air sampler with Staplex filter paper as medium. Sampling was done for a period of one hour at a known flow rate in the breathing zone. The type of operations in the workplace include most of the wet operations indicated in Table 1. In these operations there is likelyhood of thorium and thoron getting airborne. Gross alpha counting of the filter papers was done using an alpha counter after time delay of 180, 240 & 300 mins. for thoron daughter products estimation. The filter papers were again counted after a time delay of 2-3 weeks for estimation of long lived thorium. Corrections were applied for filter paper collection efficiency, transmission efficiency and counting efficiency of the alpha counter. Battery operated personal air samplers (indigenous) make with a flowrate of 2 litre per minute were used for personnel. The filter papers were collected and counted in an alpha counter, calibrated using a reference alpha source.

In order to check the efficiency of containment in the workplace surface contamination was checked at various locations. The surfaces were directly counted under an alpha monitor. In most of the institutions there were no separate rooms available for

storage of bulk quantity of thorium nitrate and finished products. The surface dose on the packed mantles was also measured. In order to have information of the exposure levels, the levels were measured using survey meters and also by fixing TLD badges in appropriate locations like storage area, processing area, cutting area etc. over a one month period. Samples of gas mantle with different candle powers were collected, so also solution samples and effluent samples were collected. Gas mantles and effluent samples were counted in HPGe spectrometer and activities of thorium were estimated by counting the energy ranges 580-590 kev, 910-920 kev and 2610-2620 kev.

Results and Discussion

Thorium nitrate is handled in large quantity by mantle manufacturers. The cycle of operations indicates that thorium can get air borne and there is a continuous release of thoron. Air monitoring is important because inhalation is the main route of intake of radioactive dust by persons handling thorium compound. Air monitoring was done in workplace where processing work was done. The results of the air monitoring showed 30% of manufacturing units exceeding Derived Air Concentration (DAC) of long lived thorium indicating poor ventilation(Table 2). In some of the units there were no exhaust fans available, even if exhaust fans were fitted in some units, they were not in proper location. From the air activity data, working level values for thoron daughter products were estimated, considering the occupancy period or working hours of the workers. The exposure in WLM ranged from 1.4E-3 WLM to 0.47 WLM.

In some of the industries, especially with smaller working areas there was no segregation of wet and dry operations resulting in widespread contamination. The surface contamination detected is tabulated in Table 3. Lack of good housekeeping and proper workpractices have also lead to the spread of contamination. Maximum surface contamination was in processing area, because the working surface or the flooring was not smooth. This further confirmed that there is a likelihood of increase in external exposure levels. Further, movement of persons across the contaminated floor with alpha emittersreleases into air unbound fraction of alpha emitting radioactive substances(2). As an example a single person crossing a relatively small non-ventilated room with its floor contaminated with one unit of radioactivity per square meter would cause an increase in the air borne radioactivity by 4.0E-3 units/cu.m. With a higher level of surface contamination the air contamination is likely to increase, confirming the fact that there is likelihood of internal contamination of workers and there is need for corrective actions to be taken.

The results of area monitoring evaluated from TLD badges fixed at various locations for a period of one month are presented in Table 4. The radiation levels are significant in storage and finished product area. The surface exposure levels measured on the packed mantles indicated 8-9 microSv/h on 10 boxes of 100 mantles each and 12-13 microSv/h on 20 boxes of 100 mantles each. The exposure at 1 metre distance varies between 0.8 - 1 microSv/h. The packages were safe for transport as excepted package but it was generally observed that workers remained in closed proximity of stacked mantles, receiving external exposure due to beta and gamma radiations. Since gas mantles come under the category of consumer porduct as per Atomic Energy Regulatory Board (AERB) safety

Standard Specifications (1) mass of thorium per product is restricted based on the candle power. Specification of average quantity of thorium in a mantle is between 600mg - 800 mg. In order to ensure the compliance of manufacturers to the specified levels, samples of gas mantles were collected during radiological protection surveys. Ten brands of mantles were counted in HPGe spectrometer. All of the gas mantles were within the prescribed limits of standard specification. Effluent samples counted indicated higher concentrations of Th-232 than Th-228 because most of Th-228 daughters, especially Ra-228 get dissolved in water much faster resulting in high concentration of Th-228 in the solution and higher concentration of Th-232 in effluent.

Conclusion

Radiological Protection Survey provided information regarding lack of ventilation and primary containment in workplace which would result in internal contamination and external exposure of handling personnel.

Separate storage rooms for bulk quantity of thorium and finished product was recommended, which would reduce the external exposure. Other recommendations regarding facilities required for safe handling like smooth work surfaces, protective clothing, adequate ventilation, segegation of areas were also made. This was ensured by followup survey. Where the conditions were satisfactory, permission was given to handle increased quantity of thorium nitrate.

To ensure safety of the public we have recommended that manufacturing of gas mantles should be done only in industrial areas and not in residential areas. Existing facilities were asked to shift their premises to industrial areas and 60% of them have already shifted. Inside the workplace, facility should be available for the outlet pipeline from the wet operation areas to be directly connected to the main sewerage to stop the flow of effluent in public areas. Waste collection and disposal methods were also corrected. Thus a significant improvement in the radiological safety could be achieved using the data collected during the protection survey.

References:

1. AERB, Atomic Energy Regulatory Board, 1991.
Safety Series-4,'Standard Specifications for Radiological
Safety in the Design & Manufacture of Consumer Products
Containing Radioactive Substances.'

2. Handbook of Radioactive Contamination and Decontamination.
J.Severa and J.Bar.

Table 1

Steps in the manufacture of gas mantle

1. Weighing of silk hose
2. Preparation of solution (thorium & other salts)
3. Dipping of hose in solution,squeezing & collecting excess liquid.
4. Drying of hose.
5. Treating in ammonia.
6. Rinsing the hoses & drying.
7. Cutting to suitable length based on candle power.
8. Colouring one side of the hose.
9. Stitching the mantle.
10. Ironing & Packing.

Table 2

Air Concentration - Long lived thorium

Number of Institutions	
< DAC	> DAC
17	5

Derived Air Concentration (DAC) = 0.04 Bq/cu.m

Table 3

Area Monitoring Results (over a period of one month)

Location	Number of Institutions		
	0.1-2mSv	2.1-5mSv	5.1-20mSv
Storage (bulk + finished product)	0	2(1)	7(1)
Processing area	3	7(5)	4
Colouring area	4	1(1)	2(2)
Drying area	1(1)	1	1(1)
Cutting, ironing, packing area	5(7)	0(3)	1

Note: Figures in paranthesis indicate beta dose

Table 4

Surface Contamination Monitoring Results

Location	Levels in dpm/sq.cm
Solution preparation	53-2115
Squeezing of hose	50-290
Colouring	15-730
Cutting	14-210
Drying	2-120
Packing	140
Exit	6-125

MONTE CARLO TECHNIQUE APPLICATIONS IN THE FIELD OF RADIATION DOSIMETRY AT THE ENEA RADIATION PROTECTION INSTITUTE: A REVIEW.

G. F. GUALDRINI*, L. CASALINI**, B. MORELLI*
*ENEA-AMB 8 v.le Ercolani (I) 40138 BOLOGNA ITALY
**ENEA-ERG 4 v.Martiri di Monte Sole (I) 40129 BOLOGNA ITALY

1-INTRODUCTION

At the ENEA (Ente Nazionale per le Nuove Tecnologie, l'Energia e l'Ambiente) Institute of Bologna (Italy) since many years various activities have been carried out in the field of experimental dosimetry and radiation protection.

As far as the external radiation monitoring is concerned, these activities dealt with the design development and type test of photon personal dosemeters as well as routine reading and control of dosemeters, calibration activities etc.

As far as the internal dosimetry activities are concerned a whole body counter has been built and used since many years both for research activities and for routine assessment of internal doses. The WBC has been extensively used in the recent years, especially after the Chernobyl accident, to assess doses from intake of radioactive nuclides for Italian workers employed in Russia as well as normal population mainly leaving in the north-eastern Italian areas.

In the recent years, the necessity of improving the general dose assessment capabilities and to provide accurate field parameters and operational quantities, according to the new international recommendations, outlined the importance of coupling experimental work with Monte Carlo radiation transport modelling.

In this framework the code employed in the calculations was the general purpose Monte Carlo code MCNP (Monte Carlo for Neutrons and Photons) /1/ developed at the Los Alamos Scientific Laboratory (USA). This code, that makes use of a point-wise cross section library for photons with data derived from Hubbell et al. /2/ is provided with a very powerful geometry package, allowing complex geometries to be described and with a large variety of variance reduction techniques (Cell Splitting and Russian Roulette being the most important). The code is one of the most widely used instrument in the OECD countries and outside for neutron, photon and electron transport calculations. Since many years the code has been used at ENEA in the field of reactor physics and shielding design, deep penetration problem solution as well as dose assessment of radioactive material transport packages. Some improvements were also included, like the capability to treat electrons based on multiple scattering algorithms according to the Moliére theory /3/ /4/ (that was included before the release of MCNP-4 in order to treat coupled photon-electron transport problems) and the splitting parameter optimization routines in space and energy based on the DSA method /5/.

The present paper summarizes some studies carried out with Monte Carlo in the framework of the ENEA contribution to the activities of the EURADOS Working Group 4 (Numerical Dosimetry): they are concerned with computations of field parameters and operational quantities for the ICRU sphere with reference photon beams and modelling and calculations for photon internal and external dose assessment with the ADAM anthropomorphic phantom.

2-MONTE CARLO CALCULATIONS OF FIELD PARAMETERS AND OPERATIONAL QUANTITIES FOR THE ICRU SPHERE WITH REFERENCE PHOTON BEAMS FOR THE DESIGN AND CALIBRATION OF PERSONAL DOSEMETERS

The publication in 1985 and 1988 by the International Commission on Radiation Units and Measurements of Reports 39 /6/ and 43 /7/ stimulated attention being given to the appropriate procedure for the calibration of personal dosemeters.

According to these documents the calibration must be performed by placing dosemeters on an appropriate phantom exposed to X and gamma reference radiations as recommended by ISO

(International Organization for Standardization) or, in particular cases, BIPM (Bureau International des Poids et Mesures) reference X-ray radiations originally employed for primary calibration.

The Italian regulations in the field of calibration of personal dosemeters do not at the moment comply with the mentioned recommendations (calibrations of photon personal dosemeters being performed in terms of photon exposure): a Task Group has been however set up by the Government to formulate a new National Regulation in the spirit of the CEC directives.

In this framework numerical studies for the characterization of radiation fields produced by the reference radiations as well as calibrations on tissue equivalent phantoms have been started since some years at the ENEA Secondary Standard Dosimetry Laboratory in Bologna, as a feasibility study.

Following the previously mentioned recommendations, the ICRU sphere was taken as a suitable phantom for calibration purposes, whilst in the last years, ICRU has proposed a slab PMMA 30 cm X 30 cm X 15 cm phantom /8/ and very recently ISO proposed a 30 cm X 30 cm X 15 cm water phantom with a front face consisting of a 2.5 mm thick PMMA plate and the other phantom sides consisting of 10 mm thick PMMA plates /9/. This new proposals were formulated when the work herewith summarized was already in progress.

The criticism concerning the adoption of the ICRU sphere as a suitable phantom for calibration purposes was motivated by practical reasons: no commercial material can really be considered as a perfect substitute of the ICRU theoretical material, the sphere does not allow contemporary calibration of many dosemeters and, moreover, the non physical effects due to the spherical shape of the phantom (the so-called "ears" effect) are encountered in calculating conversion coefficients especially for higher energies.

Leaving out the quite troublesome discussion on "the most suitable phantom", our numerical evaluations and experimental verifications on reference X-ray beams, with the addition of ^{137}Cs and ^{60}Co sources, concerned principally /10/:

(1) Determination of air kerma backscatter factors and their dependence on the incident angle of the beam in an expanded and aligned field for the ICRU sphere, together with an extensive comparison of the results with those obtained in other European Laboratories /11/.
(2) Monte Carlo calculations of spectral physical parameters, i.e. the backscattered radiation mean energy for the ICRU sphere and its dependence on the beam incident angle.

Moreover a Monte Carlo evaluation of backscattered radiation spectra in front of the ICRU sphere was performed /12/.
(3) Comparison of experimental and calculated backscatter factors (with also their dependence on the beam incident angle) using the RS-1 sphere which is composed of a nearly tissue-equivalent material /13/. The study enabled the code and its associated interaction coefficients library in the range of energies from 30 keV to ^{60}Co to be validated /14/.

Finally a Monte Carlo study of the air kerma to directional dose equivalent conversion factors at the three depths of 7 mg/cm^2, 300 mg/cm^2 and 1000 mg/cm^2 in the ICRU sphere were performed /15/.

All the calculations were carried out in the so-called KERMA approximation, i.e. the secondary electron transport was not taken into accont and the problem mock-up was simplified neglecting the presence of air (to fulfil the definition of aligned field).

2-A Backscatter factor calculations and measurements

The air kerma backscatter factors for the ICRU sphere were calculated for the four ISO X-ray refecence series (High Air Kerma Rate Series, Low Air Kerma Rate Series, Wide Spectrum Series and Narrow Spectrum Series) and the BIPM Series at three distances from the phantom surface, i.e: 0 mm, 5 mm and 10 mm. In Figure 1 the energy dependence of the air kerma backscatter factor for the Wide Spectrum Series is presented for a normally incident photon beam.

Figure 2 shows an example of comparison between measured and calculated values for the same ISO Series.

Fig. 1: Wide Spectrum Series:
Backscatter factor versus equivalent energy at various distances from the ICRU sphere

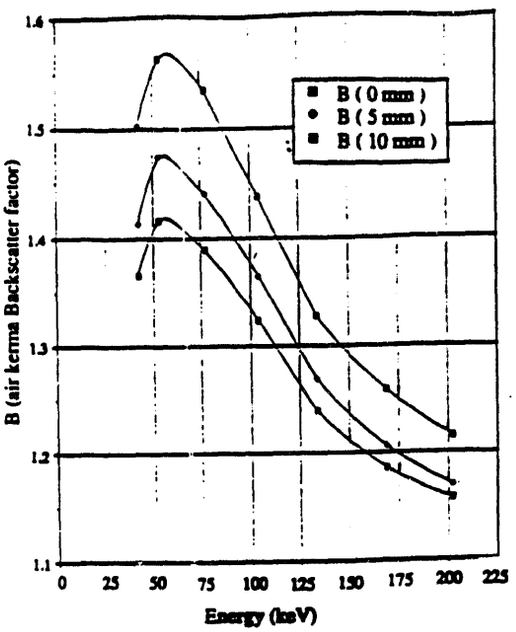


Fig. 2: Wide Spectrum Series:
Comparison between experimental and calculated Backscatter factors

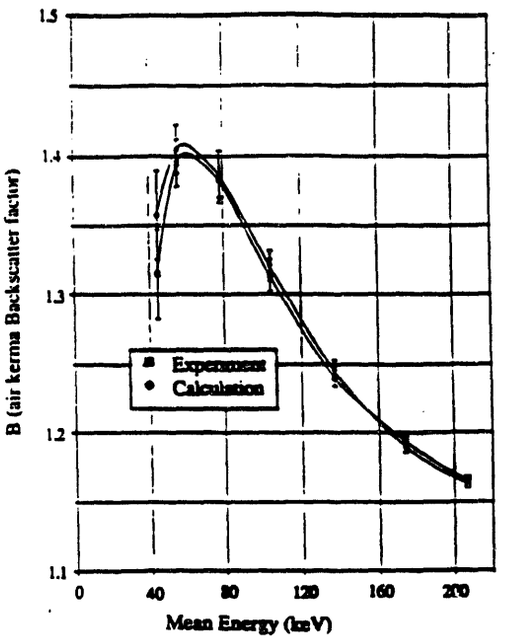


Fig. 3: Wide Spectrum Series (300 kV):
Photon fluence in presence of the ICRU sphere

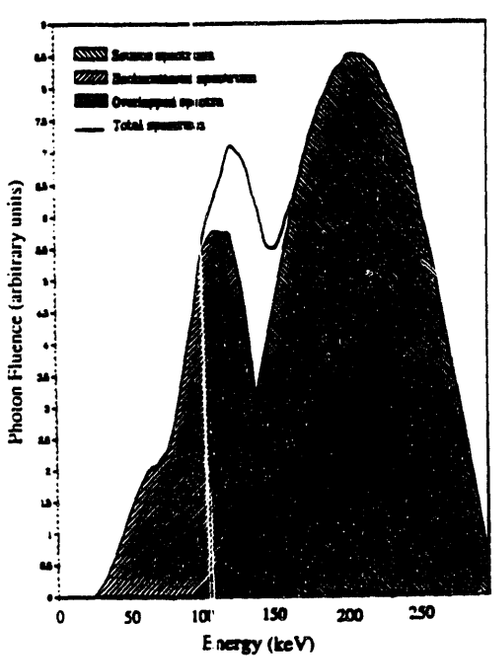
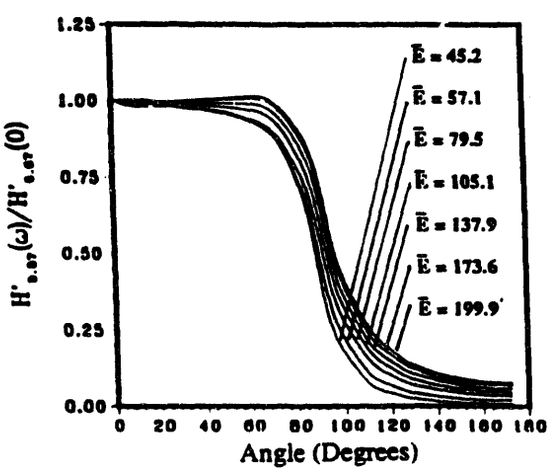


Fig. 4: H' 0.07 (w)/H' 0.07 (0) dependence on the radiation incident direction for Wide Spectrum Series photon beams



2-B Energy distribution of backscattered radiation

The mean energy of backscattered radiation as a function of incident angle was determined. This information, together with the fluence backscatter factor at the same angle, provides information on the average radiation field (in terms of energy) impinging on the detector. Figure 3 supplies the spectrum at 0 degrees incident angle for the same photon beam in front of the ICRU sphere. The convolution of incident and backscattered spectra using the fluence backscatter factor as normalization coefficient determines the mixed spectrum.

2-C Fluence to directional dose equivalent conversion coefficients

For this kind of operational quantities a certain number of data have been published concerned with both monochromatic energies and X-ray reference photon beams. These data are nevertheless incomplete, being referred mainly to normally incident beams. In our work we tried to supply a rather complete set of $H'(d,\omega)$ (both in tabular and graphical form) at the three mentioned depths together with families of depth dose curves for the various radiation incident angles. Figure 4 shows the angular dependence curves for 7 mg/cm^2.

Assuming, as mentioned above, the ICRU sphere as a suitable phantom for individual monitoring, so that the dosemeter design can be performed in terms of $H'(d,\omega)$ (that, in this case, corresponds to $H_S(d)$ and $H_p(d)$), the relationship between the dosemeter response and the operational quantity can be expressed by a semi-empirical formula, based on the theoretical expected interactions on the dosemeter when placed on the phantom and irradiated with a known photon beam as well as on the experimental energy response of the bare detector when irradiated free in air with the same photon beam /16/. The same phylosophy can of course be applied when using reference phantoms other than the ICRU sphere.

3-APPLICATIONS OF SABRINA AND MCNP TO DOSE ASSESSMENT STUDIES WITH THE ADAM ANTHROPOMORPHIC PHANTOM

Anthropomorphic phantoms play a very important role for the dose assessment in accidental irradiation conditions as well as in the dose evaluation to the patient during diagnostic and therapy treatments.

A large variety of phantoms has been proposed in the last thirty years, characterized by various degrees of complexity (sex and age-dependent).

A study has been therefore started concerned with the preparation of geometry packages for MCNP describing complex anthropomorphic phantoms. The male phantom was firstly implemented using the ADAM mathematical model /17/, based on the MIRD-5 pamphlet /18/.

The ADAM phantom is a simplified description of the standard western European male: the version that has been studied and implemented /19/ for MCNP is represented by 60 cells defined by 170 surfaces (planes, cylinders, cones, spheres, ellipsoids and torii), modelling the various organs, that are composed by four tissue materials: skin tissue (ρ=1.105 g/cm^3), lung tissue (ρ=0.296 g/cm^3), skeleton tissue (ρ=1.486 g/cm^3) that is an homogenized mixture of bone and bone marrow, and finally soft tissue (ρ=0.987 g/cm^3). The ADAM phantom was implemented for MCNP and the geometry could be checked using the SABRINA code, created at the Los Alamos Scientific Laboratory /20/. A series of accurate tests and Monte Carlo preliminary analyses for internal and external dosimetry problems have been performed /21/.

3-A Graphical display and geometry check of ADAM using the SABRINA code

The SABRINA code (LANL) was implemented on a VAX-9000 computer and the graphical studies were performed on a TEKTRONIX 4225 colour terminal connected with a PHASER-II DX colour printer. The code allows three-dimensional geometries to be reproduced (see in figure 5 the external view of the ADAM phantom). It is furthermore designed in order to point out geometry inconsistencies through an "error test", that directly displays on the terminal the geometry areas affected by the error itself. Sectional views and geometry cuts with appropriate bodies, besides the graphical display of the various body organs employing different colours, are also allowed.

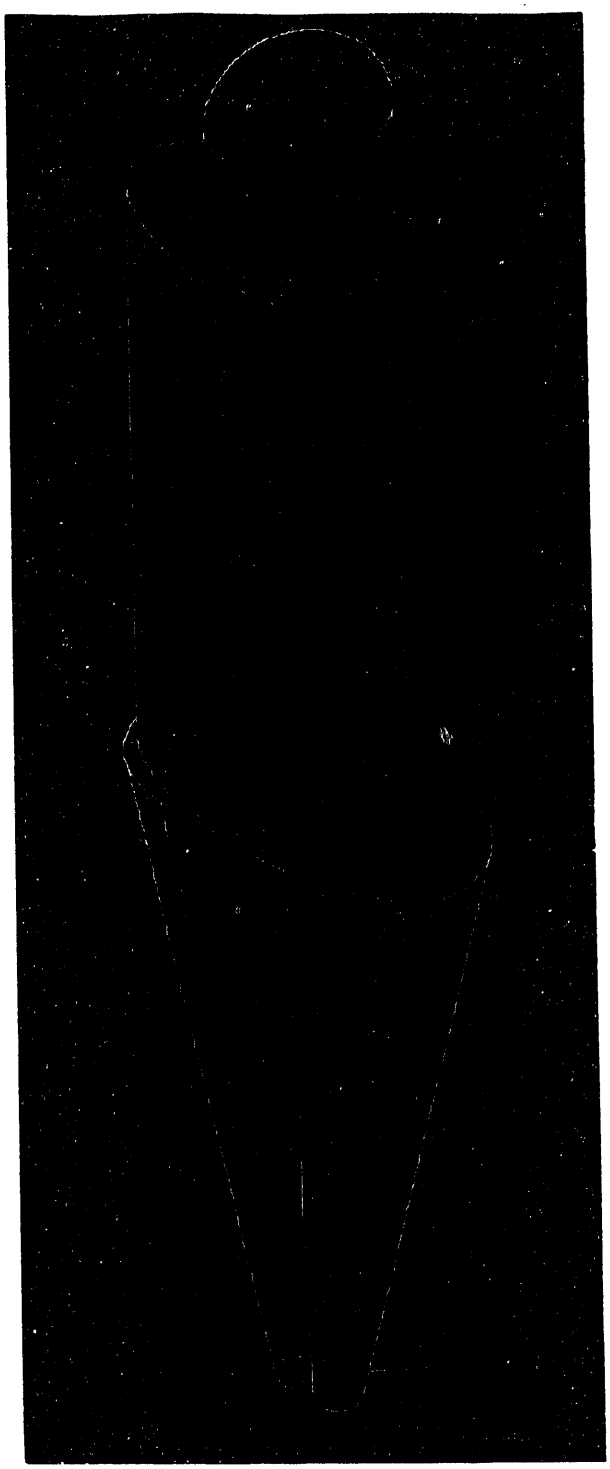


Fig. 5: External view of the ADAM phantom as produced by the SABRINA code.

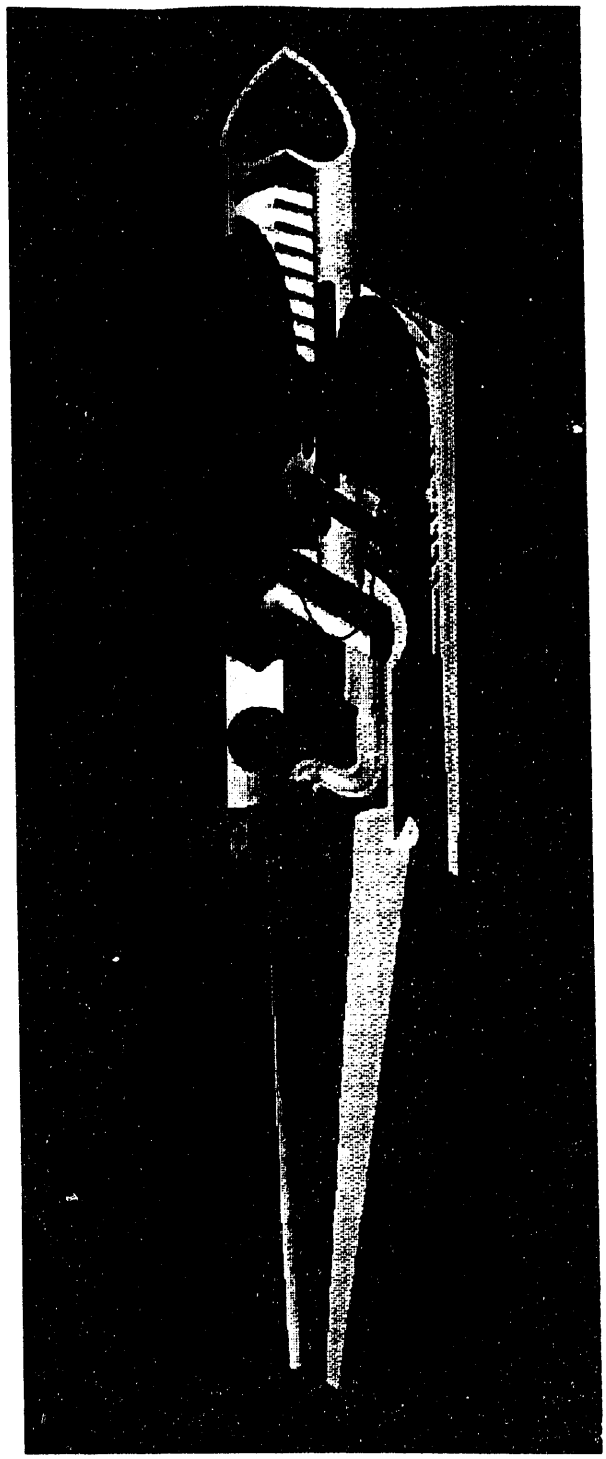


Fig. 6: Sectional view of the ADAM phantom with internal organs as produced by the SABRINA code.

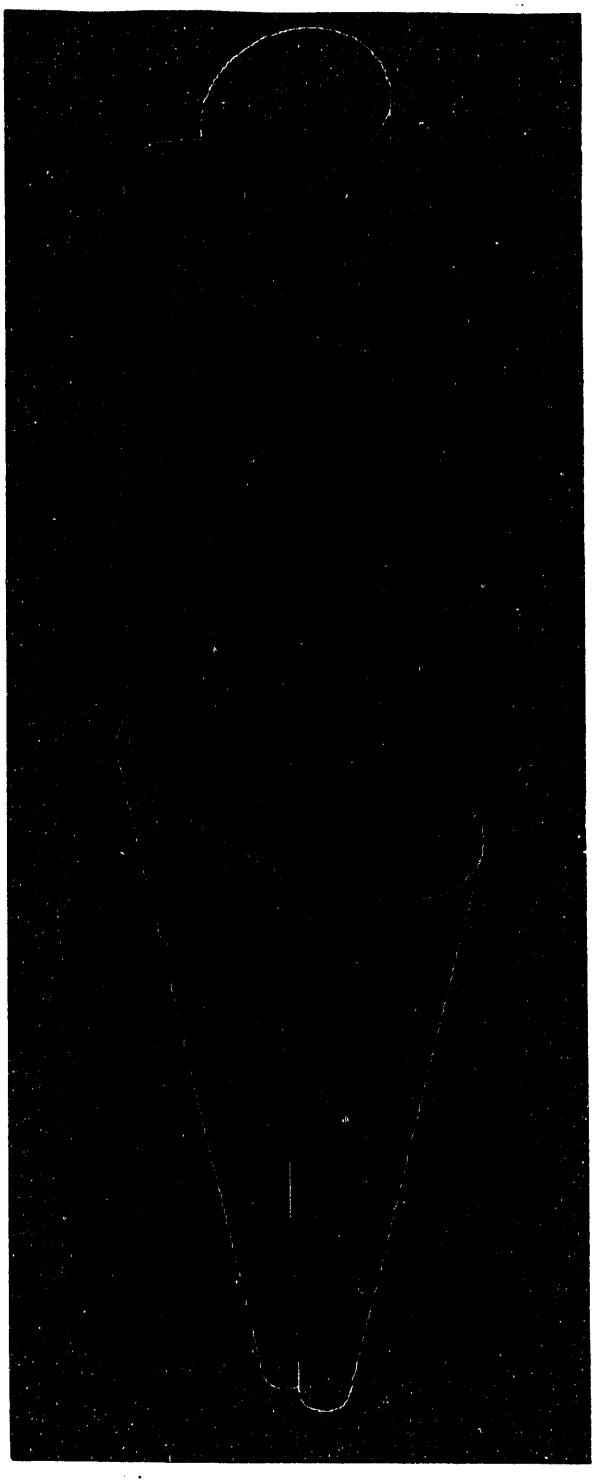


Fig. 5: External view of the ADAM phantom as produced by the SABRINA code.

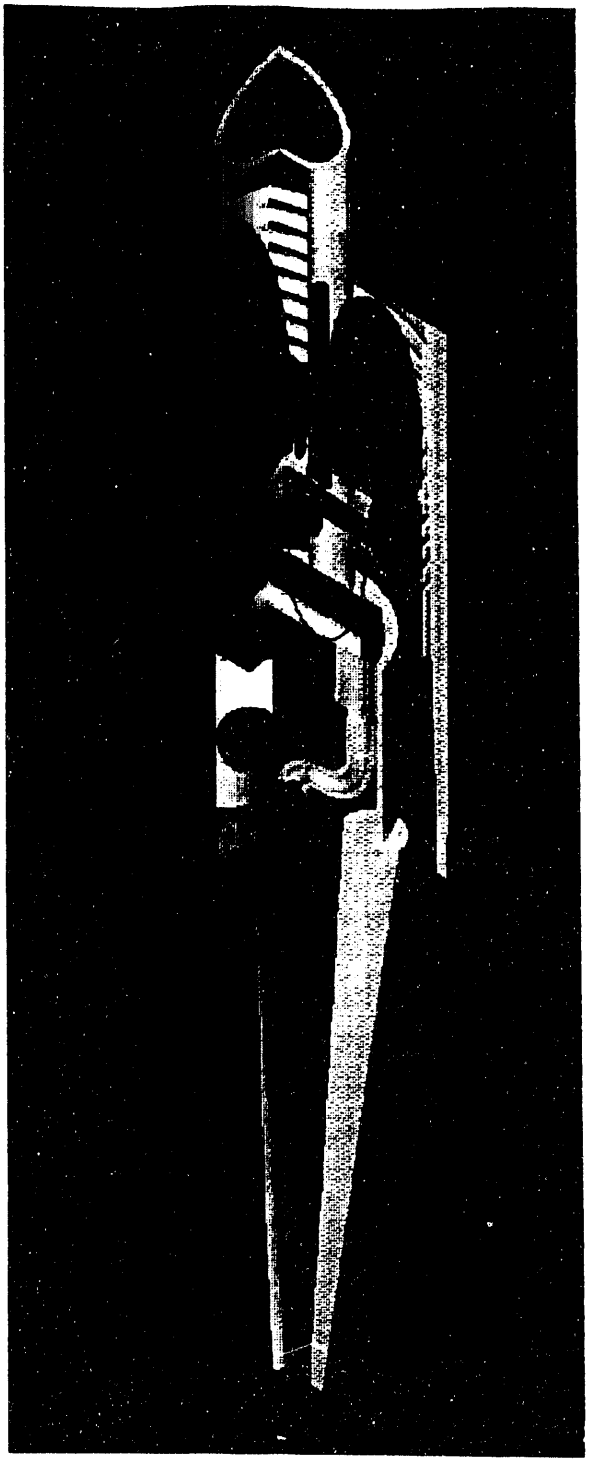


Fig. 6: Sectional view of the ADAM phantom with internal organs as produced by the SABRINA code.

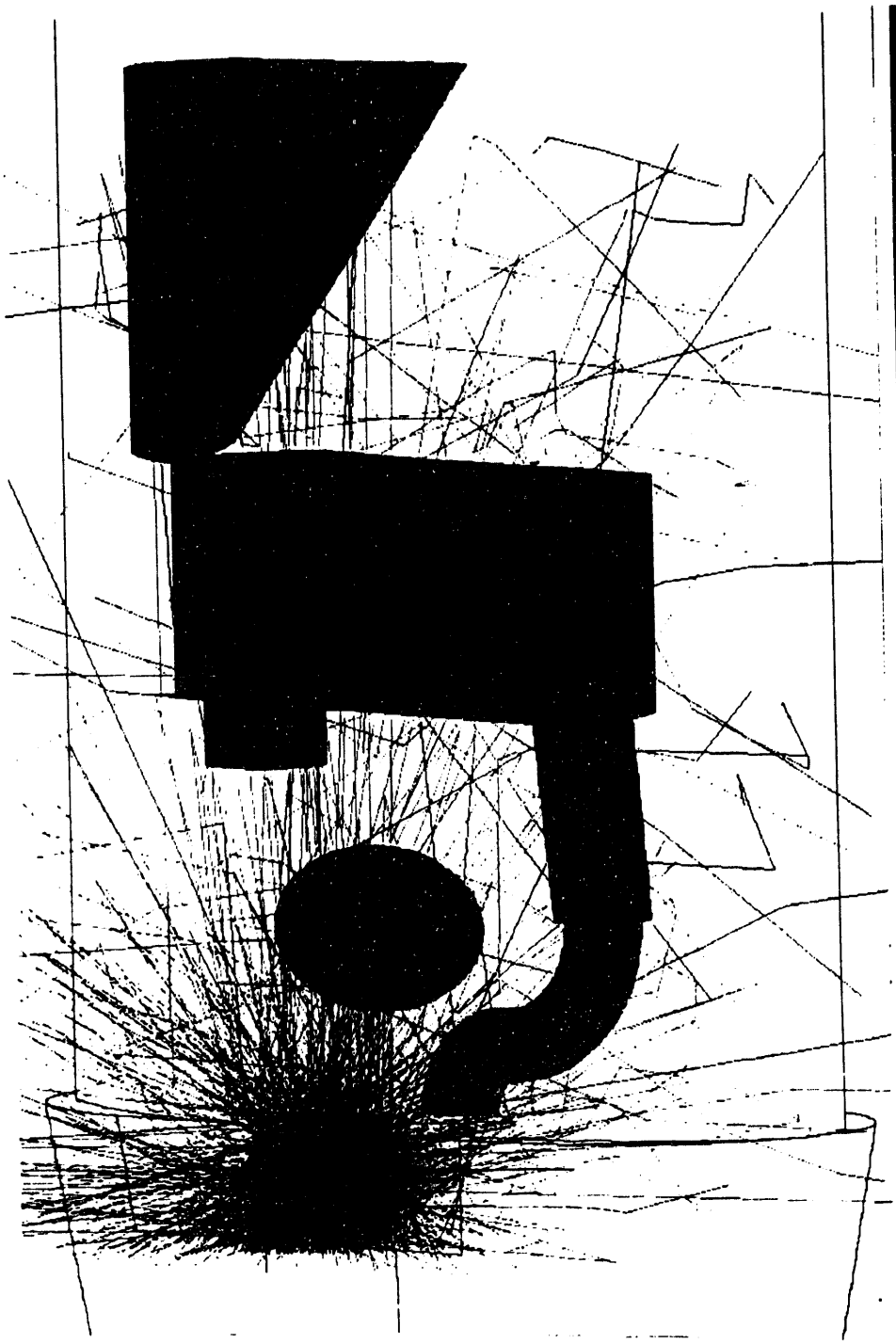


Fig. 8: Effect of the DXTRAN sphere application to the improvement of the particle population in the testes due to the ^{131}I irradiation. The source is located in the content of the seven organs: urinary bladder, sigmoid colon, descending colon, ascending colon, transverse colon, small intestine and liver.

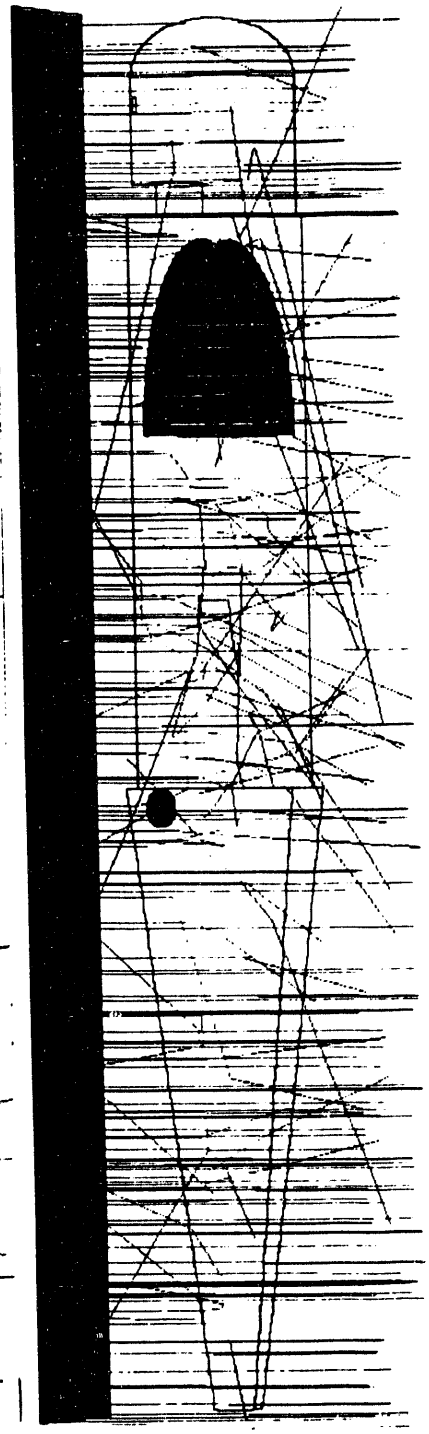


Fig. 7: ADAM phantom geometry and 1 MeV photon radiation tracks for an A/P irradiation of the human body.

Tab. 2: MCNP results of the specific energy deposition E_{dep} (MeV/g ± 1 relative standard deviation) in the testes due to the irradiation by a uniformly distributed ^{131}I source located in seven human organs
(total source strength = 1 gamma s^{-1})

	TOTAL
Edep (Mev/g ±1σ)	7.05E-7 ±1.8%
Source Volume (cm^3)	3454.9

Source organ: urinary bladder content		%
Edep (Mev/g ±1σ)	3.67E-7 ±1.9%	52.1
Source Volume (cm^3)	203	5.9

Source organ: sigmoid colon content		%
Edep (Mev/g ±1σ)	6.51E-8 ±1.9%	9.3
Source Volume (cm^3)	34.6	1.0

Source organ: descending colon content		%
Edep (Mev/g ±1σ)	3.19E-8 ±5.4%	4.5
Source Volume (cm^3)	104	3.0

Source organ: small intestine		%
Edep (Mev/g ±1σ)	1.75E-7 ±5.6%	24.8
Source Volume (cm^3)	1060	30.6

Source organ: ascending colon content		%
Edep (Mev/g ±1σ)	2.03E-8 ±6.6%	2.9
Source Volume (cm^3)	96.3	2.8

Source organ: transverse colon content		%
Edep (Mev/g ±1σ)	1.14E-8 ±4.7%	1.6
Source Volume (cm^3)	127	3.7

Source organ: liver		%
Edep (Mev/g ±1σ)	3.36E-8 ±5.3%	4.8
Source Volume (cm^3)	1830	53.0

A first approach was to consider the nuclide as uniformly distributed in the content of the following seven organs: urinary bladder, sigmoid colon, descending colon, small intestine, ascending colon, transverse colon and liver, and to calculate the specific energy deposition (in MeV g^{-1}) in the target organ, represented by the testes. Of course this calculation is not exhaustive for the dose assessment, that should require, besides other irradiation conditions, the study of the self absorption of the testes both from β and gamma emission from the blood vessels.

Several assumptions have been made to model the problem and to obtain acceptable standard deviations on the estimated quantities. As far as the source was concerned the line photon spectrum has been explicitly treated in the Monte Carlo calculation and for variance reduction purposes a series of facilities have been employed: spatial and energy biasing with the addition of the DXTRAN sphere. This method, provided in MCNP, is a way of increasing the particle population in a small region of interest (like testes). A visual idea of the particle increase in the testes area due to the DXTRAN sphere application is shown in figure 8.

The calculation was carried out in only one run of several hours computer time on an IBM-3090/XA mainframe corresponding to more than 2.5 10^6 photon histories.

A summary of the computed values is presented in table 2. For each source organ the percentage contribution to the energy deposition in the testes is presented. It has to be pointed out than 50% of the testes absorbed dose is due to the urinary bladder, as on the other hand qualitatively expected, small intestine more than 24%, sigmoid colon about 9%, descending colon and liver about 4-5%, ascending colon 3% and finally transverse colon less than 2%: liver that is 53% of the total source volume contributes to the response for less than 5%, introducing problems of source sampling optimization. Very reasonable standard deviations, ranging from 2% to 7%, were nevertheless obtained taking advantage of the extensive use of variance reduction techniques.

A spectral information is also supplied: for each source organ as well as for each energy bin (from 45.6 keV to 723 keV) the percentage contribution is supplied. These supplementary information can be useful in order to optimize the calculation and to allow necessary comparisons with the MIRD-5 pamphlet.

Table 3, e.g., shows a comparison in terms of specific energy fraction deposited in testes (g^{-1}) for four photon spectrum lines (the ENEA values can be compared by interpolation with those of ref. /18/). The agreement is satisfactory, except for the liver values. For this organ the ENEA results are however to be considered as more reliable. The values reported in ref. /18/ are in fact affected by a high statistical error when calculated with the Monte Carlo method, or rather approximate when determined with the "build-up factor method".

The comprehensive study for the dose assessment will include the treatment of a series of stationary conditions (during the distribution of the nuclide in the body as a function of time) obtained from ^{131}I kinetics model and direct measurements carried out on the patient.

Tab. 3 : Comparison of the deposited energy fractions in 1 g of testes for various photon energies.

Source Organ	Specific energy fraction deposited in testes (g^{-1}) and relative σ (%)							
	MCNP ENEA calculation				data from ref. /18/ (*)			
	0.17 MeV	0.36 MeV	0.50 MeV	0.63 MeV	0.10 MeV	0.20 MeV	0.50 MeV	1.00 MeV
Urinary Bladder Content	1.76E-5 (2.9)	1.70E-5 (2.5)	1.76E-5 (3.5)	1.67E-5 (1.3)	1.88E-5 (7)	1.59E-5 (8)	1.75E-5 (10)	1.57E-5 (12)
LLI Content (Des+Sig Colon)	6.46E-6 (4.2)	6.65E-6 (3.9)	6.60E-6 (3.8)	6.38E-6 (3.1)	6.27E-6 (11)	7.25E-6 (13)	7.14E-6 (16)	4.86E-6 (19)
ULI Content (Asc+Tra Colon)	1.04E-6 (7.1)	1.32E-6 (7.8)	1.61E-6 (9.5)	1.54E-6 (6.4)	9.33E-6 (29)	1.15E-6 (31)	1.78E-6 (28)	1.92E-6 (34)
Small Intestine	1.49E-6 (8.6)	1.55E-6 (7.4)	1.60E-6 (7.7)	1.62E-6 (4.2)	1.10E-6 (23)	1.28E-6 (27)	1.24E-6 (30)	1.79E-6 (35)
Liver	1.01E-7 (14)	1.61E-7 (7.2)	1.92E-7 (7.7)	2.52E-7 (8.0)	1.90E-7 (a)	3.05E-7 (a)	3.92E-7 (a)	8.76E-7 (48)

(*) The values have been obtained using Monte Carlo methods with the exception of those marked with (a) that have been calculated with the "build-up factor method".

4-FINAL REMARKS AND FUTURE DEVELOPMENTS

In the framework of the ENEA Radiation Protection Institute activities Monte Carlo numerical evaluations are being progressively coupled with experimental work. These techniques are demonstrating their high effectiveness in solving a large variety of problems. For the future further extensions in the use of codes as well as more complex phantoms is planned.

REFERENCES

/1/ "MCNP. A General Monte Carlo Code for Neutron and Photon Transport" Los Alamos Nartional Laboratory Report: LA-7396-M rev. 2, Sept 1986
/2/ Hubbell J. H., et al. "Atomic Form Factors, Incoherent Scattering Functions, and Photon Scattering Cross Sections." J. Phys. Chem. Ref. Data 4, 471 (1975)
/3/ Ferrari A., Sala P., Guaraldi R. and Padoani F. "An Improved Multiple Scattering Model for Charged Particle Transport.", Nucl. Instr. Meth. B71 (1992), pp. 412-426
/4/ Guaraldi R. and Padoani F. "Implementation of Algorithms Based on a New Electron Model (underpinned by the Molière Theory) in MCNP." forthcoming ENEA Report.
/5/ Burn K. W. "Implementation of an Extended Cell Model DSA including Particle Bifurcation between the Splitting Surfaces." Proc. of the ICRS-8, Arligton Texas, p. 1154 (April 1994)
/6/ ICRU 39 "Determination of Dose Equivalents resulting from External Radiation Sources." Bethesda Maryland (1985)
/7/ ICRU 43 "Determination of Dose Equivalents resulting from External Radiation Sources." Part 2 Bethesda Maryland (1988)
/8/ ICRU 47 "Measurement of Dose Equivalents from External Photon and Electron Radiations." Bethesda Maryland (1992)
/9/ Bohm J. "Minutes of the ISO/TC85/SC2/WG2 Meeting in London on 25-28 October 1993." PTB Braunschweig (November 1993).
/10/ Gualdrini G. F., Lembo L., Monteventi F. and Padoani F. "Monte Carlo Calculations of Field Parameters for the ICRU Sphere with Reference Photon Beams." Radiat. Prot. Dosim. 46, 5-13 (1993)
/11/ Gualdrini G. F. "Field Parameters and Operational Quantities for the ICRU Sphere with Reference Photon Beams; Part 1. Monte Carlo Calculations of Angular Dependence of Backscatter Factors." ENEA RT/AMB/92/12
/12/ Gualdrini G. F., Padoani F. and Morelli B. "Field Parameters and Operational Quantities for the ICRU Sphere with Reference Photon Beams; Part 2. Monte Carlo Calculations of Backscattered Spectra and Backscattered Mean Energy Angular Distribution." ENEA RT/AMB/92/13
/13/ Hermann K.P. and Harder D. "Production and Use of a Polyethylene-based Tissue-equivalent Spherical Phantom Substituting the ICRU Sphere for Photons." Radiat. Prot. Dosim. 28, 73-76 (1989)
/14/ Gualdrini G. F., Monteventi F. and Sermenghi L.. "Field Parameters and Operational Quantities for the ICRU Sphere with Reference Photon Beams; Part 3. Experimental and Computational Analyses on the Tissue Substitute Material RS-1." ENEA RT/AMB/92/30
/15/ Morelli B., Gualdrini G. F. and Monteventi F. "Field Parameters and Operational Quantities for the ICRU Sphere with Reference Photon Beams; Part 4. Monte Carlo and Experimental Evaluation of Angular Dependence of Dose Equivalent Quantities." ENEA RT/AMB/94/(in press).
/16/ Fantuzzi F., Gualdrini G. F., Morelli B. and Monteventi F. "Monte Carlo Computed Field Parameters for the Design of Photon Personal Dosemeters." Proceedings of the Austrian-Italian-Hungarian Radiation Protection Symposium, Obergurgl (Austria) 28-30 April 1993 pp. 107-110
/17/ Kramer R., Zankl M., Williams G. and Drexler G. "The calculation of Dose from External Photon Exposures Using Reference Human Phantoms and Monte Carlo Methods. Part 1 The Male (ADAM) and Female (EVA) Adult Mathematical Phantoms." Report GSF-Bericht S-885, Munchen Reprinted Jan. 1986
/18/ Snyder W. S., Ford M. R., Warner G. G. "Estimates of Specific Absorbed Fractions for Photon Sources Uniformly Distributed in Various Organs of a Heterogeneous Phantom." nm/mird Pamphlet n° 5, Health Physics Division, ORNL Oak Ridge TN 37830, Jan 1978
/19/ Kopec M. private communication
/20/ West J. T. "SABRINA: An Interactive Three-Dimensional Geometry Modeling Program for MCNP." Los Alamos National Laboratory Report LA-10688-M, October 1986
/21/ Casalini L. "Applicazione dei codici SABRINA e MCNP al Fantoccio Antropomorfo ADAMO." ENEA-ERG RTI - CT WCD 00005, 1994 (in press)
/22/ Morelli B. "Valutazione di Dose da Irraggiamento Fotonico su Fantoccio Antropomorfo Mediante Tecniche Monte Carlo." Tesi Scuola di Specializzazione in Fisica Sanitaria Bologna(I) July 1994
/23/ ICRP Publication 51 "Data for use in Protection Against External Radiation." March 1987
/24/ Handelsman D. J. and Turtle J. R. "Testicular Damage after Radioactive Iodine (I-131) Therapy for Thyroid Cancer" Clinical Endocrinology (1983) 18,465-472

THE IMPLEMENTATION OF NEW RADIATION QUANTITIES IN NUCLEAR POWER PLANTS IN TAIWAN*

C.J. Tung, H. Niu (National Tsing Hua University), T.J. Chen (Radiation Protection Association), T.L. Chou, W.W. Yeh and R.Y. Liao (Taiwan Power Company)

The International Commission on Radiological Protection (ICRP) and the International Commission on Radiation Units and Measurements (ICRU) recommended basic and operational dosimetric quantities for external radiation protection. These quantities include the equivalent dose to an organ or tissue, H_T, the effective dose, E, the ambient dose equivalent, H*, the directional dose equivalent, H', the individual dose equivalent-penetrating, H_p, and the individual dose equivalent-superficial, H_s. In the general principles of monitoring for radiation protection of workers, ICRP recommended: "At low dose equivalents (corresponding say to those within Working Condition B) dosimetric quantities might be used directly to assess exposure, since accuracy is not crucial. At intermediate dose equivalents (corresponding say to Working Condition A and slight overexposures) somewhat greater accuracy is warranted, and the conversion coefficients from dosimetric to radiation protection quantities should be applied. For significant exposures that are deemed abnormal, actual absorbed doses in the body, from an assessment of the accident, should be used." In order to determine radiation protection quantities and actual absorbed doses in the body, information on the energy and irradiation geometry of the incident radiation is required. In this work, we surveyed high radiation areas in all three nuclear power plants in Taiwan. We measured energy and angular distributions of photons in some workplaces by a portable NaI detector. We then analyzed the irradiation geometries according to ICRU classifications, i.e. AP, PA, LAT, IS, etc. Applying these results, the body doses may be more accurately evaluated for workers exposed to high-level radiation. In this work, we have also assessed the performance of instruments currently used by Taiwan Power Company for their suitability of measuring new quantities. The energy response of an instrument for the measurement of H*(10), for instance, should be converted from exposure to ambient dose equivalent using appropriate conversion coefficients. Only when the relative response is within say $\pm 30\%$ over a wide energy range, the instrument is acceptable to measure the new quantity H*(10).

*Research sponsored by the National Science Council of the Republic of China.

OCCUPATIONAL RADIATION EXPOSURES TO RAILROAD WORKERS FROM SHIPMENTS OF RADIOACTIVE MATERIALS

D.E. Fields and W.D. Cottrell (Health Sciences Research Division; Oak Ridge National Laboratory; Oak Ridge, Tennessee 37831)

Fissile and high-level radioactive wastes are currently transported over long distances by truck and by rail transportation systems. The primary form of fissile material is spent reactor fuel. DOE projected increases in the rate of shipments have generated concern by railroad companies that railroad workers may be exposed to levels of radiation sufficiently high that a radiation protection program may need to be implemented. We have estimated doses to railroad workers for two exposure scenarios that were constructed using worker activity data obtained from CSX Transportation for crew and maintenance workers. This characterization of railroad worker activity patterns includes a quantitative evaluation of the duration and rate of exposure. These duration and exposure rate values were evaluated using each of three exposure rate vs. distance models to generate exposure estimates.

Several recommendations follow from the results of this study:

- Doses to maintenance workers who service multiple shipments of legal limit shipments may approach annual limit values. Consideration of this possibility suggests that special instructions requiring monitoring of repair operations might be included with shipping papers.

- Doses from neutron exposures, both to railroad workers and to the general public, should in general be given more attention than has been the case.

- Radiological survey monitoring of fissile and high-level radioactive waste shipments appears to consist primarily of alpha monitoring (smear samples) and gamma radiation monitoring. This practice is appropriate for most shipments, but should probably be supplemented by neutron exposure monitoring for some shipments including, most notable, spent fuels.

- A study similar to this should be undertaken to examine the doses to repair and transport personnel who handle fissile and high-level waste shipments that are routed by truck.

FIELD EXPERIENCE WITH REMOTE MONITORING

Arthur E. Desrosiers
Bartlett Services, Inc.

Abstract

The Remote Monitoring System (RMS) is a combination of Merlin Gerin detection hardware, digital data communications hardware, and computer software from Bartlett Services, Inc. (BSI) that can improve the conduct of reactor plant operations in several areas. Using the RMS can reduce radiation exposures to radiation protection technicians (RPTs), reduce radiation exposures to plant maintenance and operations personnel, and reduce the time required to complete maintenance and inspections during outages. The number of temporary RPTs required during refueling outages can also be reduced. Data from use of the RMS at a two power plants are presented to illustrate these points.

Equipment Configuration

Both sets of data presented here were obtained during outage activities at PWRs. One case involved cutting and removal of RTD piping and the other involved ISI of steam generators. In both cases, one WRM radio receiver was placed in containment. Three of four LEA boosters insured radio coverage of the entire containment. Display terminals were placed at RP control point outside containment. A computer multiplexer in containment connected all of the in-containment devices to the main computer located at the main RP control point. Thus, only a single data cable was required to connect the devices in containment to the outside. The RP control points inside containment were also equipped with closed circuit video equipment and the RPTs had voice radio communication with the workers in the loop areas. The workers wore four or five transmitting dosimeters connected to a multiplexer and transmitter. Dosimeters were also mounted on the steam generator platforms to provide area monitoring for the ISI work.

Dose Savings to RPTs

The use of the RMS allowed RPTs to control the workers' radiation doses while working in a low dose area. In the case of RTD pipe cutting, the RPTs were able to work in a 2 mrem/h field while the pipe cutters were in a 500-1000 mrem/h field. Dose saved was estimated to be approximately 30 rem. In the case of ISI, the RPTs were similarly working from a low dose area outside the bioshield wall. The use of telemetry for area monitoring also allowed RPTs to perform routine surveillances from a low dose area.

Field Experience with Remote Monitoring

Dose Savings to Workers

The use of RMS allows RPTs to accurately monitor dose and dose rate in situations that would not be possible with traditional means of monitoring. Whenever a worker is near collimated sources, point sources, or line sources, monitoring of multiple whole body locations is necessary. If the work activity requires the worker to change position near the source, it is extremely difficult to track multiple whole body locations with time and motion techniques. Therefore, stay time limits are imposed to control dose. Although stay time limits are effective in limiting dose, this technique tends to require multiple trips into the high radiation area to complete the work, because the stay time limit is necessarily conservative. Also, the use of stay times does not, by itself, control the worker's dose rate.

The RMS allows an RPT to control the dose rate during the work activity, even when dose rates are rapidly changing and the worker has multiple dosimeters. The RPT also monitors the dose to each dosimeter, thereby allowing a worker to complete the job with a single entry to the high radiation area in many cases.

Figure 1, for example shows data from RTD pipe cutting. The worker placed his right are close the RTD pipe. The RP technician noticed a dose rate alert at 3000 mrem/h and directed the worker to move his arm away from the pipe. The RPT was located outside the work area, but was able to control the radiological conditions using video, voice radio, and RMS.

Figure 2 shows a more complicated series of events while "Worker T" was cutting RTD pipe. Shortly after beginning the cut, he moved his head and right arm closer to the pipe. The RPT noticed the increased dose rates on the RMS monitor and requested that he move back. The worker complied immediately. He subsequently kept his head back from the pipe, but later his right arm crept back to 1000 mrem/h again. The RPT again requested that he move his right arm back and continued to monitor the right arm closely during the remainder of the cut.

Figure 3 shows data from monitoring "Worker M" during RTD pipe cutting. This worker would alternately move his right thigh, his left thigh, or both thighs closer to the pipe. The RPT repeatedly monitored the dose rate to all five dosimeters on this worker and adjusted the positions of the worker's thighs to reduce the dose rates.

Field Experience with Remote Monitoring

These data demonstrate conclusively that an RPT can reduce a worker's dose by detecting high dose rates during a work activity and reducing the dose rate as the work is in progress. The most important method of reducing a worker's dose is to ensure that the worker does not inadvertently place his or her body in a radiation field that is unnecessarily high. Real time monitoring allows the RPT to reduce the worker's dose because the high dose rates are detected while the worker is in the high radiation area.

In situations that require exposure control via stay time limits, the RMS can constantly monitor dose and dose rate so that workers can complete a task in one entry without exceeding administrative limits. This results in fewer entries to the radiation area and less dose received while entering and exiting. When multiple whole body dosimeters are required, the RMS provides a tool to help the RPT prevent one dosimeter reading significantly higher that the others. This reduced the overall whole body dose.

The RMS can also reduce overexposures due to inadequate surveys. The common ionization chamber survey meter will significantly underestimate the dose rate from point sources at distances less than 15 cm. This occurs due to the well known geometry effect. The RMS' detectors are more accurate under such conditions because the detector is small, similar to the size of a TLD chip.

Preventing Overexposures

Figures 4 is an example of how RMS can prevent overexposures. Figure 4 shows the case where a worker on a steam generator platform made an unauthorized partial entry into the steam generator bowl. The unauthorized dose rate to his arm was rapidly detected as the RMS monitor alarmed and the worker was removed from the platform.

Saving Outage Time

The time required for maintenance or inspection activities can reduced because fewer entries are required into radiation areas. If the radiation area is also contaminated; if respiratory protection is required; or if ALARA briefings are required, the time required for an entry can easily be three or four times greater than the time required to perform the physical work. Reducing multiple entries can remove days from an outage schedule.

Figure 5 gives an example where an individual made two successive full entries into a steam generator bowl. The RMS was used to carefully control the individual's dose to within 200 mrem of the regulatory limit.

Field Experience with Remote Monitoring

Having one individual perform two successive entries resulted in a lower overall dose because it saved the dose associated with multiple trips to the steam generator platform. This procedure also saved the dose to support personnel who would have accompanied the worker into the loop area for multiple entries. In addition, the work was completed in less time.

The earlier examples of RTD pipe cutting also demonstrate an outage time savings. In this case, all of the RTD pipe was cut in one work shift. This time savings occurred because the workers were able to complete multiple cuts in each trip to the work location. Since the workers were being monitored with RMS, there was no need to come down from the platform and check "sacrificial" dosimeters after each cut.

In these examples, the RPTs were working from control points in containment. However, some plants have used RMS to move their control points completely outside containment. This can allow the RPT to work in a relatively quiet location without contamination or respiratory protection controls. This environment can improve coordination and other work groups so that work flows without interruption. The productivity of the RPT can also be increased by working from a control point outside containment. Of course, using RMS, one technician may be able to cover work in multiple locations.

Conclusion

In addition to the obvious fact that using the RMS can save dose to RPTs, there are significant opportunities to reduce workers' doses, reduce outage time, and reduce outage budgets.

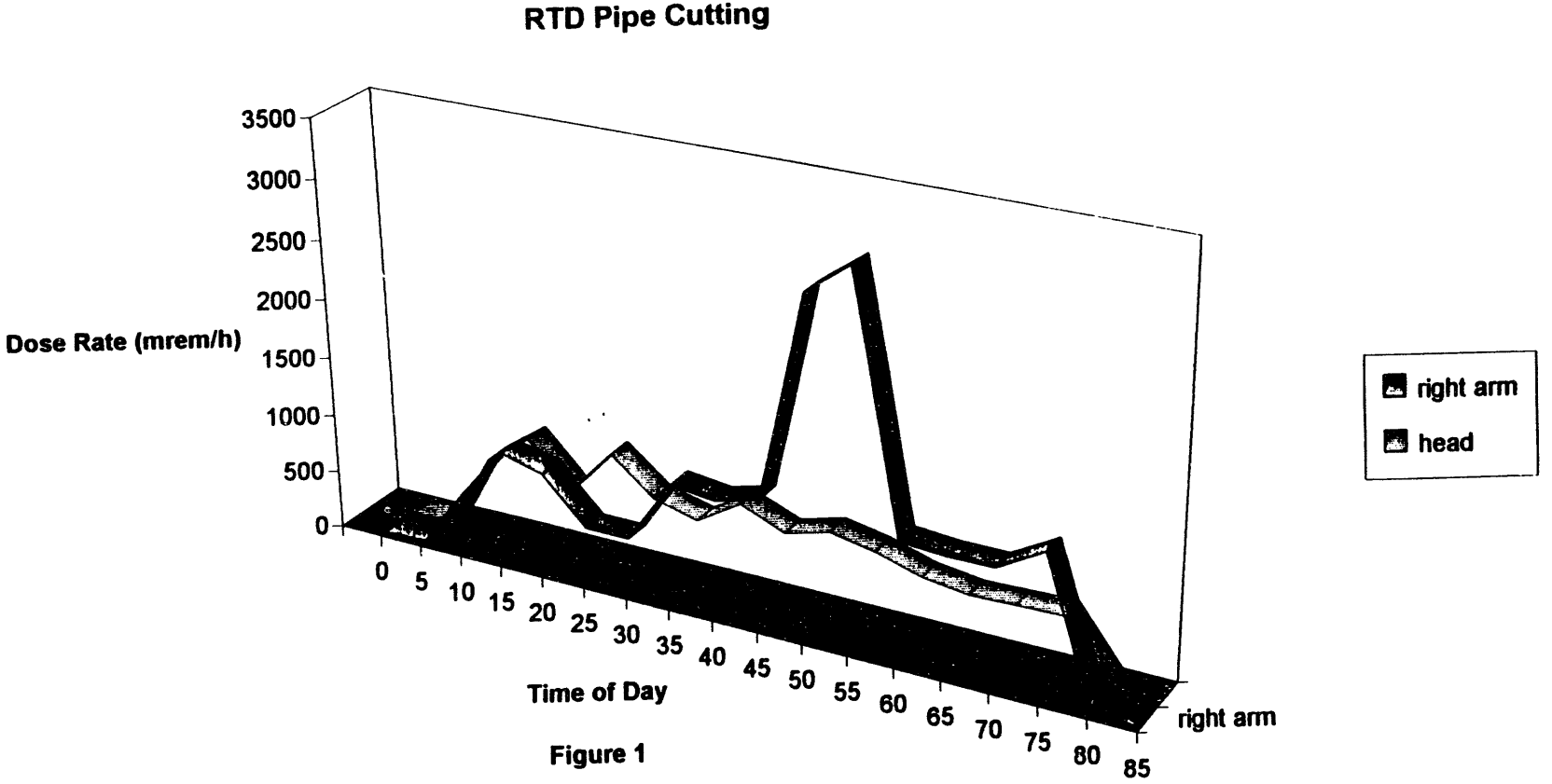

RTD Pipe Cutting
Dose Rate (mrem/h)
3500
3000
2500
2000
1500
1000
500
0
0 5 10 15 20 25 30 35 40 45 50 55 60 65 70 75 80 85
Time of Day
right arm
right arm
head

Figure 1

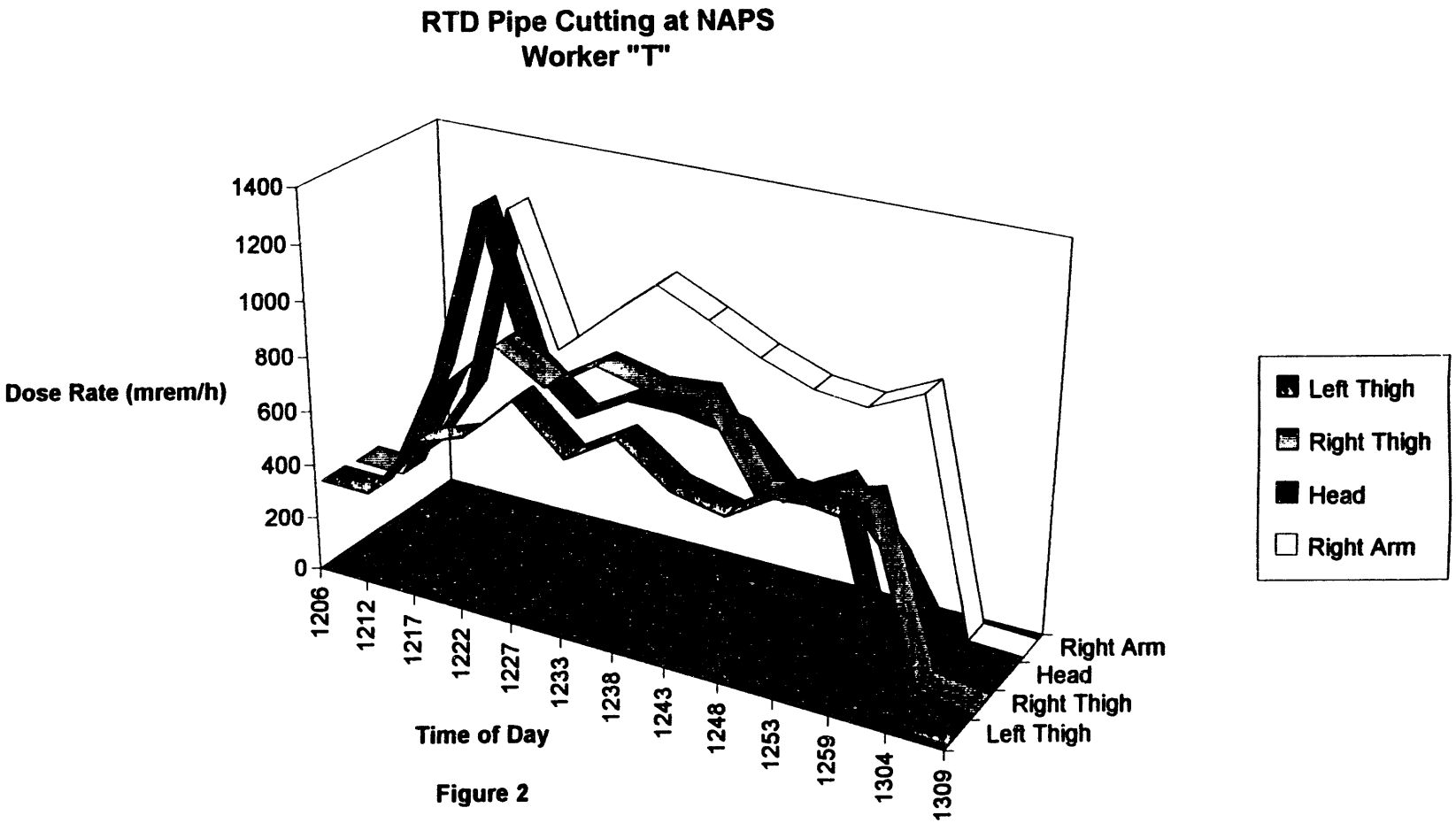

RTD Pipe Cutting at NAPS
Worker "T"
Dose Rate (mrem/h)
1400
1200
1000
800
600
400
200
0
1206
1212
1217
1222
1227
1233
1238
1243
1248
1253
1259
1304
1309
Time of Day
Left Thigh
Right Thigh
Head
Right Arm
Right Arm
Head
Right Thigh
Left Thigh

Figure 2

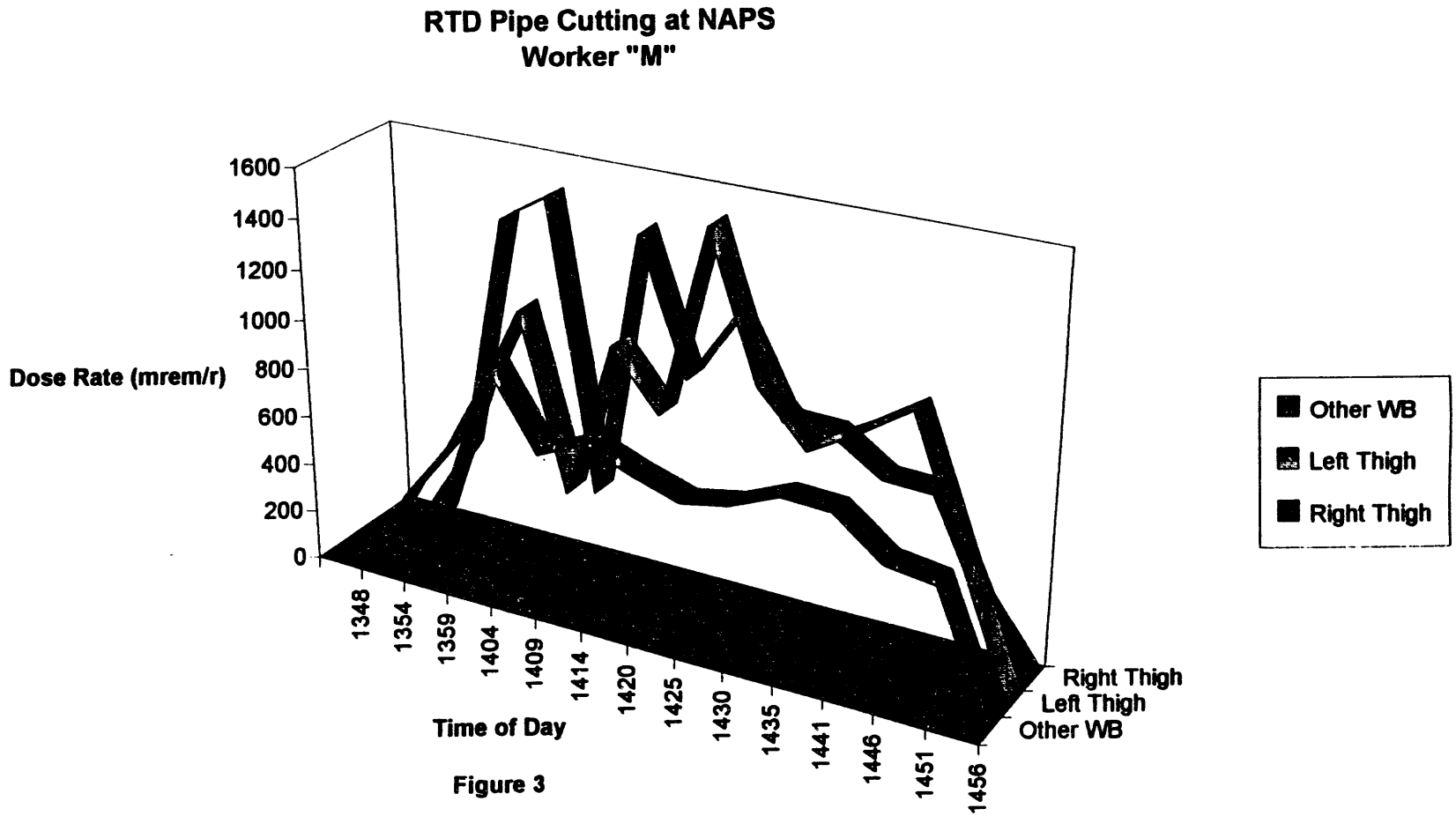

RTD Pipe Cutting at NAPS
Worker "M"
Dose Rate (mrem/r)
1600
1400
1200
1000
800
600
400
200
0
1348
1354
1359
1404
1409
1414
1420
1425
1430
1435
1441
1446
1451
1456
Time of Day
Right Thigh
Left Thigh
Other WB
Other WB
Left Thigh
Right Thigh

Figure 3

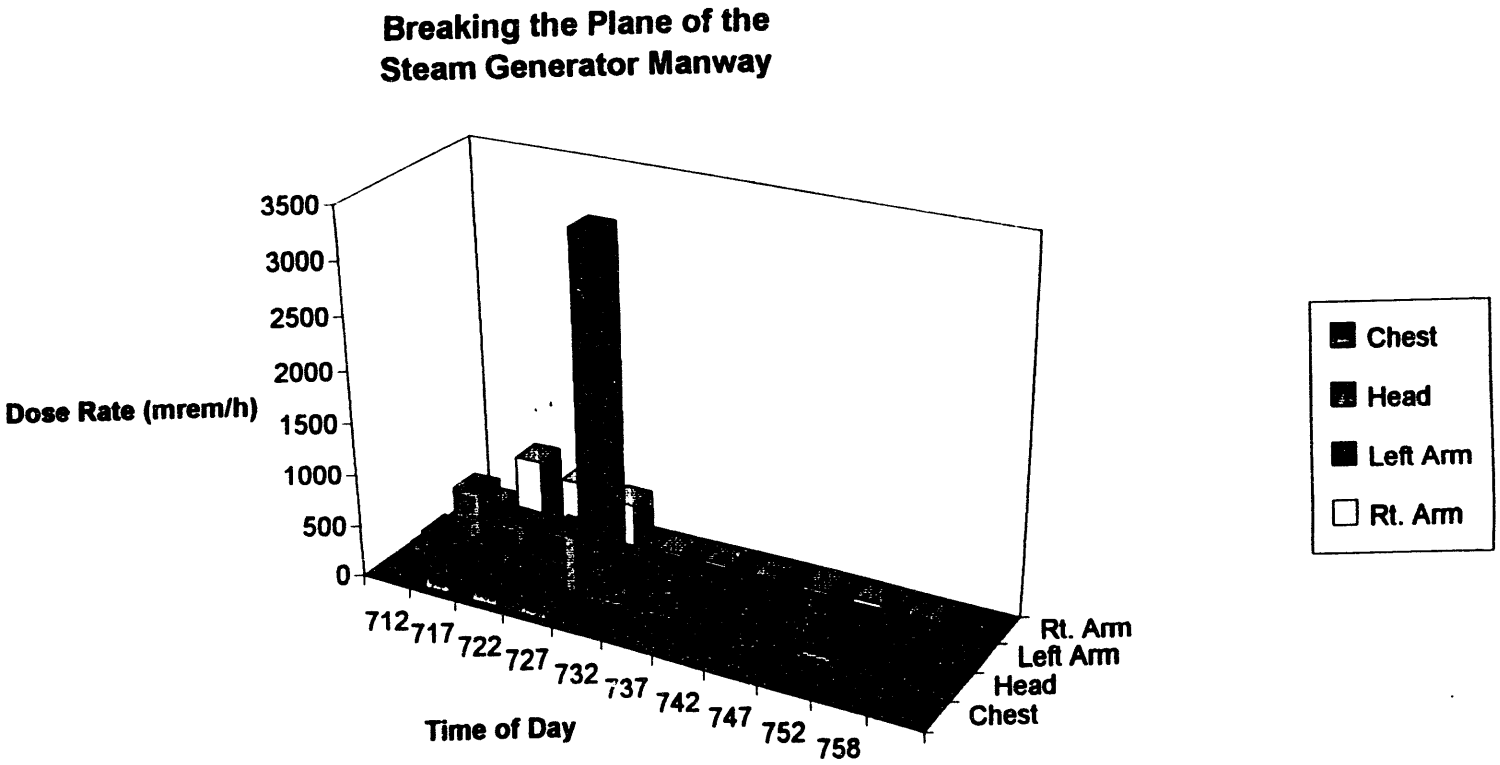

Breaking the Plane of the
Steam Generator Manway
Dose Rate (mrem/h)
3500
3000
2500
2000
1500
1000
500
0
712
717
722
727
732
737
742
747
752
758
Time of Day
Rt. Arm
Left Arm
Head
Chest
Chest
Head
Left Arm
Rt. Arm

Figure 4

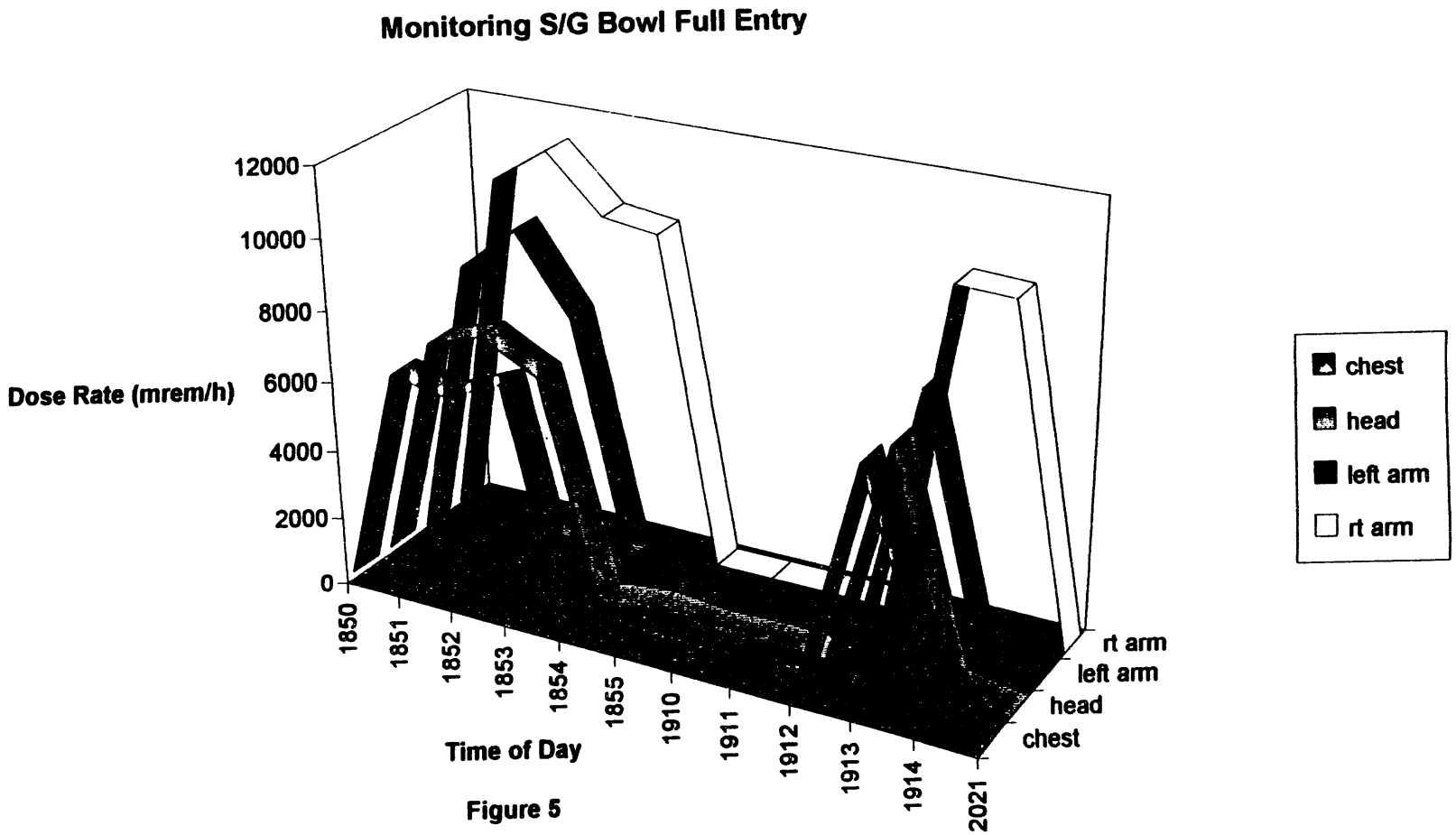

Monitoring S/G Bowl Full Entry
Dose Rate (mrem/h)
12000
10000
8000
6000
4000
2000
0
1850
1851
1852
1853
1854
1855
1910
1911
1912
1913
1914
2021
Time of Day
rt arm
left arm
head
chest
chest
head
left arm
rt arm

Figure 5

IMPLEMENTATION OF A SELF-DIRECTED WORK TEAM IN A TLD PROCESSING CENTER

A.A.Arnwine, R.S. Bogard, N.A. Teasley, D.E. Somers, and M.L. Souleyrette (Martin-Marietta Energy Systems, PO Box 2008, Bldg 9711-1, MS-8105, Oak Ridge, TN 37831)

In an effort to maintain productivity with a decreasing work force, the Oak Ridge Y-12 Plant has adopted the concept of Self-Directed Work Teams in various disciplines. The plant's Health Physics Department was able to eliminate a layer of front-line supervisors by establishing four self-directed work teams. Each team was able to choose their method of implementation. The TLD Processing Center Team chose to use project management tools to ensure a smooth transition from the traditional work group to a self-directed approach. This process focused on establishing responsibilities, determining training requirements, determining a leadership style for the group, and performing a potential problem analysis for the transition. The transition also reviewed interface issues that could occur with upper management, matrix management, technical oversight, and organizational peers. The team's experience is also evaluated in comparison to other Self-Directed Work Teams.

EXPERIENCE WITH REIRS FOR THE REVISED 10 CFR 20

Derek A. Hagemeyer (Science Applications International Corporation-SAIC)

The Nuclear Regulatory Commission's (NRC's) Radiation Exposure Information Recordkeeping System (REIRS) was recently updated to accommodate the changes required by the revised 10 CFR 20. A brief history of the REIRS database will be presented, along with a summary of the changes that were implemented to change from the old §20.406-407 reporting requirements to the new §20.2104 and §20.2106 requirements. The status of the REIRS will be discussed including the current process for submitting data, correcting previous data, and requesting dose history reports.

Several licensees have already submitted test data files in the format defined in Appendix A of Regulatory Guide 8.7, *Instructions for Recording and Reporting Occupational Radiation Exposure Data*. However, several problems were experienced with these test files. Most of these problems fall into two categories: (1) the handling of non-numeric dose codes (e.g., NC, ND, and NR) and their associated arithmetic rule, and (2) data formatting problems. This paper will discuss these problems and how to avoid them in future NRC submittals. The advantages of submitting these electronic files in lieu of hardcopy NRC Form 5s will also be discussed.

Additionally, this paper will summarize the NRC sponsored Radiation Exposure Monitoring and Information Transmittal (REMIT) computer program, which is a PC-based, menu-driven tool that facilitates the manipulation of occupational radiation exposure data, computes internal doses from intake estimates, and produces hardcopy NRC Forms 4 and 5, as well as data files in Reg. Guide 8.7 Appendix A format. A brief demonstration of this program will be given, along with availability and technical support information. The status of the Department of Energy Radiation Exposure Module (REM) system will also be discussed, including plans to upgrade it to be more consistent with the NRC REIRS.

A FEW EXPERIENCES AND LESSONS LEARNED IN INSTALLING RADIOLOGICAL ACCESS CONTROL SYSTEMS

Robert Gunn Benson, Aaron Clemmons and Peter Clemmons (Pro-Tem, Inc.)

Unforeseen obstacles are often encountered during the installation of any information system. Radiological access control systems add unique complications. Many costly events can be averted if appropriate action takes place prior to installation and system startup.

Based upon experiences gained from installing systems into radiological environments since 1980, several key areas are addressed with recommendations on how to avoid these pitfalls.

These areas include hardware considerations, working with vendors and customers, implementation schedule pitfalls, system design considerations for successful startup, user and system training (especially dosimetry), the value of factory acceptance testing, and the importance of user support at the sight. Actual examples from installations at several nuclear facilities will be presented.

SYSTEM INTEGRATION FOR RADIATION RECORDS

Brian J. Lawson, Linda Farrell, Clifford Meacham, Jane Tapio (Martin Marietta Corporation - Knolls Atomic Power Laboratory, Inc., PO Box 1072, Schenectady, NY 12301)

System integration is the process where through networking and/or software development, necessary business information is available in a common computing environment. System integration is becoming an important objective for many businesses. System integration can improve productivity and efficiency, reduce redundant stored information and errors, and improve availability of information.

This paper will discuss the information flow in a radiation health environment, and how system integration can help. Information handled includes external dosimetry and internal dosimetry (in vivo and in vitro).

The paper will focus on an ORACLE based system integration software product. The complete system includes:

- the ORACLE application software,
- Harshaw 8800 external dosimetry workstations with data acquisition and analysis computer software,
- Canberra Industries invivo data acquisition and analysis computer software,
- and a computer network supporting data transfer.

SESSION II.
TLD Materials and Dosimeter Design

Christopher Soares,
Chairman

A NEW COMBINATION BETA/GAMMA/NEUTRON WHOLE-BODY DOSIMETER

J.M. Hoffman, M.W. Mallett, H.H. Hsu, T.E. Buhl, D.G. Vasilik (Los Alamos National Laboratory, Health Physics Measurements Group), R.A. Tawil (Harshaw/Bicron Corporation)

A new combination beta/gamma/neutron TLD and track-etch whole-body dosimeter and associated dose algorithm is described. This whole-body dosimeter consists of two Harshaw/Bicron TLD cards and two NE Technology PN-3 track-etch detectors. One Harshaw/Bicron TLD card is designed to perform beta and gamma dose determination at 7 mg/cm^2 , 300 mg/cm^2 , and 1000 mg/cm^2. The beta/gamma TLD card consists of two thin (6 mil) high sensitivity ^{7}LiF:Mg,Cu,P TLD chips, one 15 mil ^{7}LiF:Mg,Cu,P TLD chip and one 15 mil CaF_2:Mn TLD chip with all four chips mounted bare on Kapton. The 15 mil LiF and CaF chips are covered with 600 mg/cm^2 ABS plastic filters. These two chips provide for a measure of the photon energy incident on the dosimeter and allow for calculation of the photon dose at the three depths of interest. In addition, this information is used to strip the photon response from the two thin LiF chips. One thin chip is covered only with an aluminized Mylar window while the second thin chip is covered with a 40 mg/cm^2 ABS plastic filter. Once the photon response is stripped, the remaining signal is due only to beta radiation. The small differences in filtration allow for an approximate measure of the average beta energy. This information is used to calculate beta doses at 7 mg/cm^2 and 300 mg/cm^2.

The remaining Harshaw/Bicron TLD card is used for neutron dosimetry. This card contains two pairs of TLD-700 and TLD-600 chips. One TLD-700 and TLD-600 pair is covered with 21 mil of cadmium on the front while the other pair is covered with 21 mil of cadmium on the back. The TLD-700 chips are used to subtract the photon response from the associated TLD-600 chips. The TLD-600 with the cadmium on the front is a classic albedo neutron detector while the TLD-600 with cadmium on the back could be called an anti-albedo detector. The relative net neutron response of the albedo TLD-600 versus the anti-albedo TLD-600 yields a measure of the average neutron energy and is used to determine a correction to apply to the albedo TLD-600 to derive dose. The result is a smooth exponential function which starts flat at very moderated neutron energies and rises steeply near bare fission spectral energies. The track-etch detectors are utilized based on two criteria: (1) the net neutron signal on the albedo detector is above a given threshold and, (2) the albedo/anti-albedo ratio indicates neutron exposure above a given energy.

DESIGN, MODELING, AND IMPROVEMENTS TO THE LOS ALAMOS NATIONAL LABORATORY TLD BASED NEUTRON DOSIMETER

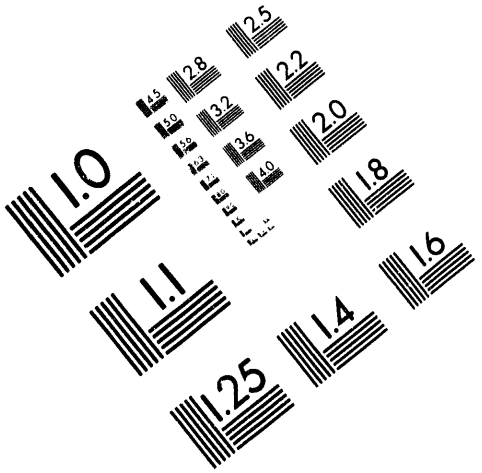
W.H. Casson, T.E. Buhl, R.T. Devine, J.M. Hoffman, H.H. Hsu, M.W. Mallett, and D.G. Vasilik (Health Physics Measurements Group, Los Alamos National Laboratory, Los Alamos, NM)

The response of a TLD based neutron dosimeter has been modeled in detail using a Monte Carlo code to predict the energy response. Detailed measurements have been made of the response of a track etch component. The results of the two efforts have been combined into an improved dosimeter unit with dose equivalent response from thermal up to approximately 20 MeV. The response above 20 MeV has been estimated. The response has been calculated for various isotopic neutron sources as well as typical work area spectra around glove boxes and hot cells. The new dosimeter design, which does not require a premeasured neutron correction factor for each neutron field measured, will replace a single TLD-600 chip system currently in use.

TLD SYSTEM ENDOVA-20 FOR INDIVIDUAL MONITORING ACCORDING TO THE ICRU RECOMMENDATIONS

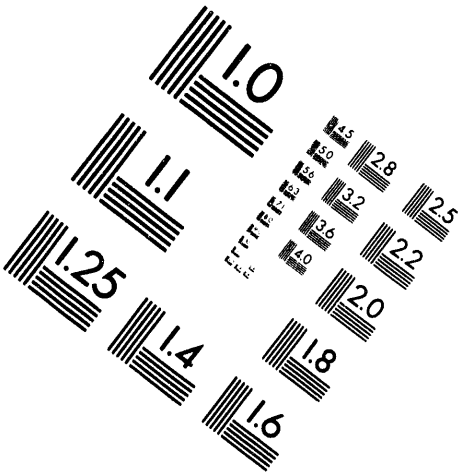
Jan Loez, Georg Holzapfol (ENDOS Gmbll, Potsdamer Str. 18A, D-14513 Teltow, FRG)

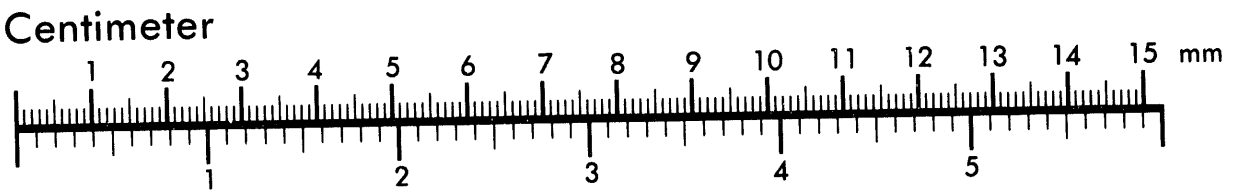
Following the current trends in personal dosimetry, a TLD system, ENDOVA-20, has recently been constructed at ENDOS, the performance of which, as well as the results of the type testing measurments at the Physikalisch-Technische Bundesanstalt are going to be presented.

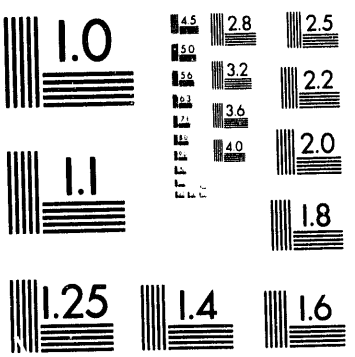


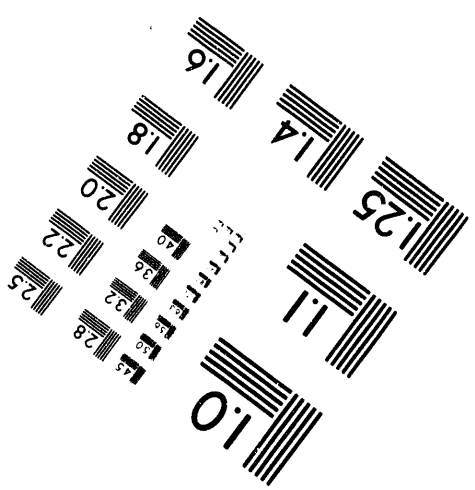


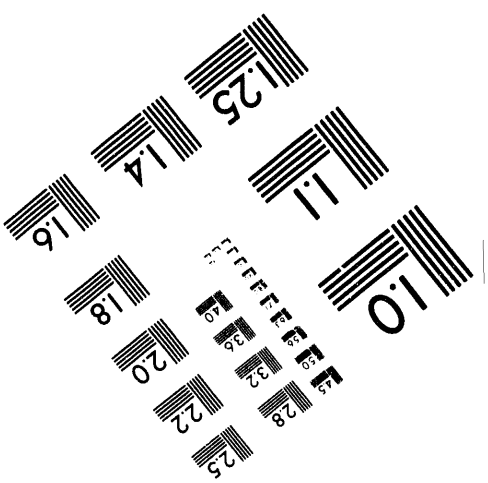
Association for Information and Image Management
1100 Wayne Avenue, Suite 1100
Silver Spring, Maryland 20910
301/587-8202











MANUFACTURED TO AIIM STANDARDS
BY APPLIED IMAGE, INC.

2 of 6

A COMPARISON OF HYPERSENSITIVE TL MATERIALS IN CARD CONFIGURATIONS

K. J. Velbeck, Y. Tan, and R. A. Tawil (Harshaw/Bicron Radiation Measurement Products, 6801 Cochran Road, Solon, OH 44139)

There has been great interest expressed in hypersensitive thermoluminescent (TL) phosphors such as Al_2O_3:C, CaF_2:Dy, CdF_2:Cu, and particularly the newly developed LiF:Mg, Cu, P. These materials exhibit sensitivities one to two orders of magnitude greater than the most commonly used phosphor, LiF:Mg,Ti (TLD-100). This greater sensitivity results in improved signal-to-noise ratios and consequently lower detection thresholds, making the material ideal for low-dose applications such as environmental monitoring. To date, most of these TL phosphors have been utilized only in loose solid forms. For reasons of convenience, built-in identification, and adaptability to automatic readout, it is desirable to mount the phosphors in card format. A series of tests has been conducted to characterize the performance of these materials in card format using a Harshaw Model 8800 Automatic TLD Card Reader. Because of the sensitivity of LiF:Mg,Cu,P to temperatures above 240°C, special precautions must be taken when mounting the material into a card in order to preserve the material trap structure and sensitivity. Accordingly, a process has been implemented whereby the various phosphors are affixed to a polyimide film, then mounted into cards. This paper describes the method used and presents the results from the tests. These tests provided data on minimum detectibility, reproducibility, residual effects, sensitivity to ambient light, and linearity. A comparison of the various materials' sensitivity to ionizing radiation is also presented. All tests were conducted using LiF:Mg,Ti (TLD-100) as reference.

USING THE HIGH TEMPERATURE THERMOLUMINESCENCE PEAK OF ZrO_2 FOR THE PRECISION DOSIMETRY OF UV RADIATION

Ching-shen Su (Institute of Nuclear Science, National Tsing Hua University, Hsinchu, Taiwan, R.O.C 30043)

The thermoluminescence (TL) peak of ZrO_2 at high temperature was found stable with good linear response to exposure to ultra-violet (UV) radiation . If the UV radiation measurement is made to read the TL peak of an irradiated detector at a pre-determined temperature rather than to scan in a temperature range with certain rates of temperature increment, then the error resulting from the TL scan can be eliminated and precision radiation dosage can be measured.

This method depends on the thickness of detector, also the precision temperature of the reader, these can all be made easily within required accuracies. The use of ZrO_2 as a detector for UV radiation measurement via the 210 °C TL peak was proposed. The linearity of the UV radiation response was shown to be better than those at the 90 and 135 °C TL peaks for the ZrO_2 sintered at 1,100 °C. Better sensitivity was also obtained when the ZrO_2 was doped with impurity Er_2O_3 of 1 mole %.

ULTRAVIOLET AND LASER RADIATION DOSIMETRY USING PHOTOSTIMULATED THERMOLUMINESCENCE IN $CaSO_4$:Dy

Ademar J. Potiens Jr., and Leticia L. Campos (Instituto de Pesquisas Energéticas e Nucleares - CNEN/SP) Caixa Postal 11049 - CEP 05422-970-São Paulo, SP - BRAZIL.

The photostimulated thermoluminescence (PSTL) is a technique that was developed through the study of light effects in thermoluminescent materials. In its applications are included the possibility of making high dose dosimetry, dose reevaluation, ultraviolet (UV) and laser radiation dosimetry. The objective of this work is to study the PSTL in $CaSO_4$:Dy in serveral UV wavelengths of interest and laser radiation. The $CaSO_4$:Dy is an extremely sensitive thermoluminescent material that has a dosimetric peak at 220 °C and is successfully used in gamma radiation dosimetry. The $CaSO_4$:Dy produced at IPEN was used in teflon pellet form. The teflon pellets were annealed at 300 °C for 15 min before the irradiations and exposure to UV light. A 15.0 TBq source of ^{60}Co was used for sample irradiation. A system containing a Hg lamp, Bausch & Lomb SP-200, under high pressure and a Kratos GM-200 monochromator were used for UV radiaion exposure. For the thermoluminescent measurement, a TL reader, Harshaw model 2000 AB with temperature range from 200 to 360 °C and heating rate of 10 °C/s, was used. The PSTL response was observed for gamma irradiation from 2.58 x 10^{-1} C/kg (10^3 R) to 2.58 C/kg (10^4 R). The PSTL response dependence with light wavelength was studied from 230 to 570 nm. The time of exposure and the wavelength was determined in order to obtain better resolution. The PSTL response linearity with exposure time for light wavelength was verified. The obtained results show that $CaSO_4$:Dy teflon pellets presents a good performance to PSTL to be used in UV and laser dosimetry.

Work partially support by CNPq - Conselho Nacional de Densenvolvimento Cientffico e Tecnológico, Brazil.

A PRECISION BROAD-RANGE DOSIMETER BASED ON CERIUM DOPED YTTRIUM ALUMINUM PEROVSKITE (YAP)

A.A. Fyodorov*, M.E. Mattson, W.P. Trower, and R.F. Zuevsky*
Physics Department, Virginia Tech, Blacksburg VA 24061

(*Abstract*)

Among the properties of YAP relevant for dosimetry are its rapid (~ 28 ns) dominant (97%) bright ($\sim 40\%$ of NaI:Tl) decay with negligible afterglow as well as its physical ruggedness and chemical nonreactivity. Our recent success with YAP-based x-ray, γ-ray, and alpha particle detectors encouraged us to use a YAP scintillator in a broad range (20-3,000 keV) portable dosimeter. Its large Compton-to-photoabsorption cross section ratio makes YAP response relatively energy insensitive and so it becomes a promising phosphor for accurately measuring exposure, equivalent, and absorbed doses.

Its stopping power and speed allow a YAP-based dosimeter to operate over more than five decades of exposure dose (5 μR/h to 1 R/h) using only a single small (25 mm diameter, 15 mm thick) crystal. In a radiation field of ~ 10 μR/h (~ 20 counts/s) a statistical precession of $\sim 15\%$ can be obtained in ~ 10 s.

In implementing our broad-range YAP-based dosimeter we have used spectrometric signal processing and a measured absorbed energy data correction algorithm which provides the possibility of reducing the measured dose energy dependence to $\pm 10\%$ over the full energy range. We have verified our instrument using usual γ-ray sources. To extend the dosimeter range down to ~ 5 keV we are constructing a combination YAP-plastic scintillator.

I. Introduction

Of those materials used to convert γ-ray energy to electronic signals -- gas-filled chambers, semiconductors, and scintillators -- none is ideal for γ-ray dosimetry [1]. Gas chamber signals are weakly energy dependent if the fill gas effective atomic number approximates that of air when measuring exposure dose, and that of the human body when determining absorbed dose. A single gas-based dosimeter, which is capable of detecting photons with energies as low as a few keV, is unable to cover a wide intensity range because of gas degradation, small absorption power (low radiation levels require large chambers), and slow response (high radiation levels require small chambers).

Germanium and silicon semiconductors require cooling to liquid nitrogen temperatures to attain their full energy resolution and so are large, cumbersome, and not suitable for field work [2]. Room temperature semiconductors such as cadmium telluride have yet to be realized in large crystals and possess spectrometric properties only comparable with those of sodium iodide scintillators.

Two classes of scintillators, organic and inorganic, are used in dosimetry [3]. Of the organic scintillators a variety of plastics are widely employed because their atomic number ($Z \sim 6$) is close to that of air ($Z \sim 8$). Further, because of their small stopping power, their ability to register very low energy photons is limited only by the light yield of the specific plastic.

Inorganic scintillators are single crystals with high density whose large stopping power allows small detectors with high count rates to be made. Sodium iodide was the first of these materials [4] and is still by far the most widely used while applications requiring greater stopping power now depend on bismuth germanate.

We are developing a rugged, portable, high-rate, broad-band, high-resolution γ-ray dosimeter based on a new, fast, heavy, bright inorganic scintillator Yttrium Aluminum Perovskite, $YAlO_3:Ce^{+3}$ [5], whose properties we list in Table I below with those of three common dosimetric scintillators: the standard sodium iodide, a representative plastic - NE104, and the sometimes used bismuth germanate.

Table I. Properties of Scintillators for Dosimetery.

	NaI	YAP	Plastic	BGO
Stoichiometry	NaI	$YAlO_3$	$(CH)^k$	$Bi_4Ge_3O_{12}$
Activator	Tl	Ce	--	--
Z_{eff}	50	36	6	74
ρ(g-cm^{-3})	3.67	5.55	1.03	7.13
dE/dx_{min} (MeV-cm^{-1})	4.1	6.6	1.9	8.1
Moliere radius (cm)	4.3	3.1	??	2.3
Critical energy (MeV)	12.5	~ 19	103	8.8
r.l. (cm/g-cm^{-2})	2.6/9.5	2.9/16.0	42.4/43.8	1.1/7.9
Brightness (% of NaI)	100	40	25	13
Risetime (ns)	~ 8	0.4	~ 1	~ 1
a.l. at 511 keV (cm)	3.05	2.24	10.5	1.11
λ_{max} (nm)	415	347	406	480
τ (ns)	230	28/170	1.9	60/300
Branching (%)	100	97/3	100	9/91
Photons/MeV (x10^3)	38.0	19.7/0.6	~ 10	0.7/7.5
Photons/MeV/ns	165	703/3	5,000	12/25
Afterglow (% at 3 ms)	0.5-5.0	~ 0	0	0.1
$(\%\Delta E/E)_\gamma$ at 511/ 60 keV	6.5/15	7/18	10/25	13/30
Refractive index at λ_{max}	1.85	1.94	1.58	2.15
Hardness (Mho)	2.0	8.5	~ 3	5.0
Melting point (K)	924	1,853	350	1,323
Radiation resistance (Mrad)	0.01	1.0	~ 1	0.01-10
Chemical reactivity	significant	slight	some	slight
Hygroscopic	very	no	no	no

Like sodium iodide, YAP's large Compton cross section and small energy dependence, seen in Fig. 1 below, makes it ideal for a wide variety of dosimetry tasks. The lower energy of its K-edge and somewhat larger cross section gives YAP a marginal advantage over sodium iodide. However, the speed with which YAP decays, 28 ± 3 ns for $\sim 97\%$ of its light [7], sets it apart from sodium iodide. A second mode with $\sim 170 \pm 30$ ns accounts for the remaining 3% of its light. YAP has no measurable afterglow after ~ 500 ns. Finally, the YAP signal risetime is ~ 400 ps.

YAP is only $\sim 40\%$ as bright as sodium iodide and its emission spectrum is centered well into the ultraviolet thus requiring windowless or quartz windowed PhotoDiodes and UV transmitting glass enveloped PhotoMultiplier Tubes. For

exposure to γ-rays YAP's radiation hardness is substantially better than sodium iodide [8] and far superior when exposed to neutrons.

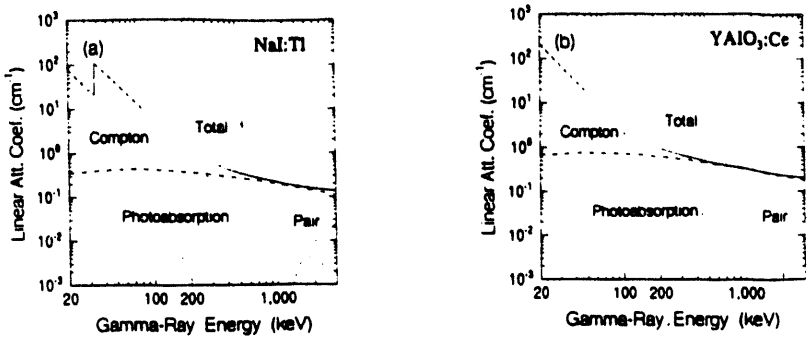


Figure 1. Linear attenuation coefficient for (a) NaI:Tl and (b) YAP.

YAP is a hard glass-like material which enters into few chemical reactions, absorbs little of anything, has a very high melting point, and whose signal strength is only weakly temperature dependent [9]. Sodium iodide, on the other hand, is a brittle, easily fractured material which when exposed to moist air is reduced to a liquid, thus limiting its applications to those in which bulky encapsulated monoliths can be tolerated.

II. Dosimetric Potential of YAP:

Having established YAP's intrinsic superiority to sodium iodide we now discuss how YAP can be employed to realize a rugged broad-band high-rate dosimeter. For inorganic scintillators the absorbed γ-ray energy, from a few keV to tens of MeV, is proportional to the number and summed energy of the photons produced in the scintillator. Thus, the charge collected from the detector PMT anode is proportional to the energy of the incident γ-ray. In air the absorbed dose for a spectrum of γ-rays with energies E_γ over time T is

$$D_{air} = \int\int I_O(E_\gamma)\ \mu_{air}(E_\gamma)\ dE_\gamma\, dT\,, \tag{1}$$

and the exposure power is

$$P_{air} \equiv \int I_O(E_\gamma)\ \mu_{air}(E_\gamma)\ dE_\gamma\,, \tag{2}$$

where I_O is the incident γ-ray intensity and μ_{air} (l_{air}) the mass (linear) attenuation coefficient for air. For a specific scintillator S, the dosimetric sensitivity, S_S, can be defined as the average PMT anode current $\langle I_A \rangle$ per exposure power,

$$S_S \equiv \langle I_A \rangle / P_{air} = C(E_\gamma)\ \{\ [1 - e^{-l_S t}]\ /\ [l_S t]\ \}\ \{\ \delta_S / \delta_{air}\ \} \tag{3}$$

where t is the cylindrical thickness, δ_S the mass absorption coefficient, and l_S the linear attenuation coefficient of the scintillator. $C(E_\gamma)$ is an energy dependent proportionality

constant. The Analog-to-Digital Converter representation of the average anode current is

$$\langle I_{ADC} \rangle = \Sigma N_i \alpha_i \ , \qquad (4)$$

where N_i is the count rate in the i'th channel and α_i the pulse amplitude which is proportional to the channel index, i, for a linear ADC. For thin scintillators having $[l_S\ t] << 1$, the energy dependence is solely determined by the ratio of mass absorption coefficients, δ_S/δ_{air}. Figure 2 below shows the mass attenuation and energy absorption coefficients for YAP and air for photon energies from 20 to 3,000 keV.

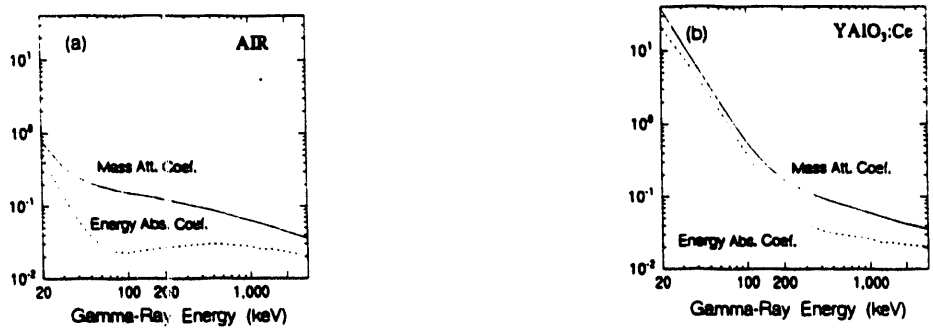


Figure 2. Mass attenuation and energy absorption for (a) air and (b) YAP [6].

Figure 3(a) below shows the energy dependence of dosimetry sensitivity for three thicknesses of YAP scintillators. For a 1.5 cm thick YAP scintillator the energy dependence is constant to within $\sim \pm 10\%$ between 0.3 and 3.0 MeV. However, for energies between 20 and 300 keV correction is needed. Our recent measurements are consistent with the calculations shown.

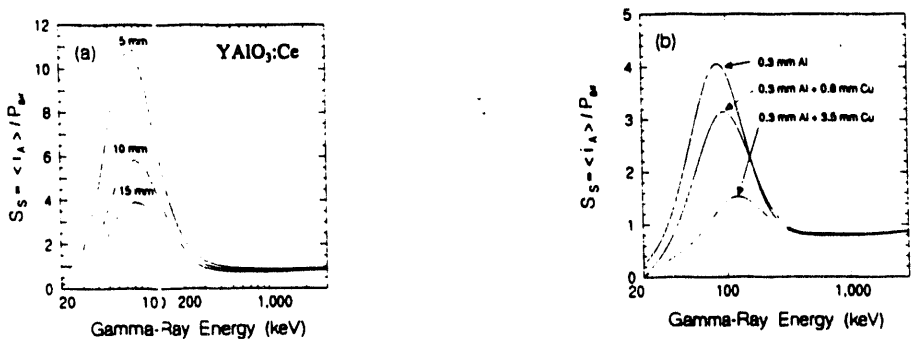


Figure 3. (a) YAP dosimetry sensitivity and (b) three shielding schemes.

The energy dependence for heavy scintillators where $Z_{eff} > Z_{air}$, can be compensated by attenuating the γ-rays with shielding. In Fig. 3(b) above, three shielding variants are calculated: (1) 0.3 mm of aluminum wrapping the crystal; then adding (2) 0.8 mm of copper shielding over half the scintillator surface; or adding (3) 3.5 mm of copper shielding over 2/3 of the surface. Since decreasing the energy dependence at ~ 80 keV decreases the sensitivity at ~ 40 keV, it is not possible to

correct for the energy dependence using shielding alone.

Therefore, to use YAP's excellent scintillation properties for dosimetry we must determine the energy dependent correction, $C(E_\gamma)$, with which to convert doses measurements into true doses. We approach this problem by rewriting Eq. (3),

$$P_{air} = \langle I_{ADC} \rangle / S_S = [\Sigma N_i \alpha_i] / S_S \quad . \tag{5}$$

Since the energy deposited in the scintillator depends on the incident γ-ray energy we must know its value to calculate S_s. For E_γ above ~ 250 keV, S_S is fairly constant, so in this region we use the average value $\langle S_S \rangle$. S_S varies dramatically from 20 to 250 keV and so a correction is more difficult to determine. Further, YAP has very little photoabsorption above 250 keV so we can not use the absorbed energy to determine the correction. For $E_\gamma \sim 1$ MeV, $S_S \sim 0.75$, but only ~ 80 keV is absorbed which gives S_S of ~ 4, or ~ 5x larger than the correct value.

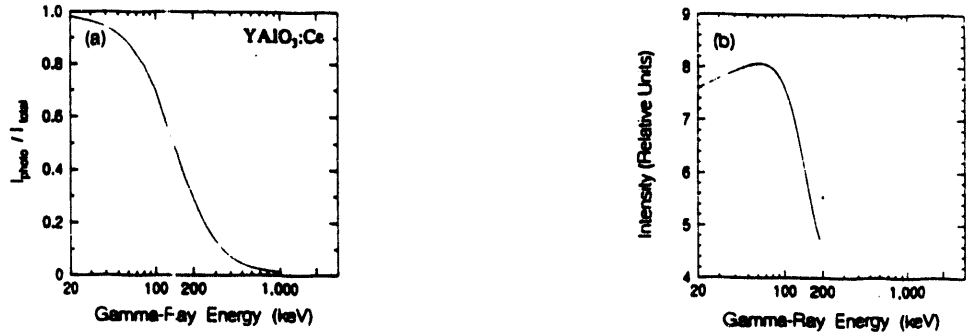


Figure 4. (a) YAP photo-to-total efficiency and (b) shape of Compton contribution.

$C(E_\gamma)$ compensates for the nonuniform energy dependence of the system and is determined empirically by the energy deposited by photoabsorption and Compton scattering. Figure 4(a) above shows the energy dependence of the photo-to-total efficiency ratio, I_{photo}/I_{total}, for a 25 mm diameter YAP right cylinder, 15 mm high. For γ-ray energies between 20 and 80 keV almost all interactions are photoabsorption which alone determines the absorbed energy and, thus, the value of S_S. Figure 4(b) above shows the contribution from Compton photons, which has little variation out to ~ 250 keV where it rapidly decreases. Although it is not possible to assign individual events with a given absorbed energy to having been photoabsorbed or Compton scattered, from the shape of the spectrum we can reconstruct the incident photon spectrum and thus calculate the coefficient $C(E_\gamma)$, or determine its value experimentally.

From these spectra we compare theoretical expectations for $\langle I_{ADC} \rangle$ with those measured. We have constructed such a prototype detector with holes distributed symmetrically on the top and sides and exposed it to americium-241, cobalt-57, cobalt-60, cesium-137, and manganese-54 sources of known strength. The inverse compensation coefficient, plotted in Fig. 5 below, is divided into seven regions, each of which is characterized by an average value of $C(E_\gamma)$. This procedure provides for the calculation of the exposure power to within $\pm 10\%$ of the measured value. For backgrounds of ~ 10 μR/h the count rate was ~ 20 counts/s and so a measurement with statistical precision of $\sim 15\%$ was obtained in ~ 10 seconds.

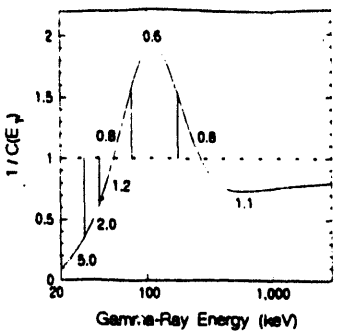


Figure 5. Shielding energy dependence.

The success of our compensation scheme lies in the copper and aluminum shielding and the shape of the Compton contribution to the photon spectrum. As previously explained, the shielding reduces the variation in the energy dependence of the sensitivity. Furthermore, because the shape of the Compton spectrum varies only slightly from source to source out to ~ 250 keV, only a single set of compensation coefficients need be determined.

Combination ZnS:Ag-plastic scintillators are used to measure α and β radiation [10,11]. Here the signals from a single PMT are routed to a pulse shape discriminator which determines if the incident particle was an α or a β particle. Following this lead we are constructing a Phosphor sandwich by placing a small YAP ($Z_{eff}>Z_{air}$) crystal in a plastic scintillator ($Z_{eff}<Z_{air}$) well, the combination viewed by a common UV transmitting PMT. Since plastic absorbs little at wavelengths where YAP emits, we may decrease the energy dependence. Our pulse shape discrimination operates with two time constants, one consistent with the decay luminescence of YAP, ~ 30 ns, and the other with that from plastic, ~ 2 ns.

Such a YAP-plastic Phoswich detector has two advantages: (1) Low energy photons are preferentially absorbed in the plastic which has a weaker energy dependence than YAP at these energies and thus, compensating the energy dependence using the method described above is easier; and (2) The plastic can be used as an anti-coincidence shield to reject signals from charged particles, a feature useful when making measurements in mixed radiation fields.

References and Footnotes:

* Permanent address: Institute for Nuclear Problems, Belarus State University, Minsk, Belarus.

1. V.I. Ivanov, Course in Dosimetry (Atomizdat, Moscow, 1970) p. 100-103. (in Russian).
2. Yu.K. Akimov, O.V. Ignatiev, A.I. Kalinin, and V.F. Kushniruk Semiconductor Detectors in Experimental Physics (Energoatomizdat, Moscow, 1989) p.108-112. (in Russian).
3. G.F. Knoll, **Radiation Detection and Measurement**, 2nd Edition (John Wiley, New York, 1989).
4. R. Hofstader, Phys. Rev. **74** (1948) 100.
5. W.P. Trower, in Scintillators and Phosphor Materials, edited by M.J. Weber, P. Lecoq, R.C. Ruchti, C. Woody, W.M. Yen, and R-y. Zhu (Material Research Soc., Pittsburgh, 1994) in press.
6. PHOTOCOEF code(1993), ACI, Grafton MA 01519.
7. S.E. Derenzo, private communication (1993).
8. J.A. Kierstead, S.P. Stoll, and C.L. Woody, in ref. 5.
9. A.A. Fyodorov, M.V. Korzhik, S.A. Smirnova, and G.Yu. Drobyshev, IEEE Nucl. Sci. Symp. Conf. Rec. 93CH3374-6, 1, 668 (1993).
10. HARSHAW/QS Handbook, Saint-Gobain Ceramiques Industrielles (1992) and SILENA Handbook, Silena GmbH (1991).

NRC-04-94-037

LETTER PROGRESS REPORT #1 - Phase I SBIR

1 July - 31 August 1994

AN YTTRIUM ALUMINUM PEROVSKITE BASED GAMMA-RAY DOSIMETER

W. PETER TROWER, Inc.
1105 Highland Circle
Blacksburg VA 24060

(31 August 1994)

Technical Objectives:

(1) Construct and evaluate the dosimetric potential of YAP-plastic combination detectors with both photomultiplier tube and photodiode readout; and

(2) Design a dosimetric detector array optimized for sensitivity and energy independence using Monte Carlo computer simulations.

In our proposal we asserted that the bright, fast, and flat energy dependence of $YAlO_3:Ce^{+3}$ (YAP) scintillator signals will allow us to construct a γ-ray dosimeter with the properties:

(1) $20\ keV \leq E_\gamma \leq 3\ MeV$;
(2) $5\ \mu R/h \leq A_\gamma \leq 1\ R/h$;
(3) $50\ nSv/h \leq D_\gamma \leq 10\ mSv/h$; and
(4) $50\ MHz \leq dN_\gamma/dt$.

We describe here our progress towards achieving these goals in these first two months which falls basically into three activity categories:

(1) Detailed recalculation of the proposal assertions. We completed this exercise and found to our relief that what we had proposed was essentially correct with some modifications and substantial clarification of details all of which will aid us in realizing our technical goals.

This material is based on work supported by the Nuclear Regulatory Commission under contract NRC-04-94-037. Any opinions, findings, and conclusions or recommendations expressed in the publication are those of the authors and do not necessarily reflect the views of the Nuclear Regulatory Agency.

(2) Acquiring equipment for the experimental studies.

- We set up a computer-based multichannel analyzer using an existing Nucleus PCA board in the backplane of a IBM 286 computer.
- We bought from Hamamatsu a 1" high gain photomultiplier tube with an ultra-violet transmitting glass envelope which has outstanding linearity, R-269.
- Stan Majewski at CEBAF gave us a special FET stabilized voltage divider base which complements the linearity of our tube (R. Wojcik, et al. *SPIE Medical Imaging Conference 1994* in press.)
- Radiation Instruments & New Components delivered to us the first set of YAP crystals - 1" diameter right cylinders of three heights.
- Compensating metal cans of copper and aluminum were constructed.
- NE 110 plastic scintillator disks of several thicknesses have been prepared for the phoswich versions of the dosimeter.
- We have acquired/evaluated ultraviolet transparent optical coupling materials.
- We have acquired/evaluated ultraviolet reflecting coating materials.
- Several additional radioactive sources have been identified which are needed for the compensation measurements and will be acquired shortly.
- NE 110 plastic scintillator disks of several thicknesses have been prepared for the phoswich versions of the dosimeter.

(3) Preparing talks/perfecting publications. Concurrent with tendering our NRC proposal we submitted abstracts of this material to two conferences as talks and both have been accepted prior to the start of this contract. Thus we have prepared two essentially identical papers for the respective proceedings in which we have not attributed support to NRC nor have we sought NRC clearance. The first paper will be presented by Trower at the **Fourth Conference on Radiation Protection and Dosimetry** to be held 23-27 October 1994 in Orlando, Florida and whose proceedings will be published by Oak Ridge National Laboratory as a TM. A copy is appended to this report for your information. The second, also to be presented by Trower, will be at **IEEE Nuclear Science Symposium** to be held 30 October - 5 November 1994 in Norfolk, Virginia and whose manuscript will be published in the *Conference Record* and submitted to *Transactions on Nuclear Science.*

In this next two months we will construct/evaluate prototype dosimeters.

UV RADIATION IMAGE SENSOR UTILIZING PHOTOSTIMULATED LUMINESCENCE

A.Kalninsh (a), I.Plavina (a), A.I.Popov (b) and A.Tale (b)
(a) Institute of Physics, Latvian Academy of Sciences LV-2169, Salaspils-1, Latvia
(b) Institute of Solid State Physics, University of Latvia, 8 Kengaraga str., LV-1063, Riga, Latvia

1. INTRODUCTION

Today an increasing demand for fast, efficient and cost-effective two-dimensional radiation detectors with a high detective quantum efficiency, high spatial resolution and a wide dynamic range arises steadily in the various application fields of medicine, material science, high energy physics and biology.

In the last decade a new type of X-ray detectors based on the photostimulated luminescence (PSL) has gained considerable importance, especially in the medical diagnostics, crystallography and biology [1-6]. PSL phosphors have replaced expensive silver chloride films as the X-ray image receptor in digital radiography systems. PSL phosphors record and store X-ray images until they are read using either visible or infrared laser light.

The principal purpose of this paper is to describe the novel type of the luminescent sensor for measurements of a UV-radiation images. The idea of this luminescence sensor is based on the photostimulated luminescence phenomenon. It should be mentioned that the PSL method was proposed for a recording and reproducing of radiation images in our laboratory ready in 1969 [7]. As these PSL phosphors, alkali halides doped with ns^2-ions were considered (KI-Tl, KCl-Pb).

In our recent endeavor to use alkali halide crystals as photostimulated storage materials, we have carried out the detailed investigations of PSL in alkali halides doped with ns^2-ions. It has been found that the KBr crystal doped with In^+ ions possess prominent PSL ideal for He-Ne laser stimulation. The detailed PSL and TSL properties of KBr-In crystals have been reported in [6.8-11], where UV-light was used as a source of radiation.

Thus, the object under study and the most important part of the luminescent sensor is the imaging plate made of the KBr-In crystal.

2.EXPERIMENTAL

The KBr-In monocrystalline sample with activator concentration of ~ $1x10^{17}$ cm^3 was studied. Physical experiments were carried out at room temperature (RT) with a conventional equipment for the luminescence investigations. In the present

experiments special attention was paid to a reduction of the scattered F-light intensity and homogenization of the incident F-light intensity [8]. A specially designed UV-radiation image recording and reproducing device was used to determine technical characteristics [9].

3. RESULTS AND DISCUSSION

UV irradiation of a KBr-In in the exciton fundamental absorption band at RT leads to the energy accumulation in the form of F,In^{2+} defect pairs, which are responsible for the distinctive PSL. This is composed spectrally of the intrinsic In^{+} ion emission revealing its main maximum at 2.8 eV and a shoulder at 2.4 eV. (Fig.1.). Thus, during UV radiation exposure a certain fraction of the energy proportional to dose is deposited and stored [6-11] and, thus, a stable latent image in created in the from of F,In^{2+} defect pair distribution [6,8,10]. The PSL of such pairs is utilized for recovering the stored UV radiation image. By scanning a focused He-Ne laser light (630 nm), a stable latent image is destroyed thus giving the characteristic In^{+} luminescence (420-530 nm). The interesting feature of the PSL of F,In^{2+} pairs under constant F-light stimulation is the dependence of the decay time τ of the PSL recovery on the F-light intensity I_F : $\tau=1/\sigma I_F$ [6,8,10].

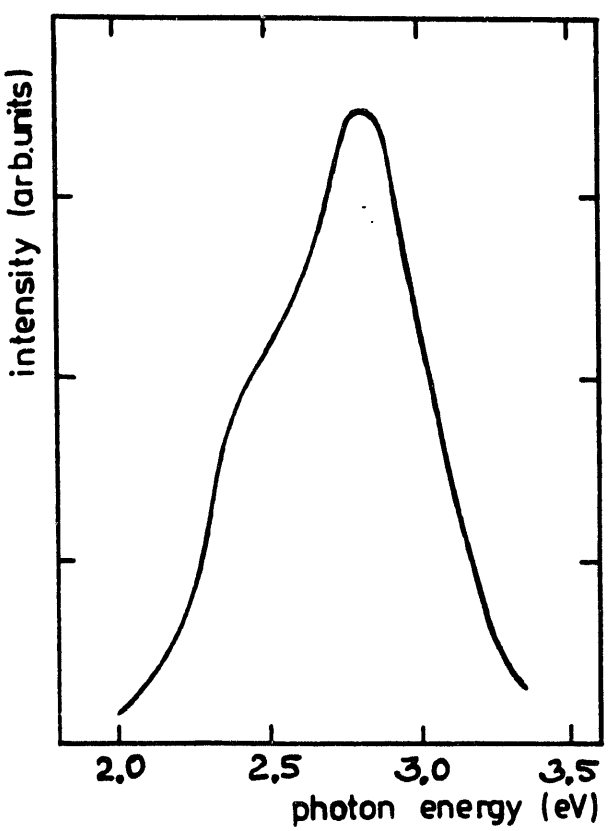


Fig.1. The photostimulated luminescence spectrum of a KBr-In crystal at RT.

As it was found, during the PSL decay (the optical recovery is induced by the F-light) several exponential components with $\tau_i=1/\sigma_i I_F$ appear, where σ_i is the absorption cross section for the F-type centers and I_F the intensity of the F-light. The spectral dependence of σ on two of the most intense components in the case of a middle - dose UV irradiation is presented in Fig.2.

One conclusion can be drawn here - namely that the PSL recovering rate (readout) is determined by the F-light intensity and limited by the intrinsic lifetime of In^*-ion excited state.

One of the most important characteristics of the radiation detector is the dose linearity or dynamic range. It shows directly the range of recordable energy variation within which an output signal is identically determined by the energy converted.

Particularly for the PSL storage materials, the relation of the energy dose of incident radiation to the intensity of the response signal of the PSL shows linearity extending over a wide range. For instance, one of the now most widely used materials, BaFBr-Eu [2,3,5] is notable for the dynamic range of five orders of magnitude at the resolution of 50x50 μm^2 if X-ray [3,12] or electron [13] flux energy have been stored.

Recently the investigations of PSL of the powdered KBr-In phosphor layers, irradiated with X-ray, used in medical diagnostics have exhibited a good linearity with the exposure [14] and a high sensitivity $\approx 10^{-12}$ $J/mm^2/mR$ [15]. A wide dynamic range (12 orders of magnitude) was also predicted [15]. Therefore, it was proposed that the powdered KBr-In phosphors in analogy to the commercially employed X-ray storage phosphor BaFBr-Eu [2,3,5,12,13], could be efficiently used as a material for image plates.

Our recent investigations of PSL of KBr-In crystals using UV radiation as a recordable radiation, have established also a good linearity within wide dynamic range (ranging over seven orders of magnitude at the above mentioned resolution [6]). The PSL intensity, which is proportional to a dose, is measured for each spot of imaging plate.

A wide-range photomultiplier tube was used to convert the luminescence signal to the electric ones. It was shown that the output electric signal Ψ^2 (Ψ is the signal-to-noise ratio) measured with UV radiation image device [9] shows a linear dependence in the range of $1\text{-}7x10^8$, where as the UV-light input signal is varied within the range of $4x10^{-13}$ to $3x10^{-4}$ J/cm^2, for the spot square is $2x10^{-4}$ cm^2 (Fig. 3.). This is definitely the outstanding property and is much better then that reported for thermostimulated luminescent MgO dosimeter, where the UV light exposure range was 10^2 to $4x10^5$ $\mu J/cm^2$ (i.e. 10^{-4} to $4x10^{-1}$ J/cm^2) [16].

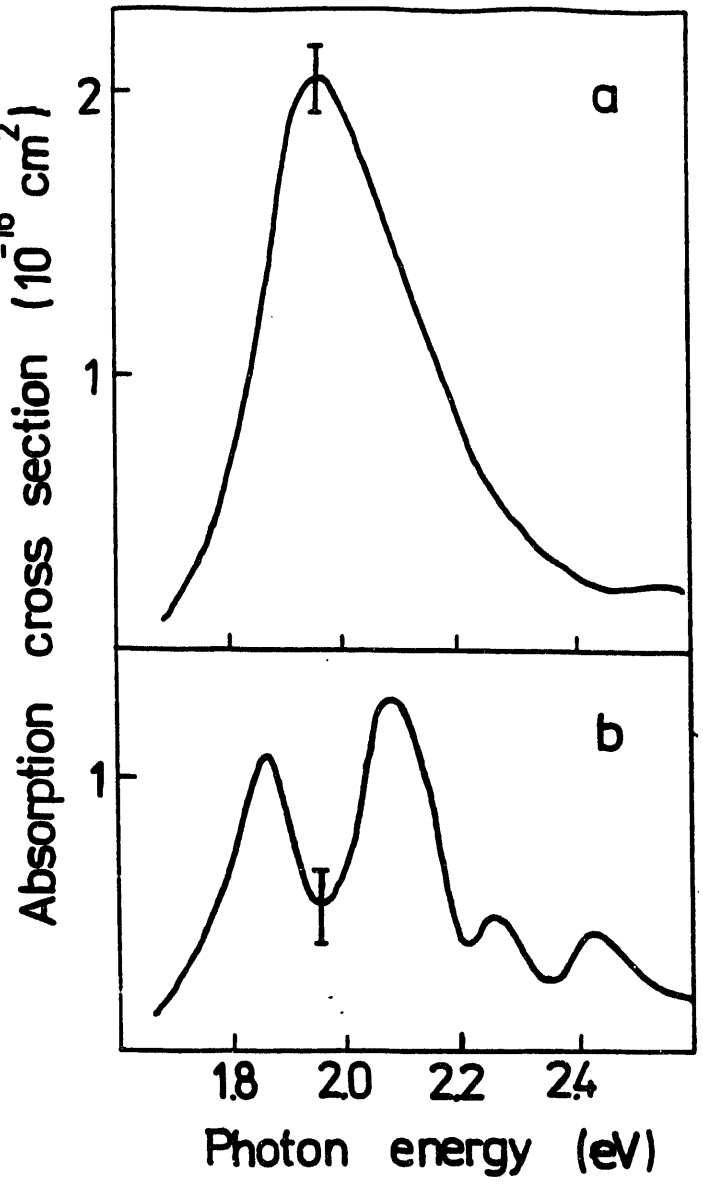


Fig.2. Stimulation spectra (in terms of optical absorption cross-section as a function of the stimulating light energy) of the middle (a) and slow (b) components of the PSL.

The highest value of the analogous part of the output signal ($7x10^8$) may be split up into $8.6x10^3$ step-bits. Hence it is easy to estimate that the highest possible value of information density in the proposed sensors reaches about $4x10^7$ bit/cm^2 for the spot square of $2x10^{-4}$cm^2, the energy expenditure being $1x10^{11}$ J/bit.

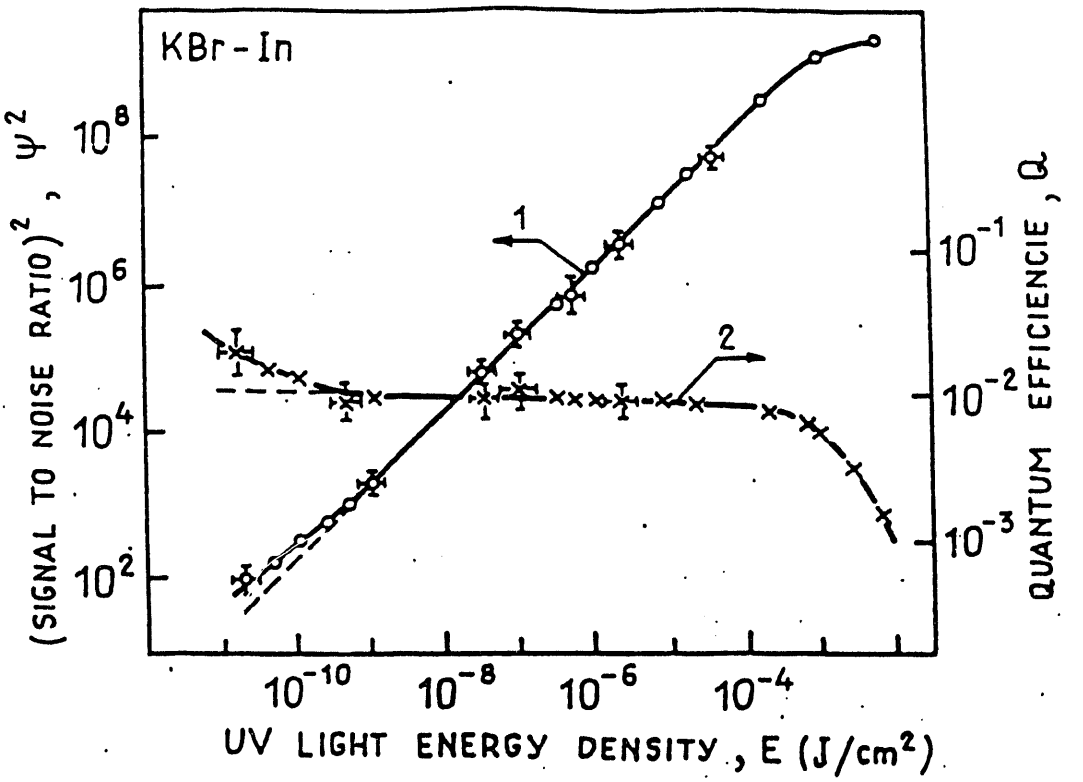


Fig.3. The dependence of KBr-In technical characteristics on energy density E of the input UV light (1 - ouput signal Ψ^2; 2 - resulting quantum efficiency Q).

It is clear that the readout processes may be fulfilled by means of the stimulating F-light beams with various diameters (spot squares) allowing, therefore, to vary both the information density and energy expenditure.

In conclusion, we would like to discuss the procedure of the sensitization of the PSL properties of KBr-In. As has been reported in [8], this procedure means the enhancement of the PSL - active centre production and allows us to eliminate the partial degradation of the PSL properties of the storage materials. It consists of the performance of two subsequent irradiation, firstly, the KBr-In sample is irradiated at RT in the region of the C-band (λ_{max}=245 nm). As a result, the excited electrons from In^+ ions are partly released into the conduction band and are captured in excited states of the lattice imperfections (anion vacancies etc.). Thus, In^{2+} hole centres and electron centres are created. Secondly, the sample is irradiated in the F-band region. Although, such irradiation in the F-absorption band leads to the destruction of some part of the A^{2+} centres, a certain amount of the A^{2+} centres survives, nevertheless, as if nothing had happened. Its influence on the exciton decay lead to a

considerable enhancement of the PSL light-sum [8,17,18].

REFERENCES

[1] G.Vlasov, R.Kalnins, L.Nagli, V.Objedkov, I.Plavina and A.Tale, Avtometrija 1 (1980)66.

[2] M.Sonoda, M.Takano, J.Miyahara and H.Kato, Radiology 148(1983)833.

[3] J.Miyahara, K.Takahashi, Y.Amemiya, N.Kamaya and Y.Satow, Nuclear Instruments Methods Phys. Research A 246 (1985) 572.

[4] K.Amitani, A.Kano, H.Tsuchino and F.Shimada, Konica Technical Report 1 (1988) 120.

[5] M.K.Crawford and L.H.Brixner, J.Luminescence 48&49 (1991) 37.

[6] P.Bratslavets, A.Kalnins, I.Plavina, A.I.Popov, B.Rapoport, A.Tale and B.Zeigurs, In: "The Advancement of Imaging Science and Technology" (Pergamon-CNPIEC Joint Venture) 1990, 474-476.

[7] I.Plavina, V.Obyedkov, V Chernak, G.Balandin, B.Sestroretsky, Proc. Latv. Academy of Sciences, 5 (1969) 67.

[8] A.Kalnins, I.Plavina, A.I.Popov, A.Tale, Latv. J.Phys and Techn. Sci. 3 (1992) 3.

[9] P.Bratslavets, B.Zeigurs et all, Preprint LAFI-115. Institute of Physics, Latvian Academy of Sciences, Salaspils, 1987.

[10] P.F.Braslavets, A.Kalnins, I.Plavina, A.I.Popov, B.Rapoport and A.Tale, Phys.Stat.Sol. (b) 170 (1992) 395.

[11] A.I.Popov, Nuclear Instruments Methods Phys.Research B 65 (1992) 521.

[12] A.Yoshiyki, K.Shunji, M.Tadashi, S.Yoshinori and A.Masami, Rev. Sci. Instr. 60 (1989) 1552.

[13] N.Mori, T.Oikawa, Y.Harada and J.Miyahara, J.Electron. Microsc. 39 (1990) 433.

[14] A.Kalnins, I.Plavina and A.Tale, Nucl. Instr. and Meth. in Phys. Res. B 84 (1994) 95.

[15] A.Kalninish, I.Plavina, A.I.Popov and A.Tale, Nucl. Instr. and Meth. in Phys. Res. B (submitted).

[16] A.K.Dhar, L.A.DeWerd and Th.G.Stoebe, US Patent 3,924,135 (Dec. 2, 1975).

[17] I.Plavina and A.I.Popov, Phys. Stat. Solidi(b) 176 (1993) 255.

[18] I.Plavina and A.I.Popov, Radiation Effects and Defects in Solids 128 (1993) 27.

OPTIMIZATION OF A NEW TLD ANNEALING PROCEDURE

René Michel[1], Fred N. Eichner[1], Joseph C. McDonald[1], Patrick J. Papin[2]

[1]Pacific Northwest Laboratory, P.O. Box 999, Richland, WA 99352
[2]Department of Physics, San Diego State University, San Diego, CA 92182

ABSTRACT

The response and sensitivity of LiF thermoluminescent materials exposed to high levels of gamma radiation was studied for different annealing procedures in which the presence of nitrogen or air was controlled. After studying different time, temperature, and atmosphere profiles, an annealing procedure consisting of heating TLDs for 2 hours in a N_2 atmosphere oven at 400° C, followed by one standard cycle (1 hour at 400° C followed by 2 hours at 100° C in air) was identified as the most cost-effective process tested. Moreover, this procedure still provided very good results, recovering the original sensitivity, and obtaining reproducible glow curves of TLDs exposed to high levels of ionizing radiation.

INTRODUCTION

It is well known that the sensitivity of thermoluminescent (TL) materials is reduced considerably after exposure to high levels of ionizing radiation (i.e., air collision kerma greater tham 1 Gy). Annealing procedures have been studied and proposed with the objective of restoring, to a certain extent, the basic conditions of the TL detectors (TLDs) after irradiations. An annealing process has two basic purposes: to empty the electron traps after irradiation, and to obtain reproducible glow curves even after repeated irradiations and thermal treatments.

Studies of the annealing characteristics of lithium fluoride (LiF) TLDs (Zimmerman et al. 1966; Harris and Jackson 1970; Spanne and Carlsson 1971) have led to an annealing procedure that has been well accepted and used as a "standard" in many laboratories: heating the LiF materials for 1 hour at 400° C and then, for 2 hours at 100° C in air. This procedure provides good results for exposures less than 1 Gy. Nevertheless, for higher values, this procedure does not completely empty the trapped electrons to restore the original sensitivity of the TL materials.

Eichner et al. (1973), and Horowitz et al. (1980) have recommended annealing in an inert nitrogen atmosphere. The former used a nitrogen anneal at a positive pressure of about 1.3×10^5 Pa and obtained good results emptying electron traps, but the TLD sensitivity was found to be reduced by about 30%. It was reported by Oberhofer and Scharmann (1986) that the absence of air exchange (oxygen) caused losses in the sensitivity of the TL material. Horowitz (1984) explained that impurity ions incorporated without the presence of oxygen inhibited TL emission. Moreover, Rossiter (1970, 1971) found that far less light was emitted from vacuum-grown material compared with the same material grown in air. Thus, it was reasoned that annealing in

a nitrogen atmosphere would provide good results in emptying deep traps but that an air exchange would also be necessary to recover the sensitivity of TLDs. By combining these ideas, a new annealing procedure was proposed and studied (Michel et al. 1994). This new process consists of annealing the TLDs for 4 hours at 400° C in a nitrogen atmosphere followed by two standard anneal cycles which would aid in reintroducing oxygen into the material.

As shown in Figure 1, the nitrogen plus air annealing cycle gives us a better response after irradiation compared to the standard or nitrogen anneal only. Moreover, as shown in Figure 2, the nitrogen plus air anneal provides better results restoring the original conditions of the TL materials after being subjected to high levels of radiation. However, if we consider the total time required to complete this procedure (10 hours), this is impractical since it takes more than a working day to complete the process, not to mention the extreme thermal stress to which the crystals are subjected.

We propose that TLDs do not need to be annealed for such a long time to obtain good results. For this reason, the purpose of this study is to test some alternative time-temperature treatments which could lead to a more cost-effective nitrogen plus air annealing procedure.

MATERIALS AND METHODS

The TL material used in this study was in the form of 0.32 x 0.32 x 0.089 cm chips of ^{7}LiF:Mn,Ti.[1] Each chip was produced from the same batch, screened to less than 3% variance, and had never been exposed to doses higher than the background accumulated during its storage. The exposures were made as recommended by the American National Standards Institute (ANSI N13.11 1983) by attaching the crystals on one of the faces of a polymethylmethacrylate phantom slab having dimensions 30 x 30 x 15 cm. The detectors were positioned at a distance of 1 m from a ^{60}Co gamma ray source with a calibration traceable to the National Institute of Standards and Technology (NIST).

The thermoluminescence of the TLDs was measured by heating them individually up to a temperature of 400° C at a constant rate of 7° C s^{-1}. A Model 2000-A system and a Model 2080 glow curve analyzer were used for glow curve analysis. All readings were performed in an oxygen-free nitrogen gas flow in the heating compartment to reduce possible incandescence, as recommended by Petrock and Jones (1968). All anneals were performed with an inert gas oven with a calibrated temperature of 400° C and flushed with pure N_2 gas from liquid nitrogen at a positive pressure of about 1.3 x 10^5 Pa. Two (air) ovens, calibrated at 400° C, and at 100° C were also used. The different time-temperature annealing cycles that were studied are the following:

- The original nitrogen plus air process (4 hour period in a N_2 atmosphere oven at 400° C followed by two standard anneal cycles) labeled as procedure A.

[1] Harshaw /Bicron, 8601 Cochran Rd., Solon, OH 44139

- A 4 hour period in a N_2 atmosphere oven at 400° C followed by one standard anneal cycle labeled as B.
- A 4 hour period in a N_2 atmosphere oven at 400° C followed by 2 hours at 100° C in an air oven labeled as C.
- A 2 hour period in a N_2 atmosphere oven at 400° C followed by one standard anneal cycle labeled as D.
- A 2 hour period in a N_2 atmosphere oven at 400° C followed by 2 hours at 100° C in an air oven labeled as E.

Before use, all the LiF crystals from this study were "standard" annealed and separated into five different groups according to the annealing procedure to which they were going to be subjected. TLDs in each group (A, B, C, D and E) were separated in six subgroups of five each plus a control for each group. The subgroups were irradiated to different known values of ^{60}Co gamma radiation, ranging from 1 mGy up to 700 Gy. The first subgroup was irradiated to an air collision kerma of 1 mGy, the second group to 1 Gy, and so forth. The crystals were read after a 2 day period to permit the emptying of unstable shallow traps (Oberhofer and Scharmann 1986).

After the readings, the TL detectors were annealed by the different processes mentioned above and irradiated to 5 mGy from a ^{60}Co gamma source, in order to study how the TLD calibration factor was affected by the accumulated radiation absorbed and the effects of the different annealing processes.

RESULTS

The calibration factor (ratio of air collision kerma by the TLD light output in terms of charge) of TLDs for the different annealing processes are plotted versus the air collision kerma in Figure 3. As shown in the figure, it was not possible to achieve enough reoxidation by annealing for 2 hours at 100° C in an air oven after either nitrogen anneal (group C and E). However, a 2 hour period in a N_2 atmosphere oven at 400° C is sufficient to restore the expected sensitivity by emptying electron traps (as shown in curves A, B and D).

CONCLUSIONS

After comparing the different processes mentioned above, it may be concluded that process D (a 2 hour period in a N_2 atmosphere oven at 400° C followed by one standard anneal) is the most efficient of the procedures tested. By using this process, results are obtained (restore, to a certain extent, the basic conditions of the TLDs after irradiations) similar to those obtained with the original nitrogen plus oxygen process in the shortest time.

REFERENCES

American National Standards Institute. American National Standard for dosimetry-personnel dosimetry performance-criteria for testing; ANSI N.13.11-1983.

Eichner, F. N., G. W. R. Endres, and L. L. Nichols. 1973. "Annealing TLDs Exposed to High Levels of Neutron and Gamma Radiation." Report No. BNW-SA-4526, Battelle Northwest. Richland, Washington.

Harris, A. M., and J. H. Jackson. 1970. "On the Low Temperature Annealing of TLD LiF." Health Phys. 18:162-164.

Horowitz, Y. S., J. Falef-Ezra, M. Moscovitch and H. Pino. 1980. "Further Studies on the Non-Universatility of the TL-LET Response in Thermoluminescent LiF and $Li_2B_4O_7$: The Effect of High Temperature TL." Nucl. Instrum. Methods 172: 479.

Horowitz, Y.S. 1984. "Thermoluminescence and Thermoluminescent Dosimetry." CRC Press Inc. Boca RatonVolume I: 95-96.

Michel, R, F. N. Eichner, J. C. McDonald, and P. J. Papin. 1994. "Sensitivity Recovery of LiF Thermoluminescent Material by a New Annealing Procedure." Presented at the 39th Annual Meeting of the Health Physics Society, San Francisco, California.

Oberhofer, M., and A. Scharmann. 1986. "Applied Thermoluminescence Dosimetry." Bristol: Adam Hilger Ltd.

Petrock, K. F., and D. E. Jones. 1968. "Hot Nitrogen Gas for Heating Thermoluminescent Dosimeters." In: Proc. 2nd Int. Conf. on Luminescence Dosimetry. Gatlinburg, Tennessee: USAEC Rep. CONF 680920; 652-69.

Rossiter, M. J., D. B. Rees-Evans, and S. C. Ellis. 1970. Preparation of Thermoluminescent LiF. J. Phys. D. 3:1816.

Rossiter, M. J., D. B. Rees-Evans, S. C. Ellis, J. M. Griffiths. 1971. "Titanium as a Luminescent Center in Thermoluminescent Lithium Fluoride." J. Phys. D. 4: 1245.

Spanne, P., and C. A. Carlsson. 1971. "Efficiency Variations of Thermoluminescent LiF Caused by Radiation and Thermal Treatments." In: Proceedings of the Third International Conference on Luminescence Dosimetry. Riso Report #249, Part I: 48; Riso.

Zimmerman, D. W., C. R. Rhyner, and J. R. Cameron. 1966. "Thermal Annealing Effects on the Thermoluminescence of LiF." Health Phys. 12: 525.

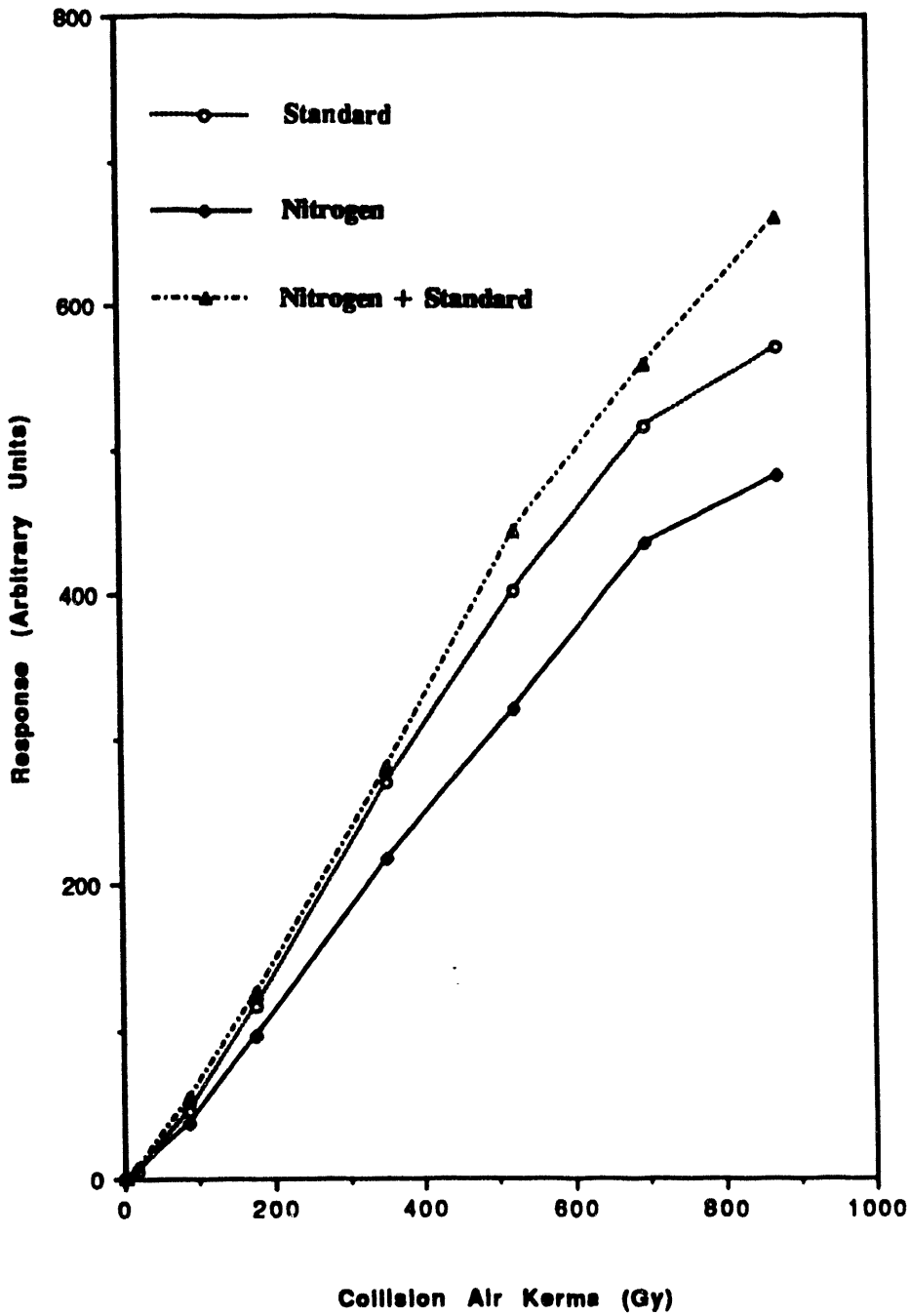


Fig. 1. Response of TLDs for the different annealing groups after being exposed to gamma rays for the second time.

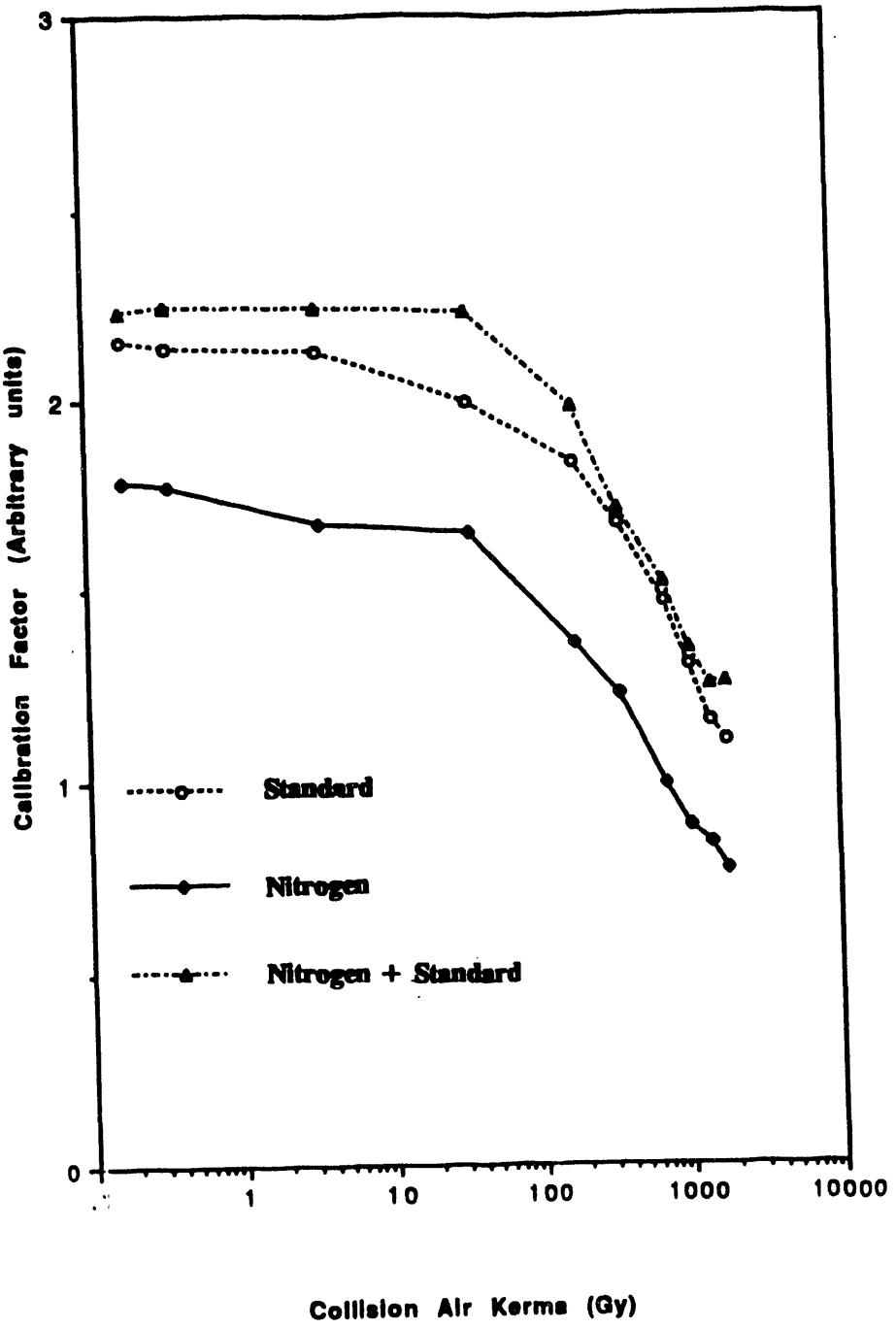


Fig. 2. Calibration Factor of TLDs after accumulation of high levels of gamma radiation (Chips were exposed to 0.05 Gy)

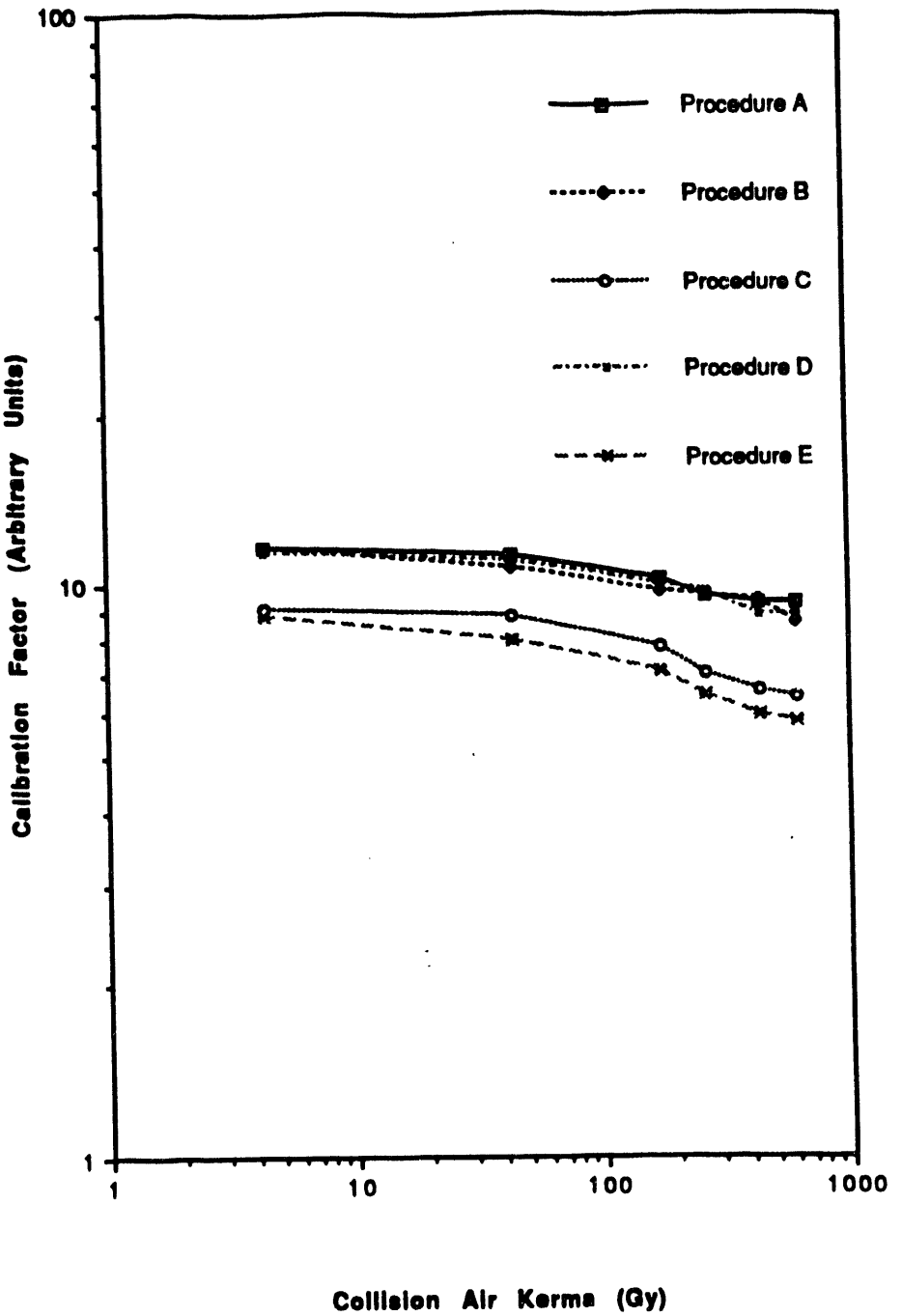


Fig. 3. Calibration factors of TLDs for the different annealing groups (A to E) after exposure to high levels of gamma radiation.

SESSION III.
External Dosimetry

C. P. Sims,
Chairman

ESTIMATES OF BIAS AND UNCERTAINTY IN RECORDED EXTERNAL DOSE

Jack J. Fix, Ethel S. Gilbert and William V. Baumgartner
Pacific Northwest Laboratory
Richland, Washington

INTRODUCTION

A study is underway to develop an approach to quantify bias and uncertainty in recorded dose estimates for workers at the Hanford Site based on personnel dosimeter results (Fix, Gilbert, and Baumgartner 1994). This paper focuses on selected experimental studies conducted to better define response characteristics of Hanford dosimeters. The study is more extensive than the experimental studies presented in this paper and includes detailed consideration and evaluation of other sources of bias and uncertainty. Hanford worker dose estimates are used in epidemiologic studies of nuclear workers (Gilbert 1991b, Gilbert et al. 1993). A major objective of these studies is to provide a direct assessment of the carcinogenic risk of exposure to ionizing radiation at low doses and dose rates. Considerations of bias and uncertainty in the recorded dose estimates are important in the conduct of this work (Gilbert 1991a).

The method developed for use with Hanford workers can be considered an elaboration of the approach used to quantify bias and uncertainty in estimated doses for personnel exposed to radiation as a result of atmospheric testing of nuclear weapons between 1945 and 1962. This approach was first developed by a National Research Council (NRC) committee examining uncertainty in recorded film badge doses during atmospheric tests (NRC 1989). It involved quantifying both bias and uncertainty from three sources (i.e., laboratory, radiological, and environmental) and then combining them to obtain an overall assessment.

Sources of uncertainty have been evaluated for each of three specific Hanford dosimetry systems (i.e., the Hanford two-element film dosimeter, 1944-1956; the Hanford multi-element film dosimeter, 1957-1971; and the Hanford multi-element TLD, 1972-1993) used to estimate personnel dose throughout the history of Hanford operations. Laboratory, radiological, and environmental sources of bias and uncertainty have been estimated based on historical documentation (Wilson et al. 1990) and, for angular response, on selected laboratory measurements.

BIAS AND UNCERTAINTY

Assessment of overall bias and uncertainty involves an evaluation for each specific dosimetry system, type of radiation, energy level, and exposure geometry. For each potential source of bias, a factor B_i is determined, where B_i is defined as the ratio of the dose that would be recorded using standard procedures to the "true" measure of dose. The overall bias from all sources is the product, B, of the B_i from all sources, and B is the factor by which one would divide the recorded dose to obtain an unbiased estimate of the true measure of dose.

Determination of the factors B_i has been made based on evaluation of relevant data and on expert judgment. Because the B_i factors are typically

not known with certainty, it has been assumed that uncertainties in B_i follow lognormal distributions. Ninety-five percent uncertainty factors K_i have also been estimated. These factors are determined such that the interval obtained by multiplying the true value by $(1/K_i)B_i$ and K_iB_i is thought to cover 95% of the estimated values. The values of K_i satisfying this relationship are referred to as 95% uncertainty factors (NRC 1989).

In most cases, data that would allow rigorous determination of uncertainties are not available. Thus, the uncertainty factors presented reflect subjective judgments of the authors regarding the extent to which a particular bias factor is known. These uncertainty factors at least give a sense of how well a particular bias factor is known. They allow one to distinguish those values that are known very precisely from those about which there is considerable uncertainty. In several instances, data are available only for selected energy-geometry combinations, and one must extrapolate to determine other values; in these cases, the combinations with actual data are naturally judged more certain than those with no data.

LABORATORY MEASUREMENTS

Laboratory experiments were made to evaluate dosimeter angular response because of its significance as a source of bias and uncertainty. The Hanford multi-element film dosimeter, used from 1962 until 1971, and the Hanford multi-element thermoluminescent dosimeter (TLD), used from 1972 until the present time, were used in the experiments. These dosimeters were placed on the anterior chest area of a male anthropomorphic phantom, essentially the same as for dosimeters worn by personnel. The measured response of dosimeters on this phantom in known radiation fields is expected to simulate the response of dosimeters worn by Hanford personnel.

Dosimeter irradiations were conducted using two geometries: 1) anterior-posterior and 2) rotational. Personnel who work routinely with radioactive material using a fume hood or a glove box would generally be exposed in the anterior-posterior geometry, whereas personnel working within a radioactive storage area would most likely be exposed in the rotational geometry. Average dosimeter response for most Hanford personnel is likely a combination of these two geometries.

In the anterior-posterior geometry, exposures were made of dosimeters placed on the anterior of the phantom facing the source (referred to as the 0° position). For the rotational geometry, exposures were conducted of dosimeters affixed in the same position but with the phantom (and dosimeter) rotated within the beam. The following angles of rotation were used: 0° (front of dosimeter perpendicular to the source), ±45°, ±90°, ±135° and 180°. In all exposure geometries, the same distance was maintained between the source and the center of the dosimeter. This was done to eliminate uncertainty that would occur if the dosimeter were located at a different distance from the source for each angle of rotation. Ten dosimeters were exposed at 0° and three dosimeters were exposed at each of the other angles. The angle of rotation was horizontal in all cases.

Three sources of photon irradiation, traceable to the National Institute of Standards and Technology, were selected to conduct these measurements as follows:

Filtered x-rays

M150 (70-keV effective energy)
H150 (120-keV effective energy)

Monoenergetic gamma

^{137}Cs (662 keV)

The two filtered x-ray beams (M150 and H150) were selected to evaluate the dosimeter response near the 100-keV threshold considered in the analysis. The M150 beam has an effective energy of 70 keV (i.e., penetrating capability of x-rays from this source is equivalent to a 70-keV monoenergetic photon) and the H150 has an effective energy of 120 keV. For the monoenergetic gamma source ^{137}Cs, all photons have an energy of 662 keV. This source was chosen because of its easy availability, significant contribution to the exposure of Hanford personnel, and predominant role in dosimeter performance evaluations for the past decade. Results of these measurements are presented in Table 1. Calculation of dose for all dosimeters was based on dosimeter response to a deep dose of 1 rem from a ^{137}Cs irradiation of dosimeters placed on the anterior of an anthropomorphic phantom. This is typical of the practice followed for each of the Hanford dosimetry systems, with the understanding that a radium source was used prior to 1977 (Wilson et al. 1990).

TABLE 1. Measured Angular Response of Hanford Dosimeters to Three Radiation Sources Using an Anthropomorphic Phantom, Expressed as a Bias Relative to the Normal Position (i.e., 0°)

	Hanford Multi-element Film Dosimeter			Hanford Multi-element Thermoluminescent Dosimeter		
Angle of Exposure	M150	H150	^{137}Cs	M150	H150	^{137}Cs
180°	0.27	0.42	0.35	0.11	0.16	0.36
-135°	0.27	0.55	0.23	0.11	0.14	0.33
- 90°	(a)	(a)	0.88	0.87	0.95	1.01
- 45°	1.01	0.88	0.96	0.98	1.00	0.98
0°	1.00	1.00	1.00	1.00	1.00	1.00
+ 45°	0.94	0.67	0.98	0.97	0.98	1.01
+ 90°	(a)	(a)	0.98	0.66	0.66	0.98
+135°	0.30	0.36	0.45	0.12	0.15	0.37

(a) For these angles (±90°), the film response would have been noted as an obviously abnormal result because the metallic filter image would not have been observed on the film.

The dose level measured at the posterior dosimeter locations, where the radiation beam must transverse the body, was always lower, with the effect most pronounced for the lower energy radiation (i.e., M150). All measured doses with the Hanford multi-element TLD followed a uniform pattern. The highest response was observed in the anterior position, with gradual decrease as the dosimeter locations progress to the posterior. However, the film

dosimeter exposed at the 90° position showed a significant abnormality, which is most pronounced at the lower energies (i.e., M150 and H150). This abnormality, which would have been detected by dosimeter processing staff, occured because radiation was striking the film obliquely and was not transversing the metallic filters. The lack of the metallic filter image in the normal location on the film would quickly demonstrate to dosimetrists that the result must be investigated. The effect occurs because of the significant over-response of film compared to tissue, which is more pronounced as the energy of the photon decreases. A similar effect was not observed with the TLD because this material more nearly simulates the response of tissue at all photon energies.

Data for the 0° and 180° exposure angles for the Hanford multi-element dosimeter were used to estimate values for the original Hanford two-element dosimeter. This was done because the original dosimeter, unlike subsequent multi-element dosimeters, was completely surrounded by 1 mm of silver. There were no individual metallic filters as used in the multi-element dosimeters. As such, it is expected that the film response is similar regardless of exposure angle; however, shielding by the body, as represented by the 180° angle, would have a significant impact. It should also be noted that all Hanford personnel dosimeters were constructed with filters on both the back and front, and for the two-element dosimeter on all sides, which minimizes dosimeter response from secondary radiation backscatter from the body.

For the anterior-posterior geometry, there is no bias for angular response (as shown in Table 1 for 0°). To simulate the effect of the rotational geometry on dosimeter response, an average dosimeter response was calculated using an evenly weighted average of dosimeter results for all exposure angles shown in Table 1. This was done for each exposure source, and the results are presented in Table 2. Also shown in Table 2 are estimates of the response for the Hanford two-element dosimeter, based an arithmetic average of the 0° and 180° degree response of the multi-element dosimeter to the M150, H150, and ^{137}Cs irradiations.

The uncertainty in the factors presented in Table 2 is estimated to be 1.4 for the two-element film dosimeter, 1.3 for the multi-element film dosimeter, and 1.2 for the TLD, and applies only to the rotational geometry.

TABLE 2. Estimated Bias Resulting From On-Phantom Angular Response of Hanford Dosimeters for Evenly Weighted Contribution from Angles Presented in Table 1[a]

Source	Hanford Two-element Film Dosimeter	Hanford Multi-element Film Dosimeter	Hanford Thermoluminescent Dosimeter
M150 (70 keV)	-0.64[b]	0.64[c]	0.60
H150 (120 keV)	-0.71[b]	0.65[c]	0.63
^{137}Cs (662 keV)	-0.68[b]	0.73	0.76

(a) Divide recorded dose by tabled value to estimate deep dose.
(b) Values estimated from 0° and 180° irradiations of Multi-Element film dosimeter.
(c) Data for 90° exposure angles were not used (see text).

HANFORD DOSIMETER UNCERTAINTY

The measured response of Hanford multi-element film and thermoluminescent dosimeters, exposed on an anthropomorphic phantom to M150 and H150 filtered x-rays and ^{137}Cs gamma rays and documented energy response information for each of the Hanford dosimetry systems (Wilson et al. 1990) were used to determine the bias in the recorded dose as an estimate of deep dose for selected photon energies. Table 3 presents the calculated bias for each of the three Hanford dosimeters based on energy and angular response characteristics of the respective dosimeters. Data from the laboratory experiments were used to estimate the bias for M150, H150, and ^{137}Cs, while information obtained from historical data was used to estimate the bias for other energy levels.

Data are provided for both the anterior-posterior and rotational geometries. For the rotational geometry, it was necessary to assume that the relationship between recorded dose and exposure was the same as that for the anterior-posterior geometry. For this analysis, it would be preferred that measured dosimeter response in the rotational exposure geometry be available in addition to the measured dosimeter response for the anterior-posterior exposure geometry. However, historical data of this type were not available, and it was not feasible to conduct new experiments at several angles. Thus, anterior-posterior dosimeter response was assumed to simulate the response in the rotational geometry. This introduces additional uncertainty regarding the bias from photon spectra for the rotational geometry.

Dosimeter response at different photon energies has a significant impact on the estimated bias. This is particularly evident for the two-element dosimeter and for lower photon energies. For example, the significant change in bias for the two-element-dosimeter deep-dose response to the M150 beam, in either the anterior-posterior or rotational exposure geometries, results directly from the rapid decrease in the response of the dosimeter to photons less than 100 keV. Based on this information, it is evident that, for the anterior-posterior exposure geometry, the bias decreased with implementation of the multi-element film dosimeter in 1957 and even further with the multi-element TLD in 1972. Uncertainty in the magnitude of the bias factors is

TABLE 3. Estimated Bias in Recorded Dose Based on Energy Response of Hanford Dosimeters[a]

Energy, keV	Anterior-Posterior Exposure Geometry			Rotational Exposure Geometry[b]		
	Film Dosimeters		Thermoluminescent Dosimeter, 1972-Present	Film Dosimeters		Thermoluminescent Dosimeter, 1972-93
	Two-element, 1944-56	Multi-element, 1957-71		Two-element, 1944-56	Multi-element, 1957-71	
70 (H150)[c]	0.7	0.70	0.95	1.31	1.31	1.77
100[d]	1.7	0.8	1.0	3.16	1.49	1.86
120 (H150)[c]	1.6	0.64	0.87	3.00	1.20	1.64
200[d]	1.4	0.8	1.0	2.38	1.36	1.70
300[d]	1.3	1.0	1.0	2.13	1.64	1.64
500[d]	1.0	1.0	1.0	1.53	1.53	1.53
662 (^{137}Cs)[c]	1.0	1.0	1.0	1.46	1.46	1.46
800[d]	1.0	1.0	1.0	1.42	1.42	1.42
1000[d]	1.0	1.0	1.0	1.39	1.39	1.39

(a) Divide recorded dose by table value to estimate deep dose.
(b) Based on the assumption that the relationship of recorded dose and exposure is the same for the rotational geometry as for the anterior-posterior geometry.
(c) Based on 1993 laboratory study and factors normalized to a 1-keV ^{137}Cs exposure response.
(d) Based on historical documentation (Wilson et al. 1990).

reduced with the implementation of the succeeding dosimeter types, each with improved energy-response characteristics.

For the anterior-posterior geometry, our assessment of the magnitude of bias in recorded dose was based on the laboratory measurements. Thus, the uncertainty from this source for any specific energy is minimal. Uncertainty factors of 1.3, 1.2, and 1.1 are estimated for the Hanford two-element film, multi-element film, and thermoluminescent dosimeters, respectively. However, for rotational geometry, there is additional uncertainty because direct measurements were not available. Thus, for rotational geometry, uncertainty factors of 1.4, 1.3, and 1.2 are estimated for the two-element film, multi-element film, and thermoluminescent dosimeters, respectively. For a specified energy, uncertainty from this source will be highly correlated across time and across workers.

SUMMARY

Observations made from analysis of the data collected at this time include the following:

> The effect of exposure angle is most pronounced at lower energies and for the film dosimeter.

- The calculated dosimeter response for the rotational geometry, based on an arithmetic average of each dosimeter response for each of the exposure angles, is approximately two-thirds of the anterior-posterior dosimeter response for all of these dosimeter types and photon energies.

- There are no significant abnormalities in the TLD data regardless of exposure angle or energy. This is directly attributable to the close similarity of the dose response between the TLD and tissue (i.e., deep dose).

- The film dosimeter provides a significant amount of data that is typically qualitatively evaluated. For example, the image of the metallic filter on the film can be used to determine exposure angle and, in the extreme, whether the film was exposed without any filter present, such as in the case of the ±90° exposure angle. Undoubtedly, this information was used by dosimetrists to evaluate unusual data.

REFERENCES

Fix, J. J., E. S. Gilbert and W. V. Baumgartner. 1994. An Assessment of Bias and Uncertainty in Recorded Dose from External Sources of Radiation for Workers at the Hanford Site. PNL-10066, Pacific Northwest Laboratory, Richland, Washington.

Gilbert, E.S. 1991a. "Accounting for Bias and Uncertainty Resulting from Dose Measurement Errors and Other Factors." In Proceedings of The Future of Human Radiation Research, Scloss Elmau, Federal Republic of Germany, March 4-8, 1991. British Institute of Radiology, London.

Gilbert, E.S. 1991b. "Studies of Workers Exposed to Low Doses of External Radiation." In Occupational Medicine: State of the Art Reviews, vol. 6, no. 4, October-December 1991, pp. 665-680. Hanley & Belfus, Inc., Philadelphia.

National Research Council (NRC), National Academy of Science (NAS). 1989. Film Badge Dosimetry in Atmospheric Tests. National Academy Press, Washington, D.C.

Wilson, R.H., J.J. Fix, W.V. Baumgartner, and L.L. Nichols. 1990. Description and Evaluation of the Hanford Personnel Dosimeter Program from 1944 Through 1989. PNL-7447, Pacific Northwest Laboratory, Richland, Washington.

EXPOSURE REDUCTIONS ENCOURAGED BY THE DETERMINATION OF THE EFFECTIVE DOSE EQUIVALENT FOR NON-UNIFORM EXTERNAL EXPOSURES

Matheny, M.D., Brown, C.G., and Dyer, S.G.
Westinghouse Savannah River Company

DOE Order 5480.11 requires calculation of the effective dose equivalent (EDE) due to non-uniform radiation fields using ICRP-26 weighting factors. To comply with this requirement, Westinghouse Savannah River Company (WSRC) developed a simple dose calculation scheme based on a draft report by the External Dosimetry Working Group of the Health Physics Society Standards Committee. Their report is entitled, "Criteria for Performing Multiple Dosimetry." The calculations involved are fairly simple and provide a conservative dose estimate. The resulting EDE estimate provides a much better representation of the risk to the monitored individual than the more prevalent practice of assigning the highest measured dose. Details of the dose assessment methodology are included as an attachment.

In addition to providing an improved dose assessment, the calculation of EDE has prompted new and innovative exposure reduction techniques at the site. For example, it is now standard practice to wear lead aprons when collecting waste from glove boxes in the site's plutonium-238 processing facility. Because of the need to physically handle and bag the waste, other shielding techniques are considered impractical. The lead apron proved particularly effective due to the low energy photon associated with plutonium-238.

The following is a comparison of average doses received by employees performing plutonium-238 waste handling operations.

Compartment	No Lead Apron	With Lead Apron
Head	18 mrem	26 mrem
Chest	36 mrem	3 mrem
Arms	26 mrem	40 mrem
EDE	**36 mrem**	**5 mrem**

While it is no surprise that the use of a lead apron significantly reduced the dose that personnel received, it is important to recognize that the aprons would not have been used without the ability to calculate an effective dose equivalent. If forced to assign the highest measured dose to the whole body, the lead aprons would have been judged inappropriate since there would be little, if any, recordable dose savings. The cost of the aprons, the minor job delays associated with apron use and the minor discomfort

placed upon those having to wear the aprons would have been justification to reject the projected dose savings.

Another benefit from the calculation of EDE is the avoidance of administrative overexposures. For example, earlier this year several riggers were removing a pump from a high level waste tank. Dose rates at waste tank openings can exceed 100 rem/hour, with extreme gradients around the openings. Because of the high dose rates and the large dose gradient, multiple dosimetry was employed. The rigger with the highest dose equivalent during the pump removal received 1273 mrem to his head but only 103 to his chest. The assigned EDE was 187 mrem. Had the dose to the head been inappropriately assigned as the dose to the whole body, the dose of record would have been in excess of the site administrative dose limit of 800 mrem. Such events often lead to added costs due to heightened attention from management and the media Increased oversight in the form of reviews, audits, and investigations are also likely. By avoiding such distractions, the company was able to proceed with the necessary work and implement appropriate corrective actions to reduce future doses.

Although there is some additional effort required on the part of the dosimetrist to determine the EDE, the reduced risk for employees, the more accurate record of dose, and the reduced cost for the company are compelling arguments for use of the concept. The technique described in the attachment provides a simple approach that is easily defended and implemented.

Attachment

Calculation of Effective Dose Equivalent

For routine monitoring purposes, a dosimeter is always placed at the chest location. The necessity for additional dosimetry is determined based on the dose rate in the work area, dose gradient, and total dose expected. Those areas of the body anticipated to receive the highest dose are included when selecting additional monitoring locations to augment the normal chest dosimeter. In accordance with ICRP 26[1] and ICRP 51[2], the highest measured dose for each compartment is conservatively assigned to all tissues in that compartment.

ICRP 26[1] also states, "A practical radiation protection system needs to be based on certain simplifying assumptions if it is to be applied effectively." At the Savannah River Site (SRS), the methodology for determining effective dose equivalent is based on the division of the whole body into seven compartments. In general terms, a compartment is any region or section of the whole body. The seven specific compartments adopted at SRS are the head and neck, thorax, abdomen, the upper right and left arms (including the elbows), and the upper right and left legs (including the knees).

The head and neck compartment includes tissue at or above the junction of the cervical vertebrae and the thoracic vertebrae. It includes the skull, cervical vertabrae, and the thyroid.

The thorax compartment begins with the thoracic vertebrae at the base of the neck. It includes the clavical, scapula, and the chest cage and its contents. The base of the thorax compartment is defined by the dome shaped diaphragm. The diaphragm is attached to the xiphoid process and follows the bottom of the chest cage. The diaphragm is the recognized division between the abdominal and thoracic cavities and as such is the logical division between the two compartments. With the use of this natural division each major tissue resides entirely within a given compartment regardless of anatomical variations or physical activity. Since any difference in dose between the two compartments is actually represented by a gradient rather than a step function, the use of a fixed but yielding division represents the same level of accuracy as other options.

The abdomen is defined as the trunk below the thorax. It contains the digestive system, excluding those organs or tissues above the stomach; the urogenital system; the lumbar vertebrae; and the pelvic girdle. The equation used to calculate personnel effective dose equivalent is as follows:

$$H_E = \sum w_T * H_T = \sum w_C * H_C$$

H_E: The effective dose equivalent. This is equal to the sum of the products of the dose equivalent in a tissue and the corresponding weighting factor for that tissue.

w_T: The weighting factor for a given tissue or organ. ICRP 26[1] weighting factors are listed in Table 1.

Table 1 Tissue Weighting Factors

Tissue (H_T)	w_T
Gonads	0.25
Breast	0.15
Red Bone Marrow	0.12
Lung	0.12
Thyroid	0.03
Bone Surfaces	0.03
Remainder	0.30

H_T: The dose equivalent to a given whole-body tissue or organ. For external exposures, ICRP 26[1] and ICRP 51[2] allow the use of the highest measured dose at a depth of 1 cm to represent the maximum dose to underlying organs and tissues.

H_C: The dose equivalent to a given whole body compartment. Consistent with the definition of H_T, the highest measured dose for each compartment is conservatively assigned to all tissues in that compartment.

w_C: The weighting factor for a given compartment of the body. The whole body is broken into 7 compartments each containing organs or parts of organs from the above list. Table 2 provides a summary of the specific compartment weighting factors. Tables 3 through 5 provide the derivation information for compartmentalization of the Red Bone Marrow, Bone Surfaces, and Remainder Organ weighting factors. Use of the following compartment factors guidelines yields the appropriate effective dose equivalent value.

TABLE 2 Compartment Weighting Factors (w_C)

Compartment (H_C)	Tissue	w_C
HEAD	thyroid	0.03
	red bone marrow	0.02
	bone surface	0.006
	remainder	0.002
Total for Head		**0.06**
THORAX	breast	0.15
	lung	0.12
	red bone marrow	0.037
	bone surface	0.008
	remainder	0.069
Total for Thorax		**0.39**
ABDOMEN	gonads	0.25
	red bone marrow	0.057
	bone surfaces	0.006
	remainder	0.30
Total for Abdomen		**0.61**
UPPER ARMS	red bone marrow	0.002
	bone surfaces	0.002
	remainder	0.008
Total for Upper Arms		**0.01**
UPPER LEGS	red bone marrow	0.005
	bone surfaces	0.008
	remainder	0.030
Total for Upper Legs		**0.04**

To determine the dose to a given compartment, the highest dosimeter result for a compartment is used. If the compartment was not monitored, the result for the nearest compartment monitored is assigned. For the abdomen, the highest adjacent compartment dose is assigned. By procedure the chest compartment is always monitored.

Determination of Compartment Weighting Factors for Red Bone Marrow

Table 31 in ICRP 23[3] lists the percent of total body red marrow for different body bones. By summing the percentages for bones in each compartment, compartment percentages are determined. The compartment percentage is multiplied by the red bone marrow weighting factor (0.12) to determine the compartment weighting factor (w_C).

TABLE 3 Compartment Weighting Factors (w_C) for Red Bone Marrow

Compartment (H_C)	Bone(s)	Percentage	w_C
HEAD	head	13.1	
	vertebrae (cervical)	3.4	
Total for Head		16.5	0.02
THORAX	upper limb girdle	6.4[(a)]	
	sternum	2.3	
	ribs	7.9	
	vertebrae (thoracic)	14.1	
Total for Thorax		30.7	0.037
ABDOMEN	vertebrae (lumbar)	10.9	
	sacrum	13.9	
	lower limb girdle	22.3[(a)]	
Total for Abdomen		47.1	0.057
UPPER ARMS	humerus	1.91	
Total for Upper Arms		1.91	0.002
UPPER LEGS	femur	3.83	
Total for Upper Legs		3.83	0.005

(a) The limb girdles as listed in ICRP 23[3] include the humerus and the femur. However, since these appendages represent separate compartments, the corresponding percentages were removed from the thorax and abdomen compartments and placed in the appropriate compartments.

Determination of Compartment Weighting Factors for Bone Surfaces

Although ICRP 23[3] specifies a total skeletal surface area of 11.2 m^2, it does not provide data for the distribution of this surface area over the bones of concern. From Table 16 of ICRP 23[3], the total (cortical + trabecular) bone mass and the trabecular bone mass are listed for the bones of significance in each compartment. In addition, ICRP 23[3] specifies that 50 % of total bone surface is accounted for by each of the two bone types. Since all cortical bone is similarly structured, determining the relative mass of cortical bone in each bone gives a reasonable estimate of the relative cortical bone surface area, RA(%). A similar approach can be used to determine the relative trabecular bone surface area of each bone. Since each type accounts for half the total bone surface area of the whole body, the relative fractions can be weighted by 50 % and then added to give the total relative bone surface area for each bone, TRA(%). By summing the fractions for the bones in each compartment and then multiplying by the weighting factor for bone surfaces (0.03) compartment weighting factors can be determined. Results are listed in Table 4.

TABLE 4 Compartment Weighting Factors (w_c) for Bone Surfaces

Compartment (H_C)	Tissue	Mass(g)	RA(%)	TRA(%)	w_C
HEAD	skull	671\35	24\5	14.5	
	cerv. vertebrae	14\55	0.5\7	4	
Total for Head				18.5	0.006
THORAX	chest cage	740\25	27\3	15	
	thor. vertebrae	50\160	2\21	11.5	
Total for Thorax				26.5	0.008
ABDOMEN	innominates	352\40	13\5	9	
	sacrum	73\25	3\3	3	
	lumb. vertebrae	57\115	2\15	8.5	
Total for Abdomen				20.5	0.006
UPPER ARMS	humerus	234\60	9\8	8.5	
Total for UA				8.5	0.002
UPPER LEGS	femur	524\260	19\33	26	
Total for UL				26	0.008

Mass(g): The total cortical and "\" the total trabecular mass in grams.
RA(%): The fraction of cortical bone surface area in the dosimetric whole body and "\" the fraction of trabecular bone surface area in the dosimetric whole body.
TRA(%): The fraction of total bone surface area in the dosimetric whole body.

Determination of Compartment Weighting Factors for Remainder

ICRP 26[1] requires that a weighting factor of 0.06 be applied to the 5 organs of highest dose not otherwise included in the list of organ weighting factors. Since it is impossible to predetermine which 5 organs will receive the highest dose, each compartment is weighted as if it received the highest compartment dose. This results in slightly conservative results in the overall calculation. However, it provides a simplified calculation methodology that is clearly consistent with ICRP 26. Organs included in the remainder are based on the practice in ICRP Publication 51[2] *Data for Use in Protection Against External Radiation* to use the list of remainder organs identified in ICRP Publication 30[4] *Limits for Intakes of Radionuclides by Workers.*

The relative abundance of muscle in each compartment is based upon the distribution of skeletal muscle mass as given in ICRP 23[3]. With the exception of muscle, each of the other "remainder" organs reside wholly within specific compartments. A list of the remainder organs, and their distribution, and the resulting weighting factors is provided in Table 5.

TABLE 5 Compartment Weighting Factors (w_c) for Remainder Organs

Organ	% Head	% Thorax	% Abdomen	% Upper Arm	% Upper Leg
Bladder			100		
Adrenals			100		
ST				100	
SI				100	
ULI			100		
LLI			100		
Kidneys			100		
Liver			100		
Muscle	4	15	13	18	50
Pancreas			100		
Spleen			100		
Thymus		100			
w_T	0.002	0.069	0.30	0.008	0.03

References

(1) ICRP Publication 26, *Recommendations of the International Commission on Radiological Protection*, 1977

(2) ICRP Publication 51, *Data for Use in Protection Against External Radiation*, 1987

(3) ICRP Publication 23, *Reference Man Anatomical, Physiological, and Metabolic Characteristics*, 1975

(4) ICRP Publication 30, *Limits for Intakes of Radionuclides by Workers*, 1978

DEVELOPMENT OF NEW METHODOLOGY FOR DOSE CALCULATION IN PHOTOGRAPHIC DOSIMETRY

Teresinha F.L Daltro and Letícia L. Campos (Instituto de Pesquisas Energéticas e Nucleares - CNEN/SP) C.P. 11049, CEP 05422-970-São Paulo-SP, Brazil)

A new methodology for equivalent dose calculation has been developed at IPEN-CNEN/SP to be applied at the Photographic Dosimetry Laboratory using artificial intelligence techniques by means of neural network. The research was orientated towards the optimization of the whole set of parameters involved in the film processing going from the irradiation in order to obtain the calibration curve up to the optical density readings. The learning of the neural network was performed by taking the readings of optical density from calibration curve as input and the effective energy and equivalent dose as output. The obtained results in the intercomparison show an excellent agreement with the actual values of dose and energy given by the National Metrology Laboratory of Ionizing Radiation.

Work partially supported by CNPq - Conselho Nacional de Desenvolvimento Científico e Tecnológico, Brazil

ENERGY DEPENDENCE OF PEN DOSEMETERS FOR X-RAYS (20-60 kV)

Eliane C. Oliveira, Marcos Xavier and Linda V.E. Caldas (Instituto de Pesquisas Energéticas e Nucleares-CNEN/SP, Caixa Postal 11049 - CEP 05422-970 - São Paulo, SP, BRAZIL)

The pen dosemeters are specially important for individual radiation monitoring because they allow direct and rapid exposure measurements. Three kinds of pen dosemeters, designed A, B and C (different manufactures), were tested in low energy X radiation fields (radiation protection level) of the Calibration Laboratory of São Paulo, in order to verify their energy dependence. Two pen dosemeters were each time simultaneously exposed to X radiation with energies varying between 15.7 and 37.6 keV. They were irradiated free in air for the energy dependence study and in front of a PMMA phantom (30x30x15 cm) with the objective to establish the backscattering contribution to their responses. All of them were tested in both studies in five different standard radiation qualities. The dosemeters of type A and C presented the highest radiation sensitivity of the investigated energy range. Short-term stability tests were performed and the results depend on the dosemeter type and the energy: the highest and lowest variations were obtained respectively for the type C pens (15% and 15.7 keV) and type B pens (0.93% and 37.6 keV). All dosemeters presented high energy dependence, varying for type B pens between 98% (15.7 keV) and 64% (37.6 keV). In the case of the backscattering response contribution study with the phantom the type C pens showed the largest values (45%, 15.7 keV). These high values are probably due to their strong radiation sensitivity. The obtained results showed consistency with literature data. All tested pen types must be used very carefully for X radiation detection in the investigated low energy range using convenient correction factors.

Work partially supported by CNPq - Conselho Nacional de Desenvolvimento Científico e Tecnológico, Brazil

ELECTRONIC PERSONNEL DOSIMETER USE IN LOW ENERGY PHOTON AND BETA ENVIRONMENTS FOR LOW EXPOSURE DOSE TRACKING AND CONTROL.*

T. E. Goff, C. F. Wu (Waste Isolation Pilot Plant, P. 0. Box 2078, Carlsbad, NM 88221) and T. R. Ohlhaber (Siemens Dosimetry Services, 2501 N. Barrington Rd., Hoffman Estates, IL 60195)

Electronic Personnel Dosimeters (EPDS) are emerging as supplement to other dosimeters for personnel monitoring. The radiation sources expected at the Waste Isolation Pilot Plant (WIPP) will yield low energy photons and beta from the transuranic wastes. This study evaluates the Seamens EPD for low dose ALARA tracking and control at the Waste Isolation Pilot Plant.

Current plans at WIPP are to use Geiger-Mueller tube based dosimeters to track and control exposures. EPDS, however, use multiple sensors with varying shielding similar to thermoluminescent dosimeters (TLDs). Their internal algorithms will provide more accurate dose estimations from the low energy photon environments than a single sensor system can.

This study also evaluates the possibility of adjusting EPD responses with radiological survey based factors. This methodology may provide better dose results than using the EPD internal algorithm alone. These factors could be included in access control systems as part of Radiation Work Permit data files.

*(Work supported by the U. S. Department of Energy under DOE Contract No. DE-AC04-86AL31950)

NEW PHOSPHATE GLASS DOSEMETER SYSTEMS FOR ROUTINE INDIVIDUAL AND ENVIRONMENTAL MONITORING

B.Burgkhardt, E. Piesch, S. Ugi (Karlsruhe Nuclear Research Centre, Germany)
T. Ishikawa, T. Ikegami, T. Omori, (Toshiba Glass Tokyo, Japan)

Abstract

Two recently developed photoluminescent dosemeter (PLD) systems are now commercially available which similar to conventional TLD systems allow a fully automatic readout and data evaluation: (a) The one-element dosemeter SC-1 makes use of a perforated tin filter for the simultanious measurement of the exposure X and $H_p(10)$ in the photon energy range 25 keV and 12 keV to 1.3 MeV, respectively, allowing in addition an automatic scanning of the glass, horizontally and vertically, for estimating radiation quality and direction of radiation incidence. The system is pattern approved by the PTB and applied by two German dosimetry services. (b) The four-element dosemeter GD-400 uses metal and plastic filters of different thicknesses. The linear combination of the detector readings allows the energy independent measurement of exposure X or $H_p(10)$ for photons and $H_p(0.07)$ for beta rays and photons.

The pulsed UV laser excitation permits a suppression of the intrinsic pre-dose reading and for annealed glasses the coefficient of variation is 10% at 30 µSv. Routine results are presented for PLD and electronic personal dosemeters worn simultaneously in controlled areas of nuclear power stations. With respect to long-term environmental monitoring PLD and TLD systems are compared in the temperature dependent fading characteristics, the self-irradiation and the response to cosmic rays.

1. Introduction

Silver activated metaphosphate glass dosemeters, developed by Schulmann in 1951 and finally improved in the glass composition by Yokota in the 1960s, have been the first solid state dosemeters applied in a large scale use mainly for military purposes [1,2]. Even in the last years Toshiba Glass produced more than two millions of glasses. In the lower dose range, however, in particular the high pre-dose of about 1 mSv and glass cleaning before readout prevented a large scale application [3,4]. In routine personal monitoring the actual progress in the field of photoluminescence dosimetry (PLD) started in the 80s, when pulsed UV laser of high intensity were available [5] and a modern evalution technique combined with a fully automatic readout system was developed within a cooporation project between KfK and Toshiba Glass [6-8]. After extended tests also in routine monitoring and the German PTB pattern approval in 1992 [9], glass dosemeters have been successfully applied at the official personnel dosimetry service at Karlsruhe. Since this time about 20,000 dosemeters are used in personnel dosimetry as well as in environmental monitoring. The paper discusses the various, recently developed dosemeters and readout systems and the practical experience with the new dosemeter types.

2. UV excitation and readout technique

PLD is based on the formation of fluorescence centres in glass dosemeters. When exposed to UV-light, radiation induced PL fluorescence light is emitted, the intensity of which is proportional to the dose. Optical filters reduce the intrinsic PL intensity and within a second light path a photo diode allows to correct fluctuations of the laser pulse intensity (Fig.1). Automatic glass scanning, horizontally and vertically, is realized by moving two diaphragms D_1 and D_2 [7,15].

Table 1: Photoluminescence dosimetry systems for fully automatic readout

	One-element dosemeter	Multi-element dosemeter
Reader type (continious readout)	FGD-10 (500x) FGD-203 (20x)	FGD-601 (500x) FGD-501 (10x)
Dosemeter type	SC-1	GD-403 1)
ID number glass card capsules	20 bits 8 digits	24 bits 14 digits
Filter position		
1	Sn/Plastic	Sn
2	---	Al
3	---	Plastic 38 µm
4	---	Plastic 250 µm
Readout position	1	1, 2, 3, 4
Energy range H_x 2) $H_p(10)$ $H_p(0.07)$	 E_γ: 25 keV - 1.3 MeV E_γ: 12 keV - 1.3 MeV E_γ: 25 keV - 1.3 MeV	 E_γ: 30 keV- 1.3 MeV E_γ: 20 keV- 1.3 MeV E_γ: 20 keV- 1.3 MeV $E_{\beta max}$: 0.5 - 2.3 MeV
Indication of radiation quality	automatically	automatically
Minimum scale unit	1 µSv	1 µSv
Dose range	30 µSv - 10Sv	30 µSv - 10 Sv
Quality assurance	German PTB pattern approval	

1) Dosemeters GD-401 and GD-402 use modified filters for optional detection of photons only (without beta window) or photons and thermal neutrons (Cd filter)
2) $H_x = k \cdot X$ with $k = 0.01$ Sv/R

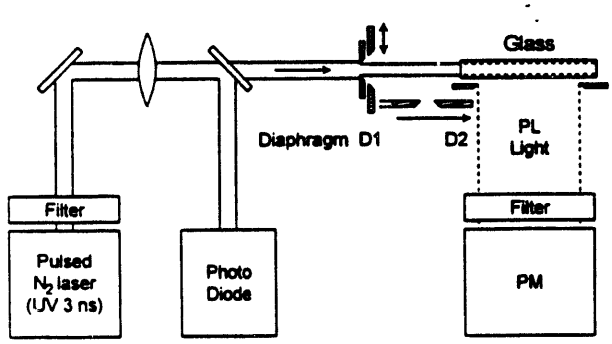


Fig. 1 Principles of phosphate glass measurement using UV excitation and photoluminescence (PL) readout

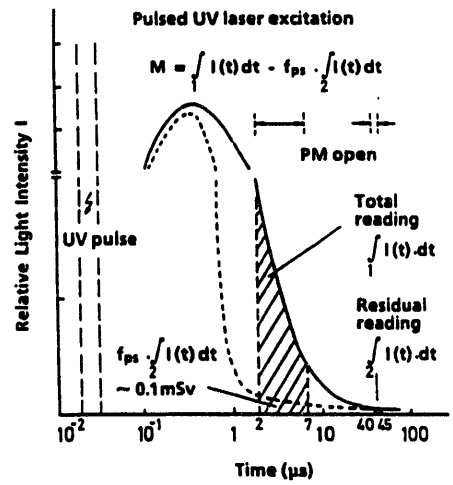


Fig. 2 Short-term PL light intensity after pulsed UV laser excitation used for the subtraction of the residual dose reading

The readout technique separates the intrinsic individual pre-dose from the radiation induced reading. Fig. 2 shows typical PL intensity curves I(t) of an annealed and irradiated glass, respectively, immediately after UV pulse excitation of 3 ns. The time dependent PL intensity I(t) is integrated in two different periods, namely the radiation independent long-term component of the residual reading in the period 2 between 40-45 µs and the short-term component in the period 1 between 2-7 µs. A multiple f_{ps} of the measured residual dose is subtracted from the total short-term reading resulting in the radiation induced reading M. The pre-dose suppression factor, f_{ps}, is measured once after the first annealing. In order to exclude negative readings of the pre-dose, the pre-dose setting at about 30 µSv is conservative and could be reduced, in principle, to a value of 10 µSv.

3. Dosimetry systems

Two different dosimetry concepts have been realized so far (Fig.3 and Table 1) using the glass dosemeter types SC-1 and GD-400.

The one-element dosemeter SC-1 offers in individual and environmental monitoring the most attractive solution for a low photon energy and angular dependence by using a capsule with an optimized energy compensation filter. For the measurement of the dose $H = N \cdot M$ the lowest uncertainty is expected due to the single readout M and the only calibration factor N. The detection of beta-rays is not of interest for whole body exposures.

The flat glass dosemeter SC-1 consists of a glass element (16 x 16 x 1.5 mm^3) fixed in a stainless steel card and a plastic encapsulation (40 x 30 x 9 mm^3) with energy compensation filters of tin and plastic on both sides. This dosemeter is used in a plastic bag. For large scale use, the fully automatic readout system FGD-10 provides, (a) magazines for dosemeters (capsules) as well as for annealed glass cards for an optional exchange of high-dosed glasses, (b) unlocking and opening of dosemeter capsules, (c) continious readout up to 500 dosemeters (20 s each), (d) reading ID numbers of the dosemeter capsule and the glass card, (e) above a variable dose threshold the automatic glass scanning for the immediate indication of radiation quality and the interpretation of radiation angle, (f) data handling of 50,000 dosemeters. For small dosimetry services the automatic readout system FGD-203 provides the continuous readout of 20 dosemeters (10 s each) and the same features except (a) and (c).

The multi-element dosemeter GD-400 adapted the commonly used technique of film and TL dosemeters to reduce the photon energy and angular dependence by using a linear combination of two from four readings M_i ($H = N_1 \cdot M_1 + N_2 \cdot M_2$). Some modified capsule types containing thin plastic windows, Al and Cd filters (see chapter 4) allow the simultanious indication of the beta-ray or thermal neutron component tolerating a higher uncertainty of measurement. These readouts serve more or less for an indication of a relevant beta or neutron exposure, which then calls for finger ring dosimetry or neutron dosimetry using a dosemeter with a sufficient response over the total energy range.

The glass dosemeter type GD-400 series consists of a glass card (40 x 14 x 2 mm^3) with four detection positions, the plastic capsule (60 x 25 x 9 mm^3) with four corresponding filters and a capsule holder for the use in routine monitoring. The FGD-601 readout system has been outlined for large scale dosimetry services and provides the features (b) to (d) and (f) of the FGD-10 system. For small dosimetry sevices, the compatible reader FGD-501 allows the continious readout of 10 dosemeters.

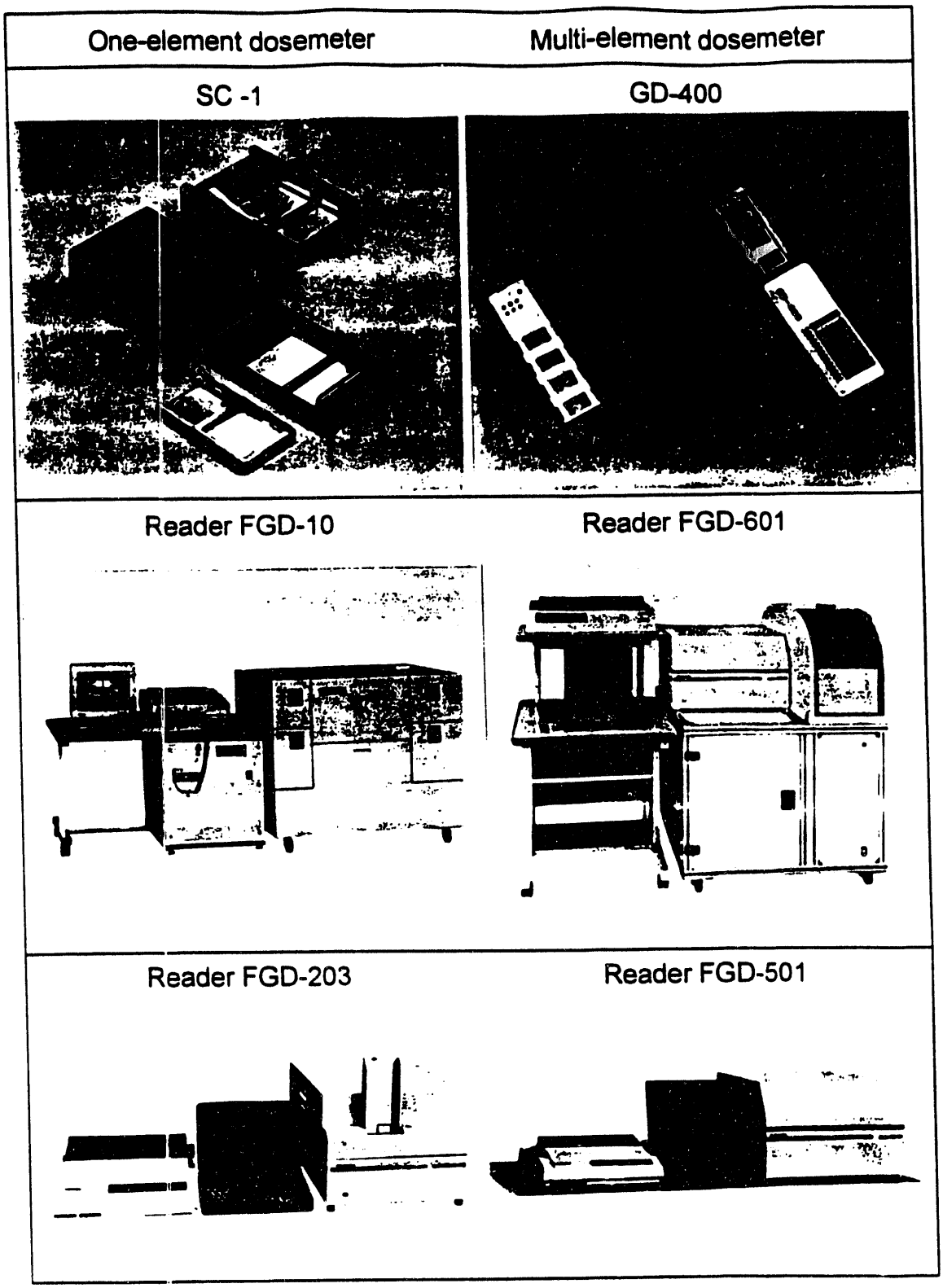


Fig. 3 Commercially available glass dosemeter types and readout systems

4. Dosimetric properties

The selected dosimetric properties of phosphate glass dosemeters presented here are results of laboratory tests, intercomparisons, the PTB pattern approval and the quality assurance during routine application. One of the most essential advantages of the PLD systems is the individual measurement of the pre-dose as well as the low standard deviation between 1 µSv and 2 µSv of annealed glasses (about 10% at 30 µSv). The glass-specific ability of repeated readouts allows the dose accumulation and the easy reader calibration using the same glass over periods of more than three months.

In routine monitoring, therefore, the actual dose contribution is given by the difference of two consecutive readouts at the beginning and the end of the monitoring period. The readout program automatically subtracts the pre-dose of the last readout H_0 and the contribution of the natural background radiation, H_{nat}, in the period between the last and the actual readout, M, resulting in the actual dose $H = N \cdot M - H_0 - H_{nat}$.

The random uncertainty of dose measurement vs. dose was experimentally determined using random batches of 10 dosemeters (Fig. 4). With annealed glasses (pre-dose of 0.03 mSv) or batches which previously accumulated 3 mSv, a dose of 0.1 mSv can be measured with a coefficient of variation of 3% and about 25%, respectively. At higher doses the v-value is about 1%. According to the requirements of the PTB for the pattern approval, the dose range is 0.1 mSv to 8 Sv for personal dosemeters, and when annealed before use, 0.03 mSv to 8 Sv for area dosemeters [9]. The long-term stability of the PLD system and the linearity of dose measurement are shown in Fig. 5.

Another advantage of the SC-1 flat glass dosemeter is the simultanious indication of both dose quantities, namely the exposure, X, free in air, and the new ICRU quantity personal dose equivalent, $H_p(10)$, defined in a tissue depth of 10 mm using a calibration on a slab phantom. In order to indicate $H_p(10)$, the Cs-137 calibration factor free in air has to be increased by a factor of 1.07. For Film, TLD and electronic personal dosemeters, however, there is, in general, the need to change the energy compensation filters and/or the evaluation technique. In Fig. 6, the photon energy response of glass dosemeters are presented for H_x and $H_p(10)$. For $H_p(10)$ and the SC-1 dosemeter, for instance, the energy response is within ± 10% in the energy range from 12 keV - 1.3 MeV and the angular response increases this value to about 25%. Results of the IAEA intercomparison have shown that the SC-1 dosimeter is also able to indicate

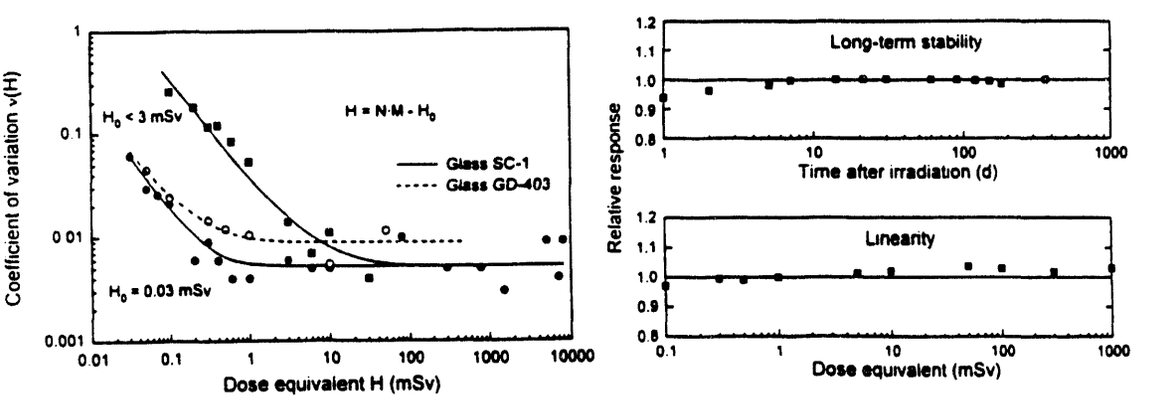
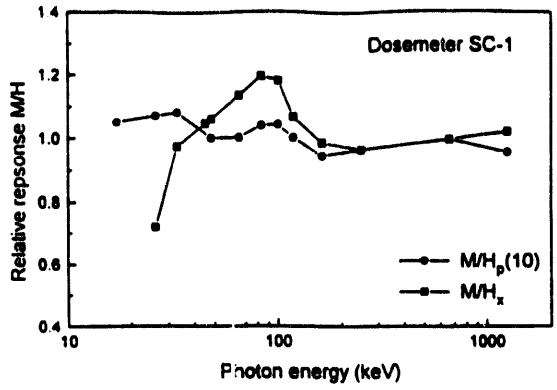


Fig. 4 Coefficient of variation for the measurement of dose using batches of annealed glasses (pre-dose 0.03 mSv) and glasses with an accumulated dose of 3 mSv

Fig. 5 Long-term stability of the GD-403 glass dosemeter reading at room temperature (a), and linearity of dose reading (b)



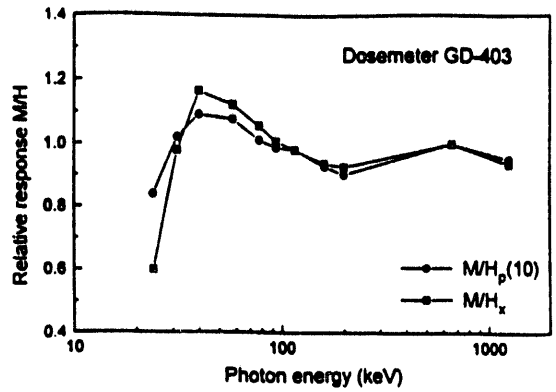


Fig. 6 Energy response of the flat SC-1 glass dosemeter; frontal irradiations on a slab phantom for measuring $H_p(10)$, and H_x free in air (with 0.01 Sv/R)

Fig. 7 Energy response of the GD-403 glass dosemeter; frontal irradiations on a slab phantom for measuring $H_p(10)$, and H_x free in air (with 0.01 Sv/R)

quantitatively radiation quality, and in most cases also qualitatively the angle of radiation incidence which both, however, are not used for the evaluation of the dose [11,15].

For the GD-400 glass dosemeter series, where the dose evaluation is based on four readouts behind different filters, another evaluation algorithm has to be used for $H_p(10)$ (see Fig. 7). GD-403 is capable of separating the beta-ray from the photon contribution by using the difference in the reading between the plastic filters, namely M_3 (38 µm) and M_4 (250 µm). After subtracting the energy dependent gamma contribution M_2, the energy dependent beta correction factor $f_\beta = f\,[(M_3 - a \cdot M_2) / (M_4 - b \cdot M_2)]$ and thus the skin dose is $H_\beta(0.07) = N_{Cs\text{-}137} \cdot f_\beta \cdot (M_3 - a \cdot M_2)$. Table 2 presents beta energy response factors. Because of the photon energy dependence of the "uncovered beta detector" (factor 30 for film compared to factor 3.6 for glass) glass dosemeters, in general, are more suitable for the indication of beta-ray exposures than film dosemeters. Compared to thin detectors of tissue equivalent material, the estimation of a beta dose suffers, however, from the effective detector thickness of about 0.5 mm. In mixed photon and beta radiation fields and for $E_{\beta max} < 0.5$MeV, the uncertainty for indicating beta doses is, therefore, significantly higher, but sufficient for the rough estimation of a beta-ray contribution using a whole body dosemeter.

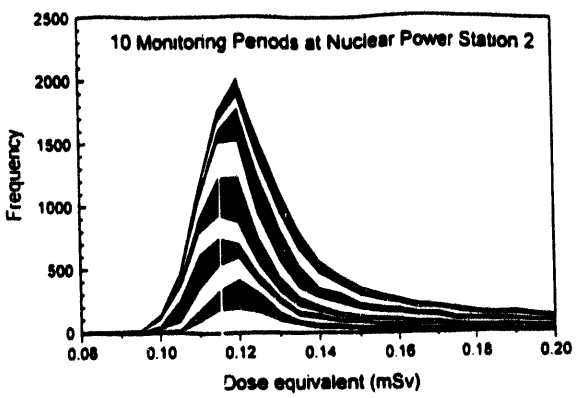
Table 2 : Relative beta energy response to $H_p(0.07)$ of glass dosemeter GD-403

Radionuclide	$E_{\beta max}$	$R_\beta / R_{\beta Sr}$
$^{90}Sr/^{90}Y$	2.28	1.00 ± 0.03
^{204}Tl	0.76	0.97 ± 0.03
^{147}Pm	0.225	1.03 ± 0.19[1]

[1] Recommended energy range excludes ^{147}Pm

5. Individual monitoring

After the PTB pattern approval and the decisions of the German Federal State Committee of Atomic Energy, the flat glass dosemeter is now applicable as an official dosemeter by governmental services for individual monitoring, also in the field of me-



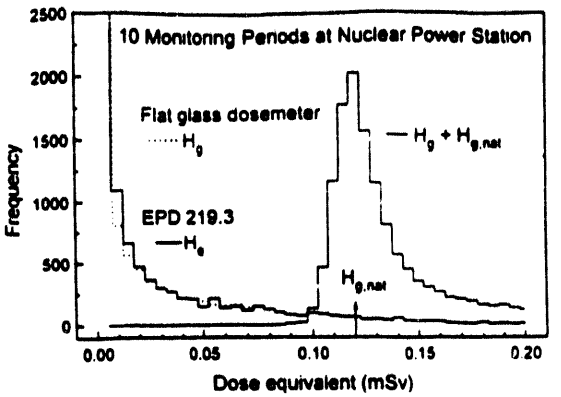


Fig. 8 Dose results of glass dosemeters ($H_g + H_{nat}$) below 0.2 mSv accumulated over 10 months within routine monitoring in a nuclear power plant

Fig. 9 Frequency distribution of the dose results of electronic personal dosemeter (H_e) and glass dosemeters before ($H_g + H_{nat}$) and after (H_g) subtracting H_{nat}

dical application. At the Karlsruhe personnel dosimetry service flat glass dosemeters SC-1 have been routinely used on a monthly base since more than 2 years. With respect to the annual PTB performance test, Tab. 3 compares the deviation from the reference dose found for individual dosemeters used at the KfK service.

In a recent study, monthly results of the official German glass dosemeter (PLD) and the electronic personal dosemeter (EPD using GM tubes) have been compared at three nuclear power plants over a period of 10 months [10]. In contrast to PLD the daily measured EPD does not indicate the contribution of the natural background radiation, H_{nat}, and doses < 1 µSv per day. Fig. 8 shows the good long-term reproducibility of the frequency distribution of monthly evaluated PLD results <0.2 mSv before subtracting H_{nat}, accumulated over a period of 10 months. The asymmetry of the same peak in Fig. 9, above all the shift to higher doses indicate low dose contributions to H_{nat}. Assuming at low doses contributions by H_{nat} only , a plant- specific H_{nat}-value (here 0.12 mSv for 60 days) may be substracted. Thus, the uncertainty of dose measurement has been significantly reduced. A good overall agreement was found between the PLD and EPD results in the dose range below 0.05 mSv up to 13 mSv. Differences of about 5-10% as shown in Fig. 10 can be explained by the energy dependence of the EPD [10].

Table 3: Results of the KfK dosimetry service at the PTB annual performance test 1993

Dosemeter	$H/H_r \pm s$ [1]
Glass SC-1	1.015± 5.6%
TLD-Albedo (photons)	1.005± 15 %
Finger ring	1.101± 16 %
TLD-Albedo (neutrons)	1.122± 15 %

1) Mean and relative standard deviation

Table 4: Doses recorded for medical personnel wearing a protective lead apron

Hospital A		Hospital B	
Glass[1]	TLD[2]	Glass[1]	TLD[2]
0.63	0.75	5.6	6.25
0.20	0.15	6.98	6.95
0.49	0.40	14.0	11.1
0.38	0.35	7.96	8.95
5.18	4.5	1.48	1.85

1) accumulated over 3 months
2) sum of monthly results

As an example for an application in radiology, Tab. 4 compares individual doses recorded by SC-1 glass dosemeters and TLD badges on the neck above an apron. The photon energy indicated by glass dosemeters was found to be uniform in the range 70-150 keV for hospital A and 30-70 keV for hospital B.

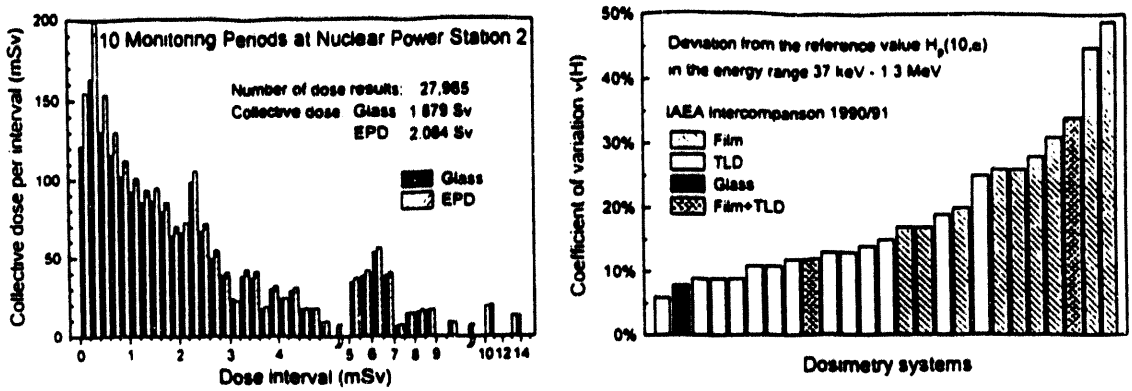


Fig.10 Collective dose per dose interval for ten months measured by glass and electronic dosemeters

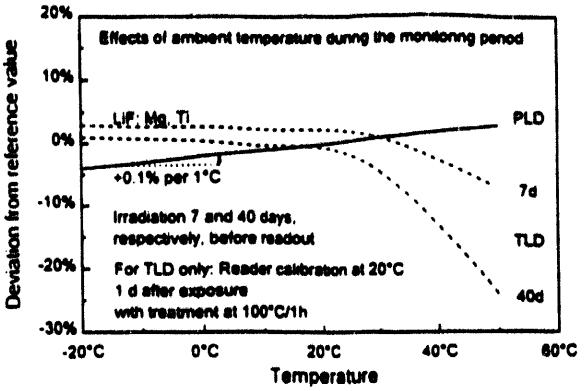
Fig.11 Frequency distribution of the coefficient of variation for the individual dosemeter systems participated in the 1990/91 IAEA intercomparison

At the IAEA intercomparison 1990/91 the optimization of the photon energy response with respect to $H_p(10)$ was investigated for various dosimetry systems confirming the dosimetric properties of the new PLD system and the advantages in competition with other systems [11]. Fig. 11 compares the results of participants, which were reported for the energy and angular dependence of their dosimetry systems, in terms of the coefficient of variation for the deviation H/H_r of the reported, H, from the reference dose equivalent, H_r. For the one-element glass dosemeter the result is comparable with those of the best TLD systems which, however, use a combination of 4 detectors of various TL materials ($Li_2B_4O_7$ and $CaSO_4$) and different shieldings on the front and rear side of the dosemeter (asymmetric albedo type dosemeter).

6. Environmental monitoring

The accuracy of dose measurement, in general, is essentially affected by the temperature during annealing, irradiation, storage as well as the readout. For elevated ambient temperatures up to 40 °C, the fading of TLD 700 chips, for instance, is up to 15% and for $Li_2B_4O_7$:Mn,Si up to 30% taking into account a short-term exposure in the period between 7 and 40 days before the readout and an optimized post-irradiation treatment (Fig. 12). For the PLD system we expect an increase in the readout of about 2% only during irradiation (0.1%/1°C). The temperature effect of glass dosemeters is thus expected to be one order of magnitude lower also at elevated temperatures. Earlier experiments indicated a long-term fading of -2% after 8 years of storage at 30 °C [12].

In the case of environmental monitoring the essential advantages of glass dosemeters are the good batch homogeneity (<1%) and the long-term stability against ambient influences of about 1%. Not considering the effect of energy and angular dependence, uncertainty of about <3% are expected. Fig. 13 shows the photon energy response of the glass dosemeter rotating free in air in two axis. In environmental monitoring, two dosemeters arranged under an angle of 90° to each other are exposed on each station using monitoring periods of 6 months. The results of routine monitoring confirm the above mentioned uncertainty of measurement [8,13]. In comparison to other dosemeters, glass dosemeters are most stable against ambient effects. Mainly the lack in the thermal stability and the sensitivity against environmental effects limits the application of TLD systems in routine monitoring.



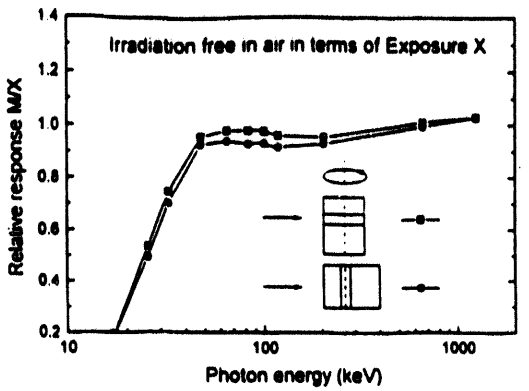


Fig. 12 Ambient temperature effects on PLD and on LiF-TLD systems vs ambient temperature within routine monitoring on a monthly basis

Fig. 13 Energy response of the flat glass dosemeter SC-1 for the measurement of H_X free in air in environmental monitoring (with 0.01 Sv/R)

The self-irradiation effect of the dosemeter itself and the response to cosmic rays have been carefully determined within a long-term experiment for different solid state dosemeters for the first time [14]. Dosemeters were exposed in the low level PTB laboratory in the Asse salt mine (9.5 µGy/a) and on the surface of a 20 m deep lake with a negligible contribution of the terrestric component. Table 5 compares the glass properties with those of different TLD systems in use at KfK. In comparison to a PE capsule and LiF:Mg,Ti with a negligible effect, the self-irradiation of a 9.5 µGy per year in the glass dosemeter is mainly caused by the tin filter. The relative response to cosmic rays is 0.91 for the glass dosemeter compared to 0.82 for LiF:Mg,Ti and a higher value of 0.95 for LiF:Mg,Cu,P because of differences in the LET response of both materials, which have been found also at low photon energies [16].

Table 5: Comparison of dosemeter reading due to exposure from self-irradiation and cosmic rays within environmental monitoring

Dosemeter type	Capsule	Air kerma (µGy/a) [1] $H_{self} \pm s$	$H_{cos} \pm s$	H_{cos}/H_{ref}
Glass SC-1	tin/plastic	9.5 ± 0.5	263 ± 1	0.91
CaF_2:Dy	tin sphere	29 ± 2	242 ± 2	0.84
^{7}LiF:Mg,Ti	PE capsule	0 ± 0.3	237 ± 1.5	0.82
LiF:Mg,Cu,P	Pl capsule	7 ± 0.5	275 ± 8	0.95
Reference		1.1 (PTB)	289	---

[1] Exposure period of 550 days in the ASSE salt mine (-775 m below see level) and on the surface of a lake (115m above see level); Standard deviation s [14]

7. Conclusion

The results of type tests, intercomparison experiments and routine monitoring point out that most of the glass dosemetric properties have been found to be superior to commonly used film and TLD systems. Advantages of glass dosemeters are the repeated readout, the simple handling, the flat energy and angular response above all of a one-element dosemeter, the reproducibility of measurement, the accurate pre-dose correction and thus the low uncertainty in the lower dose range as well as long-term

stability against ambient influences. Glass dosemeters, on the other hand, do have also the ability of indicating radiation quality and radiation angle, and using multi-element dosemeters to separate beta and photon dose contributions.

The actual variety of different PLD readout systems, on the one hand, and of different dosemeter types namely the one-element and the multi-element dosemeter, on the other hand, allows for small and large services to find out the suitable system and to compare it with commonly used multi-element dosemeters such as film and TLD systems. With the change of the legal dose quantities starting in Germany in 1995, high efforts are necessary for developing new film and TLD systems and receiving the required PTB pattern approval. The recently developed glass dosemeter is not affected by these changes.

References

[1] J. H. Schulmann,R. J. Ginther, C. C. Klick, R. S. Alger, R. A. Levy, Dosimetry of X-rays by Radiophotoluminescence, J. Appl. Phys. 22, 1479 (1951)

[2] R. Yokota, S. Nakajima and E. Sakai, High Sensitivity Silver-activated Phospate Glass for the Simultanious Measurement of Thermal Neutrons, γ- and/or β-rays, Health. Phys. 5, 219 (1961)

[3] E. Piesch, Developments in Radiophotoluminescence Dosimetry, in Attix, F. H. (Editor): Progress in Radiation Dosimetry, Vol. 1, New York, Academic Press, 461-532 (1972)

[4] J.A., Perry, RP. Dosimetry, Radiophotoluminescence in Health Physics, Adam Hilger, Bristol and Philadelphia (1987)

[5] T. Omori, T. Ikegami and T. Ai, Fluoro-Glass-Dosemeter Reader by N_2 Gas Laser Excitation, Toshiba Rev. 39, 247-250 (1984)

[6] B. Burgkhardt, M. Vilgis, E. Piesch, T. Ishidoya and T. Ikegami, Modern Automatic Readout System for Phosphate Glass Dosemeters Using UV Laser Excitation, Radiat. Prot. Dosim., 34, 369-372 (1990)

[7] E. Piesch, B. Burgkhardt, M. Vilgis, Photoluminescent Dosimetry - Progress and Present State of the Art, Radiat Prot. Dosim., 33, 215-226 (1990)

[8] E. Piesch, B. Burgkhardt, M. Vilgis, Progress in Phosphate Glass Dosimetry: Experiences and Routine Monitoring with a Modern Dosimetry System, Radiat. Prot. Dosim. 47, 409-414 (1993)

[9] P. Ambrosi, R. Neuhaus, E. Piesch, First Experience with Pattern Approvals of Dosimetry Systems in Germany, Radiat. Prot. Dosim., 47, 401-407 (1993)

[10] S. Ugi, E. Piesch, H. Briesen, J. Hastreiter, L. Izquierdo, W. Laudenklos, Vergleich der Meßergebnisse von Glasdosimetern und elektronischen Personendosimetern, Report FS-94-71-T, 535-540 (1994)

[11] P. Ambrosi, G. Buchholz, J. Böhm, R. V. Griffith, D. Herrmann and C. Strachotinsky, Results of the IAEA Intercomparison for Individual Monitoring, Radiat. Prot. Dosim., 54, 5-17, (1994)

[12] A.M. Chapuis, in Technical Recommendations for the Use of Radiophotoluminescence Dosimetry in Individual Monitoring, Report EUR 5655, Luxemburg, CEC (1977)

[13] A.Mihara, Y. Ohi, T. Tamura, T. Mochizuki, T. Numakunai, Y. Yoshida, Application of Radiophotoluminescence Dosemeters for Environmental Monitoring, Paper presented at the Asia Congress Radiation Protection, Beijing, China (1993)

[14] B. Burgkhardt, M. Budzanowski, P. Olko, W. Peßara, K. Gmür, Langzeitexperiment zur Ermittlung des Eigennulleffekts und des kosmischen Ansprechvermögens von Festkörperdosimetern - Vorläufige Ergebnisse, Report PTB to be published (1993)

[15] E. Piesch, B. Burgkhardt, and M. Vilgis, Performance of the New Photoluminescent Glass Dosimetry System at the IAEA Intercomparison 1990/91 for Individual Monitoring, to be published in Radiat. Prot. Dosim. (1994)

[16] P. Olko, P. Bilski, E. Ryba and T. Niewiadomski, Microdosimetric Interpretation of the Anomalous Photon Energy Response of Ultra-Sensitive LiF:Mg,Cu,P TL Dosemeters, Radiat. Prot. Dosim.,47, 31-35 (1993)

PERSONAL MONITORING AT ACCELERATORS USING CR-39

N. Anthony Greenhouse (Personal Dosimetry Office, Lawrence Berkeley Laboratory, Berkeley, CA 94720)

Applications of CR-39 for neutron dosimetry have been dominated by situations where neutron energies fall within the fission spectrum range. We have studied the response of this material to roughly mono-energetic neutrons of 20 to 65 MeV produced at the Crocker Nuclear Laboratory, U. C. Davis. Although the sensitivity of the material is reduced by factor of about five when compared with the response plateau at say 3 MeV, the high-energy response does appear to be useful for personal monitoring at accelerators. This paper presents work done at U. C. Davis as well as that at the 88-Inch Cyclotron, LBL. The utility of this detector for personal monitoring at facilities of similar energy was confirmed.

At least eight roughly mono-energetic neutron energies were selected at the Crocker Lab cyclotron in order to estimate the high-energy portion of the CR-39 response function. In addition, two broad spectrum exposures having endpoint energies of 30 and 65 MeV were done to compare the predicted response of this material with actual measurements. The already published lower energy response data was combined with this high energy work to produce a continuous function over the energy range of interest. Microsoft's Excel and the Statistical Sciences S-Plus library were used to fit curves to the response data, and to develop predicted dose information for the broad spectrum responses. These comparisons are presented as well.

The tentative conclusion of this work is that CR-39 is an acceptable personal monitoring device for use at accelerators of equivalent energy. Therefore it can replace Kodak's NTA film for this purpose.

This research was supported by the U.S. Department of Energy under Contract Number DE-AC03-76SF00098.

SITE-SPECIFIC CALIBRATION OF THE HANFORD PERSONNEL NEUTRON DOSIMETER

A. W. Endres, L. W. Brackenbush, W. V. Baumgartner, and B. A. Rathbone
Pacific Northwest Laboratory, Richland, Washington 99352

INTRODUCTION

A new personnel dosimetry system, employing a standard Hanford thermoluminescent dosimeter (TLD) and a combination dosimeter with both CR-39 nuclear track and TLD-albedo elements, is being implemented at Hanford. Measurements were made in workplace environments in order to verify the accuracy of the system and establish site-specific factors to account for the differences in dosimeter response between the workplace and calibration laboratory. Neutron measurements were performed using sources at Hanford's Plutonium Finishing Plant under high-scatter conditions to calibrate the new neutron dosimeter design to site-specific neutron spectra. The dosimeter was also calibrated using bare and moderated ^{252}Cf sources under low-scatter conditions available in the Hanford Calibration Laboratory. Dose equivalent rates in the workplace were calculated from spectrometer measurements using tissue equivalent proportional counter (TEPC) and multisphere spectrometers. The accuracy of the spectrometers was verified by measurements on neutron sources with calibrations directly traceable to the National Institute of Standards and Technology (NIST).

Three plutonium sources were studied: plutonium tetrafluoride, plutonium oxide, and a plutonium metal alloy. All of the sources were low-exposure plutonium containing about 5% to 6% ^{240}Pu, which is representative of the plutonium processed at Hanford in the past. The plutonium mass varied between 760 grams and 1500 grams in sealed metal containers. The plutonium fluoride source was used for primary calibration because the available source delivers a higher dose rate than the other sources and the highest neutron doses reported for personnel at Hanford historically occurred at the fluorinator hood. The fluoride source was measured at 50 cm and at 1 m, with variations in intervening plastic shielding from 0 in. to 4 in. to simulate shielded glove-box operations. The plutonium oxide and metal sources were measured only at 50 cm with no intervening shielding because of the relatively low neutron dose rates. The dosimeter results were compared with the TEPC and multisphere measurements for correlation.

METHODOLOGY

Measurements at the Plutonium Finishing Plant took place in a glove-box laboratory, which has an open area at one end sufficiently large to reduce interference from materials stored in the glove boxes. The closest glove box is approximately 4 m from the source position. The sources and phantoms were placed on aluminum stands at 1 m above a steel-reinforced concrete floor. The two closest concrete walls were approximately 3 m from the source and the other walls were approximately 8 m and 15 m from the source. The ceiling height was approximately 3 m.

The two phantoms that held the dosimeters were constructed of Lucite acrylic plastic. One phantom measured 40 cm square and the other 30 cm square, both with a thickness of 15 cm. Lucite slabs of 2.54-cm thickness (30 cm square) were taped together for the intervening shielding.

Neutron dose and spectrum measurements were performed with two different types of instruments: multisphere or Bonner sphere spectrometers and TEPCs. A brief description of these instruments is presented below; a more complete description and theory of operation is given in PNL-7881 (Brackenbush et al. 1991).

The multisphere spectrometer provides a coarse measurement of the neutron energy spectrum from thermal energies to 20 MeV, so that neutron dose equivalent can be calculated from the energy spectrum using published fluence-to-dose equivalent conversion coefficients (NCRP 1971). The multisphere spectrometer consists of a ^{6}LiI scintillator neutron detector that is inserted into polyethylene spheres of various sizes. Using the computer code SPUNIT (Brackenbush and Scherpelz 1983), it is possible to unfold an approximate neutron energy spectrum from the count rates from the different sphere sizes. The accuracy of the technique was verified by performing a spectral measurement with a NIST-traceable ^{252}Cf source and the fluence-to-dose equivalent conversion coefficient given in the National Bureau of Standards (NBS) Special Publication 633 for calibrating neutron dosimeters (Schwartz and Eisenhauer 1982). Several measurements with NIST-traceable neutron sources confirmed that the multisphere spectrometer consistently underestimated the dose equivalent rate by 9%, so the multisphere spectrometer results were increased by a factor of 1.09. The LiI crystal was slightly smaller than the one used for the response function calculations in the SPUNIT unfolding code.

The TEPC consists of a hollow sphere of tissue equivalent plastic filled with tissue equivalent (TE) gas. It measures the energy deposition in a known mass of TE gas and thus provides a direct measure of absorbed neutron dose. Using appropriate algorithms (Brackenbush et al. 1985), it is possible to determine the distribution of absorbed dose as a function of linear energy transfer (LET). Because quality factors are defined as a function of LET, it is possible to determine average neutron quality factors, and hence dose equivalent, directly from a single TEPC measurement. The accuracy of the TEPC was verified by measurements on a ^{252}Cf source with calibrations directly traceable to NIST in the Pacific Northwest Laboratory (PNL) Calibration Laboratory. At the beginning of the measurements, the dose equivalent determined by the TEPC was within 4% of the delivered dose equivalent from the NIST-traceable ^{252}Cf source. However, the TEPC experiences gain shifts with changes in temperature and impurities diffusing into the TE gas from the TE plastic wall, so accuracy deteriorates with time. In most instances, the TEPC determines dose equivalent within ±15% after several months. An internal alpha source was used to check for gain shifts before and after each TEPC measurement was completed.

The TEPCs were placed on opposite sides of the source at 1 m from the floor, and the phantoms were placed on opposite sides 90° from the TEPCs. The distance from the source varied from 50 cm to 1 m, coinciding with the distance at which the dosimeters were placed from the source. The TEPC measurements were taken with all dosimeter irradiations for the entire duration of each exposure. Irradiation times varied from overnight to more

than two weeks, depending on the source strength and the distance from the source. Background measurements with the sources removed from the room were also taken for correlation. Gamma measurements with a microrem meter were taken with each source at the same distances as above in order to quantify the contributing gamma dose. This was performed for each source and was repeated without the source for background measurement determination.

DOSIMETER DESIGN

The new Hanford neutron dosimeter consists of a package of two dosimeter designs which are physically attached to each other: 1) a beta/photon dosimeter with four TLD elements and 2) a neutron dosimeter with four TLD elements and two CR-39 foils.

The beta/photon dosimeter is based on the Harshaw 8825 design with four TLD-700 elements. The filtration is described in Figure 1 and in Table 1. The 8825 was modified from the standard design by substituting a TLD-700 for the TLD-600 neutron-sensitive element, since this dosimeter will be used only in combination with the 8816 neutron dosimeter. This allows for better discrimination of low- and mid-energy photons.

The neutron dosimeter is the Harshaw 8816 design with one TLD-700 and three TLD-600 elements. The filtration is described in Figure 2 and Table 2. Two CR-39 foils have been included in the design in order to provide capability for a technology with better neutron-energy response. The 8816 dosimeter will be used for the personnel neutron dose of record when the 8816 reports a neutron dose equivalent less than 50 mrem or greater than 1000 mrem. Otherwise, the dose equivalent calculated from the processed CR-39 elements will be used for the neutron dose of record.

DOSE CALCULATION

The basic methodology for neutron dose calculation for the 8816 dosimeter is based on the albedo effect. The NIST traceability is maintained for all sources used for beta, gamma, x-ray, and neutron calibrations.

The 8816 dose calculation algorithm can distinguish between bare and moderated ^{252}Cf spectra and will apply the appropriate calibration factors. Element 1 (TLD-700) is used for gamma background subtraction from the other three elements. After subtraction of the gamma component, the ratios of elements 2 to 4 and 3 to 4 are used for energy determination and dose calculation.

The 8825 beta/gamma dose calculation is a proprietary Harshaw algorithm that uses chip ratios to determine what calibration factors to apply.

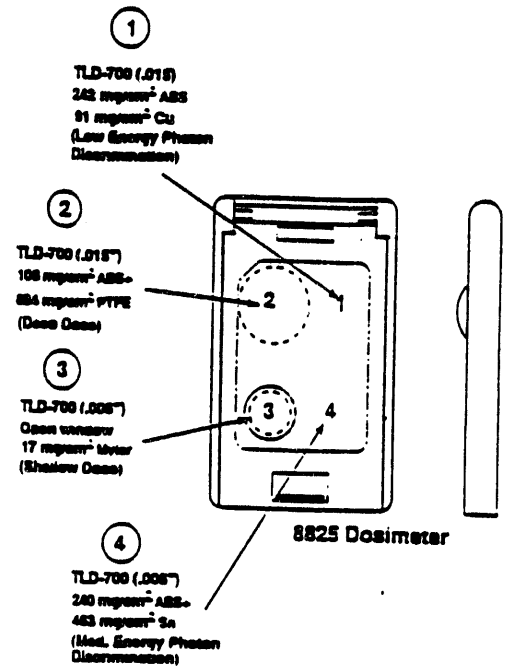


FIGURE 1. Hanford Combination Beta/Gamma Dosimeter

TABLE 1. Hanford Combination Neutron Dosimeter Holder Design

Dosimeter Position	Phosphor Type	Thickness, mil (mass density)	Total Holder Filtration[a]	
			Front	Back
1	TLD-700	15 (100 mg/cm^2)	464 mg/cm^2 Sn plus 80 mg/cm^2 ABS plastic	464 mg/cm^2 Sn plus 80 mg/cm^2 ABS plastic
2	TLD-600	15 (100 mg/cm^2)	461 mg/cm^2 Cd plus 80 mg/cm^2 ABS plastic	464 mg/cm^2 Sn plus 80 mg/cm^2 ABS plastic
3	TLD-600	15 (100 mg/cm^2)	464 mg/cm^2 Sn plus 80 mg/cm^2 ABS plastic	461 mg/cm^2 Cd plus 80 mg/cm^2 ABS plastic
4	TLD-600	15 (100 mg/cm^2)	464 mg/cm^2 Sn plus 80 mg/cm^2 ABS plastic	464 mg/cm^2 Sn plus 80 mg/cm^2 ABS plastic

(a) Values include Teflon (2 mil) used to enclose chips.

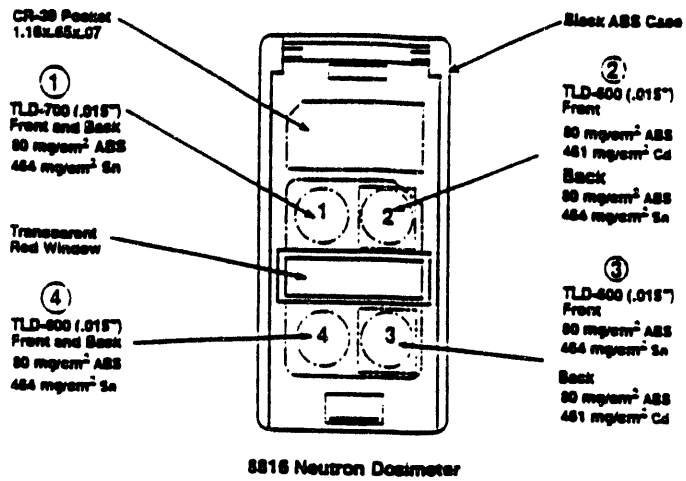


FIGURE 2. Hanford Combination Neutron Dosimeter

TABLE 2. Hanford Combination Beta/Gamma Dosimeter Holder Design

Dosimeter Position	Phosphor Type	Thickness, mil (mass density)	Total Holder Filtration[a]	
			Front	Back
1	TLD-700	15 (100 mg/cm^2)	242 cm^2 ABS[b] plastic plus 91 mg/cm^2 copper	173 mg/cm^2 ABS
2	TLD-700	15 (100 mg/cm^2)	1000 mg/cm^2 ABS and PTFE[c] plastic	173 mg/cm^2 ABS
3	TLD-700	6 (40 mg/cm^2)	17 mg/cm^2 Teflon and Mylar	173 mg/cm^2 ABS
4	TLD-700	15 (100 mg/cm^2)	240 mg/cm^2 ABS plastic plus 463 mg/cm^2 tin	173 mg/cm^2 ABS

(a) Values include Teflon (2 mil) used to enclose chips.
(b) ABS = acrylonitrile-butadiene-styrene.
(c) PTFE = polytetrafluoroethylene.

RESULTS

Table 3 shows the dose information for each irradiation that was made for each source, along with the pertinent geometry information.

TABLE 3. Dose Equivalent Rates as a Function of Distance for Shielded Plutonium Sources

Source/ Distance	Shielding	Neutron, mrem/h				Gamma, mrem/h	
		8816	TEPC	Multisphere	CR-39	8825	Rem meter
PuF_4 1 m	No shield	9.45	5.79	5.62	6.46	0.90	1.10
	1-in. shield	5.83	3.99	4.22	4.16	0.89	0.88
	2-in. shield	N/A	3.11	2.93	N/A	N/A	0.70
	3-in. shield	N/A	2.14	1.66	N/A	N/A	0.60
	4-in. shield	N/A	1.61	1.25	N/A	N/A	0.50
PuF_4 50 cm	No shield	35.4	20.6	19.6	21.5	3.10	4.00
	1-in. shield	15.5	15.2	14.9	12.8	2.90	3.20
	2-in. shield	18.0	9.93	9.46	9.94	2.80	2.80
	3-in. shield	10.3	6.21	6.50	4.97	2.22	2.10
	4-in. shield	10.9	3.94	3.83	4.08	2.12	1.90
PuO_2 50 cm	No shield	0.45	0.42	0.41	0.47	1.83	2.00
Metal 50 cm	No shield	0.70	0.53	0.50	0.59	1.76	2.20
Background (no source)		0.12	0.12	0.13	0.02	0.15	0.20
Glove Box 9		0.52	0.12	0.12	0.09	7.61	3.65

ANALYSIS

Table 4 shows the field calibration ratios of TLD results divided by measured dose for the plutonium tetrafluoride source and for the Glove Box 9 work area. Figure 3 overlays the source spectra for each of the sources used, with plutonium tetrafluoride shown as the bare source and as having 4-in. shielding.

The dosimeters are calibrated under low-scatter conditions with a bare ^{252}Cf source. This radiation geometry and low-scatter condition are required for conformance to U.S. Department of Energy Laboratory Accreditation Program (DOELAP) testing criteria. But in the workplace, dosimeters are exposed to a variety of different sources under high-scatter conditions. This is evidenced by Figure 4, which compares the measured spectra of the californium calibration source and the spectra of a glove box in the Plutonium Finishing Plant, which is representative of typical plutonium operations at Hanford. The lower energy neutrons in the workplace spectra produce a greater neutron dosimeter response per unit dose equivalent. Thus, it is necessary to introduce field-specific or site-specific correction factors to account for the differences in response to the neutron energy spectra. Note that much of the response of the TLD-albedo dosimeter originates from low-energy scattered neutrons with energies below about 10 keV. The scattering conditions in work areas are very

TABLE 4. Field Calibrations for Plutonium Tetrafluoride Source at 1 m and 50 cm and for Glove Box 9 Work Area

Source Distance/ Work Area	Shielding	8816	Average TEPC + Multisphere		Ratio
PuF_4 1 m	No shielding	9.45	5.71		1.63
	1-in. shielding	5.83	4.11		1.42
PuF_4 50 cm	No shielding	35.4	20.3		1.74
	1-in. shielding	15.5	15.1		1.03
	2-in. shielding	18.0	9.70		1.86
	3-in. shielding	10.3	6.36		1.62
	4-in. shielding	10.9	3.89		2.80
				Average	1.73
PuO_2	No shielding	0.45	0.41		1.09
Pu-Ga alloy	No shielding	0.70	0.52		1.35
Background	No source/shield	0.12	0.12		0.99
Glove Box 9		0.52	0.12		4.33

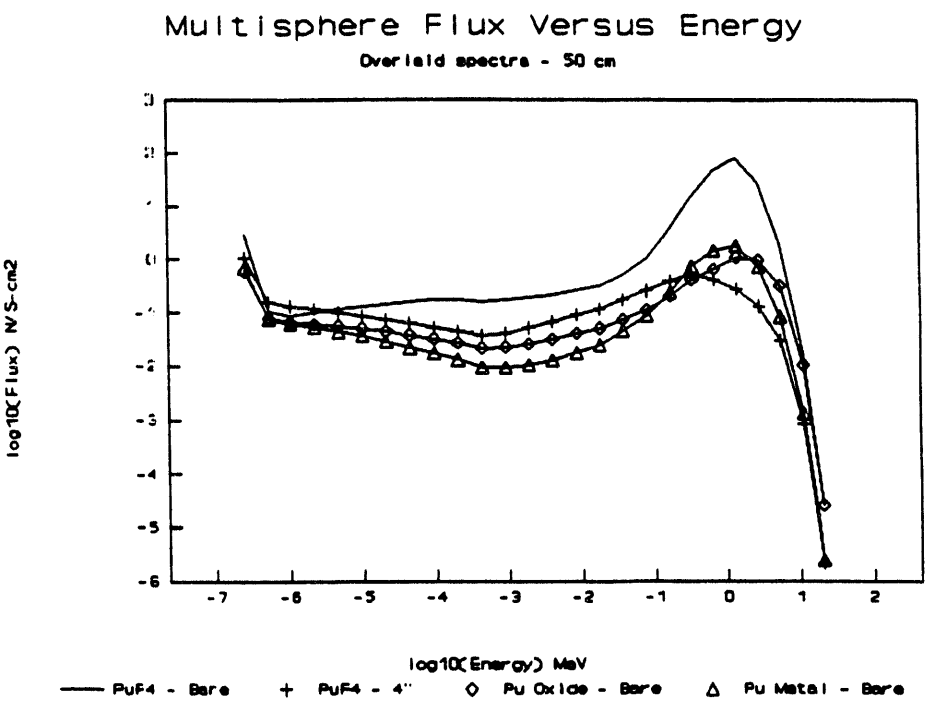


FIGURE 3. Overlaid Plutonium Source Spectra at 50 cm

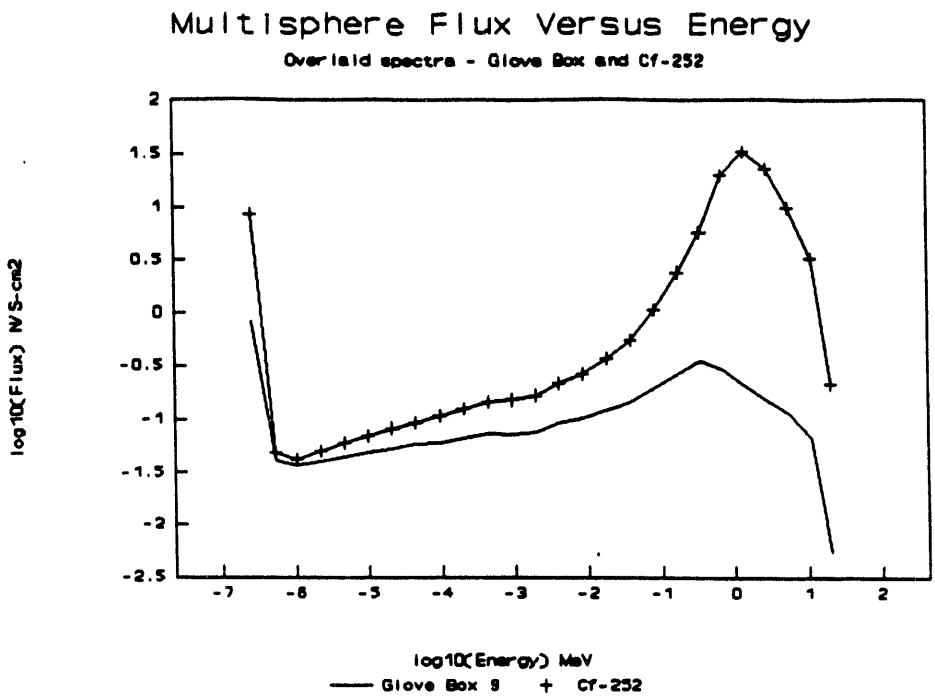


FIGURE 4. Neutron Energy Spectra from Glove Box 9 and Bare ^{252}Cf

important in determining dosimeter response. Any additional moderator, such as acrylic plastic walls of glove boxes or thick concrete floors and walls, can increase the TLD-albedo dosimeter response per unit dose equivalent.

CONCLUSION

Traditionally, the highest neutron exposures at Hanford have been the result of fluorination of plutonium. To minimize workers' doses, additional shielding has been placed around fluorination operations, which has produced changes in the neutron energy spectra and TLD-albedo dosimeter response per unit dose equivalent, as evidenced by Figure 3 and Table 4.

But the Hanford mission has changed from plutonium production, and plutonium fluoride is no longer being produced. Workers are now exposed to neutrons as the result of handling plutonium oxide or metal, and the neutron energy spectrum shown in Figure 4 is typical of glove-box operations at Hanford. Dosimeters were also exposed at 50 cm from cans of plutonium metal and plutonium oxide under the high-scatter conditions typical of workers packaging and moving plutonium. These spectra include low-energy neutrons scattered from the concrete floor and walls and room background.

The average correction factor for all of the measured spectra is 1.7 ± 0.5. When the TLD-albedo dosimeter is calibrated to a bare ^{252}Cf source at 50 cm in a low-scatter calibration facility, the indicated dose equivalent

must be reduced by a factor of 1.7 to account for the shift in neutron energy spectra.

The CR-39 dosimeters received sufficient dose to provide good counting statistics. Under these conditions, the ratio of the dose indicated by the CR-39 dosimeter divided by the delivered dose as measured by the average of the TEPC and multisphere spectrometer measurements was 0.99 ± 0.16 for all the measurements. If the delivered dose is above about 100 mrem and the sources are lightly shielded, the CR-39 dosimeter provides accurate results. But highly scattered spectra, such as those from the background measurements, have a large percentage of neutrons with energies below 100 keV. In one instance, the CR-39 dosimeter indicated a dose of 16% of that indicated by the TEPC and multisphere measurements. The CR-39 dosimeter is insensitive to neutrons below about 100 keV, so it may give questionable results. But this is an energy range in which the TLD-albedo dosimeter responds well, so that the ratio of TLD-albedo and CR-39 results may be used as a spectral indicator.

In general, the combination TLD-albedo and CR-39 nuclear track detector provided a reasonably accurate indication of dose equivalent when exposed to a wide variety of plutonium sources (metal, oxide, and fluoride) with varying amounts of moderator (0 in. to 4 in. of acrylic plastic).

ACKNOWLEDGMENTS

Pacific Northwest Laboratory is operated for the U.S. Department of Energy by Battelle Memorial Institute under Contract DE-AC06-76RLO 1830.

REFERENCES

Brackenbush, L.W., and R.I. Scherpelz. 1983. "SPUNIT, a Computer Code for Measuring Fast Neutron Flux Density." PNL-SA-11645, Pacific Northwest Laboratory, Richland, Washington.

Brackenbush, L.W., J.C. McDonald, G.W.R. Endres, and W. Quam. 1985. "Mixed Field Dose Equivalent Measuring Instruments." Radiat. Protect. Dosim. 10(1-4):307-318.

National Council on Radiation Protection and Measurements (NCRP). 1971. Protection Against Neutron Radiation. NCRP Report 38, NCRP Publications, Bethesda, Maryland.

Schwartz, R.B., and C.M. Eisenhauer. 1982. Procedures for Calibrating Neutron Personnel Dosimeters. NBS Special Publication 633, U.S. Department of Commerce/National Bureau of Standards, Washington, D.C.

FIELD EVALUATION OF BUBBLE DOSIMETERS AT LOS ALAMOS NATIONAL LABORATORY

L.L. Romero, J.M. Hoffman, and R.T. Devine
(Los Alamos National Laboratory, Los Alamos, NM 87545)

The longevity and stability of BD-100R bubble dosimeters purchased from Bubble Technology Industries have been evaluated to determine their use in personnel neutron dosimetry at Los Alamos National Laboratory. One hundred and fifteen dosimeters with varying degrees of sensitivity were evaluated over a period of one year. Fifty dosimeters were used routinely in various operations, and thirty seven dosimeters had some occasional use. Operational dosimeters were re-calibrated at three month intervals using Cf-252. The compressing mechanism of thirty two dosimeters failed after using the dosimeters over a period of time, therefore could not be re-calibrated. Preliminary results showed no significant changes in sensitivity over the one year period. However, dosimeters significantly under-responded at 350-400 bubbles per dosimeter due to the saturation associated with the image reading system.

PERSONAL NEUTRON DOSIMETRY -- CONVERSION FACTORS, CALIBRATION AND DOSIMETER PERFORMANCE

Wolfgang G. Alberts, Marlies Luszik-Bhadra and Bernd R.L. Siebert
Physikalisch-Technische Bundesanstalt, 38116 Braunschweig, Germany

Abstract

The recent recommendations on dose equivalent conventions established by ICRU and ICRP particularly affect neutron radiation. The change in the fluence-to-dose equivalent conversion factors requires a change in the desired response of a dosimeter as a function of energy of incident neutrons. This response can be investigated with monoenergetic neutron beams which are available at the PTB.

Performance of personal dosimeters with respect to the energy dependence of their response should also be tested in calibration fields providing well known, broad neutron spectra or in neutron fields encountered in routine surveillance. This can be done by calculations once the fluence response as a function of energy is known. This is demonstrated by two examples of recent investigations at the PTB involving the measurement of responses of personal dosimeters in the range from thermal neutrons up to 20 MeV, one dosimeter based on a track-etch technique and the other being a commercial electronic pocket dosimeter. The more or less strong dependence of the dose equivalent response on neutron energy favours the development of dosimeters with intrinsic spectrometric properties.

Introduction

Personal neutron dosimetry serves as a means of obtaining an estimate of the effective dose in order to limit radiation doses to individual workers and to demonstrate compliance with the full system of dose limitation (ICRP, 1982). For this purpose it has been recommended by the ICRP (ICRP, 1982) that the overall uncertainty of the estimation of the quantity to be measured should not exceed -33% or +50% (at the 95 % confidence level) where this quantity is in the order of the relevant annual limit, and -50% or +100% are considered to be acceptable where it amounts to less than 10 mSv.

The annual limits of exposure have been expressed (ICRP, 1991) in terms of the effective dose $E = \Sigma_T w_T \cdot H_T = \Sigma_T w_T \Sigma_R w_R \cdot D_{T,R}$, where w_T and w_R are tissue and radiation weighting factors, respectively. The quantity $D_{T,R}$, the mean absorbed dose *in an organ or tissue*, T, induced by radiation of Type R, cannot be evaluated experimentally (ICRU, 1993b), at least not in a mixed field, since the index R refers to type and energy of the *external radiation field*. Therefore, for radiation protection purposes, operational quantities have been introduced in terms of which dosimeters can be calibrated and which should provide a reasonable estimate of the body dose equivalents. For neutrons this was hitherto the "dose equivalent ceiling" (Harvey, 1975) which is the sum of maximum dose equivalents in a phantom generated by the energy components of the neutron spectrum using fluence-to-dose equivalent conversion factors (ICRP, 1971). Recently (ICRU, 1985, 1993b), the ambient dose equivalent, $H^*(10)$, for area monitoring and the personal dose equivalent, $H_p(10)$, for individual monitoring have been introduced. We will concentrate in this paper on the energy dependence of the response of personal dosimeters.

Although the variation of $H_p(10)$ with the directional distribution of the radiation field plays an important role, we consider energy dependence to be of prior importance. For purposes of simplification we consider here only irradiations in parallel neutron fields which are incident opposite to the reference orientation of the dosimeter.

The recent recommendations of the International Commission on Radiation Units and Measurements and of the International Commission on Radiological Protection have implications on radiation protection instrumentation. A general change is the decrease in the annual limit of the effective dose, which may require more sensitive dosimeters (Portal and Dietze, 1992). Other changes are incorporated in the neutron fluence-to-dose equivalent conversion factors and result from several changes in the dose equivalent concept:

- -- dose equivalent now at a fixed depth of 10 mm (ICRU, 1985, 1988),
- -- selection of new phantoms (ICRU sphere and ICRU slab phantom) (ICRU, 1985, 1992),
- -- formulation of a new quality factor definition, $Q(L)$, for charged particles as a function of the unrestricted linear energy transfer L in liquid water (ICRP, 1991),
- -- recommendation of new stopping powers for protons and α-particles in liquid water (ICRU, 1993a).

A detailed description of these changes has been presented elsewhere (Siebert and Alberts, 1994). The conversion factors have to be calculated since, in general, the dose equivalent $H = Q \cdot D$ also cannot be measured in mixed radiation fields. The response as a function of neutron energy can be investigated with monoenergetic neutron beams and tested with broad neutron spectra. Three examples of recent results obtained at PTB are presented in this paper.

Neutron fluence-to-dose equivalent conversion factors

Neutron dosimeters are usually calibrated in neutron fields the fluence of which is known together with its energy and angular distributions. For the calibration, fluence-to-dose equivalent conversion factors are needed in order to establish the conventional true value of the dose equivalent quantity.

Figure 1 shows the old and new fluence-to-dose equivalent conversion factors as a function of neutron energy and, for comparison, the conversion factors for the effective dose equivalent (calculated with the $Q(L)$ relation and the w_T values of ICRP 60) and the effective dose. $H_p(10)$ refers to the dose equivalent at 10 mm depth below the center of the front face of a 30 cm x 30 cm x 15 cm slab phantom made of ICRU tissue (ICRU, 1992). It is concluded from these curves that the changes of the conversion factors for the operational quantities are not dramatic. Applying the new conversion factors will result in some change of calibration factors of existing dosimeters; the change as a function of energy is in most cases less than the deviation from the desired curve of the fluence response.

Personal dosimeters and their calibration

Calibration of dosimeters means the determination of the calibration factor determined under specified calibration conditions. During the stage of development of a personal dosimeter, or during a type test, determinations of the response of a dosimeter are best performed using monoenergetic neutrons, which provide the most detailed information on physical response characteristics. The PTB maintains a complete set of such reference neutron fields. These include

- -- quasimonoenergetic reactor-based filtered neutron beams for thermal neutrons and energies of 186 eV, 2 keV, 24 keV and 144 keV (Alberts and Dietz, 1987),
- -- monoenergetic neutron fields produced with nuclear reactions using a Van-de-Graaff accelerator (Lesiecki *et al.*, 1987) for ISO energies up to 19 MeV.

The definition of the quantities in terms of which dosimeters can be calibrated is not sufficient to fully describe calibration conditions. For personal dosimeters, since most of them indicate at least partly radiation backscattered from the person or the phantom, the irradiation

must take place on an appropriate phantom; geometry and phantom have to be prescribed. The phantom used for the measurements described in this paper is a PMMA phantom having the same size as the above mentioned ICRU slab phantom. ISO is at present working on an International Standard (ISO, 1994) which defines a set of conversion factors for the reference neutron radiations (ISO, 1989) and states that, for calibration and determining the response as a function of neutron energy and angle of incidence, personal dosimeters must be irradiated on an "ISO water slab phantom" having the same size as above but consisting of PMMA walls (front wall 2,5 mm thick, all other walls 10 mm thick) and filled with water. The results shown here are believed to differ only marginally from those to be expected with the ISO phantom.

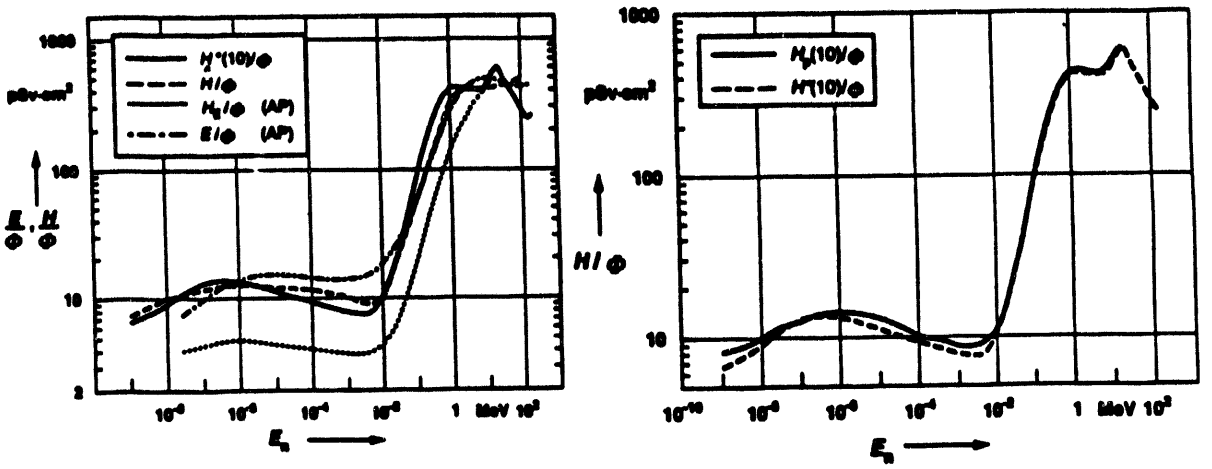


Figure 1. Left: Neutron fluence-to-dose equivalent conversion factors as a function of neutron energy E_n for the maximum dose equivalent H (ICRP, 1971), for the effective dose equivalent H_E (ICRU, 1993b) (see text) and for the new quantities based on ICRP 60 recommendations (ICRP, 1991), namely the ambient dose equivalent $H^*(10)$ and the effective dose E. Right: $H_p(10)$ is the personal dose equivalent (see text).

Such calibrations determine the fluence response $R_\Phi = M/\Phi$ (M dosimeter reading, Φ neutron fluence) as a function of neutron energy. The desirable shape of such curves would be that of the appropriate fluence-to-dose equivalent conversion factor, h_Φ: $R_\Phi(E) \sim h_\Phi(E)$. All personal dosimeters in use show responses which deviate - in most cases even markedly - from the desired shape, restricting their use (with one single calibration factor) to working environments for which an appropriate calibration factor has been established.

Recently, a passive dosimeter has been developed at the PTB (Luszik-Bhadra, 1994a, 1994b) the response of which quite well matches the desired response over the whole energy range up to 20 MeV and which in addition exhibits some spectrometric properties. A sketch of this dosimeter is presented in Figure 2: it is based on a single CR-39 etched track detector covered with three different converters thus providing three different responses at the respective sub-areas of the detector. These responses are made visible as shown in Figure 2 by three etched CR-39 detectors after irradiations with thermal, intermediate and fast neutrons, respectively. Due to the encapsulation and converters partially containing boron compounds the dosimeter is chiefly sensitive to thermal neutrons behind the "beta window" (Position 1, see Figure 2), to intermediate neutrons by means of the albedo effect at the sub-area behind the "albedo window" (Position 2) and to fast neutrons (above 70 keV) over the whole detector. Figure 3 shows the fluence response, R_Φ, of the sub-area at the "albedo position" as a function of neutron energy (Dosimeter LB2) together with the conversion factor, $h_{p\Phi}(10)$ (in pSv cm^2). R_Φ for the etched-track dosimeter is dimensionless, since it is the ratio of the track density (in cm^{-2}) and the fluence (in cm^{-2}); values between thermal and 2 keV were calculated. The response of Dosimeter LB2 is scaled to match the conversion factor in the fast-neutron region resulting in an overresponse below 70 keV.

A linear combination of the three responses in the three sub-areas shown in Figure 2 (Dosimeter LBS) can be derived (Siebert *et al.*, 1983), resulting in an optimized response as function of energy. The curve exhibits a small underresponse between about 2 keV and 100 keV. For comparison, a further curve (□) in Figure 3 shows the fluence response of a commercial, light-weight electronic pocket dosimeter (Dosimeter JPN) which has recently been tested at the PTB reference fields (Alberts *et al.*, 1994). The curve has been interpolated between 25 meV (thermal) and 186 eV in order to have a basis for the calculations described below. Since the reading of this dosimeter is in terms of dose equivalent (mSv), the fluence response is in pSv·cm^2.

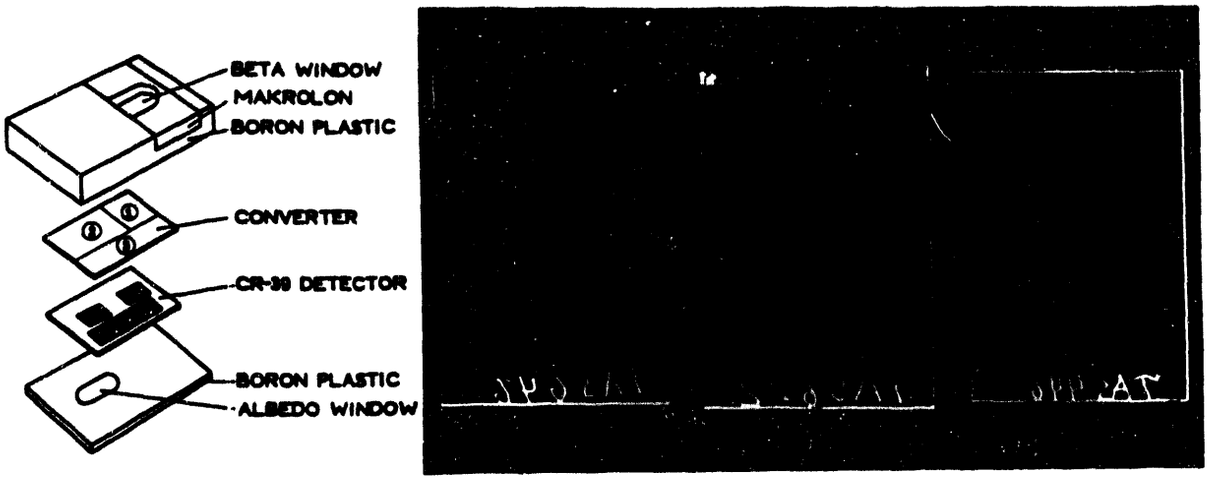


Figure 2. Sketch of the recently developed dosimeter and some etched CR-39 detectors after irradiation with (from left to right) thermal, 24 keV and 5 MeV neutrons.

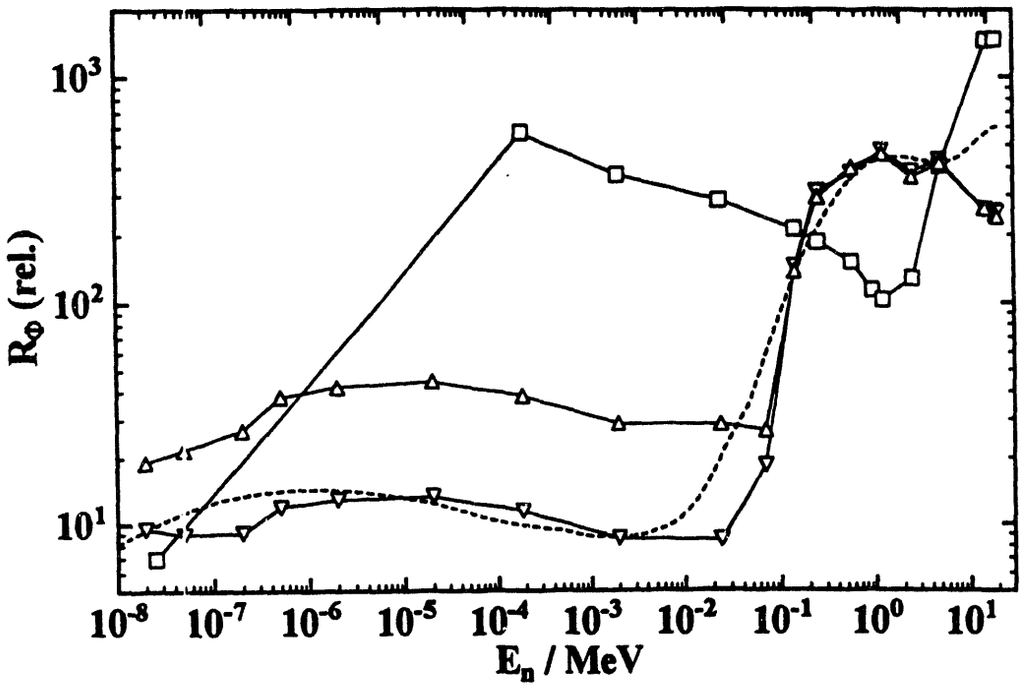


Figure 3. Fluence response of the personal dosimeters as described in the text and the conversion factor $h_{p,\beta}(10)$ as a function of neutron energy. (Δ) one-element (LB2) and (▽) three-element (LBS) etched-track dosimeter and (□) electronic pocket dosimeter.

Dosimeter performance in neutron fields with broad spectra

Whereas the information gained with monoenergetic neutrons is essential for the developer of a dosimeter, it does not immediately provide information on the expedience of its use in broad neutron spectra. Therefore, calibration laboratories provide some reference neutron fields with such spectra which should at least approximately represent spectra encountered in workplaces and which are used for routine calibrations. Four of such spectra, realized in a 7 m x 7 m and 6,5 m high concrete-walled room at the PTB (Kluge, 1984) are shown in Figure 4. They are produced by a ^{252}Cf neutron source, positioned in the middle of the room, bare or moderated by a 30-cm diameter D_2O sphere, free in air at 170 cm distance from the source or behind a shadow cone. The figure displays the fluence spectrum $\Phi_E(E)$ as well as $\Phi_E(E) \cdot h_{p\Phi}(E)$, the "personal-dose equivalent spectrum" which is the fluence spectrum weighted with the conversion factor. The spectra have been normalized to a fluence of 1 cm^{-2} and to a dose equivalent of 1 mSv, respectively. Comparison of these spectra shows the degree to which energy regions contribute to the total fluence or to the total dose equivalent.

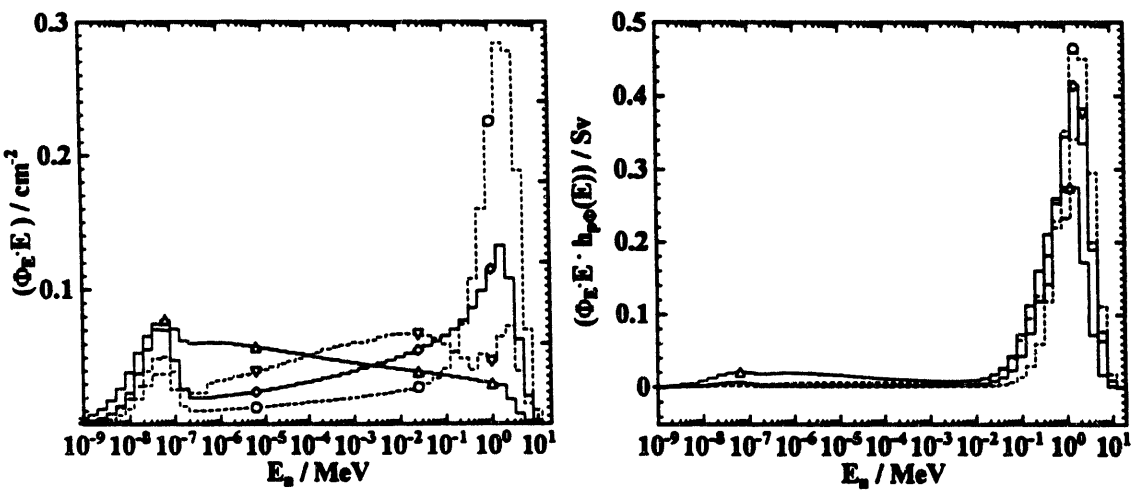


Figure 4. Fluence spectra (left) and dose equivalent spectra (right) for four reference neutron fields at the PTB calibration facility. These are (O) ^{252}Cf (bare), (∇) ^{252}Cf (D_2O-moderated), and scattered spectra produced by positioning a shadow cone between source and detector, with (◊) ^{252}Cf (bare) and (Δ) ^{252}Cf (D_2O-moderated).

Once the energy-dependent response of a dosimeter is known one can investigate its performance in broad neutron spectra by means of calculations. We have investigated the expected response in a number of spectra encountered in routine surveillance at reactors taken from Ing and Makra (1978), Griffith *et al.*, (1990) and other sources which are presently being combined into a spectrum catalogue (Naismith, 1994) in the framework of a CEC contract and under the auspices of EURADOS Working Group 7. We have added to the spectra available in that catalogue four artificial spectra which were constructed so as to approximately reproduce the relative dose equivalent proportions of realistic spectra found in Swiss reactors (Aroua *et al.*, 1994). They are displayed in Figure 5, again as fluence spectra and as "personal-dose equivalent spectra", normalized as before and denoted A to D in the order of spectrum "hardness".

The data in Table 1 characterize the spectra of Figures 4 and 5 with respect to the (spectrum-averaged) fluence-to-personal dose equivalent conversion factors, $h_{p\Phi}(10)$, which range from about 16 pSv cm^2 to 270 pSv cm^2, and the fractions of personal dose equivalent and fluence in three energy ranges.

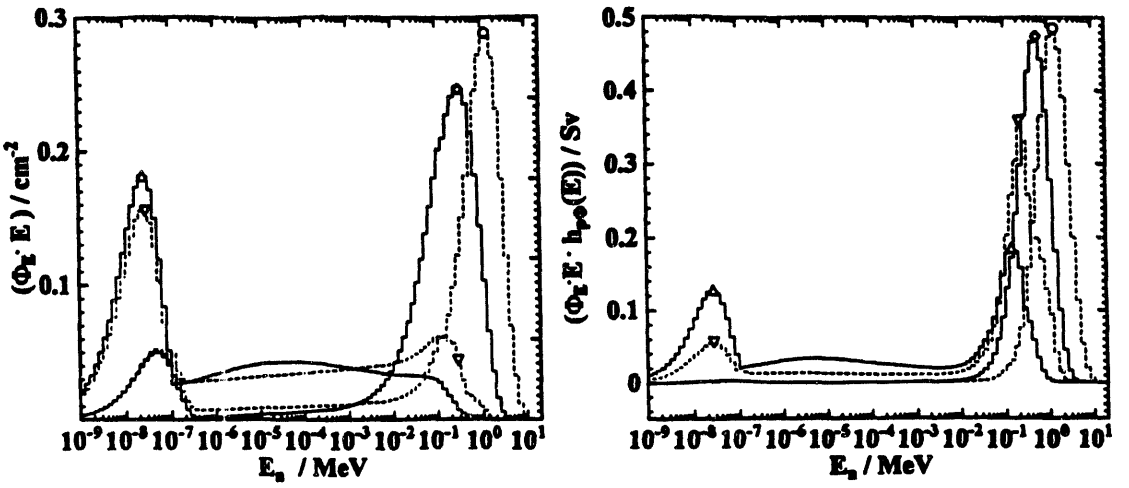


Figure 5. Fluence spectra (left) and dose equivalent spectra (right) as a function of neutron energy for four artificially constructed spectra representing the types given by Aroua et al. (1994). (Δ) Type A, (∇) Type B, (◊) Type C and (○) Type D.

Table 1. Characterization of the spectra of Figures 4 and 5. mod: moderated, sc: fields of scattered neutrons behind a shadow cone.

Spectrum	$h_{p\Phi}(10)$ in pSv·cm^2	Fraction of Dose Equivalent in %			Fraction of Neutr. Fluence in %		
		Region 1	Region 2	Region 3	Region 1	Region 2	Region 3
Calibration spectra							
Cf(mod,sc)	45,9	8	26	66	29	63	8
Cf(mod)	83,8	2	18	80	15	68	17
Cf(bare,sc)	140	2	10	88	19	49	32
Cf(bare)	269	< 1	4	96	10	26	64
Reactor spectra							
Type A	16,2	34	59	7	51	49	< 1
Type B	32,0	16	51	33	45	52	3
Type C	160	1	26	73	13	52	35
Type D	261	< 1	6	94	15	23	62

Region 1: E_n < 0,4 eV; Region 2: 0,4 eV to 0,2 MeV and Region 3: E_n > 0,2 MeV

In order to check the performance of the personal dosimeters dealt with here in the spectra of Figures 4 and 5, these spectra were folded with the energy-dependent personal-dose equivalent response ($R_H = M/H_p(10) = R_\Phi/h_{p\Phi}(10)$). Table 2 shows the results for the three dosimeters (see Figure 3).

Table 2. Relative dose-equivalent responses of three personal dosimeters in the spectra of Figures 4 and 5. mod: moderated, sc: fields of scattered neutrons behind a shadow cone. LBS and LB2 (etched-track dosimeters) and JPN (electronic dosimeter) responses are relative to that to ^{252}Cf (bare) neutrons, whereas the column JPN shows the actual dose equivalent response values (dimensionless, see text) in the various spectra.*

Spectrum	$h_{p\Phi}(10)$ in $pSv \cdot cm^2$	R_H (rel.)			
		LBS	LB2	JPN	JPN*
Calibration spectra					
Cf(mod,sc)	45,9	1,01	1,41	3.97	5,75
Cf(mod)	83,8	0,99	1,17	2,84	4,03
Cf(bare,sc)	140	1,02	1,08	1,40	2,03
Cf(bare)	269	1,00	1,00	0,70	1,00
Reactor spectra					
Type A	16,2	0,94	1,98	9,36	12,6
Type B	32,0	1,03	1,51	4,75	7,00
Type C	160	1,10	1,14	1,00	1,58
Type D	261	1,03	1,04	0,54	0,81

Figures 6 to 8 show the dose-equivalent responses in more than 100 reactor neutron spectra of the aforementioned catalogues, $h_{p\Phi}$ ranging from about 13 to 450 $pSv \cdot cm^2$. They are displayed as the dose equivalent response divided by the average fluence-to-personal dose equivalent conversion factor characterizing the respective spectrum vs. that conversion factor.

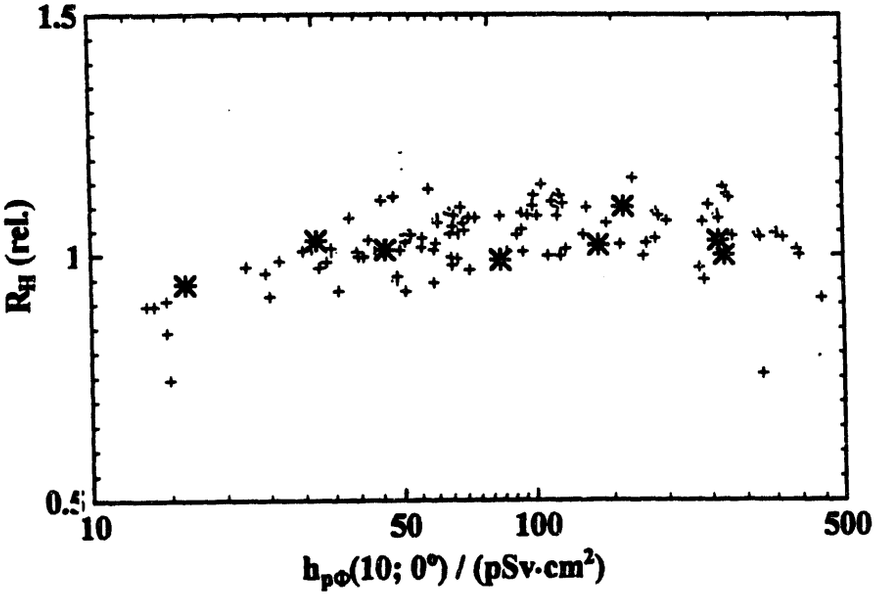


Figure 6. Dose-equivalent responses of the three-element CR-39 etched-track dosimeter (LBS) to a variety of "practical neutron spectra", ordered according to their spectrum-averaged fluence-to-dose equivalent conversion factor. The responses are displayed as ratios $R_H/h_{p\Phi}$, normalized to unity for Cf (bare) neutrons.

The points representing the responses in the four calibration fields (Figure 4) and the four representative reactor spectra (Figure 5) are marked with special symbols. The response of an ideal dosimeter should exactly reproduce the conversion factor, the respective points in the graph should all be at the value of unity. The graph therefore represents the range of deviation of the response in the respective spectra from the correct one.

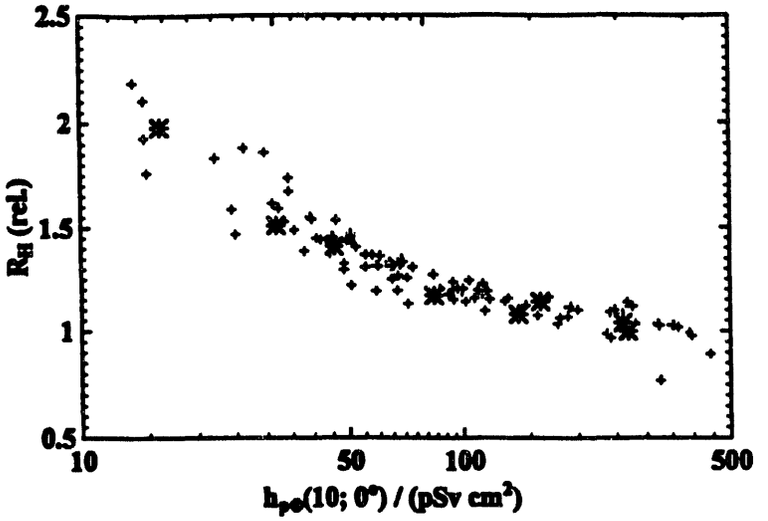


Figure 7. Dose-equivalent responses of the CR-39 detector behind the "albedo window" (LB2) of the dosimeter described in the text to a variety of "practical neutron spectra", ordered according to their spectrum-averaged fluence-to-dose equivalent conversion factor. The responses are displayed as ratios $R_H/h_{p\Phi}$, normalized to unity for Cf (bare) neutrons.

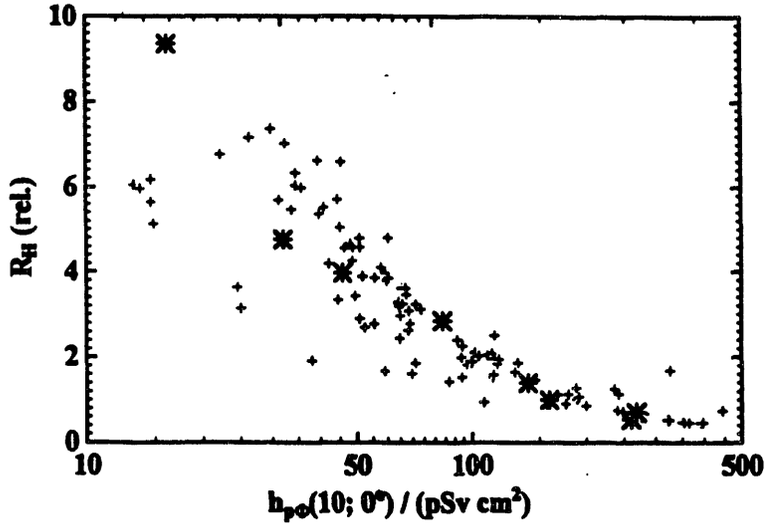


Figure 8. Dose-equivalent responses of the electronic pocket neutron personal dosimeter (JPN) to a variety of "practical neutron spectra", ordered according to their spectrum-averaged fluence-to-dose equivalent conversion factor. The responses are displayed as ratios $R_H/h_{p\Phi}$.

With two exceptions at the lower and the upper end of the range of spectra the responses for the three-element passive etched-track dosimeter (Figure 6) deviate less than 20 % from the true value if its calibration factor is unity in the "hardest" of the calibration spectra, *i.e.* that from the bare ^{252}Cf neutron source. For the element below the "albedo window" of the same dosimeter Figure 7 exhibits an increasing overresponse up to a factor of two for the "softest"spectra, which is to be expected from the overresponse below 70 keV seen in Figure 3. For the electronic dosimeter the deviations are much larger (Figure 8) as again to be expected from the response as a function of energy.

Concluding remarks

Monoenergetic neutron fields are an appropriate means for studying the response of personal dosimeters in the development stage and during type tests. Furthermore, the response as a function of energy allows a numerical evaluation of the performance of a dosimeter in a large variety of spectra using a spectrum catalogue. Such calculations provide a criterion for the deviations of the dosimeter readings in practical neutron fields. They should be verified in well known reference neutron fields with broad spectra.

Whereas the electronic dosimeter investigated here does not yield satisfactory results in reactor environments, multi-component dosimeters seem to be a promising approach towards a better response in different neutron fields. The three-element track dosimeter described in this paper furthermore allows a simple calculational adjustment of its response as a function of energy in three energy regions (thermal, intermediate and fast) without changing the design, since the response of the three components (sub-areas of the track detector to be read out individually) can be changed arbitrarily. The use of just one track detector, namely that behind the "albedo window" may also be a useful solution. This, however, will require some rough knowledge about the spectrum in which it is used, obtainable, for instance, by the ratio of the readings of two Bonner spheres (*e.g.* the 9"/3" ratio).

The new conversion functions resulting from the recent ICRP and ICRU recommendations change the required response as a function of energy, but only to a degree which does not alter the basic considerations for the design of personal neutron dosimeters.

Acknowledgement: This work was supported in part by the European Commission under Contract No. FI3P-CT92-0002.

References

Alberts, W.G. and E. Dietz (1987). *Filtered Neutron Beams at the FMRB -- Review and Current Status*. PTB-FMRB-112. Physikalisch-Technische Bundesanstalt, Braunschweig, Germany.

Alberts, W.G., E. Dietz, S. Guldbakke and H. Kluge (1994). *Response of an Electronic Personal Neutron Dosemeter*. Radiat. Prot. Dosim. 51, p. 207-210.

Aroua, A., M. Boschung, F. Cartier, M. Grecescu, S. Prêtre, J.-F. Valley and Ch. Wernli (1994). *Characterisation of the Mixed Neutron-Gamma Fields Inside the Swiss Nuclear Power Plants by Different Active Systems*. Radiat. Prot. Dosim. 51, p. 17-25.

Griffith, R.V., J. Palfalvi and U. Madhvanath (1990). *Compendium of Neutron Spectra and Detector Responses for Radiation Protection Purposes*. Technical Reports Series No. 318. International Atomic Energy Agency, Wien, Austria.

Harvey, J.R. (1975). *An Approach to the Surveying of Radiation Environments for Radiation Protection Purposes*. Phys. Med. Biol. 20, p. 1003-1006.

ICRP (1971). *Data for Protection against Ionizing Radiation from External Sources: Supplement to ICRP Publication 15*. Publication 21. International Commission on Radiological Protection, Pergamon Press, Oxford, U.K.

ICRP (1982). *General Principles of Monitoring for Radiation Protection of Workers.* Publication 35. International Commission on Radiological Protection, Pergamon Press, Oxford, U.K.

ICRP (1991). *Recommendations of the ICRP.* Publication 60. International Commission on Radiological Protection, Pergamon Press, Oxford, U.K.

ICRU (1985). *Determination of Dose Equivalents Resulting from External Radiation Sources.* Report 39. International Commission on Radiation Units and Measurements, Bethesda MD.

ICRU (1988). *Determination of Dose Equivalents from External Radiation Sources -- Part 2.* Report 43. International Commission on Radiation Units and Measurements, Bethesda MD.

ICRU (1992). *Measurement of Dose Equivalents from External Photon and Electron Radiations.* Report 47. International Commission on Radiation Units and Measurements, Bethesda MD.

ICRU (1993a). *Stopping Powers and Ranges for Protons and Alpha Particles.* Report 49. International Commission on Radiation Units and Measurements, Bethesda MD.

ICRU (1993b). *Quantities and Units in Radiation Protection Dosimetry.* Report 51. International Commission on Radiation Units and Measurements, Bethesda MD.

Ing, H. and S. Makra (1978). *Compendium of Neutron Spectra in Criticality Accident Dosimetry.* Technical Reports Series No. 180. International Atomic Energy Agency, Wien, Austria.

ISO (1989). *Neutron reference radiations for calibrating neutron-measuring devices used for radiation protection purposes and for determining their response as a function of neutron energy.* International Standard ISO 8529. International Organization for Standardization, Genève, Switzerland.

ISO (1994). *Reference Neutron Radiations: Calibration of Area and Personal Dosimeters and the Determination of Their Response as a Function of Neutron Energy and Angle of Incidence.* Working Document ISO/TC85/SC2/WG2 8529-3. International Organization for Standardization, Genève, Switzerland.

Kluge, H. (1984). *Standard Irradiation Facility for the Calibration of radiation Protection Instruments Employing Radionuclide Sources.* Compacts 6th IRPA Congress, Berlin, Germany, Vol. III, p. 1161-1164.

Lesiecki, H., M. Cosack and H. Schölermann (1987). *Monoenergetic Neutron Fields for the Calibration of Neutron Dosemeters at the Accelerator Facility of the PTB.* PTB-Mitteilungen 97, p. 373-376.

Luszik-Bhadra, M., W.G. Alberts, F. d'Errico, E. Dietz, S. Guldbakke and M. Matzke (1994a). *A CR-39 Track Dosemeter for Routine Individual Neutron Monitoring.* Radiat. Prot. Dosim. (in press)

Luszik-Bhadra, M., W.G. Alberts, E. Dietz, E. Piesch and B.R.L. Siebert (1994b). *CR-39 Track Neutron Dosemeter/Spectrometer: Investigations in the Thermal, Epithermal and Intermediate Energy Region.* 17th International Conf. on Nuclear Tracks in Solids, Dubna, Russia, 24-28 August 1994. To be published in Radiation Measurements.

Naismith, O. (1992). *Personal Communication.* National Physical Laboratory, Teddington, U.K.

Portal, G. and G. Dietze (1992). *Implications of new ICRP and ICRU Recommendations for Neutron Dosimetry.* Radiat. Prot. Dosim. 44, p. 165-170.

Siebert, B.R.L., R. Hollnagel and R. Jahr (1983). *A Theoretical Concept for Measuring Doses from External Radiation Sources in Radiation Protection.* Phys. Med. Biol. 28, p. 521-533.

Siebert, B.R.L. and W.G. Alberts (1994). *The Impact of Recent ICRU and ICRP Publications on Radiation Protection Against Neutrons.* Proc. 8th Internat. Conf. on Radiation Shielding, Arlington TX. American Nuclear Society, La Grange Park IL, p. 25-32.

ANGULAR VARIATION OF THE PERSONAL DOSE EQUIVALENT, $H_p(0.07)$, FOR BETA RADIATION AND NEARLY MONOENERGETIC ELECTRON BEAMS: PRELIMINARY RESULTS.

T. A. da Silva* and C. G. Soares
National Institute of Standards and Technology,
Gaithersburg, Maryland 20899

Abstract - Using the NIST standard beta-particle radiation sources, as well as the NIST nearly-monoenergetic electron beams, the angular variation of the personal dose equivalent, $H_p(0.07)$, was experimentally determined. Measurements were performed with the NIST standard extrapolation chambers, and with thermoluminescent detectors covered with 7-mg/cm^2 thickness of tissue equivalent material on a slab phantom. Extrapolation chamber correction factors, which are functions of energy and angle of incidence, were determined.

INTRODUCTION

The personal dose equivalent, $H_p(d)$, is the radiation protection quantity recommended by the International Commission on Radiation Units and Measurements (ICRU) for individual monitoring. $H_p(d)$ is defined in soft tissue, at a depth d below a specified point on the body. The recommended depth for beta particle and other weakly penetrating radiations is 0.07 mm for the skin. $H_p(0.07)$ can be measured with a nearly tissue equivalent detector worn on the body and covered with 7 mg/cm^2 of tissue-equivalent material. The calibration quantity to be used is $H_p(0.07)$ in an ICRU tissue phantom having the same dimensions and shape as the calibration phantom. Definition and calibration guidelines on $H_p(0.07)$ are given and discussed in several publications[1, 2, 3, 4, 5].

The value of $H_p(0.07)$ depends on the direction of the radiation relative to the phantom surface. The angular variation of $H_p(0.07)$ can be obtained with an instrument which determines the dose equivalent at the appropriate depth in the plane slab of tissue-equivalent material. An extrapolation chamber and thermoluminescent detectors were used by Christensen[6] and Böhm[7] to measure the angular dependence correction factors of $H_p(0.07)$, for the ISO reference beta radiations[8]. Recently, Monte Carlo calculations, in different phantoms, were also performed for monoenergetic electrons by Seltzer[9] and Hirayama[10].

---

* On leave from Instituto de Radioproteção e Dosimetria, CNEN, and Programa de Engenharia Nuclear, COPPE/UFRJ, Rio de Janeiro, RJ, Brazil.

The NIST standard beta-particle radiation sources[11], as well as the NIST nearly-monoenergetic electron beams[12], were used to determine the angular variation of $H_p(0.07)$. Measurements were performed with two NIST extrapolation chambers and graphite-mixed MgB_4O_7:Dy thermoluminescent detectors.

This paper presents results obtained with the $^{90}Sr/^{90}Y$ and ^{204}Tl sources and with nearly monoenergetic electron beams with average energies of 220 keV and 340 keV. The measured perturbation correction factor of the NIST extrapolation chamber is also shown for each angle of incidence and radiation energy.

MATERIAL AND METHODS

Radiation sources

The NIST standard beta-particle fields are similar to the ISO reference beta radiations[8]. The radiation fields are produced by encapsulated beta-particle sources which can be held on a stand equipped with a shutter and flattening filters. Characteristics of the NIST standard fields used in this work are shown in table 1.

The two NIST nearly monoenergetic electron beams used in this work were produced with the NIST 500-keV cascaded-rectifier electron accelerator. The irradiation setup is similar to that described by Soares[12], but, four fast plastic scintillator-plus-photomultiplier detectors were placed in the beam periphery for monitoring spatial and intensity fluctuations of the electron beam. Measurements were done with accelerator potentials of 300 kV and 400 kV. Electron beam spectra generated by both, at a distance of 30 cm from the exit window, had resolutions better than 20% and average energies of 220 keV and 340 keV, respectively.

The extrapolation chamber

The two NIST extrapolation chambers were similar to chambers designed by Böhm[13], with an entrance window of 2.6-mg/cm^2 graphite-coated polyethylene terephthalate (PTP) foil. During the measurements they were covered with 5.0-mg/cm^2 thickness of PTP foil, to simulate the depth of 7.0 mg/cm^2 in tissue. The fully automated extrapolation chamber[14] used at the beta-particle source facility allowed several sets of measurements to be made to obtain good statistics. With the manually-operated chamber, which was used in the accelerator facility, at least 5 measurements were performed at both polarities of the voltage applied to the chamber. The measured ionization current was corrected by all factors established at NIST by Pruitt[11], except for the perturbation correction factor, which was determined during this work. Extrapolation curves to determine the absorbed dose rates were obtain in the air-gap range of 0.7 mm to 1.5 mm.

Determination of the perturbation correction factor

The perturbation correction factor was determined following procedure described by Böhm[15]. Polymethyl methacrylate (PMMA) rings about 1 mm in thickness and of the same inner diameter as that of the sensitive volume of the chamber (60 mm) were fastened to the front surface of the chamber. Ionization current was measured at a fixed air gap of 0.7 mm, with +10 V and -10 V applied to the chamber. Measurements were performed for each radiation source and angles of incidence from 0° to 75°.

The ratio between the ionization current measured with no ring, I(0), and with a ring of thickness t fastened to the chamber, I(t) was measured for each radiation source at each angle. The perturbation correction, k_{pert}, was assumed to be given by $k_{pert} = 1 + bx$, where b is the slope of the straight line that fits the ratios close to a desired air gap range (usually 0.5 to 2.5 mm) and x is the air gap. Examples of the curves I(0)/I(t) versus ring thickness for the $^{90}Sr/^{90}Y$ source with the flattening filter and for the electron beam with average energy of 340 keV are shown in figures 1 and 2. The errors bars in these figures represent one standard deviation.

The measured b-values used to calculate the perturbation correction factors, for beta-particle sources at each angle of incidence, are given in table 2. They were estimated for the air gap range of 0.7 to 2.5 mm with the extrapolation chamber covered with 5.0-mg/cm^2 thickness of PTP foil. Uncertainties in b-values are given by one standard deviation.

The b-values for the electron beams could not be determined accurately due to high uncertainties in the measurements produced by instability of the electron beam. The perturbation was assumed to be negligible compared to the uncertainties for both electron beams used at angles between 0° to 60°. At 75°, b-values are 0.015 ± 0.005 mm^{-1} and 0.026 ± 0.004 mm^{-1}, for the average energy of 220 keV and 340 keV, respectively.

Thermoluminescent detectors

Graphite-mixed sintered MgB_4O_7:Dy thermoluminescent (TL) detectors with 3% graphite from Boris Kidric Institute, Belgrade, Yugoslavia[16] were used in this work. They are pellets of 4.7-mm diameter and 0.9-mm thickness with an effective thickness of 2mg/cm^2 since the graphite reduces their light transparency. A set of MgB_4O_7:Dy TL detectors was selected with dispersion (one standard deviation) lower than 2%. Individual sensitivity correction factors were determined and applied to all measurements. A 2000A Harshaw TL reader connected to a data acquisition system was used to integrate the TL signal and to record glow curves. The heating cycle of 30 s with a temperature rate of 10 °C/s between 100 °C to 300 °C was adopted. Integration of the TL signal was done between 100 °C and 225 °C. The heating cycle was enough to completely read out the

dosimeter, with no measurable residual TL signal, so no pre-irradiation annealing was needed. Only a pre-readout annealing of 100 °C for 20 minutes was used to ensure good reproducibility in the measurements.

Determination of $H_p(0.07)$ was assumed to be given by measurements with calibrated MgB_4O_7:Dy TL detectors covered with 7-mg/cm^2 thickness of PTP foil on a PMMA phantom.

RESULTS AND DISCUSSION

The angular dependence of $H_p(0.07)$ in the slab phantom is given by variation of the ratio $H_p(0.07;\alpha)$ / $H_p(0.07;0)$ at each angle of incidence, α, in degrees. Results obtained with the extrapolation chamber and with the MgB_4O_7:Dy, for the beta-particle sources, are shown in figure 3. Error bars are given by one standard deviation. Values accepted by the International Organization for Standardization (ISO)[8] are also shown for comparison purpose. Numerical values are given in tables 3, 4 and 5.

The angular variation of the $H_p(0.07)$ is a result of three competing processes: backscattering, build-up and attenuation. The angular incidence has the geometrical effect of increasing the path of the beta particles, since the actual thickness of tissue that covers the detector becomes greater than its nominal value.

Beta particles from the $^{90}Sr/^{90}Y$ source without filter reach the point of measurement without significant loss in their energy. At normal incidence, they suffer only a small absorption in the depth of 7 mg/cm^2. As the angle of incidence increases, the build-up effect occurs and after a certain angle, which corresponds to the peak in the depth-dose curve[11], attenuation is predominant. The presence of a flattening filter with the $^{90}Sr/^{90}Y$ increases the mean scattering angle and reduces the build-up effect of the beta particles that reach the detector. Results for the angular incidence of beta particles from ^{204}Tl showed that attenuation is the predominant effect.

For the beta particle sources, the ratio $H_p(0.07;\alpha)/H_p(0.07;0)$ obtained with the NIST extrapolation chamber showed good agreement with the ISO values, although deviations of about 4% were found at large angles of incidence. Results obtained with the MgB_4O_7:Dy agreed reasonably with those of the NIST extrapolation chamber (deviations about 8% were found at large angles).

The angular dependence of $H_p(0.07)$ in a slab phantom for nearly monoenergetic electron beams of 220 keV and 340 keV are shown in figure 4. Error bars for the extrapolation chamber values represent one standard deviation. Numerical values are given in table 6. Calculated values of monoenergetic electron beams, from Seltzer[10], for 100 keV, 200 keV and 400 keV are also shown for comparison purposes.

Results obtained with the MgB_4O_7:Dy showed deviations about 10% from those with the NIST extrapolation chamber, at large angles of incidence. The remarkable difference between the measured and the calculated results has not been explained. However, it might be attributed to the air scattering in the experimental beta radiation field. Calculated values were based on theoretical monoenergetic and monodirectional electron beams, where air interactions were not considered.

CONCLUSIONS

The angular dependence of the personal dose equivalent, $H_p(0.07)$, for beta-particle sources, which was measured with the NIST extrapolation chamber covered with 5.0 mg/cm^2 of PTP foil showed a good agreement with results recommended by ISO. The graphite-mixed MgB_4O_7:Dy TL detector covered with 7 mg/cm^2 of PTP foil exhibits an angular variation of response reasonably similar to that of $H_p(0.07)$. The angular dependence of $H_p(0.07)$ for nearly monoenergetic electron beams, which was also measured with both techniques, was shown to be very different from that obtained by presently available calculations. These differences may indicate the necessity to consider the influence of air scattering for low energy electron calculations.

REFERENCES

1. ICRU. Determination of Dose Equivalents Resulting from External Radiation Sources. ICRU Report 39 (1985).

2. ICRU. Determination of Dose Equivalents from External Radiation Sources - Part 2. ICRU Report 43 (1988).

3. ICRU. Measurement of Dose Equivalents from External Photon and Electron Radiations. ICRU Report 47 (1992).

4. National Radiological Protection Board (NRPB). Dose Quantities For Protection Against External Radiations. Documents of NRPB, Draft August (1992).

5. ICRU. Dosimetry of External Beta Radiation for Radiation Protection. RC on Beta Dosimetry, Draft of December (1993).

6. Christensen P., Böhm J., Francis T.M. Measurement of Absorbed Dose to Tissue in a Slab Phantom for Beta Radiation Incident at Various Angles. In: Beta Dosimetry, CEC Report EUR 11363 EN, pp. 39-75 (1988).

7. Böhm J. Standardization, Calibration and Type-Testing in Skin Dosimetry. Radiat. Prot. Dosimetry vol. 39, No. 1/3, pp. 95-100 (1991).

8. ISO. Reference Beta Radiation for Calibrating Dosemeters and Doserate Meters and for Determining their Response as a Function of Beta Radiation Energy. International Standard 6980, First Revision (1991).

9. Seltzer S.M. Dose in Water from External Irradiation by Electrons: Radiation Protection Data. NIST Publication, NISTIR 5136, Gaithersburg, MD. (1993).

10. Hirayama H. Calculation of Absorbed Dose at 0.07, 3.0 and 10.0 mm Depths in a Slab Phantom for Monoenergetic Electrons. Radiat. Prot. Dosimetry vol.51, No.2, pp. 107-124 (1994).

11. Pruitt J.S., Soares C.G., Ehrlich M. Calibration of Beta-Particle Radiation Instrumentation and Sources. NIST Special Publication 250-21, Gaithersburg, MD. (1988).

12. Soares C.G., Dick C.E., Pruitt J.S., Sparrow J.H. Development of Monoenergetic Electron Beam Sources for Radiation-Instrument Calibration. Nucl. Instrum. Methods Phys. Res. B10/11, pp.937-941 (1985).

13. Böhm J. The National Primary Standard of the PTB for Realizing the Unit of the Absorbed Dose Rate to Tissue for Beta Radiation. PTB-Bericht Dos-13, Braunschweig (1986).

14. Pruitt J.S. Automation of Extrapolation Chamber Controls. Unpublished report (1991)

15. Böhm J. The Perturbation Correction Factor of Ionisation Chambers in β-Radiation Fields. Phys. Med. Biol. vol 25 No. 1, pp. 65-75 (1980).

16. Prokić M. Graphite Mixed Magnesium Borate TL Dosemeters for Beta Ray Dosimetry. Radiat. Prot. Dosimetry vol. 6, No.1-4, pp. 133-136 (1984).

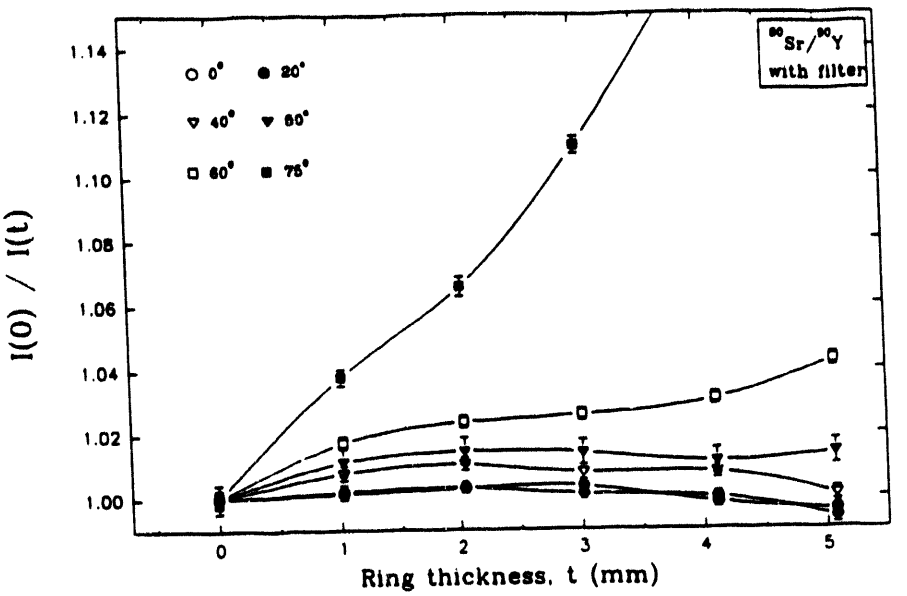


Figure 1- Ratio of the ionization current measured with and without rings fastened to the chamber (beta source: $^{90}Sr/^{90}Y$ with flattening filter).

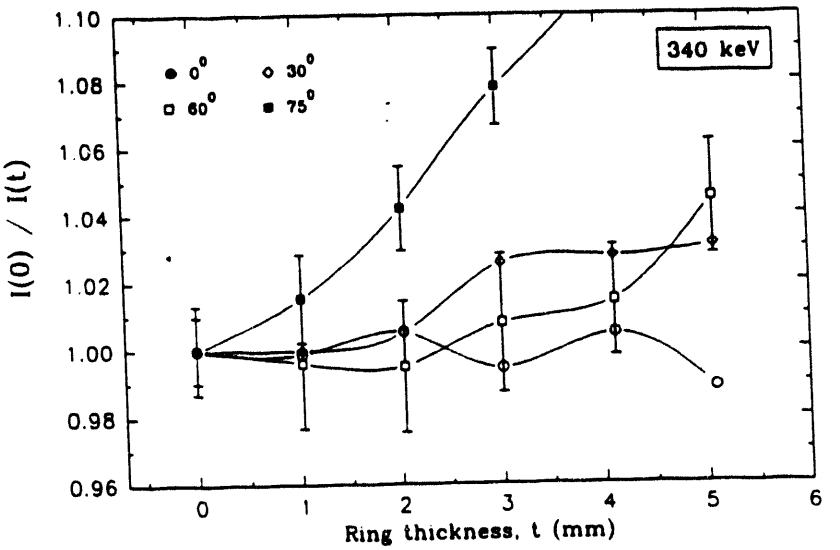


Figure 2- Ratio of the ionization current measured with and without rings fastened to the chamber (electron beam: 340 keV).

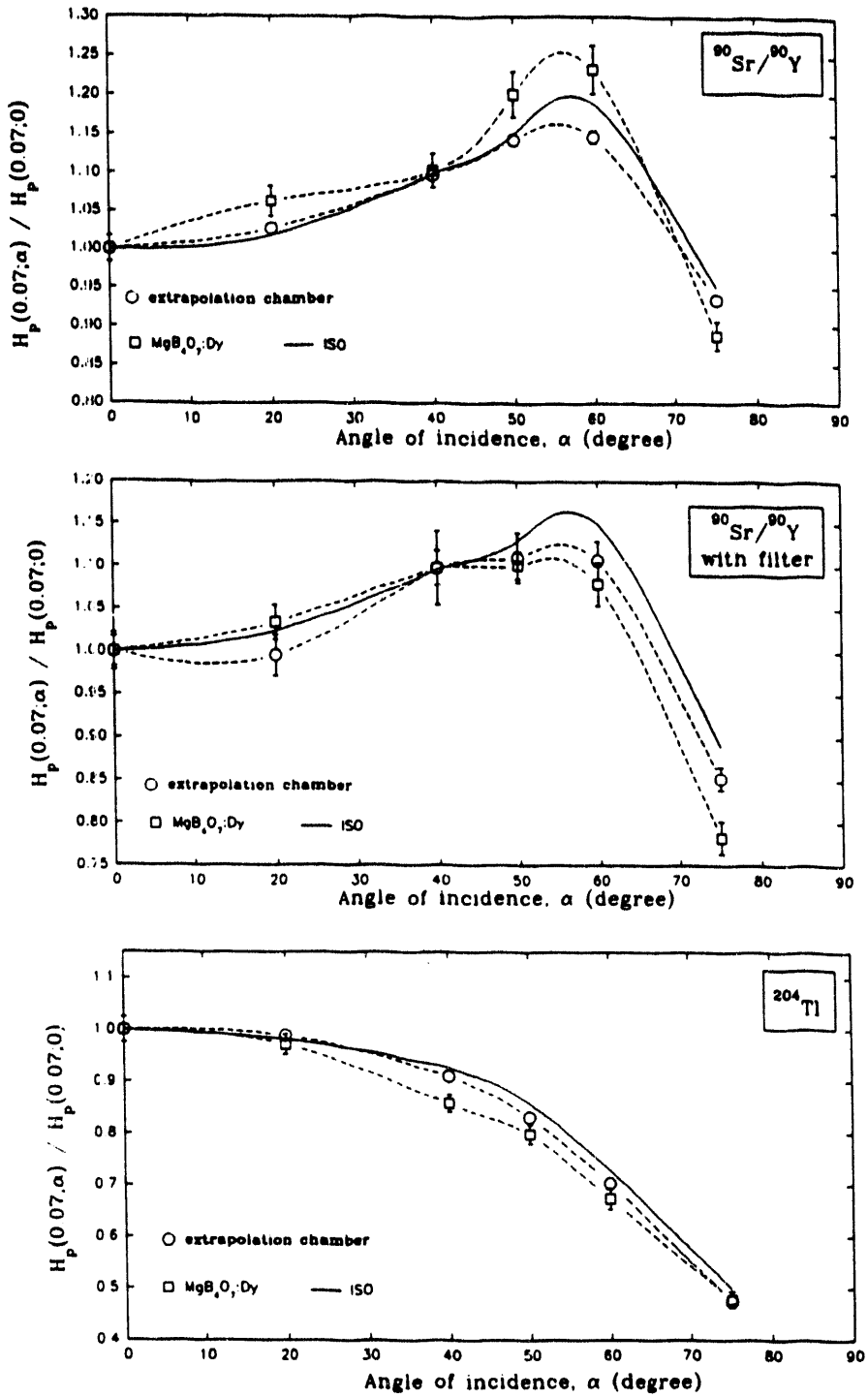


Figure 3- Angular variation of the personal dose equivalent in a slab phantom, for $^{90}Sr/^{90}Y$ and ^{204}Tl beta particle sources.

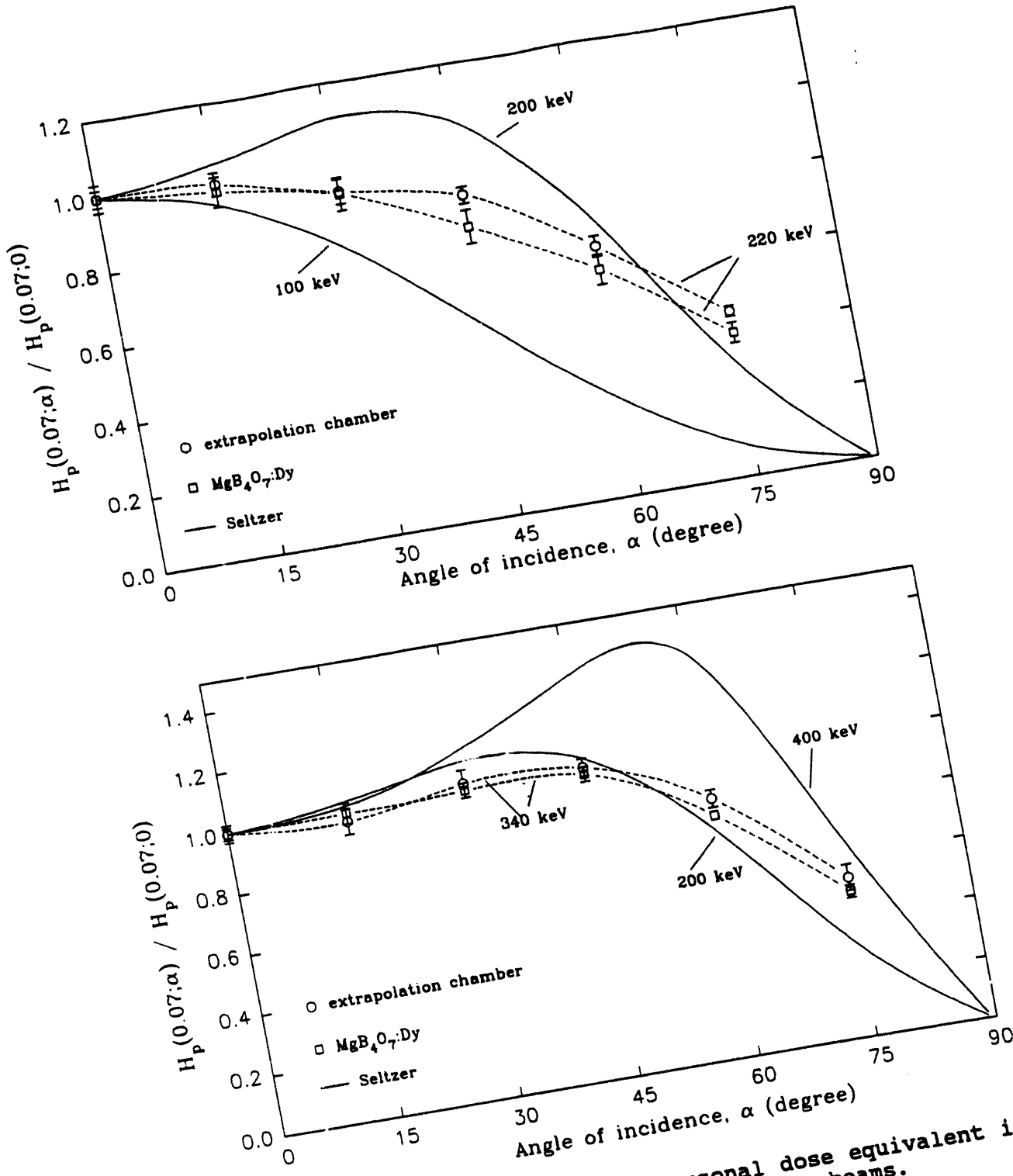


Figure 4- Angular variation of the personal dose equivalent in a slab phantom, for nearly monoenergetic electron beams.

Table 1 - Characteristics of some NIST standard beta-particle fields.

Radionuclide	$^{90}Sr/^{90}Y$	$^{90}Sr/^{90}Y$	^{204}Tl
Nominal activity (MBq)	1380	56	2000
Half-life (y)	28.5	28.5	3.78
Maximum beta ray energy (MeV)	2.274	2.274	0.763
Mean beta ray energy (MeV)	0.80	0.80	0.24
Irradiation distance (cm)	30	30	30
Flattening filter	no	yes	yes

Table 2 - Measured b-values, in mm^{-1}, to calculate the perturbation correction factors for the NIST extrapolation chamber for beta-particle sources, at different angles of incidence, α, (air-gap range: 0.7 mm to 2.5 mm, window: 7.6 mg/cm^2 of PTP foil).

	b-values (mm^{-1})		
α	$^{90}Sr/^{90}Y$	$^{90}Sr/^{90}Y$ + filter	^{204}Tl
0°	-0.0010 ± 0.0005	-0.0011 ± 0.0007	0.0011 ± 0.0001
20°	-0.0010 ± 0.0005	-0.0008 ± 0.0006	0.0012 ± 0.0005
40°	-0.0006 ± 0.0010	-0.0003 ± 0.0011	0.0031 ± 0.0007
50°	0.0011 ± 0.0011	-0.0019 ± 0.0010	0.0053 ± 0.0006
60°	0.0052 ± 0.0011	0.0057 ± 0.0009	0.0054 ± 0.0009
75°	0.0335 ± 0.0024	0.0360 ± 0.0052	0.0151 ± 0.0018

Table 3 - Ratios $H_p(0.07;\alpha)/H_p(0.07;0)$, for $^{90}Sr/^{90}Y$ source without flattening filter, at different angles of incidence, α, obtained with the NIST extrapolation chamber and the MgB_4O_7:Dy TL dosimeters, compared to those given by ISO[8].

α	$H_p(0.07;\alpha) / H_p(0.07;0)$		
	Extrapolation chamber	MgB_4O_7:Dy	ISO
0°	1.000 ± 0.005	1.00 ± 0.02	1
20°	1.027 ± 0.004	1.06 ± 0.02	1.018*
40°	1.098 ± 0.004	1.10 ± 0.02	1.101*
50°	1.143 ± 0.005	1.20 ± 0.03	1.148*
60°	1.147 ± 0.008	1.23 ± 0.03	1.19
75°	0.934 ± 0.003	0.89 ± 0.02	0.95

* interpolated values.

Table 4 - Ratios $H_p(0.07;\alpha)/H_p(0.07;0)$, for $^{90}Sr/^{90}Y$ source with flattening filter, at different angles of incidence, α, obtained with the NIST extrapolation chamber and the MgB_4O_7:Dy TL dosimeters, compared to those given by ISO[8].

α	$H_p(0.07;\alpha) / H_p(0.07;0)$		
	Extrapolation chamber	MgB_4O_7:Dy	ISO
0°	1.00 ± 0.02	1.00 ± 0.02	1
20°	1.00 ± 0.02	1.03 ± 0.02	1.024*
40°	1.10 ± 0.04	1.10 ± 0.02	1.096*
50°	1.11 ± 0.03	1.10 ± 0.02	1.130*
60°	1.11 ± 0.02	1.08 ± 0.03	1.15
75°	0.85 ± 0.01	0.78 ± 0.02	0.89

* interpolated values.

Table 5 - Ratios $H_p(0.07;\alpha)/H_p(0.07;0)$, for ^{204}Tl source with flattening filter, at different angles of incidence, α, obtained with the NIST extrapolation chamber and the MgB_4O_7:Dy TL dosimeters, compared to those given by ISO[8].

α	$H_p(0.07;\alpha) / H_p(0.07;0)$		
	Extrapolation chamber	MgB_4O_7:Dy	ISO
0°	1.000 ± 0.004	1.00 ± 0.02	1
20°	0.989 ± 0.004	0.97 ± 0.02	0.982*
40°	0.910 ± 0.005	0.86 ± 0.02	0.927*
50°	0.831 ± 0.004	0.80 ± 0.02	0.858*
60°	0.704 ± 0.003	0.67 ± 0.02	0.73
75°	0.476 ± 0.003	0.480 ± 0.02	0.50

* interpolated values.

Table 6 - Ratios $H_p(0.07;\alpha)/H_p(0.07;0)$, for nearly monoenergetic electron beams with average energy of 220 keV and 340 keV, at different angles of incidence, α, obtained with the NIST extrapolation chamber (EC) and the MgB_4O_7:Dy TL dosimeters.

α	$H_p(0.07;\alpha) / H_p(0.07;0)$			
	Avg. energy: 220 keV		Avg. energy: 340 keV	
	EC	MgB_4O_7:Dy	EC	MgB_4O_7:Dy
0°	1.00 ± 0.04	1.00 ± 0.02	1.00 ± 0.03	1.00 ± 0.02
15°	0.99 ± 0.03	0.97 ± 0.04	0.98 ± 0.04	1.01 ± 0.03
30°	0.92 ± 0.03	0.91 ± 0.04	1.04 ± 0.05	1.01 ± 0.02
45°	0.86 ± 0.02	0.77 ± 0.05	1.02 ± 0.03	1.00 ± 0.02
60°	0.67 ± 0.03	0.60 ± 0.04	0.85 ± 0.03	0.80 ± 0.01
75°	0.44 ± 0.01	0.38 ± 0.03	0.52 ± 0.04	0.48 ± 0.02

A TABULATION OF ABSORBED DOSE PER UNIT FLUENCE CONVERSION COEFFICIENTS FOR SLAB PHANTOMS OF THREE TISSUE EQUIVALENT MATERIALS FOR ELECTRON ENERGIES FROM 70 keV TO 10 MeV

G. F. GUALDRINI*, F. PADOANI** U. DE MAIO*
*ENEA-AMB 8 v.le Ercolani (I) 40138 BOLOGNA ITALY
**ENEA-ERG 4 v.Martiri di Monte Sole (I) 40129 BOLOGNA ITALY

1-INTRODUCTION

After the publication of the "1990 Recommendations of the International Commission on Radiological Protection" (ICRP 60) /1/, an ICRP/ICRU Joint Task Group was set up to revise the ICRP Publication 51 "Data for Use in Protection Against External Radiation" /2/.

In this framework a particular effort was devoted to providing new data for electron and beta radiation due to the present lack of a complete and homogeneous set of values. A subgroup of the EURADOS WG4 (Numerical Dosimetry) was therefore created as a support to the ICRP/ICRU Joint Task Group with the specific aim of providing conversion factors for operational quantities for electron and beta radiation. Six participants (from Europe, USA and Japan) gave contributions, that have been discussed by Grosswendt and Chartier in a forthcoming report /3/.

The ENEA contribution to the Task Group dealt with the Monte Carlo analyses of electron absorbed dose for slab phantoms of different compositions, which required an extended series of calculations and comparisons to be carried out. The complete set of the results is about to be published as an ENEA report /4/.

2-ABSORBED DOSE CALCULATIONS IN SLAB PHANTOMS

For individual monitoring purposes ICRU-47 /5/ defines the personal dose equivalent $H_p(d)$, i.e. the dose equivalent in soft tissue below a specified point on the body at an appropriate depth d. In the same document it is also specified that the calibration phantom should consist of 4-element ICRU tissue with a recommended slab shape of 300x300 mm face and 150 mm height. Due to the lack of an exact substitute for the 4-element ICRU tissue and since it was desirable to achieve uniformity in the calibration procedure, a PMMA phantom of the same dimensions is recommended by ICRU.

Following the operational quantity definition, the computational analyses summarised in the present paper were therefore addressed to the Monte Carlo evaluation of absorbed dose D(d) in slab phantoms to produce a complete set of fluence-to-absorbed dose conversion factors:
-for electron energies ranging from 70 keV to 10 MeV
-for different angles of incidence from 0 degrees to 75 degrees (supplementary studies for higher incident angles were performed to obtain a complete angular dependence distribution)
-for different phantom materials: water, PMMA and ICRU material

For ICRU material the absorbed dose D(d) corresponds to $H_p(d)$ by definition.

The incident electron beam was an aligned and expanded field impinging on a 300 mm x 300 mm x 150 mm phantom and the absorbed dose values had to be calculated at the centre of the 300 mm x 300 mm y - z surface at the three typical depths of 7 mg/cm^2, 300 mg/cm^2 and 1000 mg/cm^2.

Owing to the range in water at the investigated energies not exceeding 5000 mg/cm^2, the contribution of the phantom edges to the response was not considered and the irradiation geometry was described in a one-dimensional fashion with y - z infinite dimensions and a 15 cm thick tissue material in the x direction. For symmetry reasons it was demonstrated that y - z infinite scoring volumes embedded in the phantom irradiated by a point mono-directional beam provide the same results as the real finite slab with very small scoring volumes at the various depths when irradiated by an aligned and expanded field. This approach allowed considerable computer time to be saved.

3-COMPUTATIONAL METHODS AND PROBLEMS

Given the lack of experimental data, it was decided to employ two Monte Carlo codes, MCNPE-BO /6/-/9/ and MCNP4 /10/, based on two different multi-scattering theories so that a degree of confidence could be attached to the results. All the calculations were carried out with MCNPE-BO,

whilst MCNP4 was used only for the energy range most sensitive to the multiple-scattering, below 1 MeV.

The intere depth dose curve was calculated for each energy and angle. The investigated depth was divided in equal thickness cells of 1/10 range (and for some more accurate studies 1/20 range). Thinner scoring volumes of varying thicknesses were abopted around the three stated depths (7 mg/cm^2, 300 mg/cm^2 and 1000 mg/cm^2) mainly when they were located near depth dose curve sharp maxima especially occuring at high incident angles. In the majority of the situations interpolation of data performed well due to the rather smooth nature of the depth curves, with some sporadic exceptions that should need further investigations. The results at depths outside or near the end of the electron range are affected by rather high uncertainties (due to the poor sampling within the bremmstrahlung tail) and the data can be taken as reliable over certain electron energies. All the tabulated results were therefore given for electron energies over 70 keV at 7 mg/cm^2, over 800 keV at 300 mg/cm^2 and over 2000 keV at 1000 mg/cm^2. The differences in the results obtained with the two codes can be mainly ascribed to the different multi-scattering models used and a full description of their behaviour is presented in a previous paper /11/. Taking the results of the two codes as a whole, for comparable CPU times per run, they are always inside one standard deviation for energies > 0.4 MeV, while the differences are outside the statistical confidence interval at lower energies. Notwithstanding this, at lower energies the comparison is still quite satisfactory considering the critical energy range and the different algorithms used by the two codes.

The calculations were very time-consuming and many CPU hours on the IBM-3090/XA of the "C.R.E. Energia E. Clementel in Bologna" were used, mostly 1 hour for each energy at a given angle, corresponding to a number of histories varying from few thousands to tens of thousands, depending on the electron source energy. The standard deviations, usually less than 2% for normally incident electrons, were generally less than 4% for higher incident angles (reaching in particular cases values of about 10%, and more, especially for lower energies and larger depths, e.g. at 75° angle). The research of maxima as a function of depth and angle would have required an optimization of the cell thickness and a huge amount of calculations with different incident angles. A compromise had to be accepted and some discrepancies with other authors can be ascribed also to these choices. A detailed study on the angular dependence at the three stated depths was performed only for the water slab with an accurate research of maxima.

4- ABSORBED DOSE PER UNIT FLUENCE FOR NORMALLY INCIDENT ELECTRONS

The normal incidence values of absorbed dose per unit fluence are presented in Tables 1, 2 and 3 summarizing the MCNPE-BO calculations.

To start a discussion on the results it can be useful to remind that the investigated quantity during the study was the absorbed dose in the three analysed materials, according to the formula:

$$D(d) = \int_0^\infty \phi_E(d) \, [\, S(E)/\rho]_{coll} \, dE$$

where $\Phi_E(d)$ is the spectral electron fluence at the linear phantom depth d and $[S(E)/\rho]_{coll}$ is the mass collision stopping power of electrons of energy E in a material of density ρ.

This equation puts evidence on the parameters that play a critical role in the comparison of absorbed doses in different tissue equivalent materials: when dealing with linear depths one has to compare the electron fluences at that depth (that are governed by the lineal collision and radiative stopping power as well as the scattering power) and the mass collision stopping power.

These aspects have been very effectually focused by B. Grosswendt in his recent report /12/. We refer particularly to this document both to compare our results and to discuss on the two materials, water and PMMA as "well suited substitutes" for the ICRU-4 element tissue.

A first consideration is concerned with PMMA material: the absorbed doses in this material can be compared with those obtained for the other two materials (water and ICRU-4 element tissue) only at the same surface mass depths (expressed in g/cm^2) due to its ρ = 1.19 g/cm^3 compared with ρ = 1.0 g/cm^3 for water and ICRU 4-element material: the calculations were therefore performed

for 7 mg/cm^2, 300 g/cm^2 and 1000 mg/cm^2, so as to deal with comparable results.

Secondly, when the electron spectral fluences can be assumed as the same or very similar at a stated surface mass depth, the ratio of the absorbed dose values is close to the ratio of the respective mass collision stopping powers. It has to be pointed out that $[S(E)/\rho]_{coll}$ for water is about 1% larger than that for ICRU 4-element tissue, whilst $[S(E)/\rho]_{coll}$ for PMMA is about 2% smaller. This leads to the conclusion that the absorbed doses in the three materials, in the limits already highlighted, have to present a behaviour similar to their mass collision stopping powers. Figure 1 shows this behaviour for 7 mg/cm^2 compared with that proposed by Grosswendt. A substantial agreement with the data by Grosswendt has to be pointed out, apart from a too low MCNPE-BO value at 200 keV for PMMA and slightly too low MCNPE-BO estimates (for E > 2 MeV) again for PMMA. This discrepancy, that could be in some way due to our interpolation performed in the PMMA very initial layers, does not affect the overall agreement but will be investigated in detail. A better agreement of the same relative quantities has to be pointed out at 300 g/cm^2 and 1000 mg/cm^2 (not shown). The above considerations, together with graphical comparisons, are demostrating that water is a better substitute for ICRU-4 element tissue. This is confirmed by the example of figures 2 and 3, showing the depth absorbed dose per unit fluence for normally incident 10 MeV electrons incident on water and PMMA phantoms compared with the corresponding 4-element ICRU tissue depth dose data. To show how our absolute values fit in the curves proposed by other authors, figures 4 and 5 summarise some comparisons of MCNPE-BO results with data from literature /12/, /13/, /14/ for the water and the ICRU tissue slabs at the three stated depths . At 7 mg/cm^2 the results from the various authors agree within approximately 1 - 5%, with the standard deviations of the MCNPE-BO results ranging from 1 to 3%. At 300 mg.cm^{-2} and at 1000 mg.cm^{-2} the agreement with the results from the various authors is approximately within 1-4%, when the scoring depth is lower than the primary electron range; the standard deviations associated with MCNPE-BO results for these two depths are about 1%.

5-ABSORBED DOSE DEPENDENCE ON ELECTRON BEAM INCIDENT ANGLE

The angular dependence factors of the absorbed dose on the electron beam incident angle, expressed as $R(d,\theta) = [D(d,\theta)/\Phi]/[D(d,0°)/\Phi]$ were also determined and an example of comparison with other authors' results is presented in figures 6 and 7.

Figure 6 summarises the angular dependence at 7 mg/cm^2 for electron energies ranging from 80 keV to 10 MeV, whilst Figure 7 supplies the values at 1000 mg/cm^2 for electron energies ranging from 3 MeV to 10 MeV. The calculations presented were performed using MCNPE-BO in a slab water phantom. Again a comparison with literature results is shown.

It is seen that a build-up effect is contributing to the response: a qualitative explanation of the different angular behaviours with the energy at the various depths can be made considering the effect of the attenuation of the primary electrons in the material before the scoring region (which is strongly energy- and angle-dependent) and the frontal leakage from the slab (important at high incident angles of the source electrons). At a glance, taking the data as a whole, a good agreement with the data supplied by other authors may be noted. Some refinements will be nevertheless necessary, e.g. at 1000 mg.cm^{-2} for 3 and 4 MeV electrons incident at 75°.

The complete graphs showing the angular behaviours in water for 7 mg/cm^2 and for 300 mg/cm^2 are reported in figures 8 and 9. The numerical values of $R(d,\theta)$ for water are reported in tables 4, 5 and 6.

The values reported in the tables and the plots of $R(d,\theta)$ supply only information about the relative behaviour of the conversion coefficient as a function of incident angles for a stated depth and electron energy. As far as the absolute values are concerned, in Figure 10 a series of curves of fluence to absorbed dose conversion coefficients is presented as a function of energy for various incident angles at 7 mg/cm^2 for the water phantom. It has to be pointed out that the absolute values of maxima are decreasing with increasing incident angle, with a contemporary shift of the maximum towards higher energies when the incident angle is augmented. The shapes of the curves for small values of θ are quite similar to that of normal incidence (θ=0°), whilst the curves exhibit broader maxima,with increasingly different shapes from that for normally incident electrons, when

the incident angle is augmented.

Figures 11, 12 and 13 show an example of depth absorbed dose curves for water for 1.5 MeV electrons incident at 0, 30 and 75 degrees respectively.

As far as a comparison of the three material R(d,θ) is concerned, it is presented in figures 14, 15 and 16 for the three stated depths (3 MeV incident electrons). The comparison shows a generally rather similar behaviour. Taking into account the increasing standard deviations with incident angle and depth as already mentioned, and with the support of more accurate R(d,θ) analyses for the three materials, again we can canclude that water is closer to ICRU tissue also as far as the angular dependence factor is concerned. This difference, practically neglegible at low angles, becomes more evident for higher incident angles and scoring depths and is well shown in the above mentioned summary paper by Grosswendt and Chartier.

6- CONCLUSIONS

The calculations covered a wide range of energies and angles and were very expensive in term of CPU time, but the results are a quite complete set and can be of aid in the dosimetric field. A substantial agreement, in the limits already highlighted, with other authors confirms the reliability of the results obtained by MCNPE-BO and MCNP4. The differences between the two codes can be mainly attributed to the different multi-scattering theories underlying them.

This work, together with the analyses performed by other authors already mentioned, supplies further elements for the discussion on water and PMMA as suitable substitute materials for the 4-element ICRU theoretical tissue and allows to conclude that water is preferable in the investigated electron energy domain. In practice one has however to put water inside some flask (consisting of PMMA or some other plastic material) so that a new discussion rises about this practical "two material" slab, when used for low electron energies at 7 mg/cm^2.

REFERENCES

/1/ *1990 Recommendations of the International Commission on Radiological Protection*, Pergamon Press ICRP-60 (1990)

/2/ *Data for Use in Protection Against External Radiation*, Pergamon Press ICRP-51 (1987)

/3/ Grosswendt B.and Chartier J. L. *Fluence-to-Absorbed-Dose Conversion Coefficients and Angular--Dependence Factors for 4-element ICRU Tissue. Water and PMMA Slab Phantoms Irradiated by Broad Electron Beams* PTB-Report DOS-24 (1994)

/4/ Gualdrini G. F, Padoani F. and De Maio U. *Absorbed dose per Unit Fluence for Tissue Equivalent Slab Phantoms for Electrons from 50 keV to 10 MeV*, ENEA/RT/AMB/94 (in press)

/5/ *Measurement of Dose Equivalents from External Photon and Electron Radiations*, ICRU-47 International Commission on Radiation Units and Measurements - Bethesda (MD) (1992)

/6/ Guaraldi R. and Padoani F. *Implementation of Algorithms Based on a New Electron Model (Underpinned by the Molière Theory) in MCNP*, forthcoming ENEA report

/7/ Guaraldi R., Padoani F., Burn K.W., Gualdrini G.F. *Monte Carlo Applications to Photon Radiation Protection and Dosimetry at ENEA*,, Progress in Nuclear Energy 24 (1990), pp. 365-376

/8/ Ferrari A., Sala P., Guaraldi R. and Padoani F. *An Improved Multiple Scattering Model for Charged Particle Transport*. Nucl. Instr. Meth. B71 (1992), pp. 412-426

/9/ Guaraldi R. and Padoani F. *Benchmarking of the code MCNPE-BO*, forthcoming ENEA report

/10/ LANL (J.F. Briesmeister, Ed.) *MCNP - A General Monte Carlo Code for Neutron and Photon Transport version 3A* , LA-7396-M rev.2 (1986) (updated with internal Los Alamos memoranda to version 4)

/11/ Gualdrini G.F. and Padoani F.*Monte Carlo Code Comparisons for the Calculation of Absorbed Dose per Unit Fluence in Slab Phantoms for Electron Energies from 50 tkeV to 10 MeV* **Workshop on** "Individual Monitoring of Ionizing Radiation: The impact of Recent ICRP and ICRU Publications" Villigen May 5-7 th 1993. Paper accepted for Publication in Rad. Prot. Dosim.

/12/ Grosswendt B. *The Fluence-to-Absorbed-Dose Conversion Factors for 4-Element ICRU Tissue, Water, and PMMA Slab Phantoms Irradiated by Broad External Electron Beams of Normal and Oblique Incidence*, PTB-Report DOS-22 October 1993.

/13/Seltzer S.M. *Dose in Water from External Irradiation by Electrons: Radiation Protection Data* Report NISTIR 5136 (NIST, Gaithersburg, MD 20899) (1993)

/14/ Rogers D. W. O. *Fluence to Dose Equivalent Conversion Factors Calculated with EGS3 for Electrons from 100 keV to 20 GeV and Photons from 11 keV to 20 GeV*, Health Physics 46 n. 4 pp. 891-914 (1984).

Absorbed dose per unit fluence for normally incident electrons

D(7 mg/cm^2,0°)/Φ

	WATER		TISSUE		PMMA			
T(MeV)	10^{-10} Gycm^2	% σ	10^{-10} Gycm^2	% σ	10^{-10} Gycm^2	% σ	D_{water}/D_{ICRU}	D_{PMMA}/D_{ICRU}
0.07	2.14	4.0	2.51	1.8	3.8	1.2	0.853	1.514
0.08	9.66	2.3	9.74	0.9	11.5	0.6	0.992	1.181
0.09	14.7	1.4	14.5	0.7	15.5	0.5	1.014	1.069
0.1	16.2	0.4	16.3	0.7	16.0	0.8	0.994	0.982
0.2	8.65	1.0	8.57	0.8	7.60	0.9	1.009	0.887
0.4	4.51	1.6	4.49	0.7	4.27	0.8	1.005	0.951
0.6	3.65	2.2	3.57	0.8	3.41	0.6	1.022	0.955
0.7	3.41	2.1	3.35	1.1	3.21	0.6	1.018	0.958
0.8	3.27	2.4	3.19	1.1	3.06	0.6	1.025	0.959
1.0	3.04	1.2	2.99	1.2	2.89	1.7	1.017	0.967
1.5	2.81	1.4	2.74	1.3	2.69	2.0	1.026	0.982
2.0	2.78	1.6	2.76	1.6	2.62	1.4	1.007	0.949
3.0	2.75	2.0	2.74	2.0	2.60	1.7	1.004	0.949
4.0	2.77	2.3	2.69	2.2	2.58	2.0	1.030	0.959
5.0	2.70	2.0	2.67	2.0	2.56	2.0	1.011	0.959
7.0	2.71	2.5	2.67	2.3	2.54	1.8	1.015	0.951
10.0	2.76	2.8	2.68	3.0	2.57	2.0	1.030	0.959

Tab.1

Absorbed dose per unit fluence for normally incident electrons

D(300 mg/cm^2,0°)/Φ

	WATER		TISSUE		PMMA			
T(MeV)	10^{-10} Gycm^2	% σ	10^{-10} Gycm^2	% σ	10^{-10} Gycm^2	% σ	D_{water}/D_{ICRU}	D_{PMMA}/D_{ICRU}
0.8	0.418	3.9	0.50	2.2	0.80	1.5	0.836	1.600
1.0	3.01	1.0	3.08	1.0	3.55	2.9	0.977	1.150
1.5	5.30	0.8	5.23	0.8	4.94	1.9	1.010	0.945
2.0	4.78	0.9	4.72	0.9	4.36	1.5	1.010	0.924
3.0	3.72	1.1	3.67	1.1	3.44	1.8	1.010	0.937
4.0	3.35	1.0	3.31	1.1	3.22	1.4	1.010	0.973
5.0	3.16	0.7	3.12	0.7	2.98	1.5	1.010	0.955
7.0	3.07	0.8	3.07	0.8	2.92	1.0	1.000	0.951
10.0	3.01	0.9	3.01	0.9	2.92	1.0	1.000	0.970

Tab. 2

Absorbed dose per unit fluence for normally incident electrons

D(1000 mg/cm^2,0°)/Φ

	WATER		TISSUE		PMMA			
T(MeV)	10^{-10} Gycm^2	% σ	10^{-10} Gycm^2	% σ	10^{-10} Gycm^2	% σ	D_{water}/D_{ICRU}	D_{PMMA}/D_{ICRU}
2.0	0.091	5.4	0.11	7.0	0.18	10.0	0.827	1.636
3.0	3.34	1.1	3.39	1.1	3.61	3.0	0.985	1.065
4.0	4.39	1.0	4.35	1.0	4.16	3.0	1.009	0.956
5.0	4.22	0.8	4.16	0.8	3.85	1.6	1.014	0.926
7.0	3.58	0.8	3.54	0.8	3.35	1.6	1.011	0.946
10.0	3.32	0.8	3.29	0.8	3.13	1.4	1.009	0.951

Tab. 3

Energy (MeV) / Angle (°)	0.07	0.08	0.09	0.1	0.2	0.4	0.6	0.7	0.8	1.0	1.5	2.	3.	4.	5.	7.	10.
0	1.000	1.000	1.000	1.000	1.000	1.000	1.000	1.000	1.000	1.000	1.000	1.000	1.000	1.000	1.000	1.000	1.000
15	0.78	0.91	0.92	0.98	1.045	1.033	1.055	1.072	1.024	1.016	1.022	1.015	0.996	1.019	1.019	1.011	1.011
30	0.455	0.635	0.701	0.774	1.094	1.16	1.137	1.135	1.101	1.081	1.097	1.066	1.033	1.026	1.049	1.031	1.034
45	0.177	0.333	0.438	0.506	1.053	1.36	1.283	1.287	1.263	1.247	1.201	1.154	1.107	1.1	1.098	1.050	1.065
60	0.0444	0.122	0.195	0.259	0.765	1.35	1.492	1.527	1.495	1.496	1.434	1.326	1.27	1.23	1.235	1.172	1.129
75	0.00580	0.0226	0.0557	0.0786	0.284	0.632	0.929	1.090	1.160	1.355	1.631	1.641	1.559	1.485	1.489	1.412	1.354
83										0.549	0.756	0.927	1.219	1.419	1.610	1.729	1.753
37.5													1.082				
40																1.040	
53						1.470								1.138	1.129	1.087	1.078
63																1.120	
64																	1.167
66																	1.185
68										1.358	1.395						
69								1.485	1.474								
70												1.318					
72										1.519	1.639						
77.5													1.613				
79													1.633	1.620	1.645		
80												1.352			1.662		
81													1.520	1.634	1.705	1.687	
84																	1.797
85																1.436	1.723
86																	1.450

Tab. 4 :
Numerical R(d,θ) values at 7 mg . cm^{-2} in water

Energy (MeV) / Angle (°)	0.8	1.0	.5	2.	3.	4.	5.	7.	10.
0	1.000	1.000	1.000	1.000	1.000	1.000	1.000	1.000	1.000
15	0.830	0.905	0.943	1.000	1.046	1.050	1.025	1.013	1.007
30	0.407	0.648	0.817	0.949	1.124	1.131	1.129	1.062	1.026
45	0.160	0.329	0.545	0.759	1.102	1.276	1.270	1.204	1.102
60	0.0360	0.118	0.264	0.437	0.785	1.015	1.229	1.375	1.340
75	0.00600	0.0220	0.0890	0.143	0.274	0.389	0.552	0.760	1.076
83		0.00658	0.0257	0.0464	0.0887	0.128	0.163	0.234	0.333
37.5					1.137				
40								1.122	
53						1.172	1.313	1.321	1.190
63								1.323	
64									1.408
66									1.389
68		0.0543	0.155						
69	0.0160								
70				0.230					
72		0.0355	0.113						
77.5					0.213				
79					0.174	0.258	0.335		
80				0.0800			0.299		
81					0.129	0.192	0.247	0.355	
84									0.284
85								0.151	0.212
86									0.156

Tab. 5 :
Numerical R(d,θ) values at 300 mg . cm^{-2} in water

Energy (MeV) / Angle (°)	2.	3.	4.	5	7.	10.
0	1.000	1.000	1.000	1.000	1.000	1.000
15	0.789	0.890	0.959	1.012	1.019	1.023
30	0.411	0.664	0.801	0.933	1.089	1.064
45	0.137	0.333	0.526	0.712	1.032	1.190
60	0.0305	0.119	0.237	0.361	0.664	1.009
75	0.00320	0.0232	0.0624	0.102	0.206	0.355
83	0.00179	0.00550	0.0176	0.0313	0.0639	0.110
37.5		0.477				
40					1.109	
53			0.365	0.518	0.883	1.163
63					0.555	
64						0.843
66						0.777
68						
70	0.00421					
72						
77.5		0.0165				
79		0.0130	0.0363	0.0642		
80	0.00368			0.0551		
81		0.00861	0.0261	0.0459	0.0878	
84						0.0819
85					0.0353	0.0617
86						0.0433

Tab. 6 :
Numerical R(d,θ) values at 1000 mg . cm^{-2} in water

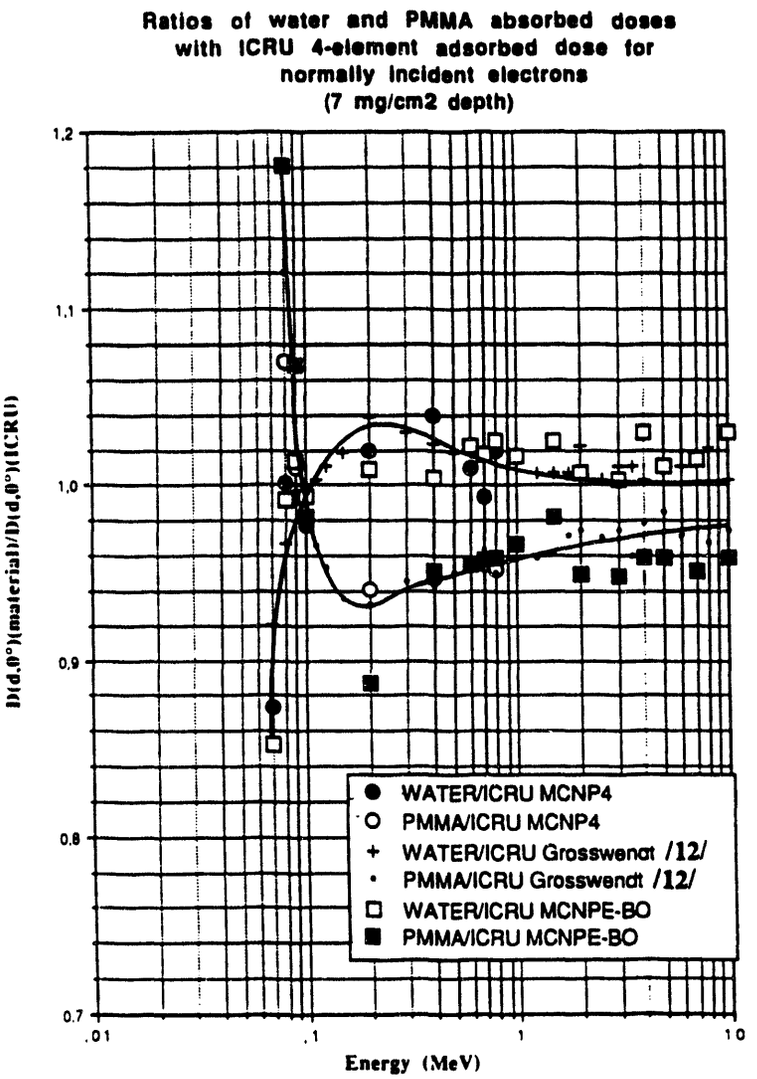

Ratios of water and PMMA absorbed doses
with ICRU 4-element adsorbed dose for
normally incident electrons
(7 mg/cm2 depth)
D(d,0°)(material)/D(d,0°)(ICRU)
1,2
1,1
1,0
0,9
0,8
0,7
.01
.1
1
10
Energy (MeV)
WATER/ICRU MCNP4
PMMA/ICRU MCNP4
WATER/ICRU Grosswendt /12/
PMMA/ICRU Grosswendt /12/
WATER/ICRU MCNPE-BO
PMMA/ICRU MCNPE-BO

fig. 1

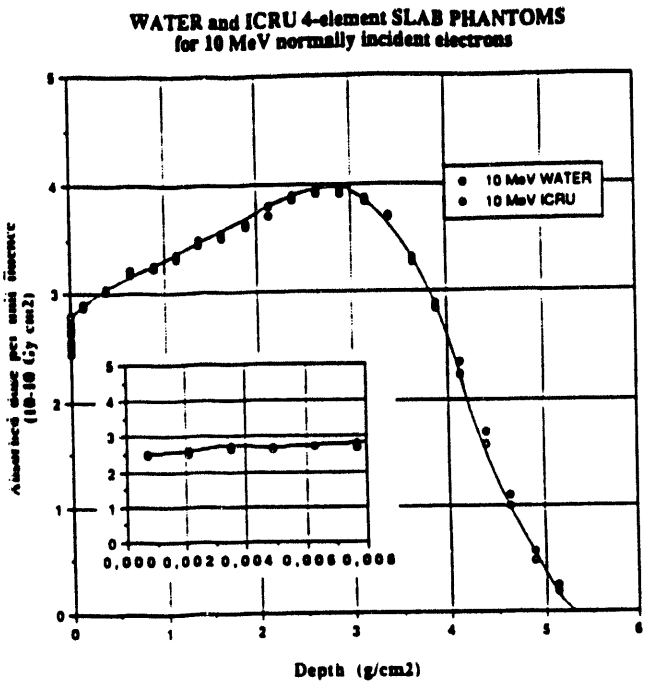

WATER and ICRU 4-element SLAB PHANTOMS
for 10 MeV normally incident electrons
10 MeV WATER
10 MeV ICRU
Depth (g/cm2)

fig. 2

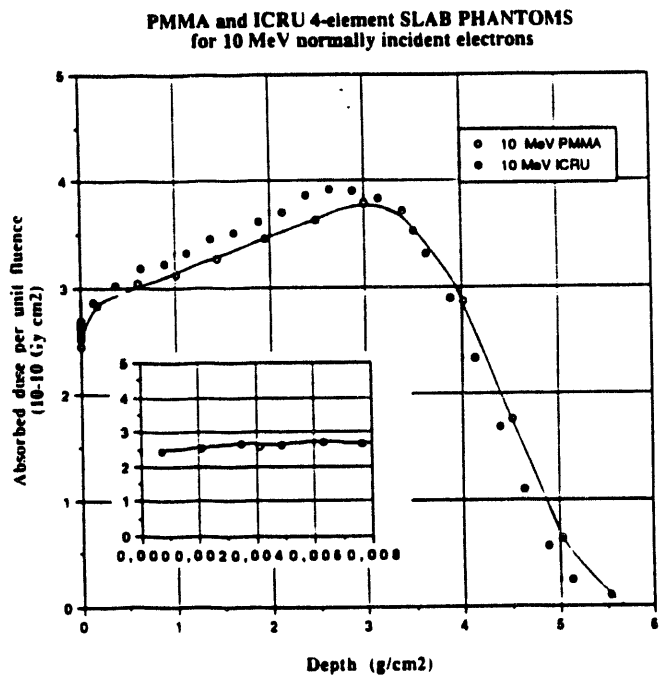

PMMA and ICRU 4-element SLAB PHANTOMS
for 10 MeV normally incident electrons
10 MeV PMMA
10 MeV ICRU
Absorbed dose per unit fluence
(10-10 Gy cm2)
Depth (g/cm2)

fig. 3

fig. 4 Absorbed dose per unit incident fluence in 10^{-10} Gy . cm^2 at 7, 300 and 1000 mg . cm^{-2}.

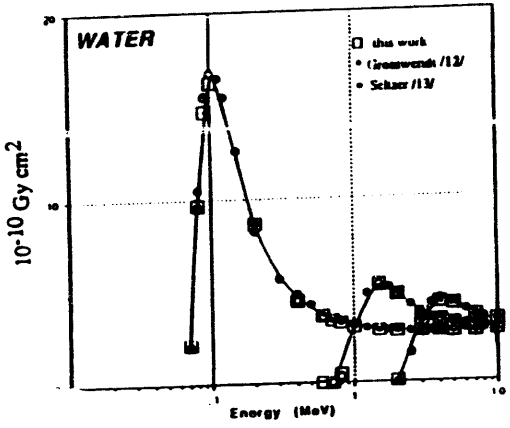


fig. 5 Absorbed dose per unit incident fluence in 10^{-10} Gy . cm^2 at 7, 300 and 1000 mg . cm^{-2}.

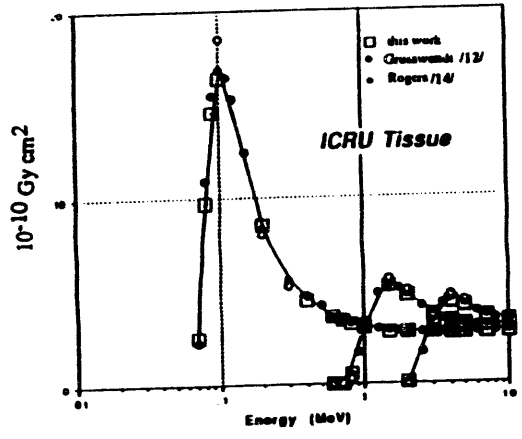


fig. 6 Angular dependence factor R(d, θ) at 7 mg . cm^{-2}: comparison with previously calculated results.

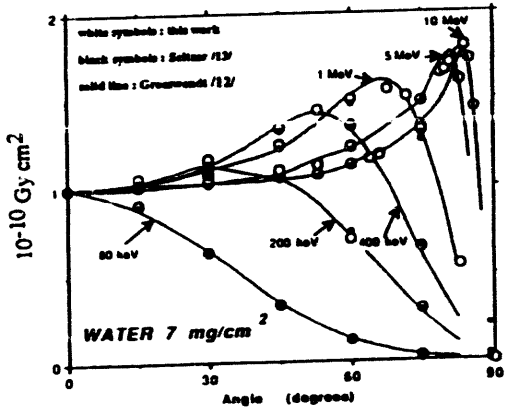


fig. 7 Angular dependence factor R(d,θ) at 1000 mg . cm^{-2}: comparison with previously calculated results.

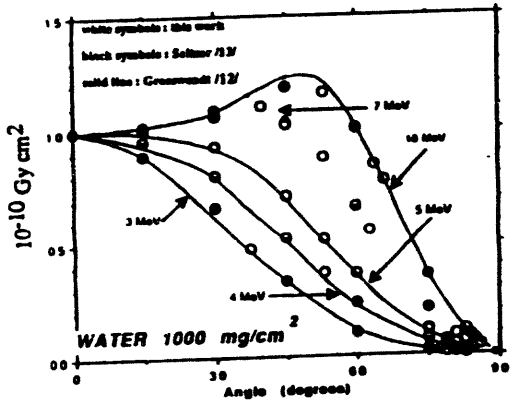


fig. 8 Angular dependence factor R(d,0) at 7mg . cm^{-2} for electron energies ranging from 800 keV to 10 MeV

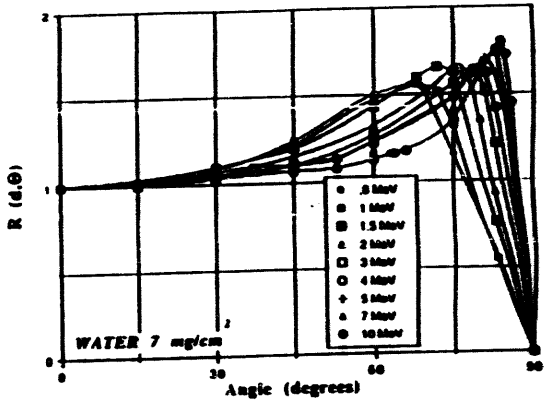


fig. 9 Angular dependence factor R(d,θ) at 300 mg . cm^{-2} for electron energies ranging from 800 keV to 10 MeV

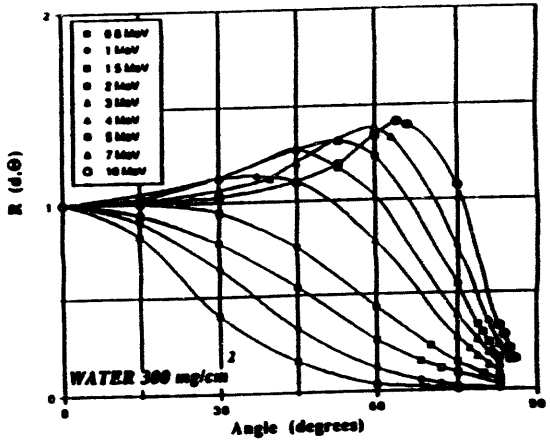
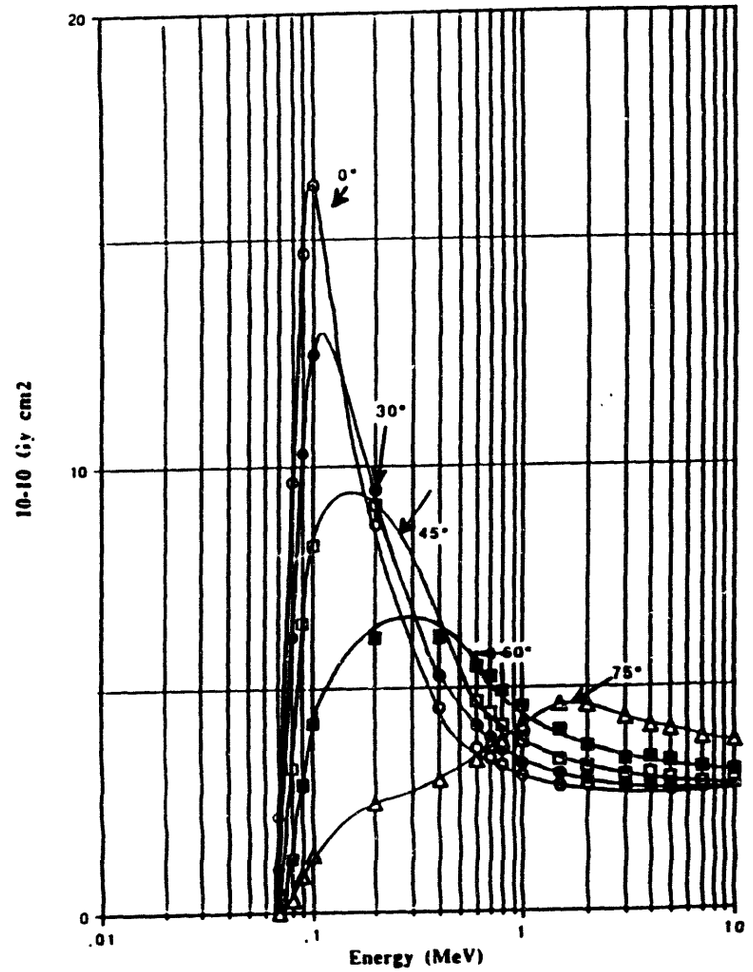


fig. 10 Fluence to absorbed dose conversion coefficient at7 mg . cm^{-2} in a water phantom as a function of energy for fixed incident angles



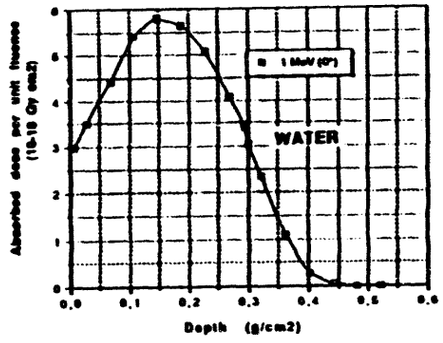


fig. 11

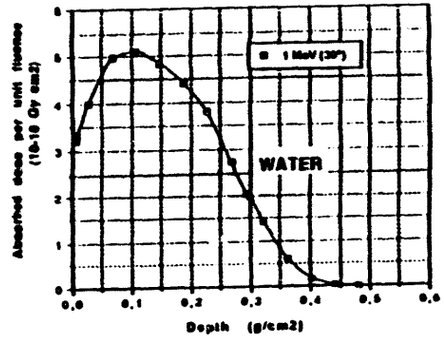


fig. 12

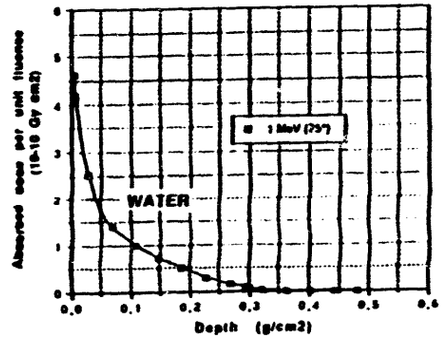
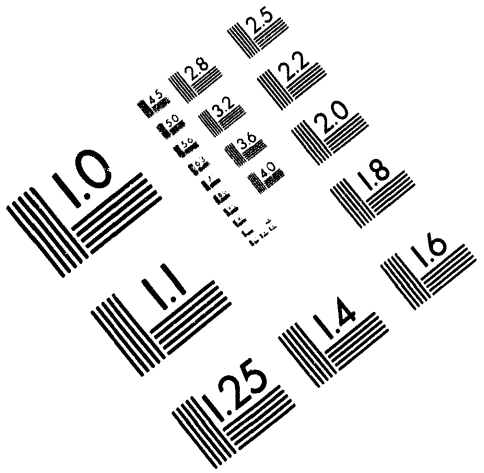
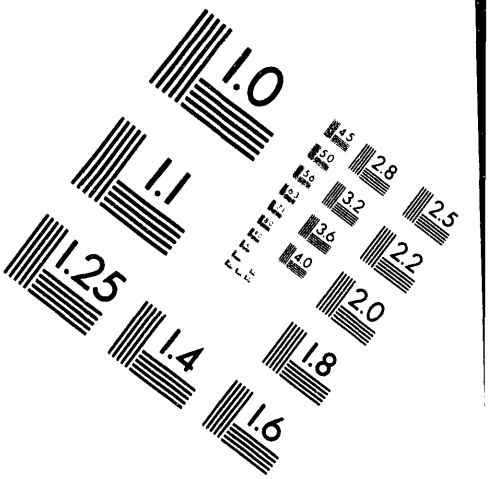


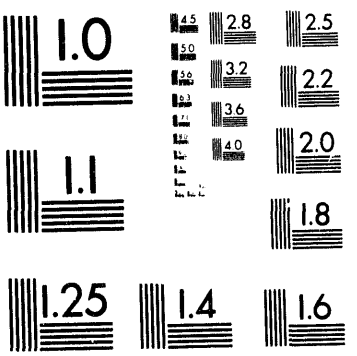
fig. 13

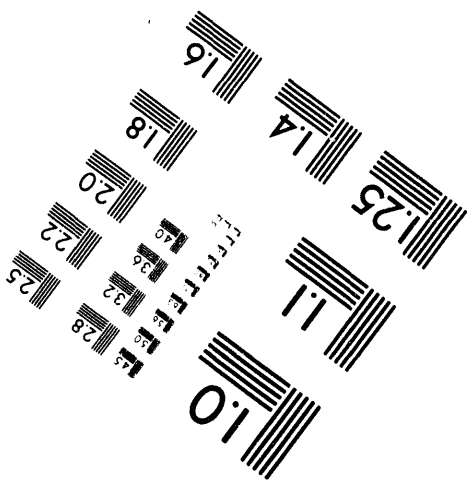


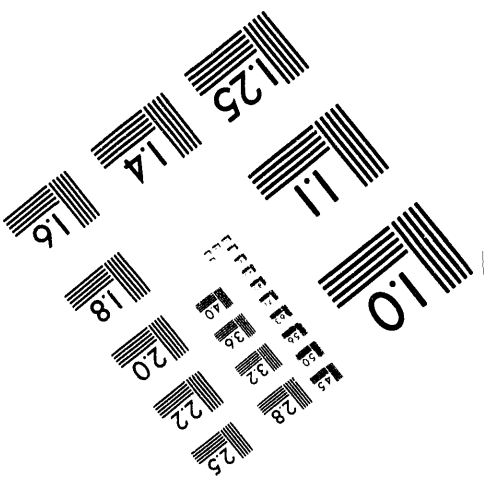


Association for Information and Image Management
1100 Wayne Avenue, Suite 1100
Silver Spring, Maryland 20910
301/587-8202









MANUFACTURED TO AIIM STANDARDS
BY APPLIED IMAGE, INC.

3 of 6

Anguiar dependence at 7 mg .cm^{-2} depth
for 3 MeV incident electrons

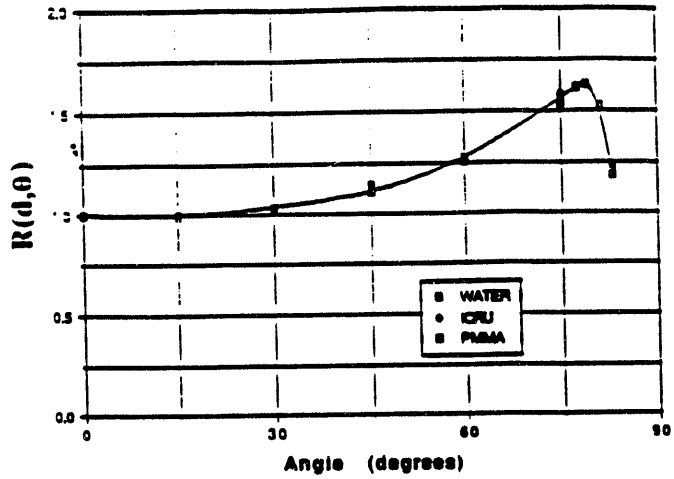


fig. 14

Angular dependence at 300 mg .cm^{-2} depth
for 3 MeV incident electrons

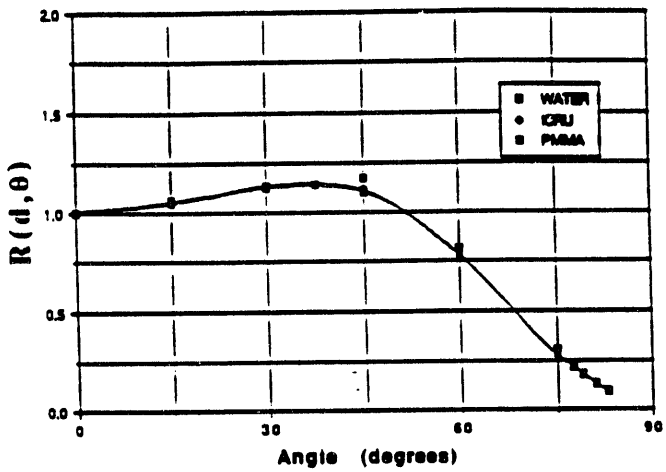


fig. 15

Anguiar dependence at 1000 mg .cm^{-2} depth
for 3 MeV incident electrons

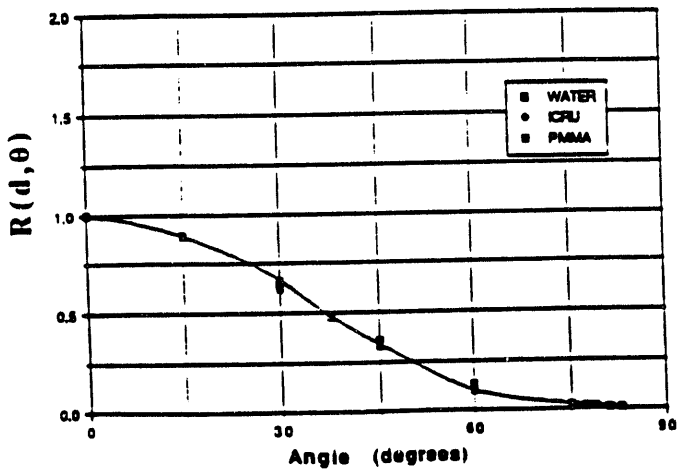


fig. 16

CONVERSION COEFFICIENTS FOR INDIVIDUAL MONITORING CALCULATED WITH INTEGRATED TIGER SERIES, ITS3, MONTE CARLO CODE

Robert T. Devine (Los Alamos National Laboratory) and Hsiao-Hua Hsu (Los Alamos National Laboratory)

The current basis for conversion coefficients for calibrating individual photon dosimeters in terms of dose equivalents is found in the series of papers by Grosswendt'. In his calculation the collision kerma inside the phantom is determined by calculation of the energy fluence at the point of interest and the use of the mass energy absorption coefficient. This approximates the local absorbed dose.

Other Monte Carlo methods can be used to provide calculations of the conversion coefficients. Rogers[2] has calculated fluence-to-dose equivalent conversion factors with the Electron-Gamma Shower Version 3, EGS3, Monte Carlo program and produced results similar to Grosswent's calculations. This paper will report on calculations using the Integrated TIGER Series[3] Version 3, ITS3, code to calculate the conversion coefficients in ICRU Tissue and in PMMA. A complete description of the input parameters to the program is given and comparison to previous results is included.

1 . Grosswendt, B. Conversion Factors for the IAEA Cube Phantom for External Photon Irradiation, Radiation Protection Dosimetry 29: 177-182; 1 989

2. Rogers, D.W.O. Fluence to Dose Equivalent Conversion Factors Calculated with EGS3 for Electrons from 1 00 key to 20 GeV and Photons from 1 1 key to 20 GeV, Health Physics 46: 891-914; 1984

3. Halbleib, J. Structure and Operation of the ITS Code System, in Monte Carlo Transport of Electrons and Photons (ed. Jenkins, T. M., Nelson, W. R. and Rindi, A., Plenum Press, New York, 1988)

AGE DEPENDENCE OF ORGAN DOSE FROM EXTERNAL PHOTON SOURCES COMPUTED USING A MATHEMATICAL PHANTOM**

Richard C. Ward
Mohammad T. Hussain*
Jeffrey C. Ryman
Computing Applications Division

Mark Cristy
Keith F. Eckerman
Health Sciences Research Division

Oak Ridge National Laboratory
Oak Ridge, Tennessee 37831

ABSTRACT

Organ dose and effective dose equivalent from external photon sources are computed using the ALGAMP Monte Carlo transport code for mathematical phantoms of various ages. Estimates of organ dose and effective dose equivalent due to isotropic field and rotational normal beam exposure for a series of monoenergetic photon sources were made for the following mathematical phantoms: newborn, 1-, 5-, and 10-year-old adolescents, and a 15-year-old male/adult female, in addition to the adult male. The existing mathematical phantoms were modified to include the esophagus and neck region for all age groups. Adjustments were required to previously defined models for the thyroid and gall bladder in the newborn phantom. The doses were calculated for monoenergetic photon sources with energies in the range 0.01 to 8.0 MeV. In this talk we compare our results with previous calculations on the adult male mathematical phantom as a function photon source energy. Our results, presented as a function of phantom mass, demonstrate that newborns and younger children are more vulnerable to the radiation from comparable photon sources than older children or adults.

*Albion College, Albion, Michigan

**Research sponsored jointly by the Great Lakes Colleges Association/Associated Colleges of the Midwest and the Department of Energy under contract DE-AC05-84OR21400 with Martin Marietta Energy Systems, Inc.

INTRODUCTION

Organ dose and effective dose equivalent have been calculated for mathematical human phantoms representing ages from newborn to adult (Cristy and Eckerman, 1987), both for isotropic field and rotational normal beam exposure to monoenergetic photon sources. This is the first calculation of dose for these types of photon sources for ages other than adult (Eckerman and Ryman, 1993) and 6-month old. The position and size of individual organs inside the mathematical phantoms and the size of the phantoms are the principal causes of variation in organ dose. The ALGAMP Monte Carlo transport code was used for the dose calculations. These calculations provide dose information useful in deriving radiation protection standards for adults in the work place, and for exposure of the public, including younger ages, to radiation.

A version of the ALGAMP (Ryman and Eckerman, 1994) Monte Carlo photon transport code was used for the calculations. The source routines for isotropic field and rotational normal beam exposures were previously developed for the calculation of organ dose from external photon sources incident on the adult phantom. Here we calculate the organ dose and effective dose equivalent for the additional mathematical phantoms: newborn, 1-, 5-, 10-, and 15-year-old/adult female, as well as for the adult phantom.

MATHEMATICAL PHANTOM

In a mathematical phantom (Fig. 1), each organ is described by a mathematical equation that roughly represents the geometrical shape of the organ (Cristy and Eckerman, 1987). The elemental compositions and densities of tissues used in the mathematical phantom are the same for all ages, with the exception of the newborn. Three kinds of tissues are represented in the phantoms: skeletal tissue, lung tissue, and soft tissue, which has a density of approximately 1 gram per cubic centimeter. The composition of skeleton and soft tissue for the newborn differed from those for the other phantoms; the density of the skeletal tissue for the newborn was 1.22 g/cc, whereas for all other phantoms, the density of skeletal tissue was 1.4 g/cc.

The external surfaces of the phantom are defined by simple geometrical shapes. The head is defined by a right elliptical cylinder covered on the top by half an ellipsoid, and the neck is a right circular cylinder. The trunk is represented by an elliptical cylinder, and the legs are represented by truncated circular cones. Individual organs are represented in much the same way. The complexity varies from a simple shape, such as an ellipsoid to represent the brain, to more complex intersections of quadratic surfaces to represent organs such as the heart.

Prior to performing the calculations, the geometry routines of the ALGAMP Monte Carlo code were tested for all the mathematical phantoms. This testing was necessary since a neck region and an esophagus model were recently added. In the testing, photon sources were randomly selected in each organ, but no transport was allowed. All collisions should then occur in the source organ if the geometry routines work correctly. The testing revealed that changes to the newborn thyroid, gall bladder, and esophagus were necessary, and that the search logic in the head and the neck region needed to be modified.

DESCRIPTION OF THE PROBLEM TO BE MODELED

We calculated the organ dose and effective dose equivalent for eighteen different photon energies, ranging from 0.01 to 8.0 MeV, and for two different photon beam orientations. The two beam orientations are **Isotropic Field**, where the phantom is exposed to a radiation field in which the fluence is uniform in every direction (Fig. 2), and **Rotational Normal Beam**, where the phantom is rotated uniformly in a broad parallel beam of radiation.

Three basic interactions take place between photons and matter:

Photoelectric Effect: A photon is completely absorbed by an atom and ionization occurs. The energy of the photon is distributed to the ionized electron and to the nucleus of the atom.

Compton Scattering: An incident photon interacts with a loosely bound electron of an atom, looses part of its energy, and scatters at a direction different from its incident direction.

Pair Production: When a photon is close to the nucleus, the interaction of the photon with the electric field can give rise to an electron-positron pair. Both the electron and the positron lose energy with the surrounding medium by collisions. When the kinetic energy of the positron approaches zero it annihilates with an electron and produces photons. The energy of the incident photon involved in the process must exceed 1.022 MeV.

The product of the attenuation coefficient (cm^2/g) for photons in isolated tissue and the photon energy (MeV) is plotted versus photon energy (MeV) in Fig. 3. Attenuation below 100 keV occurs primarily by photoelectric effect. Attenuation by Compton scattering occurs throughout the energy range, decreasing as photon energy increases. Above 1.022 MeV, attenuation is dominated by pair production.

THE MONTE CARLO TRANSPORT METHOD

The Boltzmann transport equation is used to describe the transport of photons through matter. The individual terms in the Boltzmann equation represent the birth, spatial translation, and the collision, scattering, and leakage of the particles. The organ dose due to external photon sources incident on mathematical phantom representing the human body can be approximated by solving the time-independent, neutral-particle Boltzmann transport equation (Eckerman and Ryman, 1993):

$$\bar{\nabla}\cdot\bar{\Omega}\,\Phi(\bar{r},E,\bar{\Omega}) + \mu(\bar{r},E)\,\Phi(\bar{r},E,\bar{\Omega}) = \int dE' \int d\bar{\Omega}'\,\mu_s(\bar{r},E'\to E,\bar{\Omega}'\to\bar{\Omega})\,\Phi(\bar{r},E',\bar{\Omega}') + S(\bar{r},E,\bar{\Omega}) \quad , \tag{1}$$

where $\Phi(\bar{r},E,\bar{\Omega})dEd\bar{\Omega}$ is the angular fluence at position $\bar{r}$ with energy in dE about E and direction in solid angle $d\bar{\Omega}$ about direction $\bar{\Omega}$; $\mu(\bar{r},E)$ is the linear attenuation coefficient at position $\bar{r}$ and energy E; $\mu_s(\bar{r},E'\to E,\bar{\Omega}'\to\bar{\Omega})dEd\bar{\Omega}$ is the probability per unit path length that a particle with initial energy E' and direction $\bar{\Omega}'$ will undergo a scattering collision at point $\bar{r}$ and emerge with energy in dE about E and in $d\bar{\Omega}$ about $\bar{\Omega}$; and $S(\bar{r},E,\bar{\Omega})dEd\bar{\Omega}$ is the number of source particles emitted at position $\bar{r}$ with energy in dE about E and direction in $d\bar{\Omega}$ about $\bar{\Omega}$.

In Monte Carlo transport calculations, spatial coordinates, energies, and direction cosines of a photon are sampled from distributions representing the source, transport between interaction sites, and Compton scattering. At each interaction site, the expected value of the energy that could be deposited at that site is scored (i.e., summed) in a counter for the organ in which the interaction occurred. The photon begins with an initial weight (i.e., probability of existence) of 1.0 at the source.

After each collision, the photon weight is reduced by a factor equal to the probability that it could undergo a Compton scattering. A photon is followed through the mathematical phantom until (a) it escapes from the phantom, (b) its weight becomes too low to make any

significant contribution to the dose, or (c) its energy falls below a cutoff energy (0.004 MeV), in which case the remaining energy is assumed to be absorbed at the point of last collision.

At a given interaction site, if the photon has sufficient energy (greater than 1.022 MeV) to undergo a pair production interaction, an annihilation photon of energy 0.511 MeV and a weight equal to twice the parent photon weight times the probability of pair production is generated and tracked from that site. It is assumed that the kinetic energy of the electron and positron formed by the pair production event immediately undergo annihilation without any further transport. The kinetic energy of the electron and positron are taken into account in computing the expected value of energy deposited at each collision site.

The process of following a photon trajectory, or history, is repeated many times (in this work - 100,000) which constitutes a "batch" of histories. In turn, calculations for several batches (in this work, 100) are performed. Each batch can be thought of as providing the computational equivalent of measured values of organ doses from a single experiment. The values from all batches are treated just as measured values in a physical experiment, to give an estimate of mean values of organ doses, each of which has an associated standard deviation of the mean. As in a physical experiment, the only way to reduce the uncertainty is to acquire more data points (i.e., to follow more histories). The uncertainty in the organ dose is inversely proportional to the square root of the number of histories (i.e., the number of batches times the number of photons per batch).

In calculating the effective dose equivalent we have taken into consideration the normalization factors that convert the dose per photon to a dose per fluence. For the isotropic field the normalization factor is the total surface area of the cylinder surrounding the phantom divided by four. For the rotational normal beam the normalization factor is the diameter times the height of the cylinder surrounding the phantom. The normalization factors (in cm^2) are given below:

PHANTOM	NORMALIZATION (cm^2)	
	Rotational Normal Beam	Isotropic Field
Adult male	7144	6239
15-year old	5798	5021
10-year old	3886	3355
5-year old	2499	2168
1-year old	1310	1150
Newborn	646	571

ANALYSIS

Using the ALGAMP Monte Carlo code, the **Organ Dose,** H_T (i.e. the total amount of energy per unit mass absorbed by an organ) is computed for each organ defined in the mathematical phantom. The unit of organ dose is Gray (Gy) or J/kg. The **Effective Dose Equivalent,** H_E, is computed as the weighted sum of the doses to radiosensitive tissues of the body (Eckerman and Ryman, 1993):

$$H_E = \sum_T w_T H_T \,, \tag{2}$$

where w_T are the weighting factors for the individual organs that contribute to the effective dose equivalent. The unit of effective dose equivalent is Sievert (Sv). The following weighting factors were used to compute the effective dose equivalent:

ORGAN	w_T
Lung	0.12
Thyroid	0.03
Breast	0.15
Bone Surface	0.03
Active Marrow	0.12
Gonads	0.25
Remaining Tissue	0.30

Gonad dose is taken to be the larger of the dose to the ovaries or testes at each energy. The dose to remaining tissue is calculated by averaging the organ dose for the five organs, excluding those mentioned above, with the highest doses. Note that the dose to the gonads and breast, which in the newborn are very small organs, contributes 40% to the effective dose equivalent.

Using the ALGAMP Monte Carlo code, we computed the organ dose for all the organs defined in the mathematical phantom for eighteen different photon energies, ranging from 0.01 to 8.0 MeV. Results were obtained for the newborn, 1-, 5- 10-, 15-year-old/adult female phantom and the adult phantom. Figures 4 and 5 show the dose to breast and thyroid respectively, in units of 10^{-12}Sv cm^2, plotted vs the source photon energy, in MeV, for both the newborn and the adult mathematical phantom. The breasts are on the surface of the phantom and therefore show behavior similar to the plot for isolated tissue (Fig. 3), especially in the case of the newborn. The thyroid is not as close to the surface of the phantom, so there is more shielding by other tissues at low-source photon energies. The results for the thyroid show greater variation with respect to beam orientation, the results for the isotropic field are lower than those for the rotational normal beam due to shielding by the head and torso.

Calculations for organ doses for the newborn phantom showed some anomalies at high photon energies for ovaries, testes, thyroid, and breast. The anomalies for some organs at high energy could be due to a number of reasons. To determine if the calculational method was introducing an error in certain organ doses for the newborn, we reran the case for the newborn phantom without ray tracing. Typically, the Monte Carlo calculations are made using ray tracing, which is a method in which a set of coordinates and direction cosines on the surface of the cylinder surrounding the phantom determines the location of the first interaction of the photon on the surface of the phantom. Comparisons of the organ dose to the ovaries computed with and without ray tracing suggest that the inconsistencies at high photon energies for organs of small mass were simply statistical and that the results would be improved by running more photon histories.

Using the computed organ doses and the weighting factors defined above, we calculated the effective dose equivalent for eighteen different photon energies, ranging from 0.01 to 8.0 MeV, for the adult phantom and compared those with the previously calculated effective values of Eckerman and Ryman (1993) [see also: ICRP(International Commission On Radiological Protection) publication 51]. For the adult phantom, our results are in excellent agreement with the existing data (Eckerman and Ryman, 1993). All results were within 2% of those of Eckerman and Ryman for the adult phantom.

Finally, effective dose equivalents were computed from organ doses for the newborn, 1-, 5-, 10-, 15-year old/adult female mathematical phantoms. These results for effective dose equivalent were combined with the results for the adult phantom in Figs. 6 and 7. The first plot (Fig. 6) shows the effective dose equivalent as a function of photon energy for isotropic field for all mathematical phantoms. The second plot (Fig. 7) shows effective dose equivalent versus photon energy for rotational normal beam for all mathematical phantoms. The effective dose equivalent increases with decreasing age, being highest for the newborn. These differences in the effective dose equivalent are most apparent below 100 keV.

The table below gives the effective dose equivalent versus photon energy for each of the phantoms for both the isotropic field (ISO) and the rotational normal beam (RNB) exposures. These results compare to within 2% of those obtained by Eckerman and Ryman (1993).

Effective Dose Equivalent (10^{-12} Sv*cm^2)

Photon Energy (Mev)	Phantom: Newborn RNB	Newborn ISO	1-year RNB	1-year ISO	5-year RNB	5-year ISO	10-year RNB	10-year ISO	15-year RNB	15-year ISO	Adult RNB	Adult ISO
0.01	0.301	0.260	0.189	0.167	0.140	0.119	0.118	0.098	0.019	0.016	0.014	0.013
0.015	0.421	0.361	0.341	0.273	0.279	0.226	0.251	0.210	0.092	0.076	0.075	0.063
0.02	0.457	0.370	0.358	0.289	0.312	0.255	0.276	0.236	0.159	0.131	0.139	0.119
0.03	0.463	0.389	0.366	0.292	0.316	0.259	0.282	0.229	0.223	0.184	0.207	0.172
0.05	0.380	0.325	0.342	0.283	0.317	0.256	0.291	0.243	0.258	0.214	0.246	0.204
0.07	0.366	0.322	0.349	0.292	0.341	0.280	0.315	0.266	0.292	0.244	0.284	0.235
0.10	0.443	0.382	0.429	0.364	0.414	0.346	0.398	0.333	0.376	0.311	0.364	0.305
0.20	0.898	0.793	0.880	0.758	0.845	0.737	0.842	0.695	0.757	0.644	0.734	0.629
0.50	2.45	2.27	2.42	2.10	2.31	2.00	2.19	1.95	2.02	1.77	1.97	1.74
0.80	3.80	3.53	3.56	3.23	3.70	3.15	3.46	3.13	3.23	2.87	3.10	2.79
1.0	4.69	4.39	4.41	4.01	4.26	3.92	4.11	3.81	3.92	3.53	3.79	3.43
1.5	6.37	5.76	5.99	5.72	5.96	5.48	5.84	5.45	5.40	5.03	5.38	4.92
2.0	7.72	7.54	7.64	7.43	7.26	6.85	7.21	6.68	6.80	6.40	6.78	6.15
3.0	10.65	10.30	10.15	9.77	10.23	9.40	9.12	9.02	9.30	8.70	9.03	8.36
4.0	12.77	12.51	12.25	11.79	11.77	11.20	12.04	11.40	11.46	10.77	11.16	10.52
5.0	14.43	14.28	14.67	14.17	13.93	13.09	13.87	13.33	13.47	12.54	13.29	12.52
6.0	16.80	16.67	16.47	15.81	15.55	15.77	15.87	15.40	15.38	14.38	15.17	14.07
8.0	21.24	21.07	20.27	19.41	18.99	19.14	20.31	18.48	19.67	17.99	18.85	17.81

Figure 8 shows effective dose equivalent plotted as a function of phantom mass (related to age) for two photon energies (0.05 Mev and 0.5 Mev). These plots reveal that newborns and younger children are more vulnerable to radiation than adults, attributed primarily to the smaller size of organs in young children and the newborn.

SUMMARY

We have calculated organ dose and effective dose equivalent for the phantoms representing the ages 1-, 5-, 10-, 15-year old or the adult female, and the adult. The effective dose equivalent for the adult phantom is in very good agreement with the established data for the adult phantom (ICRP Publication 51, Eckerman and Ryman 1993). Comparisons were made of the effective dose equivalent for all mathematical phantoms, including adult. The effective dose equivalent at a given photon energy increases with decreasing age, being highest for the newborn. The increase is most pronounced for photon energies below 100 keV. Statistical analysis of the Monte Carlo results showed that the largest errors occurred in computing organ doses for organs of small mass in the newborn. These errors, all within 1 standard deviation of the mean, could be reduced by computing longer photon histories for the newborn.

REFERENCES

Cristy, M. and K. F. Eckerman (1987) *Specific Absorbed Fractions of Energy at Various Ages from Internal Photon Sources. I. Methods.*, ORNL/TM-8381/V1 (Oak Ridge National Laboratory, Oak Ridge, TN).

Eckerman, K. F. and J. C. Ryman (1993) *External Exposure to Radionuclides in Air, Water, and Soil, Federal Guidance* Report #12, Environmental Protection Agency, Washington, D. C.

ICRP (1987) International Commission on Radiological Protection, "Data for Use in Protection Against External Radiation," ICRP Publication 51, *Annals of the ICRP Vol. 17, No. 2/3.*

Ryman, J. C. and K. F. Eckerman (1994) *ALGAMP - A Monte Carlo Radiation Transport Code for Calculating Specific Absorbed Fraction of Energy for Internal or External Photon Sources*, ORNL/TM-8377 (Oak Ridge National Laboratory, Oak Ridge, TN).

Fig. 1. Anterior view of the principal organs of the mathematical phantom.

Fig. 2. Mathematical phantom inside surrounding cylinder showing isotropic field.

Fig. 3. Product of the Photon attenuation (cm^2/g) and the photon energy (MeV) versus photon energy (MeV) for isolated tissue.

Fig. 4. Dose to breast ($10^{-12}Sv \bullet cm^2$) vs photon energy (MeV) for newborn and adult in both isotropic field and rotational normal beam.

Fig. 5. Dose to thyroid ($10^{-12}Sv \bullet cm^2$) vs photon energy (MeV) for newborn and adult in both isotropic field and rotational normal beam.

Fig. 6. Effective dose equivalent ($10^{-12}Sv \bullet cm^2$) versus photon energy (MeV) for all phantoms in isotropic field.

Fig. 7. Effective dose equivalent ($10^{-12}Sv \bullet cm^2$) versus photon energy (MeV) for all phantoms in rotational normal beam.

Fig. 8. Effective dose equivalent ($10^{-12}Sv \bullet cm^2$) versus phantom mass (kg) for two photon energies, 0.05 Mev and 0.5 Mev.

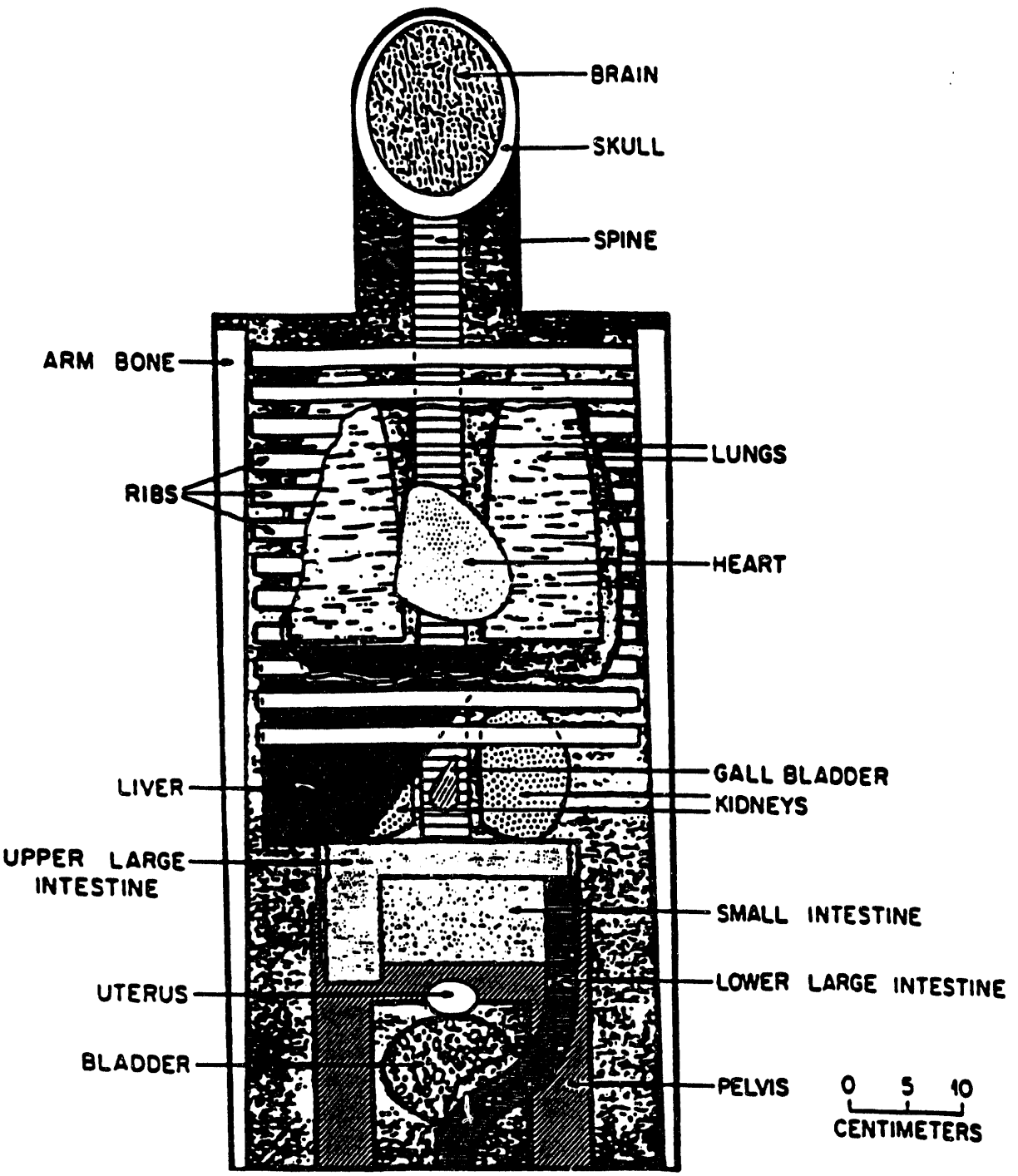


Fig. 1 Anterior view of the principal organs of the mathematical phantom

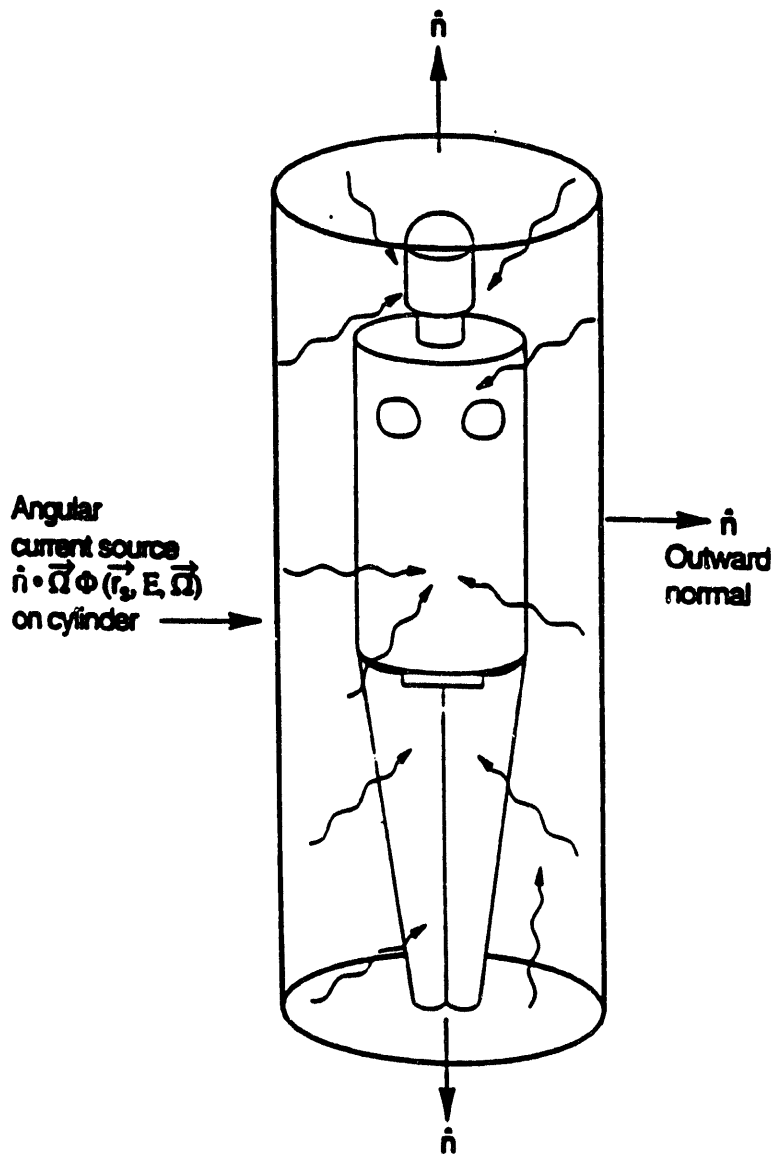
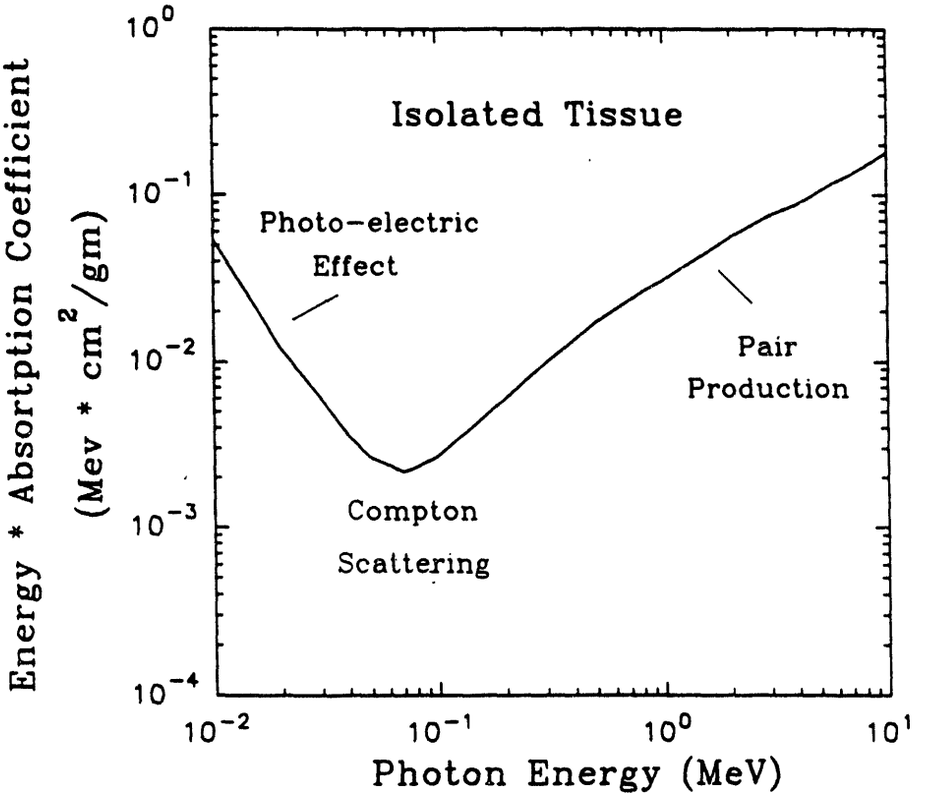
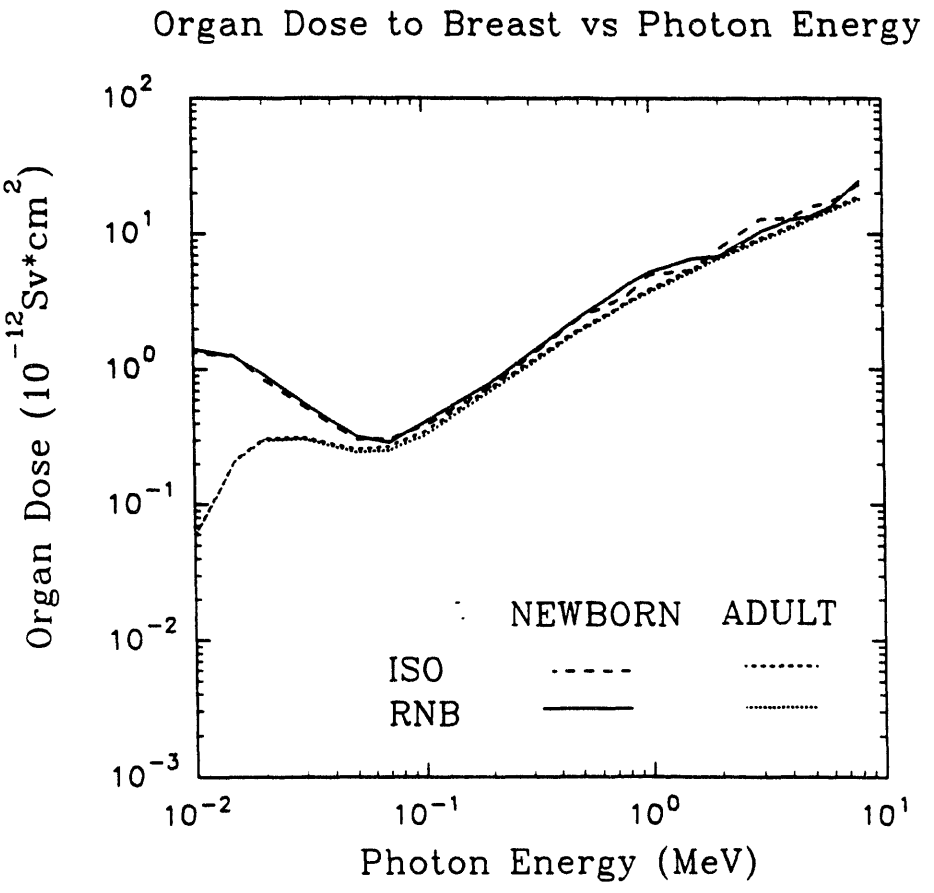
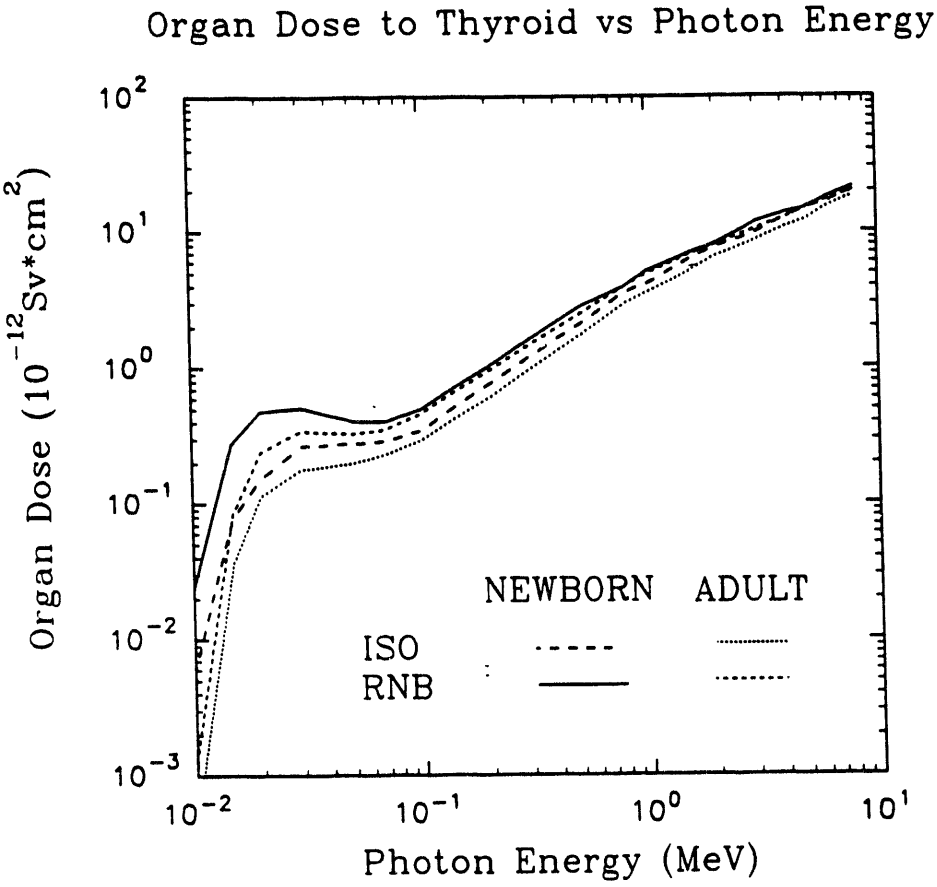
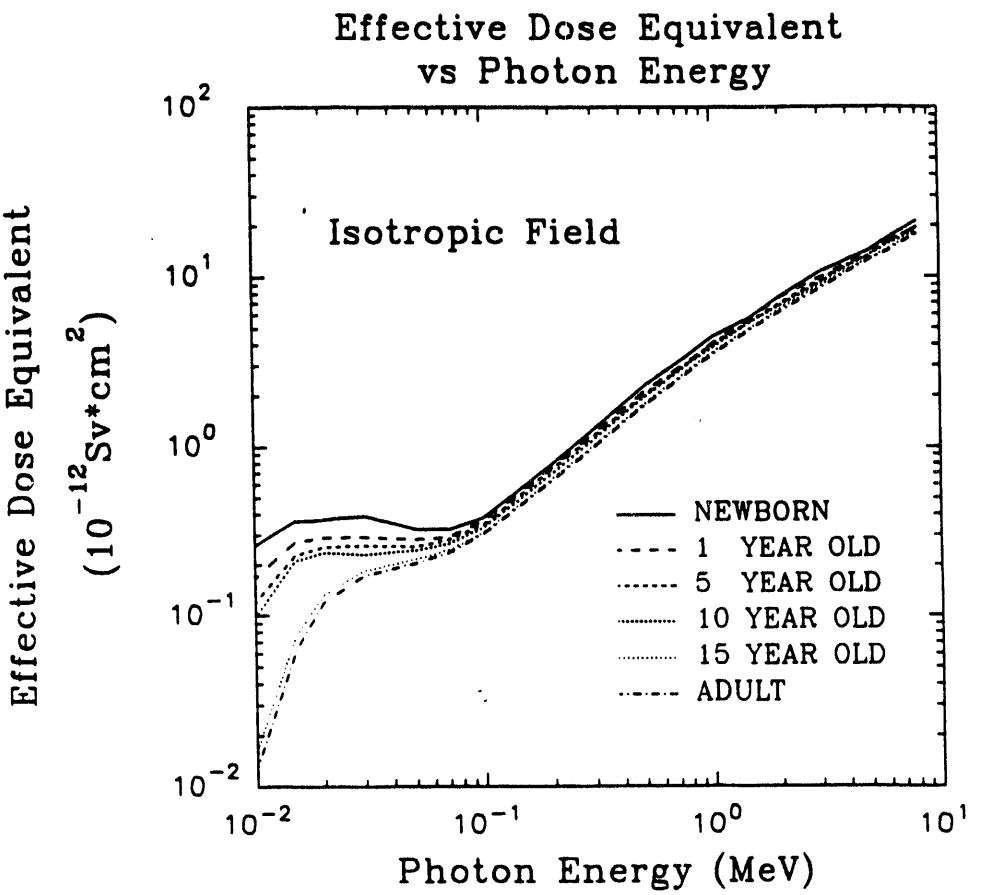


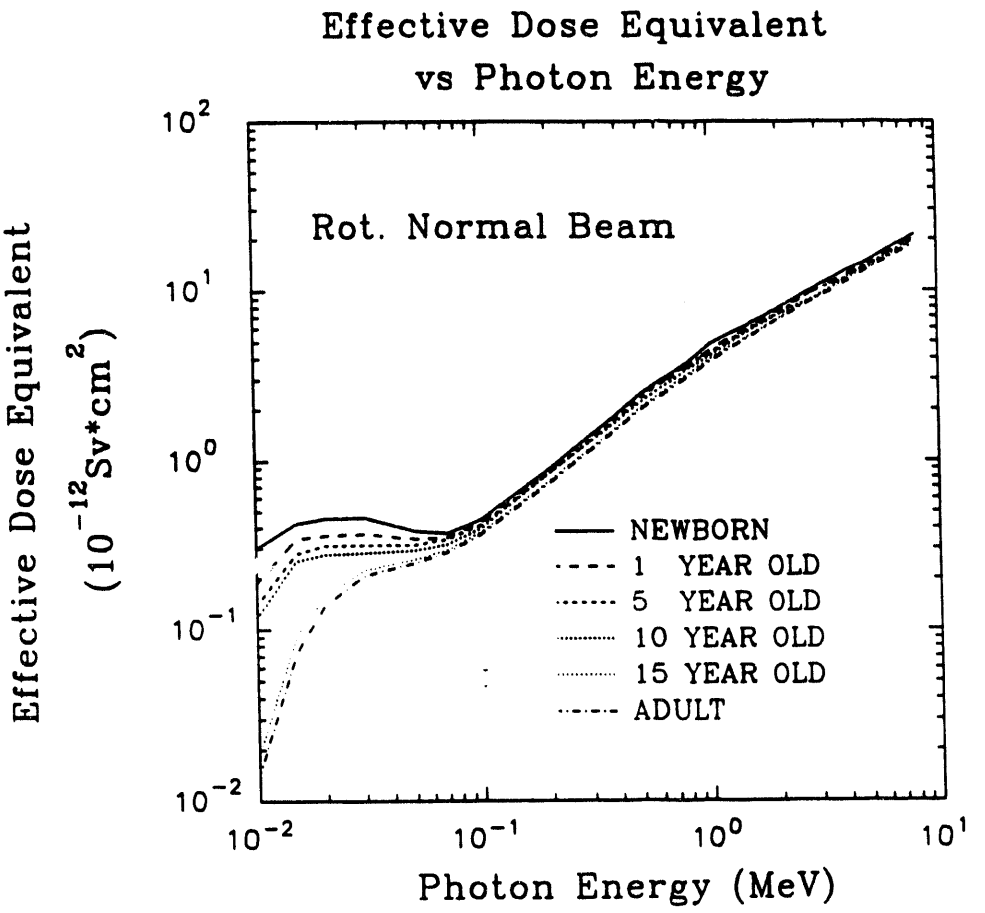
Fig. 2 Mathematical phantom inside surrounding cylinder showing isotropic field.

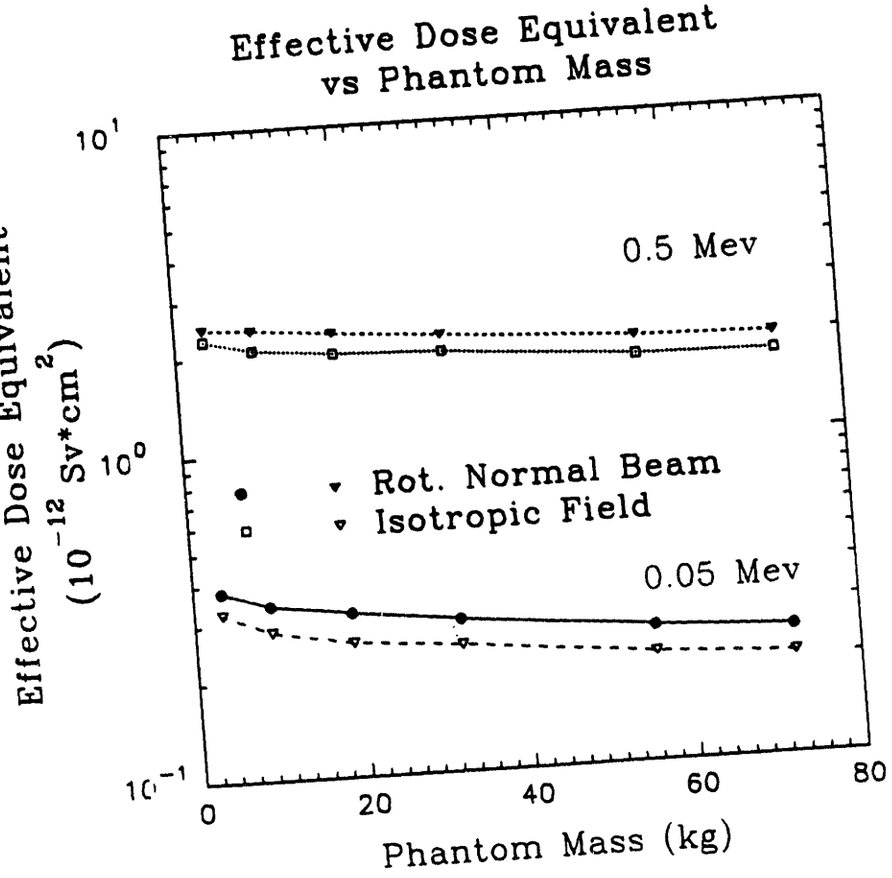

Isolated Tissue
Photo-electric
Effect
Compton
Scattering
Pair
Production
Energy * Absortption Coefficient
(Mev * cm 2 /gm)
Photon Energy (MeV)
10^0
10^-1
10^-2
10^-3
10^-4
10^-2
10^-1
10^0
10^1


Organ Dose to Breast vs Photon Energy
Organ Dose (10^{-12} Sv*cm^2)
10^2
10^1
10^0
10^{-1}
10^{-2}
10^{-3}
NEWBORN ADULT
ISO
RNB
10^{-2}
10^{-1}
10^0
10^1
Photon Energy (MeV)


Organ Dose to Thyroid vs Photon Energy
Organ Dose (10^{-12} Sv*cm^2)
10^2
10^1
10^0
10^{-1}
10^{-2}
10^{-3}
10^{-2}
10^{-1}
10^0
10^1
Photon Energy (MeV)
NEWBORN
ADULT
ISO
RNB


Effective Dose Equivalent
vs Photon Energy
Isotropic Field
NEWBORN
1 YEAR OLD
5 YEAR OLD
10 YEAR OLD
15 YEAR OLD
ADULT
Effective Dose Equivalent
(10^-12 Sv*cm^2)
Photon Energy (MeV)
10^2
10^1
10^0
10^-1
10^-2
10^-2
10^-1
10^0
10^1


Effective Dose Equivalent
vs Photon Energy
Rot. Normal Beam
Effective Dose Equivalent
(10^{-12}Sv*cm^2)
10^2
10^1
10^0
10^{-1}
10^{-2}
10^{-2}
10^{-1}
10^0
10^1
Photon Energy (MeV)
NEWBORN
1 YEAR OLD
5 YEAR OLD
10 YEAR OLD
15 YEAR OLD
ADULT


Effective Dose Equivalent
vs Phantom Mass
Effective Dose Equivalent
(10^{-12} Sv*cm^2)
10^1
10^0
10^{-1}
0.5 Mev
Rot. Normal Beam
Isotropic Field
0.05 Mev
0
20
40
60
80
Phantom Mass (kg)

SKIN DOSE DETERMINATION USING SURVEY METERS AND VARSKIN MOD 2

René Michel, John J. Fix, and Joseph C. McDonald

Pacific Northwest Laboratory, P.O. Box 999, Richland, WA 99352

ABSTRACT

Survey meters are used at almost every radiation worker exit location. These instruments are used as the first means of determining if a worker has been exposed to radiation. However, skin dose from direct skin contamination or contaminated clothing is often undetected at the time of exit because survey meters are not properly calibrated to measure radiation doses, and sometimes, the type of nuclide resident on clothes or skin is unknown. For this study we used three different survey meters, several calibrated sources, and the computer code Varskin Mod 2 to generate conservative action levels to screen radioactive contamination cases that require further analysis. Moreover, a series of tables with conversion factors were produced to determine the skin dose, once the type of nuclide was identified.

INTRODUCTION

GM pancakes and ion chambers are two of the most common detectors used to frisk personnel after working with unsealed radioactive materials. Even though these survey meters are not calibrated to measure shallow dose equivalents (skin doses) because their response is given in cpm or mR/h respectively, the response obtained from these detectors could be used to estimate accurately the skin dose. These estimations could be performed by obtaining the response of the probes to known doses, from known sources and their activities. In this study we used three different survey meters, four small beta and beta + gamma calibrated radiation sources, and the computer code Varskin Mod 2 (Durham 1993) which makes use of radionuclide point kernels to calculate the dose to the skin at the basal cell layer and the basal cell survival (Berger 1971). Using these, we can generate conservative action levels to screen cases that require further analysis as established by the Nuclear Regulatory Commission and Department of Energy (NRC 1991, DOE 1993). Moreover, a series of tables with conversion factors were produced to determine the skin dose from survey meter responses, once the type of nuclide is identified.

MATERIALS AND METHODS

For this study, four calibrated radionuclide check sources (^{36}Cl, ^{137}Cs, ^{99}Tc, and $^{90}Sr/Y$) were used to simulate contamination on a small area of the skin or clothing, a calibrated Eberline

Model 260 pancake probe[1], two calibrated Eberline Model RO-2 and RO-3B ion chambers, and a piece of overall clothing (worn by radiation workers), which when placed between the source and the detector, simulates contamination on clothing. For measurements, a source-to-detector beta window distance was set equal to 1 cm. Several readings were taken and recorded for each nuclide with and without the clothing material. The skin doses were calculated by using the 2 dimension disk geometry option from the Varskin Mod 2 computer code and the following assumptions:

- The active area of the sources is equal to 1 cm2
- The skin depth is equal to 7 mg/cm^2
- The thickness of the covering material is equal to 0 mm for bare measurements and 0.7 mm when using clothing
- Since the thickness of the clothing material is 0.7 mm, the air gap thickness used (distance between detector and source) is equal to 10 mm for bare measurements and 9.3 mm when using clothing material

The dose rates were averaged over 15.2, 38.48 and 50.27 cm^2 which are the beta window areas of the GM pancake and the two ion chambers, respectively.

RESULTS AND DISCUSSION

Table 1 shows the results obtained using the different survey meters, and the doses calculated with Varskin Mod 2. Column 1 shows the ratio of survey meter's response in cpm or mR/h and the calculated dose rates in mSv/h. The following analysis could be initiated to calculate skin doses for cases where a small area of the skin or clothing is contaminated (for a contamination larger than about five cm in diameter, slab sources could be used to better simulate the conditions).

1. Find the maximum response (cpm or mR/h) over the area contaminated using any of the three detectors.
2. Determine the skin dose (using Table 1) by dividing the maximum response by the dose rate conversion factor for the appropriate nuclide depending on the type of contamination (i.e., skin or clothing).
3. If the nuclide is unknown, the smallest response factor could be used to estimate conservatively the skin dose.

If, for example, 1 mSv is chosen as the maximum screening dose limit to be used at the exit of a contaminated area, the most conservative dose rate conversion factor (i.e., ^{90}Sr/Y with

[1] TMA/Eberline 5635 Jefferson Street, Albuquerque, NM, 87109

clothing) from the table could be used to determine the action levels for each instrument. By doing this, the following values were obtained:

Detector	Action level
Eberline Model 260 GM Pancake	2.5×10^5 cpm
Eberline Model RO-2 ion chamber	8.0 mR/h
Eberline Model RO-3B ion chamber	6.0 mR/h

Due to the nature of these detectors, this method to determine skin doses should be used only as a means to obtain a good estimation of the actual dose. More sensitive and specialized detectors such as plastic scintillators could be used to obtain more accurate results.

REFERENCES

Berger, M.J. 1971. "Distribution of Absorbed Dose Around Point Source of Electrons and Beta Particles in Water and other Media." J. Nuc. Med. MIRD Supplement No. 5, 9, 5-23.

Durham, J.S. 1993. Computer Code Varskin & Sadde Mod 2, NUREG/CR 5873. U.S. Nuclear Regulatory Commission.

10CFR20 (Subpart C, 20.1201). 1991. U.S. Nuclear Regulatory Commission.

10CFR835 Radiological Control Manual (Subpart C,845.202, Table 2-2). 1993. Department of Energy.

Table 1. Dose Rate Conversion Factors for the Different Survey Meters

Eberline Model 260 GM Pancake		
Nuclide	Skin Contamination cpm/mSv/h	Clothing Contamination cpm/mSv/h
Cl-36	12.4×10^5	10.1×10^5
Cs-137	7.6×10^5	5.6×10^5
Sr/Y-90	6.4×10^5	6.6×10^5
Tc-99	14.0×10^5	23.5×10^5
Eberline Model RO-2 Ion Chamber		
Nuclide	Skin Contamination mR/h/mSv/h	Clothing Contamination mR/h/mSv/h
Cl-36	41.0	33.1
Cs-137	26.1	23.5
Sr/Y-90	19.9	16.1
Tc-99	44.9	140.0
Eberline Model RO-3B Ion Chamber		
Nuclide	Skin Contamination mR/h/mSv/h	Clothing Contamination mR/h/mSv/h
Cl-36	37.0	31.6
Cs-137	39.4	58.9
Sr/Y-90	14.0	12.3
Tc-99	26.6	91.4

RESPONSE OF PANASONIC UD-802 AND UD-803 PERSONNEL DOSIMETERS TO FAST (PuBe) NEUTRONS

Becky S. Sobel and Kenneth A. Hardy (USAF Armstrong Laboratory/OEBD, Brooks AFB, TX)

The Panasonic UD-802 dosimeter is currently used in the USAF Personnel Dosimetry Program for neutron exposure monitoring. USAF dosimetry is NVLAP-certified for UD-802 usage, based on modersated ^{252}Cf. When exposed to highly moderated neutron fields, the UD-802 dose algorithm performs within the required margins. However, when exposed to unmoderated fast neutron sources such as PuBe, the present UD-802 dose algorithm seriously underestimates the neutron dose. It is apparent that the UD-802 dose algorithm must be modified for fast neutron spectra. Testing is currently underway to improve the UD-802 fast neutron capability using a calibrated PuBe source. In a related effort to improve fast neutron dose reliability, similar testing has also begun on Panasonic UD-809 dosimeters. The results of these measurements on the UD-802 and UD-809 dosimeters will be reported.

SESSION IV.
Instrumentation

John Frazier,
Chairman

A NEW NEUTRON DOSE EQUIVALENT RATE METER WITH IMPROVED NEUTRON ENERGY RESPONSE IN TERMS OF H*(10)

A. Klett, R. Maushart
EG&G Berthold, Bad Wildbad, Germany
B. Burgkhardt, G. Fieg, E. Piesch
Karlsruhe Nuclear Research Center, Germany

Abstract

Conventional neutron dose rate meters make use of thermal neutron detectors such as ^{3}He counters located in the center of a moderator and absorber for thermal neutrons. The various commercial types used up to now have the disadvantage that the reading is extremely energy dependent exceeding a factor of up to 15. The need to improve the energy response and the sensitivity in the lower dose rate range resulted in joint cooperation between KfK and EG&G Berthold.

On the basis of Monte-Carlo calculations and comprehensive calibrations with monoenergetic neutrons at the PTB Braunschweig, a new type of rem-counter has been optimized using a 10 cm × 4 cm diameter ^{3}He-counter. Both calculations and experiments resulted in a lower energy dependence within ±40% in the energy range 20 keV to 19 MeV. The commercially available dose rate meter of 25 cm diameter, with a weight below 10 kg and with a high neutron sensitivity of 3 counts per nSv has a dose rate range of 0.1 µSv/h - 100 mSv/h and low γ-sensitivity. With integrated electronics, this instrument is applicable for routine monitoring as well as for stationary monitoring of radiation fields near accelerators.

1. Introduction

In environmental neutron monitoring there is now increasing interest in commercially available dose-rate-meters with an instrument response tuned to ambient dose equivalent H*(10). This is because the International Commission on Radiological Protection has modified in ICRP60 [1] its recommendations on the formal relationship between the quality factors and the linear energy transfer to reflect the higher effective biological effectiveness of intermediate energy neutrons. As a consequence, the old neutron fluence to dose equivalent conversion factors based on ICRP21 [2] have to be changed. The conversion factors are shown in figure 1. As the ratio of these curves is a function of energy, existing neutron monitors can not simply be recalibrated by a trivial factor but it is necessary to develop detector systems which are optimized with respect to the new energy dependent requirements. Another objective of the development was to increase the detection efficiency considerably in comparison with competitive instruments.

2. Monte-Carlo Calculations

The energy dependence of the detector response is determined by the details of the geometrical arrangement. The most important parameters are the characteristics of the counter tube, the diameter of the moderator, and the material, position and perforated fraction of absorbing layers. To find the optimum choice for these parameters extensive Monte-Carlo calculations with the neutron transport code MCNP [3] have been performed.

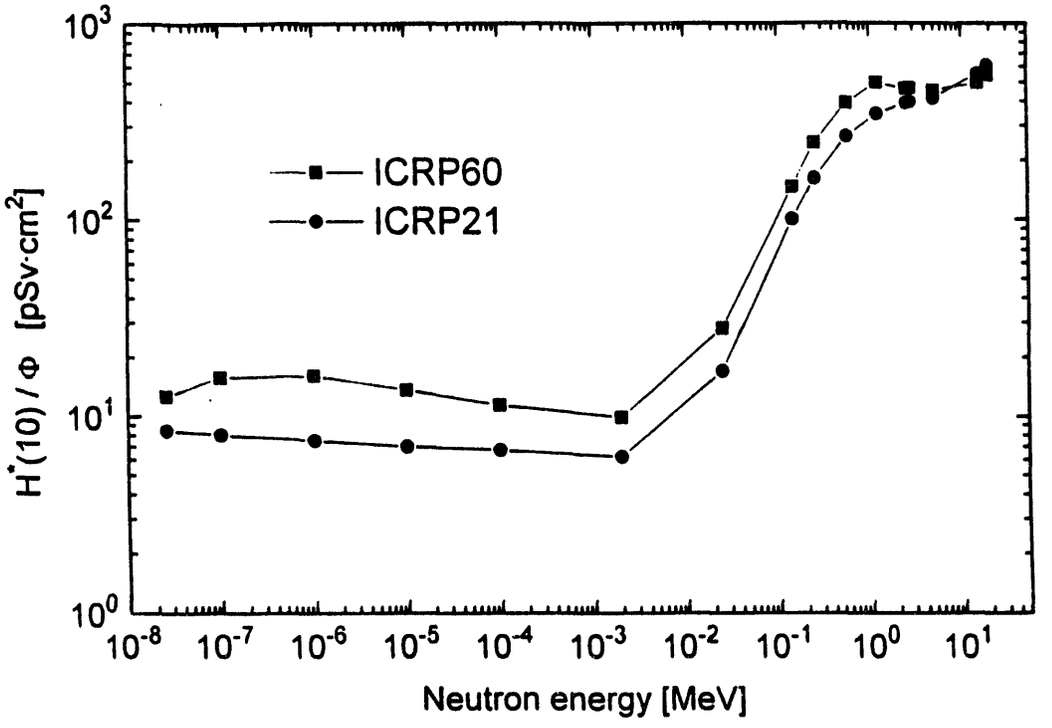


Fig. 1. Neutron fluence to ambient dose equivalent conversion factors

For the simulation in a semi-realistic model all detector components with true material compositions have been taken into account. Some parts, for example isolators, have been simplified in geometry or by homogenizing the materials. The calculations have been performed with the neutron cross section data from the latest version of the European Fusion File 1991 [4]. The differential cross sections of the neutron-proton elastic scattering have been taken as isotropic. The incident neutrons have been modelled as parallel beam. The statistical precision of the calculation was better than 8% at thermal and better than 5% at the other neutron energies.

Variation of parameters in a computer database is much easier than performing cumbersome and expensive measurements with monoenergetic neutrons and with varying detector setups. Nevertheless preliminary prototype versions had been build and tested with Am-Be and Cf-252 sources and with monoenergetic neutrons to prove the reliability of the calculation. The MC predictions had always been confirmed absolutely within 20% or better. These results have previously been reported [7].

3. Detector Description

The optimized detector setup, designated LB6411, consists of a specially developed ^{3}He proportional counter tube, a moderating sphere with internal neutron absorbers, integrated high voltage supply, signal processing electronics and a µP-controlled portable datalogger, which evaluates and displays the results of measurements.

The cylindrical ^3He proportional counter tube has size Ø4 cm × 10 cm, stainless steel walls with thickness 1 mm, Al_2O_3 ceramic isolators and 100 µm tungsten wire. The active length of the counter tube is roughly the same as the diameter to match with the spherical moderator geometry. The counter is filled with ^3He at 3.5 bar and CH_4 at 1 bar partial pressure. The methane admixture serves as quenching gas, increases the stopping-power to reduce wall effects and as a third function supplies protons to the detection volume. Neutrons at higher energies produce recoil protons which offer an additional detection mechanism. The detection efficiency for thermal neutrons is around 90%. The relatively large active volume together with the gas-filling gives rise to a high efficiency of the neutron detection system.

The moderator sphere has diameter 25 cm. Polyethylene with a small carbon admixture and density 0.95 g/cm^3 is used as a moderating material. The counter tube is located in the moderator with its active volume centered in the sphere. The ^3He detector is surrounded by 2 cm of cylindrical moderator. The surface of this internal cylinder is covered with perforated cadmium of thickness 0.5 mm. The perforated fraction of the internal neutron absorber is 10%. The complete inner assembly is embedded in the moderator sphere. The preamplifier and the high voltage supply is integrated in a small box on top of the neutron-counter. The working voltage of the detector is 2200 Volt. A cable connects the datalogger with the probe and transmits power and digitized signals.

4. Measurements

Monoenergetic neutron beams are provided by the Physikalisch-Technische-Bundes-anstalt (PTB) in Braunschweig, Germany. At the accelerator facility [5] and the research and measurement reactor facility [6] there are standard neutron fields available as recommended by the International Organisation for Standardization ISO [8]. During February 1994 the dose-rate-meter LB6411 was calibrated there.

At the accelerator facility in Braunschweig, a 3.75 MV Van de Graaff accelerator generates charged particle beams to produce neutrons via nuclear reactions such as $^7Li(p,n)^7Be$, $T(p,n)^3He$, $D(d,n)^3He$ or $T(d,n)^4He$. The neutron production target is in the center of the low backscatter experimental hall with area 24 m × 30 m and height 14 m. The neutron source and the rem-counter were at the same height 6.25 m above solid floor with a distance of 3.475 m between them. A gridded aluminium floor at height 4.5 m allows access to the experiment. The neutrons are emitted in the forward direction relative to the charged particle beam. The neutron radiation at the rem-counter's position can be considered as parallel and homogeneous. Experiments have been done at neutron energies 0.144, 0.25, 0.565, 1.2, 2.5, 5, 14.8 and 19 MeV. Contributions from scattered neutrons have been determined with a shadow cone (20 cm iron + 30 cm polyethylen) to be subtracted. As the experimental hall is designed to minimize neutron backscattering the subtracted fractions are only 7% - 22%. At 19 MeV it was necessary to measure background from the target materials using a blank target and correct for it.

The quantity of interest is the fluence response R_Φ of the neutron detector which can be calculated from instrument reading M and neutron fluence Φ by equation:

$$R_\Phi = M/\Phi$$

The PTB staff controlled the neutron fluences Φ with several independent monitoring systems and reported the values. The fluence responses of the neutron-counter are listed in table 2 together with the responses to ambient dose equivalent and the conversion factors that had been used for their calculation [9].

At the reactor facility there are several beam lines producing quasimonoenergetic neutrons between thermal energies and 144 keV by difference filtering methods. For every neutron energy, difference measurements with special filter materials had to be done. Since the cross section of the beam is smaller than the detector's dimensions, it was necessary to scan the neutron monitor. Data had been collected in a 2-dimensional grid perpendicular to the beam axis. The grid must be big enough to cover the intrument's sensitive surface into the tails of overlapping beam and efficiency profiles. The stepwidth was chosen according to the size of the beam spot. Details concernig the reactor beamlines and the scanning procedure are in table 1.

The fluence response is figured out off-line by adding up the normalized scanning results and evaluated with:

$$R_\Phi = \frac{(M_1 - M_2)}{J} \cdot \Delta x \cdot \Delta y \cdot K_D$$

where M_1 , M_2 are instrument readings with filter and difference filter respectively, J is the incident neutron rate (s^{-1}) monitored by the PTB, Δx and Δy are stepwidths of grid increments in x- and y-direction and K_D is an additional correction factor.

Table 1: Parameters of beamlines and scans at the reactor FMRB at PTB

Neutron Energy [keV]	Beam-line	Filter	Difference Filter	FWHM beam [mm]	step-width [mm]	grid area [mm]
thermal	S10	Bi	Cd	42	43	258 x 258
0.186	S4	U Ge Mn	W	84	40	400 x 400
2	S5	Sc Ti	Mn	135	80	480 x 480
24	S4	Fe Al S	Ti	84	67	402 x 402
144	S9	Si Ti	-	80	53	424 x 424

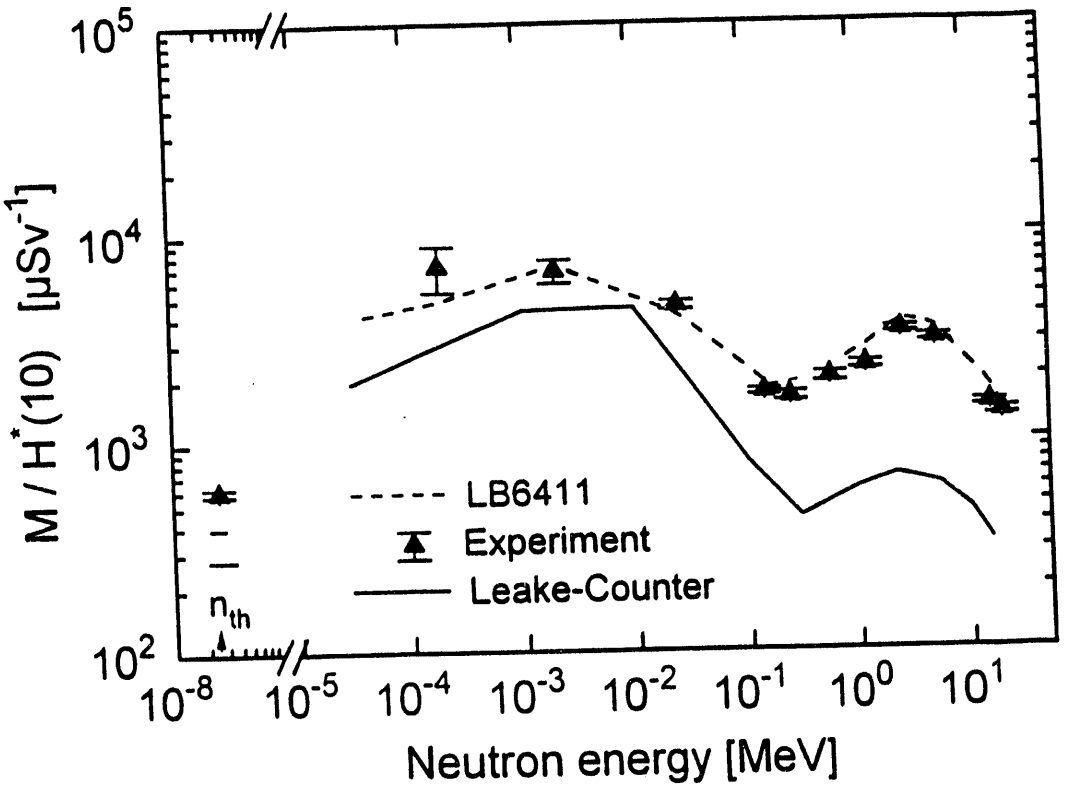


Fig. 2. Measured an calculated ambient dose equivalent response of rem-counter LB6411 and comparison with the Leake-counter.

Data had been collected at the reactor and at the accelerator with several detector orientations to determine angular dependencies. Some results are shown in figure 3. The standard orientation is called "reference direction" with irradiation perpendicular to the counter tube's axis, which defines the z-direction. Angles of radiation incidence are given as polar angles relative to this z-direction. In order to simulate isotropic irradiation also measurements with rotating neutron-counter had been done.

5. Results and Discussion

The experimental and theoretical results are shown in figure 2. The Monte-Carlo calculations shown as dashed line agree well with the experiment. In comparison with the Leake-counter the response curve of the new detector is strongly enhanced at higher neutron energies. That makes the ratios between maximum and minimum values much smaller if thermal energies are neglected. For thermal neutrons there is an underresponse, which can be accepted in practice, because the thermal neutron dose contribution at working places is usually lower than 10%. The absolute value of the response curve is approximately 3 Counts per nSv or 1 cps per µSv/h at energies of a few MeV which is a factor of 5 higher than the Leake-counter and demonstrates the increased sensitivity of the detection system. At a background counting rate of 3 cpm for the LB6411 rem-counter, neutron dose rates of 100 nSv/h can easily be measured within minutes. The numerical values are presented in table 2, first from the reactor and then from the accelerator. At 144 keV the rem-counter was calibrated at both facilities.

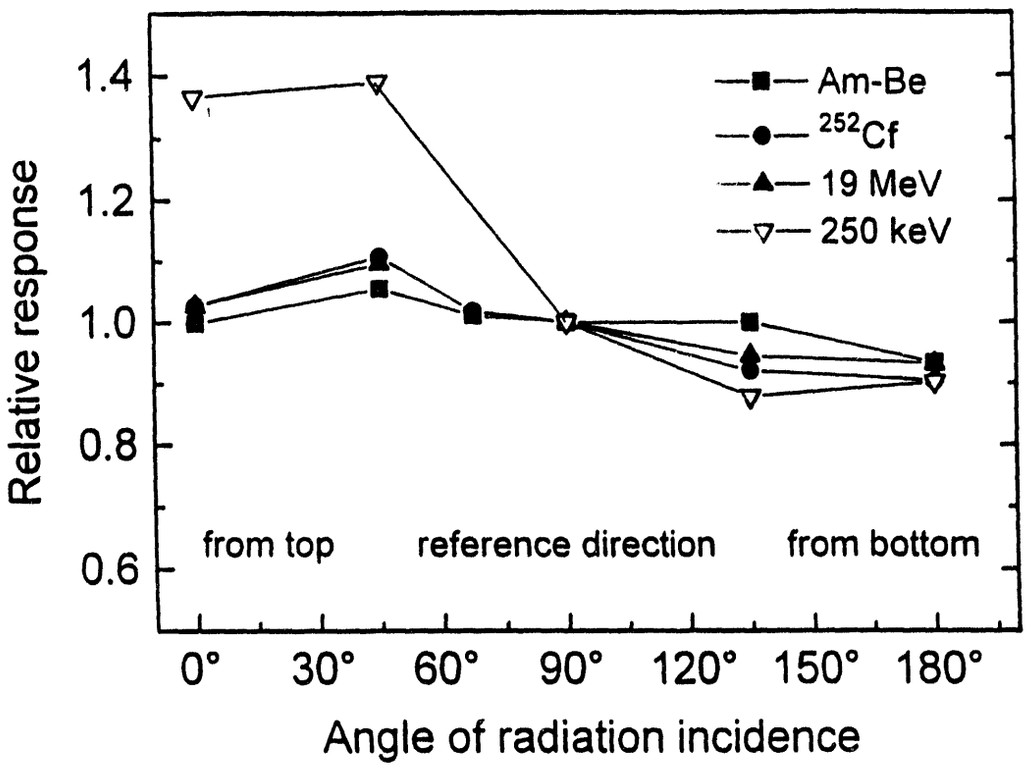


Fig. 3. Angular dependence of the response of rem-counter LB6411

Table 2: Calculated and measured response of neutron-counter LB6411

Neutron Energy	H*(10)/ϕ	Fluence Response			Ambient Dose Equivalent Response	
		exp.	error	calc.	exp.	calc.
[keV]	[pSv · cm²]	[cm²]	[%]	[cm²]	[nSv⁻¹]	[nSv⁻¹]
thermal	12.6	0.0074	3.1	0.008	0.59	0.64
0.186	9.86	0.070	25	0.057	7.1	5.63
2.0	9.9	0.066	13	0.082	6.7	8.36
24	28	0.127	4.8	0.15	4.54	5.36
144	152	0.26	15	0.32	1.72	2.10
144	152	0.27	5.2	0.32	1.78	2.10
250	241	0.41	5.2	0.47	1.70	1.95
565	393	0.80	5.3	0.87	2.04	2.22
1000	503			1.26		2.51
1200	497	1.21	4.1		2.43	
2300	466			1.69		3.63
2500	463	1.46	3.5		3.15	
5000	454	1.40	3.6		3.09	
5600	430			1.58		3.69
14800	498	0.75	3.6	0.87	1.51	1.76
19000	546	0.73	4.3	0.73	1.34	1.33

6. Conclusion

A new commercially available neutron dose-rate-meter with high sensitivity and an optimized energy dependent response according to ICRP60 has been developed. The details of the geometrical arrangements had been determined with MCNP Monte-Carlo simulations. Results of the calculations and prototype measurements have been presented. New calculations with varied parameters indicate, that the sensitivity of the neutron-counter could still be optimized further by a factor of about 2.

References

[1] ICRP Publication 60, Recommendations of the International Commission on Radiological Protection, Pergamon Press, Oxford 1990

[2] ICRP Publication 21, Data for Protection Against Ionizing Radiation from External Sources, Pergamon Press, Oxford 1973

[3] J.B. Briesemeister, ed., MCNP, A General Monte Carlo Code for Neutron and Photon Transport, Version 3A, LA-7396 M, September 1986

[4] P. Vontobel, EFF1LIB: A Enjoy Generated Neutron Data Library Based on EFF-1 for the Continuos Energy Monte Carlo Code MCNP, PSI Report No. 107, September 1991

[5] H.J. Brede, M. Cosack, G. Dietze, H. Gumpert, S. Guldbakke, R. Jahr, M. Kutscha, D. Schlegel-Bickmann, H. Schölermann; The Braunschweig Accelerator Facility for Fast Neutron Research, Nucl. Instr. and Meth. 169 (1980) 349-358

[6] W. G. Alberts and E. Dietz, Report PTB-Bericht FMRB-112 (1987)

[7] B. Burgkhardt, G. Fieg, E. Piesch, A. Klett, R. Maushart; 26. Jahrestagung für Strahlenschutz, Karlsruhe, Germany May 1994, Conf. Proc. ,1994, p. 590-595

[8] International Organisation for Standardization, ISO/DIS 8529, Geneva (1986)

[9] G. Leuthold, V. Mares, H. Schraube, Calculation of the Neutron Ambient Dose Equivalent on the Basis of the ICRP Revised Quality Factors, Rad. Prot. Dos., Vol. 40, No.2, p.77-84, 1992

RESPONSE CHARACTERISTICS OF AN EXTRAPOLATION CHAMBER MADE AT IPEN TO X RADIATION

Simone K. Dias and Linda V.E. Caldas (Instituto de Pesquisas Energéticas e Nucleares-CNEN/SP Caixa Postal 11049 - CEP 05422-970 - São Paulo, SP, BRAZIL)

Measurements of absorbed dose rates produced by beta or low energy X radiation are often difficult to obtain with accuracy. The recommended instruments for these measurements are extrapolation chambers. A plane parallel ionization chamber of variable air volume of this type was designed and constructed; its performance was tested in the radiation standard beams of the Calibration Laboratory of São Paulo. The chamber has a collecting electrode and a guard-ring of graphite. Teflon was used as insulating material between the electrode and the guard-ring. The entrance window is made of aluminized Mylar (0.84 mg/cm^2 of superficial density). The performance of the chamber was studied in relation to its response linearity and energy dependence. Extrapolation curves were initially obtained for X-rays (25 and 50 kV), varying the interelectrode distance between 0.2 and
1.0 mm and keeping the electric field constant at 10 V/mm. The calibration factors were obtained. The chamber response linearity was verified by varying the X-rays tube current between 2 and 30 mA, for 25 and 50 kV. Measurements were also taken for 25, 30, 40, 45 and 50 kV, keeping the interelectrode distance and the electric field constant at 1 .00 mm and 10 V/mm. An energy dependence of 5.2% was observed between 25 and 50 kV. The obtained results are comparable to those of commercial plane parallel chambers.

Work partially supported by CNPq - Conselho Nacional de Desenvolvimento Científico e Tecnológico, Brazil

MINIMUM DETECTABLE ACTIVITY OF PORTABLE CONTAMINATION SURVEY INSTRUMENTS

M.L. Johnson (Pacific Northwest Laboratory)

This paper describes methods for, and results from determining the minimum detectable activity of portable contamination survey instruments. The instruments examined are the "pancake" Geiger Mueller detector and a 50 cm^2 zinc sulfide alpha scintillator. This paper presents MDAs for two different survey methodologies; a scanning survey and a 5-second static count method. Determination of the MDA combines empirical measurements of the minimum count rate detectable by a technician with laboratory measurements of instrument efficiencies. Minimum detectable count rates were measured for both point and distributed sources and for both scanning and static survey methods. The MDA for the scanning survey was calculated for several scan speeds ranging from 2.5 cm/s to 20 cm/s. The results presented in this paper were used to develop a survey methodology that meets the surface contamination guideline values given in Table 2 of the DOE Radiological Control Manual.

Prepared for the U.S. Department of Energy under Contract DE-AC06-76RLO 1830.

A FILTER TECHNIQUE FOR OPTIMIZING THE PHOTON ENERGY RESPONSE OF A SILICON PIN DIODE

Richard H. Olsher (Los Alamos National Laboratory, MS G761, P.O. Box 1663, Los Alamos, NM 87545), Yosef Eisen (Soreq Nuclear Research Center, Yavne 70600, ISRAEL)

Silicon PIN diodes have become popular as radiation detectors in electronic pocket dosimeters (EPD) , where they are typically used in a pulse mode. However, current mode operation is also possible, especially at high dose rates. Because silicon is neither air nor tissue equivalent, means must be provided to flatten the dosimeter energy response. The problem is most serious in pulse mode because the count rate below 200 keV is not proportional to air dose or kerma rates.

Most EPDs use a simple filter (eg, tin) to flatten the energy response, but at the cost of sacrificing response below 60 keV. We present a new and inexpensive approach, which uses a composite filter, to extend the low-energy response of the diode to 15 keV in current mode and 25 keV in pulse mode while maintaining excellent response accuracy to 1.2 MeV in current mode and 6 MeV in pulse mode.

A Hamamatsu model S2506-01 diode was modeled in detail to include all of its essential dosimetric characteristics. Monte Carlo techniques were used to simulate the coupled electron-photon transport through the diode. The current mode response was calculated as the deposited energy in the diode's depletion layer. The pulse mode response was calculated as the number of radiation pulses depositing energy in the depletion layer in excess of the dosimeter's lower discriminator level (15 keV). The dosimeter's response was calculated over an incident photon energy range of 15 keV to 6 MeV. Each calculated response was divided by the incident air dose to obtain the energy response curve for the dosimeter.

Using these techniques, we designed and optimized composite filters for flattening the energy response of the dosimeter while preserving its low-energy response. The composite filter for current mode operation consists of a 4 mm plastic and Zr foil sandwich with a 15% areal opening. The filter for the pulse mode consists of Sn and Ta foils with a 15% areal opening, backed by a 0.13 mm copper foil. These techniques and results should be applicable to a wide variety of PIN diodes.

ROUTINE CALIBRATION OF RADIATION PROTECTION MONITORING INSTRUMENTS: A FIVE YEARS PROGRESS REPORT

Maria P.P. Albuquerque and Linda V.E. Caldas (Instituto de Pesquisas Energéticas e Nucleares-CNEN/SP, Caixa Postal 11049 - CEP 05422-970 - São Paulo, SP, BRAZIL)

Since 1980 the Calibration Laboratory of IPEN calibrates about 1000 instruments per year, at radiation protection level, belonging to industries, hospitals, clinics and other users located in São Paulo State and others in south of Brazil. The gamma radiation set-up of the laboratory consists of ^{60}Co and ^{137}Cs sealed sources with different activities. The measurement system consists of an ionization chamber, model 2581, and an electrometer, model 2502/3, both from Nuclear Enterprises Ltd. The applied technique is the use of radiation fields whose properties are well known. The tested instruments were: Geiger-Müller and ionization chamber portable instruments (59%), dose integrator detectors (36%) and alarm dosemeters (5%). The radiation detectors calibrated by the laboratory in the last five years were studied. In this period 6504 instruments were tested, but 20% did not show good enough performances to receive calibration certificates, because of a lack of scale linearity, in most cases. The tested instruments can be divided in three kinds of owners: Hospitals (20%), IPEN (14%) and Industries (66%). In order to analyze the equipments' behavior a group of instruments was selected taking into consideration the regularity of its calibration. The energy dependence (^{137}Cs - ^{60}Co range) presented variations between 0.7 and 8% for ionization chamber detectors and between 6 and 34% for Geiger-Müller detectors. Calibration factors between 0.878 and 1.18 R/(h.scale unit) were obtained. The highest difference in the calibration factors for the same instrument was 21 %.

Work partially supported by CNPq - Conselho Nacional de Desenvolvimento Científico e Tecnológico, Brazil

DEVELOPMENT OF A CALORIMETRIC SYSTEM FOR ELECTRON BEAM DOSIMETRY IN RADIATION PROCESSING

Homero E.B. Pérez and Letícia L. Campos (Instituto de Pesquisas Energéticas e Nucleares - CNEN/SP) C.P. 11049, CEP 05422-970-São Paulo-SP, Brazil)

A calorimetric system for electron beam dosimetry in radiation processing was developed. The system is composed of a graphite core calorimeter, the temperature measuring and electrical calibrating instrumentation, a microcomputer, and the software for the system automation. The research was directed towards the optimization of the project parameters, the development of advanced methodologies for calibrating the temperature sensor, the determination of the thermal capacity as a function of the temperature, the measurement of the absorbed dose, and the development of the software needed for the system operation. The operating range extends from 0.1 kGy to 30 kGy. The uncertainty in the measurement of the absorbed dose was estimated to be $\pm$ 1.8% at the 95% confidence level. Comparative tests of the absorbed dose measurements were made using the IPEN's electron accelerator. The obtained results showed an excellent agreement between the absorbed dose determined by the calorimeter and the absorbed dose calculed from the nominal power delivered by the accelerator.

USE OF PHOTOTRANSISTOR AS A RADIATION MONITOR

S. D. Dhole and V. N. Bhoraskar

Department of Physics, University of Poona, Pune 411 007, India

A sensitive device phototransistor has been used as a radiation monitor which measures the dosages in the range of 10^2 rads to 10^6 rads. The main measured characteristics of the phototransistor was the variation in the collector current (I_C) with collector to emitter voltage (V_{CE}). These parameters were measured before and after irradiation. Calibration was carried out by measuring collector current for each value of V_{CE} for different 1 MeV electron fluences. It was observed that collector current decreases with an increase in radiation dose received by the phototransistor. The other advantage in the use of this technique is that the transistor current can be changed by varying the incident light intensity which can also be used as a measure of radiation dose. Appropriate calibration of the phototransistor was made with the help of a pocket dosimeter.

INTRODUCTION

In many applications related to radiation detection,the use of semiconductor junction detectors is of great advantage[1]. It's high density and requirement of low energy for ionisation are the important properties which are specially useful in case of low radiation levels. The average energy E, necessary to produce an electron-hole pair in silicon is around 3 eV as compared with 34 eV for air. Electrical conductivity may be changed when ionising radiation either pass or absorbed in silicon through production of electron-hole pair. The induced charge in the conductivity is a function of the absorbed dose in silicon and can be therefore used to measure dose rate if appropriate calibrations are made. Devices such as JFET[2], silicon solar cell[3] and zener diode[4] have been used for the measurement of absorbed dose around 10^6 rads. Using fricke dosiemeter, the dose of 1 MeV electrons available from the race-track microtron was measured and found to be in the range of 100 rad/min to 100 Krad/min. For such low to high range of dose rate, one can not use JFET and zener diode as dosimeters. For measurement of dose rate or absorbed dose in this range, a phototransistor was found suitable. Results of this study are reported in this paper.

EXPERIMENTAL

A npn phototransitor was connected in the circuit as shown in figure - 1. Light of constant intensity from a 100 watt bulb was focused on the phototransistor to put it in conduction state, even when no voltage was applied. This set up was such that the phototransistor could also be exposed to 1 MeV electron beam, available from an electron accelerator called race-track

microtron. The I-V characteristics of the phototransistor were measured before irradiation, in which variation of I_C with V_{CE} was noted. Electron beam was made to fall on the phototransistor and simultaneously I-V characteristics were measured in steps after a fixed value of the electron fluence, measured by a Faraday cup and also wiht a induction monitor, put in the beam line.

To measure radiation dose, a pocket dosimeter was kept near the transistor at an angle 5^o with respect to the electron beam and its reading were also noted. The transistor while being irradiated, the source of light was put off. The post irradiation characteristics of the transistor were measured in absense of the electron beam but was illuminated bythe light source.

RESULTS AND DISCUSSION

Measured pre and post irradiation I-V characteristics of the phototransistor are shown in figure - 2. It is observed that the collector current decreases with increase in radiation fluence received by the phototransistor. After a dose of $5x10^{13}$ e^-/cm^2, not much variations in the collector current were observed. This trend indicates that the damage induced in a phototransistor reaches to a saturation value. The decrease in collector current 'I_C' was on account of the creation of trapping centers in the emitter and base regions. Subsequently there was an increase in the silicon resistance and hence decrease in the collector current. It was also found that when both the light as well as electrons of 1 MeV energy were made to fall on the phototransistor simultaneously, a small change in the collector

current was noted upto fluence level $2x10^{13}$ e^-/cm^2. For any further increase in the electron fluence, no appreciable change in the collector current was observed. These results show that the rate of defect production in the phototransistor reaches to a saturation limit.

The dose absorbed by the pocket dosimeter was measured simultaneously with the collector current of the phototransistor. Calibration was carried out by measuring changes in the phototransistor current with dose shown by the pocket dosimeter, results are shown in figure 3. On the basis of the measured characteristics, it is found that a phototransistor can be used as a dosimeter. From the curve shown in figure 2, it is possible to determine dose absorbed by a semiconductor device kept near or in the region of the phototransistor. This study has provided important results as regards measurement of absorbed dose in silicon which is otherwise difficult to measure in practice.

REFERENCES

1. K. Mahesh and D. R. Vij, 'Techniques of Radiation Dosimtery' Wiley Eastern Limited, (1985).
2. T. Tomimasu and T. Yamazaki, J.Appl.Phys. 47 (1976) 1732
3. A. C. Muller, F. X. Rizzo and L Galanter, BNL - 902 (T-368), (1964)
4. T. Tomimasu, T. Yamazaki and T. Mikado, Rev. Sci., Instr., 48 (1977) 312

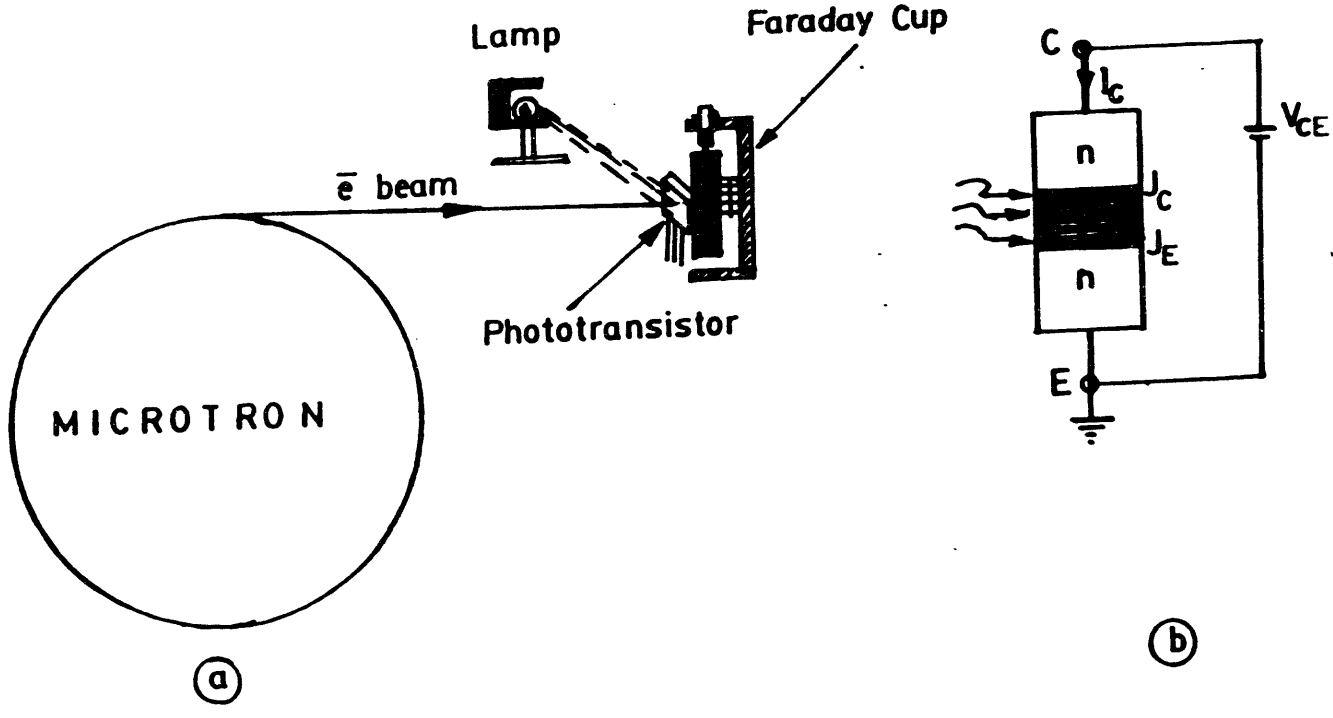


FIG-1: (a) A SCHEMATIC VIEW OF THE PHOTOTRANSISTOR UNDER 1 MeV ELECTRON IRRADIATION PROCESS.

(b) AN ELECTRICAL CIRCUIT SHOWING PHOTOTRANSISTOR CONNECTED IN COMMON EMITTER CONFIGURATION

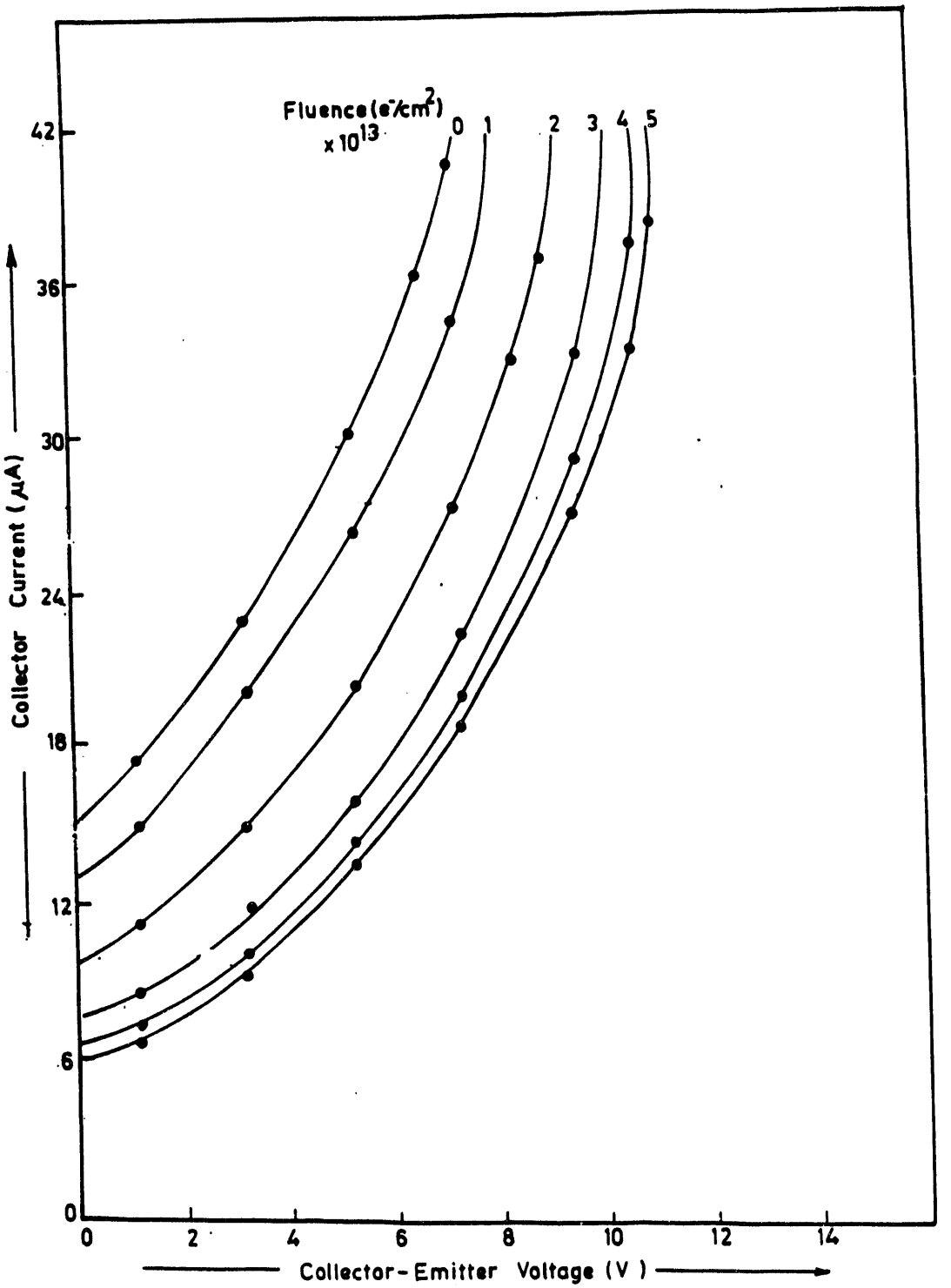


Figure - 2 : For a phototransistor variation in collector current with emitter to collector voltage, for different 1MeV electron fluences.

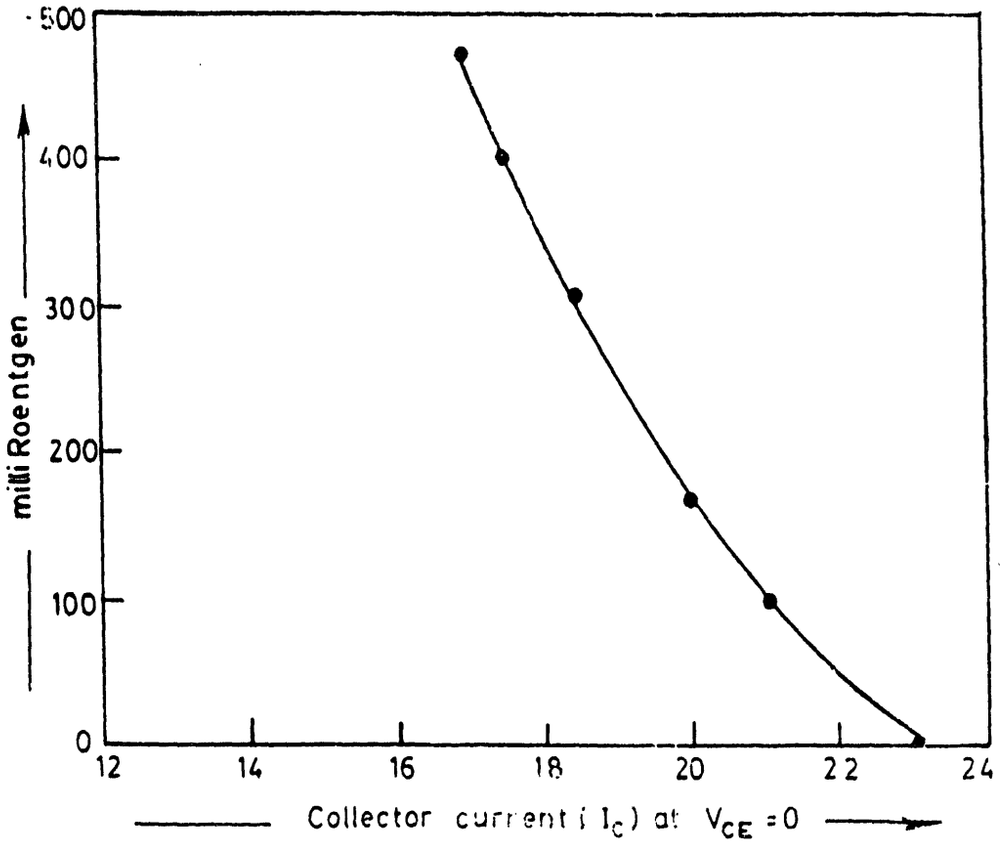


Figure 3 : Variation in collector current of a phototransistor with absorbed dose measured with a pocket dosimeter

PHOTOSTIMULATED LUMINESCENCE OF KBr-In INDUCED BY EXCITATION WITH UV RADIATION

I.Plavina[a] and A.I.Popov[b]

[a] Institute of Physics, Latvian Academy of Sciences, LV-2169 Salaspils-1, Latvia

[b] Institute of Solid State Physics, University of Latvia,8 Kengaraga str., LV-1063 Riga, Latvia

1. Introduction

In recent years the photostimulated luminescence (PSL) has the great attention of many scientists because of their application for X-radiation imaging [1-7]. For this purposes, a variety of the different PSL phosphors, such as BaFBr:Eu [3-6], RbBr-Tl [3] and KBr-In [7] etc have been considered.

It should be noted that whilst the importance of PSL is well realized in different applications in the field of X-ray imaging for medicine and biology as well as for imaging of high-energy particle radiation, the very mechanism of both the PSL phenomenon and that how defects participating in PSL are created, steel need to be better understood.

In our recent endeavor to use alkali halide crystals as photostimulated storage materials, we have carried out the detailed investigations of PSL in alkali halides doped with ns^2 - ions [1,2,7]. It has been founded that the KBr-In crystal possess a prominent PSL ideal for He-Ne laser stimulation [7,8,11-15]. The detailed PSL and TSL properties of KBr-In crystals have been reported in [7-10,14,15], where UV-light was used as a kind of radiation.

In particular, it was shown that $\{F,In^{2+}\}$ defect pairs, which are responsible for the distinctive PSL, are produced under the exciton-band excitation. Furthermore, when the number of the exciton-created photons is less than $5.0x10^{13}$ photons/cm^2 *only* the $\{F,In^{2+}\}$ pairs are formed. In order to excite the PSL of the $\{F,In^{2+}\}$ pairs, the crystal has to be illuminated with the light into the F band. As a result, the F center electrons are excited and captured by the nearby In^{2+} centers. This electron transfer from F^* to In^{2+} results in the PSL of In^+ luminescence (420-530 nm) [8].

The main goal of this paper is to present briefly new results and to analyze critically what was earlier found on the PSL studies in KBr-In crystals preliminary UV-irradiated in the

fundamental exciton absorption band [7-10,14,15]. All investigations were performed at room temperature (RT) experimental details were presented earlier for the case of UV irradiation and for X-rays.

2. Results and discussion

The KBr activated with In^+ ions is an efficient blue-luminescence material [7,8]. The emission band has its main maximum at 2.8 eV and a shoulder at 2.4 eV. It can be ascribed to a double minimum of the $^3P_1$ relaxed excited state caused by the Jahn-Teller effect.

In order to investigate the PSL process after the optical creation of the anion excitons, we measured carefully the kinetics of PSL under constant F-light stimulation. As it was shown in [7,8] the PSL of the $\{F,In^{2+}\}$ pairs is exponential in time. This process can be written schematically as

$$\{F,In^{2+}\} + h\nu_{st} \rightarrow \{v_a^+,(In^+)^*\} \rightarrow \{v_a^+,In^+\} + h\nu_{In^+} \quad (1)$$

where v_a^+ is the anion vacancy. The appropriate stimulation spectrum is presented in Fig.1. It is similar to the earlier published F band absorption spectra. Next we have found that the PSL appearing after large dose ($D > 5 \times 10^{13}$ photons/cm^{-3}) is the superposition of three exponential components, $\{F,In^{2+}\}$ pairs define the middle of them. The spectral distribution of the absorption cross-section σ of the slow component (Fig.1) looks like the M centre absorption. It is well known that the F band covers the spectral region of the transition of the M and R centers. In the case of KBr, the M band includes the M_2 and M_2' transitions (E_{M_2}=1.990 eV, $E_{M_2'}$=2.006 eV, ΔE=0.016 eV) [16]. Estimation of the the σ_{M_2} gives the values of order $1.0\ 10^{-16}$ cm^{-2}. From the stimulation spectra (Fig.1) it follows that there are two most pronounced bands; E_1=1.87 eV and E_2=2.08 eV having $\sigma_{1,2}$=$1.05\ 10^{-16}$ and $1.3\ 10^{-16}$ cm^2, respectively. These σ values are in a good correspondence with the above-mentioned estimation of σ_{M_2} values. The estimated oscillator strengths of the E_1 and E_2 bands are f_1=0.14 and f_2=0.17 with good correspondence with data [16]. Thus we can conclude that the slow component of the PSL of KBr-In crystals is due to $\{M,In^{2+}\}$ pairs and this process can be represented schematically as

$$\{M,In^{2+}\} + h\nu_{st} \rightarrow \{M^*,In^{2+}\} \rightarrow \{F_2^+,(In^+)^*\} \rightarrow \{F_2^+,In^+\} + h\nu_{In^+} \quad (2)$$

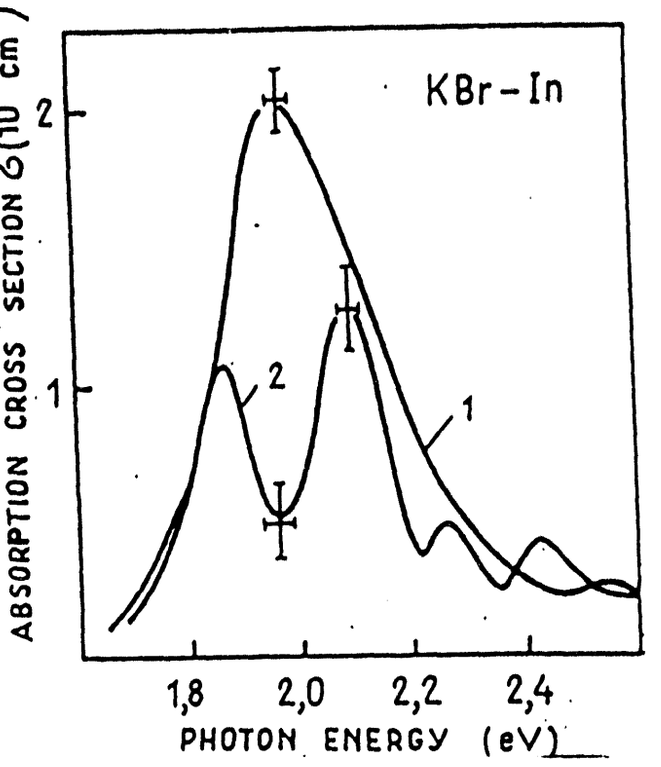


Fig.1. Stimulation spectra (in terms of optical absorption cross-section as a function of the stimulating light energy) of the middle (1) and slow (2) components of the PSL.

The origin of the shortest component of the PSL decay is not so obvious. Appearing under large irradiation doses these centers may have a complex structure. They could be the R centers as well as the F centers perturbed by some defect. The component has a spectrum shifted to the shortwavelength side to 0.1 eV compared with the F band. The pairs responsible for the shortest component will be designated as $\{DF, In^{2+}\}$. Thus we have concluded that the PSL of KBr-In crystals preliminary irradiated in the exciton fundamental absorption is due to three types of the close defect pairs, such as $\{M, In^{2+}\}$ and $\{DF, In^{2+}\}$, in which center-to-center recombination occurs. Recently we have shown that the resulting $\{V_a^+, In^+\}$ pairs may be again converted into the $\{F, In^{2+}\}$ pairs under the C-absorption band irradiation accompanied with the optical ionization of In^+ ion. The electron capture by the Coulomb field of the near anion vacancy leads to the restoration

of the $\{F, In^{2+}\}$ pair [8]. This process can be represented schematically as

$$\{V_a^+, In^+\} + h\nu_c \rightarrow \{V_a^+, e^-, In^{2+}\} \rightarrow \{F, In^{2+}\} \qquad (3)$$

The same is true for the $\{DF, In^{2+}\}$ defects, but not for the $\{M, In^{2+}\}$ ones. The last fact can be explained by the thermal unstability of the F_2^+ centre at RT. It should be noted that in the case of C - band irradiation the main part of the PSL decays in accordance with the hyperbolic law, h ~ t-1. As such irradiation leads to the optical ionization of impurity In^+ ions, the released electrons are captured by the Schottky vacancies, thus creating the F centers. Schottky vacancies are randomly distributed (at least in virgin samples !) as well as the F and In^{2+} centers are. The kinetics of the F - destruction of such randomly arranged F and In^{2+} centres differ considerably from that of $\{F, In^{2+}\}$ pairs [8].

In conclusion, in Fig. 2 we demonstrate that KBr-In is an effective UV radiation storage material with a wide dynamic

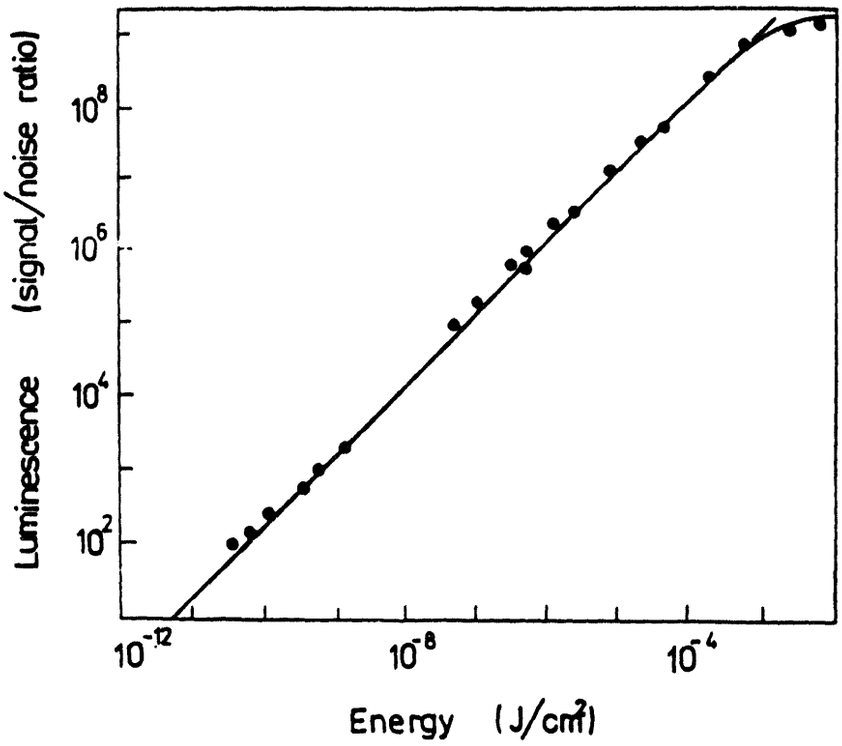


Fig.2. Dose dependence of PSL of KBr-In accumulated under UV light (λ = 195 nm).

range. A direct proportionality of the PSL intensity to X-ray exposure have been recently established over a wide dose range, viz. from 6 10^{-8} to 30 R at 44 kV voltage [12,13], that is definitely the outstanding property and is much better then that, reported for BaFBr-Eu [4]. The comparison of the stimulation energies of numerous storage of the stimulation energies of numerous storage materials also showed the advantage of the KBr-In [11].

REFERENCES

[1] I.Plavina, V.Obedkov, V.Chernyak, G.Balandin and B.Sestroretskii, Izv. Akad. Nauk Latvian SSR, Ser. fiz. tekn. nauk, No. 5, 67 (1969)

[2] G.Vlasov, R. Kalnins, L.Nagli, V.Obedkov, I.Plavina and A.Tale, Avtometriya 1, 66 (1980)

[3] H. von Seggern, A.Meijerink, T.Voigt and A.Winnacker, J. appl. Phys. 66, (1989)4418.

[4] J.Miyahara, K.Takahashi, Y.Amemiya, N.Kamiya and Y.Satow, Nuclear Instruments Methods Phys.Research A 246 (1986) 572.

[5] K.Amitani, A.Kano, H.Tsuchino and F.Shimada, Konica Technical Report vol.1 (1988) 120.

[6] M.K.Crawford and L.H.Brixner, J.Luminescence 48&49 (1991) 37.

[7] P. Bratslavets, A. Kalnins, A.Popov, B.Rapoport, A.Tale, B.Zeigurs, in: "The Advancement of Imaging Science and Technology", 1990, Int. Acad. Pub. (A. Pergamon - CNPIEC Joint Venture) p. 474-476.

[8] P.Braslavets, A.Kalnins, I.Plavina, A.I.Popov, B.I.Rapoport and A.Tale Phys. Status Solidi B 170 (1992) 395.

[9] I.Plavina and A.I.Popov, Phys. Stat.Sol. (B) 176 (1993) 255.

[10] I.Plavina and A.I.Popov, Radiation Effects and Defects in Solids. 128 (1994) 27.

[11] L.E.Trinkler, M.F.Trinker and A.I.Popov, Phys.Status Solidi B 180 (1983) K31.

[12] A. Kalninsh, I.Plavina and A.Tale, Nuclear Instr. and Meth. B 84 (1994) 95.

[13] I.Plavina, A.Kalninsh, A.I.Popov and A.Tale, Nuclear Instr. and Meth. B (in press).

[14] A.I.Popov, Nuclear Instr. and Methods Phys. Res. B 65 (1992) 521.

[15] A.I.Popov, Phys. Stat. Sol. (b) 169 (1992) K47.

[16] T.Y. Neubert, Sh. Susman, J. chem. Phys. 43 (1965) 2819.

POWDERED KBr-In AS AN EFFECTIVE X-RAY STORAGE MATERIAL WITH A WIDE DYNAMIC RANGE

A.Kalninsh(a), I.Plavina(a), A.I.Popov(b) and A.Tale (a)
(a)Institute of Physics, Latvian Academy of Sciences, LV-2169 Salaspils-1, Latvia)
(b)Institute of Solid State Physics, University of Latvia, 8 Kengaraga str., LV-1063 Riga, Latvia)

1. INTRODUCTION

In the last decade a new technique for X-ray imaging based on the photostimulated luminescence (PSL) has gained considerable importance, especially in medical diagnostics and crystallography. This technique is based on use of a photostimulable storage phosphor screen. There are several advantages of this technique over conventional techniques [1-4]. For instance, due to the higher sensitivity of detection with a photomultiplier tube compared to photographic film, the X-ray dose may be reduced. Unlike film detection, storage phosphors have a linear response with X-ray dose over several orders of magnitude, giving a much better image contrast. This wide dynamic range prevents overexposure and underexposure.

The photostimulable phosphor used at present in nearly all commercial digital X-ray imaging systems is BaFBr-Eu. This storage material has a dynamic range of five order of magnitude at the resolution of 50x50 μm^2 if X-ray [3,4] or electron flux [5] energy has been stored.

The principal purpose of this paper is to report the relation between the dose of energy stored and the PSL response for another photostimulable material - KBr-In - when the kind of energy used is X-radiation over the suitable for diagnostic medicine.

Recently we have demonstrated that KBr-In is an effective UV radiation storage material with a wide dynamic range (ranging over seven orders of magnitude at the above mentioned resolution) [6].

There is ground to suppose that physical processes with both (X and UV) radiation are predominantly the same. Therefore, it seems worthwhile to review the principal points of the interpretation concerning energy storage and photostimulated release in the case of UV irradiation [6-9].

The initial process under UV irradiation is the optical generation of anion excitons followed by the exciton decay on F and H Frenkel defects. As a result, the spatially correlated with respect to In^{2+} distribution of the F-type electron centres being

formed in the crystal [6-9]. This process corresponds to the storage of energy. Photostimulation in the F absorption band lead to the electron transfer from F centre to In^{2+} and subsequent In^{+} centre luminescence which has been detected as a response signal.

2. SAMPLES AND EXPERIMENTS

To ensure equal circumstances of observation all the experiments were performed on powdered specimens with identical specimen holders. Powdered material was obtained by grinding single crystals of KBr-In. The grain size did not exceed 100 μm. The concentration of In^{+} was evaluated from the activator absorption spectra of the single crystal before grinding and it varied from 8×10^{15} to 2.3×10^{19} cm^{-3} in the prepared powder.

Powdered KBr-In was pressed into a cylindric hole made in a plastic body. The diameter of the holes was 9 mm and the depth varied from 0.15 to 2.30 mm for different samples. The holes, after being filled with powdered KBr-In, were covered with a 2.2 mm thick plate of fused quartz in order to carry out optical examinations.

A standard somewhat rearranged, medical X-ray apparatus continuously radiating in time served as the X-ray source. The voltage on the X-ray tube could be varied from 44 to 125 kV. The intensity of X-radiation had been calibrated by means of a DKC-05 ionization dosimeter by placing its recording chamber at the position of the sample under irradiation. In order to obtain exposure smaller than 10^{-3} R, metal attenuation filters were used [10]. X-radiation in the from of a wide bundle was impinging on the sample under examination placed on a movable optical table. In this way a storage of energy in the specimens occurred. To realize readout, the table with the sample was shifted under a vertically arranged helium-neon laser, and the latter was switched on. The laser radiation (with a wavelength of 632.8 nm, a power of 1.3×10^{-3} W, and a beam diameter of 0.3 mm) gave rise to the luminescence of In^{+}, viz. PSL response, which by means of light guides was collected and directed to a photomultiplier (PM). For spectral separation of the luminescent (blue) and stimulating (red) light, blue light filters were put before the PM. There were two readout modes: (1) the scanning one when the laser was traversing across the sample in the horizontal direction with a velocity of 1 mm/s; (2) the stationary one when the laser beam was immovable relative to the sample during the readout. A filament lamp with light filters absorbing infrared radiation was used to perform a complete erasure of the information remaining in a specimen after a readout before the next irradiation.

3. RESULTS

Fig.1 shows the dependence of the PSL response on In^{+} concentration for powdered KBr-In specimens exposed to X-radiation with equal doses. The readout was made in the scanning mode. All the powdered KBr-In specimens were of the same

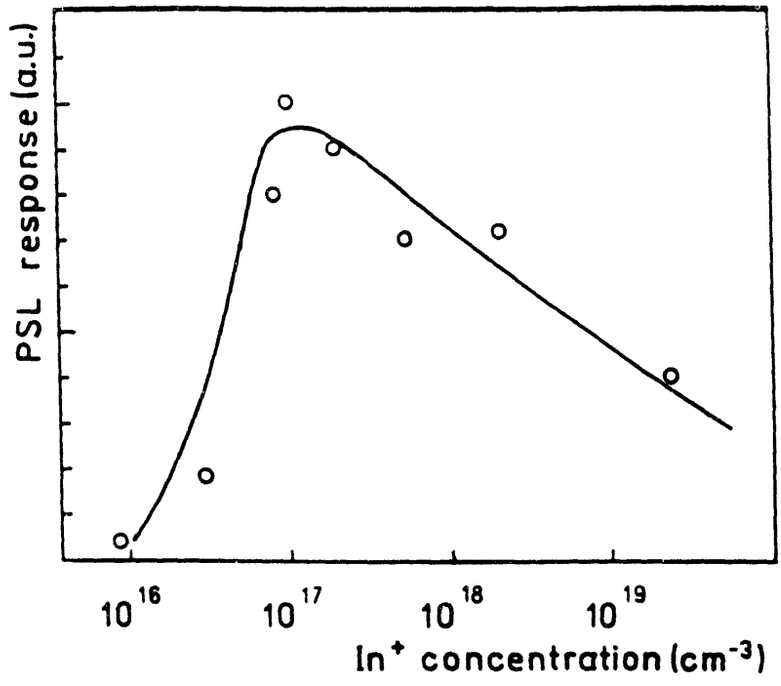


Fig.1. The PSL response of powdered KBr-In after equal exposures of X-radiation as a function of In^+ concentration.

thickness, viz. 1.0 mm. The exposure of X-radiation was $7x10^{-2}$ R at 44 kV voltage on the X-ray tube. One can see that this dependence is of an extreme character: the maximum efficiency of the response of the material to the In^+ concentration occurs at about 10^{17} cm^{-3}. Taking this into consideration, powdered KBr-In specimens prepared from single crystals having an In^+ concentration in the region of $8x10^{16}$ to $2x10^{17}$ cm^{-3} were selected for performance of all further experiments.

The dynamic range of the conversion has been examined for four different values of the voltage on the X-ray tube: 44, 57, 75 and 100 kV. For experimental simplicity, the whole range of X-ray exposures under investigation was divided into several (three to four) intervals which were chosen in a way that their utmost values should be mutually overlapping (see for details [10]). As a results, the dependence of the PSL response on the exposure was established for the voltages of 44, 57, 75 and 100 kV on the X-ray tube (Fig. 2.).

On the basis of these data the absorbed energy of X-radiation as a function of the layer thickness of powdered KBr-In plotted in Fig. 3. (the curves) for two voltages on the X-ray tube: 44 kV (d_0= 0.65 mm) and 85 kV (d_0= 1.15 mm). The

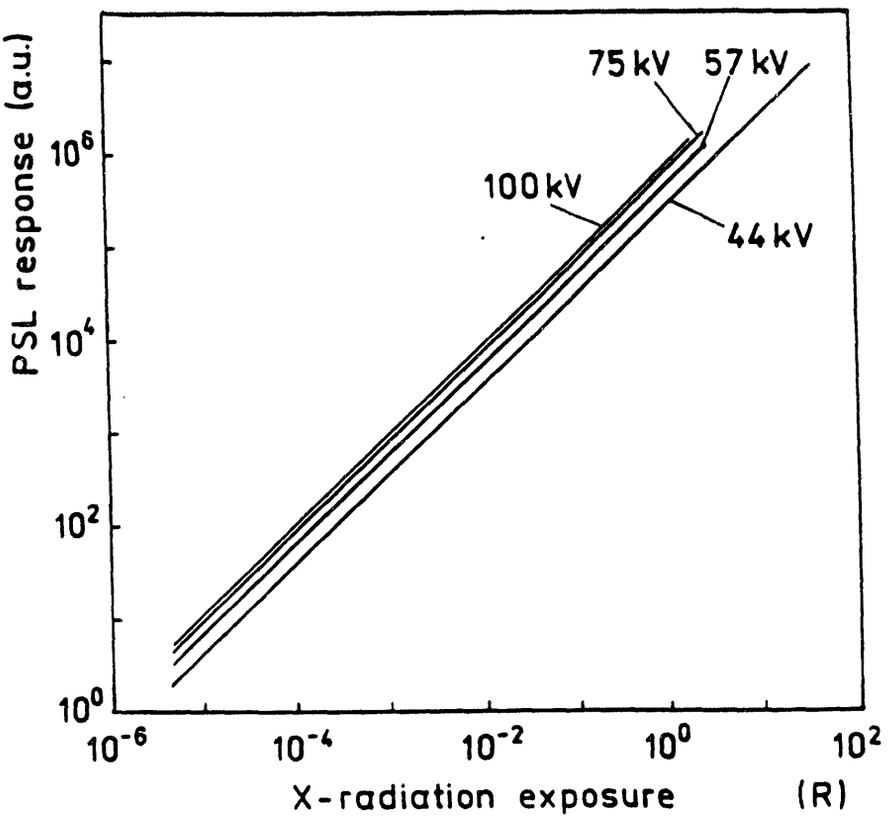


Fig.2. Dynamic range of X-ray storage in the powdered KBr-In specimen at different voltages (44, 57, 75 and 100 kV) on the X-ray tube.

experimental points in Fig. 3. indicate the PSL responses of the above-mentioned KBr-In layers for the different thicknesses after they have been exposed to one and the same dose of X-radiation ($7x10^{-2}$ R at the 44 kV voltage and $1x10^{-1}$ R at 85 kV voltage) and read out in the scanning mode with the full intensity of laser light.

The more essential result of this study concerns certainly the direct proportionality between the PSL response and the exposure of X-radiation (Fig. 2.) stated over a wide interval of dose variation ranging from $6x10^{-6}$ to 2.2 R (for 44 kV voltage even to 30 R).It should be noted that the dose interval was dictated only by conditions of a technical nature, i.e. by the sensitivity of the recording apparatus (for small doses) and by power restrictions of the X-ray apparatus (for large doses). The real region of linearity is thought to be considerably wider.

The final part of this paper is the determination of the energy and quantum yields of the PSL of KBr-In storage material.

Knowledge of absolute characteristics of material such as the energy and quantum yields of PSL, of course, makes possible further rigorous comparison of the effects of different types of irradiation of as well as behaviour of different materials under similar irradiations.

Energy yield of PSL could be calculated as a ratio of the energy (or number of photons) of PSL response to the energy (or number of photons) of exposure to X-ray, both measured at the given energy of X-ray photon (ε). It is clear that both quantities should be represented in the same energy units, e.g.

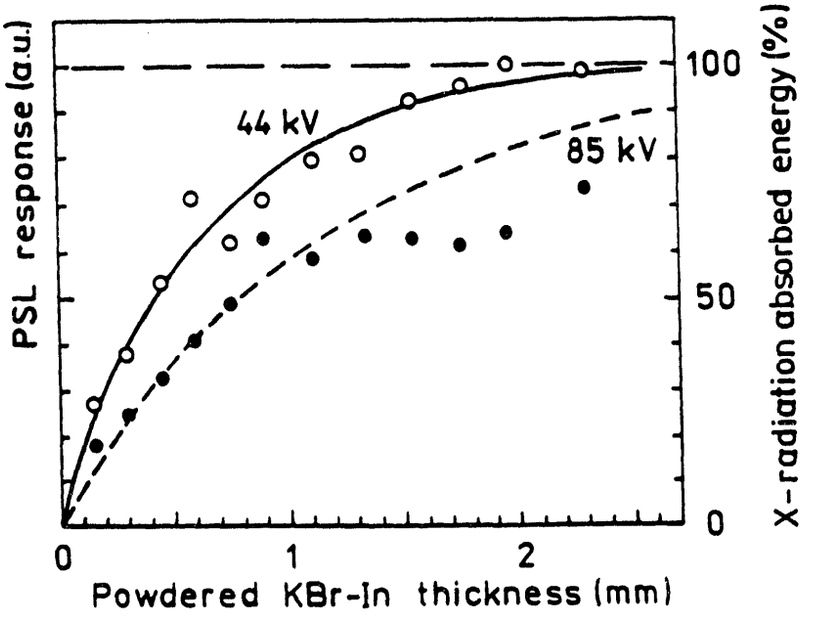


Fig.3. The energy of X-radiation absorbed (curves) and the PSL response (experimental points) as a function of thickness of the powdered KBr-In specimen obtained at two voltages: 44 (solid line, open circles) and 85 (dashed line, closed circles) kV on the X-ray tube.

in Joules (J). It is common to get PSL response in J, whereas X-ray exposure, as a rule, is measured in Rentgens (R). The proposed transition from R to I/cm^2 have been touched in [10,11].

The quantum yield of the PSL could be determined as a ratio of the number of PSL response photons per unit area after the definite X-ray exposure to the number of incident X-ray photons involved in this exposure.

The original data for the yield estimation were taken from refs. [10,11] and for illustration are given in Fig.4. Both comparable quantities - the PSL response and incident X-radiation flux corresponding to the definite exposure - are represented in

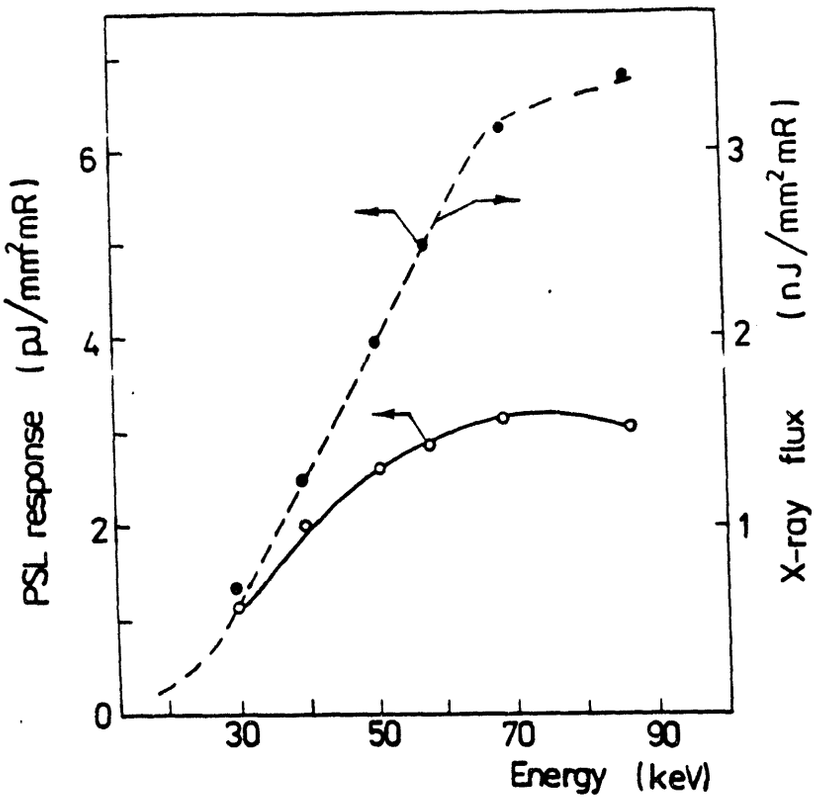


Fig.4. Dependence of the PSL response from the powdered KBr-In measured in PJ/mm^2 mR with the X-ray photon energy over the interval from 30 to 90 keV: the experimental data for a 1 mm thick sample (incomplete X-ray absorption, open circles), the data obtained from the former dependence by introducing the correction for absorption in accordance with the data of Fig. 5.

Joules (pJ and nJ, respectively) per mm^2 area and mR exposure. Note here the PSL within the total space is taken into account as the properties of material in the physical aspect is under consideration. (In ref. [9] the PSL response only within the half-space is considered, since emphasis is put there on an application of the material).

The dependence of the PSL response on the energy of X-ray photons in Fig. 4 is shown for a powdered KBr-In sample 1-mm sample, within which only the fraction of incident X-ray flux is absorbed (open circles, experiment) as well as for samples of different thickness at different energies of X-ray photons within which the whole incident X-ray flux is absorbed (full circles, calculated). The latter data were obtained using experimental curve by introducing the correction for the complete absorption in agreement with the data of Fig. 5. The dashed curve in Fig. 4. is the result of the recalculation of the data of ref. [13] for the 1 mR exposure and 1 mm^2 square.

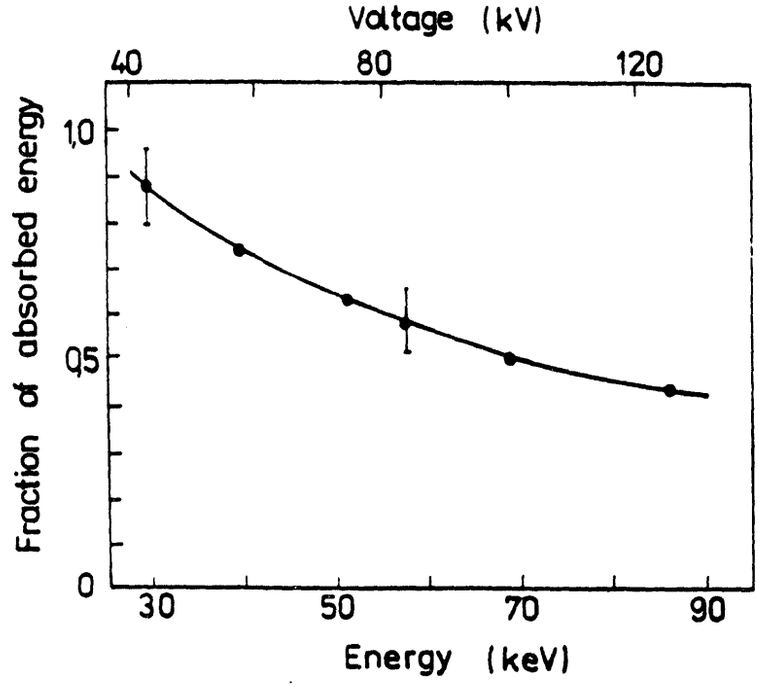


Fig.5. The fraction of incident X-ray flux absorbed in the powdered KBr-In layer of a 1 mm thickness as a function of the peak energy of the bremsstrahlung spectrum (or of the voltage on the X-ray tube).

The data of Fig. 6 which are necessary for the calculation of quantum yield of PSL were derived from the data of Fig. 5. The procedure for estimating of the PSL photon number was described in ref. [12].

Afterwards, using the data of Fig. 4. and 6. we can determine the energy and quantum yields of the PSL. As a result, one gets their dependences on the energy of X-ray photons - for both (i) incomplete (open circles in Fig. 7. and 8. and (i) complete (full circles in Fig. 7. and 8.) absorption of X-ray flux in powdered KBr-In.

Thus, the energy yield of PSL for X-ray storage upon the complete absorption within the sample was found to be constant: η_{en} = 0.20±0.06% - within region of X-ray photon energy (40 to 90 keV - Fig.7.). The quantum yield of PSL η_q in this case increases from 27 to ≈ 60; respectively - Fig. 8.

The comparison of these values with that for another radiation sources (UV - light and β - particles) have been done in [11], where physical reasons for the revealed discrepancies are proposed.

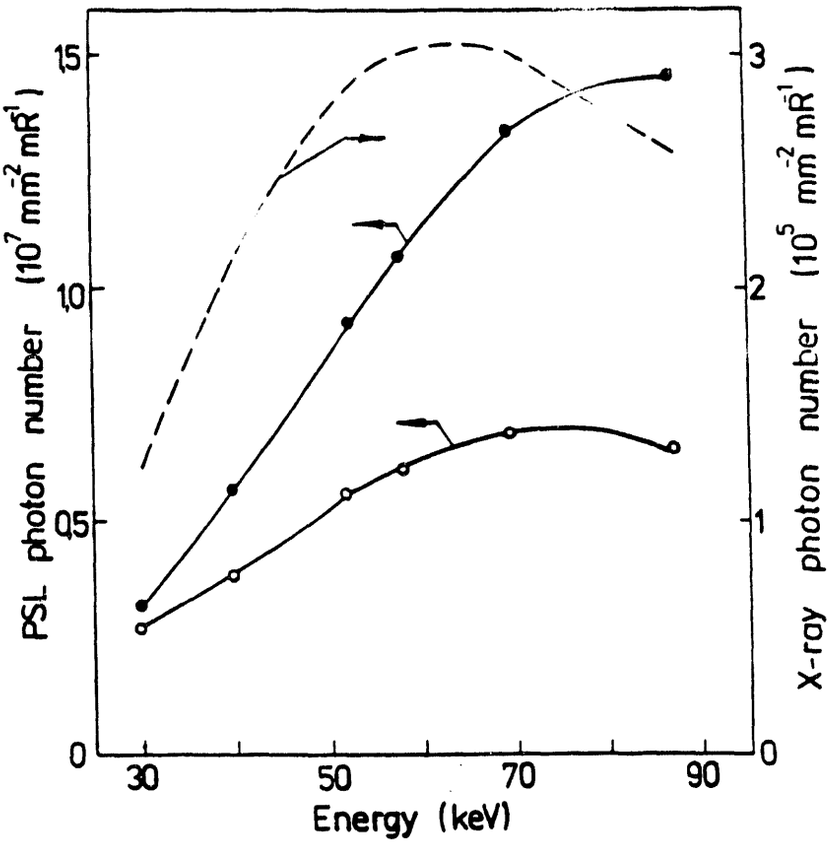


Fig.6. The PSL photon number from 1 mm^2 of the powdered KBr-In for an exposure of 1 mR as a function of the X-ray photon energy over the interval from 30 to 90 keV: incomplete absorption of the X-ray flux (open circles), complete absorption of the X-ray flux (full circles).

4. CONCLUSIONS

The main purpose of this paper was to report the relation between the dose of energy stored and the photostimulated luminescence response for photostimulable material KBr-In when the kind of energy used is X-radiation over the range suitable for diagnostic medicine.

A direct proportionality of the PSL intensity to the X-ray exposure is established over a wide dose range, viz. from 4×10^{-8} to 3 R at 57, 75 and 100 kV to 30 R at 44 kV voltage on X-ray tube.

The energy and quantum yields of the PSL and their dependence upon the energy of X-ray photons at the maximum of the bremsstrahlung spectrum have been estimated. The energy yield is

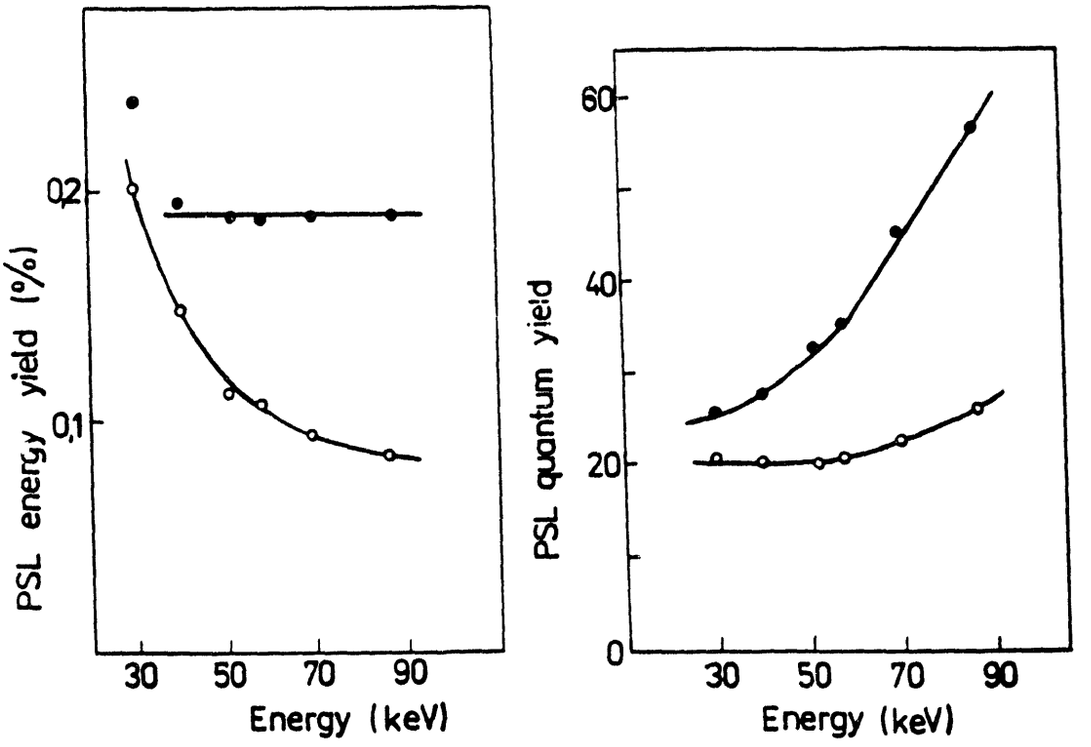


Fig.7. Dependence of the PSL energy yield for the powdered KBr-In on the X-ray photon energy: under the incomplete absorption (open circles, an accuracy in the yield determination is indicated), under the complete absorption (full circles).

Fig.8. Dependence of the PSL quantum yield for the powdered KBr-In on the X-ray photon energy: under the incomplete absorption (open circles), under the complete absorption (full circles).

found to be independent on the X-ray photon energy and equal to 0.2 %. The quantum yield under the same conditions has the values from 25 to 55 PSL photons per X-ray photon over the energy interval from 30 to 90 keV, respectively.

References

[1] M.Sonoda, M. Takano, J. Miyahara and H. Kato, Radiology 148 (1983) 833.
[2] H. von Seggern, T. Voigt and K. Scharzmichel, Seimens Res. Develop. Rep. 17 (1988) 124.
[3] J. Miyahara, K. Takahashi, Y. Amemiya, N. Kamiya and Y.Satow, Nucl. Instr. and Meth. A 246 (1986) 572.
[4] A. Yoshiyki, K. Shunji, M. Tadashi, S. Yoshinori and A. Masami, Rev. Sci. Instr. 60 (1989) 1552.

[5] N. Mori, T. Oikawa, Y. Harada and J. Miyahara, J. Electron. Microsc. 39 (1990) 433.

[6] P. Bratslavets, A. Kalnins, A. Popov, B. Rapoport, A. Tale, B. Zeigurs, in: "The Advancement of Imaging Science and Technology", 1990, Int. Acad. Pub. (A. Pergamon - CNPIEC Joint Venture) p. 474-476.

[7] A. Kalnins, I. Plavina, A.I. Popov and A. Tale, J. Phys. Condens Matter 3 1265 (1991); Proc. Intern. Conf. Luminescence, Lissabon, July 1990, (pp. 280, 281).

[8] P.F. Braslavets, A. Kalnins, I. Plavina, A.I. Popov, B.I. Rapoport and A. Tale Phys. Status Solidi B 170 (1992) 395.

[9] A. Kalnins, I. Plavina, A.I. Popov and A. Tale, Latv. J. Phys. Techn. Sci 3 (1992).

[10] A. Kalninsh, I. Plavina and A. Tale, Nucl. Instr. and Meth. in Phys. Res. B 84 (1994) 95.

[11] A. Kalninsh, I. Plavina, A.I. Popov and A. Tale, Nucl. Instr. and Meth. in Phys. Res. B 1994 (in press).

[12] I. Plavina, A. Kalninsh, A.I. Popov and A. Tale, Nucl. Instr. and Meth. in Phys. Res. B (submitted).

THE DEVELOPMENT OF A PASSIVE FIBER OPTIC SENSOR SYSTEM FOR REMOTE MONITORING IN LOW ENERGY GAMMA ENVIRONMENTS

M.A. Buckner, M.L. Bauer, D.E. Holcomb and M.L. Simpson (Oak Ridge National Laboratory, Martin Marietta Energy Systems, Inc., Oak Ridge, TN 37831-6006 USA)

A passive fiber optic sensor system (PFOSS) capable of verifying the presence of stored special nuclear materials is being developed at Oak Ridge National Laboratory. This system is being developed to reduce the costs, effort, and the exposure to employees associated with inventorying stockpiles of highly enriched uranium at the Oak Ridge Y-12 Plant. Through its research programs in scintillating materials, ORNL has developed a variety of material configurations for use in alpha-, beta-, gamma- and neutron-sensitive scintillator detectors. In addition, several concepts that arose from the innovative work with scintillating fiber optics, wavelength-shifting fibers, and plastic scintillators associated with the Superconducting Super Collider are being considered for incorporation into PFOSS. Configurations being investigated include: 1) the use of scintillating fiber optics as both radiation sensors and light pipe to external phototubes; 2) the use of bulk pieces of scintillator material (for large detection volume) coupled to wavelength-shifting fibers (for greater light transmission efficiency); and 3) the mixing of segments of scintillators, wavelength-shifters and clear fibers to optimize signal transmission over long fiber runs. The basic concept is to transmit the radiation induced light from the scintillator along a run of fiber to a remotely located monitoring station to be measured and compared to previous emission data. One of the processing schemes being explored involves monitoring both ends of a single fiber run and using time-of-flight or amplitude correlation to locate the position of the emission along the run. This technique, while enabling an unambiguous method of locating and quantifying a source of radiation, is significantly more complex and costly than deploying an array of multiple discrete sensors. The technical, economic, and system tradeoffs are discussed.

HOW HAND-HELD COMPUTERS ASSIST FACILITIES WITH FIELD INSTRUMENT SOURCE AND CALIBRATION CHECKING TO MEET THE INTENT OF 10 CFR 20 AND 10 CFR 835 REGULATIONS.

W. Henry Bailey (NFS Radiation Protection Systems, Inc.)

The paper describes an advanced computer application that utilizes PCs, hand-held computers and bar codes to collect field instrument source and calibration data. The application was developed in conjunction with 10 CFR 20 and 10 CFR 835 requirements regarding routine instrument operational checking. An advanced programming technique was incorporated which allows the user to create a sequence of specific procedures for each type of instrument. The system can manage a large number of instruments, regardless of the manufacture. These procedures are then downloaded to Intermec 9445 or the powerful Janus 2020 model hand-held computers with built-in bar code laser scanners. The instrument checking application was developed using C++ for Windows, which provides ease of use when compiling procedures. The paper describes, in detail, how the instrument checking application operates.

Instruments which were identified with an unsatisfactory operating status are immediately highlighted in the system for appropriate action. Reports and graphs can be generated that provide the user with instrument operational history. For example, the trending chart feature could assist QA programs by identifying instrument failures before they occur. The paper concludes with the level of improved efficiency and cost savings that a facility would realize by implementing an automated Field Instrument Source and Calibration system.

PENCIL-CHAMBER MEASUREMENTS OF BACKSCATTER FROM ELONGATED FIELDS OF LOW-ENERGY X RAYS

H.P. Maharaj
Department of Health, Radiation Protection Bureau, Ottawa, Canada

Abstract - To facilitate dose calculations for risk assessment purposes, the backscatter from several elongated fields was measured and comparisons were made with similar data used for superficial radiotherapy. A York fullwave rectified generator with a beryllium window x-ray tube was operated up to 81 kVp using aluminum and copper filters in the beam to provide effective energies of 27 and 73 keV. A MDH Radcal 10x5-10.3 CT ($3cm^3$) air-equivalent plastic pencil-shaped ionization chamber was utilized with a wood phantom. For x rays generated at potentials $\leq$400 kVp, the ratio of in-air measurements on the beam axis at a point in space with and without the scattering medium yields the backscatter factor (BSF). Measurements were made with the ionization chamber aligned parallel to the field length and centred on the beam axis at a tube-target-to-phantom surface distance of 50 cm, and were normalized for constant beam output using an in-beam monitor. Various fields were chosen to provide elongation (ratio of field length and width) between 2 to 23. Using the method in Appendix A of Reference 3, the test fields were converted to their equivalent square or circular field for which the corresponding BSF was determined for comparison. Differences between the mean measured BSFs and those interpolated (Fig.1.2., Tables 3.1.1 and 3.2.1 of Ref. 3) were observed to be in the range of -12.5% to 6%, and the coefficient of variation of the measured BSFs was estimated to be less than 9.5%. For field elongation >10, the mean measured BSFs were within $\pm$5% of the data in Ref. 3. Curve fitting the measured and interpolated data as a function of equivalent fields showed better agreement at 73 keV than 27 keV. The results suggest that the chamber wall is too thick causing significant attenuation of soft photons backscattered from the phantom at 27 keV, and that BSFs for elongated fields can be conveniently and reliably obtained by using the equivalent field method and data in the reference cited.

Introduction

Low-energy x rays (<400 keV) incident on a medium are scattered and absorbed by the atoms principally through coherent, photoelectric, and Compton processes. Except in a coherent interaction, energetic electrons are produced in the other two processes. These electrons ultimately deposit their energies through ionization and excitation reactions with atoms and molecules of the host media; in biological materials these reactions can cause damage, which is intimately associated with the dose, that is, the amount of energy absorbed per gram of material. The dose to a tissue or organ is often needed for radiation protection and radiotherapy purposes, but since its direct measurement is not always possible calculational methods based on simple and reliable data are desired.

In radiotherapy, in-air measurements, such as exposure[1] are made at a particular reference point and then translated to yield absorbed doses by the application of certain factors, one of which accounts for radiation backscattered from underlying tissues. This factor, called the backscatter factor (BSF), is defined as the ratio of the absorbed dose in a small mass of tissue at the depth of electronic equilibrium in a phantom and the absorbed dose in the same mass of tissue at the same position in free space[2]. For photon energies up to 400 keV, the depth of electronic equilibrium is practically zero and is located on the phantom surface[3]. BSFs for low energy x rays are typically >1.0 since the radiations are scattered more laterally and can reach the detector whereas for higher energy x rays the scatter is more forward peaked and less low energy x ray scatter returns to the surface. Extensive backscatter measurements have been undertaken and their results compiled for use in clinical radiotherapy[3]. While BSFs are provided for several standard (square and rectangular) fields, the field elongation (defined as the ratio of field length and width) is seldom greater that 2. However, for non-standard fields, approximations are made using the equivalent field method, which, in principle means the equivalent field (square or circular) that has the same backscatter at the surface as the non-standard field[3].

Improved information-to-noise ratio in imaging, realised from fan beams in computerized tomographic (CT) techniques, has resulted in many industrial machines employing similar imaging technology and utilizing low energy x rays that are collimated to dimensions >60 cm in length and >0.7 cm in width. To facilitate dose calculations, this paper discusses the backscatter from elongated fields at two beam energies and makes comparisons with similarly published data. The intent is to have simple and reliable backscatter data from which dose estimates can be made.

Materials and Methods

The experimental setup is shown schematically in Fig.1. A York x-ray machine (model 3225) equipped with a beryllium window x-ray tube capable of operating up to 110 kVp was used as the source of x rays. The x-ray tube output was monitored with a thimble ionization chamber (NEL, England; Farmer 0.6 cc chamber) fixed on the primary collimator. A 0.64-cm thick adjustable lead diaphragm was used to define the field sizes on the surface of the phantom. All measurements were done at a source to phantom surface distance of 50 cm. Added filters were positioned near the diaphragm to obtain 27 and 73 keV effective energy beams (Table 1), and were maintained at 24 cm from the pencil chamber in order to minimize extraneous scattering effects.

Measurements were made with an air-equivalent plastic ionization chamber typically used for x-ray output evaluations of CT equipment (RadCal MDH 5-10.3). This pencil chamber has an internal diameter of 0.62 cm, a wall thickness of 0.04 cm, a length of 10 cm and a volume of 3.0 cc. There are no metal parts on the chamber that can shield radiation below it or cause scatter into it; hence stem effects are virtually eliminated.

Eleven maple-wood slabs (density 0.73 g/cc), each measuring 60 cm x 15.2 cm x 2.54 cm, were stacked together to provide a 27.9 cm thick phantom, a thickness sufficient to ensure maximum backscatter. A groove was made on the slab nearest the x-ray source to ensure closer contact between the pencil chamber and the wood surface. The chamber was always oriented with its long axis perpendicular to the central ray and centred on the phantom, but parallel to the long side of the radiation fields.

Twelve fields were chosen to provide elongations that ranged from 2 to 23. For each field size and beam energy, five consecutive irradiations were carried out with the phantom firmly in contact with the pencil chamber, and readings of the in-beam monitor and pencil chamber were recorded simultaneously; this procedure was repeated with the phantom completely removed from the beam. The ratio of the pencil chamber averaged readings, normalized for beam intensity variations (<3.0%), with and without the phantom yielded the BSFs. Two independent sets of measurements were used, but if the BSFs were not within 10%, measurements were repeated to enable estimates of the standard deviations. Comparison of the BSFs was achieved by converting the elongated fields to their equivalent circular or square fields using the method in Appendix A of the British Journal of Radiology (BJR) Supplement 11[3], and consulting Figure 1.2 of BJR (2 mm Al HVT, ~ 28.5 keV) and Tables 3.1.1 and 3.2.1 (~73 keV) for the appropriate values.

Results and Discussion

Mean BSFs with a coefficient of variation (standard deviation/mean) better than 9.5% are indicated in Table 2, including the percentage differences with the BJR values. Differences ranged from -12% to 0.9% and -12.3% to 5.6% for 27 and 73 keV, respectively. The percent differences as a function of field elongation are shown in Fig.2. For field elongation >10, it is apparent that the experimental BSFs are within $\pm$5% of the BJR values at both energies. This result suggests that the BJR can be used for BSFs associated with highly elongated fields. For fields of smaller elongation, the discrepancies are larger ($<\pm$13%).

The BSFs are shown as a function of equivalent fields in Fig.3 where the data were fitted to a logarithmic regression formula *(y=a+b(ln x))*. There was good agreement between the experimental BSFs and the BJR values at 73 keV, and this implied that BJR values can be used for x-ray beams of higher energies. However, agreement was not as good at 27 keV, suggesting that the chamber wall was probably too thick in which case it would cause increased attenuation of the low energy x rays backscattered from the phantom.

It is not easy to compare BSFs at 27 keV with those of other investigators because of differences in experimental conditions. In Fig. 4(a), the experimental BSFs at 27 keV are indicated as a function of field area. Also shown are Quimby's data obtained at 2 mm Al half value layer (equivalent to 28.5 keV effective), using a presswood phantom and a Failla-designed parallel plate extrapolation chamber

(of 0.2 mm electrode thickness) placed at 70 cm from the x-ray tube[4]. Quimby's data showed a remarkably good fit to the logarithmic regression line in comparison with the experimental values. Assuming that the wood phantoms exhibited comparable scattering properties, the low experimental BSFs were probably attributed to the thicker chamber wall of the pencil detector and to differences in beam quality at 50 cm and 70 cm from the x-ray tube.

In Fig. 4(b) the experimental BSFs at 27 keV are shown as a function of the square root of the field area to facilitate comparison with Johns's data. The latter were obtained from measurements made with a thimble ionization chamber (air-wall thickness of 0.5 mm) at source to chamber distances of 35 and 50 cm in a water phantom at a beam quality of 2 mm Al half value layer[5]. Johns's data fitted the logarithmic curve very well, but the experimental values were low by 10-15%. In principle, the pencil chamber would record more low energy backscattered photons since its wall (0.04 cm) is thinner than the 0.05-cm-thick-wall chamber used by Johns, but the scattering differences between the wood and water phantoms were difficult to elucidate here.

In spite of the preceding uncertainties, the experimental BSFs obtained in this work overall were comparable to within 15% of those of other investigators and those in the BJR. Considering that the BJR was compiled from data of various authors all of which were in reasonable agreement and is a widely accepted source of backscatter and depth-dose data routinely used for radiotherapy dose calculations, it is not necessary to generate BSFs specific to x-ray equipment presented with elongated fields. The BSFs for such fields may instead be obtained by using the equivalent field method described in Appendix A of the BJR[3] and then consulting the appropriate equivalent square or circular field for the beam energy involved.

Conclusions

The results suggest that the chamber wall of the pencil detector is too thick causing significant attenuation of soft photons backscattered from the phantom. Overall the BSFs in this work were comparable to within 15% of those of other investigators and those in the BJR. The BSFs for elongated fields can be conveniently and reliably obtained by using the equivalent field method and data in the BJR.

Table 1: Irradiation parameters for backscatter measurements.

Operational Technique Irradiation parameters				
Potential (kVp)	Current (mA)	Time (s)	Added filter[a]	Effective energy[b]
30.0	25	15	0.35 mm Cu+ 1.0 mm Al	27.0
80.5	25	15	5.05 mm Cu+ 3.0 mm Al	73.0

[a] Filters indicated are aligned in order from the source out to absorb the characteristic radiations from the copper.

[b] Obtained by determining the linear attenuation coefficient from the measured half value layer in copper and consulting published attenuation data[2].

Table 2: Backscatter factors for various fields at 27 and 73 keV.

Field		Backscatter factors					
		27 keV			73 keV		
Size (cm x cm)	Elongation	Expt.	BJR[a]	% Diff.[b]	Expt.	BJR[c]	% Diff.[b]
10 x 1	10	1.06	1.07	-0.9	1.08	1.10	-1.8
15 x 1	15	1.08	1.07	+0.9	1.14	1.11	2.7
20 x 1	20	1.08	1.07	+0.9	1.10	1.11	-0.9
23 x 1	23	1.07	1.07	0	1.12	1.12	0
10 x 3	3.3	1.03	1.17	-12.0	1.07	1.22	-12.3
15 x 3	5.0	1.16	1.18	-1.7	1.31	1.24	5.6
20 x 3	6.7	1.09	1.18	-7.6	1.26	1.25	0.8
23 x 3	7.7	1.12	1.19	-5.9	1.28	1.25	2.4
10 x 5	2	1.17	1.21	-3.3	1.25	1.29	-3.1
15 x 5	3	1.15	1.22	-5.7	1.28	1.31	-2.3
20 x 5	4	1.11	1.23	-9.8	1.37	1.32	3.8
23 x 5	4.6	1.15	1.26	-8.7	1.31	1.34	-2.2

[a] Values interpolated from BJR[3], Figure 1.2, by determining the equivalent diameter of the rectangular field using Table A.1 in the reference cited.

[b] Difference between the experimental and BJR values, expressed as a percentage.

[c] Values interpolated from BJR[3], Tables 3.1.1 and 3.2.1; equivalent squares were obtained from Table A.2 in BJR for the field size used.

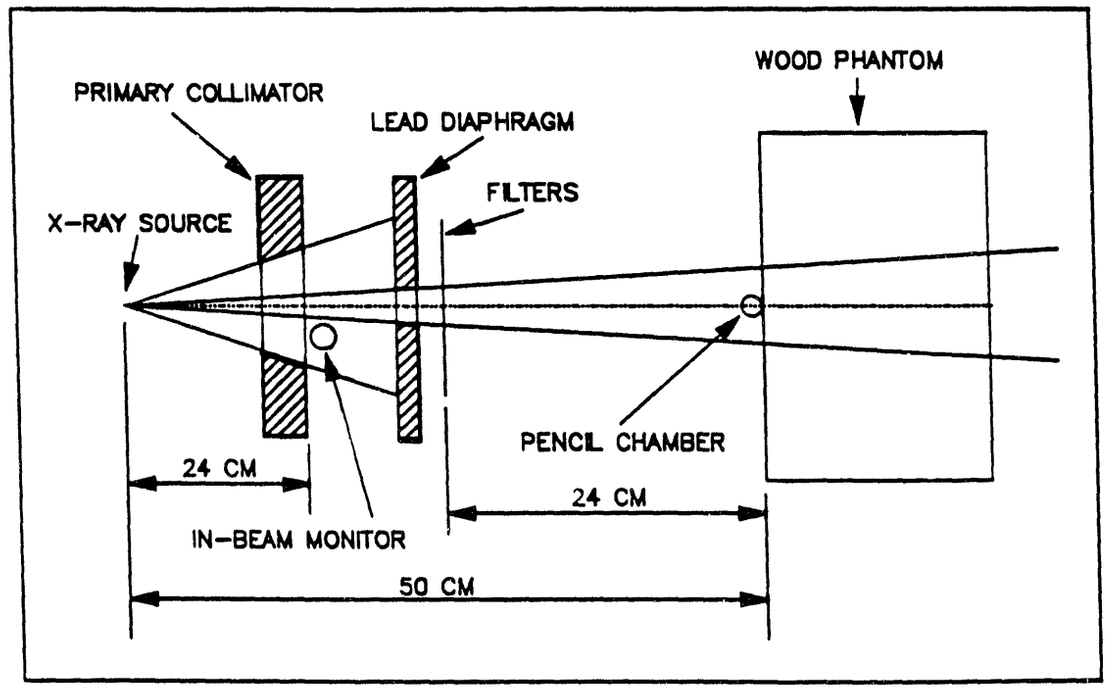


Figure 1: Schematic diagram of experimental setup used for backscatter measurements.

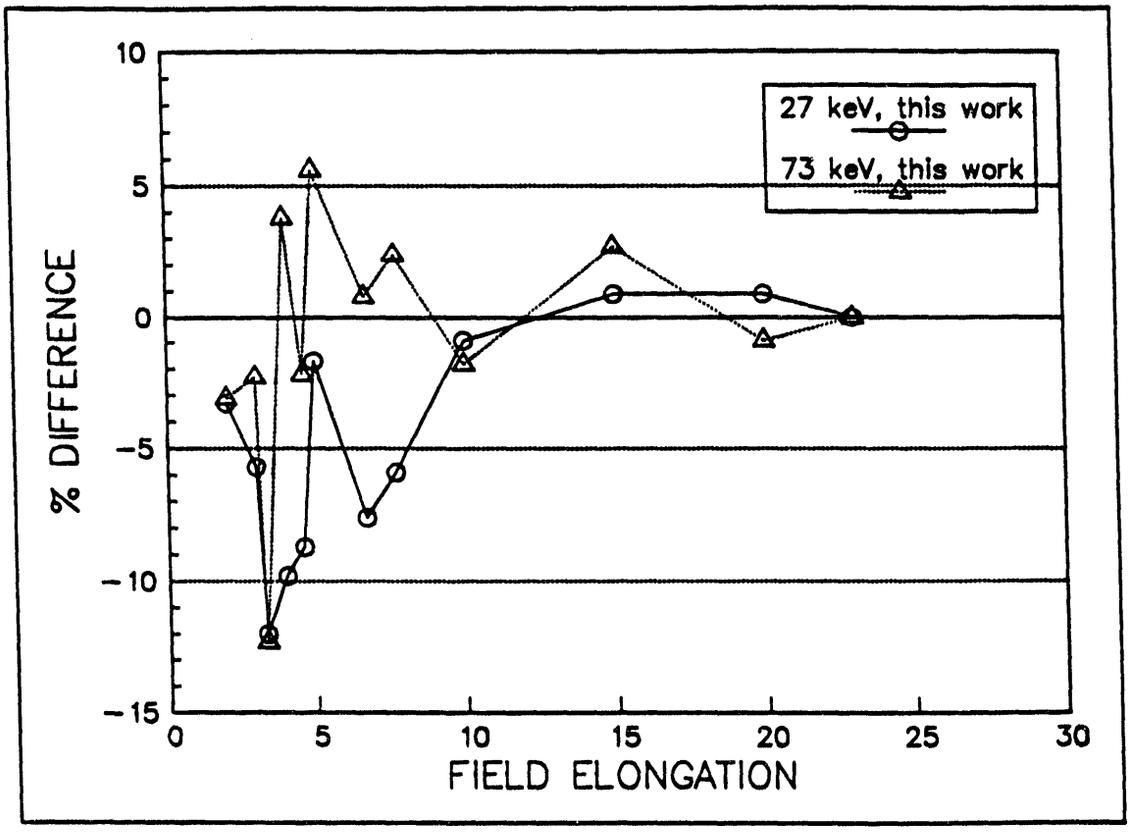


Figure 2: The variation of percentage difference between the experimental BSFs and the BJR values with field elongation.

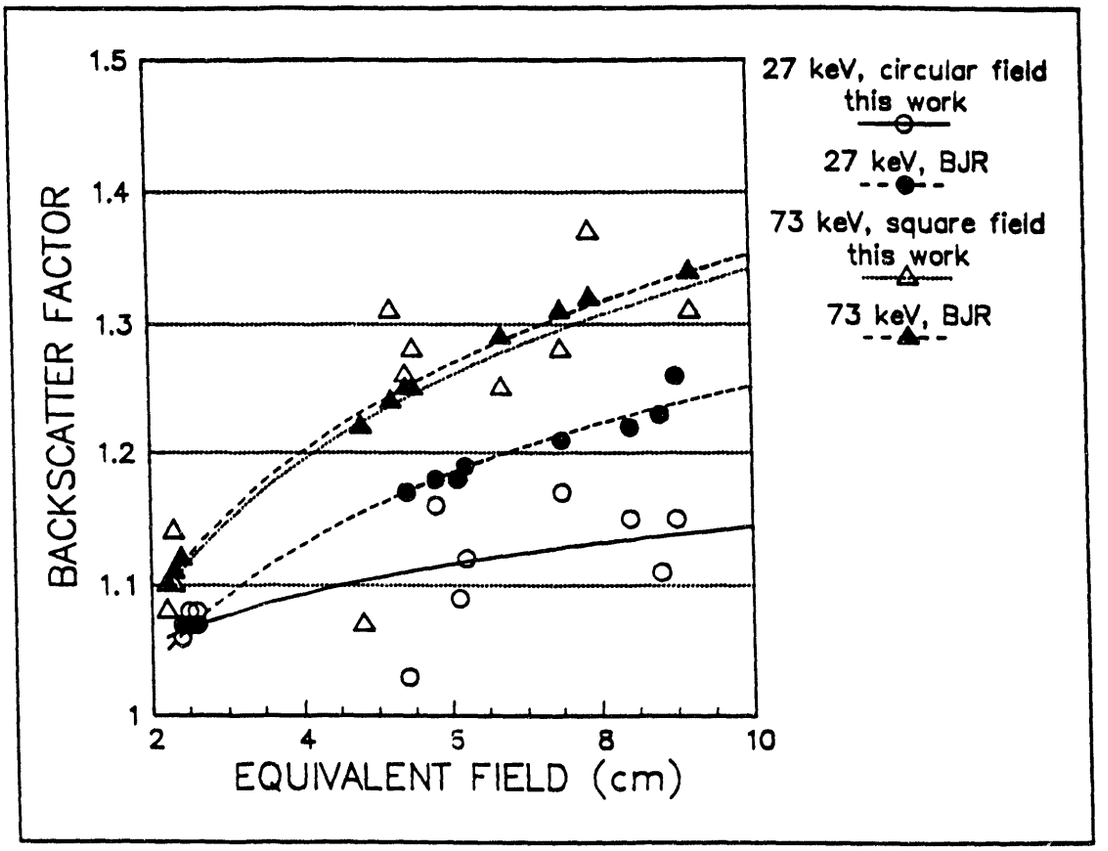
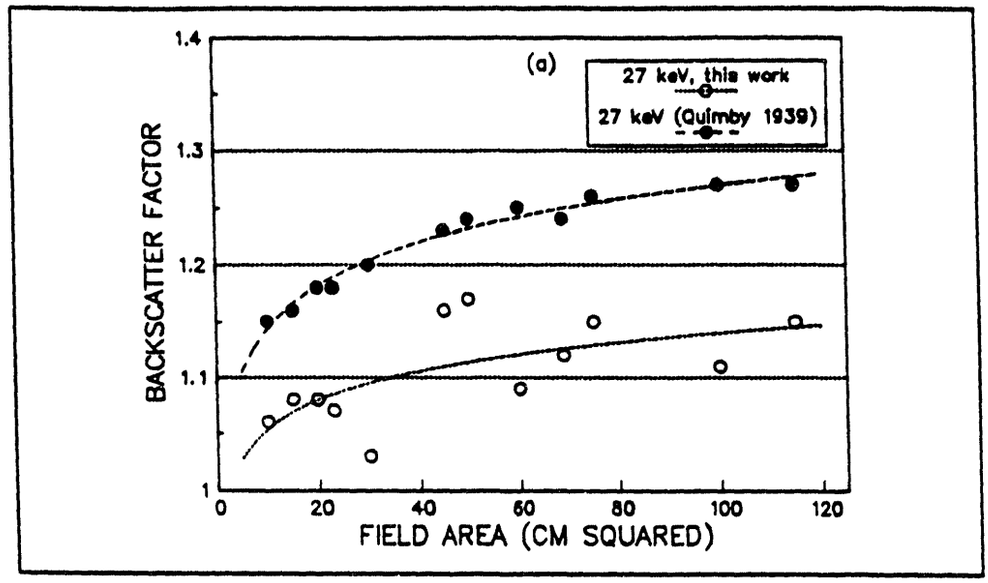


Figure 3: Backscatter factors versus equivalent fields for 27 and 73 keV beams.



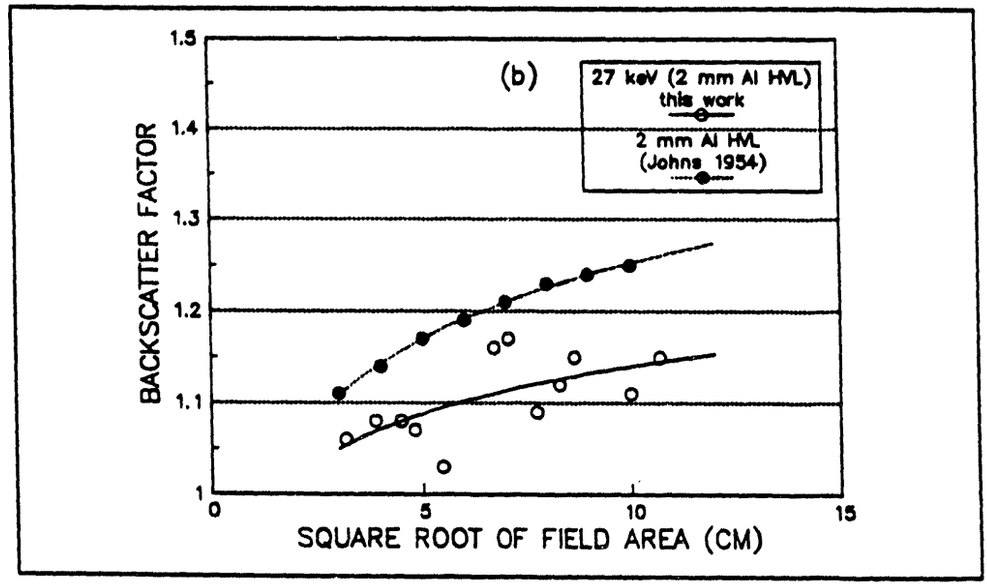


Figure 4: (a) shows the variation of backscatter factor as a function of field area for a 27 keV beam and (b) shows the variation with respect to the square root of field area. For comparison, Quimby's data[4] is shown in (a) and Johns's[5] data in (b).

References

[1]ICRU, "Radiation Dosimetry: X rays and gamma rays with maximum photon energies between 0.6 and 50 MeV," ICRU Report No. 14, 1969.

[2]H.E. Johns and J.R. Cunningham, The Physics of Radiology, 3rd Edition (Thomas, Springfield, IL,) 1980.

[3]BJR, "Central axis depth dose data for use in radiotherapy", Supplement No. 11 (BJR, London), 1972.

[4]E.H. Quimby, L.D. Marinelli, J.H. Farrow, "A study of back-scatter", Amer.J. Roent., 39, 799-815, 1939.

[5]H.E. Johns, J.W. Hunt, S. Fedoruk, "Surface back-scatter in the 100 kV to 400 kV range", Brit.J. Rad., 27, 443-448, 1954.

RADIATION IMAGE SENSOR UTILIZING PHOTOSTIMULATED LUMINESCENCE

A.Kalninsh, I.Plavina (Institute of Physics, Latvian Academy of Sciences LV-2169, Salaspils-1, Latvia), A.I. Popov and A. Tale (Institute of Solid State Physics, University of Latvia, 8 Kengaraga str., LV-1063, Riga, Latvia)

In this abstract the novel type of luminescent sensor for measurement of a UV radiation image based on the photostimulated luminescence (PSL) phosphor KBr-In is described.

The most important part of the luminescent sensor is the imaging plate consisting of a KBr-In crystal. When a KBr-In crystal (as well as other alkali halide crystals) is exposed to UV radiation a certain fraction of energy proportional to dose is deposited and stored [1]. Thus, a stable latent image is created in the form of close radiation defect pairs [2]. Each pair consists of F center (electron trapped by anion vacancy) and ionized impurity ion (In^{2+}). PSL of such pairs is utilized to recover the stored UV radiation image. By scanning a focused He-Ne laser light (630 nm), a stable latent image is destroyed giving the characteristic In luminescence (420 + 530 nm).

The PSL intensity, which is proportional to the UV radiation dose, is measured for each spot on the imaging plate. A wide-range photomultiplier tube is used to convert the luminescence signals to electric ones. It is shown that the output electric signal Ψ^2 (Ψ - the signal to noise ratio) shows a linear dependence in the range of 1 - 7 x 10^8, where the UV-light input signal is varied within the range of 4 x 10^{-13} to 3 x 10^{-4} J /cm^2, (for the spot square is 0.0002 cm^2). The highest value of the analogous part of the signal (7 x 10^8) may be split up at least into 8.6 x 10^8 step-bits; hence, it is estimated that the highest possible information density in the proposed sensors reaches about 4 x 10^7 bit/cm^2, the energy expenditure being 1 x 10^{-11} J/bit.

Some other experimental results and sensor characteristics are also presented.

1. P. Bratslavets, A.Kalnins, I.PLavina, A.Popov, S.Rapoport, A.Tale, B. Zeigurs in "The Advancement of Imaging Science and TechnoLogy", 1990, Int. Acad. Publ. (A. Pergamon-CNPIEC Joint Venture), p.474-476.
2. P. Bratslavets, A.Kalnins, I.Plavina, A.I.Popov, B.Rapoport and A. Tale, phys. stat. sol. (b) 1992, vol. 170 pp. 395-401.

DOSIMETRY OF MIXED RADIATION USING RECOMBINATION CHAMBER

Mieczyslaw Zielczyński and Natalia Golnik
Institute of Atomic Energy, 05-400 Otwock Świerk, Poland

ABSTRACT

Advantages and shortcomings of mixed radiation dosimetry based on recombination detectors are presented. The methods considered here are particularly advantageous for radiation protection dosimetry in the vicinity of high-energy particle accelerators and in other radiation fields with a complex composition and a broad energy spectrum.

1. INTRODUCTION

Mixed radiation, i.e. an external radiation capable to create both low-LET and high-LET particles in a body tissues, is a usual case in the vicinity of heavy particle accelerators, reactors, neutron isotopic sources and also in space. The energy spectrum, as well as the proportion of fluences of different particles in mixed radiation fields are usually poorly known. In most difficult cases of stray radiation fields near high-energy accelerators we have to deal with the fields consisting of many different kinds of radiation and each of them may have an extremely broad energy spectrum. Dosimetry of such fields is still a challenging task.

The main goal of radiation protection dosimetry in mixed fields is the determination of some operational quantities, defined by ICRU and introduced to the practical use as the safe estimates of these quantities, which are subjected to limitation. Among them the ambient dose equivalent, $H^*(d)$, linking the external irradiation to the effective dose equivalent is recommended for monitoring of working places. There are several types of detectors which response corresponds to the ambient dose equivalent for mixed radiation fields of simple composition and limited energy spectrum. If the composition and the energy spectrum are complex, very broad or unknown, the detectors operated according to the definition of ambient dose equivalent can give a satisfactory response. Such detectors should be tissue equivalent, the effective wall thickness of the detector should be close to 10 mm, the angular response and the scattering properties should be similar to the properties of the ICRU sphere (which is 30 cm in diameter and 1 g/cm^3 of mass density) and the detector signal-to-absorbed dose ratio should follow the function Q(L) used in the definition of quality factor.

The above mentioned properties can be fulfilled by a recombination chamber[1]. The response of any recombination chamber can be linearly correlated with the quality factor defined in ICRP report 21. Sufficiently large recombination chamber can also approximate some properties of the ICRU sphere. It has been shown that the commercially available recombination chamber of REM-2 type has satisfactory response to the ambient dose equivalent of mixed radiation[2].

Using recombination chambers one can determine not only $H^*(10)$ but also other quantities needed in radiation protection:

- the ambient absorbed dose at an appropriate depth, e.g. $D^*(10)$;
- the near-surface dose equivalent, e.g. $H^*(3)$ or $H^*(0.07)$;
- the quality factor, Q;
- the distribution of the absorbed dose versus the restricted LET, D(L) and in particular the contribution of low-LET radiation to the total absorbed dose;
- the mean and the effective local ion density, μ, in particle tracks and the corresponding quantities, like the mean restricted LET, $\bar{L}_\Delta$, or the lineal energy, y_d;
- correction factors dependent on radiation quality, useful not only in dosimetry using recombination methods.

The recombination chamber itself does not enable to determine the energy spectrum of radiation. It does not distinguish different kinds of radiation with the same restricted LET as well.

2. CHARACTERISTICS OF RECOMBINATION CHAMBERS

Recombination chambers are ionisation chambers operated in unsaturated mode, under conditions of local recombination of ions. Usually, such chambers contain several parallel-plate tissue-equivalent electrodes, spaced by gaps having the width of a few millimetres (see Fig.1). The chambers are filled with a quasi tissue-equivalent gas mixture up to the pressure of some hundreds of kilopascals. The local recombination takes place between ions formed along the paruicle track in gas. It strongly depends on local ion density, i.e. also on LET. An appropriate dependence of the chamber response on LET can be formed by choice of voltage applied between the chamber electrodes. The electrical charge created between the electrodes is proportional to the absorbed dose, while the shape of the saturation curve of the chamber (see Fig. 2) provides information on radiation quality.

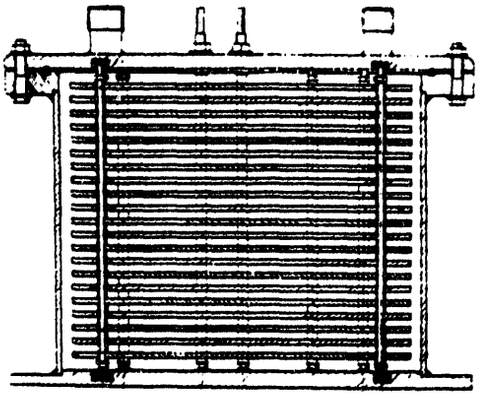


Fig. 1. Cross section of the twin recombination chamber, type KR-3

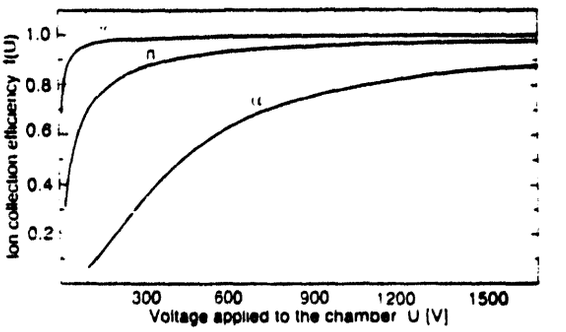


Fig. 2. Saturation curves of recombination chamber of REM-2 type for gamma (^{137}Cs), neutron (^{241}Am-Be) and $\alpha+\beta$ (^{222}Rn+daughters) radiations

Radiation quality factor can be successfully approximated by an easily measurable quantity - recombination index of radiation quality (RIQ, Q_R)[3,4]. The RIQ considered in this work is defined as:

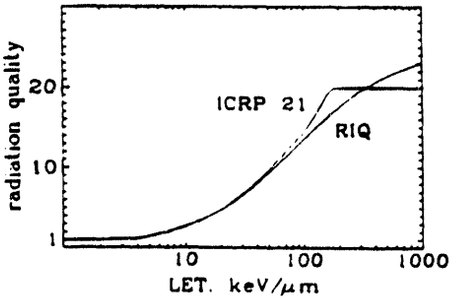


Fig. 3. Quality factor (ICRP 21) and RIQ plotted versus LET.

$$Q_R = \frac{1-f(U_R)}{1-f_\gamma(U_R)} \qquad (1)$$

where f - is the ion collection efficiency in the chamber irradiated in mixed radiation field being investigated,

f_γ - is the ion collection efficiency of the same chamber, when irradiated in a reference field of gamma radiation (^{137}Cs),

U_R - is the "recombinaton voltage" ensuring $f_\gamma \approx 0.96$.

The relation between RIQ and LET is shown in Fig. 3 together with the Q(L) funcuon. RIQ can be considered not only as the approximation of the quality factor, but also as an independent parameter of radiation quality, helpful in radiation biology, radiation therapy and in some other domaines[4].

3. PRACTICAL METHODS OF MEASUREMENTS

3.1. Determination of RIQ

For practical determination of RIQ, the ion collection efficiencies f and f_γ in relation (1) can be replaced by the appropriate ionisation current ratios:

$$Q'_R = \frac{1}{R'}\left[1 - \frac{i(U_R)}{i(U_S)}\right] \qquad (2)$$

where $R' = 1 - [i_\gamma(U_R) / i_\gamma(U_S)] \approx 0.03 + 0.05$ - is a recombination mode factor,
- i - is the ionisation current of irradiated recombination chamber,
- U_S - is the real value of high voltage applied to the chamber,
- U_R - is the recombination voltage, chosen during the calibration in a reference gamma field.

The difference between the values of Q'_R and Q_R depends on the width of the LET spectrum. In every practical situation this difference can be neglected, if the voltage U_S is high enough to ensure at least 99% of the saturation current in the reference gamma radiation field. Therefore, for determination of RIQ in mixed radiation field, it is sufficient to measure signals of recombination chamber at two voltages, sequentially applied to the chamber.

3.2. Determination of radiation quality factors

In this work we consider only the quality factor defined in ICRP report 21. However, quality factors based on other definitions (like those defined in ICRU report 40 and in ICRP report 60) can be derived from the measured values of RIQ[5,6]. The radiation quality factor Q practically does not differ numerically from RIQ defined by relation (1). Therefore, equality $Q \approx Q_R$ is recommended for practical radiation protection. It has been shown that the RIQ is the additive quantity[3], so equality $Q \approx Q_R$ is valid for every composition and every radiation spectrum. However, small differences between Q and Q_R may exist, because of :

1) non-identical dependencies on LET (see Fig. 3), especially for very low-LET and very high-LET particles,
2) possible differences in the energy spectrum of secondary ionising particles in gas of the chamber and in a tissue or in the ICRU sphere, mainly because of lack of oxygen and excess of carbon in the chamber material,
3) quality factor is related to the unrestricted LET, while RIQ is correlated rather with the restricted LET (restriction distance of order of 0.1 μm of tissue),
4) relation between Q_R and LET is slightly different from that presented in Fig. 3, if f_γ differs from 0.96.

There are also some other possibilities to determine quality factor using local recombination phenomenon, but not the RIQ concept. One of the methods is shortly described in paragraph 3.17 of this work. Other methods, based on registration of ions created in a single event, on ion equilibrium, on light emission during recombination and on investigation of the slope of the saturation curve have been reported or mentioned elsewhere [7-10], however, these methods have not found any considerable practical application up to now.

3.3. Determination of the ambient absorbed dose, $D^*(10)$

Recombination chamber can be considered as a homogenous tissue-equivalent ionisation chamber. According to cavity theories, the charge of ions created between the chamber electrodes is proportional to the absorbed dose. If the effective wall thickness and the mass of the chamber are not much different from those of the ICRU sphere, the charge is proportional to the ambient dose $D^*(10)$. The ambient dose rate can be correlated with ionisation current measured at the voltage U_S:

$$\dot{D}^*(10) = N \cdot i(U_S) \cdot \prod k \qquad (3)$$

where $N = \dfrac{\dot{D}^*_\gamma(10)}{i_\gamma(U_S)}$ - is the calibration factor established for the chamber in a reference gamma field,

$\prod k$ - is the product of correction factors.

Some correction factors can be correlated with the RIQ measured by the same chamber. The correction factor for the lack of saturation can be expressed as:

$$k_S = 1 + \frac{S(Q_R - 1)}{1 - 0.04 Q_R} \qquad (4)$$

where $S=1 - f_\gamma(U_S)$ is the lack of saturation for the reference radiation (it can be estimated by an extrapolation procedure using the saturation curve for gamma radiation measured in laboratory conditions.

The value of the saturation correction k_S can exceed 1.3 for recombination chamber filled up to high pressure (above 1 MPa) and irradiated in a high-LET radiation field.

The correction factor for the energy expended to create an ion pair can be also related to the RIQ[11]:

$$k_W = 1 + 0.008\,(Q_R - 1) \qquad (5)$$

Correction factors related to atomic composition of the chamber material and to scattering properties of the chamber, compared to that of ICRU sphere, depend generally on type and energy of radiation, but they can be also considered as dependent on RIQ for mixed radiation fields, composed mainly of neutrons and photons. It is recommended to consider together all the radiation-quality dependent correction factors established for the particular type of the chamber. For the properly designed recombination chamber the overall correction usually does not exceed some per cent.

3.4. Determination of the ambient dose equivalent, $H^*(10)$ by two sequentially applied voltages

The ionisation currents $i(U_S)$ and $i(U_R)$ are sufficient to determine not only the quality factor, but also the dose equivalent rate:

$$\dot{H} = \dot{D}Q \sim i(U_S)Q_R \sim [i(U_S) - i(U_R)] \qquad (6)$$

If the chamber is sufficiently large and its effective wall thickness is of order of 1 g/cm^2 it can give the satisfactory response to the ambient dose equivalent (rate) of mixed radiation:

$$\dot{H}^*(10) = \dot{D}^*(10) \cdot Q^*(10) = N\, i(U_S)\, Q_R \prod k \qquad (7)$$

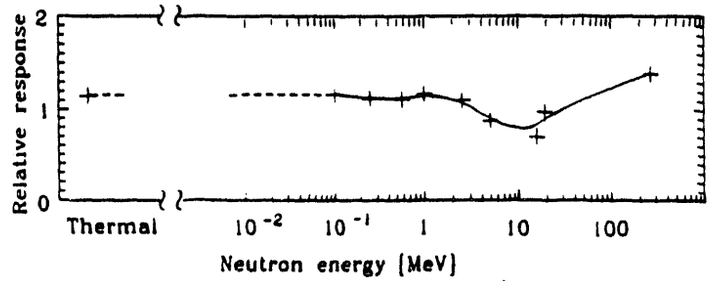


Fig. 4. Relative response of the REM-2 recombination chamber to $H^*(10)$ versus neutron energy (related to the response for ^{241}Am-Be source)

In order to ensure the same response to gamma radiation and to neutrons (e.g. from Am-Be source) it is recommended to fill up the chamber with gas containing more hydrogen than the soft tissue. The response of such a chamber to ambient dose equivalent is sufficiently independent of kind of radiation and of its energy spectrum[2]. The response of the recombination chamber of the REM-2 type to neutron radiation is shown in Fig. 4.

3.5. Continuous measuring of dose equivalent rate by means of a differential recombination chamber

As it can be seen from equation (6), the difference of ionisation currents $i(U_S) - i(U_R)$ is proportional to the dose equivalent rate of mixed radiation. Differential recombination chambers have been designed [1,12] in order to

make possible the direct measuring of dose equivalent (rate). The chamber contains at least three electrodes (usually much more), which form two equal volumes. The near-saturation voltage U_S applied to the polarising electrode of one of the volumes, while the recombination voltage U_R of opposite polarity is applied to the other polarising electrode. The differential current is measured by an electrometer, calibrated in units of dose equivalent rate (see Fig. 5).

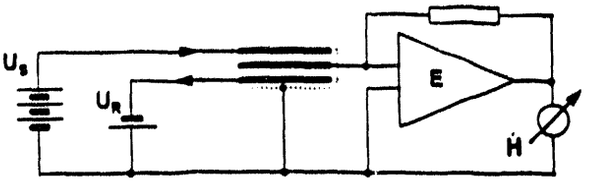


Fig. 5. Principle circuit of dose equivalent meter based on differential recombination chamber.

3.6. Measurements at unstable dose rate

The difference between $i(U_S)$ and $i(U_R)$ is correlated with the RIQ and with the dose equivalent. The relative difference is usually small - in case of low-LET radiation it does not exceed a few per cent of the saturation current. Therefore both values: $i(U_S)$ and $i(U_R)$ should be measured very precisely. Special techniques are recommended to improve the precision, particularly in situations where radiation or environmental conditions are hard.

At unstable dose rate, which is rather a usual case near nuclear installations, the use of a monitor considerably improves sequential measurements with a recombination chamber. In this case the RIQ should be determined from relation (2), but the ratios of ionisation currents (or charges) to appropriate monitor readings should be used, instead of $i(U_R)$ and $i(U_S)$. It is advantageous to make use of another recombination chamber as a monitor. This chamber can be of the same or similar type, but sometimes it is better to make use of a different gas pressure in both chambers and to perform measurements with mutual changes of the chamber positions, in order to have a good estimation of the saturation correction.

Some chambers were designed as the twin recombination chambers[13]. One part of the twin chamber can be operated as a monitor, or as one of the measuring parts for simultaneous measurements of $i(U_S)$ and $i(U_R)$, hence in this case the continuous readings of the absorbed dose and of the quality factor are possible and there is no need to use any additional monitor. The monitor is also not necessary, when a differential recombination chamber is used and the measurements are aimed at determination of the dose equivalent only. For some recombination chambers it is possible to make such connections of their electrodes[1], that the readings of the absorbed dose and the dose equivalent (rate) can be performed simultaneously (see Fig. 6).

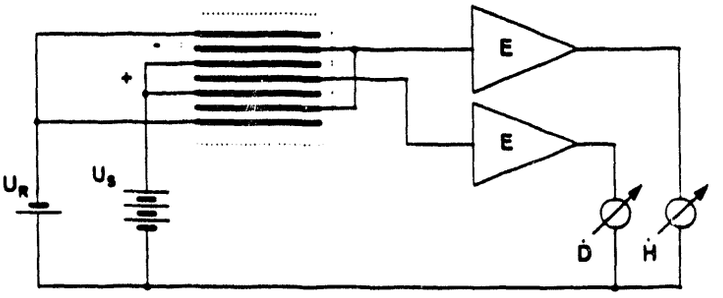


Fig. 6. Principle circuit of simultaneous measurements of the ambient dose and the dose equivalent rates using recombination chamber KR-7.

Another possibility of measurements at unstable dose rate is to make use of an appropriate time constant or of an appropriate time of measurements in the integration mode (charge measuring) and to repeat many times sequential measurements at both modes. Possibility of an automated fast switching making possible the direct reading of dose equivalent has been reported[14], however, this method needs further investigations.

3.7. Measurements at high dose rate gradients

If a differential or a twin recombination chamber is used, the number of ions collected in one volume is compared with the number of ions created in another volume. It can cause a considerable uncertainty in determinatuon of dose equivalent at spatially non uniform radiation fields. In order to reduce this uncertainty it is better to use multielectrode chambers ended on both sides by the volumes working in the same mode [1,7].

There is also the possibility of the mutual change of measuring modes in both volumes of the chamber. In this case the RIQ can be derived from measurements performed by a twin recombination chamber, using the following formula:

$$Q_R = \frac{1}{R'} \left[1 - \sqrt{\frac{i_1(U_R,t_1)\cdot i_2(U_R,t_2)}{i_2(U_S,t_1)\cdot i_1(U_S,t_2)}}\ \right] \qquad (8)$$

where i_1, i_2 - are the measured ionisation currents of both parts of the chamber
and t_1, t_2 - indicate different time of measurements.

The influence of dose rate unstability, of dose rate gradient, as well as of possible difference of the chamber volumes and difference of amplification of electrometers, can be strongly reduced using this technique of measurements.

3.8. Improvement of accuracy by using of both polarities of voltages applied

Sequential applying of both positive and negative voltages to polarising electrodes of the recombination chamber can reduce some unwanted side effects, such as an influence of electrical charges collected from side volumes of the chamber, connectors, cables and preamplifier of the electrometer if placed in radiation field , as well as to reduce the charge memory effect related to the electrical charge remaining on non conducting elements in the chamber long time after irradiation and changing the effective value of the electrical field strengths between the electrodes, especially in the recombination mode of operation. In this case the RIQ can be determined as:

$$Q_R = \frac{1}{R'} \left[1 - \frac{1}{2}\left(\frac{i(U_R)}{i(U_S)} + \frac{i(-U_R)}{i(-U_S)}\right)\right] \qquad (9)$$

It is also recommended to use the same procedure during the calibration in the reference gamma field:

$$R' = 1 - \frac{1}{2}\left(\frac{i(U_R)}{i(U_S)} + \frac{i(-U_R)}{i(-U_S)}\right)_\gamma \approx 0.04 \qquad (10)$$

3.9. Compensation of influence of unstable temperature

Both the established temperature of the chamber and the rate of the temperature changes may influence the measured ionisation currents. At saturation mode the influence of the established value of the temperature can be practically ignored - in sealed chambers this influence is caused by an absorption of gas in the electrode materials and by very small changes of the energy expended to create an ion pair in the gas. However, in the local recombination mode the temperature coefficient of the ion collection efficiency, α_f is of order of 0.1% / K and sometimes should be taken into account. It depends on the value of ion collection efficiency:

$$\alpha_f = \frac{1}{f}\frac{df}{dT} = \alpha_0(1-f) \qquad (11)$$

where T - is the temperature of gas in the chamber,
α_0 - is a constant.

An element sensitive to the temperature (e.g. a silicon diode) can be placed on the recombination chamber or inside of it and the temperature correction can be introduced to the readings. Also the temperature sensitivity of an electrometer, caused mainly by high-value resistors, can be taken into account. Usually more troubles may be caused by the temperature rate, especially if the dose rate and resulting ionisation current are low. The unwanted capacitance current appears:

$$i_T(U_S) = U_S\frac{dC}{dt} = C\,U_S\,\alpha_C\frac{dT}{dt} \qquad (12)$$

where C - is the chamber interelectrode capacity, t - is time,
and $\alpha_C = \frac{1}{C}\frac{dC}{dT}$ - is the temperature coefficient of the chamber capacity.

The capacitance current i_T should be taken into account or should be compensated automatically. It is also recommended to cover the chamber with a thermal isolation in order to prevent against high values of the chamber temperature rates.

3.10. Compensation of influence of unstability of polarisation voltage

Unwanted capacitance current appears also if the voltage applied to the chamber changes in time:

$$i_U(U_s) = C \frac{dU}{dt} \qquad (13)$$

Very stable voltage supply is required to make the value of the current i_U much lower than the value of the measured ionisation current, caused by radiation. It is also possible to compensate the capacitance current i_U using additional capacitance connected to the electrometer and to the voltage supply through a reversing follower.

3.11. Measurements at high dose rates

At high dose rates, especially if radiation is of pulsed character, the volume recombination of ions can occur between the chamber electrodes, in addition to the local one. In order to prevent this, the chamber with small interelectrode spacing should be used. Another possibility is to perform measurements at two or more dose rates, if possible, and to introduce the appropriate corrections, if necessary[15].

3.12. Measurements at low dose rates

Very stable supply source or a compensating circuit, like mentioned in the paragraph 3.10 should be used at low dose rate measurements. Better results are usually achievable if the integration mode of measurements is applied. Long time of measuring is necessary at low dose rates, because of time needed for stabilisation after moving the cables, changes of the voltage and replacement of the chamber to different temperature conditions.

The recombination chamber intended for measurements at low level of radiation should have a sufficiently large volume, the gas pressure should be also sufficiently high and the electrode spacing must not be low.

3.13. Determination of H*(0) at low dose rates and in hard environmental conditions

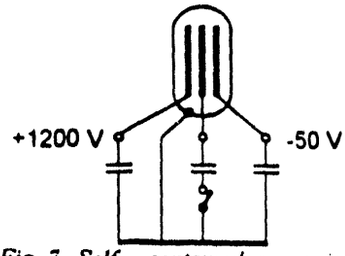


Fig. 7. Self - contained measuring system with a differential recombination chamber.

Special technique, based on a self - contained measuring system, is recommended[16] for very hard conditions of measurements, like measurements outside of buildings during winter time or measurements on board of space vehicles. The system consists of the differential recombination chamber and of 3 capacitors (Fig. 7). The special procedure of charging and reading of voltages on the capacitors is performed in laboratory conditions before and after irradiation.

3.14. Determination of depth distribution of dose equivalent in a phantom

Small recombination chambers, containing 2 or 3 parallel plate electrodes were successfully used for determination of the absorbed dose and the quality factor in phantoms[17,18]. The gap between electrodes of the in-phantom recombination chambers usually does not exceed 2 mm in order to avoid the volume recombination. The ambient dose equivalent and the dose equivalent index can be determined using the spherical phantom[19].

3.15. Determination of near-surface dose equivalents

The effective wall thickness of the recombination chambers used for the determination of near-surface dose equivalents $H^*(3)$ and $H^*(0.07)$ should not exceed 0.3 g/cm^2 and 0.007 g/cm^2 respectively. In the last case a mettalized mylar or capton foil is usually used. The wall acts also as the polarising electrode. In this case the

measuring electrode and the electrometer terminal should be placed at high electrical potential. Filling gas in the chamber cavity should have high molecular weight (like e.g. butadiene) in order to ensure conditions of local recombination at gas pressure close to the atmospheric pressure.

3.16. Measurements of personal dose equivalents, $H_p(10)$

Set of three pen-like recombination chambers, supplied from capacitors charged to the voltages U_R and U_S can be used for the determination of the personnel dose and the corresponding quality factor. The direct measurement of the personal dose equivalent, $H_p(10)$ is possible by means of the personnel dosimeter with concentric differential chamber[20].

The serious shortcoming of the personnel recombination dosimeters is the requirement of performing their reading and recharging procedures in time intervals not longer than one week.

3.17. Continuous measuring of quality factor by means of a differential recombination chamber with non equal volumes

The circuit shown in Fig. 8 presents the device which registers the quality factor continuously. Differential recombination chamber with the ratio of volumes equal to 0.87 is used in the device as a detector. High voltage U_S is applied to the smaller volume. The voltage of opposite polarity at the larger volume establishes itself automatically at the value which ensures near zero value of the differential current. This voltage is roughly proportional to the radiation quality factor[21]. The shape of relation between this voltage and LET can be changed by the appropriate choice of the value of high voltage U_S.

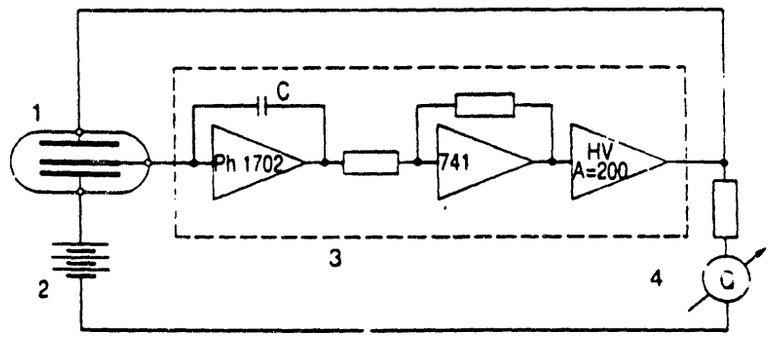


Fig. 8. Functional circuit of device with direct reading of quality factor: 1 - recombination chamber, 2 - high voltage source, 3 - high voltage electrometrical amplifier, 4 - voltmeter calibrated in units of quality factor.

3.18. Determination of the low-LET component of absorbed dose

The low-LET radiation component always exists in mixed radiation fields. Even if undisturbed radiation field contains small contribution of low-LET radiation it always arises in detectors simulating the ICRU sphere due to (n,p) reactions and generation of delta rays. At least four values of polarising voltage should be applied to the recombination chamber in order to estimate the contribution of the low-LET component to the absorbed dose. The method is based on an unfolding procedure comparing the measured ion collection efficiencies of mixed radiation with those which were previously determined in the reference gamma field[22].

Knowledge of contribution of low-LET radiation to the total absorbed dose is needed, for example, for the determination of ICRP-60 quality factors, basing on measurements of RIQ[6].

3.19. Determination of dose distribution versus restricted LET

Local recombination of ions depends on local ion density in tracks of ionising particles, which is correlated with restricted LET. The restriction radius is of order of 0.1 μm of water. Whole saturation curves, should be precisely determined in both mixed radiation field and in reference gamma field and then analysed using

an unfolding program and a formula derived from the local recombination theories[23]. The method is still under investigation.

4. COMPARISON WITH OTHER METHODS

Elaboration of recombination methods started in 1962[24,10]. Since that time the methods were successfully used in many nuclear centres. Practical evaluation of the methods can be derived from intercomparison experiments, performed in mixed radiation fields with complex composition and broad energy spectrum[25, 26].

The recombination chamber shows somewhat lower value of the ambient dose equivalent in comparison with many-detectors systems. It is easy to explain, taking into account that detectors considered as sensitive to one kind of radiation only, usually are partly sensitive also to other kinds of radiation, so the sum of ambient dose equivalent derived from readings of many-detectors system usually overestimates the true value of $H^*(10)$.

The $H^*(10)$ values, derived from measurements using recombination chambers are generally in accordance with measurements performed using tissue-equivalent proportional counters. However, some discrepancies have been noted, which can be explained taking into account differences in geometry of measurements.

Further investigations of recombination methods and intercomparison with other mixed radiation dosimetry methods are foreseen in near future.

ACKNOWLEDGEMENT

This work was supported in part by Polish State Committee of Scientific Research under the KBN contract No 2 0930 91 01.

REFERENCES

1. M. Zielczyński, K. Żarnowiecki: "A differential recombination chamber" In: "Neutron Monitoring", p. 125, IAEA Vienna (1967) (in Russian).
2. N. Golnik, M. Zielczyński: "Response of recombination chamber to ambient dose equivalent of gamma and neutron radiation" Proc. of the 17TH IRPA Regional Congress, Portsmouth 1994, p. 93, Nuclear Technology Publishing, ISBN 1 870965 32 9 (1994).
3. M. Zielczyński, N. Golnik, M. Makarewicz, A. H. Sullivan: "Definition of radiation quality by initial recombination of ions" Proc. Seventh Symposium on Microdosimetry, V. II, p. 853, Harwood Ac. Publ. for CEC, Brussels (1981).
4. M. Zielczyński, N. Golnik: "Recombination index of radiation quality - measuring and applications" Radiat. Prot. Dosim. V. 52, p. 419 (1994).
5. N. Golnik, M. Zielczyński: "Determination of the ICRU-40 quality factors by means of recombination chamber" Kernenergie, V. 34, No 7-8, p. 311 (1991).
6. N. Golnik, M. Zielczyński: "Determination of quality factor in mixed radiation fields using a recombination chamber" Radiat. Prot. Dosim., V. 44, p. 57 (1992).
7. M. Zielczyński: "The mixed radiation dose equivalent measuring methods based on analog detectors" Report of Institute of Nuclear Research, INR 1481, Warsaw (1973) (in Polish).
8. M. Zielczyński: "Determination of radiation quality by use of recombination methods" In: Biophysical Aspects of Radiation Quality, p. 125, IAEA, Vienna (1968) (in Russian).
9. D. Blanc et al.: "Sur la possibilité de mesurer de facteur de qualité des rayonnements nucleaires au moyen de chambres d'ionization remplies d'un liquide dielectrique" Health Physics, V. 11, p. 63 (1965).
10. A. H. Sullivan, J. Baarli: "An ionization chamber for the estimation of the biological effectiveness of radiation" CERN 63-17, Geneva (1963).
11. M. Zielczyński, N. Golnik: "Energy expended to create an ion pair as a factor dependent on radiation quality" In: Measurement Assurance in Dosimetry, p. 383, IAEA, Vienna (1994).
12. S. Pszona, M. Zielczyński, K. Żarnowiecki: "Methodes de mesure simultanée d'équivalent de dose et de coefficient de qualité de rayonnements mixtes" Proc. of the 1-st IRPA Congress, Perg. Press, Oxford (1968).
13. M. Zielczyński, V. N. Lebedev, M. I. Salatskaya: "Device for determination of the recommended RBE of radiation" Devices and Experimental Techniques, No. 6, p. 73 (1964) (in Russian).

14. A. H. Sullivan: "An ionisation chamber for direct measurement of dose equivalent" CERN 71-16, p. 415 (1971).
15. N. Golnik, A. Wysocka, M. Zielczyński: "Ion collection efficiency in an ionisation chamber filled with carbon dioxide up to million pascals of pressure" INR 1925, Warsaw (1982) (in Polish).
16. M. Zielczyński, N. Golnik, S. V. Shvidkij: "Possibility of space radiation dosimetry using r nbination chamber" Proc. Heavy Ions Research: Space, Radiation Protection and Therapy, Sophia - Antip 1994 (to be published in Radioprotectione).
17. M. Zielczyński et al. "Dose characteristics of 200 MeV protons" At. Energy, V. 31, No 11, p. 1971) (in Russian).
18. M. Zielczyński et al. "Investigation of detectors for determination of dosimetric parameters of edical pion and neutron high energy beams" JINR 16-80-563 (1980) (in Russian).
19. M. Zielczyński, S. Mariańska: "Device for measurement of dose equivalent index of mixed radiation" In: Advances in Radiation Protection Monitoring, p. 117, IAEA, Vienna (1979) (in Russian).
20. M. Zielczyński, S. Pszona: "Personnel dose equivalent meter for mixed radiation" CERN 71-16, p. 403 (1971).
21. M. Zielczyński, N. Golnik: "Device for direct determination of quality factor" Nukleonika, V. 38, p. 23 (1993).
22. N. Golnik: "Determination of gamma component in mixed radiation fields from saturation curve of recombination chamber" Proc. 24th Symp. Radiat. Prot. Phys., Gaussig, p. 253, TU Dresden (1992).
23. N. Golnik, M. Zielczyński: "Determination of restricted LET distribution for mixed (n,γ) radiation fields by high pressure ionisation chamber" Radiat. Prot. Dosim. V. 52, No. 1-4, p. 35 (1994).
24. M. Zielczyński: "Use of columnar recombination for determination of relative biological efficiency of radiation" Nukleonika, V. 7, No. 3, p. 175 (1962) (in Russian).
25. V. E. Aleinikov et al.: "Measurement of characteristics of JINR neutron reference fields" JINR P16-93-37, Dubna (1993) (in Russian).
26. N. Golnik: "Application of recombination chamber during the September 1993 CERN-CEC experiment" CERN/TIS-RP/TM/93-50, (1993).

EVALUATION OF THE LONG TERM PERFORMANCE OF ELECTRONIC DOSIMETERS IN THE USA

Joseph Leon (MGP Instruments, 5000 Highlands Parkway, Suite 150, Smyrna, Georgia 30082)

From 1988 to 1994, many utilities in the USA have incorporated the DMC 90/DMC 100 Electronic Dosimeters into their health physics programs. The system includes an automatic calibrator that tests the dosimeter for dose and dose rates (as a minimum). The CDM computer program keeps a full statistical database on the individual and overall performance evaluation of each unit.

Data was gathered from large-scale installations of DMC's which were used in both outage and non-outage applications. Selected graphs and data will be available. The data shows that the dosimeter population dose measurement accuracy after calibration has a standard deviation of about 1.5%.

Dose rate measurement accuracy, including the inherent statistical variations is $\pm 5\%$ at the 5000 R/hr level and $\pm 30\%$ at the 50 mR/hr level. (The inherent statistical accuracy at 5 R/hr is $\Gamma = \pm 2.8\%$ and $\Gamma = \pm 12.5\%$ for 50 mR/hr). The percentage of dosimeters requiring greater than a 5% adjustment between calibration periods is less than 20%.

After five years of operation, the overall calibration factor range (between 200 - 300 cps per Rad/hr) has not changed significantly, attesting to the stability and long range reliability of the Silicon Detector System in the DMC units. The comparison data from DMC's and the currently used primary dosimetry (TLD's) is also presented in tables.

When overall TLD vs DMC doses are compared, the correlation is within 10%; agreeing with the $\pm 5\%$ TLD and DMC cumulative statistical variance.

The accumulated data presented here can support the desire of many utilities currently utilizing sophisticated access control software and computerized databases to use electronic dosimeters as dosimetry. of record. Implementation of such a program will result in the elimination of the high expenses of maintaining NVLAP certification as well as biweekly/monthly TLD processing costs.

The data presented here also supports the idea of using the DMC series of dosimeters as dose rate instruments. Based on the stability of the DMC detector and the accuracy of the calibration procedure, the DMC can be used as a reliable and convenient dose rate detector/instrument. The configuration of the DMC dosimetry system provides exporting of dose rate data from the dosimeter to a remote display (meter). This concept enables the user to exchange/replace dosimeters (detectors) without a complete recalibration of the system.

MICRODOSIMETRY MEASUREMENTS WITH THE RME-III ON THE SPACE SHUTTLE

Kenneth A. Hardy (USAF Armstrong Laboratory/OEBD, Brooks AFB, TX), M. J. Golightly (Space Radiation Analysis Group, NASA Johnson Space Center, Houston, TX), W. Atwell (Space Transportation Systems Division, Rockwell International Corps., Houston, TX), W. Quam (E.G.&G. Energy Measurements, Inc., Goleta, CA)

Since December 1988 (STS-27) the USAF Armstrong Laboratory, in conjunction with the NASA Space Radiation Analysis Group, has been conducting microdosimetry measurements on selected high-altitude, high-inclination Space Shuttle missions with the RME-III. The RME-III is a portable, self-contained, active dosimeter system featuring a three channel tissue equivalent proportional counter (TEPC) which measures particle fluence and computes dose and dose equivalent at operator selected time intervals. The total accumulated absorbed dose and dose equivalent are displayed real time, while the data and the time of the interval dose readings are stored in memory modules for later analysis. Analysis of the time-resolved data permits correlation of the radiation exposure with geographic position, altitude, and spacecraft shielding and orientation. The RME-III has flown on 15 Shuttle missions to date. Inclinations ranged from 28.5 to 62 degrees; altitudes ranged from 250-615 km. The measured dose equivalents rates ranged from 70-5300 μSv/d. The RME-III measurements are in good agreement with other dosimetry measurements made on the Shuttle. Measurements indicate that medium- and high-LET particles contribute less than 2% of the particle fluence for all missions, but up to 50% of the dose equivalent, depending on altitude and inclination. A summary of the RME-III measurements for the missions is presented. Examples of the time resolved data analysis for different missions are also presented.

SESSION V.
Internal Dosimetry

Richard Vetter,
Chairman

DIFFERING INTERNAL DOSE CALCULATIONS FOR THE REVISED 10 CFR 20

Tony A. Rhea, CHP (Science Applications International Corporation—SAIC, 301 Laboratory Road, P.O. Box 2501, Oak Ridge, TN 37830. Phone 615/482-9031)

ABSTRACT

The revised 10 CFR 20 allows licensees several ways to calculate internal dose equivalent-related quantities. These include using the Federal Guidance Report No. 11, using the annual limit on intake (ALI), using the derived air concentration (DAC), and using the International Commission on Radiological Protection (ICRP) 26/30 methodology and metabolic models (or a commercially available software package which implements this methodology).

The difference in calculated dosimetry results can be important for demonstrating regulatory compliance, especially for significant intakes. A scenario can occur that would cause a licensees to report a significant intake as an overexposure of the applicable limit if only a rudimentary internal dose calculation is performed. An example demonstrating this problem is presented.

The simplified dose calculation methods allowed by §20.1003, §20.1202(b)(2), §20.1204(c), and §20.1204(h) are also summarized. The internal dose calculation methodology used by the NRC's Radiation Exposure Monitoring and Information Transmittal (REMIT) computer program, which many small- to mid-size licensees use for manipulating and reporting occupational radiation exposure data, is also discussed. Additionally, this paper introduces the principal references used in internal dose assessments and briefly summarizes the major changes resulting from the new Part 20.

INTRODUCTION

Regulatory Background

In 1991, the Nuclear Regulatory Commission (NRC) published a major revision to 10 CFR Part 20, *Standards for Protection Against Radiation* (10 CFR 20). This revision (often referred to as simply "the new Part 20" or "the revised 10 CFR 20") resulted in significant changes in the methods used by licensees to calculate occupational and public doses. The NRC has also issued a number of Regulatory Guides (commonly referred to as "Reg. Guides") to assist the licensee in complying with the new Part 20. The major changes introduced in the new Part 20 are:

- updated scientific methods and approaches;
- adopting the effective dose equivalent concept;
- controlling exposures based on the sum of internal and external doses;
- more consistency in the treatment of internal and external doses; and
- explicit limits on the exposure of members of the public and the embryo/fetus.

These new regulations became effective January 1, 1994 for all U. S. Nuclear Regulatory Commission (NRC) and agreement state licensees. For a section-by-section comparison of the old Part 20 to the new Part 20, see NUREG-1446, *Standards for Protection Against Radiation — 10 CFR Part 20: A Comparison of the Existing and Revised Rule* (Cool, 1991).

Internal Dose calculation changes

The determination of internal doses is the one area of radiation protection that is probably the most affected by the new Part 20. The "effective dose equivalent" concept has been adopted, which weights (or "averages") the doses to individual organs/tissues based on their relative risk of developing a specific stochastic effect (e.g., lethal cancer). The basic differences between ICRP Publication 2 (ICRP 2), which was used by the old Part 20, and ICRP Publication 30 (ICRP 30), which is used by the new Part 20, are:

- different quality factors are used;
- ICRP Publication 30 (ICRP 30) uses more detailed, multi-compartment computational models;
- the single-compartment lung model used in ICRP Publication 2 (ICRP 2) has been replaced by a multi-compartment model;
- the dose from one organ irradiating another organ is included in ICRP Publication 30 (ICRP 30); and
- ICRP Publication 30 (ICRP 30) uses new models for bone dosimetry and submersion in a radioactive cloud.

Appendix B of the new Part 20 incorporates the derived guides from ICRP Publication 26 (ICRP 26), including the ALI and DAC. Therefore, many formerly used methods for computing internal doses under the "old" Part 20 are no longer appropriate for use in demonstrating compliance with the new Part 20.

Useful references

The metabolic model for the new Part 20 is taken from ICRP Publication 30 (ICRP 30). The use of this information to calculate the committed effective dose equivalent (CEDE) is discussed in detail in Reg. Guide 8.9, *Acceptable Concepts, Models, Equations, and Assumptions for a Bioassay Program* (USNRC 8.9). The metabolic data

used in deriving the new internal exposure limits are now based on a standard or reference individual, as defined in ICRP Publication No. 23 (ICRP 23). The data in Federal Guidance Report No. 11, *Limiting Values of Radionuclide Intake and Air Concentration and Dose Conversion Factors for Inhalation, Submersion, and Ingestion* (EPA 11), are useful in determining the committed dose equivalent (CDE) for organs/tissues. Alternately, one of several available internal dose analysis computer program could be used.

A key step in calculating internal doses is to calculate (or measure) the intake of radioactive material. NUREG/CR-4884 (Lessard, 1987) contains detailed information on computing intakes from both *in vitro* and *in vivo* bioassay measurements (e.g., urinalysis and whole-body counting results, respectively). Tables useful in converting bioassay results into intake estimates are provided for several hundred radionuclides.

Once the intake is determined, internal dose may be approximated by assuming that one ALI is equivalent to 5 rem CEDE (for stochastically limited nuclides) or 50 rem CDE (for nonstochastically limited nuclides). More sophisticated internal dose assessments are possible, but this method is adequate to demonstrate compliance with the new Part 20 [see the definitions for ALI and DAC-hour (DAC-h) in §20.1003 of the new Part 20].

Reg. Guide 8.34, *Monitoring Criteria and Methods To Calculate Occupational Radiation Doses* (USNRC 8.34), ICRP Report 54, *Individual Monitoring for Intake of Radionuclides by Workers: Design and Interpretation* (ICRP 54), and NCRP Report No. 87, *Use of Bioassay Procedures for Assessment of Internal Radionuclide Deposition*, (NCRP 87) contain additional information on determination of internal doses. The proceedings of a recent Health Physics Society summer school on internal dosimetry (Raabe, 1994) are also an excellent reference and contain one of the best collections of information available on the subject.

Internal Dose Analysis Methods and Programs

Many internal dosimetry calculational models and methods are relatively straightforward, and, in many cases, hand calculations will suffice. Intake retention fractions (IRFs) from NUREG/CR-4884 (Lessard, 1987) may be applied to *in-vivo* or *in-vitro* bioassay results to estimate the intake. Once the intake is determined, dose equivalent-related quantities can be calculated by a relatively simply application of the dose conversion factors (DCFs) in Federal Guidance Report 11 (EPA 11).

Various computer codes are available to automate and refine these calculations and to aid in evaluating more complex internal exposure cases. The Radiation Exposure Monitoring and Information Transmittal (REMIT) computer program (Cale, 1993) will compute internal doses in accordance with the new Part 20, as long as the intake is known. It uses the EPA 11-based DCFs, sums internal and external doses, and NRC

Forms 4 and 5 (see USNRC 8.7). Other dosimetry codes implement numeric or analytic solutions to the ICRP metabolic models to allow interpretation of bioassay results and perform more complex assessments.

Many internal dose analysis computer programs also provide the ability to use both standard and user-defined biokinetic models based on observed retention patterns. For the initial dose calculations, the "standard man" model (ICRP 23) may be used. If follow-up sampling is performed, the biokinetic model may be adjusted by the actual data obtained for each individual to reflect the actual metabolism for a more accurate dose assessment.

No specific computer codes are endorsed by the NRC; licensees are responsible for ensuring that computer codes used are appropriate for their particular circumstances [see §C.4.2 of Reg. Guide 8.9 (USNRC 8.9)]. The cover letter published with the NUREG report (Cale, 1993) accompanying the REMIT computer program contains the following statement:

> Publication of this report does not necessarily constitute NRC approval or agreement with the information contained herein. Calculations performed by this software should be verified to the satisfaction of the licensee. Use of the REMIT software alone does not constitute a demonstration of compliance with the requirements of 10 CFR Part 20 for recording and reporting occupational radiation exposure data.

Internal Dosimetry Intercomparisons

In addition to different calculational methods allowed by the regulations, the internal dosimetrist's assumptions and methods can markedly affect internal dosimetry results. Two recent studies — one from Europe (Gibson, 1992) and one from the United States (Hui, 1994) — discuss the wide variety of results on "standard" intake scenarios. The differences arise from a variety of sources, including variations on the biokinetic models used, the different computational tools used, and the varying interpretation and statistical treatment of the data. Reg. Guide 8.25, *Air Sampling in the Workplace* (USNRC 8.25) discusses the intercomparison of air sampling and bioassay data in assessing internal doses.

Also, the impacts of the new Part 20 on internal dosimetry programs has been summarized by Poston (Poston, 1992; see also Poston, 1994).

DISCUSSION

Federal Guidance Report 11

It is important to note that the final columns in Federal Guidance Report No. 11 (EPA 11) tables, labeled "Effective", include the effective dose equivalent for every organ on the row. Be aware also that each h value in the "Remainder" column in the table in the EPA 11 report is the average over the other 5 organs (other than the gonads, breast, lung, red marrow, thyroid and bone surface) receiving the highest CDE. When h_{max} is a remainder organ, the organ is named in the column, and the h value for that organ alone is also given.

The internal dosimetry module of the REMIT computer code (Cale, 1993), which is used by many small- to mid-size licensees to assist in recordkeeping and reporting for the new Part 20, is based on the data tables in EPA 11.

Methods Authorized by the New Part 20

The new Part 20 authorizes a number of methods for internal dose calculations that *can* yield different results, as summarized below (the comment in italics is not part of the regulation):

§20.1003	(in definition of *DAC-hour*) A licensee may take 2,000 DAC-hours to represent one ALI, equivalent to a committed effective dose equivalent of 5 rems (0.05 Sv). *So 1 DAC-hour = 0.0025 rem = 2.5 mrem [see also §20.1202(b)(2)].*
§20.1202(b)(2)	(b) Intake by inhalation. If the only intake of radionuclides is by inhalation, the total effective dose equivalent limit is not exceeded if the sum of the deep-dose equivalent divided by the total effective dose equivalent limit, and one of the following, does not exceed unity: (2) The total number of derived air concentration-hours (DAC-hours) for all radionuclides divided by 2,000. *You can add DAC-hours, even though one might be limited by stochastic effects and the other might be limited by nonstochastic effects.*

§20.1204(c) When specific information on the physical and biochemical properties of the radionuclides taken into the body or the behavior or the material in an individual is known, the licensee may

(1) Use that information to calculate the committed effective dose equivalent, and, if used, the licensee shall document that information in the individual's record; and

(2) Upon prior approval of the Commission, adjust the DAC or ALI values to reflect the actual physical and chemical characteristics of airborne radioactive material (e.g., aerosol size distribution or density); and

(3) Separately assess the contribution of fractional intakes of Class D, W, or Y compounds of a given radionuclide (see appendix B to §20.1001-20.2402) to the committed effective dose equivalent.

You may adjust for actual physical and chemical properties and individual metabolic differences, adjust the ALIs and DACs given in Appendix B to the new Part 20 for particle size or density, and take credit for well-known chemical composition distributions.

§20.1204(h)(1) In order to calculate the committed effective dose equivalent, the licensee may assume that the inhalation of one ALI, or an exposure of 2,000 DAC-hours, results in a committed effective dose equivalent of 5 rems (0.05 Sv) for radionuclides that have their ALIs or DACs based on the committed effective dose equivalent. *1 ALI = 2000 DAC-hours = 5 rem for stochastically limited radionuclides.*

§20.1204(h)(2) When the ALI (and the associated DAC) is determined by the non-stochastic organ dose limit of 50 rems (0.5 Sv), the intake of radionuclides that would result in a committed effective dose equivalent of 5 rems (0.05 Sv) (the stochastic ALI) is listed in parentheses in table 1 of appendix B to §20.1001-§20.2402. In this case, the licensee may, as a simplifying assumption, use the stochastic ALIs to determine committed effective dose equivalent. However, if the licensee uses the stochastic ALIs, the licensee must also demonstrate that the limit in §20.1201(a)(1)(ii) is met. *You may use a simplifying assumption, but you must check the validity of that assumption.*

It can be seen that these regulations allow the licensee a variety of ways to calculate internal doses. For most situations, the actual differences between these methods are minor.

Evaluating Significant Intakes

Although the new Part 20 internal dosimetry concepts and models markedly differ from the old Part 20, the calculations are relatively straightforward in most cases. §2.3.1 of Reg. Guide 8.9 (USNRC 8.9) states:

> For intakes that represent a significant contribution to dose, other available data should be evaluated. If initial bioassay measurements indicate that an intake is greater than an evaluation level of 0.02 ALI, additional available data, such as airborne measurements or additional bioassay measurements, should be used to obtain the best estimate of actual intake. For radionuclides that are difficult to detect, such as alpha emitters, a single measurement may not be adequate to determine intakes.

Most NRC licensees have relatively few and relatively small intakes. Those that do have significant intakes usually have health physics staff available that can undertake a more complex analysis. This is especially true of larger nuclear facilities. However, should a significant intake occur, a smaller licensee may inappropriately use a simplified dose calculation method (perhaps out of familiarity) that, while allowed by the regulations, could result in an overexposure report per §§20.2202-20.2203. If a more thorough analysis is performed, as suggested by Reg. Guide 8.9, a better estimate of the individual's actual intake and dose is obtained.

Refinements

Refinements to initial, simplified assumptions should, of course, be made. §4 of Reg. Guide 8.9 (USNRC 8.9) discusses the use of additional or improved data for evaluating intakes. These data include:

- time of exposure
- biokinetic models
- adjustments for multiple and continuous intakes
- particle size distributions
- use of individual-specific models

Often, these can markedly improve the individual's dose estimate. Appendix A to Reg. Guide 8.9 (USNRC 8.9) includes eight example calculations for internal dose assessment, including several which demonstrate refinement of initial intake estimates. These examples fall into several broad categories:

- using standard man metabolic models for evaluating bioassay measurements;
- estimating intake from one or several bioassay measurements;
- adjusting intake estimates for multiple or continuous intakes; and
- correcting intake estimates for particle size differences.

Example

(Not available at the time this paper was going to press; please contact the author for up-to-date information.)

SUMMARY

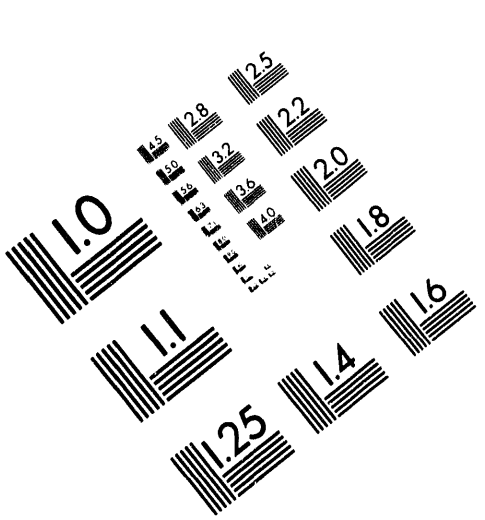
A variety of internal dose calculation methods are allowed by the new Part 20, and the difference in dosimetry results obtained by these methods can be important for demonstrating regulatory compliance. This could potentially cause some licensees to incorrectly report a significant intake as an overexposure if only a rudimentary internal dose calculation is performed. Therefore, licensees should, as recommended by Reg. Guide 8.9, evaluate significant intakes using more advanced calculational methods to ensure accurate reporting.

Some smaller licensees may not have the expertise available on their own staff for these more in-depth analyses and therefore may need to seek additional assistance in evaluating significant intakes.

REFERENCES

10 CFR 20 — United States, Code of Federal Regulations, Title 10, Part 20, *Standards for Protection Against Radiation*, Washington, DC (January 1994).

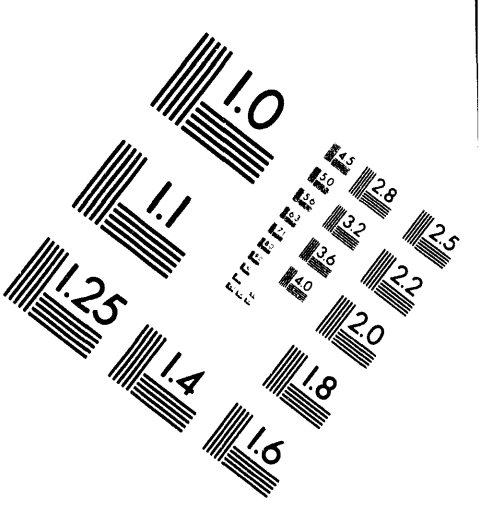
Borges, 1994 — T. Borges, R. S. Stafford, P. Y. Lu, and D. Carter, *Questions and Answers Based on the Revised 10 CFR Part 20*, United States Nuclear Regulatory Commission Publication NUREG/CR-6204, Washington, DC (1994).

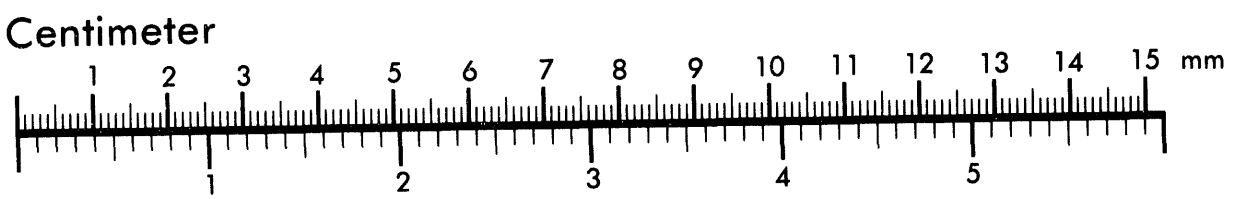


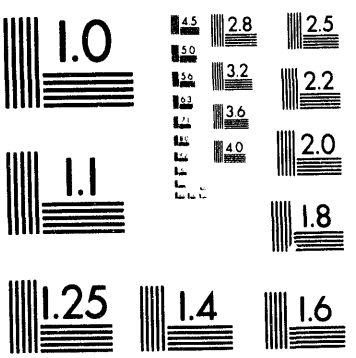
Association for Information and Image Management

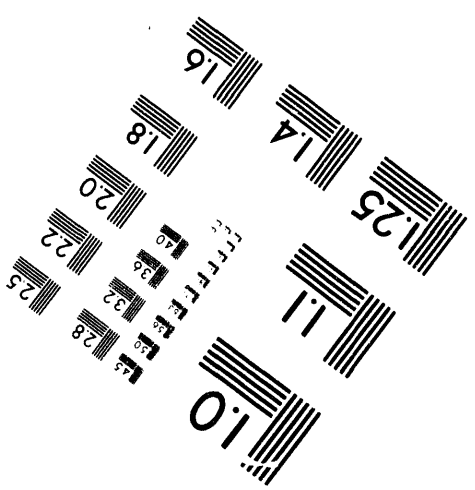
1100 Wayne Avenue, Suite 1100
Silver Spring, Maryland 20910

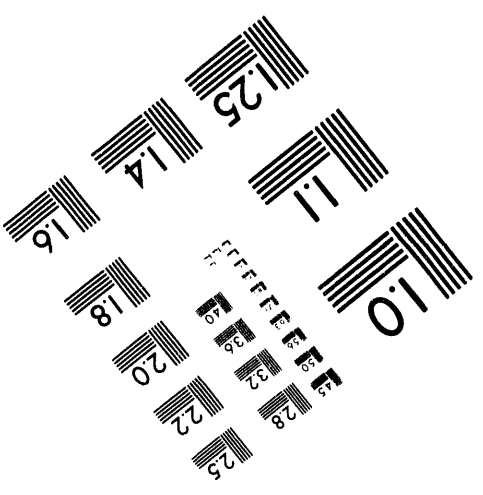
301/587-8202











MANUFACTURED TO AIIM STANDARDS
BY APPLIED IMAGE, INC.

4 of 6

Cale, 1993 — R. Cale, T. Clark, P. L[illegible]son, and D. Hagameyer, *Radiation Exposure Monitoring and Information Transmittal (REMIT) System—User's Manual*, United States Nuclear Regulatory Commission Publication NUREG/CR-6050, Washington, DC (June 1993). REMIT is available for a nominal fee from the Energy Science and Technology Software Center, P.O. Box 1020, Oak Ridge, TN 37831; phone (615) 576-2606.

Collins, 1994 — M. Collins, B. Shelton, *Guide to NRC Reporting and Recordkeeping Requirements*, United States Nuclear Regulatory Commission Publication NUREG-1460, Washington, DC (1994).

Cool, 1991 — D. A. Cool and H. T. Peterson, Jr., *Standards for Protection Against Radiation — 10 CFR Part 20: A Comparison of the Existing and Revised Rule*, United States Nuclear Regulatory Commission Publication NUREG-1446, Washington, DC (October 1991).

EPA 11 — Environmental Protection Agency (K. F. Eckerman, A. B. Wolbarst, and A. C. Richardson), *Limiting Values of Radionuclide Intake and Air Concentration and Dose Conversion Factors for Inhalation, Submersion, and Ingestion*, Federal Guidance Report No. 11, 520/1-88-020, Washington, DC (1988).

Gibson 1992 — J. A. B. Gibson, A. Birchali, R. K. Bull, K. Henricha, E. Iranzo, D. J. Lord, J. Piechowski, E. Sollett, N. P. Tancock, and C. Wernli, *A European Intercomparison of Methods Used for the Assessment of Intakes of Internally Deposited Radionuclides*, Radiation Protection Dosimetry Vol. 40, No. 4, pp. 245-257 (1992).

Hui 1994 — T. E. Hui, R. M. Loesch, C. Raddatz, D. R. Fisher, and J. C. McDonald, *An Internal Dosimetry Intercomparison Study*, Health Physics Vol. 67, No. 3, pp. 217-225 (September 1994).

ICRP 2 — International Commission on Radiation Protection Publication No. 2, *Report of Committee II on Permissible Dose for Internal Radiation*, Pergamon Press, Elmsford, NY (1959).

ICRP 23 — International Commission on Radiation Protection Publication No. 23, *Report of the Task Group on Reference Man*, Pergamon Press, Elmsford, NY (1977).

ICRP 26 — International Commission on Radiation Protection Publication No. 26, *Recommendations of the International Commission on Radiological Protection*, Pergamon Press, Elmsford, NY (1977).

ICRP 30 — International Commission on Radiation Protection Publication No. 30, *Limits for Intakes of Radionuclides by Workers*, Volumes 1-7 and Supplements, Pergamon Press, Elmsford, NY (1977).

ICRP 54 — International Commission on Radiation Protection Publication No. 54, *Individual Monitoring for Intake of Radionuclides by Workers: Design and Interpretation*, Pergamon Press, Elmsford, NY (1988).

Lessard, 1987 — E. T. Lessard, X. Yihua, K. W. Skrable, G. E. Chabot, C. S. French, T. R. Labone, J. R. Johnson, D. R. Fisher, R. Belanger, J. L. Lipsztein, *Interpretation of Bioassay Measurements*, United States Nuclear Regulatory Commission Publication NUREG/CR-4884, Washington, DC (July 1987).

NCRP 87 — National Council on Radiation Protection and Measurements, *Use of Bioassay Procedures for Assessment of Internal Radionuclide Deposition*, NCRP Report No. 87, Bethesda, MD (1987).

Poston 1992 — J. W. Poston, Jr. and J. W. Poston, Sr., *Implementation of 10 CFR 20: Potential Impacts on Internal Dose Assessment Programs*, Radiation Protection Management 9:5 (September/-October 1992).

Poston 1994 — Poston, J. W., Jr. and Poston, J. W. Sr., *Implementation of ANSI Standard N343: Potential Impacts on Commercial Nuclear Power Bioassay Programs*, Radiation Protection Management (in press, 1994).

Raabe 1994 — Otto G. Raabe, Ed., *Internal Radiation Dosimetry*, Proceedings of the Health Physics Society 1994 Summer School, Medical Physics Publishing, Madison, Wisconsin (1994).

USNRC 8.7 — United States Nuclear Regulatory Commission, *Instructions for Recording and Reporting Occupational Radiation Exposure Data*, Regulatory Guide 8.7, Washington, DC.

USNRC 8.9 — United States Nuclear Regulatory Commission, *Acceptable Concepts, Models, Equations, and Assumptions for a Bioassay Program*, Regulatory Guide 8.9, Washington, DC.

USNRC 8.25 United States Nuclear Regulatory Commission, *Air Sampling in the Workplace*, Regulatory Guide 8.25, Washington, DC.

USNRC 8.34 United States Nuclear Regulatory Commission, *Monitoring Criteria and Methods to Calculate Occupational Radiation Doses*, Regulatory Guide 8.34, Washington, DC.

Disclaimer: Material in this paper is for informational purposes only. The author assumes no responsibility for any damage or harm incurred as a result of use of this information.

THE DEPARTMENT OF ENERGY'S LABORATORY ACCREDITATION PROGRAM FOR INTERNAL DOSIMETRY

T. L. Taylor and G. E. Grothaus (Radiological and Environmental Sciences Laboratory, Dept. of Energy, Idaho Operations Office)

The U.S. Department of Energy Laboratory Accreditation Program(DOELAP) is administered by DOE's Radiological and Environmental Sciences Laboratory (RESL) at the Idaho Operations Office. DOELAP's function is to assure and improve the quality of data from DOE contractor facilities for personnel dosimetry. While the external dosimetry DOELAP has been operating for several years, the internal dosimetry DOELAP is in a pilot testing stage. Pilot tests for both indirect and direct radiobioassay programs are in different stages of completeness. Both programs have between 15 and 20 participating laboratories. The indirect radiobioassay (in-vitro) program have two testing matrices, urine and fecal. Two sets of the fecal matrix and one set of the urine matrix pilot studies have been completed.

Laboratory response (reporting results) and interest in participating has been very good. Direct radiobioassay (in-vivo) has completed the first pilot study of the bottle mannequin absorber (BOMAB) phantom. The second testing phantom is the lung phantom. This involves the participating laboratories counting the spiked lungs in their lung phantom. The pilot test is a critical link for dose assessment, a long with assuring the participating laboratory's accurate analysis.

"IN VIVO" MEASUREMENTS PERFORMED WITHIN AN INTERNATIONAL INTERCOMPARISON PROGRAM FOR WHOLE BODY COUNTERS USING A "FOUR YEARS OLD" PHANTOM

T. NAVARRO BRAVO; M.A. LOPEZ PONTE
(Whole Body Counter - Radiological Protection Division; CIEMAT - IMA, Avda. Complutense 22, 28040 Madrid, Spain)

I.- INTRODUCTION

The HML (Human Monitoring Laboratory, Ottawa-Ontario), wich is Canada's National Calibration Reference Centre for In-Vivo Monitoring, has organizated an International Intercomparison program for Whole Body Counting facilities to perform measurements with a small BOMAB phantom equivalent to a 4-year old child, constructed following the reference values of ICRP-23. The HML does not have the equipment to accurately fill a BOMAB phantom with human tissue substitute resin. The United States Department of Energy (DOE) has assisted to solve this problem performing this operation at the Battelle Pacific Northwest Laboratory. As a result of this cooperation the scope of the program was increased to cover both Intercomparison, which fulfils the HML's needs, and Intercalibration, which fulfils the DOE's needs.

There are 18 facilities enrolled in the Intercomparison program and 9 in the Intercalibration program. This is a total of 27 facilities involved (APPENDIX A). Allowing one week to perform measurements and two weeks for shipping and handling the phantom to the next facility, the program will take a minimum of 81 weeks to be completed. The program started after the Battelle Pacific Northwest Laboratory and the HML had finished the final measurements on the phantom. The target date for shipping the phantom to the first participant was the 30 April 1993.

The principal advantage of a Whole-Body Counting and the reason it is used as a control method in Radiological Protection, is that it provides a direct measurement of X and gamma radiations emitted from radionuclides internally deposited in the body by inhalation or ingestion, through a wound, or through skin absorption.

Following the Chernobyl reactor accident (April 1986) it was necesssary to monitor many children, and any Whole Body Counter that has to be used in emergency situations must have a good range of calibrations for it to be effective. The use of the 4-year old provides a lower end for the calibration set and gives the facility a chance to evaluate its own size dependency geometry factor.

II.- THE 4-YEAR BOMAB PHANTOM

A phantom can be used either to measure the background or calibrate and test a Whole Body Counter. To measure the background the phantom has to be filled with water or other tissue-substitute material (blank phantom). Phantom filled with different materials that emit photons of energies in the approximate range 200-2500 KeV (active phantom) can be used to establish the counting efficiency of the system in the desired counting geometry. This should be repeated different sized phantoms to obtain a range of counting efficiencies for a variety of different physical types.

The International Commission on Radiological Protection (ICRP) published (1975) the assigned values for most anatomical and physiological values to Reference Man, Reference Woman, Reference Child (10 years old), and Reference Infant (1 year old). The last one was too small for a BOMAB (**BO**ttle **M**annequin **AB**sorption) phantom, but it was necessary to investigate the performance of a Whole Body Counter at an extreme of the calibrations set for high-energy (>200 KeV) photon emitters. The HML chose the age of 4-year old for this purpose, obtaining an extended range of available phantom sizes to form the BOMAB phantom family. The ICRP Reference values for these groups are shown in Table I and were used to formulate the dimensions of the ellipsoidal cylinders that comprise the phantom.

Table I. REFERENCE VALUES OBTAINED FROM ICRP-23 (1975)

	MALE	FEMALE	10 years	4 years
WEIGHT (Kg)	70	58	34	18
HEIGHT (cm)	170	160	140	105
SURFACE AREA (cm^2)	18000	16000	9610	6950

The purpose of the phantoms is to calibrate and intercompare "In-Vivo" facilities and the necessary requirement is to create a series of well-defined phantoms of differing sizes that closely approximate the ICRP reference values. Values for weight, height and surface area from ICRP 23 were used to formulate the dimensions of the ellipsoidal cylinders wich compose each phantom.

The material of choice for the construction of the phantoms was hight-density polyethylene, resistant to acids and reasonable tissue-substitute material for energies in excess of 200 KeV, but is cleary not a good tissue substitute at lower energies.

The phantom of the Intercomparation Program, designated as P4C (APPENDIX B), is composed of 10 cylindrical, polyethylene pieces which simulate the physical shape of a 4-year old child, having been filled with tissue (muscle) substitute material and an unknown quantity of radioactivity. The activity in the phantom has been homogeneously distributed throughout all sections. The Activity in each section of the phantom is proportional to the volume of that section.

Table II. Dimensions and volume of the 4-year P4C phantom sections
(2a is the semimajor ellipse axis
2b is the semiminor ellipse axis
h is the cylinder heigh)

SECTION	2a (cm)	2b (cm)	h (cm)	PESO (Kg)
HEAD	21,0	15,0	12,5	3,0
NECK	9,5	8,5	5,5	0,4
CHEST	19,5	15,5	25,5	5,8
GUT	23,5	14,0	12,5	3,4
ARM	6,0	5,5	36,0	1,0
THIGH	7,0	6,5	24,5	0,8
CALF	7,0	6,5	24,5	0,8

For the performance of the calibrations of the Whole Body Counter of CIEMAT (Madrid, Spain) there is BOMAB phantom simulating the Standard Man defined by the ICRP-23. Modifications in this mannequin result in a 4-year old phantom, being the size and weight similar as the Reference values established by the ICRP-23, as follows:

SECTION	2a(cm)	2b(cm)	h(cm)	WEIGHT (Kg)
HEAD + NECK	20	15	21	3,5
TRUNCK	21	20	36	10,5
LOWER EXTREMITIES	12	15	41	4,5

III.- INTERCOMPARISON PROTOCOL

The task was to determine the identity and amount of the radionuclides. The activity in the phantom was obtained by two methods: using "normal-sized" calibration factor (this gives the size dependency for facility) and using an efficiency corrected for size. It was also requested to make an estimate of the "worst case" precision (placing the phantom in extreme positions) and to calculate a Minimum Detectable Activity for all the radionuclides detected.

Each laboratory has to perform all of the tests and any additional measurements required for the facility's needs within a one week period. The phantom should then be sent to the next facility on the List of participants. The data sheet must be completed with the values calculated after the measurements and be returned to the HML; then the laboratory will receive a preliminary report with the results. The full report will have to wait until the Intercomparison has been completed by all participants. The final report will identify facilities by a two letters code randomly assigned.

The Whole Body Counter of CIEMAT (Madrid, Spain) has already completed the measurements and has sent the results to the HML, having received a preliminary report in response. This partial report, which shows a close agreement between the estimates and the real values, was sent after the European part of the Intercomparison program had been completed.

The Whole Body Counting facility of CIEMAT consists of a shielded room whose walls, constructed with Pre-World War II steel, are thick enough to reduce backgroung radiation. The subject enters inside this room and reclines in a tilting chair. The radiation detector is a large thallium-activated sodium iodide [NaI(Tl)] crystal detector (20,3 cm diameter and 10,2 cm thick) which is correctly positioned over the subject's body. The electrical signals are transmitted from the detector to the multichannel analyzer (MCA), outside the room, that sorts the electrical pulses by voltage, which is proportional to the detected photon. When the sorted pulses are displayed they form a gamma-ray spectrum. Analysis of the energies in this espectrum identifies the radionuclides present in the body. The spectra are transfered from the MCA to a PC computer where the ABACOS-PC (CANBERRA) is the software that has been installed there. The ABACOS-PC software package consists of a set of programs written for use in the analysis of the gamma-ray spectrum to determine the identity and amount of each radionuclide present. Additionally, ABACOS-PC provides a storage facility for the result and data enabling the access of the information in the future.

1.- Identification of unknown internal contaminants

The phantom, P4C, contained an unknown number of radionuclides in the energy range 200-2000 KeV that were identified. The analysis of the measurements carried out showed that Cs-137 and Y-88 were the radionuclides present in the P4C. Both of them are gamma emitters: Cs-137 in 665 KeV (85,10%) with half life 30,17 years, and Y-88 in 898 KeV (93,4%) and 1836 KeV (99,3%) with half life 106,6 days.

2.- Determination of Activity

Two sets of 10 measurements each were carried out, the first one with a counting time of 900 s (maximun time for the measurement of a child) and the second set with a counting time of 1800 s (to minimize errors, measurements for calibration).

We were requested to obtain the Activity of the radionuclides present in the phantom by two methods:

* The **First Method** was to use the **normal "man-sized" calibration factor**. This gives the SIZE DEPENDENCY FOR FACILITY. The Activity was calculated using the Counting Efficiency obtained by the WBC of CIEMAT for the Standard-Man referenced by ICRP (APPENDIX C).

* The **Second Method** is to use an **efficiency corrected by size.** In the WBC facility of CIEMAT there were made modifications in the BOMAB phantom for the Standard Man, result in the 4-year old phantom (similar than P4C, described before). The Activity is obtained using the Counting Efficiency for the 4-years old child (APPENDIX C).

RADIO-NUCLIDE	METHOD1 - Man $\bar{A} \pm 2\sigma$	METHOD2 - 4-Year $\bar{A} \pm 2\sigma$	GEOM. (*) FACTOR
Cs-137	5950 ± 4% Bq	4407 ± 4% Bq	35 %
Y-88	6796 ± 3% Bq	5423 ± 2% Bq	25 %

(*) This factor indicates the Size Dependency Geometry Factor between Standard-Man and 4-year old sizes.

where $\bar{A}$ is the mean value of the Activities obtained from the 10 measurements set with counting time of 900 s.
2σ is the Counting Error Sigma, at the 95% confidence level.

3.- Precision of counting

Precision of counting is usually performed by counting a selected phantom repeatedly. This test was to estimate the **"Worst Case" precision** (supposing the child moves during the measurement and the counting geometry is not always the same). The phantom, P4C, is placed in extreme positions: the phantom should be counted in the normal position, in a position to the extreme left of the detector, in a position to the extreme right of the detector, and two intermediary positions between the normal and extremes. The Precision, S, is estimated by the following expression:

$$S(\%) = 100 * \frac{\sqrt{\sum_{i=1}^{n} \frac{(A_i - M)^2}{(N-1)}}}{M}$$

where A_i is the observed value
M is the mean of that data set
N is the number of measurements

The study performed for the Worst Case Precision through the 10 measurements set with counting time of 900 s, for the 4-year old child, is as follows:

	Cs-137	Y-88	Y-88
S(%):	2.5	3.2	1.8

4.- Determination of the Minimum Detectable Activity

We were requested to calculate a Minimum Detectable Activity (MDA) for all the radionuclides detected in the phantom.
A blanck phantom (4-year old size phantom) filled with KCl (36 g of potassium for a 4 years old child)) in a suitable medium (water) should be used for that purpose. The KCl in each section of the phantom is proportional to the volume of that section. Then the MDA is obtained using a background containing ^{40}K and applying the following expression to the results:

$$MDA = \frac{4.65 * \sqrt{BCKGND} + 3}{E * T}$$

BCKGND: Background Counts
E:Counting Efficiency 4-y child
T:Counting Time

RADIONUCLIDE	MDA (Tc= 900 s)	MDA (Tc = 1800 s)
Cs-137	50 Bq	35 Bq
Y-88	50 Bq	35 Bq

IV.- RESULTS FOR THE INTECOMPARISON

The Whole Body Counter of CIEMAT (Madrid, Spain) completed the measurements and sent the results to the HML, having received a preliminary report in response. This partial report shows a close agreement between the estimates and the real values:

Facility Name: **CIEMAT, Spain - PRELIMINARY REPORT (HML)**

BIAS (according to Method 1) %:	**Cs-137** **Y-88**	**34,2 % (**)** **26,1 %**
BIAS (according to Method 2) %:	**Cs-137** **Y-88**	**-0,6 %** **0,6 %**
WORST PRECISION %:	**Cs-137** **Y-88** **Y-88**	**2,5 %** **3,2 %** **1,8 %**

(**) Size Dependency Geometry Factor

$$BIAS\ (\%) = 100 * \frac{(A_i - A)}{A}$$

where A_i is the value given by CIEMAT
A is the true value of P4C

The final report will have to wait until the project has been completed and it will not be available until the end of 1994.

V.- CONCLUSION

The Whole Body Counter of CIEMAT (Madrid, Spain) has completed succesfully the measurements related with the Intercomparison Program and has sent the results to the HML, having received a preliminary report in response. This partial report, which was sent after the European part of the Intercomparison program had been completed, shows a close agreement between the estimates and the real values of the Activities in the P4C Phantom. Then, the facility disposes of a good group of calibration functions depending on the size of the subject, which make really effective the Whole Body Counter of CIEMAT.

VI.-REFERENCES

- Kramer G.H.;Inn K.G.W. A Summary of the Procedings of the Workshop on: Standard Phantoms for In-Vivo Radioactivity Measurements. Health Physics 1991;61(6)

- International Commission on Radiological Protection. Report of the Task Group on Reference Man. Oxford: Pergammon Press; ICRP-23; 1975

- Kramer G.H.;Noel L.;Burns L. The BRMD BOMAB Phantom Family, Health Physics 1991;61(6)

- American National Standards Institute Draft Document ANSI N13.30 Performance Criteria for Radiobioassay Testing, October 1992

APPENDIX A

ROUTINE FOR THE PHANTOM

1.- Battelle Pacific Northwest Laboratories, Richland, WA, USA

2.- Human Monitoring Laboratory, Ottawa, Ontario, CANADA

3.- AEA Environment and Energy, Oxfordshire, UNITED KINGDOM

4.- National Radiological Protection Board, Oxon, UNITED KINGDOM

5.- National Institute of Radiation Hygiene,DK-2700 Bronshoj,DENMARK

6.- National Institute of Radiation Protection, Stockholm, SWEDEN

7.- Finnish Centre for Radiation and Nuclear Safety, Helsinki, FINLAND

8.- GSF-Forschungszentrum fur Umwelt/Gesunheit, Frankfurt.GERMANY

9.- Centre of Radiation Hygiene, Prague, CZECHOSLOVAKIA

10.- KFKI Atomic Energy Research Institute, Budapest, HUNGARY

11.- ENEA-AMB BIO, Bologna, ITALY

12.- Paul Scherrer Institut, Villigen PSI, SWITZERLAND

13.- CEA-Cadarache, Cedex, FRANCE

14.- CIEMAT, Madrid, SPAIN

15.- Forschungszentrum Seibersdorf Ges. m.b.H., Seibersdorf, AUSTRIA

16.- Karlsruhe, GERMANY

17.- SCK.CEN, Studiecentrum voor Kernegie, BELGIUM

18.- LANL, Los Alamos, NM, USA

19.- Sandia National Laboratory, Alburquerque, NM, USA

20.- EPA, Dose Assessment, Las Vegas, NV, USA

21.- Lawrence Livermore National Laboratory, Livermo, CA, USA

22.- INEL, IdahoFalls, ID, USA

23.- Oak Ridge National Laboratory, Oak Ridge, TN, USA

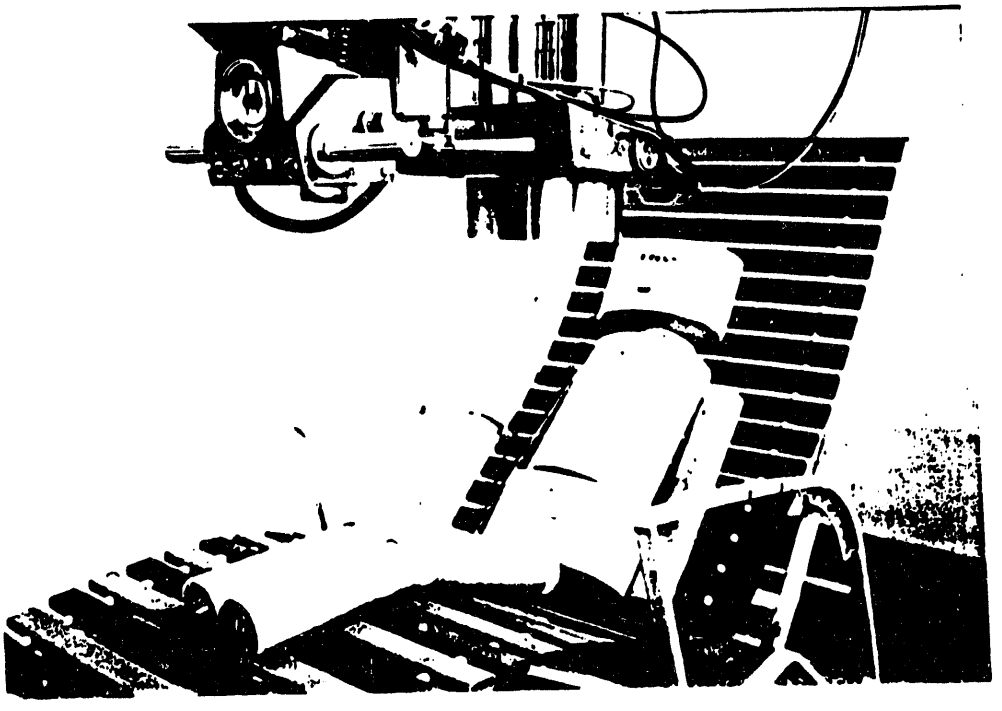
24.- Brookhaven National Laboratory, Upton, NY, USA

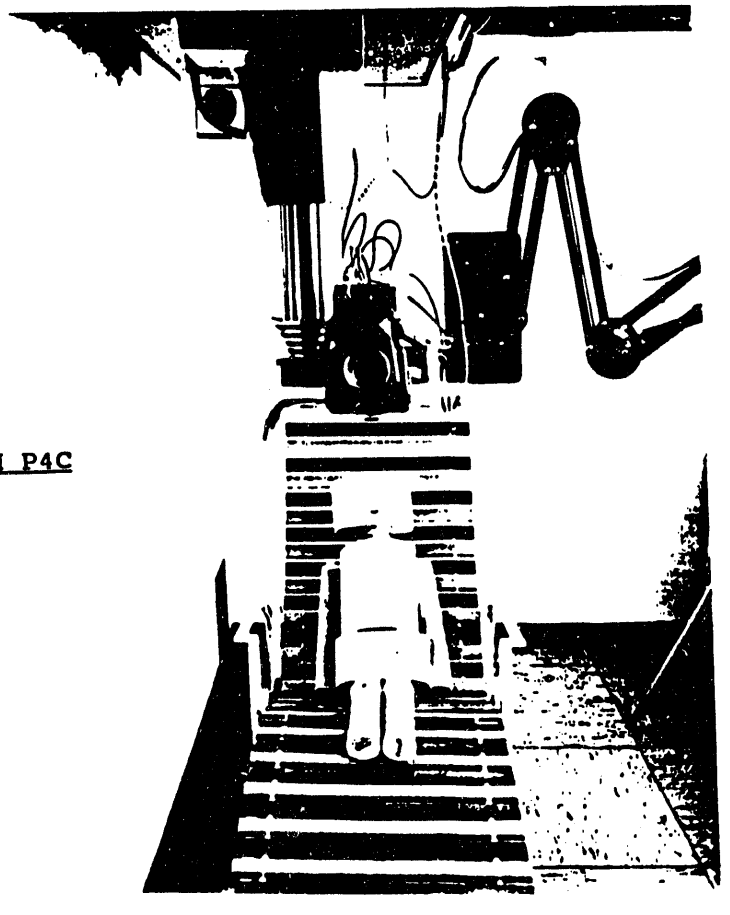
25.- CNEN, Rio de Janeiro, BRAZIL

26.- National Atomic Energy Commission, Buenos Aires, ARGENTINA

27.- NIST, Gaithersburg, MD, USA

APPENDIX B

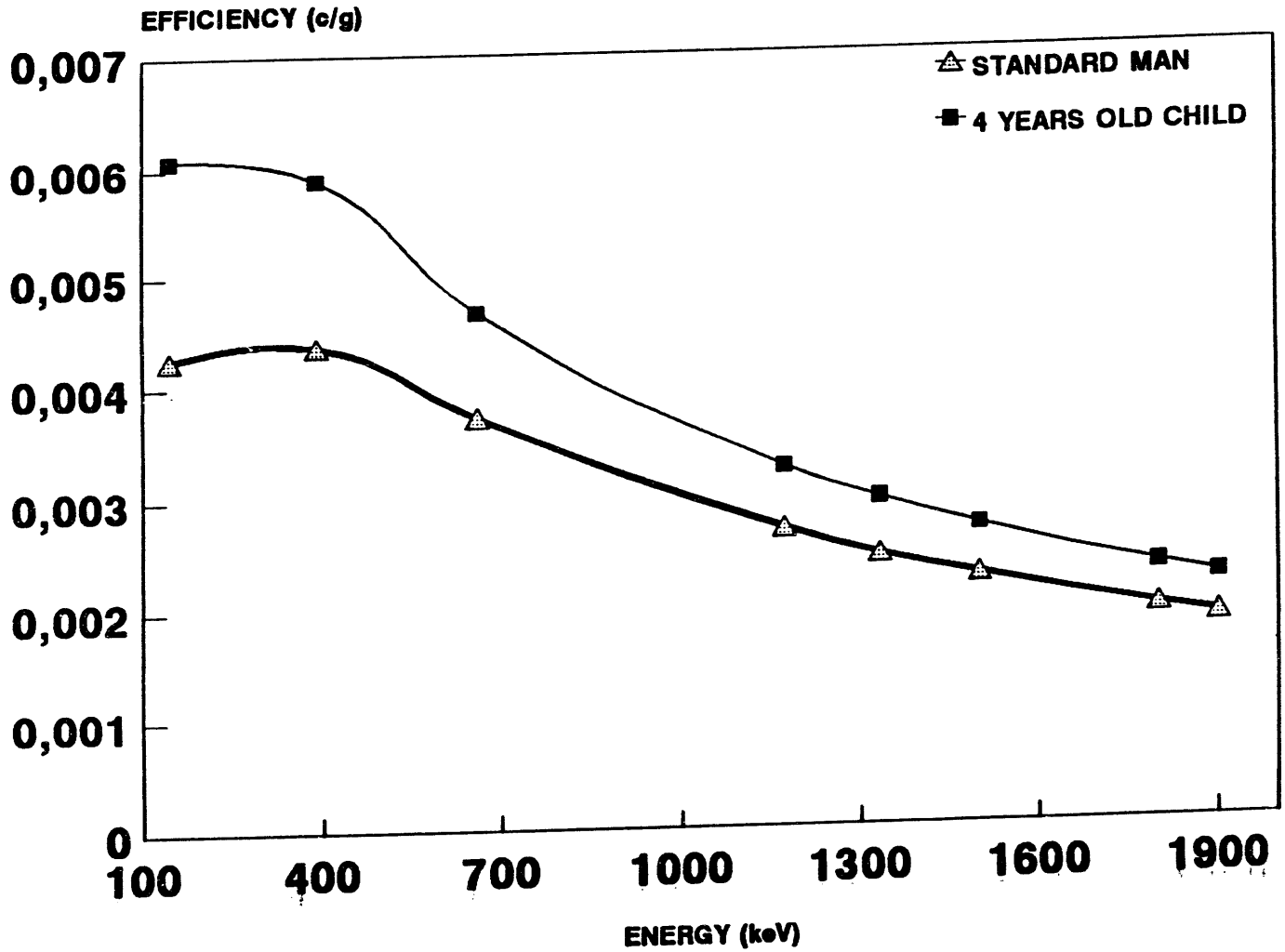




PHANTOM P4C

APPENDIX C

COUNTING EFFICIENCY FOR STANDARD MAN-4 YEARS OLD CHILD



RESULTS OF SUBSTITUTING THE NaI BY A Ge DETECTOR IN A SIMPLE SHADOW SHIELD WHOLE BODY COUNTER

P. Sahre*, Th. Schönmuth*, K. Thieme**
*Nuclear Engineering and Analytics Inc. Rossendorf, POB 510119, Dresden, 01314, Germany
**Amersham Buchler Ltd. & Co, Gieselweg 1, Braunschweig, 38110, Germany

1. INTRODUCTION

Since 1976 a whole body counter (WBC) has been used at the Rossendorf Research Centre for measuring the internal contamination of workers.
In figures 1 and 2 the WBC with the Germanium detector is given schematically and visually. The WBC is a shadow shield type with a tilted chair having only one detector. Table 1 contains the parameters of the WBC. From figures 1 and 2 and table 1 it can be seen that the WBC is a simple counter. Therefore, taking into account the experiences of McCurdy [1], a lot of improvements were expected from the simple substitution of a HP Germanium detector for a NaI (Tl) detector, i.e. despite a decrease in the sensitive detection volume, an enhancement of all quantifiable results (e.g. lower limit of detection and time for analysis of the spectrum) and above all the reliability and automation of nuclide identification were expected.

The paper describes the results of the substitution.

Table 1: Parameters of the Rossendorf Research Centre whole body counter

Type:	shadow shield, tilted chair geometry
Dimensions:	width 0.9 m, length 2.0 m, height 1.5 m
Shielding:	0.12 m old iron, seperate detector Pb-shield, shielding factor (integral 60 keV and 2 MeV): 14.3

Positioning the person: Position the person on the pulled-out tilted chair,

push in the chair, position the detector above the chest of the person (distance detector - body central axis about 0.4 m)

Detector: 1976 to 1990: NaI(Tl), 3" x 3"
fwhm = 8.8 % (662 keV) - this corresponds to 58 keV
since 1991: HP Ge detector (n-type),
efficiency 43 %
fwhm = 1.49 keV (662 keV)
1.95 keV (1332keV)

Spectrum analysis: 1976 -1990: 256 channels standard spectra for each nuclide considered, computer aided superposing of standard spectra
since 1991: 4096 channels, spectrum analysis by means of OMNIGAM [2]

2. RESULTS OF THE SUBSTITUTION

2.1. SPECTRA AND LOWER LIMIT OF DETECTION

In figures 3 and 4 spectra and pulse hight distributions resp. measured using the 3" x 3" NaI(Tl) detector and the HP Ge detector for comparable conditions are given. The obvious identification of the peaks in the case of the HP Germanium detector can clearly be seen. Furthermore the small peaks have the advantage - in contrast to the NaI(Tl) peaks - of a small peak region and therefore little disturbance due to the background. The background can also be simply eliminated by a linear background subtraction.

The efficiencies of both detectors in the measuring geometry of the WBC are given in figure 5. The efficiency of the HP Ge detector amounts to about 60 % of the efficiency of the 3" x 3" NaI(Tl) detector.

More important than the comparison of the efficiencies is the comparison of the lower limits of detection (LLD) given in figure 6. It can be seen that the HP Ge detector yields a better LLD than the NaI(Tl) detector, i.e. the HP Ge detector is more useful.

Concerning the determination of the LLD the following has to be added:

i) For reasons of comparison the LLD of the new system was also determined using the standard deviation (3σ) of the peak background value measured using a phantom.

ii) The 3σ values of the HP Ge detector correspond

approximately to the German standard DIN 25482 [3].

The good LLD of the HP Ge detector results in a reduction of the measuring time from 2000 s to 1000 s. The LLD values for a 1000 s measuring time are also given in figure 6.

2.2. SPECTRUM ANALYSIS AND CALIBRATION

In using the NaI(Tl) detector the calibration of the WBC by means of a bottle phantom and spectrum evaluation was a very time consuming process. This resulted from the very expensive computer aided spectrum analysis using the whole spectrum, not only the photo peaks. This was done in order to compensate for the small shielding (no measuring chamber, only the shadow shield). Therefore for each nuclide a so-called standard spectrum was produced. Such a standard spectrum is in turn a mean spectrum of 24 spectra representing the single measurements of the different phantom positions.

The analysis of a routine measurement was carried out off line on the research centre's central computer. The analysis results were not available until the next day.

This situation was fundamtentally improved by substituting the HP Ge detector for the NaI(Tl) detector. The significant improvement in the resolution of the detector is shown in clearly distinguished single peaks, i.e. a photo peak analysis using a commercially available spectrum analysis software can be applied.

Thus the calibration of the WBC can be reduced to determining the efficiency (see para. 2.1.), using a Eu-152 source. This source, i.e. the bottle containing the Eu-152 solution, was successively located at each position of the bottle phantom. From the resulting efficiencies a mean efficiency was calculated.

In the case of a routine measurement the spectrum evalutation (see figure 4) takes about one minute. The evaluation is shown in figure 7.

2.3. ASSESSMENT OF THE ACTIVITY DISTRIBUTION

In the above sections mean efficiencies have been constantly used. In figure 8 the efficiency of the HP Ge detector is given depending on the location of the source within the bottle phantom. As shown in the figure there are significant differences in the efficiencies in comparison to the mean efficiency (homogeneous distribution of the activity within the phantom).
An attempt was made to get further information from the spectrum in order to assess the deviation of the activity distribution from the homogeneous activity

distribution. This can be done under the following qualifications:

i) there are at least three peaks having energy distances of more than 200 keV

ii) the statistical error of the peak areas is less then 10 % for phantom positions clearly different from the homogeneous distribution (kidneys, back) resp. 2 % for not so clearly different positions (thyroid, stomach).

Because the activity distribution is only important in the case of a high incorporation the statistical error can be easier fulfilled than the demand for minimum number of peaks.

In order to use this information a computer program[4] was developed which compared the peak area ratios measured with the peak area ratios obtained from calibration which represent:

i) the peak area ratios of the homogeneous activity distribution

ii) the peak area ratios of the different phantom positions

Up to now there has been no experience in the routine use of the program, because there have been no significant incorporations during recent years.

3. SUMMARY

At the Rossendorf Research Centre a HP Ge detector (n-type, efficiency 43 %) was substituted for a 3" x 3" NaI(Tl) detector. From the simple substitution , i.e. without any modification of the WBC construction, the following improvements have been achieved:

i) clear nuclide identification

ii) decrease of the lower limit of detection from about 100 Bq to about 60 Bq (assuming a gamma ray abundance of 100 %) or reduction of the measuring time from 2000 s to 1000 s

iii) faster availability of the analysis results (1d NaI(Tl), 1 min HP Ge) by using a commerically available spectrum analysis software package

iiii) simpler calibration of the WBC due to the use of a multiline emitter.

Furthermore first steps are being taken in order to gain information from the spectrum measured on the activity distribution within the body.

REFERENCES

1. McCurdiy, D.E., Mellor, R.A., Harrington, C.L., Bard, S.T. Whole Body Counting: a New Perspective YAEC Report No. 1469, Dec. 1984

2. OMNIGAM, Gamma-Ray spectrum Analysis B30-BI Software Manual, EG&G Ortec, 1989

3. DIN-25482, Nachweisgrenze und Erkennungsgrenze bei Kernstrahlungsmessungen, Teil 5, Zählende hochauflösende gammaspektrometrische Messungen ohne Berücksichtigung des Probenbehandlungseinflusses, will be published

4. Matting, M. Untersuchungen zur Lokalisierung von Gamma-Strahlern bei einem Ganzkörperzähler mit fixer Eindetektoranordnung durch Nutzung spektraler Informationen, internal Report VKTA Rossendorf, Nov. 1991

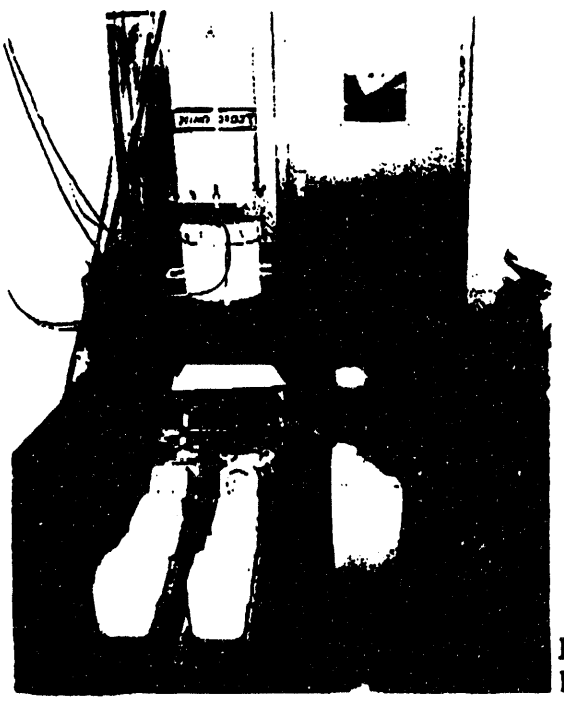


Fig. 1. Visual graph of the Rossendorf whole body counter

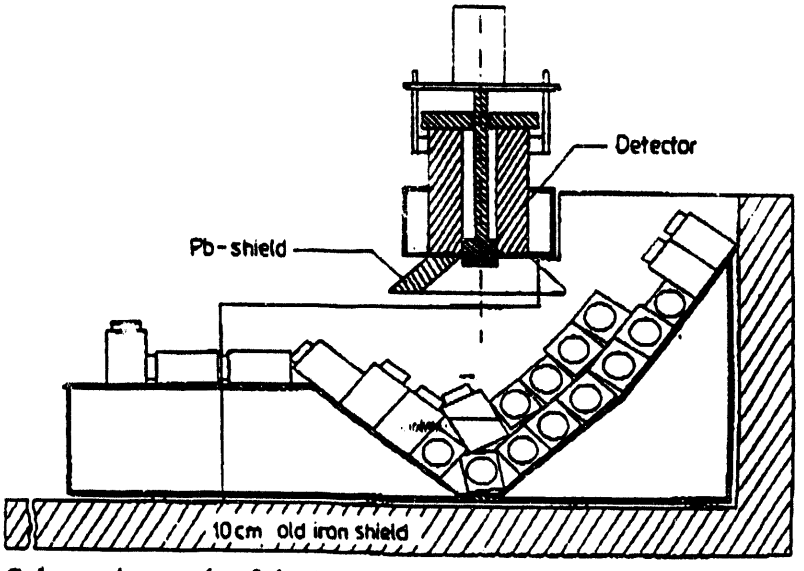


Fig. 2: Schematic graph of the Rossendorf whole body counter

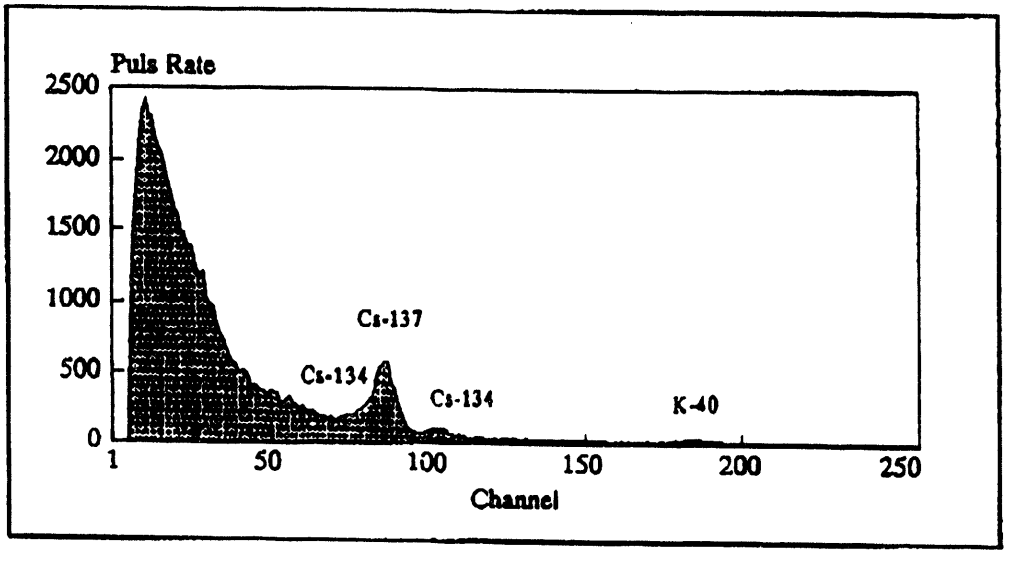


Fig. 3: Pulse high distribution of a Cs-137/134 incorporation measured with the NaI(Tl)-detector (measuring time 2000 s, activity: Cs-137 5.2 kBq, Cs-134 0.7 kBq)

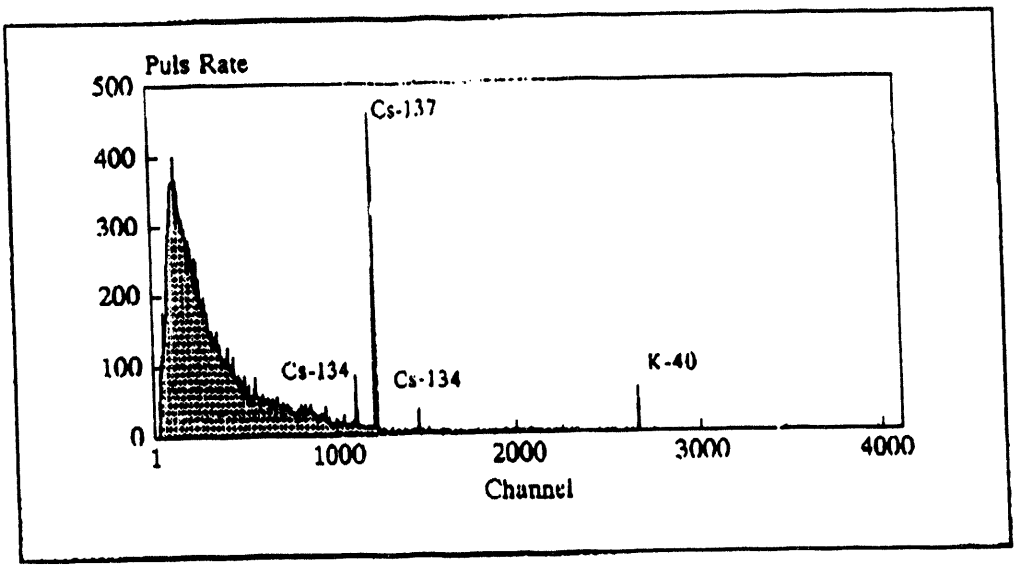


Fig. 4: Pulse high distribution of a a Cs-137/134 incorporation measured with the HP-Germanium-detector (measuring time 1000 s, activity: Cs-137 4.2 kBq, Cs-134 0.4 kBq)

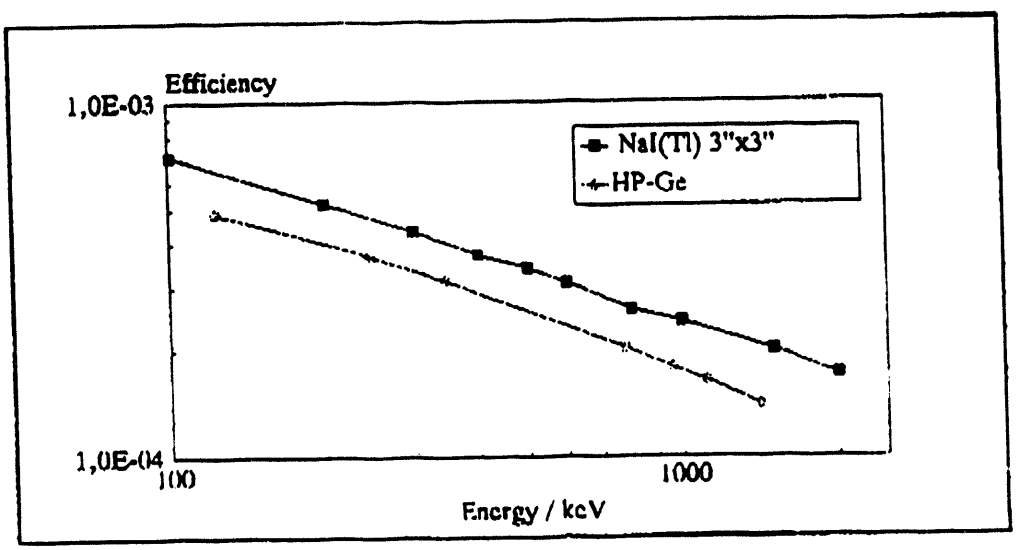


Fig. 5: Efficiency versus the gamma ray energy (100 keV to 1.5 MeV) for both detectors in WBC-measuring geometry

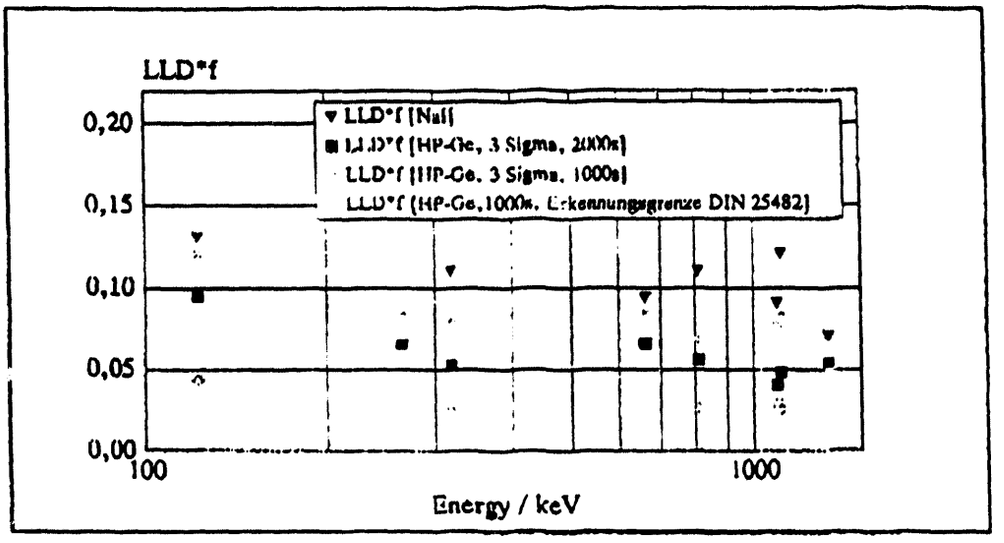


Fig. 6: Lower limit of detection (LLD) via gamma ray energy (100 % emission f) for both detectors derived from a measured spectra (for explanation see text)

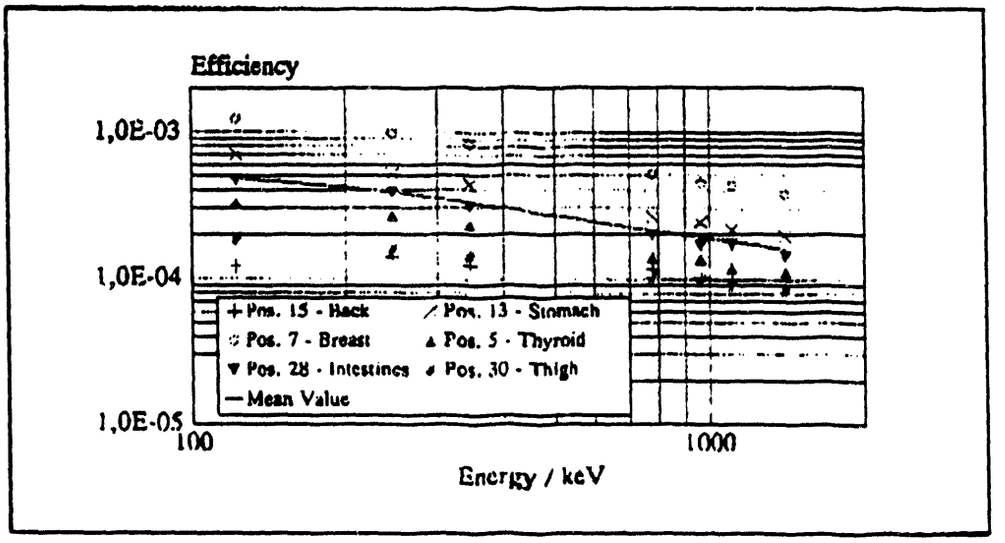


Fig. 8: Mean efficiency and efficiencies of the single bottle phantom positions

PROTOKOLL GANZKÖRPERMESSUNG

Name der Person : xxx
Vorname der Person : xxx
Geburtsdatum der Person : xxx
Körpergröße in cm : xxx
Körpermasse in kg : xxx
Entsendende Einrichtung : xxx
Art der Messung :

Resultat der Kontaminationsmessung : keine
Geduscht : ja
Möglicher Inkorporationszeitpunkt :

Spectrum Filename: 4020.SPC

Acquisition information
start time 25-MAR-92 11:11:31
Live time 1000
Real time 1001
Dead time .16%

Calibration

Filename: CALEUXX.SPC
Created: 15-NOV-91 12:28:40 & 15-NOV-91 12:31:14
Neukalibrierung 15.11.91

Zero offset -2.578 keV; Gain .550 keV/channel

Library Files
Main analysis library: GKZ.LIB

** S U M M A R Y O F N U C L I D E S I N S A M P L E **

NUCLIDE	TIME OF COUNT ACTIVITY kBq	UNCERTAINTY COUNTING 2 SIGMA	TOTAL
CS-134	3.7157E-01	21.94%	45.68%
CS-137	4.1750E+00	7.48%	40.77%
K-40	3.7216E+00	36.08%	53.93%

Fig. 7: Record of a routine WBC-measurement (for measured spectrum see figure 4)

DOSE CONTRIBUTION FROM ORGANICALLY BOUND TRITIUM AFTER AN ACUTE TRITIATED WATER INTAKE

A. Trivedi, D. Galerui and R.B. Richardson (Radiation Biology and Health Physics Branch, AECL Research, Chalk River, Ontario, Canada K0J 1J0.)

To assess the dose contribution from retained organically bound tritium (OBT), we have analyzed urinary excretion data from eight individuals who had an acute intake of tritiated water (HTO). The individuals affected had increased their water intake up to 30 d post-exposure to accelerate the turnover of tritium in the body water for dose mitigation purposes. Their urine samples were analyzed for total tritium up to 300 d post-exposure. The analysis of the bioassay data showed that the mean body water turnover half-time was 6.3 $\pm$ 1.0 d and 8.4 $\pm$ 1.9 d for the period of increased water and normal water intake, respectively. The long-term excretion of tritium was also observed (half-life 73.7 $\pm$ 18.1 d), indicting the tritium incorporation and retention in the organic components of the soft tissues. A mathematical model is proposed to estimate the dose increase from the retained OBT by examining the kinetics of tritium excretion in urine. The analysis accounts for the variable rate of water intakes. The influence of measurement errors and a limited observation time on the OBT dose assessment was assessed by theoretical means using various metabolic models that accounted for OBT excretion in urine. Based on the kinetics of tritium in urine, the average dose increase from the metabolized OBT was 6.2 $\pm$ 1.3% of the HTO dose. The uncertainty in the OBT dose estimates was calculated to be less than 50%.

NEW METHOD FOR Sr-90 DETERMINATION IN LIQUID SAMPLES BY LIQUID SCINTILLATION COUNTING.

Alvarez A., Navarro N., Salvador S.
Radiological Protecction Division
Ciemat-IMA. Avda Complutense 22, 28040 Madrid-Spain.

INTRODUCTION

Strontium-90 is a fission product with a chemical similarity to calcium and a long biological half life. For this reason, its measurement has received considerable attention for monitoring persons exposed to the risk of internal contamination. The isotopes of dominant concern for strontium internal dosimetry are ^{90}Sr and its daughter ^{90}Y. These radionuclides are found in equilibrium to each other in virtually all circunstances under which exposure is likely. Urine sample analysis is the easiest and most common bioassay method for ^{90}Sr, and therefore the urinary excretion function becomes the key for internal dosimetry evaluations of strontium. Both, ^{90}Sr and its daughter ^{90}Y, are pure beta emitters, and its determination is usually made measuring the beta total activity in a proportional gas counter, after a chemical separation. Traditionally, this separation has been performed using ion exchange columns or selective precipitations of nitrates, cromates or carbonates, being in general tedious analitycal procedures, with time-consuming.

Recently, a new chromatographic extraction material has appeared that separates quick and efectively strontium from nitric acid solutions. This material, denominated Sr.Spec is composed by macrocyclic polyethers (crown ethers) dissolved in aliphatic alcohols or ketones, and is comercially avalaible as resine or packed columns. Its application to the Sr^{90} isolation simplify considerably the analysis of this radionuclide.

In this work a new method based in the utilization of this material is proposed. The activity measurement is made by liquid scintillation technique. On this way, is possible to determine Sr^{90} activity from a quick measurement. The method has been applied to urine samples, but it is also applicable to any liquid sample.

EXPERIMENTAL

Reagents

All the reactives used were of analytical grade. Calcium carrier (40 mg Ca ml^{-1}) was made from 205 g of $Ca(NO_3)_2$ in 1 liter of deionized H_2O. The radioisotopes $^{90}Sr/^{90}Y$ and ^{85}Sr were obtained from CEA (France). The Sr.Spec columns were obtained from EIChrom Industries, Inc.(U.S.A.).

Equipment

Radiactivity measurement were performed on a liquid scintillation spectrometer Packard TriCarb 2500 TR. The quench parameter tSIE was obtained from a ^{133}Ba external γsource. A software from Packard allows to control automatically the process, fixing counting conditions.

Procedure

Urine samples, which volumes are usually higher than one litre, require a previous concentration step before chemical separation. ^{90}Sr is coprecipitated from the bulk urine sample by coprecipitation as phosphate (using Ca^{2+} as carrier). The sample was placed in a glass beaker containing a magnetic stirrer. Following, 60 ml of concentrated HNO_3 were added, and the glass was introduced in a water-bath, heating until the temperature gets 70°/80°C. Stirring continuosly, 1 ml of concentrated HNO_3 and 2 ml of $Ca((NO)_3)_2$ were added, heating at constant temperature during half an hour. After that, concentrated NH_3 was added until appearing the calcium phosphate precipitate carrying the strontium, and the sample was heated during 1 h. The stirring bar was then removed and the precipitate was allowed to settle for at least 6 h.

The supernatant liquid was decanted off and transferred to a centrifugue bottle, then spun at 2500 rpm for 10 min. The supernatant liquid was discarded and the precipitate transferred to a glass beaker with concentrated HNO_3. The beaker was heated to dryness on a hot plate. After that, several 10 ml portions of concentrated HNO_3 were added, until the sample was free of organics (if the destruction of organic matter is not complete, the residue can be calcinate in a furnace at 500°C)

The remaining residue was then dissolved in 10 ml of HNO_3 8N, and introduced in the chromatographic column.

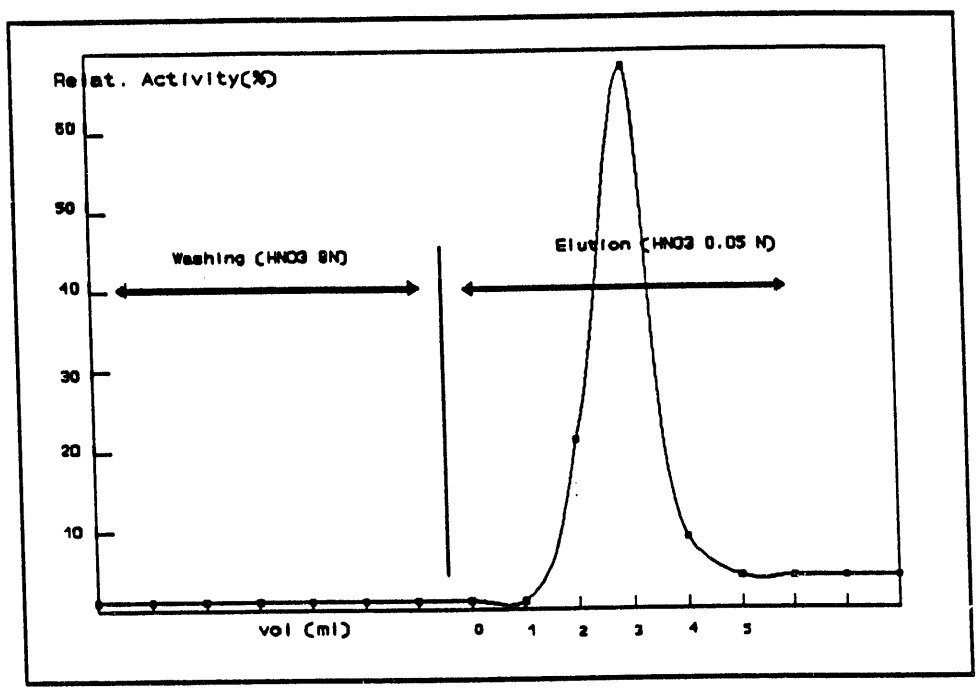
The chemical yield of the radioanalytical procedure was determinated gravimetrically, weighting the strontium nitrate precipitate obtained after elution step. This chemical yield was always in the range 80% to 90%. After that, the residue was dissolved in deionizated H_2O and mixed with the scintillation cocktail for its measurement.

The proposed method for the cromatographic separation is based on works published by Dietz and Horwitz (1). Prior to use, the columns were rinsed successively with a few milliliters of HNO_3 3N and few milliliters of loading solution (HNO_3 8N). Following, the sample is poured through the Sr.Spec column and strontium is retained in nitric acid medium. After that, the column is washed with HNO_3 8N and the strontium eluted with 5 ml of HNO_3 0.05N into a glass vial.

Elution curve

Strontium elution curve was experimentally obtained using ^{85}Sr as tracer. This is a beta/gamma emitter with a gamma emmission at 513.9 KeV (Intensity= 99.2%). The elution fraction containing the strontium was collected in small portions of 1 ml, and each vial was measured by gamma spectrometry. Figure 1 shows the results of this experiment. Almost all the strontium was eluted in the first 3 ml of HNO_3 0.05N, without loss of strontium in the scrubbing elution.

Figure 1. Sr Elution Curve.
(Sr.Spec column)



Radiactivity measurement

For samples measurement by liquid scintillation technique, 15 ml of scintillation cocktail were added to 1 ml of HNO_3 containing eluted strontium. Samples were then counted for 30 min on a Packard's counter.

Quenching is the most important interference ocurring in Liquid Scintillation Counting. It affects the efficiency of the conversion process beta particle energy to photoelectron. For this reason, the number of photons per keV of beta particle energy which reach the photomultipliers it is reduced. The result is a shift to lower amplitudes of the pulse height spectrum. Therefore the measured counts are only representative for the radioactivity of the sample if they are corrected for this quenching effect.

Obtaining a relationship between quench level in different standars and the measuring efficiency, this effect can be corrected. The calibration method applied in our case was the CIEMAT/NIST (4). By a universal curve for a stable radionuclide like tritium, a relationship between a characteristic parameter of the equipment and quench level is obtained. After that and using a series of Tables calculated for each beta emitter, is possible to obtain the efficiency of any sample.

Due to the fact that the measurement is made inmediatly after the chemical separation of ^{90}Sr and ^{90}Y, the mixture has not reach the equilibrium. This introduces a new difficulty in the measurement, since both spectras overlap. Several methods apply mathematical treatments to correct the ^{90}Y ingrowth, but in our case measurements were performed by a double-window method, stablishing counting regions for Sr^{90} and Y^{90} taking into account quench level of the samples. This procedure allows to estimate the activity of the radionuclide on a quick and simple way.

A serie of ^{90}Sr and ^{90}Y standars with different levels of quenching, were prepared to obtain efficiency curves for both radionuclides. This curves are shown in figure 2. ^{90}Sr standars allow to establish counting region for ^{90}Sr. Associating final of ^{90}Sr spectrum for each standar with its quench level, it is possible to calculate by interpolation the final ^{90}Sr spectrum for the sample. Once determined ^{90}Sr and ^{90}Y counting regions (A and B for ^{90}Sr and ^{90}Y respectively) and determining previously ^{90}Y efficiency in regions A and B, together with ^{90}Sr efficiency in the complete spectrum, activity of each radionuclide was calculated from the following expressions.

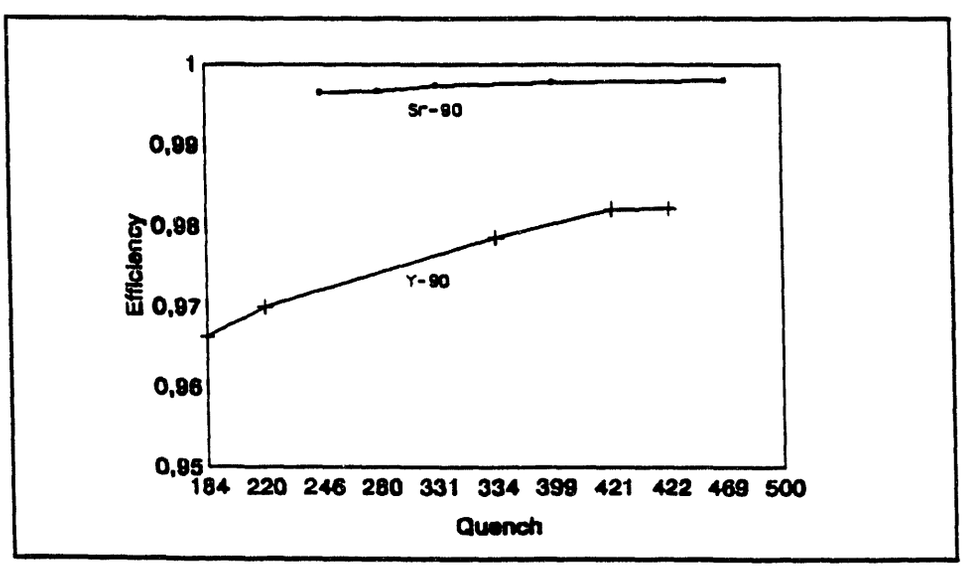
$$A(^{90}Y) = \frac{N'_B}{\epsilon_B\,(^{90}Y)}$$

N'_B = CPM in region B
$\epsilon_B(^{90}Y)$ = ^{90}Y efficiency in region B

$$A(^{90}Sr) = \frac{N'_A - A\,(^{90}Y)\,\epsilon_A\,(^{90}Y)}{\epsilon\,(^{90}Y)}$$

N'_A = CPM in region A
$\epsilon_A(^{90}Y)$ = ^{90}Y efficiency in region A
$\epsilon(^{90}Y)$ = ^{90}Sr efficiency

Figure II.
^{90}Sr and ^{90}Y Efficiency curves



Limit of detection

The limit of detection, calculated applying Currie criteria (5) and assumming a human daily excretion of 1.4 litres was $8 * 10^{-2}$ Bq/l/day. This value makes possible the aplication of this method for dossimetric purpouses.

Dosimetric application

The proposed method is adequated for ^{90}Sr dosimetric control by urine analysis. The ^{90}Sr Anual Limits of Incorporation (A.L.I) recommended by ICRP-54 (6), are $7 * 10^5$ Bq (class D) and $1 * 10^5$ Bq (class Y). In case of a quarterly routine monitoring (90 days monitoring interval), the predicted activity as fraction of intake are $3.4 * 10^{-4}$ Bq and $1.7 * 10^{-5}$ Bq for class D and Y respectively.

Considering an investigation level for routine monitoring according to the following expression;

$$IL_R = \frac{3}{10} * \frac{ALI}{N}$$

$$N = 4$$

the predicted activities in urine for this reference level would be 17.8 Bq/day (class D) and 0.13 Bq/day (class y), in both cases above the limit of detection of the proposed method.

Quality assurance

The validity of this method for the determination of ^{90}Sr in liquid samples has been sucessfully tested by good results obtained by our laboratory in the international intercomparison organized annualy by CEA-COGEMA group.

Table I reproduces results proporcionated by our laboratory for samples included in ^{90}Sr exercise, together with the real and mean values. This table shows a close agreement between these two numbers.

Sample	Real value (Bq/l)	Mean value (Bq/l)	Our laboratory (Bq/l)
Urine sample	8.93	8.58	8.5
^{90}Sr standard	13.4	13.35	13.4

CONCLUSIONS

- The presented method has been sucessfully applied to Sr^{90} determination in urine and liquid samples, although would be possible its application to any matrix with the appropiated modifications. Liquid Scintillation Technique in combination with this method, allows to obtain a limit of detection that justify its application for ^{90}Sr dosimetric control in routine monitoring programs by urine analysis.

- The application of the new chromatographic material notably improve the determination of ^{90}Sr, specially concerning time inverted in analysis. Measurement by Liquid Scintillation Thecnique allows quicker determinations, since avoids waiting until radioactive equilibrium has been reached or making complicated calculations for ^{90}Y ingrowth.

ACKNOWLEDGEMENTS: The authors wish to thank Dr. A. Grau Malonda for his assistance in this work.

REFERENCES.

(1) Dietz, M.L., Horwitz, E.P.. "An improved method for determining Sr^{89} and Sr^{90} in urine". Health PHysics. Vol 61, No 6 (December), pp.871-877. 1991.

(2) Packard Camberra Company. SpectraGraph. "Spectrum Analysis Sowftware Package. Operation Manual".

(3) Grau Carles, A., Rodriguez, L., Grau Malonda, A.. "Simultaneous Standardization of Sr^{90}-Y^{90} and Sr^{89} Mixtures". Appl. Radiat. Isot. Vol.44, No 7, pp 1003-1010, 1993.

(4) Grau Malonda, A., Coursey, B.H.. Appl. Radiat. Isot. 38, 695 (1987).

(5) Currie, LL.. "Limits for qualitative detection and quantitative determination". Anal. Chem. Vol 40, No . 1958.

(5) ICRP 54. "Individual monitoring for intakes of radionuclides by workers: Design and interpretation". Annals of the ICRP, Vol.19, No. 1-3. 1988.

DETERMINATION OF TRANSURANIC DAC EQUIVALENT FROM CE-144 CONCENTRATIONS

C. D. Stretch, Sr. Health Physicist
E. A. O'Connor, Sr. Health Physicist
Union Electric Company, Callaway Plant

ABSTRACT

The development of a reliable empirical method to determine the DAC (Derived Air Concentration) equivalent relative to observed Ce-144 concentrations for the transuranic (TRU) nuclides Pu-238, Pu-239/240, Pu-241, Am-241, Cm-242, and Cm-243/244 is documented.

The analytical methodology used to determine the relationship between TRU and Ce-144 concentrations, the practical inplant identification of TRU DAC for air samples, the DAC equivalent set point for the BAB (Beta Aerosols Beacon) Monitor, and the comparison between the observed TRU DAC and the empirical TRU DAC will be presented.

INTRODUCTION

The Callaway Plant experienced open fuel defects prior to its sixth refuel outage (Refuel 6) making it very desirable to develop a method to monitor the TRU component in the working environment. Ce-144 was selected as an acceptable indicator of the presence of TRU. (See References 1, 2 and 3.) A methodology was developed to determine the TRU DAC component based on the observed Ce-144 concentration. The bases for the Callaway Plant to calculate the non-gamma emitting nuclides was developed from the concepts presented in Reference 4.

ASSUMPTIONS

The observed Ce-144 concentration is assumed to be from fresh fuel defects. It is not decay compensated.

The Ce-144 and TRU nuclides will be in the same ratio on air samples, smears and laboratory reactor coolant filters.

METHODOLOGY DISCUSSION

A. Analytical Methodology to Determine the Relationship Between the TRU Nuclides and Ce-144

Four reactor coolant samples were filtered using 0.45 micron glass fiber filters and analyzed to determine the TRU/Ce-144 ratios. Each filter and one aliquot of filtrate were analyzed for Ce-144 utilizing gamma spectroscopy. These same samples were then analyzed for TRU nuclides by alpha spectroscopy. The TRU/Ce-144 ratio was determined by averaging the data from each of the four filters. A review of the analytical data verified that Ce-144 and TRU were greater than 95% insoluble. The results of the isotopic analysis of reactor coolant filters is shown on Attachment 1. The TRU/Ce-144 ratios are shown on Attachment 2.

B. Determination of the Equivalent TRU DAC Relative to Ce-144

The average individual nuclide ratio of TRU per unit microcurie of Ce-144 was divided by the appropriate TRU DAC to obtain the number of TRU DAC per unit microcurie of Ce-144. The TRU DACs were then summed to obtain the total number of TRU DAC per unit microcurie of Ce-144. For this study, the reciprocal of the total TRU DAC yields 3.57E-10 microcuries/cc Ce-144 per unit TRU DAC. This is shown on Attachment 3.

C. Practical Application to Air Samples

Routine 20 cubic foot air samples were obtained and analyzed using a 5 minute count time. The Ce-144 LLD (Lower Level of Detection) for the air sample counting geometry was 6.0E-10 microcuries/cc. On the basis of the empirical ratio of 3.57E-10 microcuries/cc Ce-144 per unit TRU DAC, the minimum TRU DAC capable of being identified on a routine air sample is 1.7.

D. Methodology to Determine the DAC Equivalent Set Point for the BAB

BAB continuous air monitors were used at several work sites during the Callaway Refuel 6 outage. The work sites were selected based on their potential for rapid changes in air concentration due to work evolutions being performed. These monitors are equipped with both visual and audio signals that will alarm at preset levels providing rapid local indications to the worker of increases in airborne concentrations. The lowest practical setting is 1.0E-08 microcuries/cc.

Representative air samples from Refuel 4 and Refuel 5 , as well as reactor coolant samples from Cycle 3, Cycle 4, and Cycle 5 were reviewed. The typical corrosion products distribution was then compared to that observed on the Refuel 4 routine air samples and found to be very similar in ratio and isotope mix.

With the exception of Ce-141 and Ce-144, the gamma emitting fission isotopes were in approximately the same concentration in the reactor coolant prior to the reactor shutdown for Refuel 4 as they were prior to Refuel 6. The Ce-141 and Ce-144 concentrations increased from Refuel 4 to Refuel 6, therefore it was necessary to adjust the air sample data for this increase. The Ce-144 concentration was determined to be 15.1 times greater in the reactor coolant prior to Refuel 6, consequently the Ce-144 analytical results for Refuel 4 air samples were multiplied by 15.1. The Refuel 4 Ce-141 concentrations were then corrected by multiplying the corrected Ce-144 concentrations by the maximum ratio for Ce-141/Ce-144 that will occur with fuel defects (Reference 3). A typical example is shown on Attachment 4.

A conservative approach was taken for modifying the TRU nuclides that were identified on the Refuel 4 air samples. If a TRU nuclide was not identified on the air sample, the TRU was determined by multiplying the corrected Ce-144 value by the appropriate TRU/Ce-144 conversion factor listed on Attachment 2.

The equivalent DAC for each air sample was determined by dividing the total microcuries by the sum total of the DAC fractions. The average equivalent DAC for the nine air samples is 3.78E-09 microcuries/cc. Therefore, the lowest practical BAB setting of 1.0E-08 microcuries/cc is equal to 2.5 DAC.

CONCLUSIONS

Five air samples obtained during Refuel 6 were analyzed for TRU and the total DAC was calculated for each. The actual TRU DAC component was determined for each sample and compared to the empirically derived TRU DAC. The BAB equivalent DAC value was also calculated for each of the five air samples using the methodology described above. The results of the air samples analyses are shown on Attachment 5. The results of the Refuel 6 BAB equivalent DAC data is shown on Attachment 6.

The empirically derived TRU DAC for each sample was determined to be within a factor of 2.3 of the actual TRU DAC. The average deviation between actual and empirical TRU DAC is only 1.5. The BAB equivalent DACs were determined to be within a factor of 2.6 of BAB DAC determined prior to Refuel 6. The average deviation between pre Refuel 6 BAB DAC and the and the BAB DAC determined from Refuel 6 air samples was only 1.9. The BAB DAC deviation was only 1.1 when the five Refuel 6 air sample were averaged.

On the basis of these results, it is the authors' opinion that utilization of the empirical method to determine the TRU DAC on air filters and the BAB set point calculation is an acceptable method for evaluating airborne contamination in the working environment.

REFERENCES

1. Mis, F. J.; Warren. S. B.; Harrison. M. C.; Voilleque, P. G.; Particle Size Distributions for Airborne Radionuclides in Steam Generator Work Environments; Health Phys., Vol. 56, No. 2 (February), pp. 233-238. 1989.

2. Voilleque, P. G.; Mis, F. J.; Warren. S. B.; Harrison, M. C.; Solubility of Transuranic Nuclides in Aerosols in Two Ginna Steam Generator Work Environments; Power Reactor Health Physics. Proceedings of the Twenty-First Midyear Topical Meeting of the Health Physics Society; Miami HPS Power Reactor Section; 1987:251-260.

3. Wymer, R. G.; Vondra, L. B.; Light Water Reactor Nuclear Fuel Cycle; CRC Press: Boca Raton, Florida; 1981.

4. Bray, L. G.; Copper, T. L.; Goldin, E. M.; Warnock, R. V.; Skin Dose Calculations for Fuel Particles; Radiation Protection Management, Vol. 4, No. 5 (Sep/Oct 1987), pp. 25-30.

REACTOR COOLANT FILTER ANALYSIS

FOR

TRU AND CE-144 ISOTOPES

SAMPLE COLLECTION DATE AND TIME 7/30/92, 1347

ISOTOPE	uCi/ml
Pu-238	2.70E-8
Pu-239/240	1.20E-8
Pu-241	3.50E-6
Am-241	7.25E-9
Cm-242	1.03E-8
CM-243/244	2.08E-8
Ce-144	4.31E-6

SAMPLE COLLECTION DATE AND TIME 6/14/93, 1200

ISOTOPE	uCi/ml
Pu-238	1.66E-6
Pu-239/240	3.30E-7
Pu-241	1.06E-4
Am-241	2.69E-8
Cm-242	1.33E-5
Cm-243/244	1.33E-6
Ce-144	4.11E-4

SAMPLE COLLECTION DATE AND TIME 6/14/93, 1200

ISOTOPE	uCi/ml
Pu-238	1.34E-6
Pu-239/240	2.51E-7
Pu-241	1.03E-4
Am-241	3.11E-8
Cm-242	1.24E-5
Cm-243/244	1.20E-6
Ce-144	6.75E-4

SAMPLE COLLECTION DATE AND TIME 6/14/93 1243

ISOTOPE	uCi/ml
Pu-238	7.17E-7
PU-239/240	1.22E-7
PU-241	2.66E-5
Am-241	1.42E-8
Cm-242	5.63E-6
Cm-243/244	5.78E-7
Ce-144	2.72E-4

ATTACHMENT 1

TRU/Ce-144 CONVERSION FACTORS

SAMPLE NO.	1	2	3	4	
ISOTOPE	TRU/Ce-144	TRU/Ce-144	TRU/Ce-144	TRU/Ce-144	TRU/Ce-144 AVERAGE
Pu-238	6.26E-03	4.04E-03	1.99E-03	2.64E-03	3.73E-03
Pu-239/240	2.78E-03	8.03E-04	3.72E-04	4.49E-04	1.10E-03
Pu-241	8.12E-01	2.58E-01	1.53E-01	9.78E-02	3.30E-01
Am-241	1.68E-03	6.55E-05	4.61E-05	5.22E-05	4.61E-04
Cm-242	2.39E-03	3.24E-02	1.84E-02	2.07E-02	1.85E-02
Cm-243/244	4.83E-03	3.24E-03	1.78E-03	2.13E-03	2.99E-03

Sample 1 Date/Time: 7/30/92 1347
Sample 2 Date/Time: 6/14/93 1200
Sample 3 Date/Time: 6/14/93 1200
Sample 4 Date/Time: 6/14/93 1243

ATTACHMENT 2

TRU DAC EQUIVALENT To Ce-144

ISOTOPE	µCi/cc TRU per µCi/cc Ce-144	DAC (µCi/cc)	# of TRU DAC per µCi/cc Ce-144
Pu-238	3.73E-03	8.00E-12	4.66E+08
Pu-239/240	1.10E-03	7.00E-12	1.57E+08
Pu-241	3.30E-01	3.00E-10	1.10E+09
Am-241	4.61E-04	3.00E-12	1.54E+08
Cm-242	1.85E-02	1.00E-10	1.85E+08
Cm-243/244	2.99E-03	4.00E-12	7.48E+08

TOTAL DAC = 2.81E+09

TRU DAC EQUIVALENT TO 1 µCi/cc Ce-144 = 3.57E-10 µCi/cc

ATTACHMENT 3

SAMPLE NUMBER 90-2982-H

ISOTOPE	uCi/CC	DAC uCi/CC	DAC FRACTION CONTRIBUTION	COMMENTS
Cr-51	3.77E-9	8.00E-6	4.71E-4	
Mn-54	5.72E-10	3.00E-7	1.91E-3	
Fe-59	2.33E-10	2.00E-7	1.17E-3	
Co-60	1.36E-9	1.00E-8	1.36E-1	
Co-58	6.19E-9	3.00E-7	2.06E-2	
Hf-181	2.52E-11	2.00E-7	1.26E-4	
Co-57	2.49E-11	3.00E-7	8.29E-5	
Zr-95	9.99E-10	2.00E-7	5.00E-3	
Nb-95	1.40E-9	5.00E-7	2.79E-3	
Cs-134	4.07E-11	4.00E-8	1.02E-3	
Cs-137	5.24E-11	6.00E-8	8.74E-4	
Ce-141	3.24E-10	2.00E-7	1.62E-3	Ce-144X1.2
Ce-144	2.70E-10	6.00E-9	4.50E-12	AIR FILTER Ce-144X15.1
Sn-113	6.25E-11	2.00E-7	3.13E-4	
Ni-56	1.66E-11	5.00E-7	3.31E-5	
Ru-103	1.20E-10	3.00E-7	4.00E-4	
Sb-125	5.19E-11	1.00E-6	5.19E-5	
Pu-238	1.01E-12	8.00E-12	1.26E-1	CALCULATED
Pu-239/240	2.22E-11	7.00E-12	3.17	NALYTICAL VALUE X 15.1
Pu-241	8.91E-11	3.00E-10	2.97E-1	CALCULATED
Am-241	1.24E-13	3.00E-12	4.13E-2	CALCULATED
Cm-242	5.00E-12	1.00E-10	5.00E-2	CALCULATED
Cm-243/244	9.97E-12	4.00E-12	2.49	NALYTICAL VALUE X 15.1

TOTAL SAMPLE DAC= 6.40 **PERCENT TRU DAC=96.5**

TRU DAC= 6.17 **TOTAL MICROCURIES =1.56E-8**

ATTACHMENT 4

REFUEL 6 AIR SAMPLES

SAMPLE NUMBER	SAMPLE TOTAL DAC	SAMPLE % TRU DAC	SAMPLE TRU DAC (ACTUAL)	SAMPLE TRU DAC (EMPIRICAL)	EMPIRICAL/ACTUAL
A-45	11.3	80.8	9.13	21.0	2.3
A-46	21.2	91.4	19.5	17.6	0.9
A-50	2.67	93.0	2.48	2.2	0.9
A-58	9.49	86.6	8.22	10.3	1.2
A-63	29.5	84.1	24.8	13.9	0.6

ATTACHMENT 5

RF6 BAB EQUIVALENT DAC DATA

REFUEL 6 AIR SAMPLES

SAMPLE NUMBER	RF6 BAB EQUIVALENT DAC	RF6 BAB DAC/PRE RF6 BAB DAC
A-45	4.72E-9	1.2
A-46	1.82E-9	.5
A-50	1.34E-9	0.4
A-58	3.59E-9	0.9
A-63	9.91E-9	2.6
AVERAGE	4.28E-9	1.1

PRE RF6 EQUIVALENT DAC= 3.78E-9 uCi/cc

ATTACHMENT 6

PROPOSAL OF A BIOASSAY PROGRAM FOR WORKERS OF THE THORIUM NITRATE PURIFICATION FACILITY AT THE IPEN-CNEN/SP

Janete C. G. Gaburo, Enocles E.M. Oliveira, Gian M.A.A. Sordi (Instituto de Pesquisas Energéticas e Nucleares CNEN/SP, C.P. 11049, CEP 05422---970 - SAO PAULO-SP, BRAZIL), Joyce L. Lipsztein (Instituto de Radioproteção e Dosimetria CNEN/RJ, C.P. 37025, RIO DE JANEIRO-RJ, BRAZIL.)

The operations involved in the Thorium Nitrate Purification Process at the IPEN-CNEN/SP are brieftly described. The main radioactive sources and the health physics procedures implemented are given. The techniques and the results of in vitro and in vivo analyses are shown and discussed. Finally a bioassay program for thorium workers is proposed and some recommendations are given.

Work partially suppported by CNPq - Conselho Nacional de Desenvolvimento Científico e Tecnológico, Brazil.

DOSE DEPENDENT QUALITATIVE ANALYSIS OF THE EFFECTS OF TRITIATED WATER (HTO) ON THE DEVELOPING MOUSE CEREBELLUM FROM 15th DAY POST - COITUM

NARENDRA JAIN* & A. L. BHATIA**

* Zoology Department, S. K. Government P.G College, Jaipur, Rajasthan, INDIA.

** Zoology Department, University of Rajasthan, Jaipur-302004, Rajasthan, INDIA.

INTRODUCTION

Acceptance of nuclear power as a fact of life may cause concern over the possible long term deleterious effects arising from radioactive byproducts generated in these reactors. Of concern are the possible effects from tritium in the form of tritiated water, a major byproduct of both fission and fusion reactions. As a radiation hazard of neurobiological significance, this radionuclide has largely been ignored. This neglect has been due to its low average beta energy (5.6 KeV), its rapid turnover in the body and its short range in the tissue(6.0 μm). It has, however, been demonstrated that after a protracted HTO exposure, tritium is retained in organically bound form, in large amounts and for a long duration in both adult brain (Pinson and Langham, 1957) and the developing brain of mice (Ueno and Kawamura, 1975). Various radiobiological effects of low doses of tritiated water (HTO) have been reviewed by Bhatia (1987).

An evaluation of tritium toxicity in the developing mouse brain carried out in this laboratory demonstrates that the cerebellum is fairly vulnerable to tritium exposure even in young adult mice Shishodia, 1985). In rat and mouse, the cerebellar development takes place mainly during the first few weeks after birth. The neurogenesis and migration of different cell types in the cerebellar cortex occurs during this period. The majority of the cells produced in the external granular layer (EGL) migrate to their final positions in the cortex. During this period of rapid development, proliferative and premigrative cells are very sensitive to radiations (Altman & Nicholson, 1971). The possibility of major cytoarchitectural changes in the brain therefore,cannot be safely ruled out (Bhatia, 1985). Tritium toxicity in the postnatally developing mouse cerebellum with respect to the radiopathological changes has been recently reported by Jain & Bhatia,(1993). In the absense of adequate dose response data on inhaled beta emitting radionuclides in man, it is necessary to obtain such information in experimental animals. This presentation is an attempt to look into the toxicity of tritium on the cerebellum of developing Swiss albimo mice and hence, to collect such dose response data which are necessary to establish the safety standards for the personal involved with radiation protection programs.

MATERIALS AND METHODS

Pregnant Swiss albino mice were given a priming injection of tritiated water (received from Bhabha Atomic Research Centre, Trombay, Bombay). The specific activity was 370 MBq/ml. The administered doses were 7.4kBq and 74kBq/ml. of body water respectively on the 15th day post conception. Body water was taken to be approximately 60% of the body weight. From the same day onward, the pregnant females were continuously maintained, through parturition until the last interval studied, respectively on 11.1 and 111 kBq/ml of tritiated drinking water provided ad libitum. Litters were autopsied

at 1, 2, 3, 4, 5 & 6 weeks post - partum, after cervical dislocation. The brains were removed, weighed and fixed in the Bouin's fixative. The cerebellum from each of the fixed brain was removed by cutting the cerebellar peduncles and then processed for making paraffin blocks. The sections of the cerebellar tissue were passed through a graded series of alcohol and stained in 1. Eosin & Hematoxylin (Mallory, 1944) and 2. Cresyl Violet (POWERS & Clark, 1955) for the histological studies. The qualitative studies in the treated animals have been compared with those of the sham-irradiated animals (control group).

DOSIMETRY

The dose level of 11.1kBq and 111kBq of HTO/ml in drinking water was calculated to maintain the specific activity of tritium at a constant level of 7.4kBq and 74kBq respectively per ml. of body water (supposing that the neonates would also be maintaining the same level through foster mothers). Since, 37kBq (1μCi)/ml. imparts a daily dose of 0.0028 Gy(1.28 rad), therefore, in the experimental animals, the daily dose delivered will be approximately 0.0055 Gy and 0.00055 Gy for 111kBq and 11.1kBq dose levels respectively. The total doses delivered were thus estimated to be approximately 6.55, 10.37, 14.20, 18.02, 21.84 & 25.66 mGy, respectively in the 1,2,3,4,5&6 weeks age group of mice at 11.1kBq dose and 65.5, 103.74, 141.96, 180.18, 218.4 & 256.62mGy at 111kBq dose.

RESULTS

Qualitative studies reveal that in cerebellum, of the three layers viz: Molecular layer, Purkinje cell layer and the Granular cell layer, the most radiosensitive is the Purkinje cell layer. Maximum effect has been observed here on all the studied days at both 11.1 and 111kBq dose levels. The photomicrographs of the cerebellar folia of 1, 3 & 5 weeks age groups of mice are showing the normal arrangement of the cell types (Figs. 1, 2 & 3). However, till 3 weeks of postnatal development, mild damage is evidenced in the cerebellar folia in the form of reduced number of the Purkinje cells, Separation of the molecular layer from the Purkinje cell layer, Pyknotic nuclei in the Purkinje cells, vacuolation in the inter foliar connective tissue, & loss of the Purkinje cells leading into the formation of empty basquets at 11.1kBq dose(Figs. 4&5). Relatively lesser radiopathological changes appear in 4, 5 & 6 weeks old mouse cerebellum(Fig.6). At a higher dose of 111kBq, the quality of the damage remains the same, however, it gets intensified(Figs. 7, 8,& 9). Therefore, a dose dependent behaviour so established clearly reflects that a continuous HTO exposure at a dose level 11.1kBq, though does not render an appreciable damage qualitatively, it gets intensified and causes lasting impairments at a higher dose of 111kBq/ml. drinking water.

DISCUSSION

Tritiated water (HTO) when administered by injection or ingestion replaces the body water and gets uniformly distributed in the body. It forms an endogenous source of beta rays of average energy of 5.6KeV HTO in the body water which is capable of rapid and reversible exchange with -OH, -COOH, -NH2, -NH and -SH groups of organic molecules and biosynthetic incorporation into more stable positions associated with carbon. Tritium which is incorporated into organic tissue constituents is eliminated with different half-lives ranging from less than 2 weeks to more than one year (Thompson and Ballou, 1956). The final position of tritium composed in cells is the most important factor in producing a radiobiological effect. It was reported that 40% of brain hydrogen was derived from body water as compared to 20 to 30% hydrogen in most tissue compounds after a continuous supply of tritium in drinking water. In brain, tritium is reported to be retained in larger amounts for relatively longer period after protracted exposure. The effective half-life of tritium for brain was recorded maximum (44.26 days) as compared to-21d, 28d, 36.7d and 40.13 days for liver, femoral muscles, spleen and kidneys respectively (Ueno and Kawamura, 1975). The brain has been reported as the organ most heavily exposed due to the large specific activity rates of organic tritium and its slow turnover (Bruwaene et al., 1982).

Our results clearly reflect that a dose dependent damage persists. The cerebellum is found more radiovulnerable during the early (1 to 3 weeks) postnatal intervals in comparision to the later intervals (4 to 6 weeks of age). Studies carried out by Shishodia, 1985 reveal marked histopathological changes after a continuous prenatal exposure. The neuroblasts and stem cells present in the brain of late mouse fetuses are very sensitive to radiations and are killed during the course of the exposure. In addition, cell necrosis and pyknosis have also been reported. Our results are in good agreement with these findings. Cellular events in the developing rat cerebellum exposed to X-rays on day 17 of gestation have been studied by Das, 1977. Purkinje cells showed a wavy and tortuous laminar organisation, a feature common in our findings as well. Purkinje cells might play a dominant role in the development of the cerebellum. As the normal migratory behaviour of Purkinje cells may be hindered by irradiation, the abnormal clustering of these cells might lead to folial malformations.

Thus, our observations reflect a cell death induction by low HTO radiation doses in the developing cerebellar cortex. This effect has been dose and dose rate dependent. This is in agreement with the findings on external irradiation by Altman and Nicholson (1971) and Cerda (1982). With regard to the dose dependent damage, the effects linearly increase with dose. With very low doses of HTO radiation, a relatively very small number of cells are killed and the signs of

inact histological architecture has been evident. This may be attributed to the fact that some cell populations (eg. Basket and Stellate cells in the molecular layer of cerebellar cortex) are few in number and their genesis is restricted in time according to a general development time schedule. If such a population gets affected,the number of lethally damaged cells would be much higher which in turn could result in a higher risk for later disfunction. The other consideration refers to DNA injury that does not result in cell death. This injury might be expressed in the surviving cell at the functional level.

Our results are in good agreement with those of Inouye (1979) who exposed pregnant wKA/Hok rats to 100R or 200R X-irradiation on one of gestation days 16 through 21 and examined the cerebellum at 60 days of age. Histologically, Purkinje cells were ectopically scattered in the granule cell layer and white matter of the cerebellar cortex of rats treated on gestation day 20 or 21. Similar types of neuropathological lesions have been noted in our studies as well, but the dose of 111kBq/ml. drinking water imparting 550mrads per day is very low in comparision to 200R as used by Inouye,(1979). In spite of this , a correlation exists in the type of damage incurred at the low dose and the high dose. Moreover, there has been a continuous exposure from 15th day of gestation in our experiment and the resulting injury at the studied intervals may be accounted owing to the cumulative dose. Such findings have also been dealt in the studies carried by Jain and Bhatia (1991 and 1993) on the cerebellum of Swiss albino mouse.

Thus, low doses of tritium beta radiations are equally harmful to the developing animal cerebellum as are deuterons, X- or γ rays, P32, P0210 etc. Hence the tritium induced hazards to the other aspects of physiology, ethology or morphology should not be overlooked.

SIGNIFICANCE AND JUSTIFICATION OF THE INVESTIGATION

The potential for human exposure to beta emitting radionuclides accidentally released from the operation of nuclear reactors and also formed in the upper atmosphere dictates concern for the relationship between radiation dose and the resultant biomedical response. Such data are needed for 1. developing standards that provide for maximum safety and effectiveness in the conduct of nuclear operations and 2. estimating health consequence costs of nuclear operation.

Though, situation need not be alarming with tritiated water, the studies on various parameters have given evidence of radiation damage. Though, according to the NCRP report number 63 (1979a) it appears unlikely that tritium in the form of water in the environment from natural source and from nuclear installation at presently projected levels would ever produce deleterious, detectable effects, however, studies made after 1979 requires a further evaluation. The information obtained from the results of the undertaken investigation will greatly help to the personnels charged with the responsibility for setting maximum permissible levels and other safety standards with regard to tritiated water (HTO).

ACKNOWLEDGEMENT

The authors thank Mrs. Archana Jain for the technical assistance in preparing this manuscript. Partial financial assistance from the Council of Scientific and Industrial Research, New Delhi is gratefully acknowledged.

REFERENCES

Altman, J., and Nicholson, J.L. (1971) Radiat. Res., 46: 476-489.

2. Bhatia, A. L. (1985) Invited lecture, Proc. Symp. Assess Environ. Pollut., 20-22 Dec., 1994, Univ. of Aurangabad, 29-39.

3. Bhatia, A. L. (1987) Indian Rev. Life Sci. 7: 117

4. Bruwaene, R. Van, Gerber, G. B., Kirchman, R. et al. (1982) J. Radiat. Res. 91: 124.
5. Cerda, H. (1982) Cell Pyknosis manuscript, GW I.

6. Das, G. D. (1977) J. Comp. Neurol., 176: 435-452.

7. Fisher, R. A. in Statistical methods for research workers (Oliver and Boyd, London, 1950).

8. Inouye, M. (1979) Teratology, 20: 353-364.

9. Jain, N. and Bhatia, A. L. (1991) Proc. Symp! Radioresistance of human tumors: Mechanisms and prediction. 13-14 July, Montreal, Canada.

10. Jain, N. and Bhatia, A. L. (1993) Proc. Symp. Biological effects of low doses of radiations & related agents. 12-16 Oct., China, p-92.

11. Mallory, F. B. (1944) In: Animal tissue techniques. (Eds: G. L. Humason. W. H. Freeman & Co., San Francisco, 150.

12. NCRP (1979a) In: Tritium in the environment, NCRP report No. 63.

13. Pinson, E. A. and Langham, W. H. (1957) J. Appl. Physiol., 10:108.

14. Powers, M. and Clark, G. (1955) Stain Technology, 30: 83-92.

15. Shishodia, R. (1985) Ph. D thesis submitted to the Univ. of Rajasthan, India.

16. Thompson, R. C. and Ballou, J. E. (1956) IAEA Report HW-42200.

17. Ueno, Y. and Kawamura, K. Health Phys. 29: 413, (1975).



Fig. 1.
Photomicrograph of the cerebellar folia of1 week old control mice showing the normal arrangement of cells. X 10.

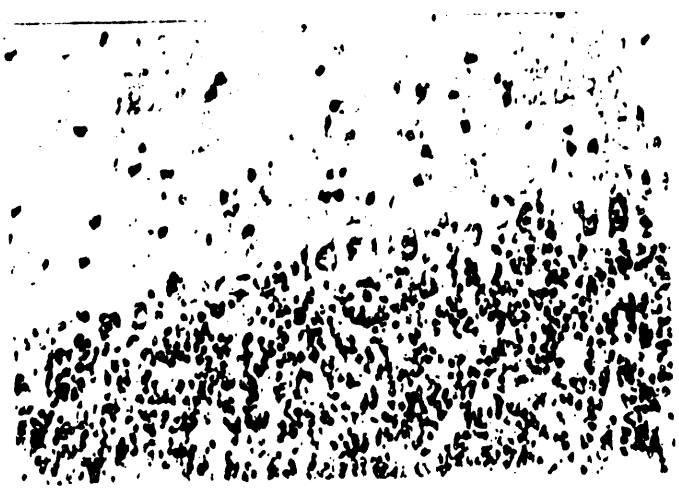


Fig. 2.
Photomicrograph of the cerebellum of 3 week old mice (control) showing distinctive granular, molecular & Purkinje cell layers. X 20

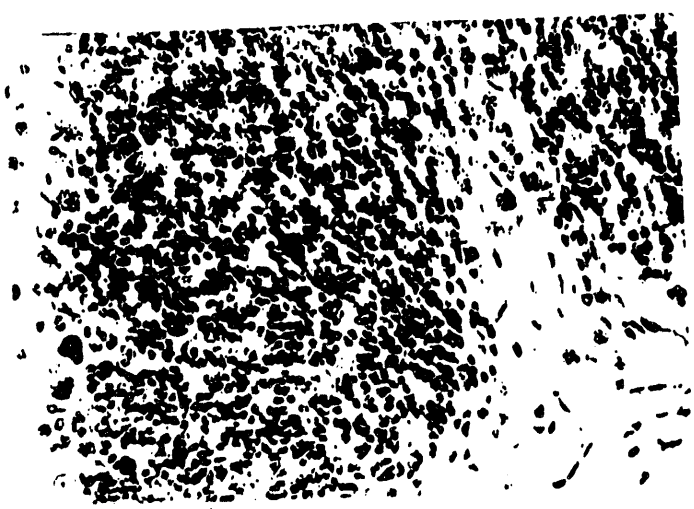


Fig. 3.
Photomicrograph of the cerebellum of 5 week old control mice showing a higher density of granule cells. X 20.



Fig. 4.
Photomicrograph of t
cerebellar folia of eek
old mice continuousl
exposed with 11.1 kB dose
from 15th day of gestation
showing pyknotic nuclei. X 40.

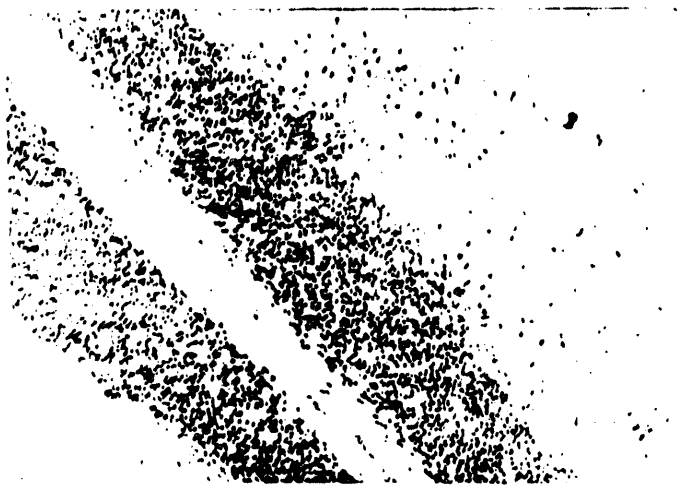


Fig. 5.
Photomicrograph of the
cerebellar folia of 3 week
old mice continuously exposed
with 11.1kBq dose from 15th
day of gestation showing
vacuolation of the inter-
foliar connective tissue. X 10



Fig 6.
Photomicrograph of the
cerebellar folia of 5 week
old mice continuously exposed
with11.1 KBq dose from 15th
day of gestation showing the
loss of Purkinje cel_ only at
1 or 2 places. X 10.

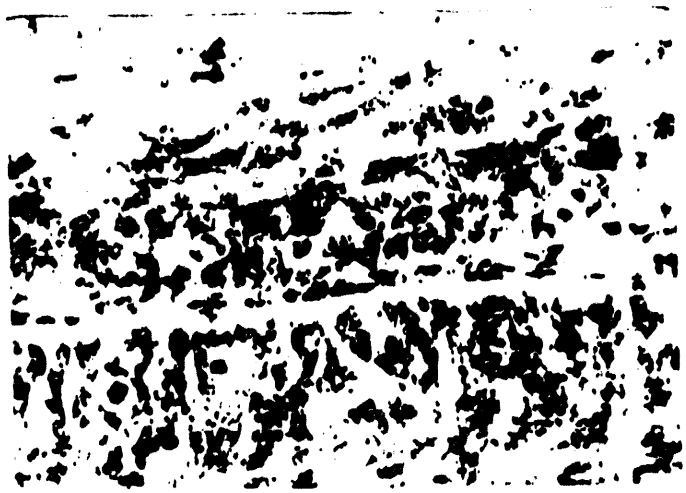


Fig. 7.
Photomicrograph of the cerebellar folia of 1 week old mice continuously exposed to 111kBq dose from 15th day of gestation showing pyknotic nuclei & degeneration of the tissue. X 40.



Fig. 8.
Photomicrograph of the cerebellar folia of 3 week old mice continuously exposed to 111kBq dose from 15th day of gestation showing degenera ting Purkinje cells with extensive vacuolation in the interfoliar connective tissue. X 20.

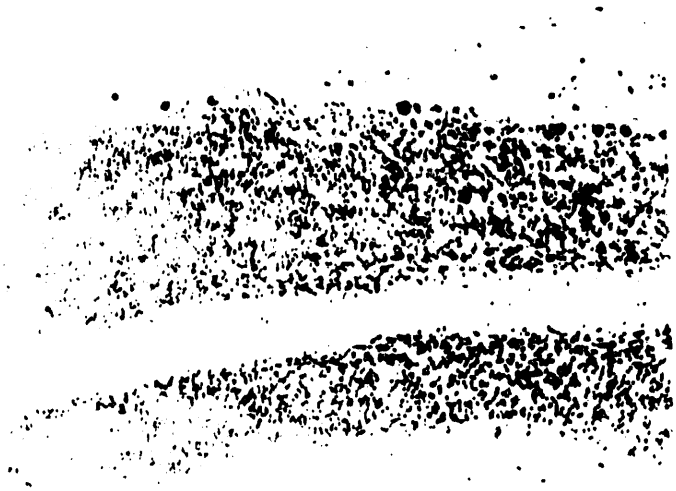


Fig. 9.
Photomicrograph of the cerebellar folia of 5 week old mice continuously exposed to 111kBq dose from 15th day of gestation showing empty basquets instead of the Purkinje cells. X 10.

SESSION VI.
Environmental

Richard E. Swaja,
Chairman

EXTERNAL EXPOSURE TO ARBITRARY DISTRIBUTIONS OF RADIONUCLIDES IN SOIL

Jeffrey C. Ryman and Keith F. Eckerman (Oak Ridge National Laboratory)

Dose coefficients for external exposure relate the doses to organs and tissues of the body to the concentrations of radionuclides in environmental media. The time-independent dose coefficient for external exposure, h_T represents the dose to tissue T of the body per unit time-integrated exposure, expressed in terms of the *time-integrated concentration of the radionuclide*. During the preparation of *Federal Guidance Report No. 12*, dose coefficients were computed for external exposure to photons and electrons emitted by radionuclides uniformly distributed in air, water, and soil. The methodology used for *Federal Guidance Report No. 12* has been extended for radionuclide sources in soil to include both an exponential distribution and an arbitrary distribution as a function of depth, for sources as deep as four mean free paths below the surface of the soil.

The uncollided and scattered angular fluences from unit isotropic plane sources of photons were computed as a function of energy, angle, and height above the air-ground interface using a specialized one-dimensional discrete ordinates transport code. These basic radiation field data were developed for twelve monoenergetic sources from 0.01 to 5.0 MeV and for six source depths from zero to four mean free paths below the air-ground interface. From these fluence data, angular current sources were constructed on the surface of a cylinder surrounding the adult Cristy phantom. The ALGAMP Monte Carlo photon transport code was used to calculate organ doses from the equivalent surface source for each of the 72 combinations of source energy and plane source depth. These doses are the organ dose coefficients for the original planar sources.

Skin dose coefficients for a series of monoenergetic electron emissions were computed with the DOSFACTER code of Kocher, which uses the electron scaled point kernel data of Berger. The depth of a planar source in soil was converted to an equivalent air thickness. Calculations were performed for planar sources ranging from the surface to a depth beyond the range of the electrons.

A program has been developed for MS-DOS personal computers which can generate dose coefficients for arbitrary distributions of radionuclides as a function of depth below the air-ground interface, using superposition of the dose coefficients for the monoenergetic planar sources. Coefficients can be computed for any of the 825 radionuclides having decay data in Publication 38 of the International Commission on Radiological Protection (ICRP). Uniform and exponentially-distributed analytical source distributions are also available between any two depth boundaries. Coefficients are available both in SI and traditional units for individual organ, for effective dose equivalent as formulated in ICRP Publication 26, and for effective dose as formulated in ICRP Publication 60.

EVALUATION OF NEW AND CONVENTIONAL THERMOLUMINESCENT PHOSPHORS FOR ENVIRONMENTAL MONITORING USING AUTOMATED THERMOLUMINESCENT DOSIMETER READERS

B. A. Rathbone, A. W. Endres, and E. J. Antonio
Pacific Northwest Laboratory, Richland, Washington 99352

In recent years, there has been considerable interest in a new generation of super-sensitive thermoluminescent (TL) phosphors for potential use in routine personnel and environmental monitoring (Akselrod et al. 1993; Bacci et al. 1993; Horowitz 1993; Prokic and Botter-Jensen 1993; Zha et al. 1993). Two of these phosphors, α-Al_2O_3:C and LiF:Mg,Cu,P, are evaluated in this paper for selected characteristics relevant to environmental monitoring, along with two conventional phosphors widely used in environmental monitoring, LiF:Mg,Ti and CaF_2:Dy. The characteristics evaluated are light-induced fading, light-induced background, linearity and variability at low dose, and the minimum measurable dose. These characteristics were determined using an automated commercial dosimetry system (Harshaw System 8800) and routine processing protocols. Annealing and readout protocols for each phosphor were optimized for use in a large-scale environmental monitoring program.

The use of TL phosphors in the Harshaw system requires mounting of the phosphors on a substrate such as polytetrafluoroethylene (PTFE) or polyimide (e.g., Kapton) film and suspension of the film in a rigid card structure with bar code label. The mounting of phosphors in cards poses limits to the oven-annealing and readout temperatures that may be applied. The inability to clear high-temperature traps in LiF:Mg,Ti, in LiF:Mg,Cu,P, and in CaF_2:Dy can result in significant residual. The inability to clear high-temperature traps in α-Al_2O_3:C can result in significant light-induced background in chips with large dose histories (Akselrod et al. 1993). The manual handling of cards required during loading and unloading of dosimeter holders and the loading and unloading of the reader introduces the potential for contamination and requires some exposure to light. Significant light-induced fading has been reported for Al_2O_3:C (Mosovitch et al. 1993; Musk 1993).

MATERIALS AND METHODS

All thermoluminescent dosimeter (TLD) cards used in this study were manufactured by Bicron for use in the Harshaw Model 8800 TLD reader. The α-Al_2O_3:C TL phosphor used in these cards is manufactured as single crystal chips by Urals Polytechnical Institute, Ekaterinburg, Russia, and marketed by Bicron under the product name TLD 500. For convenience, this phosphor will be referred to as TLD 500. The LiF:Mg,Cu,P phosphor used in these cards is manufactured as hot-pressed chips by Solid Dosimetric and Method Laboratory, Beijing, Peoples Republic of China, under the product name GR 207 and marketed by Bicron as TLD 700H. For convenience, this phosphor will be referred to as TLD 700H. Both the TLD 700H phosphor and TLD 700 have a Li^6 abundance of 0.007%. The CaF_2:Dy and LiF:Mg,Ti phosphors used in these cards are manufactured and marketed by Bicron under the product names TLD 200 and TLD 700, respectively, and will be referred to by these names for convenience.

The TLD 200 and TLD 700 chips (3 mm x 3 mm x 0.9 mm) were mounted between two layers of PTFE film to form TL elements on Bicron's standard type 8807 Environmental TLD card, having two TLD 200 and two TLD 700 elements per card. The TLD 500 chips (5 mm x 0.5 mm) were adhesively bonded to Kapton substrate to form TL elements, with four elements mounted per card. The TLD 700H chips (3 mm x 3 mm x 0.5 mm) were also adhesively bonded to Kapton to form TL elements with four elements per card. Thus, the TLD 500 and TLD 700H phosphor types were represented by their own card types.

The readout equipment used was the Harshaw Model 8800 TLD reader. This is a large-capacity automated reader that uses heated nitrogen gas to heat the chips according to a user-programmable linear time-temperature profile (TTP).

The anneal and readout protocols used for all experiments described in this paper were designed to optimize dosimetry performance while maintaining reasonable throughput and handling convenience in a large-scale program. For each phosphor type, the same anneal and readout protocols were used for all experiments. The time-temperature profiles used for each phosphor type are shown in Table 1. For the TLD 200 and TLD 700 chips, separate TTPs were used for annealing and for dosimetric readout. For these phosphors, the anneal procedure consisted of readout under the anneal TTP followed by a 16-hour oven anneal at 80°C. Oven annealing reduces the traps available for peaks 2 and 3 in TLD 700, thereby improving fade characteristics but has no effect on the TLD 200 chips, which are on the same card. For TLD 500, annealing consisted of one reading using the TTP for dosimetric readout, with no oven anneal. For TLD 700H, annealing consisted of two readings with the dosimetric TTP and no oven anneal. This TTP was chosen after our own studies on sensitivity loss with reuse as a function of maximum readout temperature showed no significant loss of sensitivity with up to 100 readouts at 270°C. This readout temperature gives a residual of less than 1%, which was considered adequate for environmental dosimetry. These results are in agreement with those of other investigators (Oster et al. 1993).

The TLD 500 and TLD 700H elements were calibrated using a ^{90}Sr card irradiator. The TLD 200 and TLD 700 elements were calibrated in air using a ^{60}Co source. The calibration process provides an element correction coefficient (ECC) for each chip that normalizes its sensitivity to the mean sensitivity of the population of calibration chips in the same position. These ECCs were applied to all readings.

For each experiment, the reader was calibrated to provide reader calibration factors (RCFs) for each TTP used. These RCFs were based on the response of calibration cards exposed in the ^{90}Sr card irradiator. This irradiator is calibrated to provide dose in generic units (gU), where one generic unit is approximately equivalent to one millirad or 10 μGy. The RCFs based on this irradiator, therefore, have units of nC/gU. These RCFs were applied by the reader to all card readings.

TABLE 1. Time-Temperature Profiles

TLD Phosphor Type	TLD 200	TLD 200 (anneal)	TLD 700	TLD 700 (anneal)	TLD 500	TLD 700H
Preheat temperature (°C)	160	50	50	50	50	160
Preheat time (sec)	25	0	0	0	0	5
Temperature rate (°C/sec)	20	20	10	10	5	20
Maximum temperature (°C)	300	300	300	300	300	270
Acquire time (sec)	20	40	33.3	33.3	60	16.6
Anneal temperature (°C)	0	0	0	300	0	0
Anneal time (sec)	0	0	0	6	0	0

Light-Induced Fading

White, yellow, and red lighting environments were constructed in the laboratory to produce uniform lighting at a level of 300 lux on designated work surfaces. The white lighting was provided by standard 40-watt warm white fluorescent tubes; the yellow lighting was provided by General Electric F40GO gold fluorescent tubes; the red lighting was provided by incandescent red bulbs. All lighting was filtered by transparent ultraviolet (UV) blocking film. Cards containing each chip type were annealed, then exposed to 100 gU (1 mGy) using a ^{90}Sr card irradiator. Five cards of each type were exposed for durations of 1, 3, 10, 30, 100, and 300 minutes to the warm white source. Five cards of each type were also exposed to the yellow and red light for the same durations. The same day, cards of each type were read together along with a set of controls of each card type exposed to the ^{90}Sr source but not to light.

Light-Induced Background

Groups of five TLD 500 cards were annealed, then exposed to red, yellow, and warm white light at an illumination level of 300 lux for durations of 1, 3, 10, 30, 100, and 300 minutes and read the same day with unexposed controls. To the author's knowledge, each of these chips had a cumulative radiation dose history of 1 Gy or less before performing this experiment. Throughout each of these light experiments, great care was taken to avoid unnecessary exposure to light.

Linearity and Variability at Low Dose

After annealing, cards of each type were loaded into Harshaw 8807 Environmental Dosimeter holders to minimize exposure to light. The holders used for the TLD 500 cards and for the TLD 700H cards provided 80 mg/cm^2 of ABS plastic filtration. The holders used for the 8807 card (TLD 200 and TLD 700) provided 422 mg/cm^2 Ta + 58 mg/cm^2 Pb filtration over front and back sides of the TLD 200 elements in addition to the 80 mg/cm^2 ABS over all elements. Groups containing 10 dosimeters of each type (8807, TLD 500, TLD 700H) were exposed to 0.1, 0.3, 1.0, 3.0, 10.0, 30.0, and 100.0 mR in air from a ^{137}Cs source. The estimated error in the applied exposure in all cases was less than 5%. A group containing 10 dosimeters of each type was designated as a control and accompanied the experimental dosimeters to and from the irradiation facility. Card annealing was performed the day before irradiations and readout was conducted on the same day as the irradiations.

Minimum Measurable Dose

The standard deviation of control dosimeters in the linearity test was used to calculate the minimum measurable dose for each phosphor type.

RESULTS AND DISCUSSION

Light-Induced Fading

The results of the light-induced fading experiments are summarized in Table 2. All readings were obtained with ECCs and RCFs (nC/gU) applied. To obtain the fade factor, the mean result for each chip position in an exposure group was normalized to the mean of exposed control chips in the same position. The fade factors for all chip positions were averaged to obtain the single fade factor shown in Table 2. Thus, for TLD 500 and TLD 700H, the fade factor was based on 20 data points per exposure condition. For TLD 200 and TLD 700, the average was based on 10 data points per exposure condition. The relative standard deviation was calculated for each chip position and the average reported in Table 2. In general, the results were as expected. The only phosphor to show significant fading was the TLD 500. The data for this phosphor are plotted in Figure 1. Other investigators have reported strong light-induced fading in TLD 500 for white and yellow light. It is interesting to note the superior performance of red lighting at the same level of illumination as the other sources. Other investigators have reported significant UV light-induced fading in TLD 200. The fact that none was observed in the present experiments attests to the effectiveness of the UV filter employed. Minimal sensitivity to visible light has been reported in the literature for both TLD 700 and TLD 700H, which is consistent with the data in Table 2.

TABLE 2. Light-Induced Fading

Time, min	Red		Yellow		White	
	Avg	%Std	Avg	%Std	Avg	%Std
			TLD 200			
1	0.99	2.8	1.00	2.7	1.00	2.5
3	0.99	1.9	1.01	3.5	0.99	1.5
10	1.01	2.3	1.00	2.2	1.00	2.0
30	0.99	3.2	0.99	2.0	0.98	2.5
100	1.00	1.1	1.01	2.2	1.00	1.6
300	1.00	1.9	1.00	2.1	1.01	1.3
			TLD 700			
1	1.00	1.2	1.00	1.3	0.99	1.3
3	0.99	1.0	1.00	1.1	1.00	1.4
10	1.00	1.0	1.00	0.6	0.99	1.8
30	0.99	1.4	1.00	1.2	1.00	1.6
100	1.00	1.3	1.00	2.3	1.00	1.7
300	1.00	0.9	1.03	2.3	1.01	1.7
			TLD 500			
1	1.01	0.6	1.00	0.6	1.00	0.6
3	1.00	0.4	1.00	0.5	1.00	1.5
10	1.00	0.5	0.98	0.5	0.97	0.9
30	0.99	0.8	0.94	1.4	0.91	2.6
100	0.93	1.7	0.82	4.0	0.73	6.2
300	0.80	5.1	0.58	12.1	0.42	25.6
			TLD 700H			
1	0.99	1.3	1.01	1.3	0.98	1.8
3	0.98	2.0	0.99	2.4	0.98	2.8
10	0.98	1.9	0.99	2.4	0.98	1.7
30	0.99	1.8	0.99	2.0	0.99	2.3
100	0.99	1.9	0.97	2.6	0.99	2.9
300	1.00	2.4	0.96	2.0	0.98	1.3

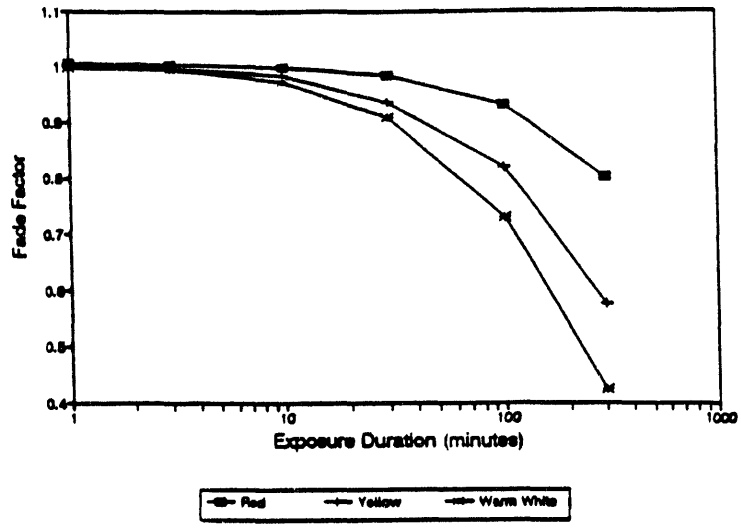


FIGURE 1. Light-Induced Fading in TLD 500, Illumination = 300 lux

Light-Induced Background

The cards were read on a reader previously calibrated with cards exposed to 100 gU with the ^{90}Sr card irradiator. The ECCs and RCFs were applied to all chip readings. For each exposure group (five cards) the mean and standard deviation for each chip position were calculated and the results averaged to obtain a single mean and standard deviation value for the group. The results are shown in Table 3 and Figure 2. Even though the cards had a prior dose history of less than 0.01 Gy, a small background effect is evident. It is believed that the light-induced background in TLD 500 results from light-transferred sensitivity from higher temperature traps and that the background effect will be greater with larger cumulative doses on the chip.

TABLE 3. Light-Induced Background in TLD 500 at 300 lux, μGy

Exposure, min	Red		Yellow		White	
	Avg	%Std	Avg	%Std	Avg	%Std
0	2.90	0.27	2.90	0.27	2.90	0.27
1	3.24	0.29	2.90	0.19	3.09	0.36
3	3.17	0.53	3.00	0.27	3.07	0.28
10	3.20	0.32	3.04	0.43	3.78	0.86
30	2.94	0.38	3.05	0.38	4.48	1.38
100	3.27	0.38	3.28	0.43	5.50	2.13
300	3.43	0.33	3.78	0.64	9.25	4.27

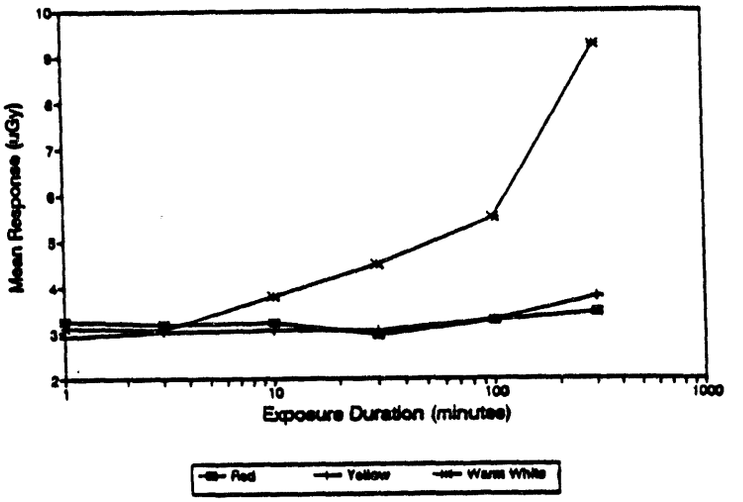


FIGURE 2. Light-Induced Background in TLD 500, Illumination = 300 lux

Linearity and Variability at Low Dose

Cards were read on a reader calibrated using the ^{90}Sr irradiator, and ECCs and RCFs were applied to all chip readings by the reader. For each chip type, the zero dose reading from the set of control dosimeters was subtracted from the reading of each experimental dosimeter and the net reading adjusted by a one-point calibration factor (gU/mR) derived from the response of the dosimeters exposed to 100 mR. For each group, the mean and standard deviation of these net adjusted readings were calculated from all chips in an exposure group without regard to chip position to obtain a single value for the exposure level and chip types. The results are shown in Tables 4 and 5. Linear regression analysis was performed on the mean adjusted readings in Table 4; the results are shown in Table 6. These results show excellent linearity for all phosphor types. The relative standard deviation in percent as a function of exposure is plotted in Figure 3. The standard deviation values in Table 5 and Figure 3 are for <u>net</u> responses. It should be noted that the TLD 500 and TLD 700H chips were calibrated using a ^{90}Sr card irradiator having close geometry. Because of the field gradient, and the nonpenetrating nature of beta radiation, small variations in chip positioning and chip thickness on the card can result in measurable random error in the ECC. This error is evident in the fact that the standard deviation for TLD 500 is on the order of 0.5% (Table 2) when irradiated with the ^{90}Sr irradiator used for ECC generation. The true variability for TLD 500 at exposures above 1 mR is probably less than 1%.

TABLE 4. Mean Adjusted Readings, mR

Exposure Level, mR	TLD 200	TLD 700	TLD 500	TLD 700H
0.1	0.099	0.096	0.105	0.100
0.3	0.289	0.246	0.299	0.298
1.0	0.975	1.002	1.004	1.005
3.0	2.957	2.972	2.997	2.943
10.0	9.879	9.979	9.978	10.032
30.0	29.929	30.031	29.894	30.464
100.0	100.000	100.000	100.000	100.000

TABLE 5. Percent Coefficient of Variation for Adjusted Readings

Exposure Level, mR	TLD 200	TLD 700	TLD 500	TLD 700H
0.1	17.801	307.348	20.622	111.102
0.3	6.110	33.337	6.659	37.820
1.0	1.968	16.983	3.202	16.962
3.0	2.336	5.477	2.678	4.328
10.0	2.025	1.371	2.055	3.148
30.0	1.510	0.927	1.754	2.576
100.0	0.605	1.274	1.104	2.008

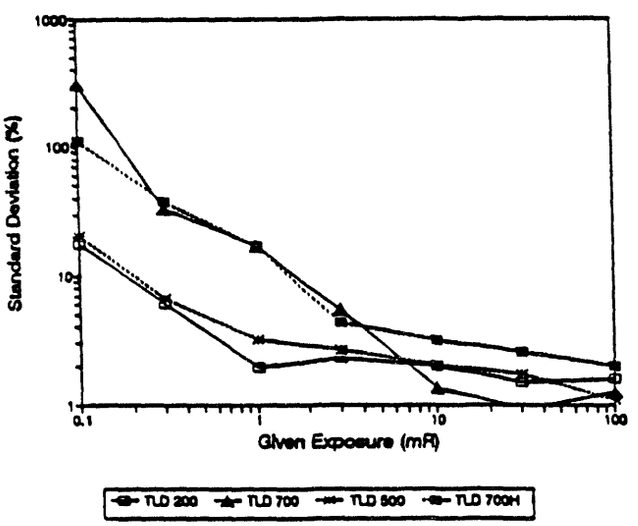


FIGURE 3. Variability at Low Dose for TLD 200, TLD 700, TLD 500, and TLD 700H, Net Response

TABLE 6. Linear Regression Data

	TLD 200	TLD 700	TLD 500	TLD 700H
Constant	-0.04468	-0.01586	-0.01515	0.050512
Standard Error of Y Est.	0.047256	0.027233	0.043896	0.194348
R^2	0.999999	1.000000	0.999999	0.999977
Number of Observations	7	7	7	7
Degrees of Freedom	5	5	5	5
X Coefficients	1.000267	1.000264	0.999888	1.000617
Standard Error of Coefficient	0.000527	0.000304	0.00049	0.002169

Minimum Measurable Dose

The standard deviation of unexposed control dosimeter readings expressed in mR was used to calculate the minimum measurable dose (MMD) for each phosphor type. Using the relationship MMD = $3\sigma_B$, where σ_B is the standard deviation of the zero dose reading, the MMDs were calculated for Table 7. For the anneal and readout protocols used, the sensitivity of each phosphor relative to 15-mil TLD 700 (3 mm x 3 mm x 0.4 mm) is shown in Table 7. These sensitivities are based on the phosphor response to ^{137}Cs gamma radiation.

TABLE 7. Sensitivity and Minimum Dose

Phosphor Type	Dimensions, mm	Reader Calibration Factor, nC/mR	Relative Sensitivity	Minimum Measurable Dose, mR
TLD 200	3 x 3 x 0.9	8.0	40	0.051
TLD 700	3 x 3 x 0.9	0.45	2.25	0.645
TLD 500	5 x 0.5	9.8	50	0.063
TLD 700H	3 x 3 x 0.5	1.5	7.5	0.306

CONCLUSIONS

All phosphors exhibited excellent linearity down to 0.1 mR. All phosphors exhibited good reproducibility above 10 mR while TLD 200 and TLD 500 appear to be better choices for exposures below 10 mR (monthly or weekly monitoring). Only TLD 500 showed significant light-induced background or fading under laboratory lighting. Special lighting and handling will be

necessary for use of this phosphor in a routine program. Yellow and red lighting appear to offer adequate handling time for loading and unloading of dosimeter holders and TLD readers with the TLD 500 card.

ACKNOWLEDGMENTS

Pacific Northwest Laboratory is operated for the U.S. Department of Energy by Battelle Memorial Institute under Contract DE-AC06-76RLO 1830.

REFERENCES

Akselrod, M. S., V. S. Kortov, and E. A. Gorelova. 1993. "Preparation and Properties of α-Al_2O_3:C." Radiation Protection Dosimetry 47(1-4):159-164.

Bacci, C., L. D'Angelo, C. Furetta, and S. Giancola. 1993. "Comprehensive Study on LiF:Cu,Mg,P (GR-200 A)." Radiation Protection Dosimetry 47(1-4):215-218.

Horowitz, Y. S. 1993. "LiF:Mg,Ti Versus LiF:Mg,Cu,P: The Competition Heats Up." Radiation Protection Dosimetry 47(1-4):135-141.

Moscovitch, M., R. A. Tawil, and M. Svinkin. 1993. "Light Induced Fading in α-Al_2O_3:C." Radiation Protection Dosimetry 47(1-4):251-253.

Musk, J. H. 1993. "Time Dependent and Light-Induced Fading in Victoreen Model 2600-80 Aluminum Oxide Thermoluminescence Dosemeters." Radiation Protection Dosimetry 47(1-4):247-249.

Oster, L., Y. S. Horowitz, and A. Horowitz. 1993. "Glow Curve Readout of LiF:Mg,Cu,P (GR-200) Chips at Maximum Temperatures Between 240°C and 280°C: Elimination of the Residual Signal." Radiation Protection Dosimetry 49(4):407-411.

Prokic, M., and L. Botter-Jensen. 1993. "Comparison of Main Thermoluminescent Properties of Some TL Dosemeters." Radiation Protection Dosimetry 47(1-4):195-199.

Zha, Z., S. Wang, W. Shen, J. Zhu, and G. Cai. 1993. "Preparation and Characteristics of LiF:Mg,Cu,P Thermoluminescent Material." Radiation Protection Dosimetry 47(1-4):111-118.

HARSHAW/BICRON 8807 ENVIRONMENTAL DOSEMETER - IMPLEMENTATION ISSUES

Brian J. Lawson, Mark Moleski, Robert Karandy, Charles R. Phillips, Robert Champagne, Richard J. Winslow

(Martin Marietta Corporation - Knolls Atomic Power Laboratory, Inc., PO Box 1072, Schenectady, NY 12301 USA)

This paper provides details regarding implementation of the Harshaw/Bicron 8807 dosemeter for field use in an environmental monitoring program. The paper discusses special precautions which must be taken to ensure accuracy and reproducibility. Specifically, light sensitivity should be eliminated and temperature dependent fade accounted for. Seasonal bias of +15% to +50% can result if this is not done.

INTRODUCTION

The Harshaw 8807 environmental dosemeter card contains two (2) LiF (TLD-100) and two (2) CaF elements (TLD-200) (figure 1). Because of fade differences between LiF and CaF, the LiF elements are most useful in long term environmental monitoring situations (e.g. 90 day field cycles), while the CaF elements are most useful for short monitoring periods. The LiF elements are used for the generation of routine environmental monitoring data. The active elements are encased in teflon, and then sandwiched between two aluminum sheets as part of the dosemeter card manufacturing process. A barcode label, which is both human and barcode reader readable, is applied to the card (figure 2).

A dosemeter card is placed inside a dosemeter case which provides appropriate radiation filtration of the dosemeter card elements and protection from the weather when on station. The standard 8807 dosemeter case supplied by Harshaw provides a clear plastic window so the barcode label of the dosemeter card inside the dosemeter case can be scanned.

Harshaw 8807 dosemeter cards are processed through Harshaw 8800 thermoluminescent dosemeter readers. The 8800 reader is a hot nitrogen gas, non-contact reader. The reader is operated by a personal computer running Harshaw's TLD-REMS data acquisition software. The computer stores time-light output (i.e. glow curves) and time-temperature profiles for each dosemeter element processed. The time-light data is corrected for element manufacturing differences via element correction coefficients (ecc) and for a reader calibration factor (RCF). Dose is calculated by processing a time-light data file through a dose algorithm on the computer. The dose algorithm permits background subtraction and application of fade corrections, and converts the corrected light output to NIST traceable dose results.

The dosimetry system works well for Harshaw 8806 type neutron dosemeters and the 8802 family of beta-gamma-neutron dosemeters. In order to implement the 8807 environmental dosemeter, two additional factors must be compensated for in order to ensure accurate and reproducible results; teflon light sensitivity and temperature dependent LiF fading.

TEFLON LIGHT SENSITIVITY AND THE 8807 DOSEMETER CASE

Harshaw/Bicron has determined that teflon used in dosemeter card manufacturing contains traces of chemicals used in the teflon manufacturing process. These chemicals are photosensitive. If cards are exposed to light, they will read artificially high because of light induced signal. This light induced photoluminescence is measured as radiation induced photoluminescence when a card is processed through a dosemeter reader. The effect can be pronounced

(526 μGy [60 mR], (figure 3) if the teflon is not pre-treated by heating prior to use in manufacturing. For heat treated teflon, the effect decreases to a constant value of about 18-26 μGy [2-3 mR] equivalent after processing through a reader several times (figure 4).

It is typical for dosimetry programs to subtract environmental radiation from personnel monitoring results. Facilities using the 8806 and 8802 family of Harshaw dosemeters for personnel monitoring end up eliminating the teflon effect by subtracting background dosemeter results. The subtracted values include background radiation and light induced signal. This leaves only operational radiation induced signal remaining. There is no background subtraction process for environmental dosimetry programs. Any light induced signal will be reported as measured radiation. Therefore, it is essential that the 8807 dosemeter card be protected from light. Dosemeter case design is crucial to achieving this.

The original 8807 dosemeter case delivered with the dosimetry system is shown in figure 5. Note the clear plastic window permitting the barcode on the dosemeter card to be scanned. Unfortunately, the clear window also provided a direct pathway for light to enter the dosemeter case and generate light induced signal. The 8807 dosemeter cases with clear windows were replaced with solid black 8807 dosemeter cases (figure 6).

Paired comparison testing (difference in means) was conducted to determine differences in light induced signal for the clear window case (Group E), the clear window case with the dosemeter wrapped in a single layer of aluminum foil (Group F), the all black case (Group G), and the all black dosemeter case with the dosemeter wrapped in a single layer of aluminum foil (Group H). Twelve dosemeters of each type were exposed to strong light for 140 hours. Then the dosemeter cards were removed and processed through the reader. Results (in generic units (gU)) are shown in Table 1. Statistical analyses of the mean differences are provided in Table 2.

The results of these comparisons clearly indicate additional protection from light is required beyond the dosemeter case design capability. The original case design with foil wrapped dosemeter (Group F) and the new case design with foil wrapped dosemeter (Group H) do not differ. This is as expected. Surprisingly, the old case (Group E) and the new case (Group G) with no foil wrapping on the dosemeter card did not differ significantly either. Significant differences were noted for the old and new design with and without foil wrapping.

An additional study was conducted to verify the observations noted above. Thirty solid black dosemeter cases were loaded with ASA50 film in a dark room. These cases were then placed in the environment in direct sun for two hours. Film packs, as controls, were loaded with the same type film and placed next to the dosemeters in the environment. The dosemeter cases and film packs

were then retrieved. The film was removed in a dark room and developed. The film packs indicated no exposure to light. All thirty films in the dosemeter cases indicated significant exposure to light. The study was repeated using three foil wrapped films in solid black dosemeter cases and a non-foil wrapped film as a control. The three foil wrapped films indicated no exposure to light. The film which was not foil wrapped indicated significant exposure to light.

The conclusions are:

1.)The dosemeter case design does not preclude light from entering. Therefore additional protection of the dosemeter from light is required.

2.)Reproducibility is better when cards are foil wrapped and the light effect is eliminated.

TEMPERATURE DEPENDENT LiF FADE

LiF fade is temperature dependent. Figure 7 shows a typical glow curve for LiF shortly after irradiation. Note that five (5) distinct peaks are visible. The peak number, anneal temperature and half life are given in Table 3.

Environmental dosemeters see a wide variation in temperature. In the Northeastern United States, temperatures can range between -34.4 °C to 37.8 °C during the year. A winter glow curve (figure 8) looks very different from a summer glow curve (figure 9). Placing dosemeters in the environment in winter conditions tends to "freeze" signal in the low temperature traps. Conversely, summer temperatures tend to anneal peaks 1,2 and 3. Signal for a given amount of radiation will vary depending on whether it is a winter glow curve (i.e. more signal) or a summer glow curve (i.e. less signal). The effect of this difference was measured by conducting the following experiment.

Temperature Dependent LiF Fade Test

During the fourth quarter of 1992, three insulated containers were set up in one location to provide a common environmental radiation level. One container simulated summer conditions by the addition of a low wattage light bulb for a heat source. One container was not heated or cooled, but allowed to follow ambient temperatures. The third container was kept cold by the regular addition of ice packs. Materials used in any specific container for temperature control were added to the other containers to ensure all environmental factors were kept identical. For example, uncooled ice packs were kept in the "hot" and "ambient" box, and sections of wire and a light bulb (not turned on) and socket were placed in the "cold" box and the ambient box. Dosemeters were wrapped in household aluminum foil, placed inside solid black dosemeter cases, and then placed inside each insulated container. The three containers were rotated

in position every 15 days to ensure uniform radiation in the environment.

Temperatures in the containers were monitored during each 15 day test period. The minimum temperature recorded in the cold box during the 90 day test was -13 °C. The maximum temperature recorded in the hot box was 38.4 °C. Table 4 provides average minimum and maximum temperatures recorded for each 15 day period.

Dosemeters were withdrawn from each container over a period of about eight days, two at a time. The dosemeters were then read sequentially within a 30 minute period. This permitted the analysis of the effect of time between removal from the environment and read time. The results of the study are shown in Table 5.

Table 5 indicates that if a dosimetrist uses a room temperature calibration, environmental monitoring results will differ by about 35 μGy [4 mR] between the summer and winter due solely to temperature dependent LiF fade. Further, the results indicate there is no advantage to waiting a period of time between removing the dosemeters from the environment and reading them. The results will be essentially the same.

In order to get the correct environmental dose result, the dosimetrist must either:

1.) calibrate the reader using calibration dosemeters stored under the same environmental conditions as being measured, or

2.) calibrate the reader using room temperature calibration dosemeters and then apply an environmental correction factor in the Harshaw 8807 dose algorithm.

For either 1 or 2 above, dosemeters are placed in the field and retrieved mid-cycle (i.e. 45 days into a 90 day field cycle). The dosemeters are then exposed to a known local source and immediately returned to the field. At the end of the field cycle they are processed through the reader. We have found that option 2 provides us with the most flexibility. (We can read dosemeters stored in the environment plus dosemeters stored in laboratory conditions.)

Environmental correction factors will actually exceed 1.0 for certain seasons (winter), and be less than 1.0 (summer) for others. The calculated factor is entered in the Harshaw 8807 environmental dosemeter algorithm by selecting "FADE" from the menu selection, followed by "KNOWN". The value is then entered. This value is applied to all dosemeters in the group (i.e. data) file processed through the algorithm.

INDEPENDENT TESTING

The 10th International Intercomparison Environmental Dosemeter Study (IIEDS) provided an independent test of the implementation of the

Harshaw 8807 environmental dosimetry system. All dosemeters were submitted with the dosemeter cards wrapped in a single layer of aluminum foil and inserted in solid black 8807 dosemeter cases. The study included low and high dose gamma laboratory irradiations and dosemeters placed in the environment in Idaho winter conditions for about 100 days. Table 6 provides the results of the study for the dosemeters submitted.

The results of this study were calculated using the local winter calibration. Idaho and upstate New York winter temperatures are similar. This study occurred prior to the development of laboratory calibrations and the measurement of environmental correction factors. As can be seen, the field results are excellent because the calibration mimics the field conditions. On the other hand, the laboratory stored dosemeters came out low because the calibration dosemeters contained peaks 2 and 3, and the laboratory dosemeters did not. This study convinced us of the need to be able to read both types of dosemeters (field and laboratory), and apply specific environmental correction factors as needed in the dose algorithm.

CONCLUSION

The Harshaw 8807 environmental dosimetry system can be used to accurately measure environmental radiation doses. Additional protection from light for the dosemeter card must be provided and temperature dependent LiF fade must be compensated for to ensure accurate results. Failure to account for these two effects can lead to monitoring differences of between 26 to 70 μGy [3 to 8 mR], depending on the season of the year. Assuming a true environmental radiation level of about 158 μGy [18 mR], total bias could range between +15 to nearly +50%.

Figure 1

Harshaw/Bicron 8807 Dosemeter Card/Case Configuration

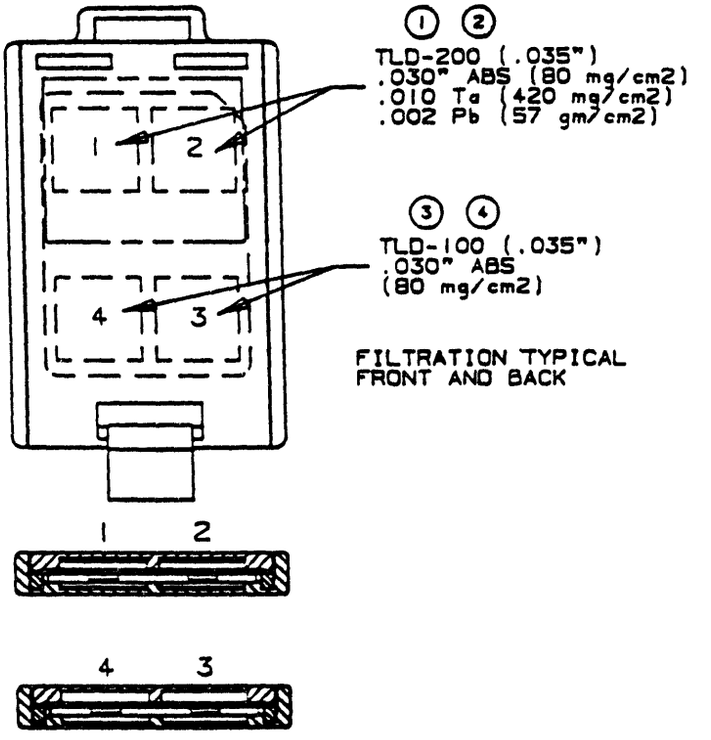


Figure 2

Harshaw/Bicron 8807 Dosemeter Card

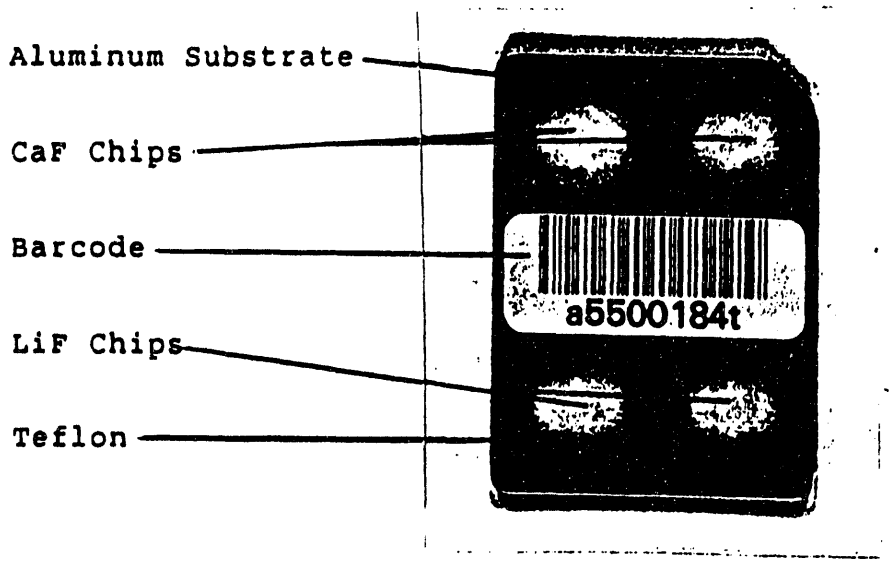


Figure 3

Non-Heat Treated Teflon Lots - Light Sensitivity

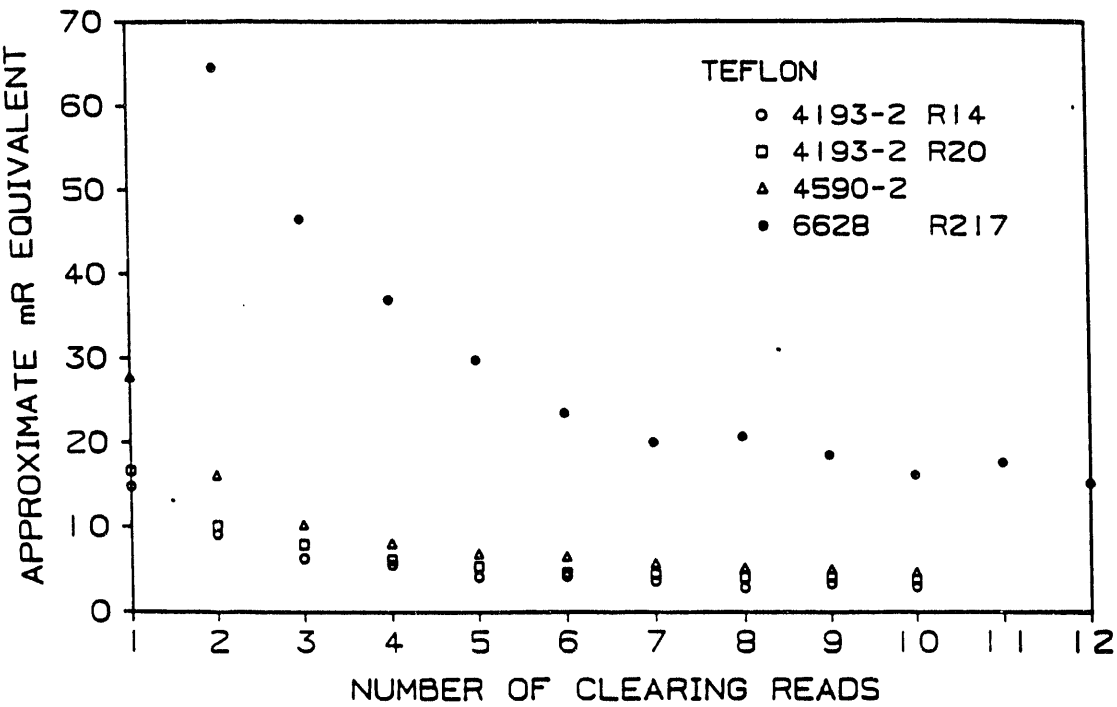


Figure 4

Comparison of Heat Treated vs. Non-Heat Treated Teflon Lots

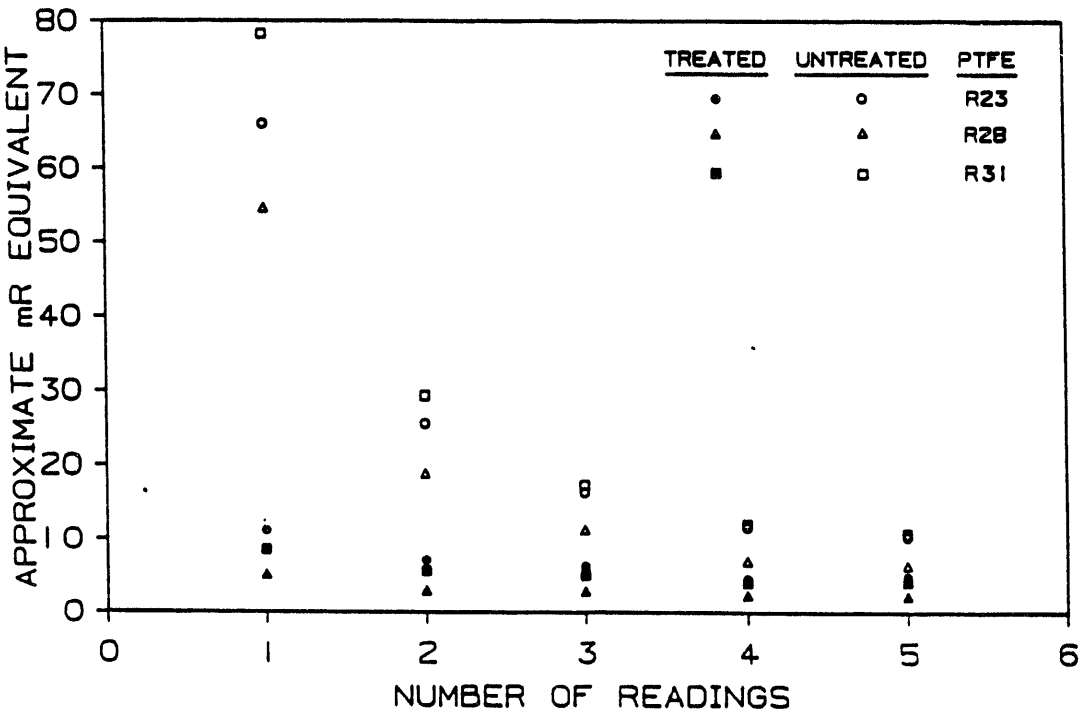


Figure 5

Harshaw/Bicron 8807 Dosemeter Case with Clear Window

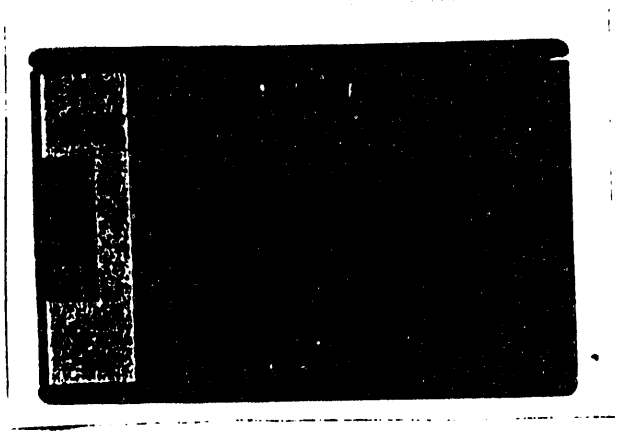


Figure 6

Harshaw/Bicron 8807 Solid Black Dosemeter Case



Table 1

Light Output in Generic Units (gU) After Exposure to Fluorescent Light for 140 Hours

Group E	Group F	Group G	Group H
2.55	2.14	2.20	2.15
2.17	1.93	2.31	2.22
3.03	2.26	3.03	2.07
3.40	2.2	2.34	2.12
2.69	1.97	3.14	2.03
3.34	2.05	2.70	2.21
2.97	2.18	2.23	2.06
2.6	1.95	2.39	2.15
2.9	2.22	2.96	1.99
3.99	2.26	2.32	2.25
2.37	1.99	2.87	2.08
3.68	2.15	2.32	2.22
Average = 2.97 ± 0.54	Average = 2.11 ± 0.12	Average = 2.65 ± 0.40	Average = 2.13 ± 0.08

Key to Table 1 and 2

Group E	Clear Window
Group F	Window c Foil
Group G	Solid Black
Group H	Black c Foil

Table 2

Results of Comparison Testing Between Windowed and Solid Black Harshaw/Bicron 8807 Dosemeter Cases ($t_{\alpha/2}$=2.074)

Group 1 - Group 2	Test Statistic *t*	Result	Mean Difference Confidence Interval
Group E - Group F	5.37	Reject Null Hypothesis	0.87 ± 0.33 gU
Group E - Group G	1.66	Accept Null Hypothesis	0.32 ± 0.40 gU
Group E - Group H	5.31	Reject Null Hypothesis	0.84 ± 0.33 gU
Group F - Group G	-4.50	Reject Null Hypothesis	-0.54 ± 0.25 gU
Group F - Group H	-0.48	Accept Null Hypothesis	-0.02 ± 0.09 gU
Group G - Group H	4.44	Reject Null Hypothesis	0.52 ± 0.24 gU

Figure 7

LiF Glow Curve Immediately After Irradiation

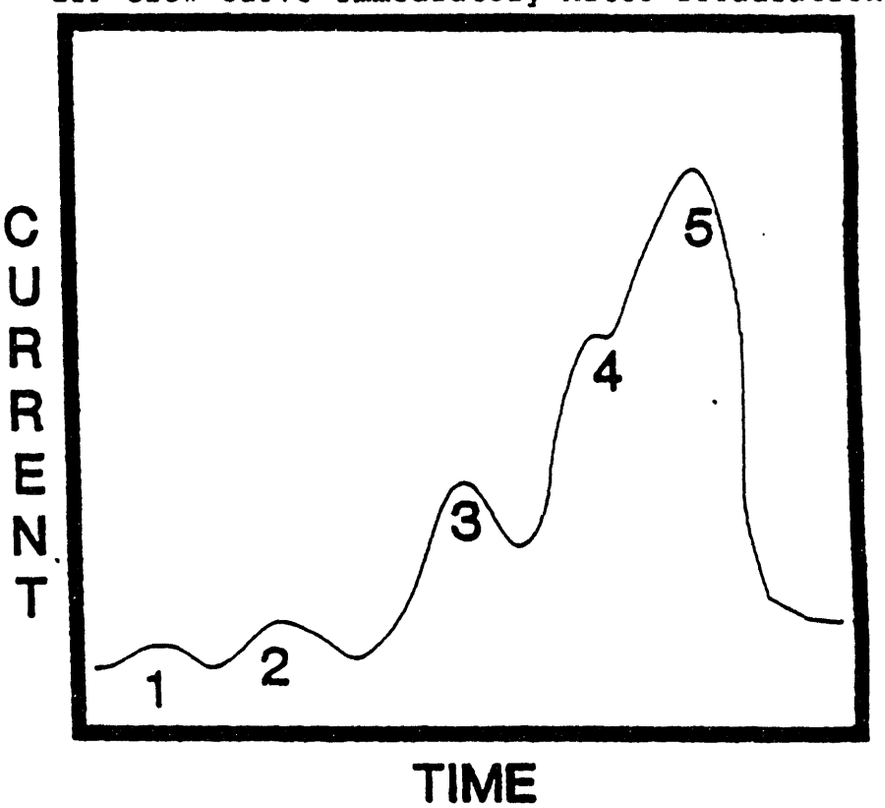


Table 3

LiF Glow Curve

Peak	Anneal Temp	Half Life
1	59° C	20sec-5min
2	120° C	10 hours
3	137° C	0.5 year
4	170° C	7 years
5	195° C	80 years

Figure 8

TLD-REMS Output for "Winter" Dosemeter

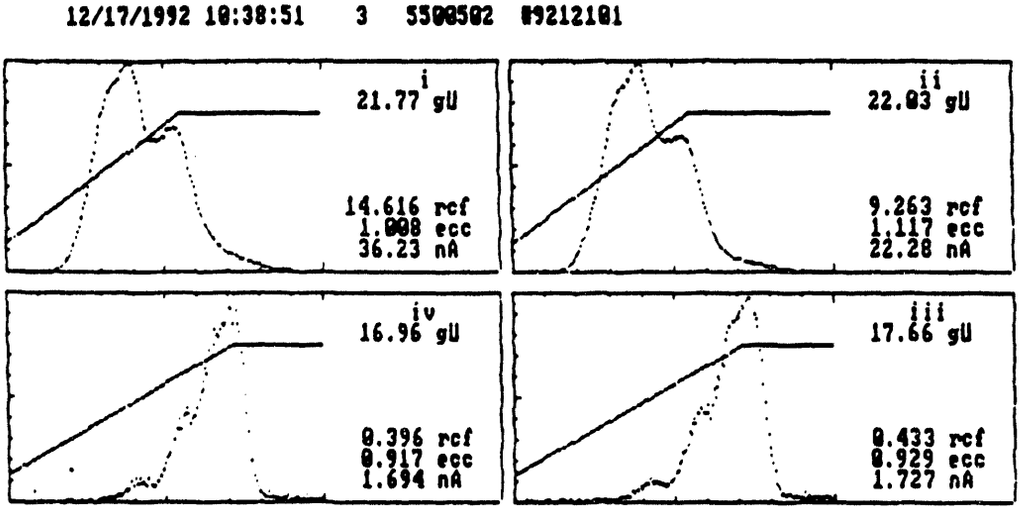


Figure 9

TLD-REMS Output for "Summer" Dosemeter

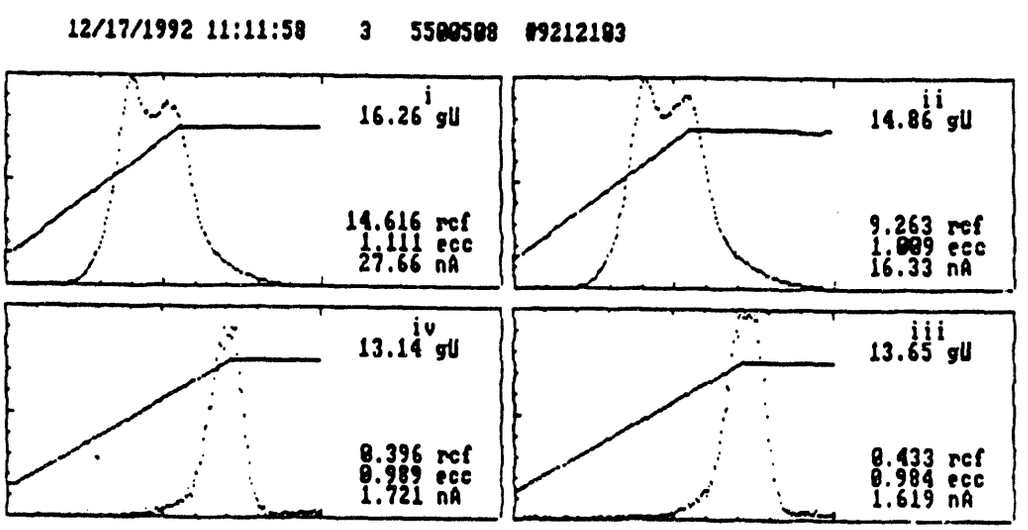


Table 4

Average 15 Day Temperature Minimums and Maximums

Period	Cold (° C)		Ambient (° C)		Hot (° C)	
	Avg Min	Avg Max	Avg Min	Avg Max	Avg Min	Avg Max
1	-0.7	6.8	10.4	16.6	13.9	32.2
2	0.1	6.5	8.2	15.7	13.0	29.1
3	-0.9	3.1	3.3	6.8	14.2	34.8
4	-1.8	1.4	1.2	4.9	14.8	34.7
5	-1.7	1.0	2.0	4.8	16.3	35.6
6	-4.4	-0.6	-3.3	-0.1	12.1	34.2

Table 5

Results of Temperature Dependent Fade Study

Time Delta (hr)	Cold (μGy)		Ambient (μGy)		Hot (μGy)	
186	140	149	131	131	96	96
108	149	131	131	140	96	105
66	131	131	131	123	105	105
24	131	131	131	131	105	105
4	140	131	131	149	105	114
Mean Response	140		131		105	

Note: 8.76 μGy = 1 mR (μ = micro)

Table 6

Field Dosemeter Results - 10th IIEDS

Measurement	Actual Dose	Reported Dose	Bias%
Lo Dose Cs-137	227 μGy	191 μGy	-15.9
High Dose Cs-137	637 μGy	532 μGy	-16.5
Field	237 μGy	233 μGy	- 1.7

Test of New Solid Black Case - Differing Gaskets

Gasket Type - with or without Aluminum Foil	gU
Rubber Gasket-Without Aluminum Foil	12.7
Rubber Gasket-with Aluminum Foil	10.0
Foam Gasket-Without Aluminum Foil	10.1

METHODOLOGY FOR PERFORMING SURVEYS FOR FIXED CONTAMINATION

J. S. Durham, Ph.D.
Pacific Northwest Laboratory, Richland, Washington
D. L. Gardner
Westinghouse Hanford Company, Richland, Washington

SUMMARY

This report describes a methodology for performing instrument surveys for fixed contamination that can be used to support the release of material from radiological areas, including release to controlled areas and release from radiological control. The methodology, which is based on a fast scan survey and a series of statistical, fixed measurements, meets the requirements of the *U.S. Department of Energy Radiological Control Manual* (RadCon Manual) (DOE 1994) and DOE Order 5400.5 (DOE 1990) for surveys for fixed contamination and requires less time than a conventional scan survey. The confidence interval associated with the new methodology conforms to the draft national standard for surveys. The methodology that is presented applies only to surveys for fixed contamination. Surveys for removable contamination are not discussed, and the new methodology does not affect surveys for removable contamination.

The methodology first requires evaluating the material for potential contamination. Material can be released without an instrument survey if its documented history ensures 1) that it has never been used or stored in an area controlled for contamination purposes (i.e., a contamination area [CA], high-contamination area [HCA], or airborne radioactivity area [ARA]); 2) that it has never come into contact with unsealed radioactive sources; and 3) that it has not been stored or used in a radiological buffer area (RBA) surrounding a CA, HCA, or ARA. If the material was used or stored in one or more of these areas, or if the material's history cannot be determined, an instrument survey is performed. The instrument survey consists of a fast scan of the entire accessible surface of the material at a rate that can measure, with 67% confidence, contamination at three times the guideline values tabulated in the RadCon Manual (DOE 1994). For Hanford instrumentation, the fast scan speed has been empirically determined to be 15 cm/s (6 in./s). After completing the fast scan survey, a series of twenty-two 5-sec fixed measurements is taken at random over the surface of the material. If no measurements are above background following an appropriate survey for removable contamination, the material may be released to radiologically controlled areas. If no measurements are above background following an appropriate survey for removable contamination, and the potential radioactive contaminant is listed in Table IV-1 of DOE Order 5400.5 (DOE 1990), then the material may be released from radiological control. The fast scan measurements ensure, with 67% confidence, that none of the material's surface is contaminated above three times the guideline value. The statistical measurements ensure, with 67% confidence, that 95% of the material's surface is not contaminated above the minimum detectable activity (MDA) for a 5-sec fixed measurement. If the surface area of the material is less than 4.6 m^2 (50 ft^2), the requirements for release of material tabulated in the RadCon Manual (DOE 1994) and DOE

Order 5400.5 (DOE 1990) will be met. For material with a surface area larger than 0.56 m^2 (6 ft^2), the time required to perform an instrument survey using the new methodology is less than the time required to perform a conventional scan survey.

INTRODUCTION

It is often necessary, and usually desirable, to release materials used within radiologically controlled areas at nuclear facilities for either controlled or uncontrolled use. Prior to their release, however, the materials must be evaluated for surface contamination. The goal of the evaluation process, which may include measurements, is to prevent the release of any material that contains surface contamination above the guideline values for surface contamination specified in the *U.S. Department of Energy Radiological Control Manual* (RadCon) (DOE 1994) and DOE Order 5400.5 (DOE 1990). (In the following text, the surface contamination guideline values listed in the RadCon Manual [DOE 1994] are denoted as the guideline values.) The guideline values for fixed contamination are summarized in Table 1.

Material that leaves a radiologically controlled area is typically evaluated for the presence of surface contamination by means of an instrument survey. The survey for fixed contamination requires passing an appropriate radiation detector over the material's surface at a rate of 5 cm/s (2 in./s) at a maximum distance from the surface of 0.6 cm (0.25 in.). The purpose of this paper is to describe a new methodology for performing surveys for fixed contamination that meets the requirements of DOE orders and reduces the time required to perform the surveys.

This paper only discusses surveys for fixed contamination of material with potential surface contamination and does not discuss surveys for removable contamination. It does not apply to surveys of bulk contamination, such as soil; surveys of material that has been activated through irradiation; surveys of personnel and their effects; or surveys of buildings and other properties. Likewise, the methodology does not apply to automated radiation-detection equipment such as tool monitors and laundry monitors. For this document, material consists of equipment, furniture, tools, etc., that are portable or transferrable.

The new survey methodology has three components: material evaluation, scan survey for fixed contamination, and a statistical survey for fixed contamination. The methodology ensures, with 67% confidence, that the guideline values of DOE Order 5400.5 (DOE 1990) and the RadCon Manual (DOE 1994) are met. If no measurements are greater than background following an appropriate survey for removable contamination, the material is not considered to be contaminated with fixed contamination and may be released for controlled use. If no measurements are greater than background following an appropriate survey for removable contamination, and guideline values for the contaminant are listed in Table IV-1 in DOE Order 5400.5 (DOE 1990), the material may be released from radiological control.

TABLE 1. Summary of Contamination Values

NUCLIDE (See Note 1.)	TOTAL (FIXED + REMOVABLE) (dpm/100 cm^2) (See Note 2.)
U-natural, U-235, U-238 and associated decay products	5,000 alpha
Transuranics, Ra-226, Ra-228, Th-230, Th-228, Pa-231, Ac-227, I-129 (See Note 3.)	500
Th-nat, Th-232, Sr-90, Ra-223, Ra-224, U-232, I-125, I-126, I-131, I-133	1,000
Beta-gamma emitters (nuclides with decay modes other than alpha emission or spontaneous fission) except Sr-90 and others noted above. Includes mixed fission products containing Sr-90.	5,000 beta-gamma
Tritium organic compounds, surfaces contaminated by HT, HTO, and metal tritide aerosols (See Note 3.)	10,000

Notes:

1. The values in this table apply to radioactive contamination deposited on, but not incorporated into the interior of, the contaminated item. Where contamination by both alpha- and beta/gamma-emitting nuclides exists, the limits established for the alpha- and beta/gamma-emitting nuclides apply independently.

2. The levels may be averaged over 1 m^2 provided the maximum activity in any area of 100 cm^2 is less than three times the values in Table 1.

3. Surface contamination guidelines for these radionuclides are reserved in DOE 5400.5 (DOE 1990). For these radionuclides, the surface contamination guidelines in the RadCon Manual (DOE 1994) are included. These guidelines refer only to release of material to controlled areas.

Both the typical procedure and the new methodology have a 67% confidence interval associated with the measurements. A minimum confidence interval of 67% is recommended by both the American National Standards Institute (ANSI) draft standard ANSI 13.12 (ANSI 1978) and the Health Physics Society (HPS)

Standards Committee[a] for performing radiation surveys. No other guidance is available on which to base a confidence interval for material release surveys.

For reasons detailed later, this methodology is applicable to material that has a surface area between 0.56 m^2 (6 ft^2) and 4.6 m^2 (50 ft^2). Material with a surface area of less than 0.56 m^2 (6 ft^2) can be surveyed faster, and with equal confidence, using a scan survey at a scan rate of 5 cm/s (2 in./s). Material that has a surface area greater than 4.6 m^2 (50 ft^2) must be separated into 4.6 m^2 (50 ft^2) partitions, and the methodology should be applied to each partition independently.

Inherent in the methodology is the ability of the instrument to measure contamination levels below the guideline values during a 5-second fixed measurement. Some radionuclides, notably tritium and some isotopes of iodine, cannot be adequately measured with portable instruments. The following methodology should not be applied when performing release measurements of material that has potentially been exposed to significant quantities of these radionuclides.

MATERIAL EVALUATION

Determination of the potential that material is contaminated is based on a process termed *material evaluation*. In this process, the evaluator considers previous known uses of the material, as well as typical uses and the environment in which the material was used. Material evaluation places the material into one of two categories: not potentially contaminated or potentially contaminated.

Material is not potentially contaminated and can be released without an instrument survey if 1) it has never been used or stored in an area controlled for contamination purposes (i.e., a contamination area [CA], high-contamination area [HCA], or airborne radioactivity area [ARA]); 2) it has never come into contact with unsealed radioactive sources; and 3) it has not been stored or used in a radiological buffer area (RBA) surrounding a CA, HCA, or ARA. This material may be considered to be nonradioactive material for which the RadCon Manual (DOE 1994) does not require an instrument survey. A material history release form is used to document the release of material that is known to be free of contamination by its history of use. If a material history release form cannot be completed, or if the history of the material is unknown, the material is potentially contaminated and an instrument survey must be made of the material. Material released from RBAs surrounding CAs, HCAs, or ARAs should also be evaluated using an instrument survey.

Material that is known to have resided in a CA, HCA, or ARA and that contains instrument-inaccessible areas may not require an instrument survey of the inaccessible areas. If a material history release form can be used to document that the inaccessible areas could not become contaminated without

---

(a) Health Physics Society (HPS) Standards Committee. 1987. *Surface Radioactivity Guides for Materials, Equipment, and Facilities to be Released for Uncontrolled Use.* Draft.

contaminating the accessible areas, then only the accessible areas need to be surveyed.

The material evaluation process should also consider the nuclides to which the material was potentially exposed. If the material was exposed to significant quantities of difficult-to-detect nuclides, including tritium, ^{125}I, or ^{129}I, this methodology should not be applied.

INSTRUMENT SURVEYS

A survey for fixed contamination of material that is potentially contaminated is performed using a new survey methodology. This methodology consists of a scan survey for fixed contamination of the surface area of the material, followed by a statistical survey of the surface area. These surveys are discussed in detail in this section.

Scan Survey for Fixed Contamination

A scan survey for fixed contamination requires passing the detector of an alpha and a beta/gamma survey instrument, as applicable, over the entire accessible surface of the material. The detector is moved at a constant rate that allows detection of contamination at a level equal to three times the guideline value. Note 2 in Table 1 states that the maximum activity in any 100-cm^2 area must be less than three times the guideline values. For Hanford instrumentation, the scan rate has been empirically determined to be 15 cm/s (6 in./s). The maximum source-to-detector distance during the scan should be 0.6 cm (0.25 in.). If a change in the audible output of the instrument is heard (that is, if the number of clicks increases noticeably), the area under the window of the instrument is resurveyed using a stationary measurement for 3 sec to 5 sec. If the elevated counts persist, the material is contaminated and it should not be released. If the increase does not persist, the scan continues, and the fixed measurement should be counted as one of the required 22 measurements that comprise the statistical survey for fixed contamination. This procedure is followed until the entire surface of the material has been surveyed.

The scan survey for fixed contamination ensures that none of the surface of the material is contaminated above three times the guideline value. If no contamination above background is detected during the scan survey, a statistical survey for fixed contamination is performed. If contamination above background is detected, then decontamination of the material should be considered and the methodology described in this paper is not applicable.

Statistical Survey for Fixed Contamination

The survey for fixed contamination of material that is potentially contaminated is based on a statistical sampling of measurements obtained on the surface of the material. A series of 22 fixed, random measurements should be made over the area of the material. Each fixed measurement should be 5 sec in duration, with the detector in contact with the surface of the material, providing it has been determined that no removable contamination exists on the material. The maximum area of material that may be surveyed is based on the MDA of the instrument being used, as discussed below. The survey methodology

should be used for both beta/gamma and alpha contamination, unless only one type of contaminant exists in the facility. If a survey for removable contamination has been completed and no measurements above background are observed, the material may be released to a controlled area. If the potential contaminant is not reserved in DOE Order 5400.5, then the material may be released from radiological control. The statistical survey provides assurance, with 67% confidence, that no more than 5% of the surface of the material is contaminated above the guideline values (Owen 1986).

The fixed survey measurements should be chosen using random detector placements over the entire surface of the material. It may be prudent to bias some of the measurements toward those areas that are more likely to be contaminated, including handles, horizontal surfaces, stains, cracks, and other surface anomalies in which foreign material typically accumulates. This type of selection bias will further increase the confidence associated with the statistical survey method. A minimum of 22 fixed measurements must be maintained for all material that has a surface area greater than 0.56 m^2 (6 ft^2). For material that is smaller in area than 0.56 m^2 (6 ft^2), scanning at a rate that enables measurement of contamination at the guideline values (typically 5 cm/s [2 in./s]) is faster than the statistically based methodology.

DETERMINATION OF MAXIMUM MATERIAL AREA

DOE Order 5400.5 (DOE 1990) states that "the [contamination] levels may be averaged over 1 square meter provided the maximum activity in any area of 100 cm^2 is less than three times the [guideline] values." To meet this requirement, a maximum material area must be determined. The maximum material area, A_{max}, is based on the MDA of the instrument for a 5-sec fixed count.

After following the above methodology, and if the MDA for a 5-sec measurement is known (expressed as a fraction of the guideline value), then it can be stated that a maximum of 5% of the material is contaminated above the MDA but not above 3 times the guideline value. The remaining 95% of the material is contaminated at or below the MDA of the instrument. In the worst-case scenario, all of the contamination resides within a single square meter of the material's surface; 5% of the entire surface of the material is contaminated at three times the guideline value; and the remaining portion of the square meter is contaminated at the MDA of the instrument. For this worst-case scenario, the following equation can be written for a 1-m^2 area:

$$3 \cdot GV \cdot x + MDA(1-x) = GV \qquad (1)$$

where GV is the guideline value in dpm/100 cm^2, x is the fraction of 1 m^2 that is contaminated at 3 times the guidelines value, and MDA is the MDA in dpm/100 cm^2 for a 5-sec fixed measurement. The first term in Equation 1 ($3 \cdot GV \cdot x$) represents the amount of activity on the 1-m^2 area that is contaminated at 3 times the guideline value. The second term in Equation 1 [MDA(1-x)] is the amount of activity on the remaining fraction of the 1-m^2 area that is contaminated at the MDA value. Finally, the right side of Equation 1 is the guideline value averaged over 1 m^2. Rearranging Equation 1

and solving for x gives

$$x = \frac{1-\frac{MDA}{GV}}{3-\frac{MDA}{GV}}. \quad (2)$$

Because x represents 5% of the total surface area of the material in m^2, the maximum area, A_{max}, is given by

$$A_{max} = \frac{1-\frac{MDA}{GV}}{0.05\left(3-\frac{MDA}{GV}\right)}. \quad (3)$$

Equation 3 establishes a limit on the area of the material to which the statistically based methodology can be applied, and this limit is based on the measurement capabilities of the instruments used in performing material release surveys. Measurements of the detection capabilities of Hanford portable instrumentation for various radionuclides have been completed for both point and distributed sources. For most of the radionuclides listed in the RadCon Manual (DOE 1994), Table 2 gives the maximum material area for surveys for fixed contamination. Note that the difference in minimum and maximum material areas between separated $^{90}Sr/^{90}Y$ and $^{90}Sr/^{90}Y$ as a mixed-fission product are a result of different guideline values for the two forms. In addition, the guideline values for separated $^{90}Sr/^{90}Y$ can only be measured using a 100-cm^2 gas proportional counter, and this instrument is recommended for use during surveys for separated $^{90}Sr/^{90}Y$ at the Hanford Site.

If separated ^{99}Tc is excluded, limits on the area of the material can be determined based on the data in Table 2. Because ^{99}Tc and $^{90}Sr/^{90}Y$ are seldom encountered in their separated form, excluding them from the general methodology is warranted. The most limiting material area for applying the statistically based methodology to surveys for fixed contamination is 4.6 m^2 (50 ft^2).

DISCUSSION

The goal of the proposed methodology is to meet the requirements in DOE Order 5400.5 (DOE 1990) and the RadCon Manual (DOE 1994) for performing surveys for fixed contamination while reducing the time that is currently required to survey material at 5 cm/s (2 in./s). For most radionuclides, a survey using a scan rate of 5 cm/s (2 in./s) will measure contamination at the guideline values with a confidence of 67%. A confidence interval of 67% is recommended by both ANSI and HPS for radiation surveys. The statistically based methodology significantly reduces the time required to survey the material.

TABLE 2. Maximum Material Area for Surveys for Fixed Contamination

Nuclide	MDA[a] (distributed source), dpm/100 cm^2	Maximum Material Area, m^2 (ft^2)
U-natural, U-235, U-238	140	6.5 (71)
Pu-239, Ra-226, Th-230, Th-228, Pa-231, Ac-227	140	5.3 (57)
Th-natural, Th-232 Ra-223, Ra-224, U-232	140	6.0 (65)
Separated Sr/Y-90	210[b]	5.7 (61)
Sr/Y-90	1700	5.0 (54)
Tc-99	2600	3.9 (42)
Cs-137	1900	4.7 (51)

(a) Johnson, M.L. 1994. "Survey Speeds to Detect One Times and Three Times DOE RadCon Manual Table 2-2 Total Contamination Values," presented at this conference.
(b) MDA for a 100-cm^2 gas proportional counter.

Using the proposed methodology will eliminate the dependence on a slow, time-consuming scan rate. After using the methodology, it can be stated, with 67% confidence, that no 100-cm^2 area of the material is contaminated above three times the guideline value, and that the contamination level averaged over any 1 m^2 is below the guideline value. By biasing the statistical survey measurements toward those areas that are more likely to be contaminated, the confidence associated with the methodology is further increased. Thus, for the "unreserved" radionuclides listed in DOE Order 5400.5 (DOE 1990) (with the exception of difficult-to-detect radionuclides), all of the requirements for release are met and the material may be released from radiological control after an appropriate survey for removable contamination. Because the RadCon Manual (DOE 1994) contains guideline values for the "reserved" radionuclides in DOE Order 5400.5 (DOE 1990), material that may have been exposed to reserved radionuclides may be released for controlled use by following the proposed methodology.

In order to compare the time required to survey a hypothetical piece of material using the traditional scan survey versus using the statistically based methodology, the following exercise was completed. Consider the survey of a flat piece of material that is 13 cm (5 in.) wide. This width is chosen because it corresponds to the largest dimension of the window of a Hanford portable alpha monitor (window area of 50 cm^2); thus, only a single pass of

the alpha detector is required to survey the material. The estimates were made by assuming that the material is surveyed by both an alpha probe and a pancake G-M probe (window area of 15 cm^2), and that the G-M probe requires three passes for each pass of the alpha probe (to allow for some overlap between passes). Table 3 presents a comparison of using the conventional scan procedure and the new methodology. It should be noted that the guideline values for detection of ^{230}Th and ^{231}Pa cannot be measured with 67% confidence using a 5 cm/s (2 in./s) scan rate, and a slower scan rate is required for these radionuclides. The new survey methodology is able to measure the guideline values for all radionuclides with 67% confidence, with the exception of the previously noted hard-to-detect radionuclides. The results of the comparison show that the statistical method is significantly faster than the scanning method for material with a surface area greater than 0.56 m^2 (6 ft^2).

TABLE 3. Comparison of Survey Times for Different Survey Methodologies

Material Area	2-in./s Scan	Statistical Methodology
0.56 m^2 (6 ft^2)	5.8 min	5.9 min
2.3 m^2 (25 ft^2)	24 min	12 min
4.6 m^2 (50 ft^2)	48 min	20 min

CONCLUSION

Implementation of the proposed methodology with a confidence interval of 67% will meet the material release requirements in DOE Order 5400.5 (DOE 1990) and the RadCon Manual (DOE 1994). The material evaluation process will allow material that has not been exposed to contamination to be released from radiological control without a survey. For potential radioactive contaminants that are not reserved in DOE Order 5400.5 (DOE 1990), the methodology will allow material to be released from radiological control after performing a suitable survey for removable contamination. For other radionuclides, with the exception of some difficult-to-detect radionuclides, material may be released for controlled use. Compared with current techniques, the proposed methodology will reduce the amount of time required to perform surveys for fixed contamination.

ACKNOWLEDGMENT

The authors would like to acknowledge significant contributions to this report provided by Thomas J. Froelich, Louis Jensen, and Leo H. Munson. Without the leadership and input of these three individuals, completion of this report would not have been possible. The authors would also like to acknowledge Jackson Ellis, David Ottley, and George Vargo for their technical review of the document. Finally, the authors would like to thank Donald J.

Hanley and Marianna Cross for their support during the production of this document. Pacific Northwest Laboratory is operated for the U.S. Department of Energy by Battelle Memorial Institute under Contract DE-AC06-76RLO 1830.

REFERENCES

American National Standards Institute (ANSI). 1978. *Draft American National Standard Control for Radioactive Surface Contamination on Materials, Equipment, and Facilities to be Released for Uncontrolled Use.* ANSI N13.12, 1430 Broadway, New York, New York.

Owen, D. B. 1986. *Handbook of Statistical Tables.* Addison-Wesley Publishing Co., Reading, Massachusetts.

U.S. Department of Energy (DOE). 1990. *Radiation Protection of the Public and the Environment.* DOE Order 5400.5, Washington, D.C.

U.S. Department of Energy (DOE). 1994. *U.S. Department of Energy Radiological Control Manual.* DOE/EH-0256T, Washington, D.C.

CALIBRATION OF SURFACE CONTAMINATION MONITORS AT IPEN/SÃO PAULO

Linda V.E. Caldas and Marcos Xavier (Instituto de Pesquisas Energéticas e Nucleares-CNEN/SP Caixa Postal 11049 - CEP 05422-970 - São Paulo, SP, BRAZIL)

The need for effective monitoring of surface contamination is quantified in terms of activity per unit area; this quantity is used to specify the derived limits, that are incorporated in the national regulations of radiation protection. These regulations recommend the calibration of all health physics instruments every 12 months. In the case of surface contamination monitors, a special set-up and a method were developed at the Calibration Laboratory of São Paulo, using standard alpha and beta radioactive sources. The international recommendations approve the use of ^{241}Am and $^{90}Sr + ^{90}Y$ (or ^{204}Tl) sources in the calibration procedures for this case. At São Paulo, the monitors are being calibrated in the standard radioactive fields of ^{241}Am, ^{14}C, ^{36}Cl and $^{90}Sr + ^{90}Y$ sources, and the instrument efficiency is determined for each case in the range 0.5 to 1.5 cm (alpha radiation) and 0.5 to 5.0 cm (beta radiation). Moreover, all instruments are being normally tested also with ^{241}Am sources of different activities (response linearity) and with ^{137}Cs, ^{244}Cm, ^{233}U, ^{238}Pu and ^{239}Pu sources (energy dependence). Instruments of different manufacturers and types were used for this study.

Work partially supported by CNPq - Conselho Nacional de Desenvolvimento Científico e Tecnológico, Brazil

AUTOMATED RADIOACTIVE CONTROL SYSTEM OF THE MOSCOW MESON FACTORY'S RELEASES.

S.V.Serezhnikov and V.E.Stepanov (Institute for Nuclear Research of the Russian Academy of Sciences, 60oh October Anniversary prospect 7a, 117312, Moscow, Russia.)

At the last conference we had reported about the investigation of radiation environmental effects from the high current proton accelerators /1,2/. On the basis of this investigation, now we are creating an Automatic Radioactive Control System of the Moscow meson factory's releases (ARCS) into the atmosphere /3/. The composition of the releases consists primarily of the short-lived radioactive gases C, N, O, O. About 10 % of the releases consist of Ar and about 2 % - another radionuclides. The continual sampling of the released mixture results from the pressure difference existing in the ventilation system. The mixture sampling network includes the filters, the ionization and the measuring chambers, where gamma-rays with energy of 0.511 Mev and 1.29 Mev are measured with the scintillation gamma spectrometer. Besides the system measures gross gamma and beta activity, the speed of the selected mixture, the speed of the released mixture, the speed and direction of the wind, the vertical gradient of the temperature and the humidity of the released mixture. The results of the measurments needed for sight and population dose model calculations /1,4/ are written into a database of ARCS.

REFERENCES

1. I.N.Kopeikin, S.V.Serezhnikov, and V.E.Stepanov. "Anticipated Radiation Environmental Effect From the Moscow Kaon Factory". In Proceedings of the Third Conference on Radiation Protection and Dosimetry.Orlando,Florida.153-161 (1991).
2. I.N.Kopeikin, S.V.Serezhnikov, and V.E.Stepanov. "Environmental Effect of Airborne Radioactivity Releases From High Current Proton Accelerators". Radiation Protection Dosimetry.V.46,N.2,79-88 (1993).
3. *Automated Radioactive Control System of the Moscow Meson Factory Release Project.* Environmental Monitoring Ltd.(in Russian),(1994).
4. A National Standard of Canada. CAN/CSA-N288.1-M87.

RADIUM EQUIVALENT ACTIVITY OF BUILDING MATERIALS AND GAMMA RAY DOSE RATES IN ORDINARY HOUSES OF SÃO PAULO, BRAZIL

M.P. Campos and B.R.S. Pecequilo (Instituto de Pesquisas Energéticas e Nucleares, P.O. Box 11049, São Paulo 05422-970, Brazil)

The major contribution to the radiation exposure received by the general population is due to natural sources, which include external sources such as cosmic radiation and radioactive nuclides present in building materials and internal sources from inhalation and ingestion of naturally occurring radionuclides in air and diet. The external radiation exposure from natural radioactivity represents, approximately, 50% of the average annual dose caused to the human body by all natural and artificial radiation sources. Natural radioactivity in building materials is the most important source of external radiation exposure in dwellings because of the gamma rays emitted from ^{40}K and members of the uranium 238 and thorium 232 decay chains.

The specific activity of building materials determined in many countries shows that concrete is one of the most potential sources of elevated radiation exposure. However, very little is known about the natural radioactivity of Brazilian construction materials and, in 1991, our group was charged by the Santo André district of São Paulo, Brazil, to predict the exposure rates of several ordinary houses built almost of concrete, knowing the activities of the building materials.

A total of 38 samples of 6 different materials (4 raw and 2 building products) were collected and prepared for activity concentration measurements by using high resolution gamma-ray spectrometry.

Since ^{226}Ra is fairly the most critical radionuclide for radiation exposure considerations, the radium equivalent activity was calculated for all the 38 samples, in order to compare the specific activities of the construction materials containing different amounts of radium, thorium and potassium. The results varied from 90.7 Bq/kg (concrete beam) to 242.2 Bq/kg (concrete). The effective dose equivalent rate due to the indoor gamma radiation from the building materials was performed following the 1988 UNSCEAR procedures. The values obtained ranged from 4.0×10^{-3} mSv/y (concrete beam) to 0.3 mSv/y (concrete) which is below the 2.4 mSv/y assumed UNSCEAR value for natural radiation sources.

MICROCLIMATIC EFFECTS ON OUTDOOR RADON AND ITS PROGENY IN A LONG-TERM STUDY

M. Schütz, G. Keller, R. J. A. Kappel

(Institute of Biophysics, University of Saarland, 66421 Homburg, Germany)

Abstract

The dose due to the long term radon exposure is estimated from the radon concentration and from an equilibrium factor that in the literature is reported with a wide uncertainty. Therefore the radon equilibrium factor outdoors and its dependence on climatic effects should be investigated in a long-term study.

Both the outdoor concentrations of radon and of its progeny near Ellweiler/Hunsrück were measured continuously during 12 months and the resulting equilibrium factors were determined. Simultaneously to the every 2 hour's radon data many meteorological parameters as temperature and relative humidity of the air, barometric pressure and duration and amount of rainfall were recorded. At a height of 6 meters above ground and in 10 minute intervals the local wind direction and velocity were registered. By that a set of more than 3000 single measurements of the equilibrium factor and of the corresponding weather conditions was collected.

In the inspected area the outdoor radon level averaged about 27 Bq/m³ and mostly during the nights short-term peak values of more than 160 Bq/m³ occurred. The statistical analysis of the data yielded a significant correlation between radon and progeny concentrations and some meteorological factors as for example wind velocity or rainfall. Analogously to the daily and annually changing of the weather conditions varying radon and progeny concentrations were observed.

The overall mean equilibrium factor in the outdoor air was settled F = 0.26. Obviously it depended not significantly on the observed weather conditions. Therefore the inhalation dose may reliably be estimated from the measurements of the radon concentration and a mean equilibrium factor.

Introduction

The soil is the natural and the main source of all the radon in the air. Therefore a concentration gradient may establish in the atmosphere with the higher concentrations near the ground. By diffusion and convection the radon rich air in the lower layers mixes with radon free air of higher layers. As a consequence in many cases the radon concentration throughout the atmosphere is diluted and hardly can be detected even with extended measuring times. Under certain conditions radon may accumulate to values that normally occur indoors.

Beside the radon concentration also the concentration of its progenies varies. The detection of these daughter products forces a more sophisticated measuring technique than that of the radon gas itself. A way out is to suppose an equilibrium factor (called F-factor) by which the progeny concentration and finally the health risk due to radon may be estimated. F-factors indoors average at

about 0.3 ± 0.1 (1), but a great variance from 0.01 to 0.9 is reported (2). Even little detailed information is available about meteorological parameters that possibly influence the F-factor (3, 4). Some measurements indoors and outdoors came out with a correlation between the aerosols in the air and the F-factor (5), but are there any other parameters as for example temperature, barometric pressure or wind to influence the behavior of the F-factor? This question is the main focus of our measurements of the concentration of the radon gas, that of its progenies and of many meteorological parameters that we carried out at a fixed site in the south-western part of Germany over the period of a whole year.

Measuring methods

Our measuring station laid in the midst of a 2 km long valley that stretches from north to south. The borders of that 200 m broad valley are covered with forest and abrupt rocks dot about them. The soil of this region is known for its high content of uranium and radium and not far away there are small uranium dumps that have been covered with foils and a thick layer of clay. Thus a raised radon concentration in the atmosphere may be awaited. The complete supply to measure radon, progenies and the meteorological figures was installed inside a weather station 2 m above ground, except the velocity and the direction of the wind that was registered at a height of 6 m.

A radon monitor of „Alnor"-type hourly recorded the radon activity in the air. Its technique bases on the electrostatic precipitation of the first daughter product onto the covering of a silicon surface barrier detector and following alpha spectroscopy. This method allows to proof radon concentrations of 2 Bq/m³ with integration times of 1 hour. Concurrently a radon daughter monitor of „Silena"-type sampled the attached fraction of the radon progenies on a filter and counts the emitted alpha particles. With sampling periods of 15 minutes and counting intervals of some more than 1 hour the concentration of each individual radon daughter was calculated with 0.5 Bq/m³ as the lower limit of detection. Hence the equilibrium factor in the atmosphere was resolved every second hour. The following meteorological data were noted every 10 minutes:

- temperature (°C), barometric pressure (kPa) and relative humidity (%) of the air
- velocity (m/s) and direction (0°-360°) of the wind
- duration (percentage of 10 min.) and amount (mm) of the precipitation.

For its north to south extension the wind was blowing most of the time from north or from south through the valley. At the measuring station these winds were twisted by nearby buildings. The rough surface -trees and buildings- caused a lot of whirls and zones of calm. The narrowness of the valley with its steep borders diminished the duration of sunshine at the bottom of the valley. Thus typical microclimates arose at the measuring station that may be completely different from the global weather condition.

Results

From March to next February - only during March and July the radon monitors sometimes failed to record - more than 6000 single radon data and 3000 data of the progenies were collected. The mean annual radon concentration sets up at 27 Bq/m³. The radon concentrations follow a log-normal-distribution thus the median value is determined lower, at about 22 Bq/m³. Short term radon concentrations limit at 160 Bq/m³. The concentrations of the radon daughter products also match the log-normal-distribution with a mean value of 7 Bq/m³ and a median of 4 Bq/m³. Finally a mean annual F-factor F = 0.26 and a median of F = 0.17 is determined from all single data.

During one single day the concentration of radon and the progenies differ at large as the temperature of the air or the velocity of the wind does. Three representative patterns of weather conditions in different seasons are presented which display clearly the correlations between meteorological parameters, radon concentrations and F-factors.

The first model was recorded during autumn. The weather was sunny or partially cloudy and it did not rain. The barometric high-pressure fluctuated between 97.3 kPa and 98.6 kPa. The temperatures rose up to 25°C at noon or shortly after and cooled down to the freezing-point at about 5 a.m. every morning. As figure 1 displays the radon concentration modulated during each day in the same rhythm as the temperature but with the opposite sign and with a slight lag. The minimal values of approximately 15 Bq/m³ occurred in the afternoon, topmost concentrations of 90 Bq/m³ arose at 6 a.m.. Two distinct radon levels came out: a high-level phase during the night with radon concentrations above 50 Bq/m³ and a low-level phase in the afternoon with radon concentrations below 20 Bq/m³. Concentrations between these two plateaus were of short term around the hours of sunrise and sunset.

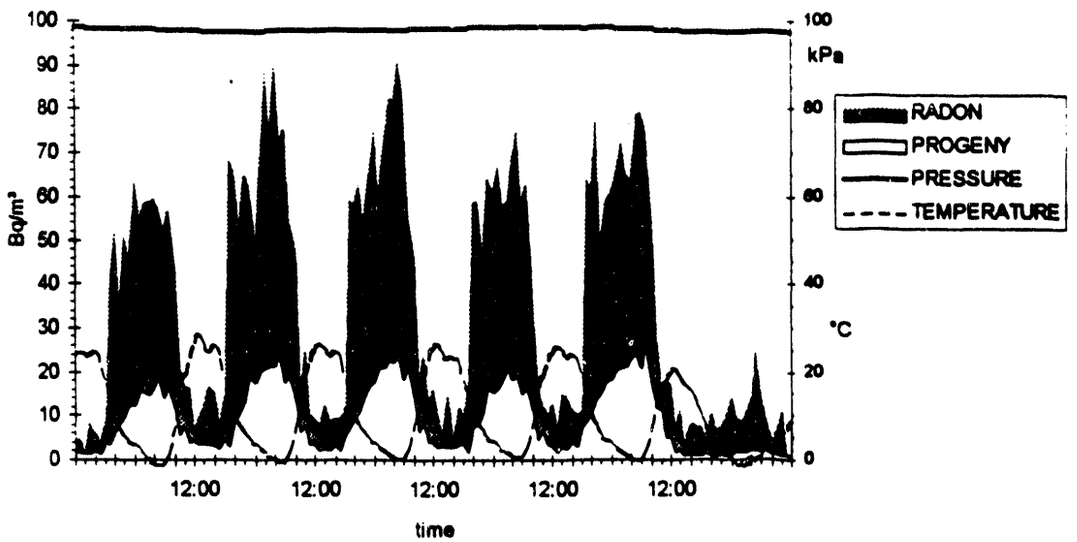
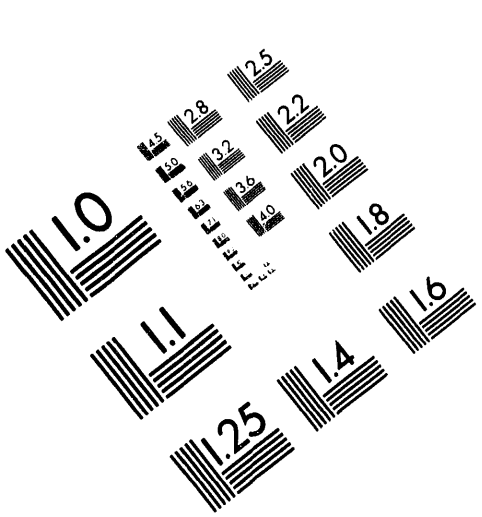


Figure 1: Concentration of radon and progeny, air temperature and bar. pressure in autumn

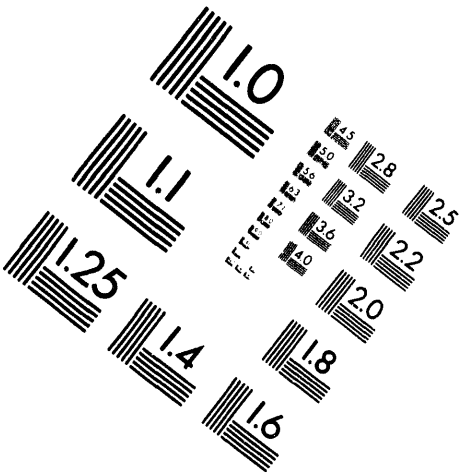
Although two corresponding levels of the air temperature were hardly marked, a certain correlation was visible: the low-level of radon appeared at temperatures above 15 °C and whenever temperature dropped below 12 °C the high-level of radon came into view. A similar correlation existed between the radon daughter products and the air temperature: the higher the temperature the less the concentration of the radon progeny in the air.

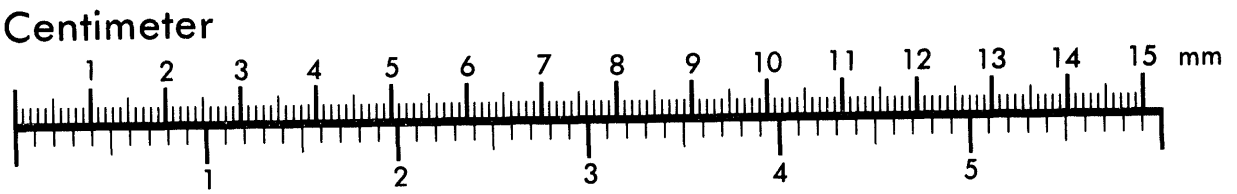
The mean radon concentration during this investigated week amounted to 27 Bq/m³ and the progeny averaged at 10 Bq/m³. This resulted in a mean F-factor of F = 0.37 in the atmosphere that exceeded the above mentioned annual mean by about 50%. Although the concentrations of radon and its progenies varied widely and periodically the F-factor was almost constant and showed not that „wave-like" behavior. Any correlation between the F-factor and the temperature could not be found from the data of this week nor from all the data of the year. The question for the causal connections between radon concentration and air temperature shall be explained in the section to follow.

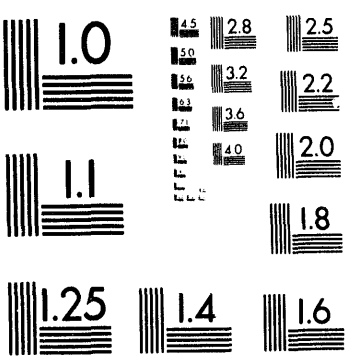


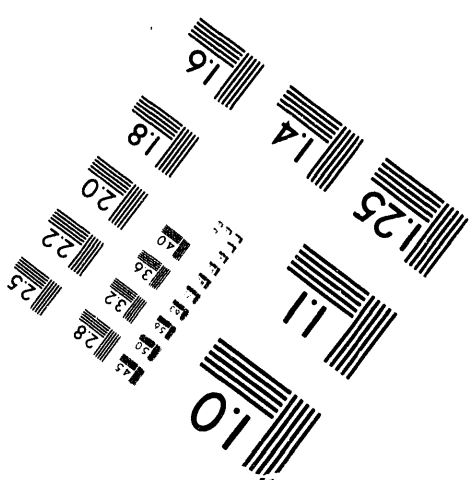


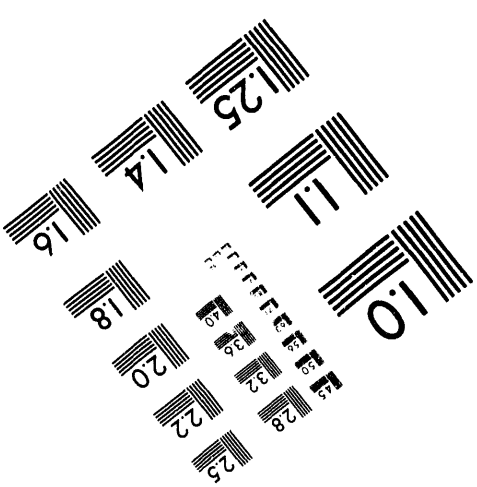
Association for Information and Image Management
1100 Wayne Avenue, Suite 1100
Silver Spring, Maryland 20910
301/587-8202











MANUFACTURED TO AIIM STANDARDS
BY APPLIED IMAGE, INC.

5 of 6

The second example was taken in the cold season and shows two different weather conditions that many times occur during winter. The first two days were characterized by cloudy skies. Under the cloud cover the temperatures did not change throughout day and night. An icy wind from north brought these constant air temperatures below 0°C. During this period the radon concentration kept low at about 10 Bq/m³. And this contradicts to the correlation given in the first example, that saw such low radon concentrations only at temperatures above 15 °C. As to see in figure 2, the wind velocity during the first two days averaged at a fairly constant value of 5 m/s. This suggests the hypothesis that the wind speed is causally correlated with the radon concentration and not the temperature itself.

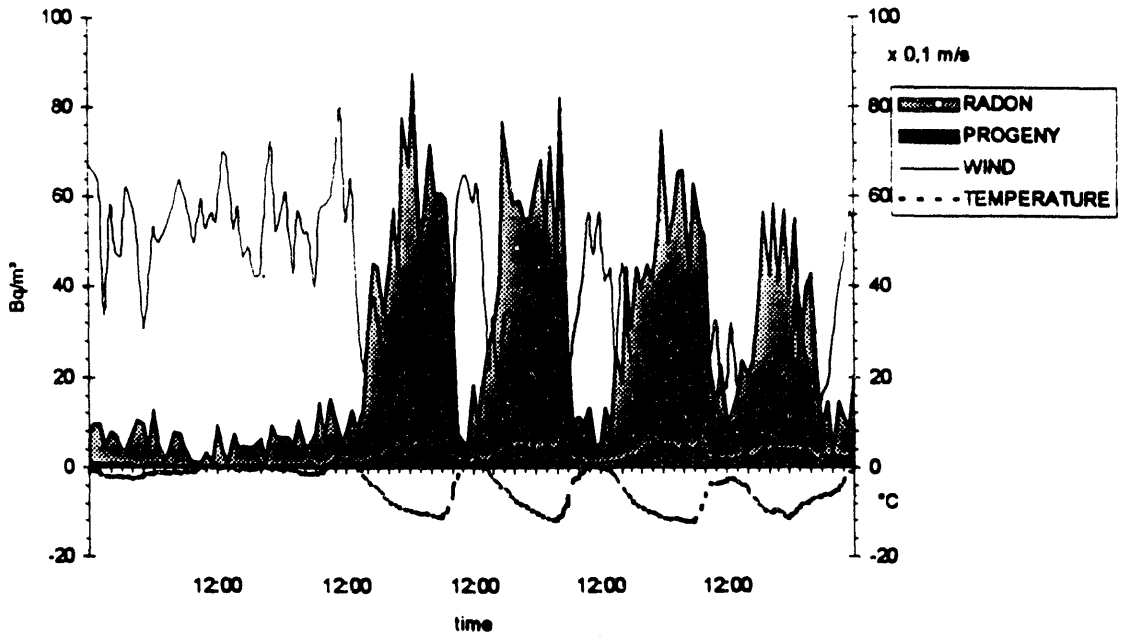


Figure 2: Concentration of radon and progeny, air temperature and wind velocity in winter

The further development of the radon concentration in figure 2 is consistent with the prediction, that the low radon concentrations appear simultaneously with the high wind speeds. During the last 4 days in figure 2 a daily up and down of the wind velocity was observed and concurrently the radon concentration and the concentration of the progeny varied. From that moment when the wind calmed, the radon concentration increased instantaneously to maximum values of 70 Bq/m³. Oppositely when wind arose the radon concentration went back again to the low-level of about 10 Bq/m³. This completely reflects the behavior performed in the first example. Moreover the daily fluctuations of the air temperature correspond to the above stated relation: the higher the temperature the less the concentrations of radon and its daughter products. In this example the air temperature varied between 0°C and -10°C whereas in the first example it varied from 0°C to 25 °C, but the radon concentrations always took the same two levels - a high level at about 70 Bq/m³ and a low level at about 10 Bq/m³.

Thus it is not the temperature itself to directly influence the radon concentration. The soil is heated by the sunshine and this implies an increase of the air temperature starting from near the ground. By that solar heating, temperature gradients in the atmosphere are induced and force the warmer air near the ground to ascend. The loss of the radon rich air near the ground is balanced by fresh and radon poor air form anywhere around. This process happens every morning after sunrise -

provided that no clouds shelter the solar heating of the soil- and results in the dilution of the radon concentration in the lower layers of the atmosphere. After sunset many times calms establish and radon that exhales from the soil will accumulate in the air above.

Figure 3 displays a scatterplot of radon concentration against wind speed and clarifies this deduction. At a wind velocity of more than 4 m/s the radon concentration does not exceed 20 Bq/m³, vice versa at lower wind velocities radon may accumulate. Furthermore there cannot be a simple functional relation between radon concentration and wind velocity, because the longer a calm continues the more radon may accumulate, which involves the time as a cofactor.

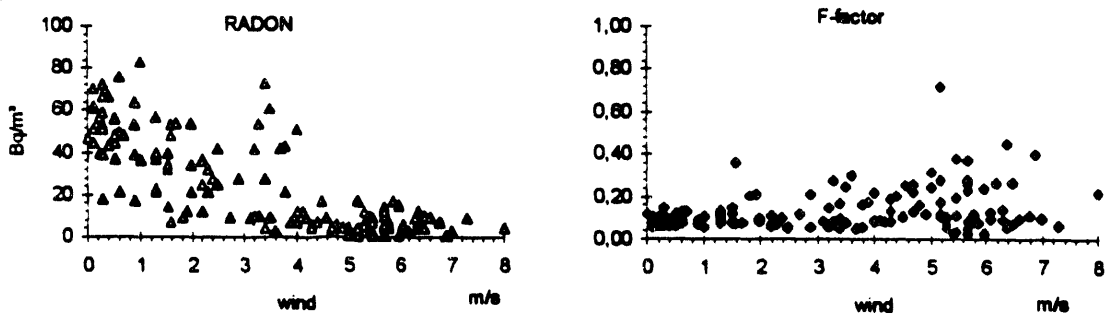


Figure 3: Scatterplot of radon concentration and F-factor against wind velocity

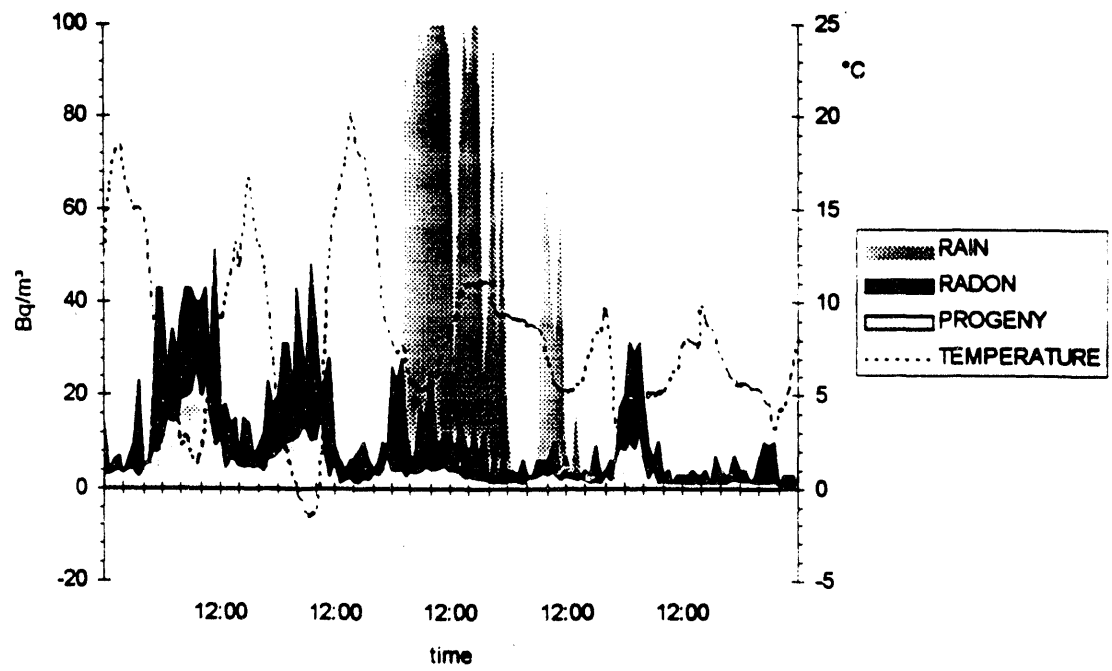


Figure 4: Concentration of radon and progeny, air temperature and rain in spring

The mean radon concentration during this week in winter amounts to 25 Bq/m³ and equals the annual mean value. The 2 Bq/m³ as the mean concentration of the radon progeny yield an equilibrium factor F= 0.09, which is half the annual mean. Figure 3 displays the scatterplot of the F-factor against the wind velocity. There is no marginal influence detectable except a broadening of the distribution of the F-factors at higher wind speeds.

The third example -see figure 4- now makes clear the influence of rain on the radon concentration. It was shot during springtime. For the first 2 days the well-known day-night-variation of the radon concentration showed again. During the 3rd night it started to pour with rain. Instantaneously the radon concentration decreased to less than 10 Bq/m³ and did not reach the high level of 70 Bq/m³ anymore. The radon concentration reacted immediately to the changed weather, but there was no straight effect on the F-factor to notice as to see in figure 5. Although the F-factor considerably varied during that week - between F = 0.15 and F = 1 - these variations were of the same extent both before, during and after the rainfall.

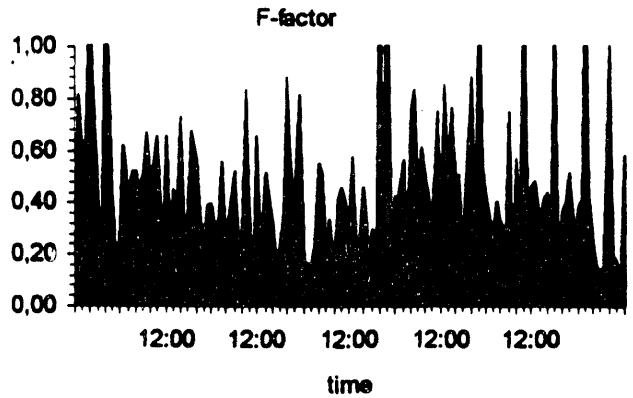


Figure 5: The F-factor before, during and after the rainfall (taken from figure 4)

The mean radon concentration during that week in spring amounted to 13 Bq/m³ and is far below the annual mean value. The mean F-factor F = 0.4 resulted from the elevated radon progeny concentrations.

Conclusions

Both the concentrations of radon and its progeny as well as the F-factors follow a log-normal distribution. During each of the 3 presented typical weather conditions totally different mean F-factors were measured and they do not represent the mean annual F-factor. During the summer months - May, June, July- the mean monthly F-factors were 2 to 3 times higher than during the winter months -November to February. Figure 6 shows the monthly averaged F-factors, their monthly minima and maxima and -as lines- the mean and median annual F-factor in the atmosphere.

The three presented examples demonstrate that the mean annual F-factor may not be determined by a single measurement campaign over several days. A reliable estimation of it can be achieved only by taking all the different typical weather conditions into account. During a single day wide variations of the F-factor are quite normal. The best daytimes to measure the F-factor are those hours when the radon concentration is relatively constant, for example during the night or in the

afternoon. Due to changing weather conditions steep and fast increases or decreases of the radon concentration occur. These hours are not suitable to determine the equilibrium factor in the atmosphere.

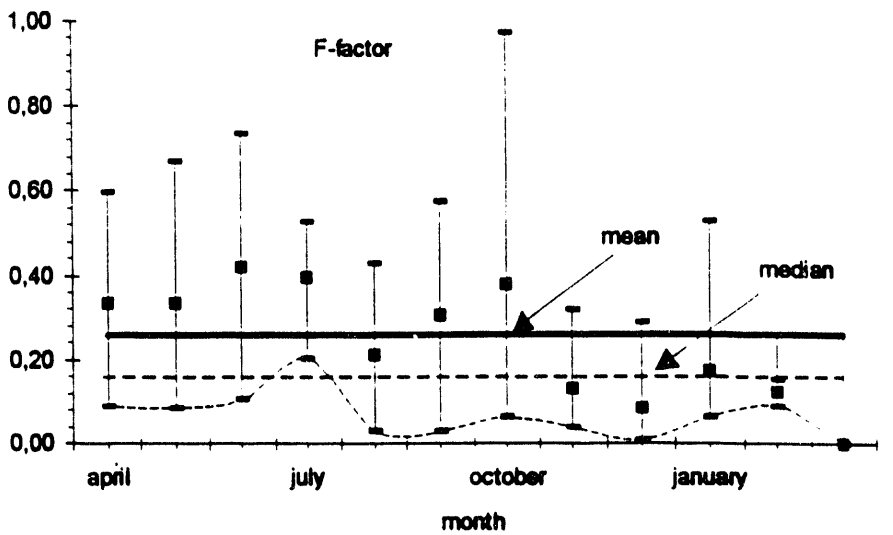


Figure 6: Monthly mean, minima and maxima of the equilibrium factor F

The observed meteorological parameters as barometric pressure, temperature or relative humidity of the air and speed or direction of the wind do not seem to influence the F-factor. But to a certain degree they can be used as indicators for the change in other unknown parameters as e.g. the concentration of aerosols in the atmosphere. Thus during the dry season we found that there was apparently more dust in the air that could be the explanation for the elevated F-factors.

References

1. Israeli, M. (1985), Deposition rates of Rn progeny in houses, Health Physics 49, 1069
2. George,A.C., Knutson, E.O., and Tu,K.W. (1983) Radon daughter plateout- I: measurements, Health Physics 45, 439
3. Swedjemark, G.A., (1983), The equilibrium factor F, Health Physics 45, 453
4. Gesell, T.F., (1983), Background atmospheric ^{222}Rn concentration outdors and indoors: a review, Health Physics 45, 289
5. Porstendörfer, J.(1984), Behavior of radon daughter products in indoor air, Radiation Protection Dosimetry 7, 107

INTERCALIBRATION OF VARIOUS TYPES OF PASSIVE RADON DOSIMETERS EMPLOYING PARTICLE TRACK DETECTORS

A.A. Qureshi, K. Jamil, Daiss Al-Ahmady*, Fazal-ur-Rehman and H.A. Khan (Radiation Physics Division, PINSTECH, P.O. Nilore, Islamabad, Pakistan)

Radon (^{222}Rn) and its progenies, known to be carcinogenic, are a matter of great concern specially in energy conserved air tight houses. A number of dosimeters have been devised to measure radon concentration using particle track detectors.

This paper describes the intercalibration of various types of dosimeters, currently in use in various countries. The present work includes, Box-type (1). Cup-type (2), Pen-type (3), Tube-Type (4), Bare-type (5), and Circular-type (6) dosimeters using CR-39 and CN-85 particle track detectors. Experiments have been carried out in a custom designed exposure chamber connected to a radon source. The calibration results, determined in terms of Bq/m^3 with respect to Box-type dosimeter, are useful for intercomparision and standardization of measured radon concentrations by various types of passive radon dosimeters in various laboratories.

(1) After L. Tommasino: ENEA-DISP, Via V Brancati 48, 00144, Rome, Italy.
(2) After E. Piesch: Health Physics Division, Karlssruhe, Nuclear Research Centre, Germany.
(3) After R. Brandt, H.A. Khani Kernochomic, Philipps, University, Marburg, Lahn, Germany.
(4) After H.A. Khan: Radiation Physics Division, PINSTECH, P.O.,Nilore, Islamabad, Pakistan.
(5) Used by Various Laboratories.
(6) After J. McLayhln: University College Dublin Department of Experimental Physics, Belfield, Dublin 4, Ireland.

*202 NSC, The University of Florida, Gainesville, FL 32611, USA

SESSION VII.
Calibration, Standards, & Accreditation

John Poston,
Chairman

STATUS OF THE REVISION OF ANSI N13.27, "PERFORMANCE SPECIFICATIONS FOR POCKET-SIZED ALARMING DOSIMETERS/ RATEMETERS"

Bogard, J. S. (Oak Ridge National Laboratory, P.O. Box 2008, Oak Ridge, Tennessee 37831-6383)

A working group of the Health Physics Society Standards Committee (HPSSC) was formed in June, 1993, to revise ANSI N13.27-1981, "Performance Specifications for Pocket-Sized Alarm Dosimeters and Alarm Ratemeters." The existing standard was written to address the performance of pocket ionization chambers and 'chirpers' used for exposure control purposes, but is inadequate to address performance capabalities of electronic personnel dosimeters (EPDs). Neither ANSI N13.11-1983, "American National Standard for Dosimetry - Personnel Dosimetry Performance - Criteria for Testing," nor the recently issued draft ANSI N13.11-1993 address this class of dosimeter at all. The recent evolution of EPDs to include dose conversion algorithms and microminiaturized logic control circuitry, coupled with advanced communications technology, have made these devices attractive for use in applications which generate doses of record, as well as for exposure control.

The working group (WG) composition reflects a cross-section of organizations that will manufacture, test, use, or regulate the use of alarming dosimeters and ratemeters for personnel radiation dosimetry and radiation protection programs. Foreign and domestic manufacturers, commercial dosimetry services, the U.S. military, the U.S. Nuclear Regulatory Commission, U.S.N.R.C. licensees, and National Laboratories of the U.S. Department of Energy are all represented. Each member has either management responsibility for personnel radiation monitoring programs or unique technical expertise essential to the Working Group; many have both. Members of the WG and their employers are shown in Table 1. The WG is located organizationally in the Instrumentation Section of the Health Physics Society Standards Committee (HPSSC). Harley V. Piltingsrud is Chairman of the HPSSC, and Joseph J. Shonka is Chairman of the Instrumentation Section. The WG held its organizational meeting in July, 1993. Additional meetings to review and comment on drafts have coincided with the Annual Meeting of the Health Physics Society, the Council on Ionizing Radiation Monitoring Standards (CIRMS), and the Health Physics Society Midyear meeting.

Initial N13.27 drafts have drawn heavily from two other standards, the

International Electrotechnical Commission Standards (IECS) draft Revision of Document 45B(Central Office)94, "Direct Reading Personal Dose Equivalent and/or Dose Equivalent Rate Monitors for X, Gamma and High Energy Beta Radiation," and ANSI N13.11-1993, "American National Standard for Dosimetry - Personnel Dosimetry Performance - Criteria for Testing." Technical issues which must be addressed by the WG are primarily related to the development of suitable performance tests for active devices which estimate and record both dose and dose rate while, at the same time, providing alarming capabilities for exposure control, since the most well-developed performance standards available are applicable to passive integrating devices with limited utility for real-time exposure control. Some more interesting examples of specific issues being addressed by the WG are listed below:

- Electronic personnel dosimeters (EPDs) tend to respond with much greater precision than thermoluminescent (TL) or film dosimeters. What quantity of EPDs is appropriate for a statistically meaningful performance test?

- EPDs are much more sophisticated than the precursor chirpers and pocket meters. How should the user verify that the unit is working properly before use; is proper monitoring of background radiation a sufficient criterion? What verification and validation requirements are appropriate for the software or firmware that estimate dose?

- The conventionally true value of dose in performance tests for TL and film dosimeters is determined at the phantom face, but EPD active elements may be located at a sufficient distance from the phantom face during testing that significant systematic error is introduced. How should the conventionally true value of dose be determined in such a case?

- Mixed-field testing of passive dosimeters can be simulated by exposing first to one (pure) field and then to another, but mixed-field testing of active dosimeters cannot be accomplished in this way. Can mixed-field performance tests for EPDs be provided using existing standard exposure protocols, or must new protocols be addressed?

- Intense interest exists in the possibility of using EPDs for generating doses of record. What controls are necessary to ensure that doses stored in memory are inaccessible to tampering by unauthorized personnel?

The original goal of the WG was to provide a final draft of the revision to N13.27 to the Health Physics Society Standards Committee in July, 1994. It appears now that a more

realistic goal is to provide the final draft by December, 1994. The draft will then require approval by the HPSSC before balloting by the American National Standards Institute and release as an ANSI standard.

Table 1. ANSI N13.27 WORKING GROUP MEMBERS

Name	Affiliation
James S. Bogard, Ph.D., C.H.P. (Chairman)	Oak Ridge National Laboratory
Stephen A. Browne	Carolina Power & Light Company
W. H. Casson, Jr., Ph.D.	Los Alamos National Laboratory
Maj. Lawrence Donovan	Armstrong Laboratory (AFMC), Brooks Air Force Base
Joseph Leon	Merlin Gerin, Inc.
Robert M. Loesch (Consultant)	U.S. Department of Energy
Charleen T. Raddatz	U.S. Nuclear Regulatory Commission
Mark C. Simpson	Public Service Electric & Gas Company
Kenneth L. Swinth (Consultant)	Battelle Pacific Northwest Laboratories
Robert P. Ulman	Dosimeter Corporation
Joseph Zlotnicki	Landauer, Inc.

THE DOE LABORATORY ACCREDITATION PROGRAM PERFORMANCE TESTING LABORATORY AUTOMATED CALIBRATION VERIFICATION PROGRAM

Rick Cummings and Rich Kershisnik (U.S. Department of Energy, Idaho Operations Office, 785 DOE Place, MS-4149, Idaho Falls, ID 83401), Randy Holloway (EG&G Idaho, Inc., P.O. Box 1625, MS-4149, Idaho Falls, ID 83415)

The Performance Testing Laboratory for the Department of Energy Laboratory Accreditation Program (DOELAP) resides at the Radiological and Environmental Sciences Laboratory (RESL) on the Idaho National Engineering Laboratory (INEL). A system has been developed to verify the calibration of ^{137}Cs irradiators using a reference class ionization chamber under computer control. The measurement system consists of irradiators, a Victoreen Model 415 ionization chamber, a Keithley Model 617 electrometer, a high voltage power supply, a VAXLAB microVAX II processor controller, a Fluke digital thermometer, a Heise digital barometer and an Optomux interface between the computer and irradiator. The ionization chamber is placed in an irradiation fixture which is affixed to the dosimeter phantom stand. The computer then executes a variety of steps to conduct the irradiation and measurement. The data taken over the last six months indicate that all of the irradiator geometries meet requirements in the governing standards.

THE DOE LABORATORY ACCREDITATION PROGRAM 8 YEARS LATER

Rick Cummings, Rich Kershisnik, Tansy Taylor and Gary Grothaus (U.S. Department of Energy, Idaho Operations Office, 785 DOE Place, Idaho Falls, ID 83401), Robert M. Loesch (U.S. Department of Energy, Office of Health Physics and Industrial Hygiene Programs, EH-411, Washington D.C. 20545)

The Department of Energy Laboratory Accreditation Program was implemented in 1986. Currently, the program is conducting its seventeenth performance testing session for whole body personnel dosimeters. All but two DOE laboratories have gained accreditation for their whole body personnel dosimetry systems. Several test situations which were anticipated in the early stages of DOELAP have not materialized. In addition, the testing standard for whole body personnel dosimetry systems is under review and revision. In the near future, the accreditation programs for extremity dosimetry and bioassay will be implemented. This presentation summerizes the status and anticipated direction of the DOE whole body and extremity dosimetry and bioassay laboratory accreditation programs.

RECENT CHANGES IN ACCREDITATION PHILOSOPHY

R.M. Loesch, (U.S.Department of Energy, EH-41, Washington, DC 20585)

In the past few years, several significant changes have developed which could impact the accreditation of personnel dosimeters within the US.

A revised ANSI N13.11 was finally published in 1993, which incorporated several changes, including the addition of AmBe in lieu of ^{252}Cf as a bare neutron source. In 1993, ISO Working Group 2 approved several new phantoms to be used for all radiations in the accreditation of personnel dosimeters. With these phantoms came a recommendation as to the proper use of correction factors. ISO WG15 is also developing a standard for the accreditation of personnel dosimeters. However, in concert with European community philosophy, the standard will distinguish between type testing and accreditation. In 1994, a proposal was put forth to the Council on Ionizing Radiation Measurements and Standards (CIRMS) that the US also take this approach.

These and other recent changes including recommendations of the ICRU and the increasing interest in electronic dosimeters are currently being considered in the rewrite of the DOE's Standard on the Accreditation of Personnel Dosimeters.

NEUTRON FIELD CHARACTERIZATION FOR A CALIBRATION LABORATORY

A.J.P. Ghilardi (Universidade de Sao Paulo, Ribeirao Preto, SP 14040-901, Brasil), E.B. Lee (Department of Nuclear Engineering, University of Tennessee, Knoxville, TN 37831-6379, USA), W.H. Casson (Los Alamos National Laboratory, Health Physics Measurements Group, HS-4, Los Alamos, NM 87545, USA), J.S. Bogard (Oak Ridge National Laboratory, Health Sciences Research Division, Oak Ridge, TN 37831-6383, USA.)

When measurement instruments for neutrons are calibrated with a isotopic neutron source in a calibration room, the response is not only to direct radiation from the source but also to neutrons scattered by the air and room. The calibration should be corrected using the vacuum source spectrum as a reference value, which would exclude neutron scattering processes which affects the total fluence and the neutron spectrum which hits the detector. The objective of this research is the neutron source caracterization for different irradiation conditions by using a multisphere spectrometer and others types of neutrons detectors.

Computational methods are necessary to determine the fluence, dose and dose equivalent (direct and scattered) at the detector position. Appropriate corrections are introduced for air and room neutron scattering specific for the subject detector.

*(Research sponsored by the U.S. Department of Energy with Martin Marietta Energy Systems, Inc. and Research National Council of Brazil.)

NEUTRON CALIBRATION FACILITIES

Gordon K. Riel (Naval Surface Warfare Center, R36, Silver Spring, MD 20903-5640)

We just built two neutron calibration facilities: one for monoenergetic neutrons, and one with an AmBe source that operates in high and low scattering environments. We have standard fields for calibrating dosimeters and challenging spectra for assessing their performance in the real world. One may wonder why a dosimeter that passes NAVLAP, or DOELAP tests needs to prove itself in other spectra. One detriment of any minimum standard is that it leaves no motive for excellence. For example: Suppose you enrolled in a course, and learned that the final exam had only two questions. So, you ask the professor "Life is short. Please jut tell me the answer to those two questions". If he did, would you have mastered the subject? So, a dosimeter that works in two fields may not work in all fields.

The NSWC Tandem Accelerator produces monoenergetic neutrons by bombarding Lithium (Li) with protons. Neutron energies from 0.2 to 2.5 MeV are produced by protons of 2.0 to 4.5 MeV. Thick Li targets produce a maximum fluence of 1×10^6 n/s/cm^2 at one meter, but the spectrum is almost flat from the threshold to the maximum energy. Thin targets produce monoenergetic neutrons, for example from 780 to 800 KeV, but the fluence falls to 3×10^5 n/s/cm^2. The nearest wall is five meters from the target. We can accommodate remmeters and other large devices, such as a 40X40X20 cm phantom for albedo dosimeters.

The calibration laboratory is about eight meters square by seven meters high. It is divided into low and high scatter bays by a light metal grid at ground level. A light metal building covers the upper low scatter bay. Concrete walls with an inner surface of steel plates line the high scatter bay, which extends three meters into the ground. The storage pit for the 0.2 TBq (5Ci) AmBe source is in the center of the bottom. A pneumatic actuator moves the source from shielded, through highly scattered, to the low scattering environment. Some scattering cannot be avoided, but we find the response to unscattered radiation by a regression of response with distance. We make energy corrections to report ^{252}Cf response in the AmBe field. Comparisons with NIST, DOD, and DOE calibration laboratories give us confidence in the results.

The high scatter area simulates real environments in both energy and direction. Ordinarily, one produces low energy neutrons by surrounding the source with a moderator. However, real environments produce low energy neutorns by scattering at a distance. Thus, scattered neutrons differ from source neutrons in direction as well as in energy. We reduce the source neutrons by distance and shielding and enhance the scattered neutrons by distance and reflection. Thus we produce a realistic field for tesing personnel dosimeters.

CALIBRATION OF REFERENCE NEUTRON FIELDS FOR DOSIMETER AND CRITICALITY ALARM VALIDATION AND INTERCOMPARISON

Michael B. Stanka and Richard C. Harrison
USA Combat Systems Test Activity
Army Pulse Radiation Facility
Aberdeen Proving Ground, MD USA 21005

I. Introduction.

The APRF operates a fast burst reactor for radiation hardening of electronics, radiation transport code validation, and dosimetry testing. Radiation environments have been developed for the validation and intercomparison of personnel dosimeters and criticality alarm systems. These fields can be varied in their dose rates, neutron to gamma-ray ratios, and time profiles.

For personnel dosimeters, the emphasis has been on developing well-characterized, stable fields with appropriate neutron and gamma dose levels. This has been achieved by adding material between the reactor and the dosimeter. Also, the distance from the reactor to the dosimeter may be varied. For criticality monitor testing, the time history of the applied dose is of more significance. Dose profiles may be provided through steady-state, short pulse, wide pulse, or fast ramp operations. Combinations of converters and time profile may be combined in almost any combination to supply the desired environment for a given test.

II. Reactor Description.

APRF is an advanced version of the Health Physics Research Reactor (HPRR) and produces the same neutron and gamma radiation fields. The reactor is mobile and manipulated by a movable gantry. The core is a right circular cylinder of enriched uranium with 10% molybdenum for structural strength.[1] The reactor is housed in a silo, 30 meters in diameter and 26.2 meters high, which is constructed out of thin aluminum sheeting. The floor of the reactor building is borated concrete. These features result in a low scatter, low neutron activation environment.

III. Modification of Reactor Environments.

A. Neutron to Gamma Ratio.

The free-field reactor environment is characterized by a neutron to gamma ratio of approximately 11. This factor is the ratio of the neutron tissue kerma to the gamma-ray tissue kerma. In order to meet the requirements of test programs, alternative environments with differing neutron to gamma ratios were developed.[2] Typically, these alternative environments are characterized by smaller neutron to gamma ratios. The neutron to gamma ratio is modified by using a converter which increases the gamma-ray kerma through the production of neutron capture gamma-rays. The converter currently used at the APRF consists of cadmium loaded (5 wt%) polyethylene. The thickness of the converter and cadmium loading can be customized to meet test requirements. Conversely, lead or lead-bismuth converters can be used to enhance the neutron to gamma ratio.

B. Time Profile of Irradiation.

The APRF can be operated in either the steady-state or pulse mode. In the steady-state mode, the reactor can be operated at power levels up to 200 kW for approximatley one minute, at 10 kW for several minutes and at 7 kW continuously. The limiting factor for steady-state operations is the fuel temperature. In the pulse mode, there is a maximum pulse yield of 1.5×10^{17} fissions. The pulse width can be varied from approximately 50 μsec to 10 milliseconds. The reactor can also be operated on a fast exponential ramp with a period of 5 seconds.

IV. Reactor Environments.

A. NATO Dosimeter Intercomparison Environments.

APRF radiation environments have been established within the NATO community as reference fields for the intercomparison of battlefield dosimeters and radiation shielding studies. To date, two NATO dosimetry intercomparisons have been conducted in September 1986 and in March 1992. The radiation environments were established with the following criteria:

1. The radiation fields must be sufficiently large and uniform to permit the exposure of multiple dosimeters.
2. The radiation fields must be calibrated traceable to national standards.
3. The radiation fields must have a high simulation fidelity (neutron to gamma ratio).
4. The dosimeters must be irradiated at several levels ranging from a few cGy to 10 Gy.

The geometry of the exposure fields are shown in Figures 1 and 2. All irradiations are made 165cm from the reactor core centerline and at a height of 200cm above the borated floor. Four configurations are used. In the first geometry, the dosimeters are irradiated free-in-air. In the second geometry, the leakage spectrum is perturbed by using a 12.7 cm thick by 46 cm high converter which consists of polyethylene loaded with cadium oxide (5% by weight)[3]. This converter reduces the neutron kerma and alters the neutron spectrum to give the the neutron to gamma ratio of the radiation field 1 km from a tactical weapon detonation. The third and fourth geometries are the same as the first two except that the dosimeters are now exposed on polyethylene phantoms.

Reference dosimetry measurements for the second intercomparison were made by scientists from the Etablissement Technique Central de l'Armement (ETCA), Arcueil-Cedex, France, Armed Forces Radiobiology Research Institute (AFRRI), Bethesda, Maryland, and Army Pulse Radiation Facility (APRF). Measurements were made with the detectors listed in Table 1.

Table 1. Detectors Used in Calibration.

Organization	Detectors
ETCA	TE-Mg IC, TE-Al IC, TE-C IC, Np FC, Silicon Diodes, Rh foils, Al_2O_3 TLD
AFRRI	TE-Mg IC
APRF	TE-Mg IC, CaF TLD

The results of the reference dosimetry measurements are shown in Table 2. The results shown are the numerical averages and standard deviations of the detectors listed in Table 1. The uncertainties represent only the consistancy of the various measurements, not the accuracy. As indicated by the data for the bare reactor, there is excellent agreement in the measured neutron kerma; however, the standard deviation of the gamma-ray kerma is greater due to the difficulty associated with measuring a small gamma-ray component in a mixed neutron and gamma-ray field. The effect of the converter is to reduce the neutron kerma and enhance the gamma-ray kerma. For these environments, the standard deviation of the gamma-ray kerma measurements is decreased significantly with the error associated with the neutron kerma increasing. There appears to be no effect on the neutron kerma due to backscattering from the phantoms; however, the neutron interactions with the phantoms does increase the gamma-ray kerma.

Table 2. Reference Neutron and Gamma-Ray Kermas.
(cGy(Ti) per kWmin)

Configuration	Neutron Kerma	Gamma-Ray Kerma	n/r
Bare Rx, FIA	20.4 ± 1%	1.75 ± 13%	11.6
Bare Rx, Phantoms	21.4 ± 1%	4.53 ± 5%	4.7
Converter, FIA	3.57 ± 6%	4.70 ± 1%	0.76
Converter, Phantoms	3.53 ± 7%	5.53 ± 4%	0.64

For a radiation field to be valid as a reference field, the field must be reproducible. Table 3 compares the results above with measurements made during the First NATO Battlefield Dosimeter Intercomparison for the reactor with the converter, free-in-air environment. Agreement is within 2% for this geometry.

Table 3. Reproducibility - Converter, FIA Configuration.
(cGy(Ti) per kWmin)

Data Set	Neutron Kerma	Gamma-ray Kerma	n/r
1986	3.51	4.65	0.76
1992	3.57	4.70	0.76
Ratio	1.017	1.011	—

B. Calculated and Measured Neutron Spectra.

Neutron and gamma-ray spectra have been measured and calculated for a number of reactor environments. Figure 3 shows the DORT[4] calculations of Kaul[5] for the bare reactor. These spectra illustrate the change in the shape, softening, of the neutron spectrum with distance. Figure 4 details the calculations of Nurdin[6] which show the affects of 12.7cm cadmium loaded polyethylene converter on the neutron spectrum. This spectrum corresponds to the converter free-in-air geometry described above. The polyethylene in the converter reduces the fast portion of the spectrum by moderating the neutrons allowing these less energetic neutrons undergo an (n,r) reaction with the cadmium. Recent measurements of the neutron leakage spectrum using proton-recoil techniques agree with the DORT calculations.[7]

C. Criticality Monitor Testing Environments.

American National Standard ANSI/ANS-83-1986, *Criticality Accident Alarm System*[8], establishes the performance criteria for criticality alarms used in monitoring operations with plutonium, ^{233}U, uranium enriched in ^{235}U, and other fissionable materials in which an accidentaly excursion would cause the exposure of personnel to high levels of radiation. This standard defines a minimum detection criterion for a monitor in terms of a minimum accident of concern. In areas where the materials described above are handled or processed with nominal shielding, the minimum accident of concern is assumed to deliver an absorbed dose (neutron and gamma-ray) 20 cGy at 2m from the material in 60s. A criticality monitor, therefore, must activate when the dose rate equals or exceeds a value of equivalent to 20cGy/min at 2m from the reacting material. This standard also states that a criticality monitor must be able to detect a radiation transient of 1 ms. Depending upon the mechanics of the criticality excursion, the neutron to gamma ratio may vary from 0.30 for moderated assemblies[9] to 10-12 for an unmoderated, unreflected metallic assembly such as the APRF. This range of neutron to gamma ratios and dose rates can be spanned through the use of the bare reactor and the reactor with converters and by varying the type of reactor operation.

Figure 5 illustrates various gamma dose rate profiles available at 1 meter from the reactor center line. Pulse Operation P93-35 illustrates the free field behavior while P93-38 shows the increased gamma dose rate with the 10 cm neutron to gamma converter. The pulse width of these operations are 68 and 60 μsec respectively. These environments correspond to over-testing of the monitor to very short radiation transients. P93-69 is the output of the reactor when it is deliberately slowed down with reflected thermal neutrons. The pulse width for this operation is 2.3 msec and corresponds to testing at the level required by the ANSI standard. Steady-state Operation SS93-127 is the output from a high level steady state run at 150 kilowatts for 30 seconds. All of these operations result in approximately $1x10^{17}$ fissions. Figure 6 shows a typical instrument response test with a gamma sensitive ion chamber located 10 meters from the reactor core driving a logarithmic picoammeter.

For tests at more modest levels and slower rates, subprompt critical ramps with a stable positive period can be used to approach the trip point. Figure 7 illustrates a reactor power ramp with a 0.2 second period.

V. Conclusions.

A number of different radiation environments have been validated at the APRF for use in dosimeter intercomparison and calibration of criticality monitors. These environmenmts have been utilized for two intercomparisons of NATO personnel dosimeters and for testing criticality monitors. By using converters and varying the type of reactor operation, the APRF can provide radiation environments which have different spectra, neutron to gamma ratios, and time histories.

VI. Acknowledgements.

This work was supported in part by the Radiation Environments Program (REP) of the Defense Nuclear Agency, and in support of the objectives of NATO AC/243(Panel 8) Research Study Group 23 on the Assessment, Prophylaxis, and Treatment in Nuclear Environments.

VII. References

1. Kazi, A.H., *Operation of the Army Pulsed Radiation Facility Reactor Core*, Trans. of Amer. Nucl. Soc., 14:313, 1971.

2. Hazi, A.H., et. al., *Characteristics of Pulsed Fast Neutron-to-Gamma-Ray Converters*, Nuclear Technology, 25, 1975.

3. Ibid.

4. Rhoades, W.A. and Emmet, M.B., "DOS: The Discrete Ordinates System," ORNL/TM-8362, Oak Ridge National Laboratories, Oak Ridge,TN, 1982.

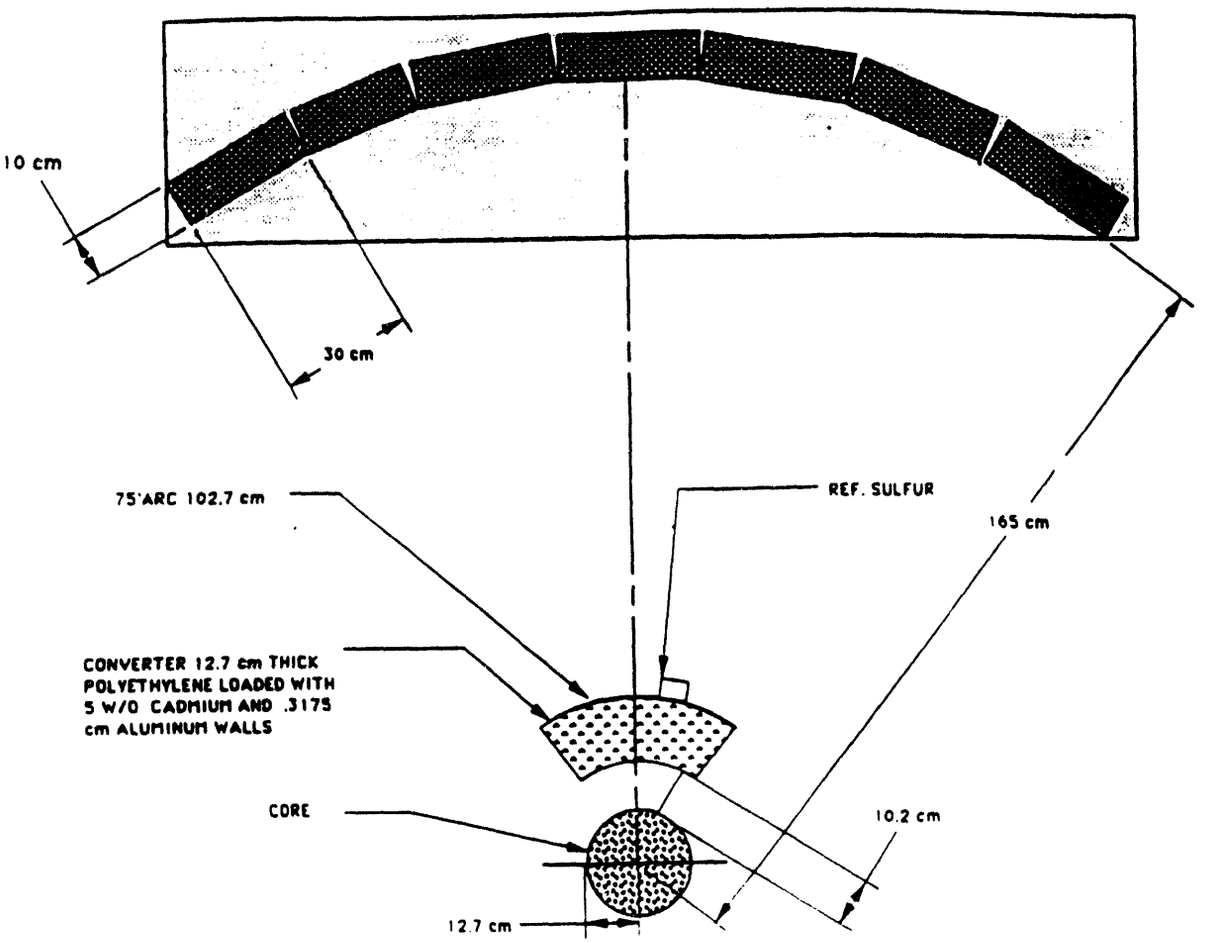
5. Kaul, Dean C. and Egbert, Stephen D., *Radiation Leakage from the Army Pulse Radiation (APRF) Fast Reactor*, Science Applications International Corporation, SAIC-89/1423, May 1989.

6. Nurdin, Guy, *Short and Long Distance Radiation Transport Calculations at APRF*, Etablissement Technique Central de l'Armement, July 1992.

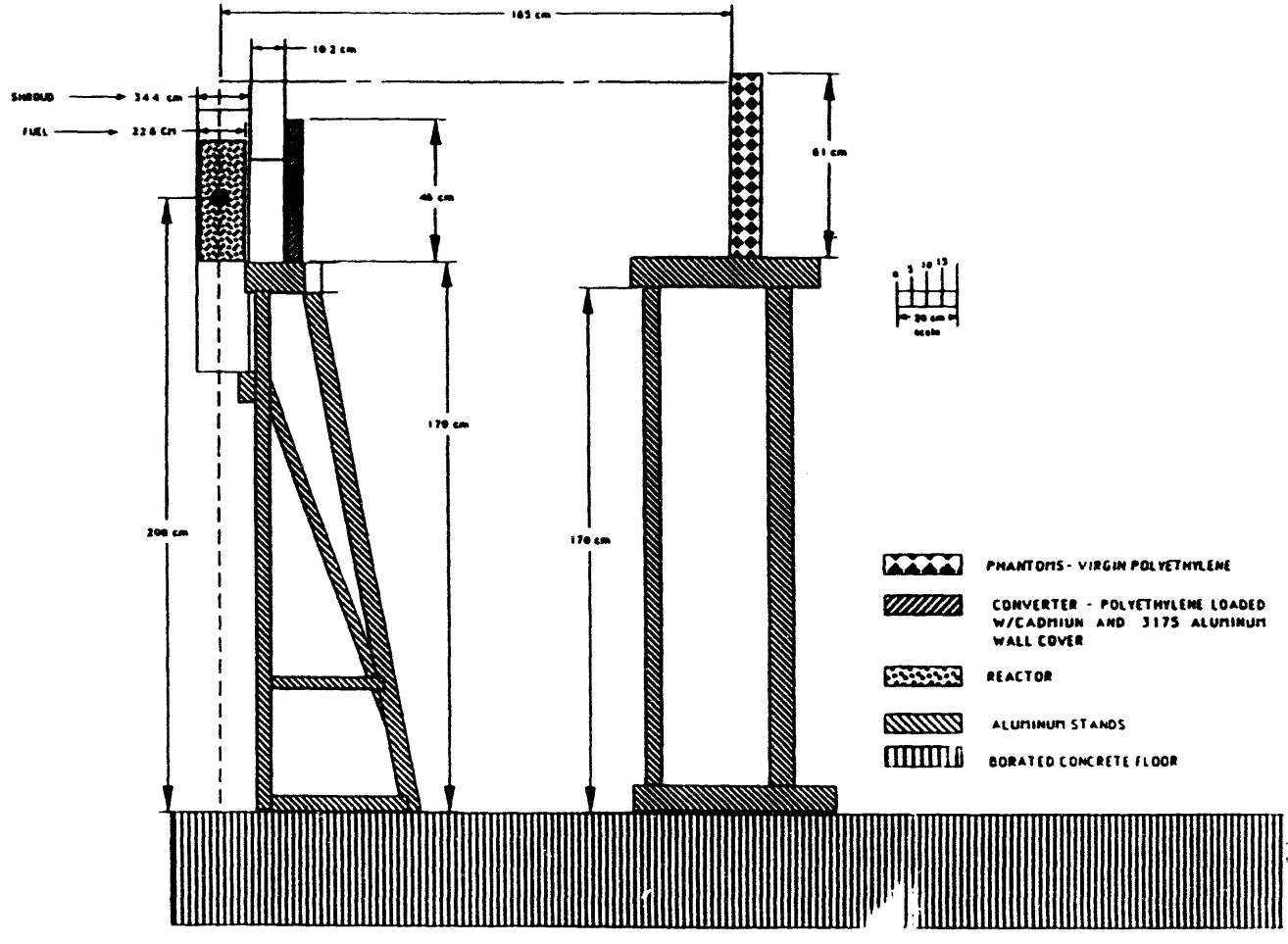
7. to be published.

8. ANSI/ANS Standard 8.3-1986, *Criticality Accident Alarm System*, American Nuclear Society, August 1986.

9. Hurst, G.S., Ritchie, R.S., and Emerson, L.C., "Accidental Radiation Excursion at the Oak Ridge Y-12 Plant, Part III, Determination of Radiation Doses," Health Physics, 2, 121(1959).



EXPOSURE CONFIGURATION WITH CONVERTER AND SLAB PHANTOMS -TOP VIEW



EXPOSURE CONFIGURATION WITH CONVERTER AND SLAB PHANTOMS- SIDE VIEW

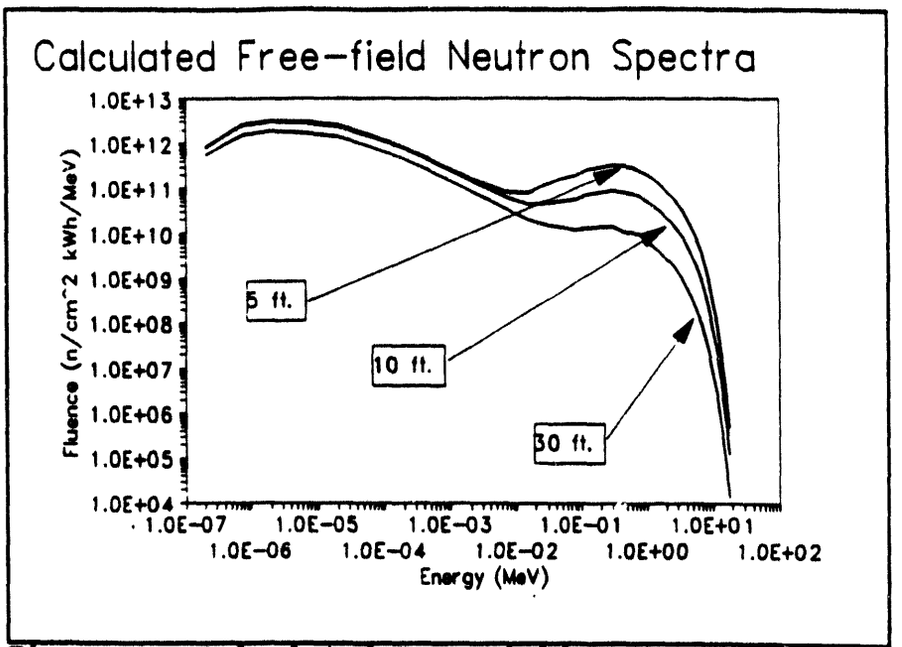


Figure 3. Calculated Free Field Neutron Spectra.

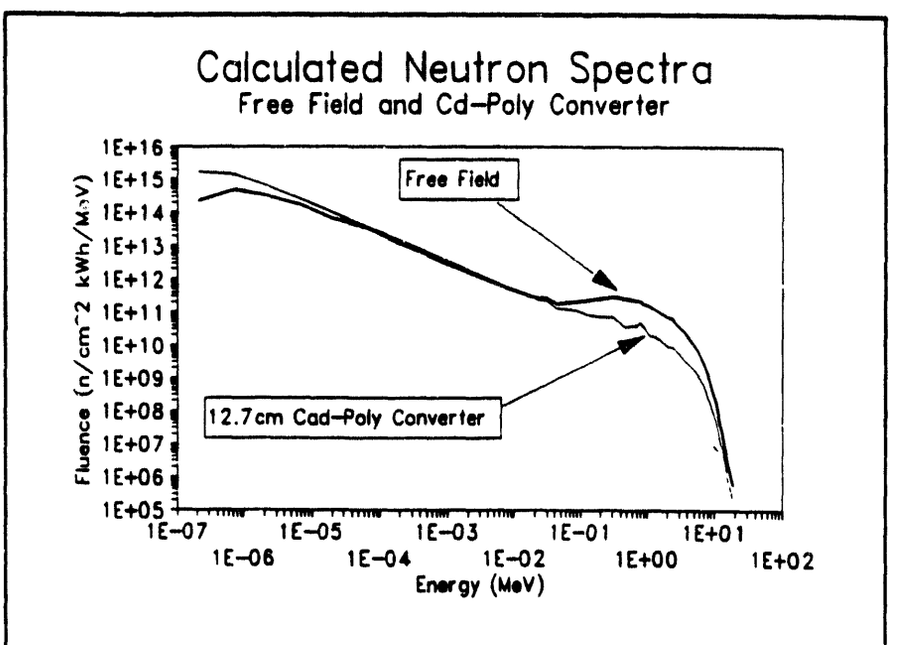
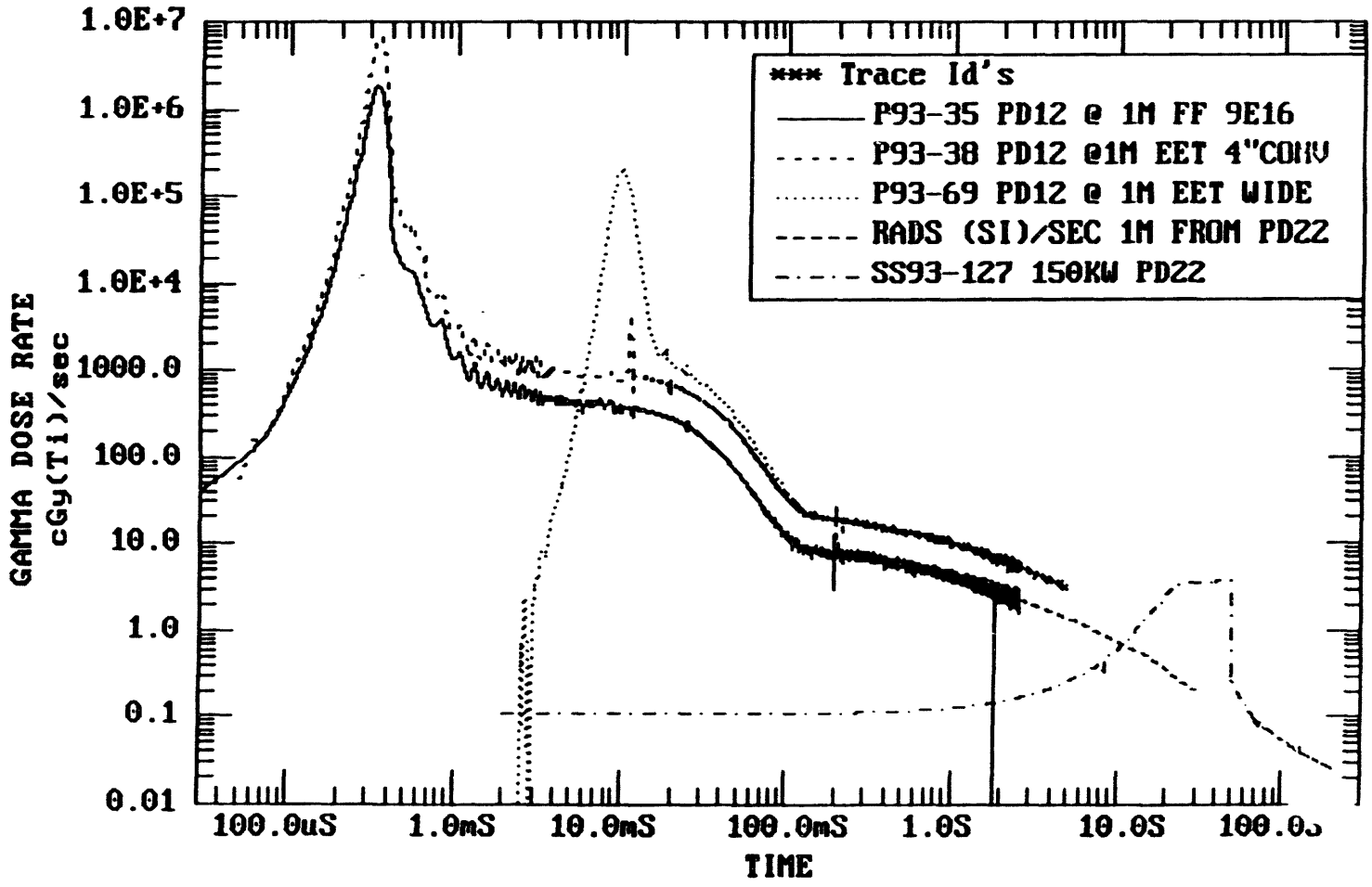
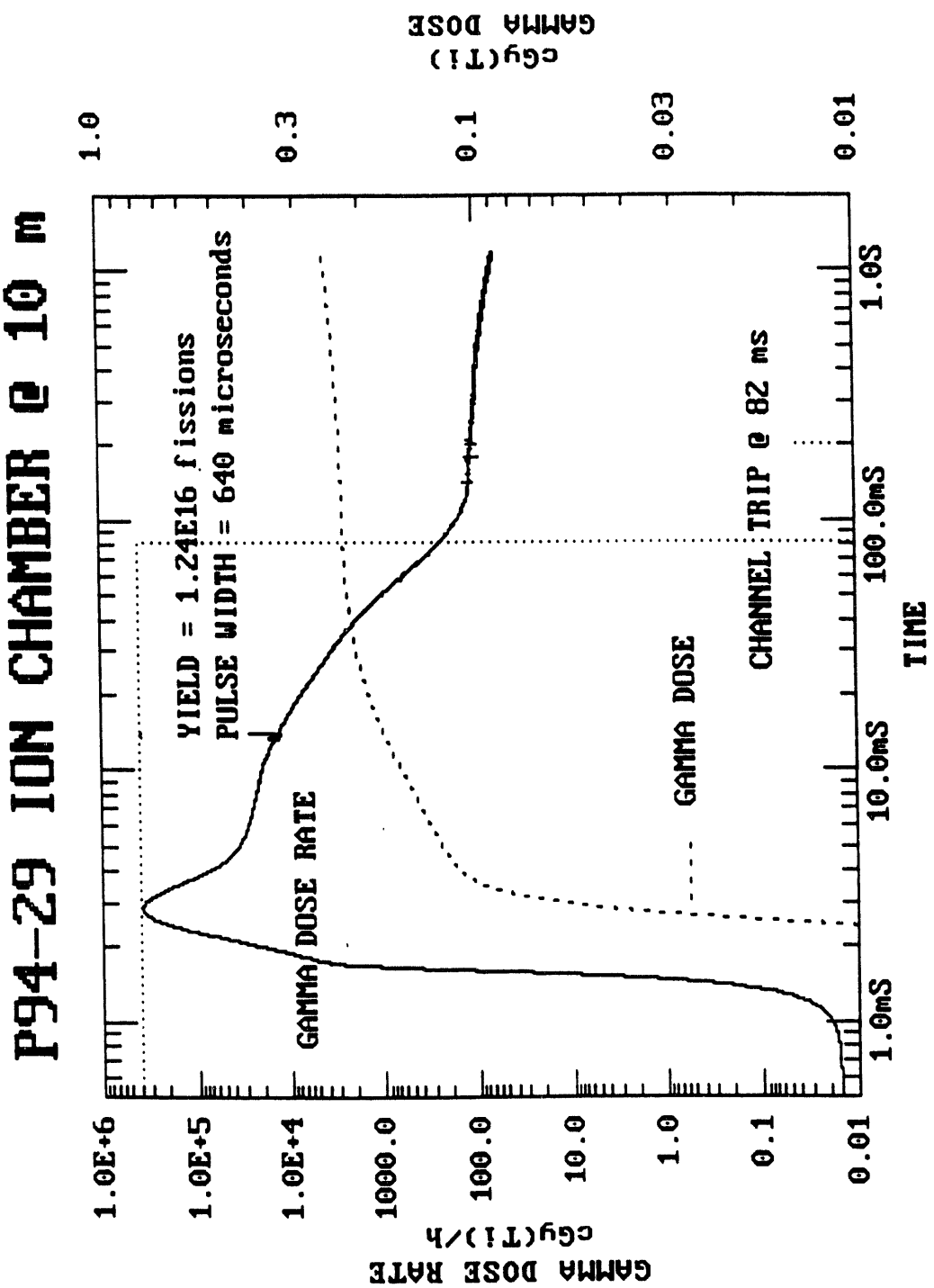


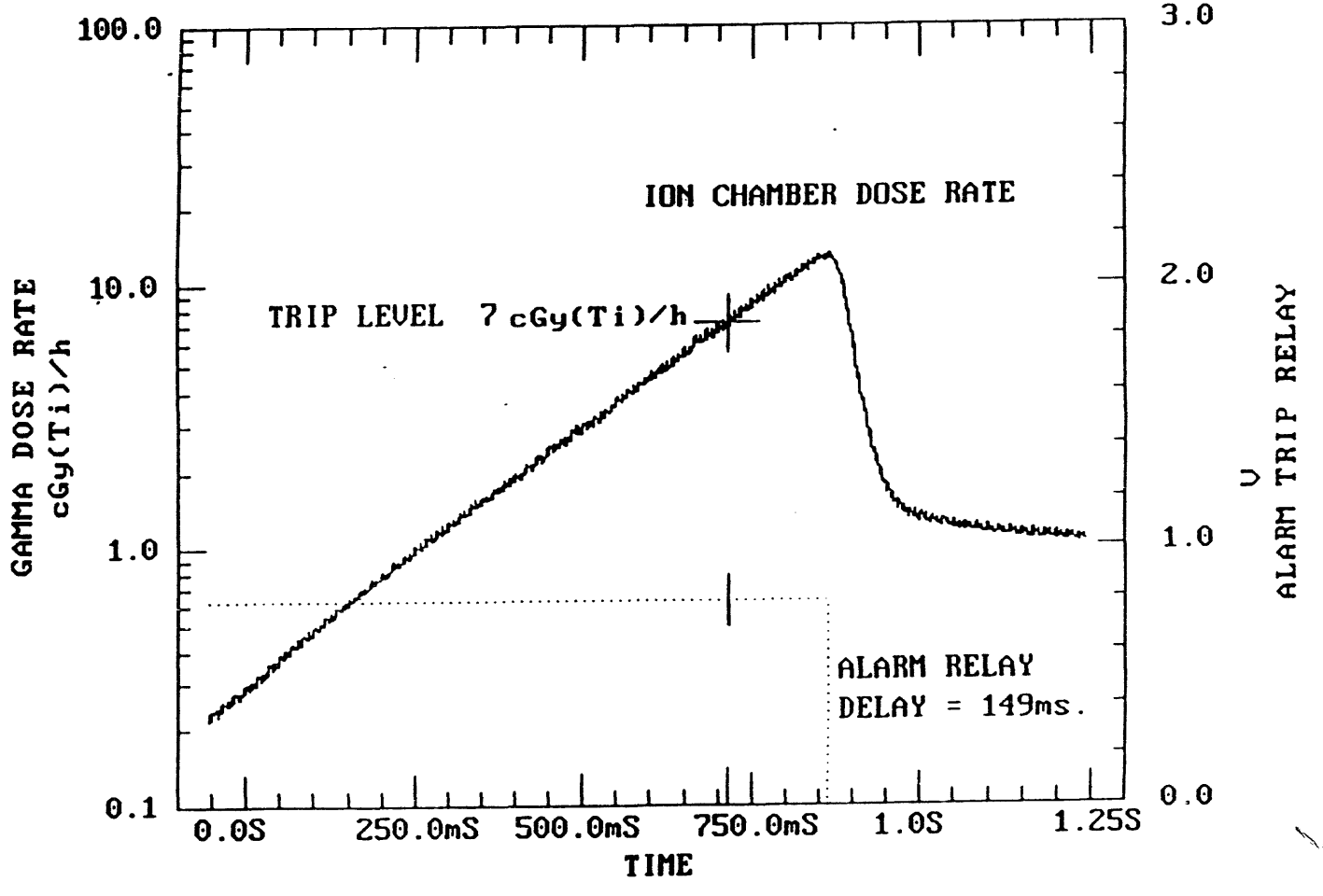
Figure 4. Effects of a Cd-Poly Converter on the Neutron Spectrum.

REACTOR GAMMA DOSE RATE PROFILE




P94-29 ION CHAMBER @ 10 m
YIELD = 1.24E16 fissions
PULSE WIDTH = 640 microseconds
GAMMA DOSE RATE
GAMMA DOSE
CHANNEL TRIP @ 82 ms
GAMMA DOSE RATE
cGy(Ti)/h
GAMMA DOSE
cGy(Ti)
TIME
1.0E+6
1.0E+5
1.0E+4
1000.0
100.0
10.0
1.0
0.1
0.01
1.0
0.3
0.1
0.03
0.01
1.0mS
10.0mS
100.0mS
1.0S

MINIPULSE FOR P94-28



ESTABLISHING A ^{252}Cf SOURCE FOR NEUTRON IRRADIATIONS OF DOSIMETRY AT THE IDAHO NATIONAL ENGINEERING LABORATORY

Orval R. Perry
Idaho National Engineering Laboratory

Paul E. Ruhter
Idaho National Engineering Laboratory

The neutron monitoring program at the Idaho National Engineering Laboratory (INEL) was developed in the early 1970s and has essentially remained unchanged since its implementation. The program is based on the albedo neutron detections methods and dosimeter of Mr. Dale Hankins[3]. The INEL dosimeter design is identical to that constructed by Mr. Hankins while at the Los Alamos National Laboratory (Los Alamos Scientific Laboratory at the time). The dosimeter uses 3 LiF (TLD-700) "chips" and 3 LiF (TLD-600) "chips" positioned on the center axis of a polyethylene lined cadmium enclosed 10.1 mm X 19.4 mm X 31.8 mm box. The neutron dosimeter is attached to and worn with a neutron insensitive beta/gamma dosimetry badge.

Neutron dosimeters are processed on a Harshaw Atlas hot gas reader. The neutron dose is interpreted by a correction factor that is applied to the difference between the mean responses of the TLD-700 (photon sensitive) and TLD-600 (photon + neutron sensitive). The correction factor is interpreted from the Hankins curve[3] based on a 9 inch to 3 inch Rem-meter ratio.

The neutron quality assurance program includes dosimeters irradiated on a monthly basis. Historically, the dosimeters were irradiated by DOE-ID personnel using an Am-Be source located at the Radiological and Environmental Sciences Laboratory (RESL) at the INEL. The DOE personnel providing the irradiation services also provided the DOE oversight to the EG&G operated dosimetry program as well as being part of the DOELAP program. A 1991 DOE Tiger Team review of the dosimetry operations concluded that the DOE providing both a program Overview and dosimeter irradiations to the EG&G program constituted a potential conflict of interest. Consequently, the Operational Dosimetry Unit (ODU) of EG&G moved the neutron irradiation program from the RESL Am-Be source to a ^{252}Cf source located in the Health Physics Instrument Laboratory (HPIL).

To accomplish this move the ODU designed a DOELAP equivalent PMMA neutron phantom, designed and constructed an irradiation platform at HPIL, and developed a neutron correction factor based on ^{252}Cf for interpreting phosphor output. In addition, to facilitate dosimeter change-out, the central 20 cm X 20 cm area of the phantom was designed to be

removable which required validation that an interchangeable slide area would not measurably affect the albedo effect provided by the phantom.

The 160 micro-gram ^{252}Cf source at HPIL is stored underground in a .91 meter diameter X 3.05 meter long tank containing DI water and is raised by chain and stepping motor to an irradiation position through an aluminum tube that extends vertically to just beneath the ceiling area of a 12.8 meter long X 8.53 meter wide X 9.75 meter high room. The normal irradiation height is 4.27 meters above the floor in the approximate mid-point of the room. The facility purpose is to calibrate neutron instruments, and an instrument positioning linear track system (4.88 meters long) and operator control area and walkway was available at the normal irradiation height. The height of the center-line of the neutron phantom and maximum height the source could be raised precluded the use of the installed linear track system for phantom mounting; consequently a separate aluminum platform was constructed using the walkway rails as a foundation. The platform was sized to permit irradiations from approximately 30 cm to 100 cm from the source. The platform includes phantom base orientation rails to ensure axis and positioning duplication for neutron irradiations.

ODU first attempted to construct the 40 cm X 40 cm X 15 cm phantom using 3 PMMA slices and bonding the slices together. The end product contained extensive air bubbles at the bonding junctions. The bubble formation most probably resulted from three conditions that should be noted (1) as-purchased PMMA slabs were used and were probably not totally flat - oversized slabs should be used and milled flat, (2) an insufficient amount of bonding agent was used to dissolve enough plastic at the junctions, and (3) The clamping process did not exert enough force to completely remove air from the junction area - the process should be pressed instead of clamped. The slab phantom was discontinued and a poured single piece phantom was purchased from a commercial plastics vendor. The phantom was mounted on a 1.27 cm thick X 30.3 cm wide X 61 cm long aluminum base. The base dimensions were selected to prevent the phantom from inadvertently toppling during positioning. The phantom base slides in the platform guide rails for ease of positioning. One face of the phantom was milled with slots to accept a 0.5 cm thick slide covering the central 20 cm square surface of the phantom. The intent of the slide was to be able to perform multiple irradiations by simply inserting and removing pre-constructed dosimeter slides.

A testing protocol was constructed to develop a neutron correction factor for interpreting QA/QC dosimeter results. The protocol accomplished the following objectives.

1. Verify that dosimeters positioned in the central 20 cm X 20 cm region of the phantom demonstrated a uniform response.

2. Verify that the removable slide did not measurably affect dosimeter performance.

3. Establish a correction factor relating TL output (nano-coulombs) to dose at a phantom position of 100 cm from the center-line of the source.

4. Validate the correction factor with TLDs randomly selected from the field population.

5. Establish a correction factor relating TL output (nano-coulombs) to dose at a phantom position of 40 cm from the center-line of the source and compare the factor to that generated by Dale Hankins using Rem-meter 9" to 3" ratios.

The fifth objective was designed to validate the appropriateness of using Eberline HP-280 probes and PNR-4 Rem-meters currently in use at the INEL with the Hankins curves for determining correction factors. The close geometry at 40 cm from the source would introduce large errors due to minor distance discrepancies between the 9" and 3" sphere center-lines. To reduce these discrepancies, a special irradiation jig was designed to ensure consistent alignment of the sphere-centers with the source.

The first objective was accomplished by positioning 17 neutron dosimeters at 10 cm intervals on the face of the phantom with 1 dosimeter at the center of the phantom. With this arrangement 5 dosimeters were within the central area and 12 dosimeters were outside the central area. The dosimeters were irradiated with the phantom at 100 cm from the source center-line. The TL output in nano-coulombs was recorded for each TLD "chip" in each dosimeter. The 5 dosimeters located in the center region of the phantom were evaluated using a single factor analysis of variance[1,2] (F test) on the gamma compensated output of all TLD-600 phosphors. The critical value ($F_{0.05,(1),(k-1),(N-k)}$) for the 95% confidence level was established as 3.48 (k-1 = 4, N-k = 10) and the calculated F value was 1.27. From the F test results it was concluded that a uniform beam existed in the central area of the phantom. An F test of all dosimeter positions determined that a uniform beam did not exist across the entire face of the phantom. As expected the results of the dosimeters within 5 cm of the phantom edge demonstrated a markedly lower TL output. The F test results demonstrated that (1) the platform and phantom mounting system was adequate to position the central area of the phantom at the approximate source center-line, (2) the phantom demonstrated the expected albedo effect, and (3) the selected TLD-600 and 700 phosphor sensitivities were similar enough not to introduce an unreasonable bias to the test.

The second objective was accomplished by reversing the phantom and presenting the back of the phantom (solid area) to the source with the back face 100 cm from the source center-line. The dosimeters located in the central area of the front face of the phantom during the first test were located in the same position with the phantom reversed. The dosimeters were irradiated to dose levels similar to the first test. The TL output was normalized to the first test by the ratio of the delivered dose (test 1)/delivered dose (test 2). A "t" test was used to evaluate the similarity of TLD response between the back (solid) and front (slide) of the phantom.

The null hypothesis for the "t" test is described as the mean TLD response of position j equal to the mean TLD response of position j'($u_j = u_{j'}$) and the alternative is that the mean TLD response of dosimeter position j is greater than or less than j' ($u_j < u_{j'}$ or $u_j > u_{j'}$). The critical t values for a two-sided 5% level of significance with 4 degrees of freedom are 2.776 and -2.776. The t value between equal positions (j and j') on the phantom is determined by:[1,2]

$$t_{j,j'} = \frac{\bar{X}_{i,j} - \bar{X}_{i,j'}}{s_p \sqrt{\frac{1}{N_j} + \frac{1}{N_{j'}}}}$$

Where,

$$s_p = \left[\frac{\sum_{i=1} X_{i,j}^2 - \left[\frac{(\sum_{i=1} X_{i,j})^2}{N_j}\right] + \sum_{i=1} X_{i,j'}^2 - \left[\frac{(\sum_{i=1} X_{i,j'})^2}{N_{j'}}\right]}{N_j + N_{j'} - 2}\right]^{\frac{1}{2}}$$

$$\bar{X}_{i,j},\ \bar{X}_{i,j'} = \frac{\sum_{i=1} X_{i,j}}{N_j},\ \frac{\sum_{i=1} X_{i,j'}}{N_{j'}}$$

$X_{i,j}$ = [*TLD-600 chip i position j output (nC)* - *Control*] γC - [$\overline{\text{TLD-700}}$ - *Control*]

$X_{i,j'}$ *is solved the same as* $X_{i,j}$ *above*

i = *TLD-600 chip* 1, 2, 3

j = *B2, B3, C2, C3,* 0

j' = *B2', B3', C2', C3',* 0'

γC = *TLD-600/TLD-700 photon sensitivity adjustment factor*

N_j, $N_{j'}$ = *Number of TLD-600 chips at Position j, j'*

The calculated "t" values for the five dosimeter positions varied from -2.363 to 0.964. The results of the "t" tests indicated the mean response between duplicate dosimeter positions on the back of the phantom and front of the phantom were the same. Thus, the addition of the slide did not significantly impact the albedo effect of the phantom with respect to TLD detection.

The third objective was to generate a neutron correction factor for a phantom face position 100 cm from the center-line of the source. The correction factor was established using the data obtained from the 5 dosimeters in the central 20 cm X 20 cm area of the

phantom during the first test. The correction factor is the quotient of the ratio:

$$\textit{Derived Neutron Correction Factor (NCF)} = \frac{\bar{X}_L\ (\gamma\ CF)}{\textit{Delivered Neutron Dose} - \textit{Transient Dose}}$$

Where,

γ *CF = Cs-137 equivalent units factor (mrem / nano- coulombs)*

$\bar{X}_L$ *= mean neutron TL (nano- coulombs)*

$$\bar{X}_L = \frac{\sum_i \sum_j n_{i,j}}{N}$$

i = Dosimeter chips 1, 2, 3, *output (nC)*

j = Dosimeter Positions 1 - 5

N = The total number of chips = 15

The correction factor was determined to be 0.156. In this form, the neutron TL (difference between the TLD-600 and TLD-700 response) must be converted to equivalent ^{137}Cs units before the neutron correction factor is applied. This is the same convention used by Hankins in generating his 9" to 3" correction curves.

Note that the denominator of the ratio includes a transient dose to account for neutron dose accumulation on the TLDs during source positioning. The transient dose was a conservative estimate from simple numerical integration of dose rate and time. For an irradiation time of 60 minutes the transient component is approximately 1% of the total dose at 100 cm from the source.

The fourth objective was tested by using 5 dosimeters placed in the phantom central irradiation area. The phantom face was placed 100 cm from the center-line of the source and the dosimeters were irradiated to 104.4 mrem total dose. The measured mean of the dosimeter group was 105.2 mrem with a standard deviation of 5.9 mrem. The acceptance criteria was that the sum of the absolute value of the group bias and 1 standard deviation (σ) was less than or equal to 15% of the delivered dose. The value of this sum was less than 7% of the delivered dose. Since this met the acceptance criteria, the derived correction factor for QA/QC neutron dosimeters irradiated on phantom face at 100 cm from the center-line of the source was acceptable.

The fifth objective of the protocol was to establish a neutron correction factor at 40 cm from the source and compare the factor to that derived from the Hankins curve[6] using a 9" to 3" Rem-meter ratio. Five dosimeters were prepared and placed in the center region of the phantom. The face of the phantom was positioned 40 cm from the center-line of the source and the dosimeters irradiated to 720.2 mrem. The correction factor was established

in a manner analogous to the derivation at 100 cm.

The empirical neutron correction factor was determined to be 0.1364. As with the correction factor established at 100 cm from the source, the neutron TL (difference between the TLD-600 and TLD-700 response) must be converted to equivalent ^{137}Cs units before the neutron correction factor is applied.

The correction factor taken from the Hankins curve used the PNR-4 Rem-meter response ratio of the 9" to 3" spheres with the sphere center-line 41.4 cm from the source center-line. The 41.4 cm distance was dictated by interference of the HPIL instrument positioning track with the positioning jig developed by ODU. The source beam axis for the jig was identical to that used for the phantom irradiations. The sphere ratio at 41.4 cm was considered acceptable for comparison purposes in that no significant ratio change was anticipated over a 2 cm distance. The 9" to 3" sphere ratio was established as 1.833. The Hankins correction factor corresponding to this ratio was 0.1357.

The neutron correction factors established by the Rem-meter ratio method and empirically by TLD results deviated by $< 1\%$. Figure 1 replicates a portion of Hankins neutron calibration factor curve and annotates the Rem-meter sphere ratio and empirical TLD correction factor intersection with the curve.

The results of this test concluded that the INEL dosimeter design and portable instrumentation currently in use were satisfactory for using the Hankins neutron calibration curve.

Hankins Neutron Calibration Curve
Comparison Of Rem-meter And TLD Fit

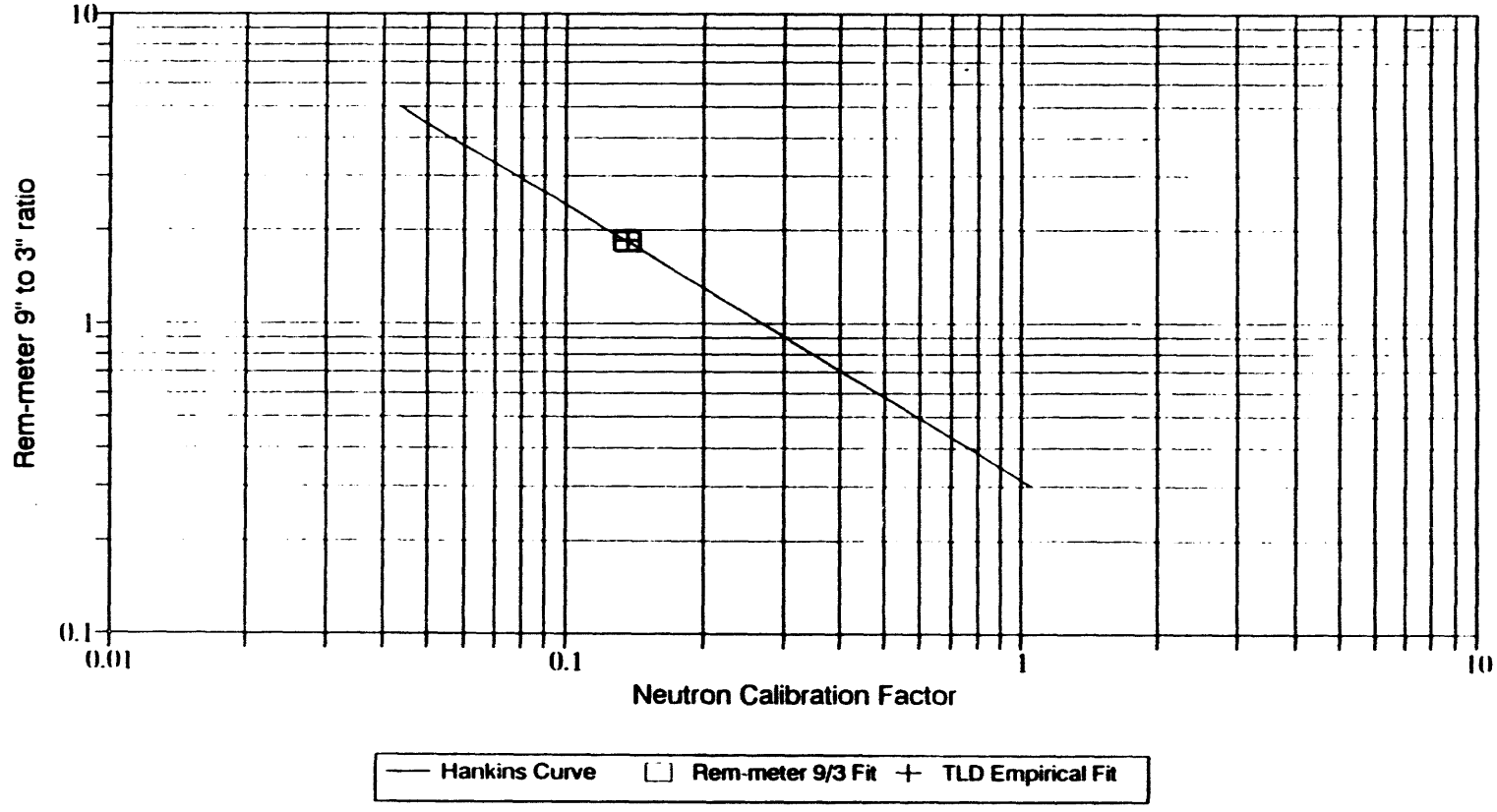


Figure 1. The Rem-meter sphere ratio and empirically derived TLD correction factor intersection with Hankins curve.

References

1. Jerrold H. Zar, Biostatistical Analysis, Prentice-Hall, 2nd edition, 1984.

2. W. J. Dixon and F. J. Massey, Jr., Introduction To Statistical Analysis, McGraw-Hill Book Company, Third Edition, 1969.

3. D. E. Hankins, A Small Inexpensive Albedo Neutron Dosimeter, Los Alamos Scientific Laboratory report, LA-5261, 1973.

COMPARISON OF NIST AND ISO FILTERED BREMSSTRAHLUNG CALIBRATION BEAMS

C. G. Soares and M. Ehrlich
Ionizing Ra· :ion Div., National Institute of Standards and Technology, Gaithersburg, MD 20899.

HISTORICAL BACKGROUND

For radiation-instrument calibration to be generally acceptable in the United States, direct or indirect traceability to a primary standard is required. In most instances, one of the primary standards established at NIST is employed for direct traceability. The National Voluntary Laboratory Accreditation Program (NVLAP) [ANSI 1983, ANSI 1994] and the Department of Energy Laboratory Accreditation Program (DOELAP) [USDOE 1986], are examples of programs employing dosimetry based on the NIST primary photon-, beta particle- and neutron-dosimetry standards.

The current NIST primary dosimetry standards for bremsstrahlung [Lamperti et al. 1988, Simmons 1991] were first established in the 1950s. They have been updated since then on several occasions, most recently in 1983. For use in the US, radiation instruments are presently calibrated at NIST or approved secondary laboratories, in these standard bremsstrahlung beams in terms of the quantities air kerma or absorbed dose. Where required, the user converts from the calibration quantities to the ones of interest in his field of application. In other countries, bremsstrahlung standards as a rule developed separately, with little or no attempt for international uniformity. However, in the 1970s, Technical Committee 85 of the International Organization for Standardization (ISO) started its work on establishing sets of internationally acceptable, well-characterized photon beams for the calibration of radiation-protection instruments [ISO 1983]. This work was based on data obtained by the Gesellschaft für Strahlen- und Umweltforschung (GSF) [Seelentag et al. 1979]. An additional set of bremsstrahlung beams is being added in the present update of ISO 4037 [ISO 1993]. The ISO beams have been widely accepted by ISO Member Nations and also by other international groups, e.g., the International Atomic Energy Agency (IAEA). However, up to now, there have been only minimal attempts in the United States to adopt the internationally accepted calibration beams. This is in contrast to the situation with beta particles and neutrons, where international standards [ISO 1984, ISO 1989] are followed in the U.S.

STATEMENT OF PROBLEM

The traditional indifference of the U.S. to international standards did not pose a difficulty in the field of the calibration of radiation-protection instrumentation until the International Commission on Radiation Units and Measurements (ICRU) recommended new quantities for use in practical radiation-protection dosimetry [ICRU 1985, ICRU 1988, ICRU 1992], which are to approximate the equivalent dose [ICRP 1991] by readily measurable, operational quantities. Inasmuch as two of the operational quantities (the directional and personal dose equivalent) take on different values not only for different photon energies, but also for different directions of photon incidence, the conversion coefficients from photon fluence and air kerma to the recommended operational quantities are functions of photon energy and angle of photon incidence. Therefore, instrument calibration in terms of the operational quantities involves a computation of conversion coefficients for the photon beams and the geometry employed in the particular calibration.

Conversion coefficients from fluence and air kerma to personal dose equivalent applicable to the ISO calibration beams and various calibration geometries in practical use are available in the literature [Grosswendt 1990, Grosswe 1991, Grosswendt 1992]. However, when the committee of the American National Standards Institute (ANSI) revising the standard ANSI N13.11 [ANSI 1983, ANSI 1994] which in the United States is the basis for the National Voluntary Laboratory Accreditation Program (NVLAP) for dosimetry, decided to require compliance testing in terms of the operational quantities recommended by the ICRU, they had to initiate their own computation of conversion coefficients [Zeman et al. 1991]. The reason for this was that the bremsstrahlung beams required for traceability to NIST in most instances are different from the ISO beams. Similarly, DOELAP, which also desires to express the results of its compliance tests in the future in terms of the applicable operational quantities and has selected NIST beams different from the ones selected for NVLAP, will have to compute its own conversion coefficients. The same procedure would have to be followed by all U.S. organizations interested in using the operational quantities for instrument calibrations with one or the other of the NIST calibration beams different from the ISO beams. These special laborious computations could be avoided if NIST agreed to offer at least some sets of ISO photon beams for which conversion coefficients are available in the literature. Recently, DOE was the first government agency to propose that NIST add ISO beams to its standard beams, and subsequently gave NIST a detailed list of the ISO beams that would be desirable to DOELAP. Also, in a recent radiation protection dosimetry conference, a need was expressed for greater international uniformity in photon beams used for instrument calibrations [Sims and Swaja 1992].

SCOPE OF THIS WORK

In the following, a review is presented of available data for the calibration beams in use in different countries. The two main methods of specifying beam quality are discussed and examples are given for the measurement precision of the parameters employed in either. Finally, there is a presentation of the current NIST endeavor to produce and characterize a series of ISO bremsstrahlung beams for instrument calibration in the United States.

Specification of Beam Quality

There are two comparable systems for specifying x-ray spectra. The traditional method [ICRU 1962] has been to measure narrow beam attenuation in a well-characterized material such as Cu or Al and then to determine the thicknesses needed to attenuate the primary beam by one half and again by one half (first and second half value layers, respectively). The first HVL is an indication of the overall beam hardness (average energy), while the ratio of the first and second HVLs, known as the homogeneity coefficient, is an indication of the spectral width, with a ratio of unity expected for monoenergetic photons. HVL measurements are difficult and time consuming, and proper geometry is crucial for successful measurements. In addition, the problem of the energy dependence of the instrument used to measure the air kerma rate of the transmitted beam must be addressed since the transmitted spectrum is changed ("hardened") by the added absorbers. For these reasons, rather high limits of tolerance are often placed on HVL measurements, as for example $\pm 5\%$ on first HVL and ± 7-10% on homogeneity coefficient [ANSI 1983, ANSI 1994, Eisenhower 1991].

A more modern and effective way of specifying beam spectra is actual measurement of the spectrum. With a knowledge of the spectrum, the average energy and the spectral width can be calculated directly. Spectral measurements are now accomplished using high-resolution photon counting detectors such as intrinsic Ge detectors. However, such measurements are count-rate limited, and hence

must be performed at very low tube currents, with very small apertures and at large distances. In addition, as described below, some unfolding of the measured pulse-height distribution is necessary to yield the fluence spectrum. There is always the caveat in such measurements on their applicability to the conditions under which the x-ray tube is ordinarily operated. A recent development which may circumvent all of these problems has been the development of the crystal small-angle diffraction spectrometer [Deslattes et al. 1994]. Such devices are now under development for higher energies (150 kV and 300 kV) [Deslattes and Kessler 1994] and promise to revolutionize the field of photon spectral measurement. Unlike counting detectors, these devices are signal-starved at normal operating currents and distances, and efforts are underway to increase the detection efficiency by modifications to the shape and structure of the diffracting crystal.

Sources for Spectral Data for Calibration Beams

The classic reference for spectral data for calibration beams remains the Catalog of Spectra compiled by the GSF [Seelentag et al. 1979] which contains plots of unfolded pulse-height distributions for 135 different spectra. Most of the ISO and NIST calibration beams are contained in this list, along with numerous others. The numerical data and three additional unpublished spectra have been made available to the authors. The measured pulse height distributions were converted to fluence using the technique of "backstripping" [Seelentag and Panzer 1979]; however detector resolution was not otherwise accounted for as can be seen from the widths of the W L-lines in some of the spectra.

All of the spectra of the calibration beams available at NIST prior to 1983 were measured by the authors [Eisenhower 1984]. Backstripping was employed to convert measured pulse-height distributions to fluence, and in addition, detector resolution was accounted for [Seltzer 1981 Seltzer 1983]. In 1983, several of the NIST beams were revised and the nomenclature was changed to the present style. Some beams were added; these latter were all based on existing ISO beams.

Several other groups have measured ISO spectra and have published tables of fluences [Read and Hagreen 1987, Peaple et al. 1989, Laitano et al. 1990, Bueerman et al. 1994]. What is known about these measurements is summarized in Table 1. Finally, Iles [Iles 1987, Iles 1991] has performed calculations of expected bremsstrahlung spectra for the ISO beams of 40 kV and above. These spectra are shown in the revised ISO 4037 [ISO 1993].

Comparison of Current NIST Techniques[1] and ISO 4037 Techniques

It is the intent in this section to present a detailed comparison between the current NIST and the most up-to-date ISO techniques [ISO 1993]. At present, 41 bremsstrahlung techniques are specified in ISO 4037 while NIST supports a total of 32 techniques. In ISO 4037 the spectra are divided into four categories: High and Low-Air Kerma Rate, and Wide and Narrow Spectrum. In the following tables, a system of notation has been adopted for these techniques. The prefix "NS" refers to the ISO Narrow Spectrum Series, "WS" refers to the ISO Wide Spectrum Series, "HK" refers to the ISO High Air Kerma Rate Series, and "LK" refers to the ISO Low Air-Kerma Rate Series.

Similarly, the NIST techniques are categorized according to filtration employed. For these, "H"

[1]In this context, the term "technique" is generally used to signify the list of values of all parameters used to characterize a particular calibration beam.

refers to the NIST Heavily Filtered Series, "M" refers to the NIST Moderately Filtered Series, "L" refers to the NIST Lightly Filtered Series, and "S" refers to the NIST Special Filtered Series. In each case, the number following the series type indicates the tube potential in kV to be employed. The NIST and ISO series are summarized in Tables 2 and 3.

The comparison between NIST and ISO techniques is broken down by kilovoltage in Tables 4 to 17. For each kilovoltage, or range of kilovoltages, the series, technique code, the inherent filtration, and added filtration are shown. Also shown are nominal values for first and second half-value layers (HVL) in Al or Cu, as well as average energy and full width at half maximum (FWHM) calculated from spectra (where they exist). Note that the homogeneity coefficient in a material is defined as the ratio of first and second half-value layers in that material, and that resolution is defined as the ratio of the spectral FWHM to the average energy.

What is evident from Tables 4-17 is that there is already some overlap between NIST and ISO, mainly between the NIST Heavily Filtered (H) techniques and the ISO Narrow Spectrum (NS) techniques at 10, 15, 20, 30, 40, 60, 100 and 300 kV. Also there is near agreement between the NIST Moderately Filtered (M) techniques and the ISO High Air-Kerma Rate (HK) techniques at 30 and 200 kV. In addition, NIST technique M300 is identical to the 300-kV ISO Wide Spectrum (WS) technique. Given these existing equivalences, the emphasis of a NIST program for implementing ISO techniques therefore should be to extend the NIST techniques to cover more of the ISO Narrow Spectrum and High Air-Kerma Rate Series. These extensions will also allow the use of ISO beam techniques in future revisions of US dosimetry testing standards, and in this way will enhance acceptance of US test results abroad.

As examples of the relative precision with which HVLs and spectra can be measured at the national laboratory level, some comparisons were made for two narrow spectrum techniques and two high air-kerma rate techniques. Figures 1 to 4 shows plots of measured and calculated spectra from various laboratories as identified in Table 1. Tables 18 to 21 present a more detailed comparison of the results shown in the figures, giving both measured HVLs and homogeneity coefficients, as well as HVLs, homogeneity coefficients, average energies and resolutions calculated from the spectra. In addition, air-kerma weighted spectrum averages of the conversion coefficient between air kerma and personal dose equivalent at 10 cm ($H_p(10)/K_a$) in ICRU tissue are shown, obtained by using the monoenergetic photon data of Grosswendt [Grosswendt 1991] and mass-energy absorption coefficients from Hubbell [Hubbell 1982].

One of the main problems associated with the use of broad-spectral, high air-kerma rate beams at the lower kilovoltages is illustrated in Table 18. The three spectra shown are similar with respect to both the attenuation (HVLs) and spectral (average energy and FWHM) descriptors. However there is a wide variation in the calculated conversion coefficient; this is due to the steep low-energy dependence of both the conversion coefficient function and the mass-energy absorption coefficients. Thus, small differences on the low-energy sides of this spectrum have large effects on the conversion coefficients from air kerma to the operational quantities. These differences may occur between laboratories due to variations in inherent filtration, x-ray tube ageing, target angle, filter thickness, and scatter conditions.

PROGRESS IN THE IMPLEMENTATION OF ISO TECHNIQUES AT NIST

In 1993 a program was inaugurated to implement ISO bremsstrahlung techniques at NIST. As a first step, the appropriate materials were acquired to construct the necessary filters. The foil samples obtained are 10 cm by 10 cm and range from 0.01 to 2-mm in thickness. To determine average thickness, five different areas have been measured on each sample using an automated coordinate measurement machine located in the NIST Fabrication Technology Division. In addition, a sample from each lot of material was subjected to x-ray fluorescence analysis in the Inorganic Analysis Division at NIST to verify that the material satisfies the 99.9+% purity requirements in ISO 4037. Finally, samples of each lot were radiographed to verify uniform x-ray transmission and assure that the material was free from large crystals which might cause preferential x-ray transmission.

New filter wheels, used at NIST for the expedient and reproducible exchange of filters, have been designed and constructed which will allow wheels to be easily mounted and removed. This will allow NIST to support the additional ISO techniques without having to sacrifice any of the current NIST techniques. The new wheels have been designed with larger filter apertures than are currently available. This will allow NIST to have larger beam diameters at closer distances than are currently available. Finally, the edge-driven wheel mechanism is being replaced with center-driven precision rotary tables, which will allow better positioning precision and easier programming.

CONCLUSIONS

For the purposes of international uniformity it is important that a consistent set of calibration beams be adopted for widespread use. To further this endeavor, ISO developed a standardized set of bremsstrahlung beam qualities which has been adopted for use in most of the world. It is proposed that they also be adopted in the US. To hasten this adoption it will be necessary to incorporate the ISO set of beams into the NIST set of standard calibration beams and into existing US test standards.

Given the difficulty in exactly duplicating broad-spectrum beams such as M30 (see Figure 1), in future revision of such standards it is important that testing for energy dependence of response be done with spectra which are as narrow as possible. The current test beams in ANSI N13.11 [ANSI 1994] are not amenable to this concept because of their broad spectra (except H150). It is recommended that this set of spectra be replaced with the ISO Narrow Spectrum and Low Air-Kerma Rate Series. This will give the added benefit that these spectra are easier to reproduce and verify in secondary laboratories than the presently-used broad spectra, particularly at the lower energies. It is recommended that broad spectra be used only to test rate dependence. If testing for realistic spectra is desired, it is suggested that combinations of narrow spectra be used to simulate these spectra.

The use of average energy and FWHM as spectral descriptors in preference to HVLs is recommended. This necessitates the measurement of spectra, which while difficult, gives one the best assurance that one is replicating techniques used at the national level. In addition, spectral measurement is a non-invasive method to verify kilovoltage calibration when the endpoint is determined. The new generation of spectrometers described above promises to ease the spectral measurement task.

ACKNOWLEDGEMENT

This work was supported by Department of Energy Interagency Agreement #DE-AI01-93EH89321.

REFERENCES

American National Standards Institute, Inc. American national standard for dosimetry - personnel dosimetry performance - criteria for testing. New York: ANSI; ANSI N13.11-1983; 1983.

American National Standards Institute, Inc. American national standard for dosimetry - personnel dosimetry performance - criteria for testing. New York: ANSI; ANSI N13.11-1994; 1994.

Bueermann, L.; Guldbakke, S.; Kramer, H.M. To be published; 1994.

Deslattes, R.D.; Levin, J.C.; Walker, M.D.; Henins, A. Noninvasive high-voltage measurement in mammography by crystal diffraction spectrometry. Med. Phys. 21:123-126; 1994.

Deslattes, R.D.; Kessler, E.G. Private communication; 1994.

Eisenhower, E. H. ed. Quality assurance for measurements of ionizing radiation. W on, DC: National Bureau of Standards; NUREG/CR-3775; 1984.

Eisenhower, E.H. ed. Criteria for the operation of federally-owned secondary laboratories (ionizing radiation). Washington, DC: U.S. Department of Commerce; NBS Special Publication 812; 1991.

Grosswendt, B. Conversion coefficients for calibrating individual photon dosemeters in terms of dose equivalents defined in an ICRU tissue cube and PMMA slabs. Radiat. Protect. Dosim. 32:219-231; 1990.

Grosswendt, B. The angular dependence and irradiation geometry factor for the dose equivalent for photons in slab phantoms of tissue-equivalent material and PMMA. Radiat. Protect. Dosim. 35:221-235; 1991.

Grosswendt, B. Coefficients for the conversion of air-collision-kerma to dose-equivalent for the calibration on individual dosemeters in x-ray fields. Radiat. Protect. Dosim. 40:169-183; 1992.

Hubbell, J.H. Photon mass attenuation and energy-absorption coefficients from 1 keV to 20 MeV. Int. J. Appl. Radiat. Isot. 33:1269-1290; 1982.

Iles, W. J. The computation of bremsstrahlung x-ray spectra over an energy range of 15 keV to 300 keV. Chilton, Didcot, Oxon, United Kingdom: National Radiological Protection Board; NRPB-R204; 1987.

Iles, W. J. Private communication; 1991.

International Commission on Radiological Protection. 1990 Recommendations of the International Commission on Radiological Protection. Oxford: Pergamon Press; ICRP Publication 60; 1991.

International Commission on Radiation Units and Measurements. Physical aspects of irradiation. Bethesda, MD: ICRU; ICRU Report 10b; 1962.

International Commission on Radiation Units and Measurements. Determination of dose equivalents resulting from external radiation sources. Bethesda, MD: ICRU; ICRU Report 39; 1985.

International Commission on Radiation Units and Measurements. Determination of dose equivalents resulting from external radiation sources - Part 2. Bethesda, MD: ICRU; ICRU Report 43; 1988.

International Commission on Radiation Units and Measurements. Measurement of dose equivalents from external photon and electron radiations. Bethesda, MD: ICRU; ICRU Report 47; 1992.

International Standards Organization. X and gamma reference radiations for calibrating dosemeters and dose ratemeters and for determining their response as a function of photon energy. Geneva: ISO;ISO Standard 4037; 1983.

International Standards Organization. Reference beta radiations for calibrating dosemeters and doseratemeters and for determining their response as a function of beta radiation energy. Geneva: ISO; ISO Standard 6980; 1984.

International Standards Organization. Neutron reference radiations for calibrating neutron-measuring devices used for radiation protection purposes and for determining their response as a function of neutron energy. Geneva: ISO; ISO Standard 8529; 1989.

International Standards Organization. X and gamma reference radiations for calibrating dosemeters and dose ratemeters and for determining their response as a function of photon energy. Geneva: ISO;ISO Standard 4037; 1993 (unpublished).

Laitano, R.F.; Pani, R.; Pellegrini, R.; Toni, M.P. Energy distributions and air kerma rates of ISO and BIPM reference filtered x-radiations. ENEA Publication RT/AMB/90; 1990.

Lamperti, P. J.; Loftus, T. P.; Loevinger, R. Calibration of x-ray and gamma-ray instruments. Washington, DC: U.S. Department of Commerce; NBS Special Publication 250-16; 1988.

Peaple, L.H.J.; Birch, R.; Marshall, M. Measurement of the ISO series of filtered radiations. United Kingdom Atomic Energy Authority Report, R13424; 1989.

Read, L.R.; Hagreen, M. The ISO narrow spectrum series of filtered x-radiations at NPL. NPL Report RS (EXT) 92; 1987.

Seelentag, W.W.;Panzer, W.;Drexler, G.;Platz, L.;Santer, F. A catalog of spectra for the calibration of dosemeters. Munich: Gesellschaft für Strahlen- und Umweltforschung; GSF Bericht S 560; 1979.

Seelentag, W.W.; Panzer, W. Stripping of x-ray bremsstrahlung spectra up to 300 kVp on a desk type computer. Phys. Med. Biol. 24:767-780; 1979.

Seltzer, S.M. Calculated response of intrinsic germanium detectors to narrow beams of photons with energies up to ~300 keV. Nucl. Inst. Meth. 188:133-151; 1981.

Seltzer, S.M. Private communication; 1983.

Simmons, J.D. ed. NIST Calibration Services users guide 1991. Washington, DC: U.S. Department of Commerce; NIST Special Publication 250; 1991.

Sims, C.S.; Swaja, R.E. Summary statements from the Third Conference on Radiation Protection and Dosimetry. Health Phys. 63:192-194; 1992.

U.S. Department of Energy. Department of Energy Standard for the performance testing of personnel dosimetry systems. Washington, DC: U.S. Department of Energy; DOE/EH-0027; 1986.

Zeman, G. H.;Soares, C. G.;Devine, R. T. Why change the x-ray conversion factors in ANSI N13.11? Oak Ridge, TN: Oak Ridge National Laboratory; Proceedings of the 3rd Conference on Radiation Protection and Dosimetry; 1991.

Table 1. Sources of Spectra

Institution	Reference	Detector	Unfolding Technique	Measured
GSF	Seelentag et al. 1979	2.8 cc InGe	backstripping	138 techniques
NIST	Eisenhower et al. 1982	1.0 cc InGe	backstripping	pre-1983 NIST
NPL	Read, Hagreen 1987	30 cc InGe	none	ISO Narrow < 200kV
Harwell	Poeple et.al. 1989	1.3 cc GeLi		ISO < 150 kV
ENEA	Laitano et.al. 1990	0.5 cc InGe	backstripping	ISO & BIPM
PTB	Bassermann et al 1994			PTB techniques
NRPB	Ilea 1991	calculated	-	ISO > 30 kV

Table 2. Specifications of NIST Filtered Bremsstrahlung Beams

Series Name	Homogeneity Coefficient	Typical Air Kerma Rates, Gy h^{-1}
Heavily Filtered	0.88 to 1.0	4 x 10^{-3} to 2
Moderately Filtered	0.66 to 1.0	4 x 10^{-3} to 20
Lightly Filtered	0.59 to 1.0	4 x 10^{-3} to 200
Specially Filtered	0.63 to 0.75	4 x 10^{-3} to 20

Table 3. Specifications of ISO Filtered Bremsstrahlung Beams

Series Name	Resolution, %	Homogeneity Coefficient	Typical Air Kerma Rates, Gy h^{-1}
Low Air Kerma Rate	18 to 22	1.0	3 x 10^{-4}
Narrow Spectrum	27 to 37	0.75 to 1.0	10^{-3} to 10^{-2}
Wide Spectrum	48 to 57	0.67 to 0.98	10^{-2} to 10^{-1}
High Air Kerma Rate	not specified	0.64 to 0.86	10^{-2} to 0.5

Table 4. Comparison of NIST and ISO Bremsstrahlung Techniques at 10 kV

Series	Code	Inherent Filtration, mm Be	Added Filtration, mm Al	GSF Catalog Number	Half Value Layer, mm Al		Average Energy, keV	FWHM, keV
					First	Second		
NIST Lightly Filtered	L10	1.0			0.029	0.037		
ISO High Air-Kerma Rate	HK10	4.0		1	0.036	0.041	7.5	2.7
ISO Narrow Spectrum	NS10	1.0	0.1	2	0.047	0.052	8.0	2.2
NIST Heavily Filtered	H10	1.0	0.105	2	0.048	0.054		
ISO Low Air-Kerma Rate	LK10	1.0	0.3		0.058	0.058	8.5	1.8

Table 5. Comparison of NIST and ISO Bremsstrahlung Techniques at 15 kV

Series	Code	Inherent Filtration, mm Be	Added Filtration, mm Al	GSF Catalog Number	Half Value Layer, mm Al		Average Energy, keV	FWHM, keV
					First	Second		
NIST Lightly Filtered	L15	1.0		6	0.050	0.068	9.9	5.9[1]
ISO Narrow Spectrum	NS15	1.0	0.5	7	0.14	0.16	12	4.3
NIST Heavily Filtered	H15	1.0	0.5	7	0.15	0.17		

[1]Prominent L characteristic lines present from W target.

Table 6. Comparison of NIST and ISO Bremsstrahlung Techniques at 20 kV

Series	Code	Inherent Filtration, mm Be	Added Filtration, mm Al	GSF Catalog Number	Half Value Layer, mm Al		Average Energy, keV	FWHM, keV
					First	Second		
NIST Lightly Filtered	L20	1.0		9	0.071	0.093	11.4	10.5[1]
ISO High Air-Kerma Rate	HK20	4.0	0.15	10	0.12	0.16	12.9	8.8[1]
NIST Moderately Filtered	M20	1.0	0.23	11	0.152	0.19		
ISO Narrow Spectrum	NS20	1.0	1.0	13	0.32	0.37	16	5.2
NIST Heavily Filtered	H20	1.0	1.021	13	0.36	0.41		
ISO Low Air-Kerma Rate	LK20	1.0	2.0		0.42	0.42	17	3.6

[1]Prominent L characteristic lines present from W target.

Table 7. Comparison of NIST and ISO Bremsstrahlung Techniques at 30 kV

Series	Code	Inherent Filtration, mm Be	Added Filtration, mm		GSF Cat. No.	Half Value Layer, mm Al		Average Energy, keV	FWHM, keV
			Al	Cu		First	Second		
NIST Lightly Filtered	L30	1.0	0.265		20	0.22	0.37	18	14[1]
NIST Moderately Filtered	M30	1.0	0.50		21	0.36	0.56	20.1	12.85
ISO High Air-Kerma Rate	HK30	4.0	0.52		21	0.38	0.60	19.7	13.0
ISO Narrow Spectrum	NS30	1.0	4.0		26	1.15	1.30	24	7.5
NIST Heavily Filtered	H30	1.0	4.13		26	1.23	1.32		
ISO Low Air-Kerma Rate	LK30	1.0	4.0	0.18		1.46	1.46	26	5.5

[1]Prominent L characteristic lines present from W target.

Table 8. Comparison of NIST and ISO Bremsstrahlung Techniques at 40 kV

Series	Code	Inherent Filtration, mm Be	Added Filtration, mm		GSF Cat. No.	Half Value Layer, mm Al		Average Energy, keV	FWHM, keV
			Al	Cu		First	Second		
NIST Lightly Filtered	L40	1.0	0.50		31	0.49	0.86	23.4	18.6
NIST Moderately Filtered	M40	1.0	0.786		32	0.73	1.11	24.8	17.9
ISO Narrow Spectrum	NS40	3.6	*	0.21	37	2.54	2.71	32.8	9.9
NIST Heavily Filtered	H40	1.0	4.05	0.26	37	2.9	3.1	32.5	9.1

* Additional filtration added to make total inherent filtration equivalent to 4 mm Al.

Table 9 Comparison of NIST and ISO Bremsstrahlung Techniques at 60 kV

Series	Code	Inherent Filtration, mm Be	Added Filtration, mm		GSF Cat. No.	Half Value Layer, mm Cu		Average Energy, keV	FWHM, keV
			Al	Cu		First	Second		
NIST Moderately Filtered	M60	3.0	1.51		49	0.052	0.081	34.6	27.5
ISO High Air-Kerma Rate	HK60	4.0	3.2		51	0.079	0.11	36.3	25.6
NIST Specially Filtered	S60	3.0	4.0		52	0.089	0.127	38.2	26.6
ISO Wide Spectrum	WS60	3.6	*	0.30	53	0.18	0.21	44.3	20.5
ISO Narrow Spectrum	NS60	3.6	*	0.60	54	0.24	0.26	47.3	17.3
NIST Heavily Filtered	H60	3.0	4.0	0.61	54	0.24	0.27	47.3	17.1

* Additional filtration added to make total inherent filtration equivalent to 4 mm Al.

Table 10. Comparison of NIST and ISO Bremsstrahlung Techniques at 80 kV

Series	Code	Inherent Filtration, mm Be	Added Filtration, mm		GSF Cat. No.	Half Value Layer, mm Cu		Average Energy, keV	FWHM, keV
			Al	Cu		First	Second		
NIST Lightly Filtered	L80	1.0	1.284		59	0.061	0.12	40.3	34.6
ISO Wide Spectrum	WS80	3.6	*	0.50	62	0.35	0.44	56.0	29.1†
ISO Narrow Spectrum	NS80	3.6	*	2.0	65	0.58	0.62	64.6	20.9†

* Additional filtration added to make total inherent filtration equivalent to 4 mm Al.
†Prominent K characteristic lines present from W target.

Table 11: Comparison of NIST and ISO Bremsstrahlung Techniques at 100 kV

Series	Code	Inherent Filtration, mm Be	Added Filtration, mm			GSF Cat. No.	Half Value Layer, mm Cu		Average Energy, keV	FWHM, keV
			Al	Cu	Sn		First	Second		
NIST Lightly Filtered	L100	1.0	1.978			68	0.11	0.24	48.2	45.9†
NIST Moderately Filtered	M100	3.0	5.0			71	0.20	0.36	52.9	41.9†
ISO High Air-Kerma Rate	HK100	4.0	3.9	0.15		72	0.30	0.47	56.7	42.7†
ISO Narrow Spectrum	NS100	3.6	*	5.0		75	1.11	1.17	82.7	23.4
NIST Heavily Filtered	H100	3.0	4.0	5.2		75	1.14	1.21		
ISO Low Air-Kerma Rate	LK100	3.6	*	0.5	2.0	76	1.24	1.24	86.3	18.8

*Additional filtration added to make total inherent filtration equivalent to 4 mm Al.
†Prominent K characteristic lines present from W target.

Table 12. Comparison of NIST and ISO Bremsstrahlung Techniques at 150 kV

Series	Code	Inherent Filtration, mm Be	Added Filtration, mm			GSF Cat. No.	Half Value Layer, mm Cu		Average Energy, keV	FWHM, keV
			Al	Cu	Sn		First	Second		
NIST Moderately Filtered	M150	3.0	5.0	0.25		94	0.67	1.08	73.2	58.5†
ISO Wide Spectrum	WS150	3.6	*		1.0	96	1.86	2.1	103.7	56.6†
ISO Narrow Spectrum	NS150	3.6	*		2.5	98	2.36	2.47	117.2	44.6
NIST Heavily Filtered	H150	3.0	4.0	4.0	1.51		2.5	2.6	117.5	44.4

*Additional filtration added to make total inherent filtration equivalent to 4 mm Al.
†Prominent K characteristic lines present from W target.

Table 13. Comparison of NIST and ISO Bremsstrahlung Techniques at 200 kV

Series	Code	Inherent Filtration, mm Be	Added Filtration, mm				GSF Cat. No.	Half Value Layer, mm Cu		Average Energy, keV	FWHM, keV
			Al	Cu	Sn	Pb		First	Second		
NIST Moderately Filtered	M200	3.0	4.1	1.12			107	1.69	2.45		†
ISO High Air-Kerma Rate	HK200	3.6	*	1.15			107	1.70	2.40	100.3	87.2†
ISO Wide Spectrum	WS200	3.6	*		2.0		109	3.08	3.31	136.8	77.5
ISO Narrow Spectrum	NS200	3.6	*	2.0	3.0	1.0	110	3.99	4.05	164.4	48.5
NIST Heavily Filtered	H200	3.0	4.0	0.6	4.16	0.77		4.1	4.1	161.9	52.2

*Additional filtration added to make total inherent filtration equivalent to 4 mm Al.
†Prominent K characteristic lines present from W target.

Table 14. Comparison of NIST and ISO Bremsstrahlung Techniques at 250 kV

Series	Code	Inherent Filtration, mm Be	Added Filtration, mm				GSF Cat. No.	Half Value Layer, mm Cu		Average Energy, keV	FWHM, keV
			Al	Cu	Sn	Pb		First	Second		
ISO High Air-Kerma Rate	HK250	3.6	*	1.6			121	2.47	3.29	120.1	106.0†
NIST Moderately Filtered	M250	3.0	5.0	3.2			123	3.2	3.7	138.5	104.9
ISO Wide Spectrum	WS250	3.6	*		4.0		125	4.22	4.40	172.2	95.8
ISO Narrow Spectrum	NS250	3.6	*		2.0	3.0	126	5.19	5.23	208.4	57.5
NIST Heavily Filtered	H250	3.0	4.0	0.60	1.04	2.72		5.2	5.3	204.2	61.3

*Additional filtration added to make total inherent filtration equivalent to 4 mm Al.
†Prominent K characteristic lines present from W target.

Table 15. Comparison of NIST and ISO Bremsstrahlung Techniques at 300 kV

Series	Code	Inherent Filtration, mm Be	Added Filtration, mm				GSF Cat. No.	Half Value Layer, mm Cu		Average Energy, keV	FWHM, keV
			Al	Cu	Sn	Pb		First	Second		
ISO High Air-Kerma Rate	HK300	3.6	*	2.5			132	3.40	4.15	145.0	121.3†
ISO Wide Spectrum	WS300	3.6	*		6.5		134	5.20	5.34	205.8	115.2
NIST Moderately Filtered	M300	3.0	4.0		6.5		134	5.3	5.46		
ISO Narrow Spectrum	NS300	3.6	*		3.0	5.0	135	6.12	6.15	250.5	68.4
NIST Heavily Filtered	H300	3.0	4.1		3.0	5.0	135	6.2	6.3		

*Additional filtration added to make total inherent filtration equivalent to 4 mm Al.
†Prominent K characteristic lines present from W target.

Table 16. Comparison of Other NIST and ISO Bremsstrahlung Techniques Below 100 kV

Series	Code	Inherent Filtration, mm Be	Added Filtration, mm			GSF Cat. No.	Half Value Layer, mm Al		Average Energy, keV	FWHM, keV
			Al	Cu	Pb		First	Second		
ISO Narrow Spectrum	NS25	1.0	2.0				0.66	0.73	20	6.9
ISO Low Air-Kerma Rate	LK35	1.0		0.25		29	2.20	2.20	30.1	6.8
NIST Lightly Filtered	L50	1.0	0.639			42	0.75	1.29	28.0	22.7
NIST Moderately Filtered	M50	1.0	1.021			43	1.02	1.55	29.1	23.2
NIST Heavily Filtered	H50	3.0	4.0		0.10	47	4.2	4.6	39.1	14.0
ISO Low Air-Kerma Rate	LK55	3.6	*	1.2		48	6.02	6.16	47.3	10.7
ISO Low Air-Kerma Rate	LK70	3.6	*	2.5		56	9.04	9.15	60.1	13.7
NIST Specially Filtered	S75	1.0	1.504			57	1.86	2.95	39.6	35.1

*Additional filtration added to make total inherent filtration equivalent to 4 mm Al.

Table 17. Other ISO Bremsstrahlung Techniques Above 100 kV

Series	Code	Inherent Filtration, mm Be	Added Filtration, mm				GSF Cat. No.	Half Value Layer, mm Cu		Average Energy, keV	FWHM, keV
			Al	Cu	Sn	Pb		First	Second		
ISO Wide Spectrum	WS110	3.6	*	2.0			78	0.96	1.11	78.6	39.5†
ISO Narrow Spectrum	NS120	3.6	*	5.0	1.0		83	1.71	1.77	99.8	27.9
ISO Low Air-Kerma Rate	LK125	3.6	*	1.0	4.0		84	2.04	2.04	108.6	22.7
ISO Low Air-Kerma Rate	LK170	3.6	*	1.0	3.0	1.5	101	3.47	3.47	148.1	28.0
ISO Low Air-Kerma Rate	LK210	3.6	*	0.5	2.0	3.5	111	4.54	4.54	185.0	34.1
ISO Low Air-Kerma Rate	LK240	3.6	*	0.5	2.0	5.5	119	5.26	5.26	212.8	37.4
ISO High Air-Kerma Rate	HK280	3.6	*	3.0			128	3.37	3.99	144.5	79.4†

*Additional filtration added to make total inherent filtration equivalent to 4 mm Al.

†Prominent K characteristic lines present from W target.

Table 18. Comparison of NIST Moderately Filtered and ISO High Air-Kerma Rate 30 kV Spectra

Source	Measured		Calculated from spectrum		Average Energy, keV	Resolution, %	Hp(10)/Ka, Sv/Gy
	HVL, mm Al	Homogeneity Coefficient	HVL, mm Al	Homogeneity Coefficient			
NIST	0.36	0.64	0.46	0.70	20.1	64	0.448
GSF Spectrum #21			0.38	0.63	19.7	67	0.397
ENEA	0.35		0.37	0.67	19.1	64	0.378

Table 19. Comparison of ISO Narrow Spectrum 60 kV Spectra

Source	Measured		Calculated from spectrum		Average Energy, keV	Resolution, %	Hp(10)/Ka, Sv/Gy
	HVL, mm Cu	Homogeneity Coefficient	HVL, mm Cu	Homogeneity Coefficient			
NIST	0.24	0.89					
GSF Spectrum #54			0.23	0.85	47.3	36	1.652
NRPB Calculated			0.23	0.89	47.3	37	1.652
PTB	0.24		0.24	0.90	47.7	36	1.664
ENEA	0.24		0.25	0.90	48.7	35	1.689
Harwell			0.24	0.89	47.9	37	1.664

Table 20. Comparison of NIST Heavily Filtered and ISO Narrow Spectrum 150 kV Spectra

Source	Measured		Calculated from spectrum		Average Energy, keV	Resolution, %	Hp(10)/Ka, Sv/Gy
	HVL, mm Cu	Homogeneity Coefficient	HVL, mm Cu	Homogeneity Coefficient			
NIST	2.5	0.95	2.37	0.95	118	38	1.711
GSF Spectrum #98			2.29	0.95	117	38	1.716
NRPB Calculated			2.33	0.95	117	38	1.716
PTB	2.4		2.32	0.95	117	39	1.717
ENEA	2.46		2.36	0.95	118	37	1.712

Table 21. Comparison of NIST Moderately Filtered and ISO High Air-Kerma Rate 200 kV Spectra

Source	Measured		Calculated from spectrum		Average Energy, keV	Resolution, %	Hp(10)/Ka, Sv/Gy
	HVL, mm Cu	Homogeneity Coefficient	HVL, mm Cu	Homogeneity Coefficient			
NIST	1.69	0.69					
GSF Spectrum #107			1.70	0.71	102	93	1.743
NRPB Calculated			1.63	0.70	100	87	1.745
ENEA	1.70		1.76	0.71	103	83	1.733
PTB	1.7		1.54	0.67	98	89	1.747

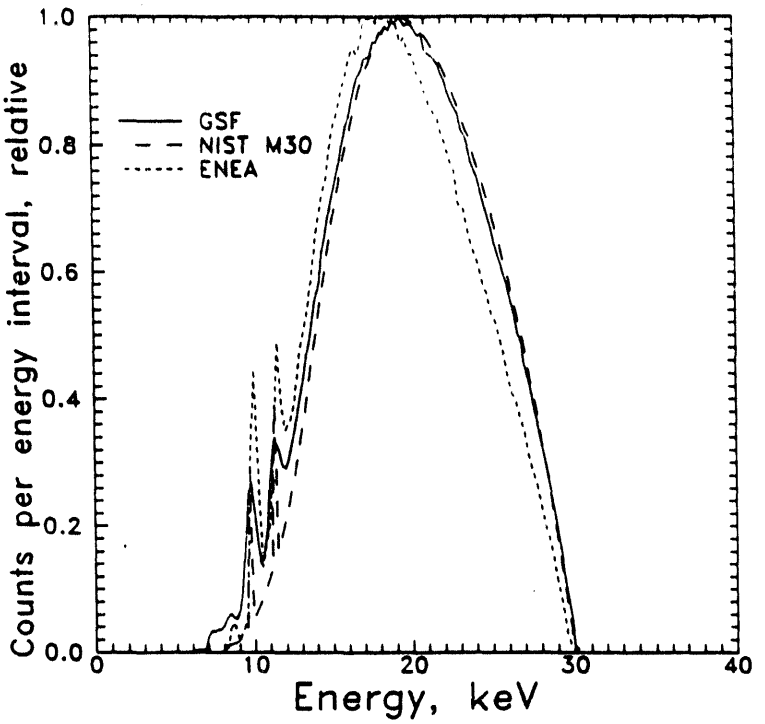


Figure 1. Comparison of NIST Moderately Filtered and ISO High Air-Kerma Rate 30 kV Spectra

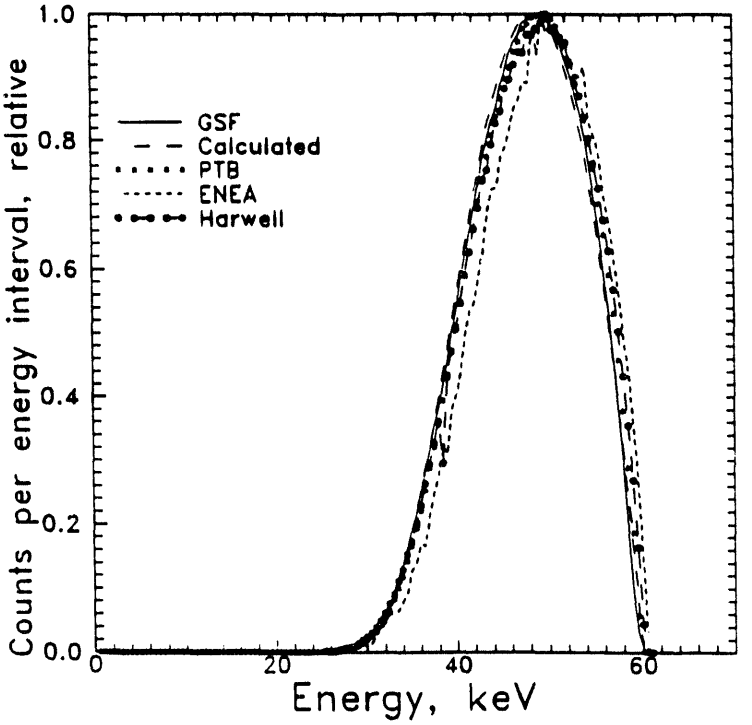


Figure 2. Comparison of ISO Narrow Spectrum 60 kV Spectra

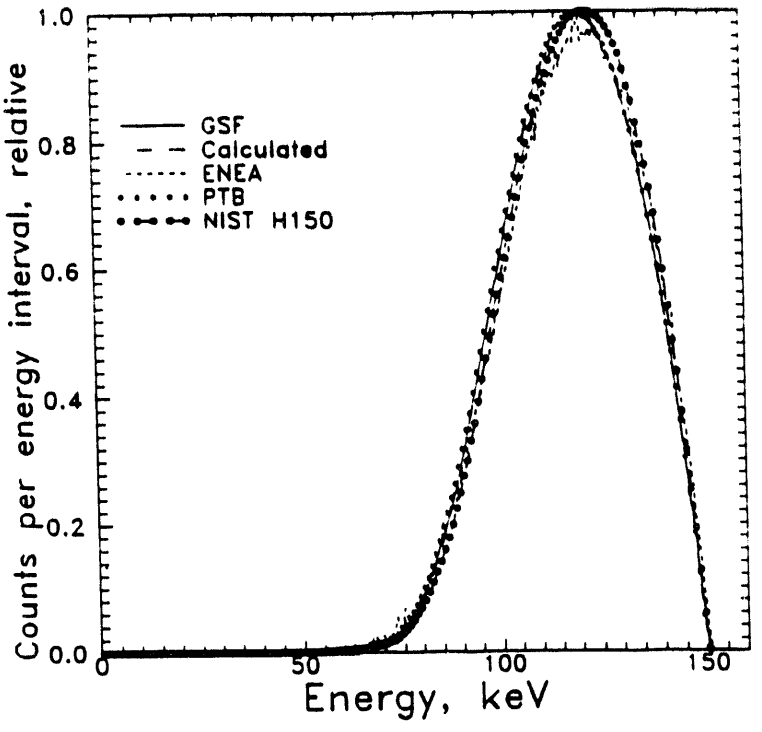


Figure 3. Comparison of NIST Heavily Filtered and ISO Narrow Spectrum 150 kV Spectra

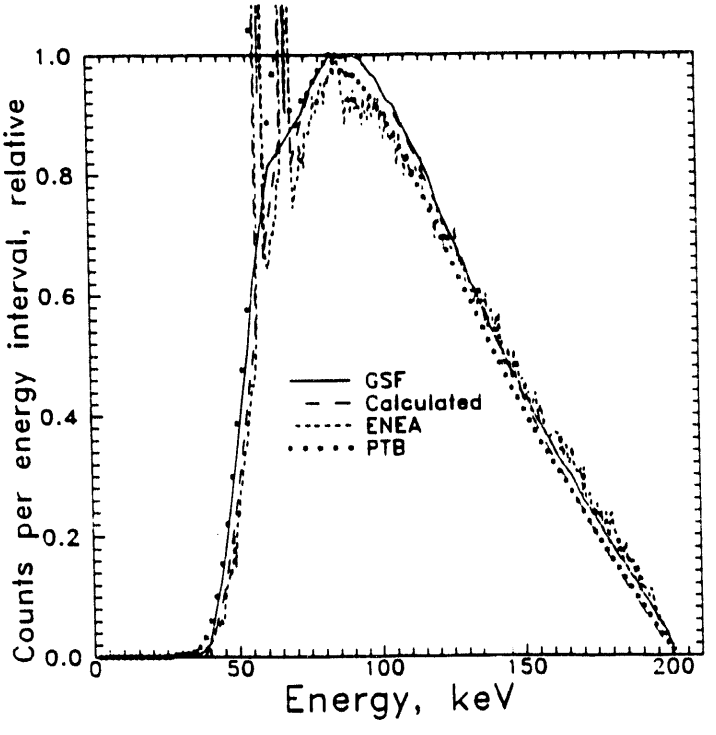


Figure 4. Comparison of NIST Moderately Filtered and ISO High Air-Kerma Rate 200 kV Spectra

OPTIMAL FILTERS FOR ISO K-FLUORESCENCE REFERENCE RADIATIONS

Jing Chen (Institute of Radiation Biology, GSF, D-85758 Oberschleißheim, FRG)
Hsiao-Hua Hsu (Health Physics Measurements Group, LANL, Los Alamos, NM 87545)

In an earlier paper[1], we presented the optimal target filter system for electron beam generated X rays. We pointed out that the system has the advantage of a very high production yield[2] . The bremsstrahlung production is proportional to Z (atomic number of the target), and the ionization cross section is proportional to Z. X ray production by direct electron beam bombardment is optimal for low Z targets. For high Z targets, one uses photons to excite target atoms. Source photons are produced by the electron bremsstrahlung process. This method is utilized by the ISO to produce ISO K-fluorescence reference radiations.

In the document ISO 4037[2], 16 radiator materials with corresponding secondary filtration and primary electron beam energy are recommended for the production of reference radiations. For the filter materials, recommendations were made only for the minimum mass per unit area, which may not be the optimal thickness to achieve the highest purity.

We used the Monte Carlo code ACCEPT of the Integrated TIGER series[3] to simulate ISO geometries. By varying the thickness of filters, we can find the optimal thickness required to achieve the highest purity for all reference radiations. For example, to produce 17.5 keV Mo Kα X rays, ISO 4037 recommends a primary electron beam energy of 80 keV and the use of Mo as the radiator with a Zr filter of 0.035 g/cm^2 (this corresponds to a thickness of 53.9 μm). Our calculations show that the optimal filter thickness is 80 μm. We can achieve a purity of 85.9%. As a comparison to electron direct excitation, we evaluated a 100 keV electron beam with a Mo target and a 40 μm Nb filter. We obtained a purity of only 43%, but almost a 1000 times higher intensity than for the ISO configuration.

1. H. H. Hsu, D. G. Vasilik and J. Chen, Health Physics Society Annual Meeting, San Francisco, June, 1994.
2. International Standard, ISO 4037-1979 (E).
3. J. Halbleib, Monte Carlo Transport of Electrons and Photons, eds., T. M. Jenkins, W. R. Nelson, A. Rindi, Plenum Press, 1987.

ESTABLISHING A URANIUM SLAB SOURCE FOR BETA IRRADIATIONS OF DOSIMETRY AT THE IDAHO NATIONAL ENGINEERING LABORATORY (INEL)

Laird C. Bean, Orval R. Perry, Paul E. Ruhter
Idaho National Engineering Laboratory

The Idaho National Engineering Laboratory (INEL) uses a DOELAP accredited Panasonic thermoluminescence dosimetry (TLD) system to provide photon and beta radiation monitoring. The Operational Dosimetry Unit (ODU) at the INEL manages the personnel dosimetry programs. As part of personnel dosimetry processing, the ODU includes TLDs that are irradiated to pre-determined dose equivalent levels using ^{137}Cs and depleted uranium sources. These pre-irradiated dosimeters serve as Quality Assurance and Quality Control indicators of system performance. Historically, the DOE-ID provided the QA/QC dosimeter irradiations to the ODU using DOELAP sources and DOE personnel. However, in 1991 a DOE Tiger Team review noted that a potential conflict of interest existed because DOE was also responsible for the oversight of ODU. As a result of the potential conflict of interest, the ODU moved from a DOE provided irradiation service to contractor controlled sources for QA/QC irradiations. To accomplish this for beta irradiations, the ODU decided to duplicate the source, source container and geometry used by DOELAP in Category VB (uranium slab). The choice of the slab geometry supports the personnel algorithm which unfolds beta dose equivalency based on slab geometries.

Four objectives were established to implement a contractor controlled source:

(1) Procure a depleted uranium source meeting the DOELAP source dimensions of 50.8 cm X 7.62 cm X 0.397 cm.

(2) Manufacture a source container to the exact dimensions of the DOELAP source container.

(3) Obtain a NIST calibration of the source surface dose rate and have NIST provide a uniformity analysis of the source.

(4) Develop and implement a protocol for establishing the dose equivalency delivered to the beta sensitive elements of the INEL dosimeter. Positions 1 (E1) and 2 (E2) will be used to determine dose equivalency. Positions E1 and E2 are $Li_2B_4O_7$ which are under 16 mg/cm^2 and 58 mg/cm^2 filtration respectively.

Both the source and source box were constructed within the INEL complex. The source was constructed using a spare uranium slab which was shaped, cut and rolled to the finished source to the DOELAP dimensions. The source was double wrapped in 3.5 mg/cm^2 mylar to prevent oxidation from the source becoming an external contamination hazard. The Engineering Services group at the INEL manufactured the acrylic source container to the exact dimensions of the DOELAP source box. The DOE irradiation jigs were also duplicated.

The source was originally manufactured under the dimensions of 50.8 cm X 7.62 cm X 0.794 cm. The manufacturer of the source had to re-cut and roll the source to the DOELAP source dimensions. When the source was delivered to the ODU, a bow was evident and had to be compressed to fit the source container. From conversations with NIST personnel, a bow is not uncommon in large slab sources and NIST can accommodate some bow without affecting the calibration.

ODU requested NIST to perform Test Number 47030C, Beta-Particle Sources Calibrated for Absolute Surface Emission Rate[1]. Calibration was done with the source wrapped in 7 mg/cm^2 of mylar and mounted in its box. Beta particle sources are calibrated by NIST for absorbed-dose rate to water. Current was measured over the central 30-mm diameter area from the source surface using an extrapolation ion chamber with a graphite-coated plastic electrode. The NIST report[2] provided the following calibration information:

$$D = \frac{33.97 \times 1.12 \times B \times U}{1.197 \times A}\left(\frac{\Delta I}{\Delta d}\right)_0$$

where,

D = the absorbed-dose rate to water in Gy/s

B = a correction factor for reduced backscatter from the collecting electrode

U = a correction factor for attenuation by the high voltage electrode

A = the area of the collecting electrode in mm^2

$\left(\frac{\Delta I}{\Delta d}\right)_0$ = the rate of change of current with an extrapolation air-gap thickness as the thickness approaches zero in nA/mm

1.197 = the density of air at standard temperature and pressure in Kg/m^2

33.97 = the energy in joules needed to produce one coulomb of ions of either sign in air

1.12 = the ratio of the mean mass stopping power of water to that of air

Two calibrations were made, one at the source surface and the other at 1.4 mm off the

source surface, to determine the average absorbed-dose rate across the central area of the source, at a depth of 7 mg/cm^2. A 30-mm diameter graphite-coated plastic collecting electrode was used to measure the rate of change of current with air-gap thickness. Currents were measured at five air gaps ranging from 0.3 to 1.1 mm and were corrected to the reference temperature and pressure. The data yielded a linear relation between corrected current and air gap.

Measurements indicate the absorbed-dose rates at a depth of 7 mg/cm^2 (the surface of the plastic cover on the source) averaged over the area of the collecting electrode, both at the source surface and at a distance of 1.4 mm off the source surface, to be 0.656 μGy/s and 0.650 μGy/s. The overall uncertainty in the calibration, with a 95% confidence interval, was estimated to be ± 10%.

In addition to the source calibration, ODU requested NIST to provide validation of uniformity using a minimum of 3 points. Because the area of the source was large, two pieces of film, each covering half of the source, were used. The two films were mounted on a 1.27-cm thick plastic plate which was then placed on the source. Both films were exposed for 22.5 hours, developed, and read using the NIST high-resolution scanning densitometer. A 39 x 212 point array of relative dose-rates spaced at 2.4 mm intervals was produced. Source uniformity was reported to be within ± 10%.

A protocol to quantify the dose rate to the shallow elements of the INEL dosimeter was designed using transfer techniques from DOELAP's uranium slab source to ODU's uranium slab source . The protocol identified the following objectives:

(1) Establish a select group of dosimeters to be exposed to the DOELAP uranium slab source using the ODU irradiation jig.
(2) Establish a correction factor for each dosimeter exposed to the DOELAP uranium slab source.
(3) Expose the group of dosimeters to the ODU uranium slab source in the same configuration used with the DOELAP source.
(4) Establish the ODU source dose rate using the dosimeter correction factors derived from the DOELAP source irradiations.
(5) Test the derived ODU source dose rate by exposing dosimeters not used in the testing protocol to a known dose level and processing the dosimeters through the normal personnel algorithm.

Appropriate precautions were noted in the protocol to minimize error while annealing, handling and processing dosimeters.

Fifty dosimeters (Panasonic 814 inserts enclosed in the INEL hanger) were exposed to 300 mrem ^{137}Cs using the Shepherd Mini AS4 irradiator. From the irradiated group, 18 test dosimeters and 4 control dosimeters were selected. The selected group demonstrated the smallest standard deviation based on the response of the beta sensitive elements of the dosimeter.

The source box was designed to accept an irradiation jig that would hold nine dosimeters. The ODU constructed two irradiation jigs and mounted nine of the test dosimeters in each jig. The dosimeters were irradiated for 1 hour on the DOELAP uranium slab source, delivering a dose equivalent of approximately 213 mrem. All dosimeters were processed on a designated Panasonic reader.

The E1 and E2 responses from the DOELAP slab source irradiation were tabulated for each dosimeter. E1 and E2 correction factors for each dosimeter were assigned based on the reader output per delivered dose equivalent of 213 mrem.

The 18 test dosimeters mounted in the irradiation jigs were exposed using the ODU uranium slab source. Dosimeters were mounted in the same jig configuration as when they were irradiated using the DOELAP source. A one hour exposure was delivered to the dosimeters. Both E1 and E2 responses for each dosimeter were recorded.

The response of each beta sensitive element was adjusted by the appropriate correction factor to derive a source dose rate by the following relationship.

$$DR_i = \frac{\text{element}_i \text{ response}}{CF_i \times \text{exposure time}}$$

where,

DR_i = element$_i$ dose rate

CF_i = element$_i$ correction factor

The average dose rate of the ODU source (206 mrem/hr) was established as the mean of the element responses (DR_i) for E1 and E2. The mean E1 responses indicated a source dose rate of 204 mrem/hr. The mean E2 responses indicated a source dose rate of 208 mrem/hr.

Nine dosimeters and 4 controls were randomly selected from the set of "field" dosimeters to validate the established dose rate. Dosimeters were positioned in jig 2, mounted on the source, and irradiated for 43 minutes and 4 seconds for a delivered dose equivalent of 147.9 mrem. The average measured dose of the 9 dosimeters were within 6% of the delivered dose equivalent of 147.9 mrem.

Dosimeters were annealed and then loaded in jig 1. The dosimeter inserts were placed with the same hangers and positioned in the same location in jig 1 as they were in jig 2. The average measured dose for the nine dosimeters were within 3% of the delivered dose equivalent of 147.9 mrem. Processing results from using each jig indicate that the sample population is representative of the whole population of field dosimeters. Results also indicate that either jig may be used to perform beta irradiations.

The ODU uranium slab dose rate of 206 mrem/hour is within 5% of the DOELAP uranium slab dose rate of 213 mrem/hour. This type of agreement is what is expected for duplicated sources and establishes both the validity of the protocol and use of the ODU uranium source for quality assurance irradiations.

REFERENCES

1. *NIST Calibration Services Users Guide 1989*, NIST Special Publication 250, pp. 93-94.

2. C.G. Soares, *NIST Report of Calibration*, DG 9699/93, October 1993.

CALIBRATION STANDARDS USING NUCLIDES INCORPORATED INTO *POLYMERIC MEMBRANES*™ or *POLYSURFACE*™

Gary E. Strathearn
Ana R. Ramirez
Aman Khan
Karl Amlauer
Isotope Products Laboratories
3017 N. San Fernando Blvd., Burbank, CA 91504.

Abstract

Nuclides can be incorporated into organic-based materials, called *polymeric membranes*™ or *Polysurface*™. These *polymeric membranes*™ have several distinct advantages over the more traditional methods of deposition, electroplating or an anodized layer. Alpha emitters can be incorporated into *polymeric membranes*™, but the best emitters for this method are beta (Sr/Y-90, Tl-204, C-14, Cs-137, Pm-147 and Ge/Ga-68) and gamma emitters (Fe-55, I-125/-129/-131, Cs-137, Am-241, Co-57 and Eu-152).

To limit beta-energy attenuation the nuclides are typically incorporated into a thin layer 1 mg/cm² thick. The organic layer is covered by a thin acrylic protection (approximately 200 µg/cm²) and a thin conductive metal layer (approximately 100 µg/cm²) of either gold or aluminum. Beta calibration of these standards is based upon electron flux from the surface of the source, and can be certified traceable to NIST. Contained activity can also be provided. Gamma calibration is based on either contained activity for high energy photon emitters or photon flux for low-energy sources.

These sources allow the problems of more traditional sources to be overcome. Deposited sources have the disadvantage of poor binding of the salt to the backing, and the potential to leak if the window is punctured. Electroplated sources are more rugged, but not all elements can be electroplated, including Sr-90, C-14 and I-129. Even when electroplated, many nuclides can still be removed by mild abrasion. Anodizing allows protection of the sources by incorporation of the nuclide into a metal layer, but has the serious limitations of selective nuclide incorporation and mass limitation permitting very low activity levels.

Polymeric membranes™ overcome these problems. The material is incorporated into a non-water leachable source which retards loss of material by abrasion, allows a wide range of nuclides to be incorporated and permits incorporation of millicurie (~50+ MBq) levels of most nuclides, if desired. The material can, if unmounted, be bent, allowing a layer to wrap cylinders or other shapes not easily available previously.

INTRODUCTION

Wide area radioactive sources for calibration have several traditional problems, especially when alpha emitters are considered. The most important factor for all source construction types (methods) is that the activity is not removable, for if it is, it becomes a contamination problem. Also, the calibration is no longer valid as activity is lost. As important, especially for alpha and beta particle emitting sources, is that minimal energy degradation of the particle occurs as it passes through and out of the active layer.

Other problems must be overcome in production of these sources, although the importance in various uses changes dramatically. For particle emitting sources an electrically conductive surface must be available to eliminate the charge from the surface of the source when using non-windowed proportional counting equipment. This layer must be thin enough so that energy attenuation of the emitted particles is not altered significantly. Also, in some counting systems, the backing material must also be electrically conductive, and developing standards worldwide are soon to require a metal backed source.

Uniformity of the source may be critical, especially when only portions of the source may be used. Calibration error is increased by the uniformity error, and hence, with non-uniform sources, may make calibrations using less than the total source meaningless.

Environmental or work conditions are especially important for some uses. These factors include stability or useful life of the source, the temperature range of use and source stability at temperature extremes outside of the use temperature, radiation resistance of the component parts, and the ability to undergo wipe (leak) tests on the source window.

The last source criterion, and often most important in the decision of source manufacture type, is whether the source can be made by that procedure. If so, what is the amount of active material, and hence activity, which can be incorporated into the active element. The maximum amount may be constrained by the self-attenuation of the material, especially in alpha and low energy beta sources. For example, for an alpha particle standard, Th-232 is a very poor calibration material because its specific activity is only 110 pCi/mg. This limits the amount of material which can be used on the source to a few disintegrations per second. The other limiting factor on mass and hence activity incorporation is the ability of the active surface to absorb or contain that nuclide if it is incorporated into an active layer, such as found in anodized and *Polysurface*™ sources. Beyond mass loading the active layer may be limiting because of energy attenuation of the emitted particles or photons.

Table 1 demonstrates these various parameters and the different source manufacturing methods. These constraints are discussed in detail below for each construction method. These methods include deposition, electrodeposition, anodized active surfaces and Isotope Products

Table 1: RELATIVE CHARACTERISTICS OF VARIOUS WIDE AREA SOURCE MANUFACTURING TECHNIQUES

Character	Deposition	Electrodeposition	Anodized sources	*Polysurface*™
Ruggedness	Poor	Moderate	High	Moderate
Temperature range	Moderate	High	High	High
Uniformity	High (see text)	Poor	Moderate - High	High
Number of nuclides incorporated	High	Poor	Poor	High
Maximum activity of nuclides incorporated	High	Moderate	Poor	High
Low attenuation of the emitted particle energy	High	Moderate	Poor - moderate	Moderate
Stability	Poor	Moderate	High	Moderate

Laboratories new *Polysurface*™ or *Polymeric membrane*™ source manufacture method.

Deposited Sources

Deposited sources are the simplest sources to make. In this system, a solution of the active nuclide, usually as a salt, is deposited into an array of grids and dried. The salt is then made more adherent, the method dependent upon both the salt used and the source manufacturer, and is usually a guarded secret.

The advantage of deposited sources are the high uniformity, the wide range of nuclides available and the high activity. The latter is theoretically limited only by the self-attenuation, although in practice limited by safety concerns. Disadvantages of this source type are numerous. The window material required for electrical conductance is usually added as a suspended layer over the source. This layer may be easily punctured by even careful handling if sharp instruments are used and the potential for material loss, contamination, and loss of calibration is high. Second, very often the salt adherence to the surface of the source is poor (again depending upon the salt and method used) allowing the salt to be displaced over time. This removes the advantage of the uniformity. The remainder of the factors (useful life and other environmental constraints) discussed above are dependent upon the source manufacture and no consistent comparisons can be made.

Electroplated Sources

The second most common wide area source manufacturing technique is electroplating. In this production method the nuclide to be electrodeposited, either by true electroplating or by the companion method of molecular deposition, is accumulated on the active surface by passing a current through the solution. This causes charged ions to migrate to

one of the charged surfaces, most often the cathode. After the electrodeposition process, further processing to increase adherence is performed, usually by diffusion-bonding.

The advantages of electrodeposition is the production of very thin adherent surfaces which are normally electrically conductive. The thin layer without cover reduces attenuation problems and generates the narrowest peak widths. This method is often required for energy calibration of alpha particles.

Again, numerous disadvantages exist. The range of nuclides which can be deposited is limited. Many of the most common beta emitters (Sr-90, Cs-137 and Na-22) cannot be electrodeposited. Uniformity is also a problem. Highly uniform sources can be made, but across large areas the uniformity of most electrodeposited sources on the market today is often worse (greater) than ± 10%. This poor uniformity is restricted by neither manufacturer nor nuclide. Additionally, the amount of material which can be electrodeposited is also limited in many cases.

Anodized Sources

Anodized sources are manufactured on aluminum surfaces in which pores have been made by the anodization of the surface. Nuclides are then incorporated into these pores and the pores are sealed either by the hydration of the aluminum closing the pores or, more commonly, by putting a thin layer of plastic, shellac or other material over the surface.

Anodized sources sealed by hydration solve many of the problems involved with wide-area sources. The ruggedness is very good as the source acts as a single piece of metal. Plus, in most sources, the temperature use-range and source maximum temperature are the largest of any source production method. In addition, radiation resistance is high and the useful life is in excess of ten years. However, the more common alternate method of manufacture alters these parameters, with those sources which are sealed with plastic or shellac being less rugged and having lower temperature tolerances than those truly sealed by aluminum hydration.

The other factors making the anodized source the optimum source configuration for most uses, up to this time, is that the active deposition has uniformity better than ± 5%. Wipe tests are easily performed. Because the aluminum provides an electrically conductive surface, no additional layer is necessary.

The drawbacks to anodized sources are as major as the advantages. The types of nuclides that are incorporated into truly anodized sources is limited and the amount of material, and hence activity, is even more limited. Thus, even when a nuclide has the ability to be incorporated, the amount of material which can be incorporated may eliminate the source from standard usage.

Additionally, the anodized source suffers from the attenuation of the emitted particles. Due to the cover, either the aluminum hydroxide in true anodized sources, or aluminum and plastic in others, attenuation is such that most alpha sources and many low energy beta sources have such wide particle energy peaks that precise calibration using these sources is not possible.

POLYMERIC MEMBRANES™ OR POLYSURFACE™

Nuclides can be incorporated into very thin layers of organic-based materials, called *polymeric membranes™* or *Polysurface™*. There are three types of *polymeric membranes™* (Table 2) and although the method of production varies, it can be generally summarized as bond formation between (1) the metal nuclide and the organic, or (2) between the organic layer and an organically-bound nuclide. The organic layer is backed by a layer of polyimide (Kapton™) or mylar which is further backed by a conductive layer of either aluminum or stainless steel. The cover of the source is varied and the conductive surfaces are made of either gold or aluminum.

The main characteristics of *Polymeric membranes™* are shown in Tables 2 to 4. The ruggedness of these wide area sources is very good, surpassed only by the truly anodized sources. The source can be wiped for leak test without damage by abrasion. The source can be punctured without loss of material, unlike the deposited or electrodeposited sources.

A major benefit of the *Polymeric membrane™* source construction is the source ruggedness and the large temperature range over which the source can be used. Although not as rugged as the anodized source, the *Polymeric membrane™* source will exceed the demands of all normal source uses. Also, all normal use temperatures are in the sources range, from the frozen winters conditions to hot, humid, tropical summers. Furthermore the sources can be exposed to water and other standard solvents and not be damaged.

The most important features of this source type are: (1) the nearly unlimited range of nuclides capable of inclusion into one of the three types of membrane; (2) the extreme uniformity meeting or exceeding that of even anodized sources; and (3) the incorporation of large nuclide masses and activities. For nuclides, Isotope Products routinely incorporates over 20 different nuclides into the *Polymeric membrane™* but the capability exists to incorporate over 80 different nuclides. The uniformity is given in table 2 and shows that the worst uniformity for any source made using *Polymeric membranes™* is ± 5% based on the standard 1 cm^2 area. However, the uniformity for most nuclides is usually ± 1.5% or better (Figure 1).

Table 4 gives the maximum available activities which can be calibrated traceable to NIST but for most nuclides this is dependent

Table 2: *POLYSURFACE*™ RADIATION MATERIALS			
Description	**Type X**	**Type F**	**Type H**
Main Uses	(1) High energy beta emitters such as P-32, Sr-90, Cs-137 (2) Most Gamma Sources (3) Any application requiring high area uniformity	(1) Low energy beta emitters (2) Low energy gamma emitters	(1) Very low energy beta emitters, such as C-14 and H-3
Backing	Kapton™ 0.003" = 0.075 mm = 11 mg/cm²	Mylar 0.004" = 0.1 mm = 15 mg/cm²	Mylar 0.004" = 0.1 mm = 15 mg/cm²
Active Layer Thickness	7 - 10 mg/cm²	4 - 5 mg/cm²	1 mg/cm²
Planar Uniformity[1]	± 3%	± 5%	± 5%
Resolution	2,000 pix/cm²	Continuous	Continuous
Covers Available	(1) 50 µg/cm² Au (<2"diameter only) (2) 80 µg/cm² Al (3) 100-200 µg/cm² acrylic (4) Kapton (various thicknesses) (5) None	(1) 50 µg/cm² Au (<2"diameter only) (2) 80 µg/cm² Al (3) 100-200 µg/cm² acrylic	(1) 50 µg/cm² Au (<2"diameter only) (2) 80 µg/cm² Al

[1] Based on 1 cm² areas, deviation from mean.

Table 3: *POLYSURFACE*™ RADIATION MATERIALS CHARACTERISTICS, CONTINUED			
Description	**Type X**	**Type F**	**Type H**
Standard nuclides available[2]	Si-32/P-32 Co-56 Co-57 Co-60 Ge-68 Sr-90 Cd-109 Cs-137 Eu-152 Tl-204	Cl-36 Fe-55 I-125 I-129 I-131 Pm-147 Tl-204 Am-241	H-3 C-14 Fe-55 Co-57 Co-60
Stability (Useful life)	5 years	10 years	10 years
Wipe Test[3]	Yes	Yes	Yes
Radiation Resistance	Testing not complete but > 3 x 10^6 rads	3 x 10^6 rads	3 x 10^6 rads
Temperature - Normal use	10° - 40° C	10° - 40° C	10° - 40° C
Maximum temperature range	-180° - 100° C (Do not expose to greater than 100° C)	-180° - 70° C[4]	-180° - 70° C[4]

[2] Other nuclides available, contact Technical Information at IPL.

[3] Based on a wiping force of less than 1 kg/cm², with standard aluminum or acrylic cover, except for type H, which has no cover.

[4] Temperatures above 70° C may cause the surface to warp but will not liberate activity until >200° C.

Table 4: CALIBRATION OF *POLYSURFACE*™ RADIATION MATERIALS, NIST TRACEABLE OUTPUT			
Description	Type X	Type F	Type H
Minimum Activity Available for NIST Calibration[1]	5 nCi β 0.2 nCi α 0.1 μCi γ	5 nCi β 0.2 nCi α 0.1 μCi γ	5 nCi β 0.2 nCi α 0.1 μCi γ
Maximum Activity Available for NIST Calibration	200 nCi α or β 100 μCi γ	200 nCi α or β 100 μCi γ	200 nCi α or β 100 μCi γ

[1] Some activities outside of this range are possible, contact Technical.

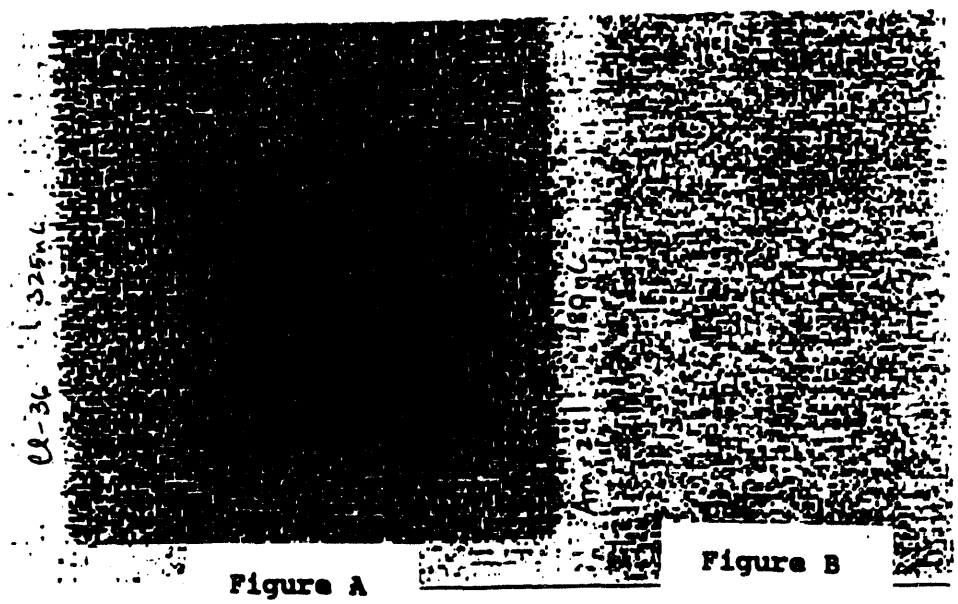
upon the counting equipment and not the loading capability. In the extreme, the beta emitter Pm-147 can be loaded onto a 100 x 100 cm area source in activities in the Curie (~100 GBq) level. Most nuclides can be incorporated in multiple millicurie amounts. It is not surprising that these methods are used for the manufacture of dose rate area sources as well.

Source layer attenuation of alpha and beta emitted particles is critical in some uses. *Polymeric membranes*™ are similar to electroplated sources or deposited sources in the low energy attenuation of these emitted particles. Figure 2 shows a common beta nuclide, Sr-90/Y-90, both in a deposited source and in a *Polymeric membrane*™. No significant energy decrease is found in the energy maxima, the average energy or the peak shape when a comparison is made. However, like any source production type, when low energy sources are examined some attenuation occurs. Table 5 give data on contained activity versus output, including backscatter, in 2 pi. At low energies only half the total emitted particles for C-14 are observed at the detector. Hence, while the *Polymeric membrane*™ technology allows for a decrease in attenuation over the anodized technology for some source types, i.e. those of lower beta energy, the problem is still significant.

Finally, the uses for sources manufactured using *Polymeric membrane*™ exceed that of other source production methods. All the traditional methods, deposition, electroplating and anodizing, require that a hard backing be present in the source. *Polymeric membranes*™ were designed, in part, to allow the solid backing to be removed from the source so the standard can be bent and shaped into different configurations. This allows the source to be used in new ways, for example, using a *Polymeric membrane*™ wrapped around or inside a pipe to simulate more easily the contamination found outside or inside the pipes.

The size which this procedure allows is also novel. While the limit to electrodeposited sources with uniform deposition is about 20 cm x 10 cm and anodized sources are limited by the anodizing cells and the cost of cell production, the upper limit to the process using *Polymeric membrane*™ technology has not yet been reached.

Figure 1: Uniformity scans of wide-area sources made using Isotope Products Laboratories Polymeric Membrane technology. (a) Shows a Cl-36 β-emitter, 325 nCi, in a 10 cm x 10 cm configuration; (b) shows an Am-241 α-emitter, 480 nCi. (c) C-14 decade standards (edges masked creating uneven borders).



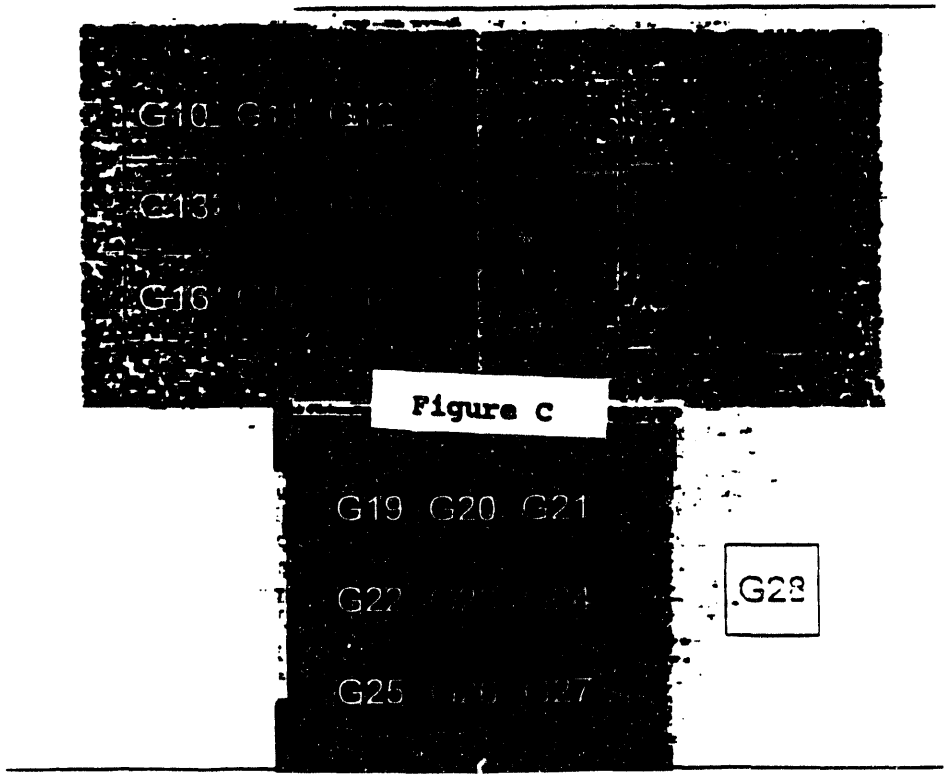
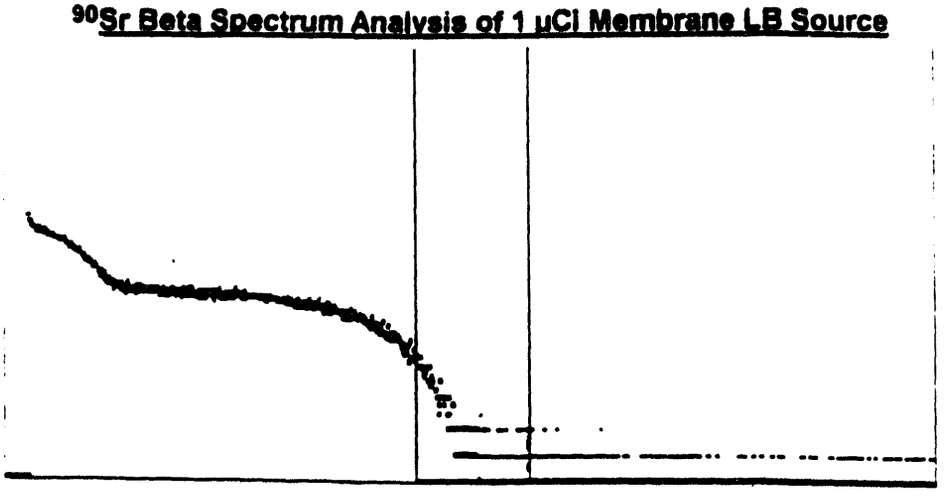


Figure 2: Sr-90/Y-90 β-spectrum in a deposited sources (no source attenuation) and in a Type X Polymeric membrane. No detectable change in the peak shape, maximum β-energy or average β-energy exists. Output from both sources is 63% (see table 5).



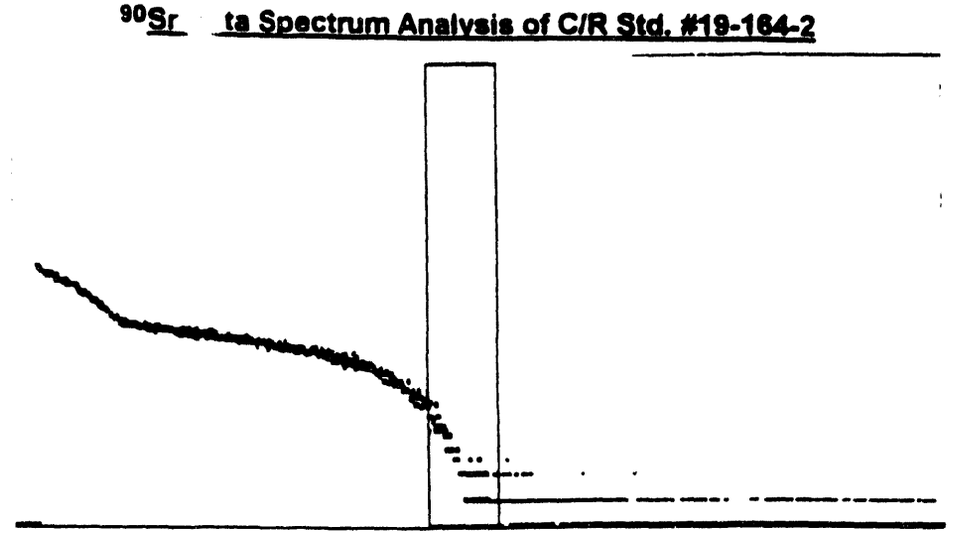


Table 5: CONTAINED ACTIVITY VERSUS BETA OUTPUT. *POLYSURFACE*™ SOURCES				
Nuclide	Average Beta Energy (keV)	Contained Activity (dps) ± 5%	β/sec/2 pi Beta Emission Rate ± 5%	Ratio Emission Rate (2 pi)/contained activity[a] ± 6%
C-14	49	11060	2828	25.6%
Co-60	96	8954	2807	31.3%
Cl-36	251	5310	3175	59.8%
Sr-90/Y-90	566	13790	8776	63.6%

[a] Includes backscatter

USE OF POLYSURFACE SOURCES™

Because of the range of environmental conditions, the wide range of nuclides and activity levels available, the low energy attenuation and good uniformity of the source, it is therefore suggested that the *Polysurface*™ source replace most other source construction types. *Polysurface*™ sources should replace all deposited sources based on personnel safety issues (contamination by window puncture). Except in the extremes of energy calibration sources, which are usually small, the uniformity found in the *Polysurface*™ sources make them the preferred source. *Polysurface*™ sources should replace anodized sources when higher activity or a greater range of nuclides is required, when reduction of energy attenuation of emitted particles is necessary or when aluminum cannot be brought into the system. Finally, *Polysurface*™ sources can be used in new applications where a NIST traceable surface is desired in a non-flat configuration or when extreme size ranges are required.

TRACEABILITY OF A PANORAMIC GAMMA IRRADIATOR USING DIFFERENT TLD SYSTEMS AS TRANSFER INSTRUMENTS

A.M. ROMERO, J.C. SAEZ-VERGARA
Radiological Protection Division
CIEMAT
Avda. Complutense 22, 28040 Madrid, Spain

Phone: 34-1-3466252
FAX: 34-1-3466393

ABSTRACT

The Quality Control Program in a TLD Personal & Environmental Dosimetry Service requires not only the calibration in a recognized reference laboratory but also large amount of additional irradiations for daily controls, individual correction factors calculation, fading corrections and other purposes.

These routine irradiations do not need metrological quality to be performed, so that auxiliary equipments such as a self-contained panoramic gamma irradiator can be employed. However, it seems reasonable to characterize the response of these equipments to the reference laboratory.

This work shows the calibration in terms of the new operational radiological quantities $H_p(10)$ and $H^*(10)$ for different TLD systems (Harshaw TLD-100 and Panasonic UD-802) used in environmental and personal monitoring programs at CIEMAT. The irradiations were performed in the Spanish Reference Laboratory in radiation protection levels, managed by CIEMAT's Metrology of Ionizing Radiations Unit.

With these data, different calibrations of a panoramic gamma irradiator in terms of the radiological quantity per unit of time were established, providing the traceability of the irradiator to the Reference Laboratory using the corresponding TLD systems as transfer instruments.

INTRODUCTION

CIEMAT's Dosimetry Service uses several personal and environmental TLD dosimetry systems calibrated in CIEMAT's Metrology of Ionizing Radiations Unit[1] in terms of the operational quantities $H_p(10)$, $H_p(0.07)$ and $H^*(10)$ recommended by I.C.R.U.[2].

For routine irradiations, such as daily controls or individual correction factors calculation, CIEMAT's Dosimetry Service employs a J.L. Shepherd model 142-S[3] gamma irradiator.

The aim of this work is to study the traceability of this irradiator to the Spanish Reference Laboratory in radiation protection levels for two different dosimetric systems: Harshaw for environmental purposes and Panasonic for personal ones.

IRRADIATION FACILITIES

Gamma Irradiation Laboratory in radiation protection levels of CIEMAT's Metrology of Ionizing Radiations Unit

CIEMAT's Metrology of Ionizing Radiations Unit is the Spanish Reference Laboratory in radiation protection levels and is traceable to international metrological laboratories as NPL in United Kingdom and BIPM in France.

The gamma irradiation laboratory has two different irradiators. One encloses a 100 TBq of Cs-137 source and the other one includes a 1.5 TBq and a 15 GBq of Cs-137 sources and a 0.74 TBq and a 7.4 GBq of Co-60 sources placed in a revolving chamber.

Radiation Protection Laboratory: J.L. Shepherd panoramic gamma irradiator

The model Mini 142-S irradiator incorporates two sources, 111 GBq and 740 MBq Cesium-137, mounted on one operating rod assembly.

This irradiator provides panoramic irradiation of TLD's, inside a completely self-shielded irradiation chamber. TLD's are placed onto mounting racks, which in turn are placed onto the turntable inside the irradiator. All operational functions for this unit, i.e. access cover, source selection and operation, turntable rotation, etc. are found on the control panel. The irradiation chamber access cover is interlocked so that the sources cannot be raised with the cover open and the cover cannot be raised with sources exposed.

The manufacturer provides the irradiator with a calibration certificate indicating that calibration is directly traceable to the National Institute of Standards and Technology (NIST).

THERMOLUMINESCENT DOSIMETRIC SYSTEMS

Harshaw Environmental Dosimetric System[4]

The Harshaw TLD-100 chips (3 x 3 x 0.9 mm^3) are used as environmental detectors. The dosemeter is formed by eight chips lodged inside a PMMA phantom with wall thickness of 600 $mg.cm^{-2}$.

Thermal treatments applied to the detectors were performed in an oven, microprocessor controlled in time and temperature.

A Harshaw reader model 4000-A was used for readouts. It was linked to a personal computer. Conventional and glow curve (200 points) data were acquired and stored in the computer. Glow curves were analyzed using a specific software[5,6] developed in CIEMAT's Dosimetry Service. This computer code performs the filtration and smoothing of the raw data, identifies characteristic points in the curve, calculates and subtracts exponential background and computes useful parameters such as the area and the maximum in the net signal.

Panasonic Personal Dosimetric System

The standard Panasonic UD-802 badge in hanger UD-874 is used. This badge has four detectors or elements of two different phosphors: $Li_2B_4O_7$:Cu (practically tissue-equivalent) and $CaSO_4$:Tm (high sensitivity TL material but with high over response to low energy photons).

The hanger offers an additional filtration in order to reach charged particle equilibrium for most of the radiation fields in routine.

These dosemeters were processed in an automatic Panasonic reader model UD-710A. The heating system of the reader is based on an infrared emission from a tungsten lamp. The reader is automatically controlled by a personal computer and a specific software[7,8], developed in CIEMAT's Dosimetry Service, which stores the data, applies quality control criteria and uses a dose calculation algorithm to evaluate results.

CALIBRATION AND TRACEABILITY

The set of operations which establish, under specified conditions, the relationship between values indicated by a measuring instrument and the corresponding known values of a quantity is called **Calibration**. The result of a calibration is usually expressed as calibration factor and it may be recorded in a document (calibration certificate). Calibration may permit the estimation of errors of the measuring system.

Radiological quantities recommended by I.C.R.U. are defined in specific irradiation conditions as normal radiation incidence on appropriate phantoms. For the calibration of the TLD systems, TL detectors are irradiated in CIEMAT's Metrology of Ionizing Radiation Unit under these conditions.

The first hypothesis is the linear dependence of delivered dose in Metrology Laboratory (**D**) on the readout in reader (**L**), i.e.,

$$D = a \cdot L + b,$$

where **a** is the calibration factor of the reader and **b** is usually negligible. This hypothesis is based on the linear response of TLD in usual environmental and personal dosimetry range.

Although irradiation conditions in the J.L.S. irradiator are

very different (panoramic beam, no phantom, scattered radiation), is possible to get a relation between both facilities using the TLD systems as transfer devices, i.e., inferring the value of the radiological quantity in the irradiator from the TL readout.

Next assumption is the linear dependence of the readout in reader (L) on the irradiation time in the J.L.S. irradiator (t), i.e. $L = a' \cdot t + b'$. This assumption is founded in the first hypothesis and the proportionality between dose delivered and irradiation time.

Accepting both hypothesis:

$$D = a \cdot L + b = a \cdot (a' \cdot t + b') + b = A \cdot t + B$$

where $A = a \cdot a'$ and $B = a \cdot b' + b$.

With this procedure the readouts of TLD irradiated in the panoramic beam can be directly related with the radiological quantity of interest (**Traceability**).

The purpose of this work is to get the values A and B of the relation $D = A \cdot t + B$, the uncertainty for this values and the dose range application of the relation for both deep personal dose equivalent $H_p(10)$ and ambient dose equivalent $H^*(10)$.

EXPERIMENTAL PROCEDURES

A group of each type of dosemeters were irradiated at CIEMAT Metrology Laboratory to known doses in the dose range of interest for each one of the quantities to study, $H_p(10)$ and $H^*(10)$.

The dosemeters where processed in the corresponding reader and the relation $D = a \cdot L + b$ was calculated by a linear regression fit of the data.

The same dosemeters where subsequently irradiated on the J.L.S. panoramic gamma irradiator to known irradiation times so that delivered dose ranges were the same as previously.

The relation of calibration was applied to the readouts of this dosemeters yielding delivered dose versus irradiation time and by a linear regression fit of this data, the relation $D = A \cdot t + B$ was obtained.

The irradiations in CIEMAT's Metrology Laboratory were performed according to the next classification:

a.- **Ambient dose equivalent, $H^*(10)$, in the range 0.01 - 1 mSv**

Several types of dosemeters (TLD-100 into environmental phantom and Panasonic UD-802 in hanger UD-874) were irradiated with a 1.5 TBq of Cs-137 source and a 0.65 mSv/h dose rate. The exposures were performed free in air.

The number of dosemeters employed in each point of measurement was eight TLD-100 detectors.

b.- **Personal dose equivalent, $H_p(10)$, in the range 0.01 - 150 mSv**

For each point of measurement, six Panasonic UD-802 in hanger UD-874 were irradiated in the range 0.01 - 7.5 mSv with the same source as previously but mounted on a PMMA phantom (30 x 30 x 15 cm^3).

In the range 10 - 150 mSv, six Panasonic UD-802 in hanger UD-874, placed on a PMMA phantom (30 x 30 x 15 cm^3), were irradiated for each point of measurement with a 100 TBq of Cs-137 source and a 19.5 mSv/h dose rate.

The irradiations in the J.L.S. panoramic gamma irradiator were performed as follows:

a.- **Ambient dose equivalent, $H^*(10)$, in the range 0.01 - 1 mSv**

Several types of dosemeters (TLD-100 into environmental phantom and Panasonic UD-802 in hanger UD-874) were irradiated with a 20 mCi of Cs-137 source in the range 0.600 - 64.000 minutes of irradiation time.

The number of dosemeters exposed for each point of measurement was eight TLD-100 detectors.

b.- **Personal dose equivalent, $H_p(10)$, in the range 0.01 - 150 mSv**

In the range 0.01 - 0.15 mSv, six Panasonic UD-802 in hanger UD-874 were irradiated for each point of measurement with the same source as previously but in a irradiation time range 0.600 - 9.500 minutes.

Six Panasonic UD-802 in hanger UD-874 for each point of measurement were irradiated in the range 0.25 - 150 mSv with a 111 GBq of Cs-137 source from 0.100 to 60.000 minutes of irradiation time.

RESULTS AND DISCUSSION

Figures 1 and 2 shows the linear regression fits and the experimental data obtained for every item object of this study. In all cases, errors for estimation of the parameters and correlation coefficients, r^2, are included. The criterion for deciding the linear fit was to considerate if the independent term was smaller than its error and, in this case, a new linear fit without independent term was adopted.

The data of very low doses (10-20 μSv) in Panasonic dosemeter were refused, as this values are very close to detection limit for these materials.

For the Panasonic TLD system, only the results for elements 3 and 4 are presented since these are the elements used for calibration and dose evaluation. In addition, systematic errors due to lack of filtration in element 1 and to the lead filter in element 4 are avoided.

As it can be seen in figures, linearity of all dosimetric

systems studied shows good correlation coefficients and relative errors in slope less than 1% in all cases.

The relative standard deviation against dose (characteristic curve) for the different dosimetric systems studied are shown in Figure 3 (Ambient Dose) and Figure 4 Personal Dose). The expected increases of the uncertainty at low doses are observed[9].

Good agreement is obtained in the comparison of the characteristic curves from both irradiation facilities for each dosimetric system. This fact confirms that irradiations in J.L.S. panoramic gamma irradiator are highly homogeneous in the dose ranges tested, since uncertainty founded is inherent in the dosimetric system independently of the irradiation facility employed.

CONCLUSIONS

This work shows that it is possible to perform **high homogeneity** irradiations with the J.L. Shepherd model 142-S[3] panoramic gamma irradiator, property of CIEMAT's Dosimetry Service; for all TLD dosimetric systems employed by this Group.

These irradiations are **traceable** to CIEMAT's Metrology Labortory in terms of the radiological quantity in which dosimetr system is calibrated, using different personal and environmental TLD systems as transfer instruments.

REFERENCES

[1] Brosed A., Delgado A. Granados C.E., " Nuevas magnitudes para la vigilancia ambiental e individual. Calibración de dosímetros personales usando haces externos de fotones". CIEMAT-605 (1987).

[2] I.C.R.U., "Determination of dose equivalents resulting from external radiation sources. Parts I, II & III". Reports 39 (1985), 43 (1988) y 47 (1992). Bethesda, MD : ICRU Publications.

[3] J.L. Shepherd & Associates, "Installation and Operation Manual for Model Mini 142-SA3 self contained panoramic gamma irradiator" (1991)

[4] Sáez J.C., "Sistema de dosimetría ambiental TL basado en LiF:Mg,Ti (TLD-100)". CIEMAT-655 (1990).

[5] Sáez J.C., "Evaluación dosimétrica basada en curvas TL. Programa GCA-DOS: Manual del Usuario", CIEMAT/UPR/DAM/01/91 (1991).

[6] Sáez J.C., "Evaluación dosimétrica basada en curvas de emisión TL obtenidas en el lector Harshaw 4000", CIEMAT/PRYMA/PR/DPE/37/90 (1990).

[7] Romero A.M., Sáez J.C., "Aplicación informática para la lectura de dosímetros personales TL en el Servicio de Dosimetría del CIEMAT. Manual de Usuario". CIEMAT/UPR/DPE/03/93 (1993).

[8] Romero A.M., Sáez J.C., "Evaluación de dosímetros personales TL en el Servicio de Dosimetría del CIEMAT". CIEMAT/UPR/DPE/02/93 (1993).

[9] Vázquez C., Sáez J.C., Labarta T., "Caracterización de un sistema de dosimetría personal termoluminiscente Panasonic". CIEMAT-638 (1989).

Figure 1.a.: TLD Calibration at CIEMAT Metrology Laboratory
Ambient Dose Equivalent (Harshaw)

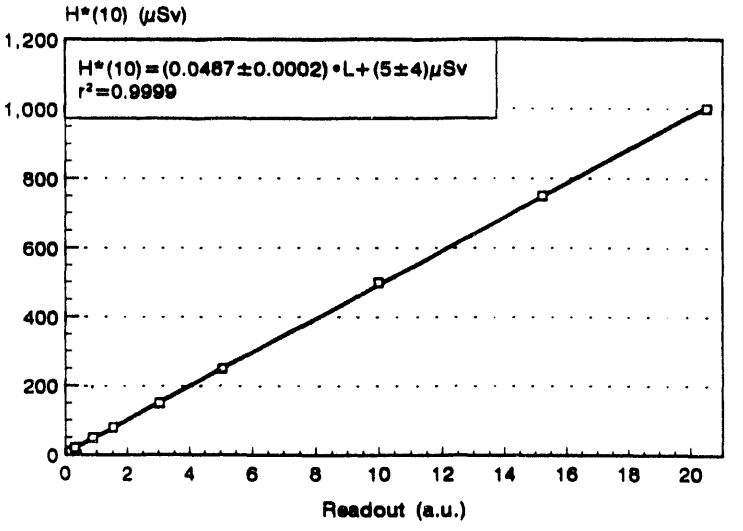


Figure 1.b.: Panoramic Irradiator Traceability (740 MBq source)
Ambient Dose Equivalent (Harshaw)

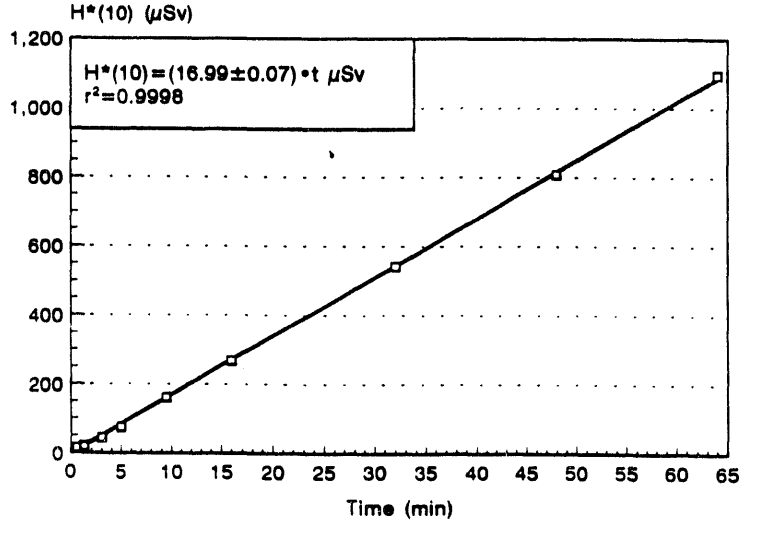


Figure 2.a.: TLD Calibration at CIEMAT Metrology Laboratory
Personal Dose Equivalent (Panasonic)

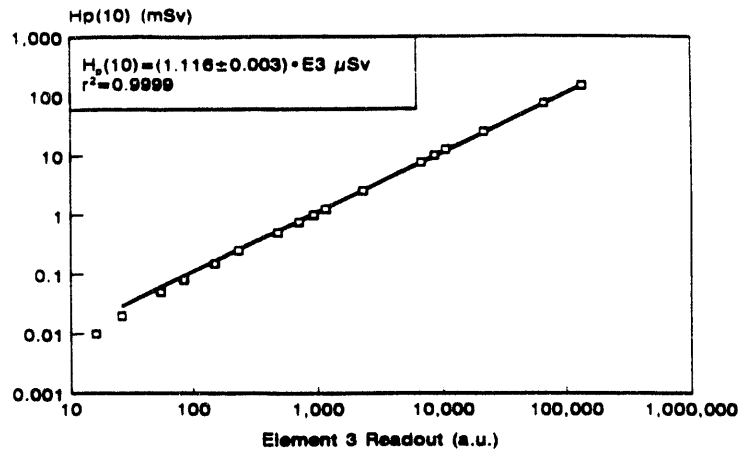


Figure 2.b.: Panoramic Irradiator Traceability (740 MBq source)
Personal Dose Equivalent (Panasonic)

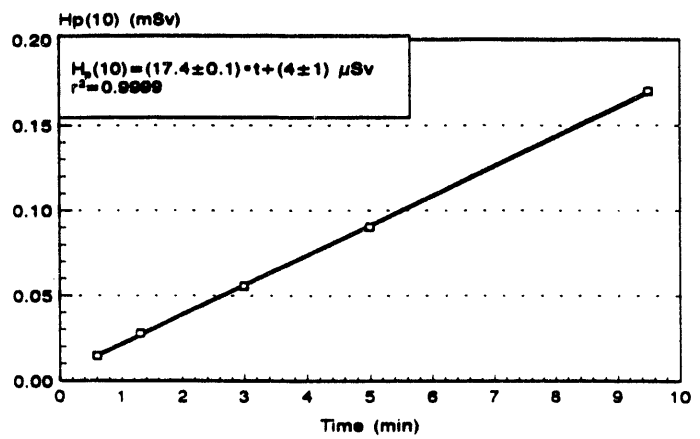


Figure 2.c.: Panoramic Irradiator Traceability (111 GBq source)
Personal Dose Equivalent (Panasonic)

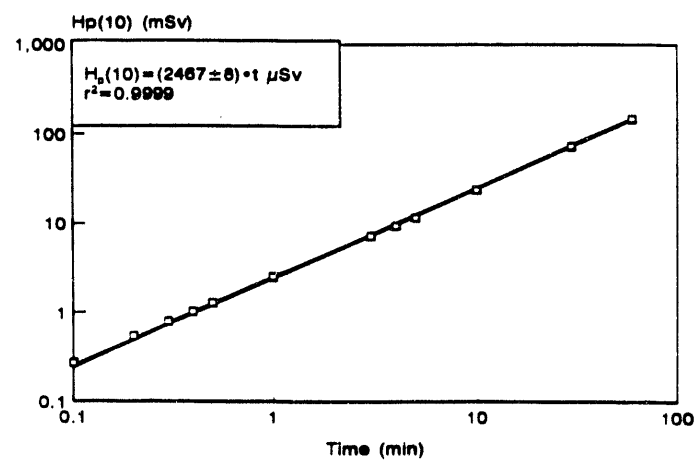


Figure 3: Reproducibility Curves
Ambient Dose Equivalent (Harshaw)

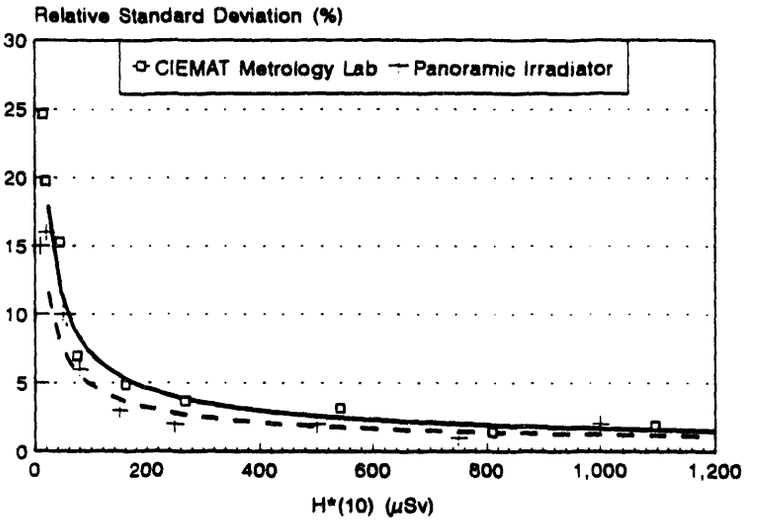
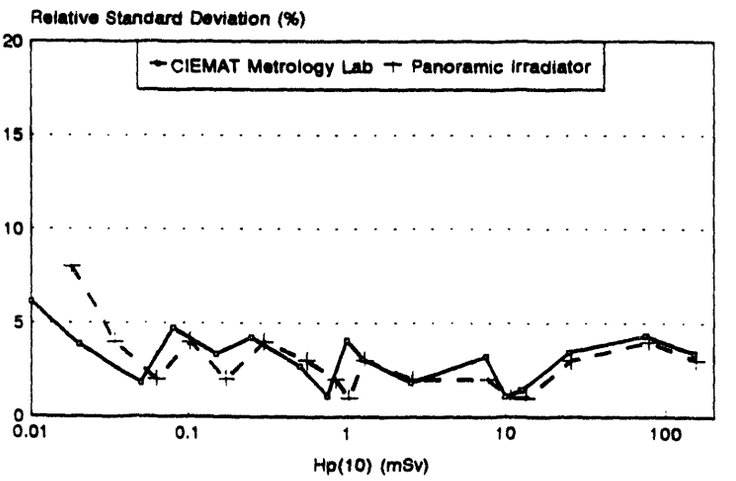


Figure 4: Reproducibility Curves
Personal Dose Equivalent (Panasonic)



SESSION VIII.
Medical, Accident, & High-Level Dosimetry

Keith Eckerman,
Chairman

THE IMPORTANCE OF RADIOPROTECTION CONTROLS IN NUCLEAR MEDICINE

Sahyun A.(IIPS), Sanches M.P.(LAS) & Sordi G.M.A.A.(IIPS)
Instituto de Pesquisas Energeticas e Nucleares - IPEN-CNEN/SP. Travessa R. 400 - 05508-900 - São Paulo, SP, BRAZIL

ABSTRACT

In nuclear medicine the main objective of radioprotection controls is to protect three people groups from external and internal radiation. To obtain this goal, the dose limitation system has to be followed firmly and for that, basic procedures have to be introduced. These basic procedures are the result of several activities which have to be balanced, one against the other to be effective.

The aims of radioprotection are to ensure that people are not exposed to doses enough to cause acute radiation symptoms and to limit the doses of radiation. This is achieved by the use of shielding, containment, careful design and operating and administrative procedures.

This paper presents a small list of general radioprotection problems found in nuclear medicine and establishes some rules related to the job schedule and control measures to be followed in favor of safety. By considering the general radioprotection problems, a number of factors of substantial relevance in the control of external and internal doses can be deduced and emphasis properly placed. Work with radioactive material should be concentrated on a limited number of work rooms. Good radioactive materials inventory are essential because of the potentially large diversity of material and users. Storage of radioactive materials ensure that the public is not unnecessarily exposed. Appropriate monitoring equipment should be available within each working site.

Line management commitment to safety has led to a heightened awareness for those control measures which encourages individuals to review and improve their own work rules. Investment in training programs, plant modifications and written procedures provide the necessary resource to support the dose reduction initiatives.

1. INTRODUCTION

Unsealed radioactive sources are used in nuclear medicine.

Radioactive sources are used in diagnostics procedures "in vivo" and "in vitro", and in some laboratories they are used in therapeutic procedures. As a consequence of the radioactive sources usage in nuclear medicine laboratory there is the risk of the external radiation and the external and internal contamination by the personnel.

In this case, the people involved in nuclear medicine laboratory job need the skill to identify the risks associated to their job and need the knowledge of radioprotection regulation and procedures to be put into practice.

2. FACILITIES REQUIREMENTS

The nuclear medicine laboratory workplace layout should be designed according to the radiation source containment principle. The workplace where the radiation exposure can overpass the 3/10 of the worker annual limits[1] should be classified as controlled, otherwise will be classified as supervised, save it is lower than the public annual limits and in this case will be considered as free.

The controlled and supervisioned workplace need to be bring together and be separated of the free workplace. They need to be well identified by visible warns and signals at the workplace entrance and inside it. The workplace entrance needs to be controlled. The workplace site needs to be ordered in such a manner that the environment of major risk will be situated inner and the other external surroundings, that is from radioactive source handling workplace to the radioactive source fraction to be administrated to the patient.

2.1. General Guidance Related to the Workplace

These guidances are essentially related for the contamination risk, which is the most dangerous.

- The surfaces should be washably and resistent to the chemical corrosion and warming.
- The walls and the ceilings should be covered with a washable, hard and non-porous paint.
- Material applied in covering should be easily decontaminated.
- The floor with such materials as linoleun, rubber tile or polyvinyl chloride and the junction of floor and the walls should be sealed and rounded in order to facilitate cleaning.
- The sinks should be provided with taps designed for operation by foot, knee or elbow, rather than by hand.
- The spouts used for radioactive material disposal should be connected to a waste collection tank of liquid wastes.
- A shower should be installed for emergency cases.
- Appropriate rooms should be designed for radioactive sources and radioactive waste storage.

2.2. Aditional Guidance for Workplace

a) Sites where radioactive material aliquotes are separated will be labeled and identified and will be provided with:

- Walls with at least 15cm of bricks thickness in order to limit the neighboor places irradiation.
- Showers should be installed for emergency situations.
- Spouts used for radioactive material disposal should be connected to a waste collection tank of liquid wastes.
- Strongbox for radioactive material storage.
- Solid-waste collection system.

b) In hospital patients submitted to therapy:

- Should be hospitalized in rooms with short dimensions.

- The rooms should be classified as controlled area.
- The room should have such walls thickness that dose rate in the exterior would be lower than 25 μSv/h..
- The urinal of those rooms should be connected to the dilution on decay[2] tank.

c) **Other places**

Depending on the activity handled and the physical and chemical properties of the radionuclides and the activities levels, these places need to be provided with a:

- Radioactive waste temporary storage place.
- Fume cupboard for radioactive material handling.
- Bench easy to be decontaminated.
- Active sinks connected to dilution tanks.

3. PROTECTION REQUIREMENTS

3.1 External Radiation in Controlled Areas

The radioprotection general guidance regarding the three basic factors, i.e, time, distance and shielding materials continues valid for external radiation.

a) **Radioprotection for external radiation.**

- The best shielding is distance until 1 meter because the dose value for this type of source depends inversely on the square distance from it. If we go from 1 centimeter to 1 meter the dose will be reduced by a factor of 10^4, but if we go from 1 meter to 4 meters the dose value decreases only a factor of 16. Work at distances over 1 meter became difficult and the dose value decreases a little. To work at a distance of 1 meter is easy because a remote-handling tong of 30cm long more 70 cm of arm perform 1 meter. This distance limitation impose very low activity sources handling and then conversely that we need to make use of the other two basic factors.
- The dose received by a person is proportional to the time of irradiation, and then will be reduced if the radioactive material handling will be done only at the time of administration to the patient and if the people incharged of the handling work in turns.
- Do not touch the flacon that contains radioactive material with the hands, because even small, distances will reduce a lot of the doses in hands.
- Use movable shielding, particularly if the activities are higher than 10 MBq. The shielding thickness depends on the activity, the types and the energy of the radiation.
- Do not use activities bigger than necessary.
- Maintain in the laboratory only the necessary number of people to avoid unnecessary irradiation.

- To prevent and to avoid the dispersion of contamination, keeping the normal condition of personal cleanliness maintaining as regular monitoring program for contamination, using protection clothes and absorbent material if necessary.

- To the controlled and supervised are look at the behavior guidance as: don't drink, don't eat, don't smoke.

- If possible, transport radioactive material in the same containment used at the reception.

3.2. Radioactive Contamination in Person

Radioactive surface contamination is unwanted radioactive material deposited in an uncontrolled manner in or on animate or inanimate objects, irrespective of their situations, in such concentrations that radiological hazard is caused. In the case of personal contamination we can distinguish the external contamination, i.e., the radioactive material is on the body surfaces, using an external irradiation and the internal contamination when the radioactive material enter the body using an internal irradiation.

The protection against radioactive contamination is assured by the availability of equipment's and by the adhesion of recommendations for radioactive products handling.

a) In the sources handling

- The sources handling needs the glove use.

- Mouth-operated equipment, e.g., pipettes, must not be used or even be present in any radioisotope laboratory.

- The source handling should be reduced at the minimum time.

- The distance operator-source should be maximized in such a manner to propiciate good operation conditions.

- The protection shielding thickness should be in accord to the radiation characteristics.

- The radiaoctive substances movement needs to be done in a containment involved in a removable absorvent paper.

- A fume cupboard is necessary for solution evaporation.

- Containment container should be removed to sinks appropriated for this purpose.

b) In source management

During the reception of radioactive products, their characteristics need to be appropriately recorded in a log-book and then put in the storage place.

- The activity decrease due to the administration to the patient or by other reasons needs to be recorded in an appropriate log-book.

- The flacon or container with radioactive material needs to be immediately identified and in a clear manner.

- The source that becomes out of use needs to be recorded immediately in its storage place.

- The radioactive substances cannot be delivered in the environment unless they attend the regulation enforced.

c) In radioactive waste management

- The radioactive waste collected must be segregated according to the peculiar characteristics of the facility[2,3,4].

- The empty package for radioactive material cannot be thrown into the normal inactive waste without any verification that is not containment and without to have removed any indication, warn or signal accusing radioactive material.

4. RADIOACTIVE WASTE

The radioactive wastes should be object of controlled elimination.

The sealed radioactive waste can be thrown into the normal inactive waste provided the regulation[3,4] permits, conversely it needs to be eliminated by an authorized service corporation.

The environment deliveries need to be according to the international recommendations.

The human excreta can be delivered in a sewage sanitary.

5. CONCLUSION

In the uncontrolled and supervised area the worker needs to know the recommendations about radioactive materials handling, at least the IAEA recommendations published in the safety series[5,6] collections, needs to wash the hands and control the surface contamination.

The dosimeter should be used in an easily looking way during his job journey.

The dosimeter needs to be maintained in an appropriate place when the user is out of the workplace. The aim is to be sure that the dosimeter was not irradiated without the presence of the user.

The radioactive wastes must be disposed in an appropriate package, classified according to their characteristics and storage in a specified and appropriate place before the disposal as normal inactive waste or an authorized activity.

6. REFERENCES

1. Safety Series number 9 - "Basic Safety Standards for Radiation Protection", IAEA, 1982.
2. Safety Series number 30 - "Manual on Safety Aspects of the Design and Equipment of Hot Laboratories", IAEA, 1981.
3. Safety Series number 12 - "The Management of Radioactive Wastes Produced by Radioisotope Users", IAEA, 1965.
4. Safety Series number 19 - "The Management of Radioactive Wastes Produced by Radioisotope Users", IAEA, 1966.
5. Safety Series number 1 - "Safe Handling of Radionuclides", IAEA, 1973.
6. Safety Series number 38 - "Radiation Protection Procedures", IAEA, 1973.

RADIATION PROTECTION IN HOSPITALS

Richard J. Vetter (Mayo Clinic/Foundation)

Hospitals contain a variety of sources that may contribute to occupational and public radiation doses. Engineering design, training, administrative controls, and quality control are used to minimize doses. Changes in consensus standards and regulations have reduced the annual permissible effective dose to members of the public and the lifetime occupational effective dose. Hospital radiation protection and monitoring programs must take advantage of the latest developments in radiation protection and radiation monitoring techniques to keep occupational and public doses as low as reasonably achievable. This paper will describe the radiation protection program of a broad scope medical licensee, describe efforts to reduce radiation doses, and discuss trends in doses to employees and the public.

OCCUPATIONAL HEALTH EXPERIENCE IN THE PRODUCTION AND DISTRIBUTION OF RADIONUCLIDES USED IN MEDICINE

GABURO, Janete C.(SBPR); SANCHES, Matias P.(SBPR) & SORDI, Gian M. A. A.(HPS)
Instituto de Pesquisas Energéticas e Nucleares - CNEN/SP, C.P. 11049, CEP 05422-970 - São Paulo-SP,Brazil

ABSTRACT

A brief description of the main operations performed in the Radioisotope Production Facility at IPEN-CNEN/SP is presented. This facility is provided with hot cells which must be periodically replaced due to deterioration by reagent processing and hard treatment to which they are submitted. When the lifetime of these hot cells are at their limit, leaking of airbone materials arises bringing forth incorporation by workers. As a safe control, a series of procedures have been implemented in a program of internal monitoring by urine sampling and external monitoring by film badge. From this program it became possible to evaluate the radiation dose received by workers. The results obtained within the last 10 years where analyzed against the lifetime of the hot cells and studies were made to verify possible explicit or implicit relations between doses and the natural stress of these hot cells. In the distribution of the effective dose equivalent among 304 workers submitted for individual monitoring of internal exposure by urine samples, some significant exposures higher than 1.5 mSv, in 126 cases were presented. From these cases, 64 had an effective dose higher than 4.5 mSv. The sum of effective doses and doses from external exposures can lead to levels close to regulatory limits. The internal effective dose equivalent is small when compared with whole body external dose equivalent, however it is not negligible.

1. INTRODUCTION

The workers exposed to ionizing radiation at the controlled area in the Radioisotope Production Facility at Instituto de Pesquisas Energéticas e Nucleares - GP-IPEN-CNEN/SP are submitted to personnel monitoring. Individual radiation exposures consist of external exposure from radiation sources outside the body and of internal exposure due to the intake of radioactive material. The radioisotope production is based upon targets irradiated either in a research reactor or in a cyclotron unit available in the IPEN-CNEN/SP facilities. The main targets irradiated in the reactor are tellurium, sodium, samallium and rhenium. The targets irradiated in the cyclotron are telhurium and zinc.

In the IPEN-CNEN/SP, the maximum activity level is limited on the basis of available processing containments. This facility not only produce radioactive materials and labelled compounds but also use them for research purposes. The main part of the radioisotope production is used in medicine. Therefore, a great part of the job is done in workplaces that may easily become contaminated as during the maintenance and other procedures. Due to the possibility of internal contamination the workers are monitored by urine sampling that are sent to the radiotoxicological laboratory at periodic intervals. Presently there are approximately 62 employees for operating, mantaining and managing the facilities. During the whole operation, workers radiation doses have been monitored and assessed to ensure that they remain well controlled.

2. METHODS AND PROCEDURES

Presently the project involves sixty two (62) workers of the GP-IPEN-CNEN/SP that cross two processing plant sites. Urine samples was collected during the work period i.e. 8 hours per day, using rigorous collection protocols to minimise the possibility of contamination. The measurement method for internal monitoring of the Iodine-131 by urine sampling is based on the use of silver chloride with the aim of separating iodine by precipitation from the sample. The detection is carried out in a NaI(Tl) scintillator counter.

The urine samples analysis frequency for the iodine-131 is twice a month or 25 analysis per person per year.It was assumed that the worker exposure to radiation is continuous during the work period and that the worker always has collected 25 urine samples per year although there may be some missing. In this case the values in the Table I are always the medium value over 25 analyses per person per year.

The external monitoring is perfomed by film badge. The measurement frequency is once a month or 12 per year.

3. RESULTS AND DISCUSSION

3.1 Urine Sampling

The Table I shows the results of Iodine-131 internal contamination monitoring by urinalysis measurements. From 1984 to 1993, 304 persons were monitored, giving a medium value of 30.4 persons per year. The reference levels, recording, investigation and intervention are annual and they are based on the ALI value for ^{131}I and taking into account 25 urinalysis per year. These reference levels were calculated considering the limit for deterministic effects on the thyroid.

Table I - Result of Urinalysis - Distribution of Internal Contamination

^{131}I in urine (Bq/L) per year	year									
	1984	1985	1986	1987	1988	1989	1990	1991	1992	1993
Recording Level <150	18	21	13	22	17	23	8	19	12	25
151 - 450	6	4	6	10	9	8	2	7	5	5
451 - 1500	3	1	4	2	9	2	7	7	2	3
> 1500	1	1	3	0	1	0	15	2	1	0
Persons Monitored	28	27	26	34	36	33	32	35	20	33
Average Intake (Bq/L) per year	250.0	397.5	468.5	152.5	355.0	165.0	1866.0	1195.0	292.5	152.5

The Table II, shows the collective committed effective dose equivalent, considering the thyroid as deposition organ.and the ratio between the number of individual monitored and the effective dose equivalent ranges.

Table II - Collective Committed Effective Dose Equivalent and Annual Effective Dose Equivalent for Internal Exposure

Year	Collective dose person x mSv	Number of Workers		
		H_e=0	1.5<H_e<4.5 mSv	4.5<H_e<50 mSv
1984	47.00	18	6	4
1985	72.71	21	4	2
1986	83.14	13	6	7
1987	35.25	22	10	2
1988	86.90	17	9	10
1989	37.02	23	8	2
1990	406.08	8	2	22
1991	284.41	19	7	9
1992	39.78	12	5	3
1993	34.22	25	5	3

From the Table II it can be seen that there were 126 cases with effective dose equivalent above the recording level, that is 1.5 mSv/y and 64 cases above the investigation level, that is 4.5 mSv/y.

The results show that 58% of the persons monitored had an effective dose equivalent lower than the recording level and therefore considered without internal exposure.

3.2 External Exposure

The Table III presents the results of external exposure monitoring for the same exposure period considered in the urinalysis samples. From 1984 to 1993, 451 persons were monitored, giving a medium value of 45.1 persons per year. The Table III shows that there are 103 cases with whole body external exposure above the recording level, that is 5 mSv/y and 32 cases above the investigation level, That is 15 mSv/y.

Table III - External Radiation Exposure - Whole Body

Annual Equivalent Dose mSv/y	year									
	1984	1985	1986	1987	1988	1989	1990	1991	1992	1993
Recording Level < 5	28	29	32	31	33	31	33	45	43	45
5 - 15	7	2	4	6	6	9	8	5	12	13
15.1 - 50	1	4	3	5	5	3	2	2	3	4
> 50	0	0	0	0	0	0	0	0	0	0
Number of Workers Monitored	34	35	39	42	43	43	43	52	58	62
Average Annual Dose (mSv/y)	4.24	4.15	4.49	4.79	5.37	5.15	4.05	3.80	4.83	5.00
Collective Dose (Person x mSv)	144.16	146.25	175.11	201.18	230.91	221.45	174.15	197.60	280.14	310.00

The results show that 89% of the persons monitored had a whole body external exposure lower than the recording level an therefore were considered without external exposure.

3.3 General Discussion

The table I shows that only a few persons has individual effective committed dose equivalent over 15 mSv/y and the Table III shows that the same occurs for external exposure. If it is considered the internal effective dose equivalent added to the external whole body dose equivalent for each individual worker no one exceeds the annual limit of 50 mSv for stochastic effects.

The Tables II and III show that both the internal and external annual collective effective dose equivalent are extremely low.

4. CONCLUSION

Internal exposure does not represent a problem on the individual committed effective dose equivalent in Radioisotope Production Facility for stochastics effects, however it is not negligible for the doses. The same, is not possible to state for the dose limits for deterministics effects in the thyroid organ.

The assessments presented in this paper demonstrate that the radiation protection mechanisms are adequate for the control of the employee exposure, considering the ICRP dose limit.

According to the results presented in Table I, in 1986 there was a dose peak.In That year the filters of the hot cells were replaced due deterioration, and the internal contamination level in 1987 became lower than 1986. In 1990 and 1991, appeared several problems in the hot cells. The safe containment, due deterioration by hard treatment that they are submitted presented failure and required maintenance. In 1992 the internal contamination level was higher than 1993 due to a small influence of the 1991 problems.

As final conclusion of this work, is possible to observe that with the increasing difficulty in the operations and in the activity level, it is more important to improve the intrinsic containment safety, instead of providing radiation protection control equipment.

5. REFERENCES

Limits for Intakes of Radionuclides by Workes. International Commission on Radiological Protection - Publication 30, 1979.

Recommendations of the International Commission on Radiological Protection - Publication 26, 1977.

Duarte, C. L; Gaburo, J. C; Rangel, E.P. Interpretação dos Dados de Análises de Iodo 131 na Urina segundo o ICRP - 35 - São Paulo, Instituto de Pesquisas Energéticas e Nucleares, 1988 - Publicação IPEN 213.

VERIFICATION OF RADIONUCLIDE CALIBRATORS USED IN NUCLEAR MEDICINE LABORATORIES IN THE CZECH AND SLOVAK REPUBLICS

J. Suran, P. Jasanovsky, and P. Dryak
Czech Metrological Institute
Inspectorate for Ionizing Radiation
Prague
Czech Republic

1. Introduction

In order to obtain a reliable diagnostic statement or to carry out an efficient therapy while keeping the unnecessary exposure of the human body as low as possible the precise activity determination of the applied preparation is necessary. The Czech Metrological Act requires regular annual check of devices measuring the activity of the diagnostic and therapeutic preparations applied to patients "in vivo". This control is performed by the Inspectorate for Ionizing Radiation (IIR) which belongs to the Czech Metrological Institute (CMI).

In the Czech and Slovak republics there are 57 nuclear medicine and therapy units using seven types of radionuclide calibrators produced in the USA: Nuclear Chicago, Picker Corporation, Victoreen, Germany: PTW Freiburg, Robotron, and Czechoslovakia: Tesla (tab. 1) and 17 radionuclides (tab. 2) in different measuring containers (tab. 3). Tab. 4 lists radionuclides used for tests of the stability of the calibrators. This paper presents results of checking their calibration constants for mostly used radionuclides 131-I and 99m-Tc.

2. Methodology

The radionuclide calibrators are usually based on an ionization chamber with a well for positioning of a container with radioactive material. Their check consists in the measurement of the activity of the reference source supplied by the IIR. These measurements were done by the users according to their methodology. The radionuclide calibrator complies the criterion of acceptance if the relative difference of its reading from the reference activity is less than 10 %.

The reference source 131-I was a solution with stabilizing chemicals free of any radioactive impurities emitting gamma radiation. From five to eight grams of this solution was precisely weighted in a "penicillin vial". The reference source activity was determined using the primary Czech standard of activity with the precision of 2 % (for the confidence level of 99 %). Because the values of commonly measured and applied activities are rather widely spread (see fig. 1), the average nominal reference source activity of 6-10 MBq has been chosen.

The use of 99m-Tc radionuclide as the reference source is not possible because it has in contrast to 131-I too short half-life. Thus the check was done by means of the comparator which is the selected radionuclide calibrator whose calibration is traceable to an absolute activity determination at the IIR. The activity of

99m-Tc equal to 100 MBq, used for calibration, was determined in the same manner as for 131-I, fig. 4. The Curiementor II was chosen as a comparator due to its frequent use and best results during the measurements with 131-I. The stability of the comparator was regularly checked by the 137-Cs source. The uncertainty of the 99m-Tc activity in a standard penicillin vial was 3.15 % for the confidence level of 99 %.

In every medical unit the 99m-Tc sample was obtained from the generator and measured in the penicillin vial by the radionuclide calibrator being checked as well as by the comparator. To estimate the additional uncertainty due to the use of different penicillin vials the activity measurement was repeated with the penicillin vial commonly used in the particular medical unit.

3. Results and discussion

The results of the "checking round" organized in 1992 with the 131-I reference source are shown in fig. 2. About 25 % of medical units were not equipped with any device complying the criterion of acceptance. The extreme relative deviations reached +33 % and -62 %. The use of devices with negative relative deviation is dangerous because it leads to overdoses of patients. These results are similar to results of first "checking rounds" carried out in Great Britain [1], Belgium [2] and Hungary [3].

From the survey of the results according to the device type as given in fig. 3 it follows that the lowest deviation is for the Curiementor II meters (PTW Freiburg), the highest for the NNG 601 meters (Tesla). The Tesla radionuclide calibrators exhibited a common technical defect: the poor tightness of the ionization chamber resulting in the decrease of the detection efficiency and therefore were excluded from use.

In 1993 the "checking round" orientated to the 99m-Tc activity determination was realized. In some cases when the radionuclide calibrator did not meet the acceptance criterion it was immediately recalibrated. Fig. 5 shows the relative deviations from the conventionally true value before and after recalibration. After the recalibration the maximum relative deviation did not exceed 5 %. Fig. 6 presents the results from all medical units. The 10 % acceptance criterion is not met for those radionuclide calibrators which were not recalibrated.

The influence of different penicillin vials on the detection efficiency of the 99m-Tc activity measured with the Curiementor II comparator is shown in fig. 7. The change of the relative detection efficiency is less than 2 % for majority of commonly used penicillin vials and even for atypical rarely used vials does not exceed 3 %. It can be therefore stated that with regard to the use of different penicillin vials by different medical units the precision of the 99m-Tc activity measurements with the comparator was better than 5 % for the 99 % confidence level.

From the survey of the radionuclide calibrators used in medical units during the first and second "checking rounds" one can see that the unreliable NNG Tesla radionuclide calibrators were replaced with the calibrators of other types (see fig. 8).

4. Conclusions

During two "checking rounds" the radionuclide calibrators of medical units were checked for two widely used radionuclides 131-I and 99m-Tc. The first "checking round" with a view to the activity of the 131-I radionuclide showed the necessity to exclude some radionuclide calibrators. The results of the second "checking round" justified this exclusion. Relative deviations of 99m-Tc activity from conventional true value met the 10 % acceptance criterion and after recalibration most of them were less than 5 %.

In both republics the supervision of the state metrological authority helped to the rapid improvement of the equipment of medical units and to the subsequent improvement of the precision of activity measurements for applications "in vivo".

References

1. Woods, M.J.: NPL Report RS(EXT)56; Intercomparison of 57Co and 125I in UK Hospitals 1980/81

2. Reher, D.D.G.; Merlo, P.: Eur. J. Nucl. Med. 17 (1990) 103-105; A Quality Control of Radionuclide Calibrators Among Belgium Hospitals

3. Szörényi, A., Vágvölgyi, J.: Int. J. Nucl. Biol. 10 (1983) 91-96; Experiences of the Metrological Supervision of Radionuclide Calibrators in Hungary

Tab 1: List of used types of measuring devices

Mark:	Type:	Manufacturer:	No. devic.
c	Curiementor	PTW Freiburg	19
m	Mediac Dose Calibrator	Nuclear Chicago	7
r	Robotron H27013	VEB Robotron (DDR)	15
n	NNG 601	Tesla Vráble	14
p	Isotope Calibrator	Picker Corporation	9
u	Corp-U-Call II	Victoreen	2
s	Scintillation probe with analyzer		1
Total number:			69

Tab. 2.
List of commonly measured radionuclides

nuclid:	n	%
99m-Tc	55	96,49
131-I	54	94,74
201-Tl	21	36,84
51-Cr	18	31,58
67-Ga	16	28,07
125-I	9	15,79
169-Yb	6	10,53
111-In	3	5,26
32-P	3	5,26
58-Co	3	5,26
113m-In	2	3,51
198-Au	2	3,51
59-Fe	2	3,51
99-Mo	2	3,51
133-Xe	1	1,75
57-Co	1	1,75
90-Y	1	1,75

n - number of laboratories
100% = 57 laboratories

Tab. 3
List of used vials

vial	n	%
ampoule	4	7,02
penicillin vials	55	96,49
syringes	40	70,18
other	5	8,77

n - number of laboratories
100% = 57 laboratories

Tab. 4:
Perceutage of devices equipped with calibration standard source

Type	n	%
none	11	15,9
137-Cs	39	56,5
226-Ra	17	24,6
57-Co	2	2,9

n - number of meas. devices

100% = 69 devices

Fig.1. Range of measured activities of 13

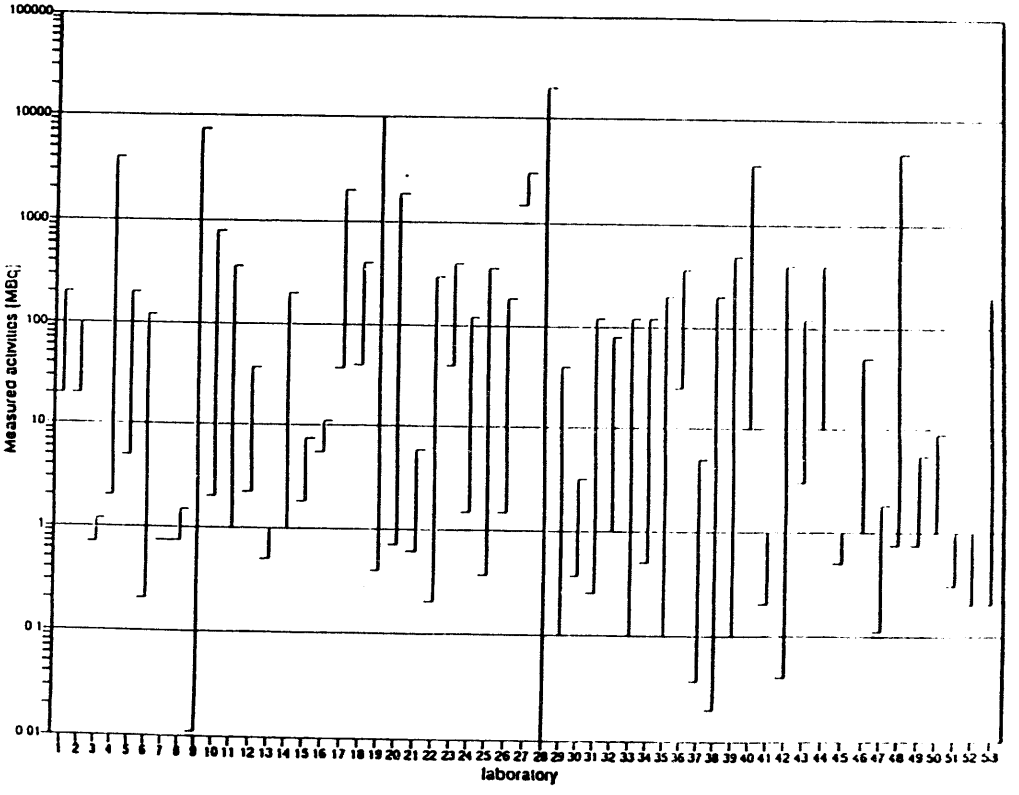


Fig.2. Penicilline vial measurement

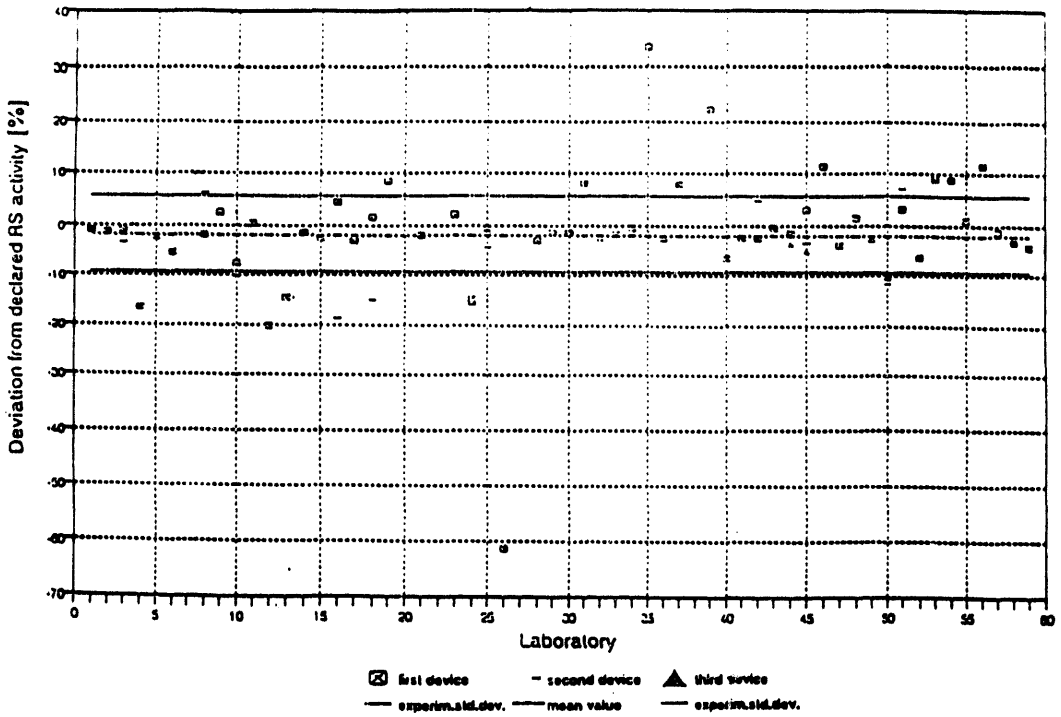
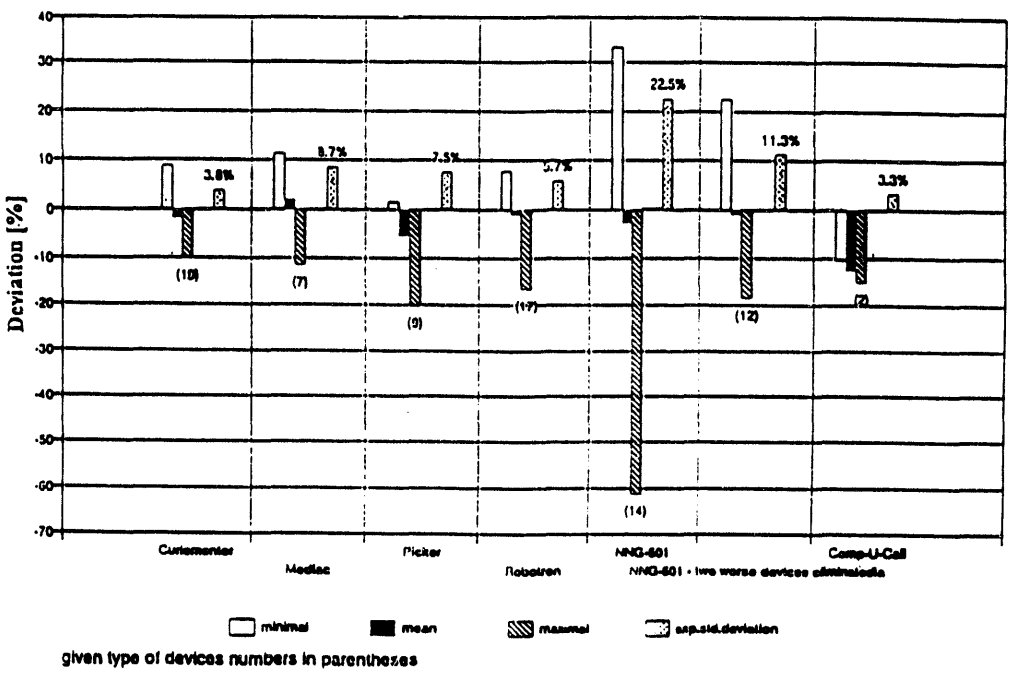


Fig.3. Deviations of individual types of devices



given type of devices numbers in parentheses

Fig.4. Range of measured activities of 99m-Tc

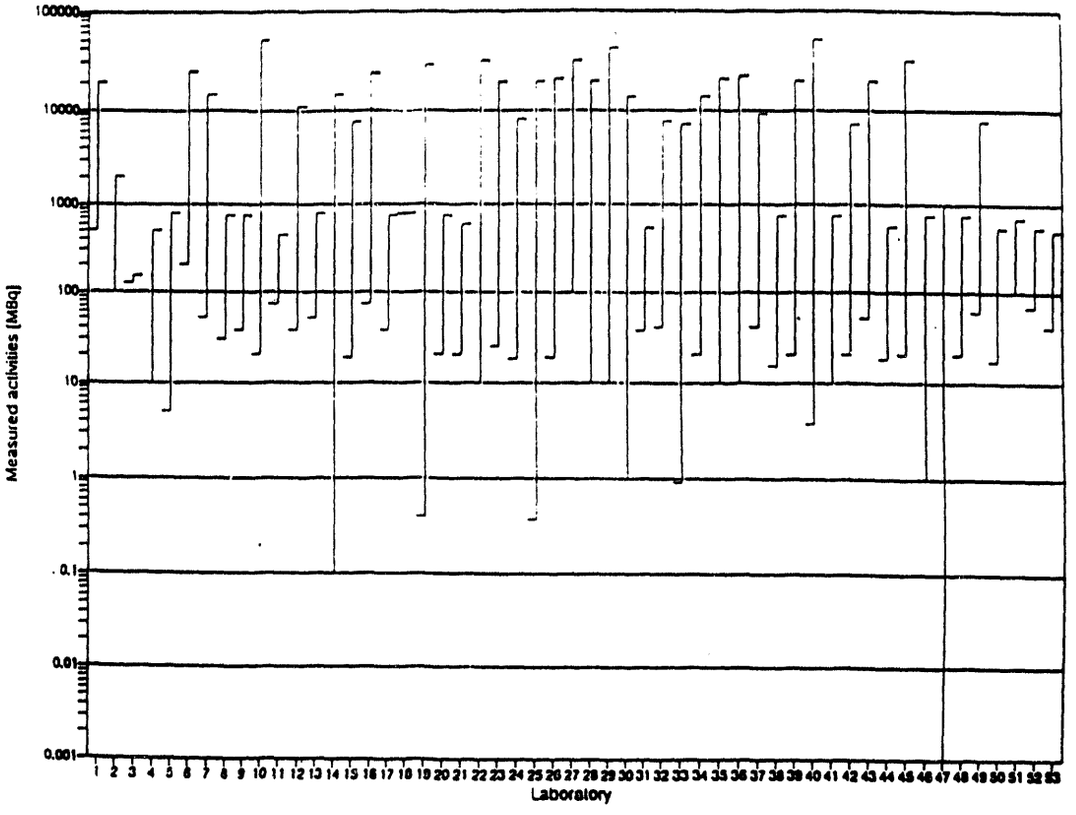


Fig.5. Comparison of deviations of recalibrated measuring devices (1993)

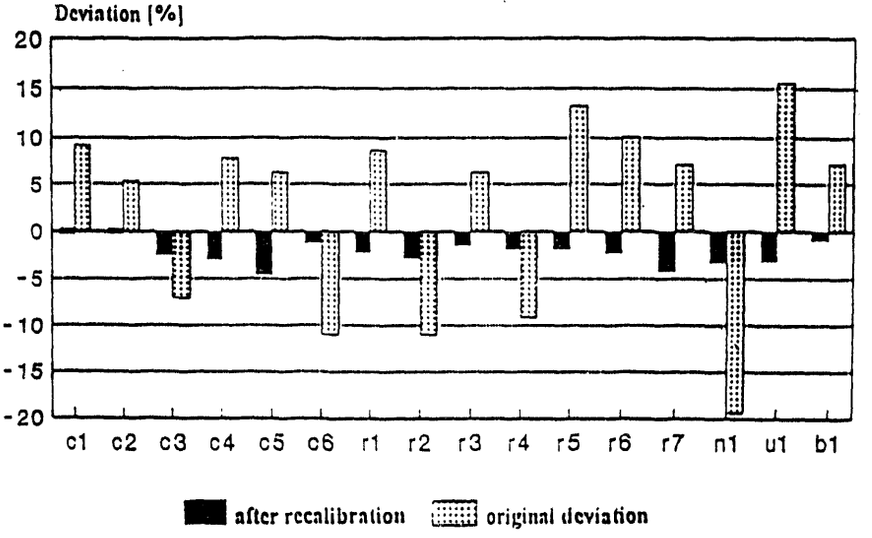


Fig.6. Evaluation of Tc - 99m

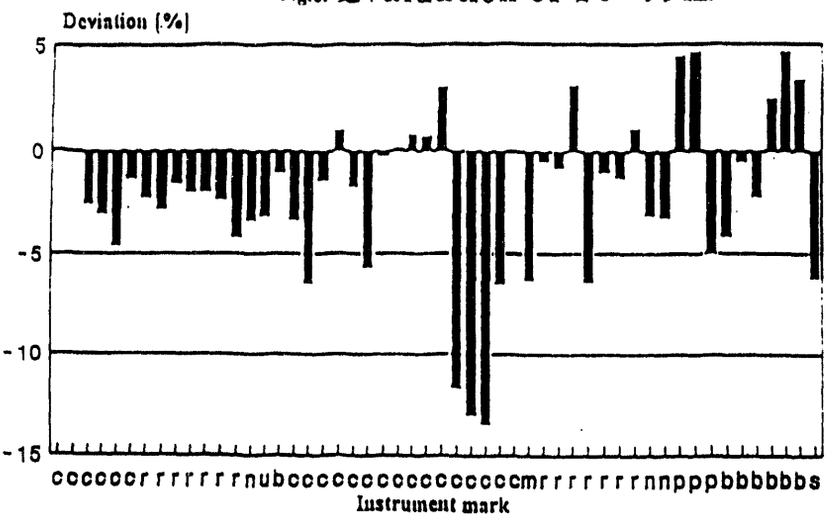


Fig.7. Comparison of the relative efficiency of comparator for various types standard penicilline vials

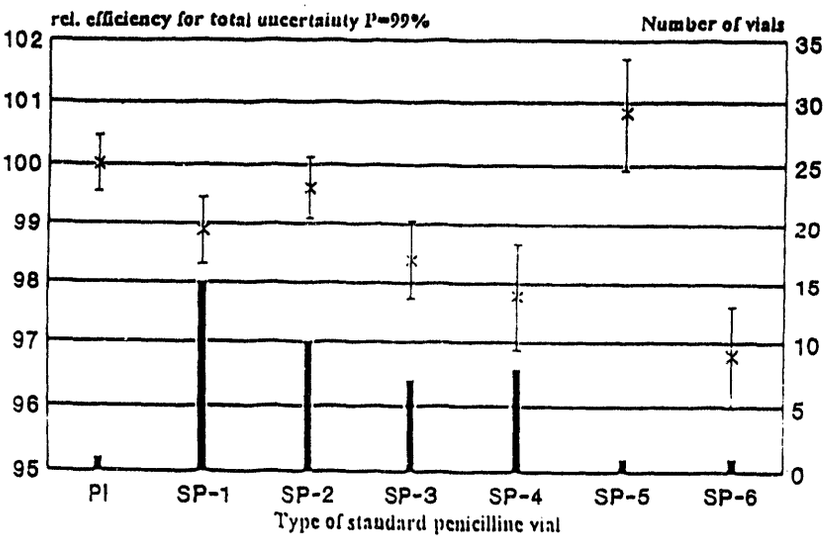
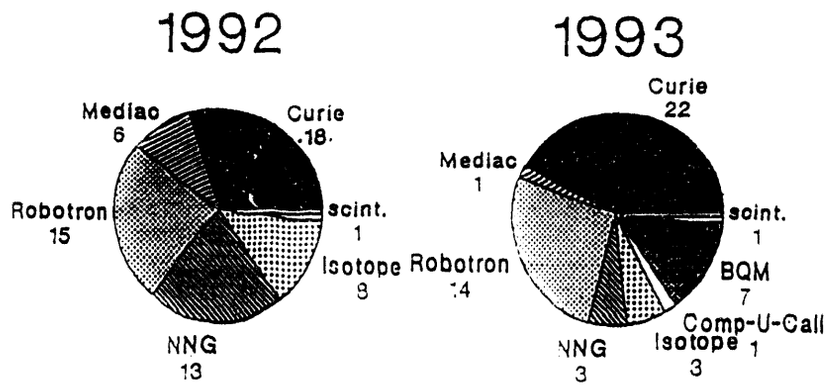


Fig.8. Change in device equipment



CALIBRATION OF CLINICAL DOSEMETERS IN THE IAEA WATER PHANTOM

Linda V.E. Caldas and Maria P.P. Albuquerque (Instituto de Pesquisas Energéticas e Nucleares-CNEN/SP Caixa Postal 11049 - CEP 05422-970 - São Paulo, SP, BRAZIL)

The procedures recommended by the IAEA Code of Practice were applied at the Calibration Laboratory of São Paulo in order to provide in the future the clinical dosemeters users with absorbed dose to water calibration factors for ^{60}Co radiation beams. In this work the clinical dosemeters were calibrated free in air and in water, and the results were compared, using conversion factors. The secondary standard dosemeter consists of an ionization chamber (NE model 2561), an electrometer (NE model 2560) and a radioactive check source (NE 2562). Its calibration factors are given in terms of exposure in air (NPL). This system participates annually of the national intercomparisons organized by the Brazilian Secondary Standard Dosimetry Laboratory (SSDL Rio de Janeiro). The experiments were all performed in ^{60}Co radiation beams (12 TBq) and the substitution technique was applied. The several tested clinical dosemeters of different manufacturers and models belong to the laboratory and to hospitals. For the measurements in water the IAEA cubic water phantom was used. The dosemeters were all calibrated free in air in terms of air kerma, and the calibration factors in terms of absorbed dose to water were obtained through conversion factors. The same dosemeters were also calibrated into the water phantom. Good agreement was found between the two methods; the differences were always less than 0.5%. The data obtained during this work show that when the dosemeters are used only in ^{60}Co radiation and the users apply in the hospital routine work the IAEA Code of Practice, the calibration can be performed directly in the water phantom. This procedure provides the useful calibration factors in terms of absorbed dose to water.

Work partially supported by CNPq - Conselho Nacional de Desenvolvimento Científico e Tecnológico, Brazil

CUTANEOUS MITOCHONDRIAL PROTECTION BY TOPICAL TREATMENT OF HERBAL ANTIOXIDANTS FOLLOWING 60 CO-GAMMA IRRADIATION

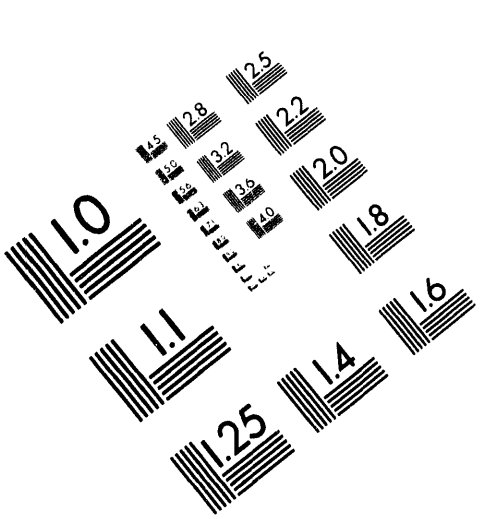
Faramarz Ashoori (Department of Plastic and Reconstructive Surgery), Rei Takahashi, Jain Zhou, Taketoshi Sugiyama (Department of Pathology of Kyoto University School of Medicine, Kyoto), and Ikuo Nishigaki (Institute of Applied Biochemistry, Mitake, Gifts, Japan)

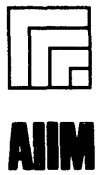
Some of herbal antioxidants have been used in traditional medicine and even for protection against sun light since long ago. We have already reported suppression of lipid peroxidation (LP) by different herbal antioxidants in in-vivo models.

To find out the effective dose to elevate the cutaneous LP at optimal level, gamma irradiation of cutaneous microsomal fraction was performed at different doses and 200 Gy was chosen. Microsomal gamma irradiation was done in the absence (control) and in the presence (test groups) of either ferulic acid, alpha-tocopherol, gallic acid, chlorogenic acid, curcumin and ellagic acid (with different structure and number of hydroxyl group which is important in free radical trapping) at different doses. Ellagic acid and curcumin at I-50 (50% inhibition of LP) doses of 10 and 20 μM, respectively, showed most strongest antioxidant effect. Therefore, they were chosen for in-vivo experiment.

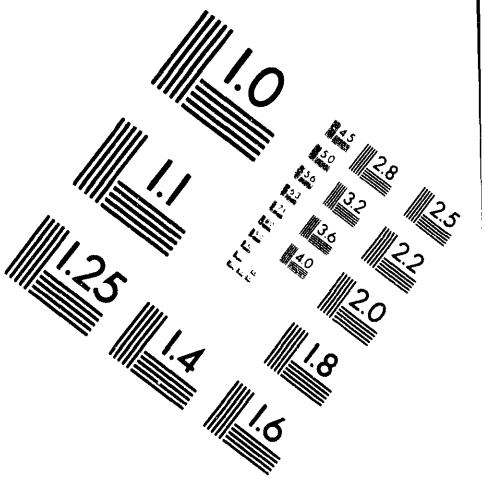
For in-vivo experiment, twice the I-50 doses of ellagic acid and curcumin were applied topically (separately) on the back skin of rats, three times a day for three days. On the fourth day, after one more application of antioxidants, gamma irradiation was done on the rats at 1, 5 and 15 Gy. 12 h after irradiation, mitochondrial fraction of the back skin which had already been treated by antioxidants were prepared. Mitochondrial fractions of unirradiated (control) and irradiated (test groups) were incubated in the presence and absence of succinate and were subjected to LP by $FeCl_3$. Mitochondrial lipid peroxide levels of unirradiated rats were significantly suppressed by succinate in antioxinat-treated rats (most) and antioxidant-untreated rats (less). In irradiated groups, succinate failed to suppress LP in antioxidant- untreated rats, dose (irradiation) dependently. Among irradiated groups which were treated by antioxidants, succinate remarkably suppressed LP. Both antioxidants acted equally, but because of lower dose of ellagic acid, it was more potential.

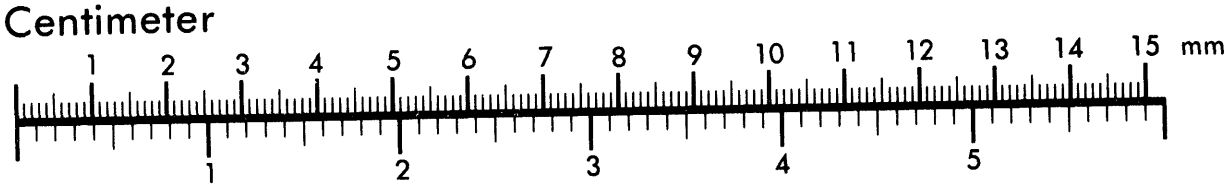
The present findings indicate that the failure of succinate in suppression of mitochondrial LP of irradiated rats might be due to diminishing of mitochondrial antioxidants which had been reduced by free radicals (generated by irradiation), since succinate suppressed mitochondrial LP in antioxidant-treated rats. From these points of view, topical application of either curcumin or ellagic acid could be beneficial in prevention of radiation skin ulcer.

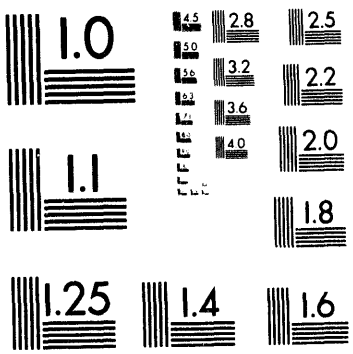


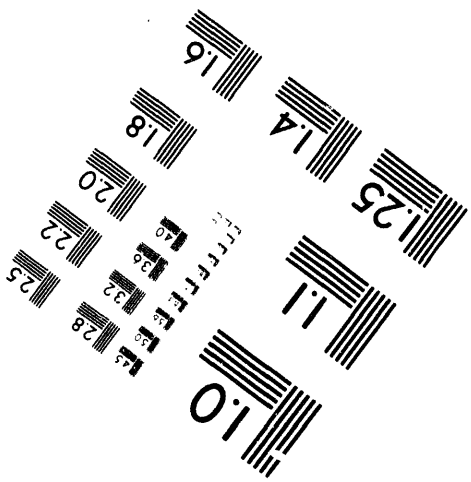


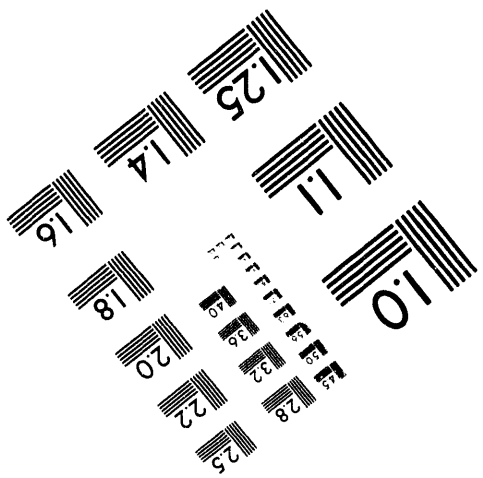
Association for Information and Image Management
1100 Wayne Avenue, Suite 1100
Silver Spring, Maryland 20910
301/587-8202











MANUFACTURED TO AIIM STANDARDS
BY APPLIED IMAGE, INC.

6 of 6

DOSIMETRY OF ELECTRON AND GAMMA RADIATION WITH DL-ALANINE

Zelia M. Costa and Leticia L. Campos (Instituto de Pesquisas Energeticas e Nucleares - CNEN/SP, Caixa Postal 11049 - CEP 05422 - 907 -Sao Paulo, SP - BRAZIL)

Alanine is a simple aminoacid, on irradiation at room temperature, predominantly free paramagnetic radicals of the type CH_3-CH-COOH are produced, which can be measured quantitatively using ESR. This paper reports the aplication of powder DL-alanine/ESR dosemeter for measurement of the absorbed dose of ^{60}Co gamma rays and electron beams. The sample preparation details are described, as well as the analysis of the ESR signal to dose, the energy response, the influence of dose rate and effect of the amibient conditions on the fading of the ESR signal. The irradiations were performed using a panoramic ^{60}Co gamma ray source and electrons emitted from an accelerator for industrial purposes. The ESR spectra was measured at room temperature using JES-ME-3X ESR spectrometer with cylindrical TE_{011} mode cavity (Jeol) operating at a frequency of 9400 MHz (X). The ESR spectra was recorded as the first derivative of the paramagnetic absorption spectra where the response of the alanine was expressed as the maximum peak to peak amplitude of the ESR spectra and measurements taken at differenct days were normalized using a Mn^{2+} reference sample. The same signal-dose relationship was obtained for both gamma rays (1.25 MeV) and electron beams (1.14MeV) and no dependence of the response on dose rate has been found in the range from 0.21 to 1.16 kGy/h. In the dose range of 10^2 to 10^5 Gy, the dose response showed a linear relationship and the precision was less than 2%. The obtained results give useful information on the care necessary to obtain the needed overall accuracy in the determination of absorbed does.

Work partially supported by CNPq - Conselho Nacional de Desenvolvimento Científico e Tecnológico, Brazil

SENSITIVITY IMPROVEMENT OF FRICKE DOSIMETER FOR 14 MeV NEUTRONS

N.NAGESH, G.R.PANSARE AND V.N.BHORASKAR

DEPARTMENT OF PHYSICS,

UNIVERSITY OF POONA

PUNE - 411007

INDIA

1. INTRODUCTION :-

Considerable work has been carried out and reported in literature on measurement of dose rate and absorbed dose measurement for thermal and slow neutrons[1]. However, very little work has been carried out in the feild of fast neutron dosimetry.

For several applications, it may be neccesary to know the neutron dose in terms of the energy deposited in a medium. Neutron flux monitors have been developed for fast neutrons, which provide information in terms of neutrons incident on the detectors, but in several cases it is difficult to distinguish fast neutron flux from that of the low energy neutrons.

In this paper , measurements of 14 MeV neutron dose using improved Fricke dosimeter system are reported. The Ferrous Sulphate dosimetry, known as Fricke dosimeter, developed by Fricke and Morse[2-4] was used for determination of dose rate and flux of the 14 MeV neutrons produced through $^{3}H(d,n)^{4}He$ reaction. Fricke dosimeter technique has gained universal importance for work in radiation physics that involves x-ray, γ-ray or any other energetic particles. However, for the fast neutrons, this technique is yet to be fully developed. Though for 14 MeV neutrons, many investigators have evaluated $G(Fe^{3+})$ values for ferrous sulphate dosimeter, in the present work,an attempt has been made to increase the G-value and in effect to improve the sensitivity for measurement of the dose for 14 MeV neutrons .

2. EXPERIMENTAL AND MEASUREMENTS

(i) OF THE METHOD :-

In ferrous sulphate dosimeter, most of the energy of 14 MeV neutrons (about 60-70%) is transferred via scattering of the neutrons and the rest of the energy is deposited via various radiation, such as γ and β rays produced through the nuclear reactions. The details of these processes can be found in the literature[1,5]. In the present work the system is modified by putting thin graphite plates in the container such that their planes are perpendicular to the incident neutrons. On interaction of the 14 MeV neutrons with the carbon nuclei , α-particles are produced through the $^{12}C(n,n')3\alpha$ reaction .The α-particles being highly ionising, the number of ferric ions(Fe^{3+})formed increases with the neutron fluence. The Carbon plate thickness is 0.2mm and therefore the α- particles produced on both the sides of the carbon plate are used in the formation of the Fe^{3+} ions. The absorbed dose is calculated from the following standard expression.

$$D_{rad} = 9.65 \times 10^{6} \frac{\Delta (O.D)}{G(Fe^{3+}) \rho d \Delta\varepsilon}$$

where d is the optical path length, 1 cm, $\Delta\varepsilon$ is the molar extinction coeficient, 2204 moles/cm, ρ is the density of fricke solution, 1.024 gm/cm^3, $G(Fe^{3+})$ is the yield of ferric ions per 100 eV absorbed energy ,8.9 $\pm$ 0.6 and Δ(O.D) is the change in the optical density of fricke solution at 304 nm. In this chemical analysis, the amount of light absorbed is measured with the help of a spectrophotometry. The Lambert-Beer law[6],which gives a relation between the light

absorbed and the concentration in terms of the optical density is used to estimate dose of the 14 MeV neutrons .

(ii) MEASUREMENTS:-

The fricke solution is prepared from analytical grade chemicals and triply distilled water. As the solution oxidises slowly with external stray radiation, each time a fresh solution was prepared and used. This has also helped to confirm the repeatability and reproducability of the measurements.

The solution, after shaking vigourously to saturate with air, was transferred into a small aluminium container, having internal dimensions of 20mm X 20mm X 20mm. The top side was kept open and in one of the vertical walls of the container, a circular hole of 15 cm diameter was made and closed with a thin mylar. This hole acted as a a window for the neutron entry. Four graphite plates each of thickness 0.5mm and dimension 20mm X 20mm were dipped vertically into the solution and fixed in the container such that separation between the two neighbouring plates was ~ 3mm. This assembly was exposed to 14 MeV neutrons through the mylar window one centimeter away from the Tritium target. The mylar window helped to minimise interaction of the neutrons with aluminium.The α-particles emitted from the graphite strips interact with the fricke solution and therefore the change in the optical density is found to be more as compared to the solution irradiated without graphite plates. Each time a fresh solution was irradiated by keeping a constant value of the neutron flux, but the time of irradiation was varied in the range five to sixty minutes. Simultaneously,neutron flux was measured irradiating a pure (99.9%) aluminium foil and the activity of the Na^{24} (1.369 MeV) produced

through $^{27}Al(n,\alpha)Na^{24}$ reaction was measured .

Optical density of the irradiated solution was measured using a spectrophotometer (Hitachi-330).The measuring setup consisted of two quartz cells each of dimension 10mm X 10mm X 40mm . In one of the cells, for reference,unirradiated solution was kept, while the other cell was filled with the irradiated solution. The wavelength of the incident light was changed from 200nm to 400nm. The optical density was noted at 304nm at room temperature, because of comparatively higher absorbance for ferric ions and least sensitivity for the impurities.

3.. RESULTS AND DISCUSSION

Figures 1 and 2 show the absorption spectra of the ferrous sulphate solution exposed to 14 MeV neutrons without and with graphite plates dipped in the chemical solution . Change in the optical density of the solution noted at 304nm for different irradiation period in the range 5-60 minutes is shown in figure 3. During this period deuterium current maintained was~ 100μA, and the neutron flux was constantly monitored by a 14 MeV neutron detector.

At a constant neutron flux of 3.3 X $10^6 n/cm^2$-sec, the estimated dose rate of 14 MeV neutron was ~ 18 rad per minute in the absence of graphite plates in the solution. Later on the value of $G(Fe^{3+})$was estimated for the system in which the graphite plates were immersed in the solution. The corresponding dose rate was maintained as per the previous value by monitoring the neutron flux..On measuring the optical densities of the irradiated solution , the value of $G(Fe^{3+})$ factor by was found to be 10.9 ± 0.3, as against the $G(Fe^{3+})$ value of 8.9 ± 0.6 which is normally used in the

conventional system. This increase in the G value amounts to enhancement in the sensitivity by 22.5%.This has been acheived due to the α-particles produced in the $^{12}C(n,n')3\alpha$ reaction having Q-value equal to -7.28MeV and cross-section of the reaction 17Ømb. Using this reaction, one gets an advantage that neutrons of energies below 7MeV do not make anychange in the sensitivity of the experiment. The improved G value 1Ø.9±Ø.3 was calculated and compared with that obtained with the conventional solution, which is 8.9± Ø.6.

These results indicate that the sensitivity and accuracy of the dose measurements of 14 MeV neutrons have been improved by increasing the $G(Fe^{3+})$ value.

REFERENCES

1. K.Mahesh and D.R.Vij , Techniques of Radiation Dosimetry, Wiley Eastern Ltd.(1985), New Delhi.
2. H.Fricke and S.Morse - American Journal of Roentgenol and Radium Therapy, 18 ,426,(1927).
3. H.Fricke and S.Morse - American Journal of Rontgenol and Radium Therapy ,18,43Ø,(1927).
4. H. Fricke and S.Morse - Phil. Mag. and S. of Science, 7, 129,(1927).
5. H.Fricke and E.J. Hart, Radiation Dosimetry (Edns. F.H. Attix. and W.C. Roesch) Vol.II., Academic press, New York (1966).
6. A. Farhat and P.J. Dyne -A. Practical course in Radiation Chemistry, Atomic Energy centre, Lahore, Pakistan (1963).

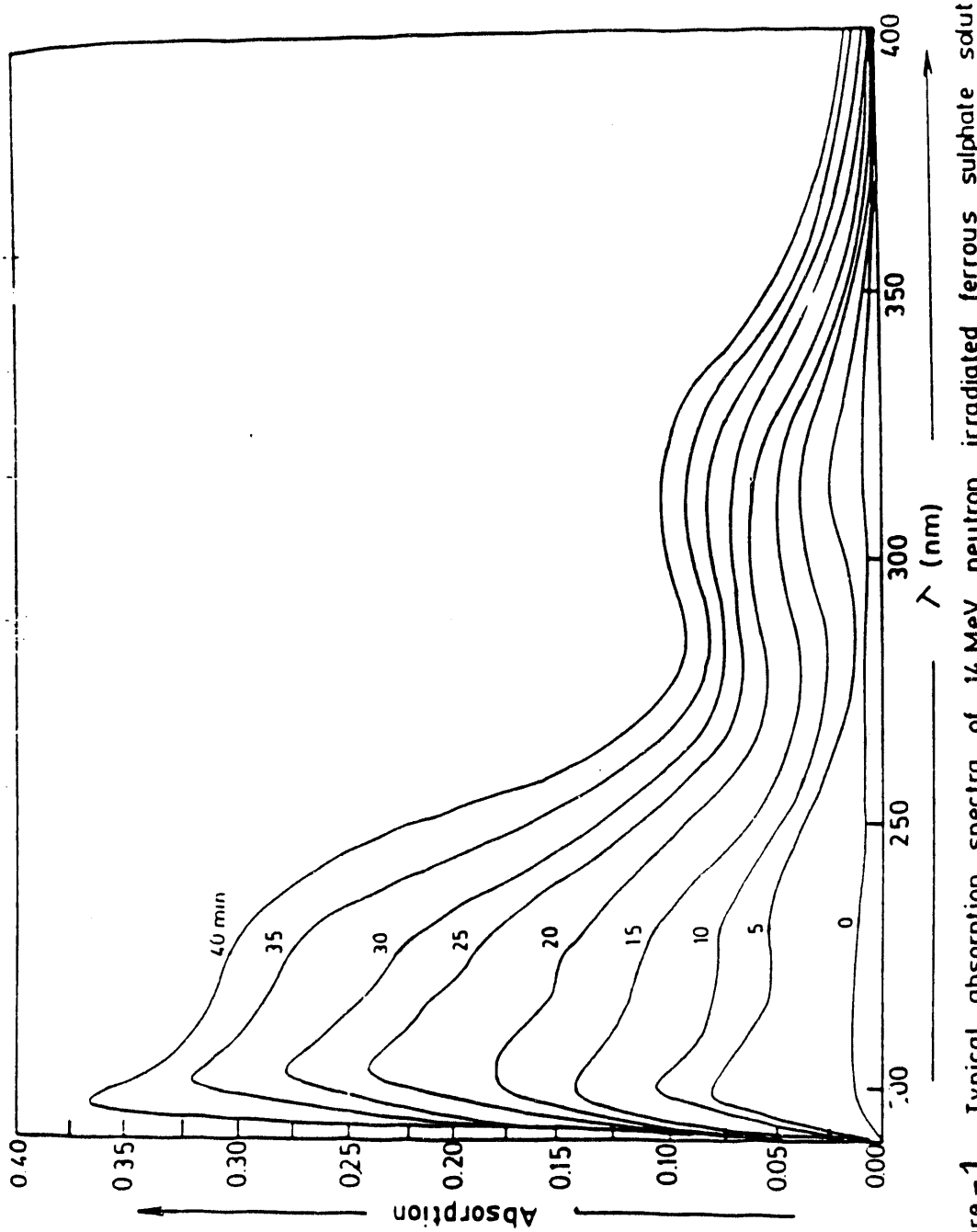


Figure-1 Typical absorption spectra of 14 MeV neutron irradiated ferrous sulphate solution without graphite plates dipped in the solution.

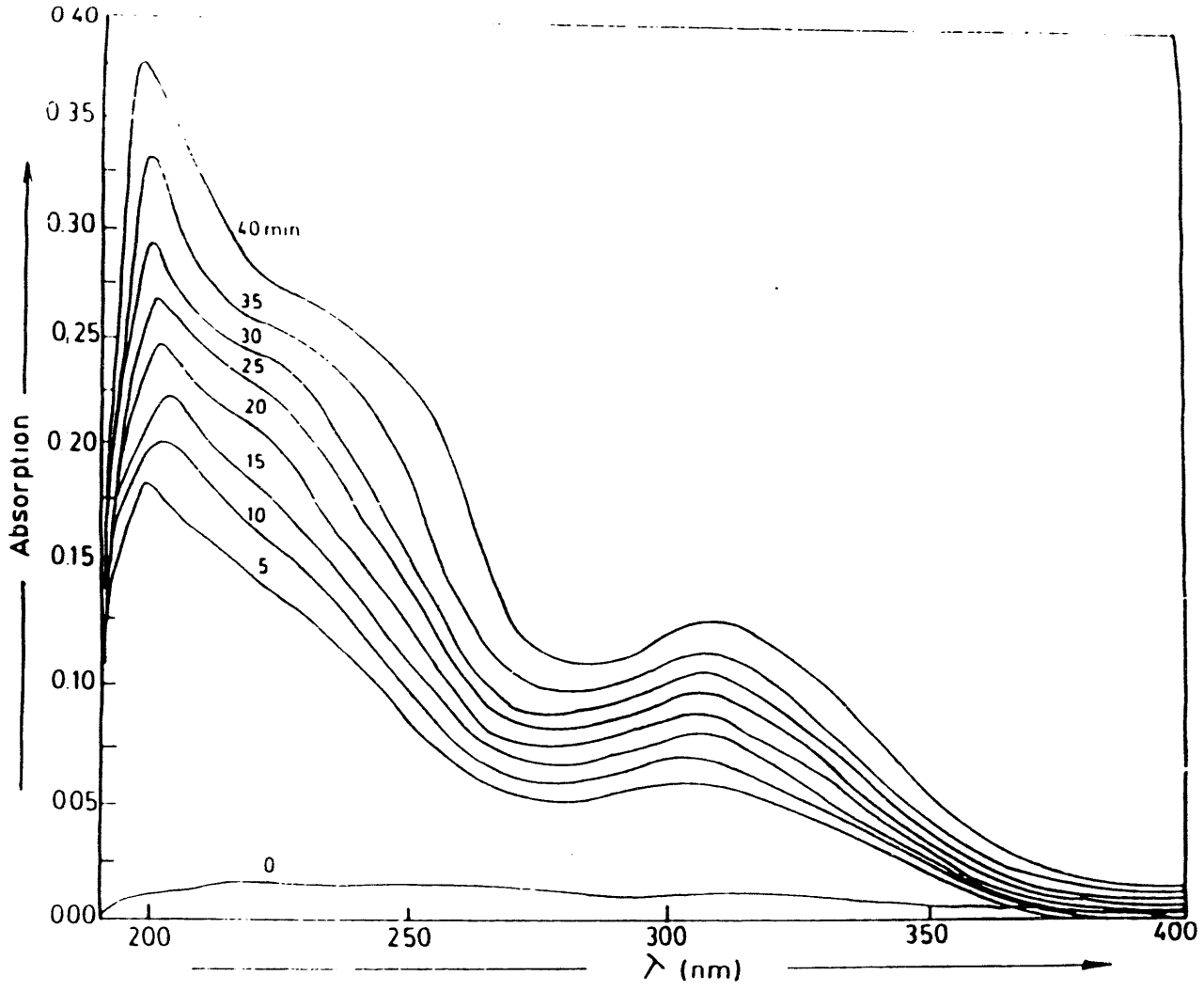


Figure – 2 Typical absorption spectra of the 14MeV neutron irradiated ferrous sulphate solution with graphite plates dipped in the solution.

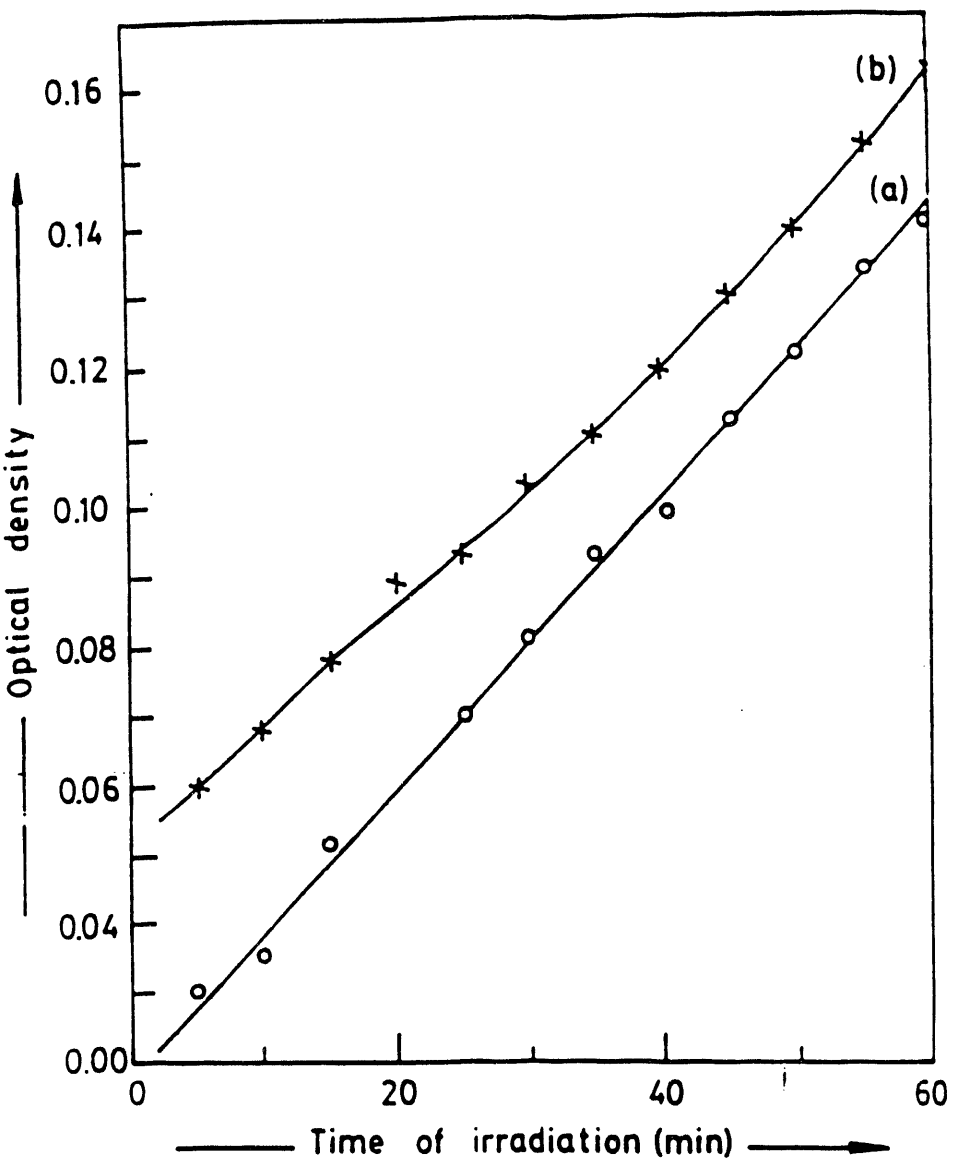


Figure-3 Variations in optical density of the ferrous sulphate solution with time of 14 MeV neutron irradiation. (a) without graphite plates, (b) with graphite plates dipped in the solution.

THE LOS ALAMOS NATIONAL LABORATORY NUCLEAR ACCIDENT DOSIMETER: OVERVIEW AND RECENT DEVELOPMENTS

T.E. Buhl, W.H. Casson, J.M. Hoffman, D.L. Upp, L.L. Romero and D.G. Vasilik (Los Alamos National Laboratory, Los Alamos, NM 87545)

The design and operation of the nuclear accident dosimeter (NAD) now being used at Los Alamos National Laboratory (LANL) will be described. The presentation will include an overview of the dosimeter and its components, a description of the methods used to analyze each dosimeter foil, and a discussion of the procedure determining the radiation dose based on the dosimeter results. A userfriendly computer program has been developed to calculate the absorbed dose using this procedure. Recent and anticipated improvements in the dosimeter will be discussed.

Results of recent exposures of the NAD using LANL's Godiva IV and SHEBA II critical assemblies will be presented. LANL is planning continued use of these assemblies, and initiating a nuclear accident dosimeter intercomparison program.

A ROUTINE CHEMICAL DOSIMETRIC SYSTEM USING THE MODIFIED CERIC SULPHATE DOSIMETER

Lucy K. Yamanaka and Linda V.E.Caldas (Instituto de Pesquisas Energéticas e Nucleares-CNEN/SP Caixa Postal 11049 - CEP 05422-970 - Sao Paulo,SP,BRAZIL)

The radiolytic reduction of the Ce4+ in a 0.8N sulfuric acid was examined, with the objective of measuring large radiation doses. The ceric sulphate dosimeter was tested in the range from 1 to 20 kGy. The 0.01 M sodium oxalate solution was chosen instead of the arsenious oxide solution (used in the conventional method), in order to obtain a less expensive dosimetric system than that normally used for routine chemical dosimetry. The absorption spectrum of the Ce^{4+} solution presents an absoption peak at 370 nm (2.99×10^{-4}M); the obtained molar extinction coefficients of Ce^{4+} and Ce^{3+} were 5670 and 2.7 M^{-1} cm^{-1} respectively. The purpose of this work was to establish a simple, reliable and inexpensive routine chemical dosimetric system for high doses.

Work partially supported by CNPq - Conselho Nacional de Desenvolvimento Cientffico e Tecnolócaldgico, Brazil

A STUDY OF IRRADIATION-INDUCED DAMAGE IN α-QUARTZ

I.Kh. Abdukadyrova

Samples of crystalline synthetic quartz were exposed in a reactor to fast neutrons with a fluence ranging from 10^{18} to 10^{21} neutron/cm^2. They were wrapped in aluminum foil and quartzous ampules. The temperatures of the samples are estimated to have been about 60° C.

As a result of the high-doses fast neutron bombardment, monocrystalline α-quartz had transformed into the amorphous phase. This process of radiation damage of crystalline structure by optical, mechanical, and roentgenographic methods has been studied. The possibility of the utilization of the structurally sensitive properties of α-quartz in neutron-irradiation dosimetry was discovered.

The mechanical and optical properties of crystal quartz irradiated by neutrons are investigated. The influence of dose on the radiation expansion along and perpendicular to the C-axis and on the density, ρ, of samples is studied. A comparison is made with the properties of the samples before irradiation. Monotonous changes of $\Delta C/C_o(F)$, $\Delta a/ a_0$ (F), $\Delta \rho / \rho_o$ (F) functions were observed following the transition to a stable measurement result at high level exposures (10^{20} - 10^{21} neutron/cm^2).

On the basis of measurements of the refractive index change, dose dependence of $\Delta n/n_o(F)$ at 589 nm was determined. The dispersion curve, $n(\lambda)$, at λ = 365-628 nm folowing irradiation of the crystals with a dose of F = 10^{18} to 10^{21} neutron/cm^2 was studied. It has been found, that when F increases, the high-level radiation effect at 365 nm is obtained. In addition, at the intense levels of radiation, induced damage on the structure in α-quartz (for higher doses) and "crystal-amorphous stage" phase transitions, and increase in the defective (amorphized) regions is produced. The growth of halos shows a dependence on $T_h(F)$ in the diffractograms with an increase of exposure to the samples (F = 4 x 10^{19} - 3 x 10^{20} neutron/cm^2).

Based on this data, the method of high-dose dosimetry of neutrons by use of the parameters (ρ,a,T_h) in α-quartz was suggested.

HERMETIC INPUTS OF POWER AND CONTROL CABLES FOR ATOM ENERGETICS

M. Muminov, M. Mukhamedzhanov, Kh.Nurmatov, Yu.Skripnikov (Institute of Nuclear Physics AS of Uzbekistan, Ulugbek 702132 Tashkent, Uzbekistan).
N.Kostyukov, N.Minakov. (Engineering Technologic Center AS of Russian, 675000 Blagoveshchensk, Russia).

This paper presents the results of testing of the inputs of the power an control cables destined for atomic electric power stations including the water-water type reactor. Several ceramics and metals were used as construction materials for being radiation hard and thermal stable till temperatures - 10000 °C and excecluding any inflammable and thermally unstable polymers and other composites. Radiation testing of the inputs was conducted under the regimes of "small" and "great" damage (break-down) having the following parameters:

parameters	"small" damage	"great" damage
Temperature, C	till 90	till 150
Pressure, MPa	0.118	0.5
Humidity	steam-air mixture	steam-air mixture
Specific active Cu/l	$1.5\ 10^{-4}$	2.5
Absorbed dose power Rad/hr	10^2	10^5
Period of a damage regime hour	5	10
Period between the regime	1 per 2 years	1 per total exploating period
Temperature after the damage, C	till 60	till 60
Pressure after the damage, MPa	0.05 - 0.12	0.05 - 0.12

During the tests the total radiation dose of $5x10^8$ R is simulated over the total expoating period (40 years) accounting for probable damages. The testing of the hermetic inputs were carried out in a special chamber invented for this purpose with a ^{60}Co gamma-source inside at the Institute of Nuclear Physics (Tashkent, Uzbekistan). The results of the testing have shown that these hermetic drivings based on metal-ceramic conjunctions maintains its working abilities after simultaneous influence of external factors having the characteristics listed in the table above. In conclusion one should note, that the modeled facility imitating the damage regimes, the probability of which is provided for the atom reactor processing, allows testing any constructions (diameter up to 300 mm and height up to 2000mm) for management, control and protection of the reactors of atomic electric power stations.

IONIZING RADIATION DOSIMETRY BASED ON OPTICAL PARAMETERS WIDTH MEASUREMENTS OF OXIDES

I.Kh. Abdukadyrova

This work is aimed at the investigation of the spectroscopic characteristics and the ^{60}Co γ-ray effects on oxides irradiated in a reactor. The purpose of this investigation is the determination of the growth kinetics of radiation damage, their stability, dependence on radiation dose, irradiation conditions and the possible use of oxides as a measurement of absorbed dose of neutron and photon emissions.

The glasses c-SiO_2 (types I and II) and $LiIO_3$ monocrystals were studied. The optical absorption spectra and RSL of the samples were measured before and after irradiatation. Absorption spectra of various glasses are measured in the ultra-violet region, the intensity change of UV-bands caused by gamma-radiation from 1Gy to 1 MGy was studied. The amount of the optical absorption change for the wavelength band at 300 nm in the irradiated samples caused by γ-rays is traced. In the range of 10^2 - 5 x 10^5 Gy for type II, the proportional growth of the bands intensity has been noted.

Such parameters as the influence of time storage (from 0.2 to 240 h), irradiation temperature (to 180°C) and exposure (to 450°C), dose power (from 20 to 3000 R/s), effects of the thickness of the sample on the measured parameter, and the possibility of the repeated use of the oxides was studied.

The optical absorption spectra of the $LiIO_3$crystals were measured in the region of 200-400 nm. The intensity change of the 340 and 640 nm peaks caused by γ-radiation in the range from 10 to 10^8 Gy was studied. The kinetics of these bands demonstrates the growth in the concentration of the coloring centers at 340 nm in the region of 1 x 10^3 + 3 x 10^5 Gy and 640 nm in the region 10^5 - 10^7 Gy.

A band at 608 cm^{-1}, connected with structure defects, was revealed by RLS spectroscopic methods near the fluence of 10^{17} $n.cm^{-2}$, which grows in intensity with fluence up to 3 x 10^{20} $n.cm^{-2}$.

Thermal and optical discoloring of the bands, used for revealing the nature of the guided centers, are studied. The possible use of these crystals and glasses in the dosimetry of neutron and gamma-radiation is suggested on the basis of a dosimetric characteristics analysis.

SESSION IX.
TLD Systems

C. Glenn Hudson,
Chairman

ANGULAR DEPENDENCE OF DOSE EQUIVALENT RESPONSE OF AN ALBEDO NEUTRON DOSIMETER

B. A. Torres (Georgetown University, Department of Radiation Science, Washington, DC), E. Boswell and R. B. Schwartz (National Institute of Standards and Technology, Gaithersburg, MD)

The American National Standards Institute (ANSI) provides procedures for testing the performance of dosimetry services. The ANSI Standard N13.11-1993 includes testing of processor performance of photon-irradiated dosimeters at nonperpendicular incidence. Although neutron dose equivalent angular response studies are not now mandated, future standards may well require that such studies be performed. Current studies with an albedo dosimeter will yield information regarding the angular dependence of dose equivalent response for this type of personnel dosimeter.

The personnel badges were mounted on the standard ANSI 40 x 40 x 15 cm phantom used for neutron calibrations. Irradiations were performed by aligning the long axis of the dosimeter vertically (vertical orientation) in the field and irradiating the dosimeters at angles from -90° to +90° in 10° or 20° increments with 0° being the angle of perpendicular incidenceto the front face of the phantom. The procedure was repeated with short axis aligned vertically (horizontal orientation).

Preliminary data for bare ^{252}Cf fluences show a marked decrease in dosimeter reading with increasing angle. The response decreased by an approximate factor of four from 0° to 80°. For the horizontal orientaion, the same response was noted from both positive and negative angles. However, for the vertical orientation, the response was assymetric. At the moment we have no explanation for this behavior.

We are also examining the response of the personnel badge in moderated ^{252}Cf fluences. Responses from the moderated and unmoderated ^{252}Cf fields and theoretical calculations of the neutron angular response will be compared. This information will assist in building a data base for future comparisons of neutron angular responses with other neutron albedo dosimeters and phantoms.

COMPARISON OF RESPONSES OF THERMOLUMINESCENT DOSEMETERS IRRADIATED BY SOFT X-RAYS AT VERY LOW AND VERY HIGH DOSE RATE LEVELS

M. Pietriková -Fárníková , J. Krása, L. Juha
Institute of Physics, Academy of Sciences of the Czech Republic
Na Slovance 2, 180 40 Praha 8, Czech Republic

Abstract: Recent great progress in construction and application of bright sources of soft X-rays gave a strong impetus for the development of methods of their dosimetric diagnostics. The soft X-ray sources are primarily represented by synchrotron radiation sources and by sources based on laser-produced plasma, including X-ray lasers. Their characteristics spread over a very wide region of photon energies, peak and average powers and densities. From our preliminary experiments it follows that thermoluminescent dosemeters can serve as a suitable tool for the determination of these characteristics. Problem lies in the fact that routine use of the thermoluminescent dosemeters for the dosimetry of soft X-rays requires their spectral calibration, which can be carried out with low peak power sources (synchrotron radiation and radionuclide sources). On the contrary, many important sources, especially these based on laser-produced plasmas, exhibit a very high peak power, i.e. dosemeters are irradiated at extremely high dose rate. In comparative experiments carried out with laser-produced plasmas and radionuclides using TLD 200 (CaF_2:Dy) and GR 200A (LiF:Mg,Cu,P) it was satisfactorily proven that total thermoluminescent signals are independent of the dose rate. Dependencies of glow curve shapes on the dose, dose rate and photon energy were equally determined.

During the last decade the intensity of studies on the interaction of soft X-rays (SXR) with matter has been rapidly growing. It was caused by an expanding development of the bright and accessible SXR sources as well as by specificity of the SXR interactions with condensed and gas systems and their consequences [1, 2].

SXR sources can be devided according to their peak power in two different groups. The first one includes sources with low peak power but relatively high average power and it is typically represented by synchrotron radiation sources. In the second one there are sources producing a high peak power but relatively low average power of SXR. Sources based on a laser-produced plasma typically represent this group. Current technical, applications motivated development of the both group of the sources focused on maximization of their average power and optimization (including the economical) of their operation causes convergence of sources power characteristics. This trend is in the first group represented by development of compact synchrotron radiation sources for microlithographical and biomedical applications [3] and in second group play the same role sources based on plasma generated on the surface of rotating target by focused radiation from high repetitive excimer [4,5] and frequency doubled neodymium [6,7] laser radiation. Though the differences in average power disappear, the peak power differences stay in a comparison to the first mentioned almost unchanged. It is connected with high difference between pulse repetition rate of these systems. Laser systems have repetition rate typically 10 - 100 Hz and synchrotron radiation sources can exhibit repetition rate higher than 100 MHz. A question of successful realization of accurate and versatile measurements of SXR fields characteristics over a very wide range of dose rate levels is still open. The problem lies in the fact, that low peak power sources (suitable radionuclides and monochromatized synchrotron radiation) are commonly used for a calibration of SXR detectors and results of these measurements are subsequently transferred to experiments occurring at a high peak power level.

SXR radiation takes an important role in contemporary radiation research which is motivated by its applications. Great progress has been achieved in the last decade in SXR microlithography [3-7], where the laser produced plasma sources are also used and so the accurate measurements of dose characteristics are needed. Single shot experiments play an important role in SXR microscopy of living organisms [8]. Cause of the exclusivity of high dose rate experiments lies here in the living cell mobility in medium which cannot affects its living functions. Using of long-term irradiation conditions requires an

immobile object. In this way the main advantage of SXR microscopy, i. e. a possibility of looking into a living cell, is lost. Current progress in the study of biological effects induced by SXR is an important and exciting part of SXR radiation research. Since the forties it is known that SXR shows an extremely high radiobiological effectiveness [9-10]. The main advantage of laser produced plasma SXR source lies here in the possibility of sample irradiation by single subnanosecond pulse, i.e. the possibility to record the image of an object in vivo moments before it is killed by the radiation overdose.

The above mentioned SXR application fields require accurate, absolutely calibrated methods for SXR dose measurement working in wide range of SXR field parameters, above all dose rate.

As SXR detectors various photodiodes are mainly used in experiments with laser-produced plasma. Their application is limited to the higher photon energies because of the relatively small thickness of their sensitive layer. The use of semiconductor photodiodes in a photoamperic mode of operation is limited by high photon flux with $\phi \sim 10^{12}$ photons/s into a diode area (DA) of ≈ 1 mm^2, because the saturation may be expected [11]. For the detection of SXR radiation from a nanosecond scale the limit falls to $\phi \sim 10^3$ photons/ns/DA. In a typical laser-plasma experiment, where line or continuum emission is detected some tens cm away from the plasma, the photon flux on the detector can reach 10^8 - 10^9 photons ns^{-1} mm^{-2}, e.g. [12]. This intense photon flux can be the cause of a non-linear response of the semiconductor detector. This effect should be amplified with decreasing photon energy because of the rapid decrease in the absorption length. Another effect which can negatively influence the diode response to the intense irradiation can be the fact that the diode time constant and the SXR pulse duration are comparable. In this case the separation of charge carriers produced by the intense SXR pulse could be longer than their generation which could result in a non-proportional diode response.

Thermoluminescent dosemeters (TLDs) generally used in personal, health and environmental dosimetry have been several times tested in a SXR region, too. Only few papers on the behaviour of TLDs irradiated by SXR have been published up to now. Horowitz and Kalef-Ezra [14] proved spectral sensitivity of TLD 100 for 4 keV radiation. For a detection of SXR emitted by high-temperature plasma TLD 200 [15], TLD 100 [16] and TL aluminium phosphate glasses [16] has been used. Dose dependence of TLD 100 resposes to 1.5 keV radiation was studied by Folkard et al. [17,18]. To our knowledge, no study of dose rate effects in TLDs irradiated by SXR has been published.

Our quest for dose rate dependence effects in TLD 200 and GR 200A irradiated by SXR was primarily carried out in the way described as follows. In each experiment one TLD 200 and one GR 200A were irradiated under the same condition either by SXR pulses from laser produced plasma (from low energy photons the crystals were shielded by 300 μm thick Be foils, mean photon energy transmitted is ~ 2-3 keV) or SXR from ^{55}Fe radionuclide preparate (photon energy is 5.99 keV). The plasma ($T_e \sim 300$ - 500 eV) was produced by focussing high power laser pulses ($E < 30$ J, $\tau \sim 1$ ns) on an 30 μm planar Al target. The attainable power density in the spot of ~ 100 μm in diameter was about 10^{14} Wcm^{-2} The doses were varied by changes of laser pulse energy and by exposure time under radionuclide. Each measured TLD 200 signal was correlated with corresponding signal of GR 200A. Results are presented in Fig. 1. We can see that correlation curves are identical for both the type of irradiation, i.e. for irradiation at low dose rate level (radionuclide)

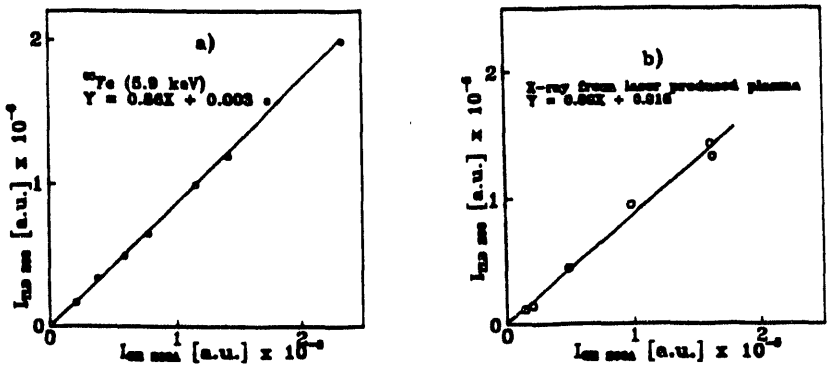


Fig. 1 Correlation of responses of TLD 200 and GR 200A to irradiation by the same doses of SXR from ^{55}Fe (a) and laser-produced plasma (b).

and very high dose rate level (laser-produced plasma). It indicates that dose rate effects could be in these dosimetric systems and under this irradiation condition negligible. We also looked for changes in the TLD 200 glow curve shapes caused by the dose rate. We found that the glow curve shapes depend on the photon energy of incident SXR. The thermoluminescence glow curves of TLD 200 were analyzed (from the six single peaks of TLD 200 glow curves only first three were distinguished at low photon energies) by us after the monocrystalic chips irradiation in the SXR range of 1 - 22.2 keV [19]. As SXR sources we used ^{109} Cd, ^{238}Pu, ^{55}Fe and high temperature dense plasma behind Be foils of a thickness 7.5 μm, 25 μm, 175 μm and 350 μm. Fig. 2 shows dependencies of the TLD 200 glow curve single peak height ratios P_1/P_3 and P_2/P_3 on photon energy. It is evident the dependencies are composed of two parts.

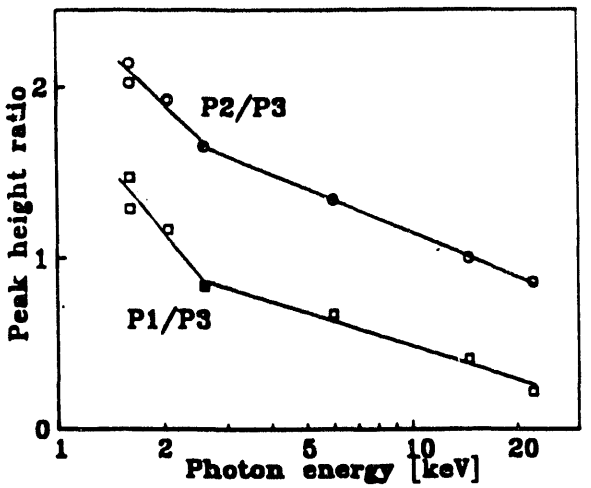


Fig. 2 Ratios of single peaks corresponding to $T_1 \cong$ 409 K, $T_2 \cong$ 437 K and $T_3 \cong$ 489 K in glow curves of TLD 200 irradiated by SXR as a function of photon energy.

At the lower photon energy region both the peak ratios decrease with increasing photon energy more rapidly than in the higher one. The break point is in both cases at about 2.6 keV. One of processes influencing the described changes in the single peak height ratios might be considered a high local dose caused by the very short absorption length which can be changed more than ten times in our conditions as a result of varying photon energy (Fig. 3). With decreasing photon energy the absorption length is decreasing and, therefore, a saturation of traps could be recognized as a result of the increasing local dose [20].

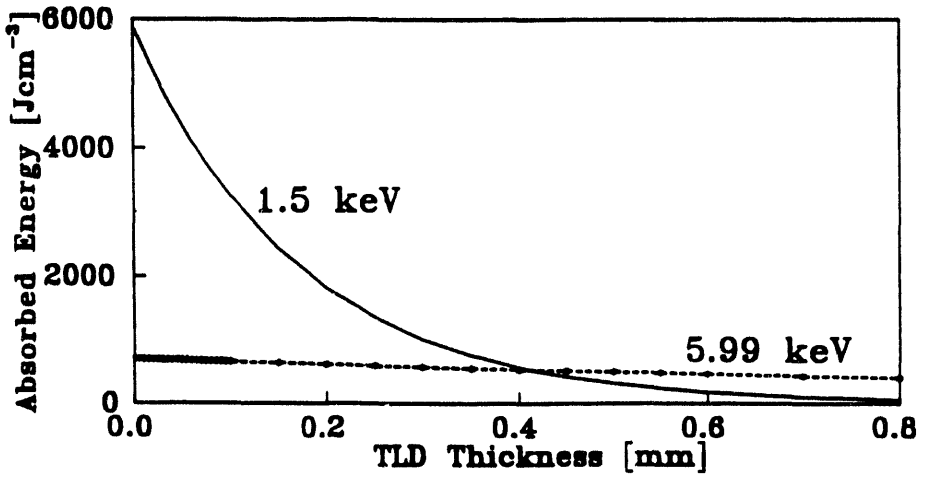


Fig. 3 Calculated absorption profiles of 1.5 keV and 5.99 keV SXR in CaF_2.

This "competing trap model" can be used for an elucidation of the increase in the ratios $P_{1,2}/P_3$ with decreasing photon energy. The "competition" of P_1 and P_2 is also observable but an increase of P_1 in comparison with P_2 is not so significant as it is in the former cases. The influence of the dose rate can be excluded because the photons of lower energies were emitted from the laser produced plasma with radiative power about twelve order higher than the one produced by the radionuclide sources used (the last three points from 5.99 to 22.2 keV). It would be useful to mention a selective enhancement of the SXR radiation absorption of photons with energies lower than 2.6 keV (the break point) by Dy having binding energies of M level electrons from 1.29 to 2.05 keV. A local high ionization density as a consequence of the Auger effect following the photoionization of Dy can play important role in the observed phenomenon. It can contribute to a nonlinear filling of the electron traps. A satisfactory interpretation of the observed break point, however, is not possible without applying an adequate computer model taking into account the mentioned effects. A simples explanation could lie in the dose effect. This possibility was tested by means of ^{55}Fe and laser-produced aluminium plasma shielded by 300 μm thick Be foil. In Fig. 4 it is shown that for both the irradiation conditions SXR glow curve shape does not depend on the dose (results of low dose rate irradiation are in the inset in Fig. 4). Comparison of the P_1/P_2 single peak ratios evaluated for TLD 200 chips irradiated by different doses of SXR from radionuclide and from laser-produced plasma is given in Fig. 5. We can say that the ratio is dose independent and there is no difference between chips irradiated at the low (radionuclide) and the very high (laser-produced plasma) dose rate levels. We can thus conclude that the results of our study on glow curve shapes indicate negligibly small dose rate dependencies of TL signals measured on TLD 200 chips irradiated by SXR.

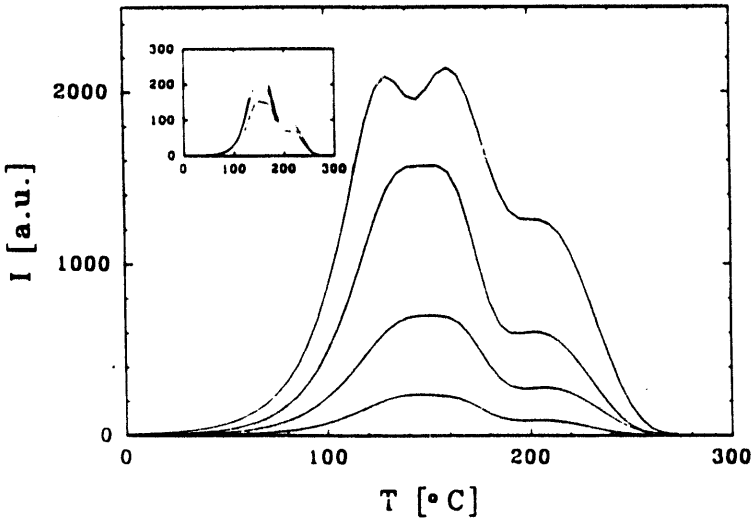


Fig. 4 Glow curves of TLD 200 irradiated by different doses of SXR from laser-produced plasma (figure) and ^{55}Fe (window).

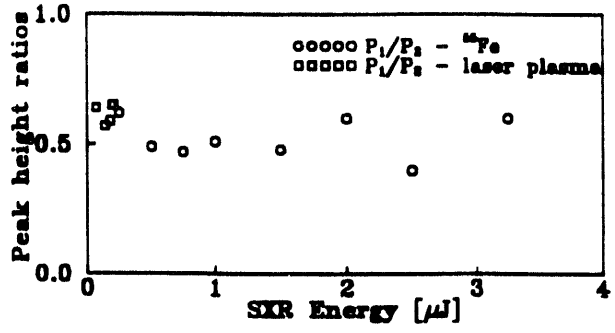


Fig. 5 Ratios of single peaks corresponding to $T_1 \cong 409$ K and $T_2 \cong 437$ K in glow curves of TLD 200 irradiated by SXR from ^{55}Fe (circles) and laser-produced plasma (squares) as a function of dose.

The present results confirm the asumption of negligible influence of the dose rate on the TLD response in the SXR region. This qualifies the TLDs for their safe calibration by monochromatized synchrotron radiation and their use for accurate SXR dose measurements in a wide range of dose rates. It equally legitimises the use of the TLDs for an absolute measurement of SXR radiation emitted from the laser-produced plasma. On the other hand, the popular Si diodes used in the laser plasma experiments seem to be sensitive to the dose rate. An indirect substantiation of this fact follows from the mesured photodiode responses to high-power SXR pulses, which may be two or three times lower than the corresponding calculated values [5] or lower than those measured by TLDs [21]. This renders an application of Si diodes for laser plasma experiments in questionable, because the diodes are usually calibrated with e.g. the synchrotron radiation at very low dose rates. A comparative measuremnet of Si diodes and TLDs responses can serve as a quality test of the diodes [22].

References

[1] Agarwal B. K.: X-Ray Spectroscopy. An Introduction. Springer-Verlag, Berlin-Heidelberg-New York 1979.
[2] Michette A. G. : Optical Systems for Soft X Rays. Plenum Press, New York-London 1980.
[3] Fleming D. et al.: J.Vac.Sci.Technol. B10,2511(1992).
[4] Turcu I. C. E. et al.: Proc. SPIE 2015, in press.
[5] Bijkerk F.: Laser Plasma Soft X-Ray Sources, Application in Microlithigraphy. Doctor Thesis, Vrije Universiteit te Amsterdam, Amsterdam 1993.
[6] Gohil P. et al.: Appl.Opt. 24,2024(1985).
[7] Bijkerk F. et al.: Microelectr. Eng. 9,121(1989).
[8] X-Ray Microscopy (Eds. Schmahl G., Rudolph D.). Springer-Verlag, Berlin-Heidelberg-New York-Tokyo 1984.
[9] Raju M. R. et al.: Radiat.Res. 110,396(1987).
[10] Kobayashi K. et al.: Int.J.Radiat.Biol. 59,643(1991).
[11] O'Neill F. et al.: Annual Report to the Laser Facility Committee 1989, Rutherford Appleton Laboratory, RAL-89-045, Chilton, Didcot, Oxon 1989, p. 331.
[12] Tegeler E., Krumrey M.: Nucl.Instrum.Meth.Phys.Res. A282,701(1989).
[13] Matthews D. et al.: J.Opt.Soc.Am. B4,578(1987).
[14] Horowitz Y. S., Kalef-Ezra J.: Nucl.Instrum.Meth. 188,603(1981).
[15] Meyer F. J., Montry G. R., Benn E.: Adv. X-Ray Anal. 18,169(1975).
[16] Basov N. G. et al.: Proc. P. N. Lebedev Phys. Inst. 203,69(1990).
[17] Folkard M. et al.: Phys.Med.Biol. 32,769(1987).
[18] Folkard M. et al.: Phys.Med.Biol. 34,707(1989).
[19] Pietriková M. et al.: Z.Phys. B93,63(1993).
[20] Chen R. et al.: Phys.Rev. B24,4931(1981)
[21] Fárníková M. et al.: unpublished results.
[22] Krása J. et al.: Proc. SPIE 1980,103(1992).

ESTABLISHING A MINIMUM REPORTING LEVEL (GAMMA) FOR THE PERSONNEL DOSIMETRY DEVICE WORN AT THE IDAHO NATIONAL ENGINEERING LABORATORY (INEL)

Orval R. Perry, Brian L. Andersen, and Paul E. Ruther (EG&G Idaho, Inc.)

The report evaluates various approaches to defining a minimum reporting level (MRL) for personnel thermoluminescent dosimetry (TLD) systems. The evaluations include the traditional statically-based approaches, using lower limit of detection and critical level as well as several unique approaches developed as part of the study. The advantages and disadvantages of each technique are discussed with the conclusion that none of the statistically based methods satisfy the need to provide accurate low-level data without being overwhelmed with apparent "false positive" values. A unique approach is presented on the premise of optimizing the accuracy of the total monitored dose. This approach requires the analysis of the distribution of TLD results around "zero" and provides some insight into the performance of TLD systems at very low dose values.

A NEW EXTREMITY SYSTEM AND PERFORMANCE AT INEL

O.R. Perry (EG&G Idaho, Inc. Operational Dosimetry Unit, P. 0, Box 1625, Idaho Falls, ID 83415-4147), R.A. Tawil, K.J. Velbeck, J.E. Rotunda (Harshaw/Bicron Radiation Measurements Products, 6801 Goonan Road, Sonon, OH 44137)

The TLD Extremity Dosimetry System described herein incorporates the components necessary for Personnel Extremity Monitoring to meet all current and proposed requirements for DOELAP, HPSSC and the HSE in the UK. The automatic, hot gas TLD reader employs a closely controlled linearly ramped readout cycle. The reader interfaces to an application software package that evaluates and manages the generated TLD data. Single and dual element TLD dosimeters and appropriate filtration comprise the extremity detectors. The TL elements are made of TLD-100 and TLD-700 material in thicknesses from 20 to 100 mg/cm^2, and are uniquely identified by individual, non removable, bar code labels. Copper and tin filtration may be used with either or both elements. A dose algorithm was developed to be used in conjunction with the dosimeters and TLD reader technology capable of reporting shallow dose, H_s at 7mg/cm^2, from betas and low and high energy photons using any combination of these dosimeters. Performance tests and results obtained by the Idaho National Engineering Laboratory (INEL) Operational Dosimetry Unit in the evaluation of a single extremity dosimeter capable of simultaneously monitoring beta and high energy gamma. Four TL materials and two filter types were tested in various combinations to ^{137}Cs photons, uranium slab and ^{90}Sr/^{90}Y beta irradiations. An overview of the current INEL system, monitoring objectives, testing and calibration is presented. Dosimeter response with and without filtration, linearity, angular dependance, residual, and effects of physical damage to the dosimeter were tested. The results of these tests lead to the preliminary conclusion that an extremity dosimeter can be constructed to simultaneously monitor beta and high energy gamma radiation. The tests, results and performance are presented in this paper.

IMPROVED BETA SENSITIVITY UNDER FIELD CONDITIONS FOR THE PANASONIC UD-807 EXTREMITY DOSIMETER

J. Robert Flood (Tennessee Valley Authority, Chattanooga, TN)

Benchmark tests were designed to characterize the sensitivity of the Panasonic UD-807 extremity dosimeter to photon and beta radiations of varying energies. The lithium tetraborate dosimeters are sealed in the plastic used in TVA facilities at the time (nominally 30 mg/cm^2) and sent to Battelle Pacific Northwest Laboratory for irradiation. Processing results showed excellent response to photons of low energy (M30 beam code) and high energy (Cs-137). The response to high energy beta (Sr/Y-90) was very good, but the tests demonstrated a strong under-response to lower energy beta radiation (T1-204).

The Panasonic, design a single element dosimeter, does not permit independent correction of beta response after exposure to mixed beta-gamma fields typical of nuclear facilities. Accordingly, tests were designed to evaluate a variety of materials with characteristics potentially suitable for field use. The ideal material would be easy for a dosimetry staff to use, be practical for users, and protect the dosimeter from moisture, dirt and light.

The materials were tested for beta response using TVA-owned sources (Sr/Y-90and T1-204) routinely used for survey meter calibration. Tests of varying thicknesses of plastic and Mylar found improved beta sensitivity, but the best materials for beta response were unsuited to easy use by the dosimetry staff. Further tests found that polyester urethane 1 mg/cm^2 thick is strong enough for dosimeter protection and thin enough for acceptable beta response at low and high energies.

TVA designed a "Band-Aid"-type holder with a dosimeter pouch that is sealed on three sides during manufacture. The pouch is easily sealed on fourth side after inserting the dosimeter. Using the "peel and stick" methodology of medical plastic strips, it can be applied to the skin of an extremity for single use or applied to a short plastic sleeve for multiple use in a ring-like configuration.

TIME-DEPENDENT, LOW-DOSE REPORTING LIMIT FOR DOSIMETERS THAT ARE TAKEN HOME AT THE END OF THE WORKDAY

Edward Sonder

ABSTRACT

In routine personnel dosimetry, it is usual to report doses only where the occupational dose (measured dose with background subtracted) is greater than a previously determined reporting limit. The reporting limit, although set administratively, should be justified by an assessment of the errors inherent in the personnel and background dose measurements, and estimates of the probability that a zero exposure will yield a dosimeter response equal to the reporting limit.

In the process of determining the best values to use for background subtraction and reporting limits, it was realized that the source of low-dose uncertainty is very much dependent on whether dosimeters are held in racks at the work site or remain with the employee. The External dosimetry Program for the Department of Energy facilities at Oak Ridge, Tennessee, is operated such that dosimeters are taken home by the employee at the end of each workday. This report is a summary of measurements of background radiation in a variety of home locations, and of calculations of the effect of the variation of this background on the uncertainty of low-level occupational dose and on the reporting level.

When dosimeters are stored at a given location (e.g., the facility gate), it is theoretically possible to determine the background there to any desired accuracy; the errors in occupational dose are then those due to measurement noise and dosimeter calibration. However, when different dosimeters are stored in different homes, the difference in background between a particular location and the average for all locations appears as an added uncertainty in the occupational dose. Moreover, since this difference is not random, but fixed for a given location, the error due to this difference increases linearly with assignment time. From the background measurements, time-dependent values of the standard deviation of occupational dose and critical levels are derived and used to define an expression for the reporting limit.

However, if dosimeters are taken to various locations (homes) during off-work periods, it is possible that the background accumulation will be different for different dosimeters. Since it is impractical to measure the background at every employee's dosimeter storage location, and an average value for background is routinely subtracted to obtain the occupational dose, these differences have to be determined and their effects have to be explicitly included in the analysis.

DETERMINATION OF RADIATION BACKGROUND AND ITS VARIATION

Seventy different home locations were selected to cover the area around Oak Ridge, Tennessee, and Paducah, Kentucky, where employees whose dosimeters we measure live. At the beginning of the study, April 1990, 12 annealed dosimeters were placed in each location, with one being retrieved each subsequent month for measurement of the accumulated background dose. Also, each month an additional, single dosimeter was placed at these locations and kept there for one month to yield differential readings.

Figure 1 shows the accumulated background dose[3] averaged for all locations. The plotted values are in units of reader response, which for our installation are calibrated to be equal to milliroentgen from one of our ^{137}Cs gamma sources. The data can be well fitted with a linear function the slope of which, as indicated, gives an average background rate of approximately 0.74 mR/week. The finite intercept (approximately 3 mR) is not due to radiation; it is due to electronic noise and small amounts of light that enter the dosimeter housing.[4] Figure 2 shows the distribution of dose rates obtained for 4, 5, and 6 months at the different locations. A reasonable Gaussian fit is possible for most of the data, as indicated in the inset. However, there are a few measurement results that are clearly higher than would fit the Gaussian. Further analysis indicated that the high data came consistently from the same locations and that, indeed, the differences in background rate, measured at different locations was much greater than the general experimental uncertainty of the measurements. This fact is clearly demonstrated by Fig. 3, in which the dose measured at three different locations is plotted vs time; the differences in slope for the three locations are obviously much greater than the point scatter.

The results described in the previous paragraph imply that the background accumulation for any specific dosimeter (location) is not equal to that of other locations or any determined average value. Therefore, use of even the most carefully determined average for background radiation produces errors in the occupational dose for all locations at which the background is not equal to the average value. Moreover, the difference in total dose between the background at a given location and the average increases with assignment time (time at that specific location). We

$$RL\ (deep) = 1.2 + 0.40 \times t \quad (4)$$

$$RL\ (shallow) = 12 + 0.32 \times t\ . \quad (5)$$

As mentioned previously, the variations that lead to our expressions for the RL stem primarily from the background (gamma-ray) radiation. Thus, the RL is independent of the type and energy of radiation that causes an exposure, and can, therefore, be applied to the measured reader response before any conversion to dose equivalent is performed (i.e., before the algorithm is applied). This makes it unnecessary to develop multiple expressions for RL for different radiation types and energies.

DISCUSSION OF REPORTING LIMIT AND LOWER LIMIT OF DETECTION

In the "Department of Energy Standard for Performance Testing"[5] (DOESPT) one requirement is the determination of a Lower Limit of Detectability (LLD). This LLD is a radiation dose for which the measuring system has a given, high probability (usually 95%, but it could be another percentage) of detecting the exposure, i.e., producing a measuring results above the RL. This is the same definition as given by Currie for his L_d. It must be reemphasized that L_c and L_d are different entities, the former being a measuring system output (labelled "a posteriori" by Currie),[1] while the latter is a radiation dose or measuring system input (labelled "a priori" by Currie).[1] Values of LLD determined by any method cannot, logically, be used as a Reporting Limit.

A procedure for determining the LLD is given in the DOESPT document.[5] This procedure has been derived[6] for two types of errors, one type being fixed, stemming mainly from equipment sensitivities, and the other type being proportional to dose, such as, calibration errors. However, errors due to background uncertainties are not included since it is assumed that background can be measured to any degree of accuracy desired. As a result, the prescribed procedure[5] is not strictly applicable to an operation such as ours, where dosimeters are taken home by employees and where background uncertainties increase with assignment time and are the dominant source of errors. For operations where dosimeters are taken home, Currie's definition of the Lower Limit of Detectability,

REFERENCES

1. L. A. Currie, "Limits for Qualitative Detection and Quantitative Determination: Application to Radiochemistry," *Anal. Chem.*, 40, 586, (1968).

2. *U.S. Department of Energy Radiological Control Manual*, DOE/EH-0256T, U.S. Government Printing Office, Washington, D.C., June 1992.

3. E. Sonder and A. B. Ahmed, *Background Radiation Accumulation and Lower Limit of Detection in Thermoluminescent Beta-Gamma Dosimeters Used by the Centralized External Dosimetry System*, ORNL/TM-11995, Martin Marietta Energy Systems, Inc., Oak Ridge Natl. Lab., December 1991.

4. E. Sonder et al., *The Effect of Visible Light on Harshaw Model 8801 Thermoluminescent Dosimeters*, ORNL/TM-11651, Martin Marietta Energy Systems, Inc., Oak Ridge Natl. Lab., September 1990.

5. *U.S. Department of Energy Standard for Performance Testing of Personnel Dosimetry Systems*, DOE/EH-0027, 1986.

6. P. L. Roberson and R. D. Carlson, "Determining the Lower Limit of Detection for Personnel Dosimetry Systems," *Health Physics*, 62, 2, (1992).

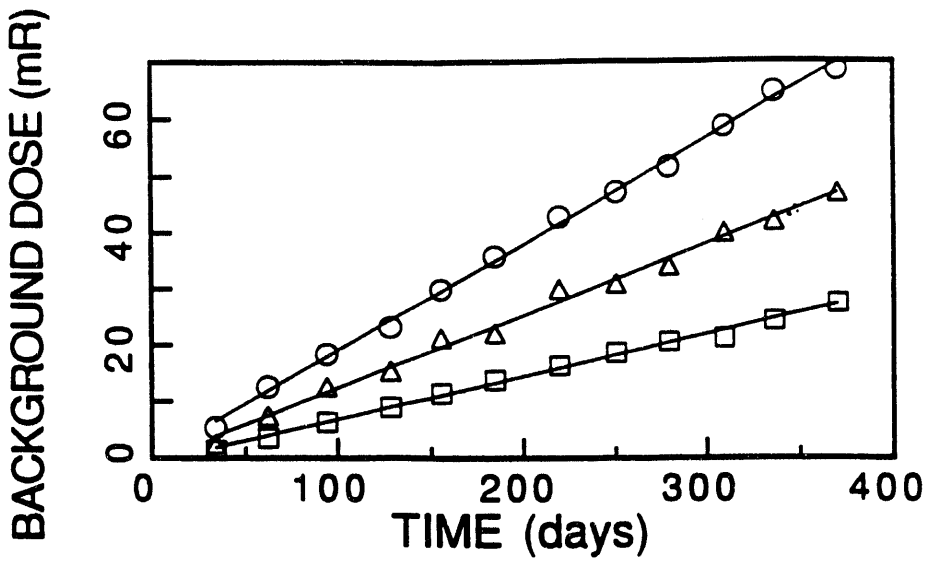


Fig. 3. Time dependence of background accumulation at three different locations. The solid lines are linear fits to the data values.

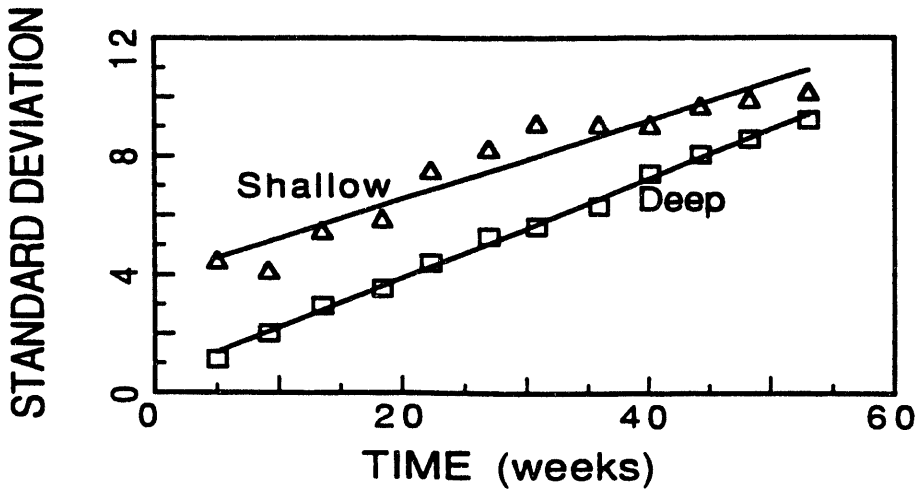


Fig. 4. Time variation of the standard deviation of background dose measured by normal and thin thermoluminescent phosphors in Harshaw/Bicron 4-chip dosimeters. The intercepts are due primarily to experimental variations while the slopes are due to locational differences in background as discussed in the text.

MODIFICATION OF DOSE ALGORITHM FOR TELEDYNE 9150 TLD SYSTEM AND PERFORMANCE TEST OF THE ALGORITHM VIA INTERCOMPARISON STUDIES

Jang-Lyul Kim, Si-Young Chang, Kyung-Won Seo
Suk-Chul Yoon, Sang-Yoon Lee and Hyung-Sub Lee
(Health Physics Dept., KAERI, P.O.Box 105, Taejon, Korea)

Abstract

To encourage dosimeter processors to evaluate personnel radiation dose more accurately, the Ministry of Science and Technology (MOST) of Korea issued an Ministerial Ordinance on the technical criteria on personnel dosimetry in August 1992 which was very similar to the ANSI N13.11 standard.

Korea Atomic Energy Research Institute (KAERI) has modified the dose calculation algorithm of our Teledyne 9150 TLD system to meet the 8 test categories specified in the MOST Ordinance since 1991, and to provide a dosimeter performance test program to all domestic dosimeter processors.

This paper describes the modified the dose calculation algorithm, radiation fields used for modifying the existing algorithm, and presents intercomparison results for the performance of the modified algorithm with Atlan-Tech Inc., Oak Ridge National Lab.(ORNL), Japan Atomic Energy Research Institute(JAERI) and Australian Radiation Lab.(ARL).

All Intercomparison results showed a good agreement between irradiated and evaluated doses within the tolerance level of MOST Ordinance.

Table 1. Filter Materials and Thickness for the PB-3 Badge System

Area	Front	Back
A 1	7mg/cm^2 Mylar film	Plastic case
A 2	Plastic case 3.2 mm of Teflon Plastic case	Plastic case
A 3	Plastic case 2.64 mm of slotted Cu 0.81 mm of Al Plastic case	Plastic case 1.02 mm of Cu 0.81 mm of Al Plastic case
A 4	Plastic case 2.64 mm of slotted Cu 0.81 mm of Al Plastic case	Plastic case 0.13 mm of slotted Cu 0.81 mm of Al 0.81 mm of Cd Plastic case

filter. The copper filter has a hole in it to provide a relative flat response for the deep dose. Since the deep response in area 3 or area 4 is not flat, a correction has to be made to the measured deep dose response to properly correct for over-response of the deep dose in area 3 and area 4 when the badge case is exposed to low energy photons. Also, in area 4, Cd filter is inserted to measure neutron dose.

3. Calibration

3-1. Radiation fields

X-ray beams were obtained by a MG-320 X-ray generator (Philips, Germany). The specifications of this generator are as follows:

- output voltage and current : 320 kV, 30 mA
- Inherent filtration : 3 mm Al
- beam angle : 40^0
- stability : < 1%
- cooling : oil (40 L/min)

The list of X-ray average energies and other sources used in this experiment are shown in Table 2.

areas of Teledyne PB-3 badge case. The Table-of-Ratio R10 to R16 and conversion coefficients CF1 and CF2 for reference are calculated by

$$R10 = E2/E4,\quad R11 = E1/E2,\quad R12 = E2^{**}2/E3^{**}2,\quad R13 = E2/E3$$

$$R14 = E3/E4,\quad R15 = E1^{*}E2/E4^{**}2,\quad R16 = E1^{**}3/E2^{*}E3^{*}E4$$

$$CF1 = E4/DEEP,\quad CF2 = SHALLOW/DEEP$$

When raw field data of 4 filter areas are read, the data are transformed to relative Cs-137 dose by calibration, then calculate conversion coefficients CF1 and CF2 for field TLD. To determine CF1 and CF2, it is used the measured ratios R10 to R16 for field data and compared to the ratios R10 to R16 in the reference Table-of-Ratio to obtain the best fit. The following formular is used to calculate the best fit.

$$BF = \sum_{i=10}^{i=16} \frac{R_{i,ref} - R_{i,meas}}{R_{i,ref}}$$

where $R_{i,ref}$ is the ratio R10 to R16 in reference Table-of-Ratio and $R_{i,meas}$ is the ratio calculated by raw field data.

For neutron, following basic concept is used to calculate neutron dose.

Neutron Dosimeter *Gamma Dosimeter*

E3 (neutron+gamma in mR) - (gamma in mR) = neutron E3 in mR(TLP)

E4 (neutron+gamma in mR) - (gamma in mR) = neutron E4 in mR(BCD)

By these two values, we have two kinds of methods for neutron dose evaluation. First, TLP is used in case of known neutron source only. Table 3 shows the dose conversion factor with neutron source. Second, BCD/TLP ratio is uesd for unknown neutron sources. Fig.1 shows the relation of BCD/TLP ratio to dose conversion factor.

5. Intercomparison Results and Discussion

Intercomparison studies were performed with ORNL, JAERI, ARL and Atlan-Tech Inc. for all 8 test categories represented in ANSI

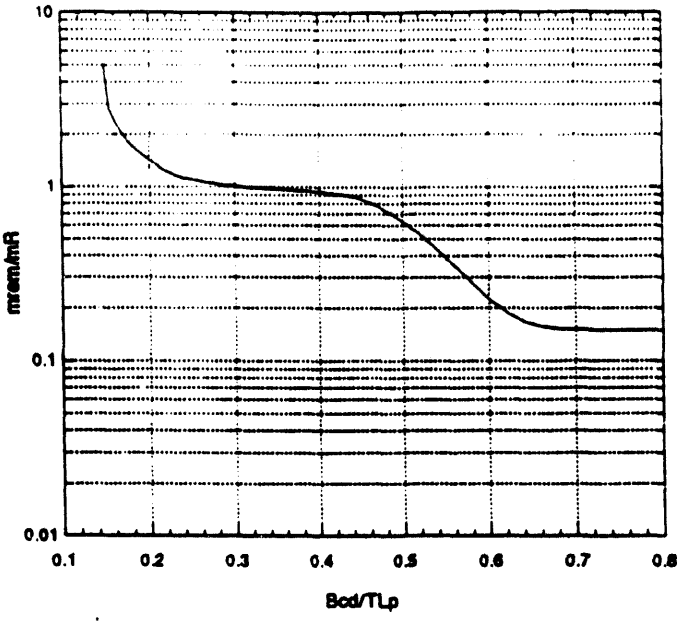


Fig. 1. Neutron mrem/mR Conversion Factor as a Funtion of BCD/TLP Ratio.

useful for known neutron sources, but BCD/TLP ratio for unknown neutron sources in Fig. 1 shows 50-80 % overestimation for application. So it is strongly requested intercomparison study by various neutron sources to improve neutron dose evaluation technique because we have only one Cf-252 source.

In conclusion, it has been confirmed that our modified algorithm for Teledyne PB-3 personnel dosimetry system allows to evaluate all of the MOST Ordinance with a good accuracy. But to improve the accuracy of the neutron dose measurement with energies, further intercomparison studies using various neutron sources are needed in future.

References

[1] International Commission on Radiation Units and Measurement, *Measurement of Dose Equivalent from External Photon and Electron Radiation*, ICRU Report 47(1992).

[2] Ministry of Science and Technology, *Technical Requirement for Personnel Radiation Monitoring*, Ministerial Ordinance(1992).

[3] American National Standard for Dosimetry, *Personnel Dosimetry Performance Criteria for Testing*, ANSI N13.11(1983).

[4] American National Standard for Dosimetry, *Personnel Dosimetry Performance Criteria for Testing*, ANSI N13.11(1993).

Table 6. Intercomparison Results for X-Ray(ANSI categories I, III)

Intercomparison with	No.of Dosi.	Energy (keV)	Delivered Dose(mrem)	Performance (IBI+S)	Tolerance Level	Remark
ORNL	3	20	68[1] (150.5)	0.08 (0.12)	0.5	PDIS18('93)
JAERI[2]	3	32.1	129	0.46	0.5	IAEA/RCA('90)
	3	64.1	58	0.06		
	3	95.5	70	0.08		
	3	161	297	0.16		
	3	36.5	35	0.12		IAEA/RCA('91)
	3	70.5	65	0.11		
	3	119	90	0.11		
	3	60.4	6270	0.29		IAEA/RCA('92)
	3	60.4	380	0.15		
	3	203	144	0.09		
ARL	3	33	26 (25.6)	0.07 (0.28)	0.5	IAEA/Asia-Pacific Region ('91)
	3	79	93.1 (84.6)	0.04 (0.10)		
	3	202	156 (150)	0.04 (0.10)		
Atlan-Tech Inc.	15	M150[3] S60	31,155 660 (767)	0.09 0.19 (0.23)	0.3 0.5	'91
	15	M150 S75	30,594 485 (583)	0.20 0.18 (0.05)	0.3 0.5	'92

(1) The values in parentheses evaluated from shallow dose equivalent
(2) Irradiated by mR not mrem
(3)Accident High Dose

A TLD DOSE ALGORITHM FOR MIXED FIELDS AT A NUCLEAR WEAPONS FACILITY

Neill Stanford (Stanford Dosimetry); Christopher N. Passmore, Mark Prather, Jerome B. Martin (Battelle Pantex)

Personnel dosimetry at a nuclear weapons facility typically involves assessment of external dose from a wide range of beta, photon and neutron fields. The nature of the facility allows the possibility that a given radiation worker may receive dose from any mixture of fields during a single monitoring period. To further challenge the system, the specific exposure conditions for any given TLD are generally unknown to the processing group. While some facilities have chosen to issue multiple dosimeter types to each worker to monitor for the different fields, this paper describes a single dose algorithm implemented at the Pantex Plant, designed to calculate external dose from an unknown mixture of these fields based on the readings of a single eight element TLD badge.

The algorithm takes advantage of the different relative sensitivities provided by the four phosphor types and six filtration configurations, to isolate responses for the photon, beta and neutron components. These isolated responses are used to characterize each of the fields, allowing the calculation of specific correction factors for each processed field dosimeter. Test results demonstrate that the design can accommodate, with no a priori information, irradiations to various mixtures of: low and high energy beta radiation, photon radiation as low as 20 keV, and a range of neutron fields from unmoderated ^{252}Cf to a ^{252}Cf source moderated with 9.5 cm of polyethylene. Results of synthetic testing as well as comparisons to field measurements are presented.

A NEW APPROACH TO TLD DOSE ALGORITHMS

Marko Moscovitch (Department of Radiation Medicine, Georgetown University School of Medicine, 3800 Reservoir Road NW, Washington, DC 20007), D.J. Rotunda (Harshaw/ Bicron, 6801 Cochran Road, Solon, OH 44139)

A new solution was designed and applied to multi-element thermoluminescence dosimetry (TLD) dose algorithm development.

A dose algorithm based on this new approach is a fundamentally different approach from conventional algorithms. The algorithm eventually is able to produce its own unique solution to similar, but not exactly the same, dose calculation problems. For personnel dosimetry, the output consists of the desired dose components: deep dose, shallow dose, and eye dose. The input consists of the TL data obtained from the readout of a multi-element dosimeter. For this application, a new architecture was developed based on this concept. This simplifies the problem and results in a relatively simple and reliable dose calculation algorithm.

A test set was composed of the response of a group of multi-element dosimeters (Harshaw Type 8825) exposed to a variety of photon-beta mixed fields. After test set, the algorithm was able to correctly calculate the dose (well within DOELAP criteria) from a set of blind dosimeters that were independent from the test set. Overall, the performance of the new dose algorithm has been shown to be significantly better than conventional algorithms.

AUTOMATIC SCREENING OF ABNORMAL LiF:Mg,Ti GLOW CURVES FOR USE IN ROUTINE DOSIMETRY

Y.Tan, L.E.Rotunda, K.J. Velbeck, and R.A. Tawil (Harshaw/Bicron Radiation Measurement Products, 6801 Cochran Road, Solon, OH 44139)

In routine dosimetry, the dosimetric information is, for practical reasons, approximated by the integral area under the glow curve. The validity of this practice is ensured by visual screening of glow curves before applying a dose computation algorithm. A simple computer program was specifically developed for large scale routine dosimetry to electronically screen abnormal glow curves of LiF:Mg,Ti mounted in cards. The method presented here identifies glow curves with abnormal patterns by examining a few key features from which information about background and thermoluminescent (TL) signals can be extracted. The underlying criteria for glow curve acceptance/rejection are discussed. These criteria are determined both from those glow curve characteristic dictated by the dosimeter and reader, and from the acceptable limits of parameter values specified by the operator through the provided user interface. The dosimeter and reader-dictated parameters, such as the glow peak locations and width, are automatically determined by analyzing the records of Quality Control (QC) cards that are in the same group as the field cards to be analyzed, thus eliminating the need for any prior knowledge of those conditions required for reference determination. The program performance was evaluated by using actual glow curve data provided by users of commercially available readers and dosimeters in routinely high-throughput operations. The initial tests showed a near 100% success rate in identifying glow curves with faulty features (no false positive results) and a minimal rate of rejection of usable glow curves. Results have shown that this method is applicable for dose levels down to 50 μSv.

SELFDOSE MEASUREMENTS IN ROUTINE PERSONAL AND ENVIRONMENTAL TLD SYSTEMS

J.C. SAEZ-VERGARA*, A.M. ROMERO*, A. DELGADO**
* Radiological Protection Division
** Basic Research Institute
CIEMAT
Avda. Complutense 22, 28040 Madrid, Spain

Phone: 34-1-3466252
FAX: 34-1-3466393

(This work has been funden by the European Community Research Contract FI3P-CT92-0018 and by the CIEMAT/ENRESA Protocol 92-94)

ABSTRACT

Passive TLD systems are widely used to measure low doses (below 0.15 mSv/month) in personal and environmental monitoring. In order to achieve enough fiability in this range it is necessary to characterize the selfdose response of the detector, including phosphor and hanger with metallic and plastic filtrations.

CIEMAT has performed different selfdose studies in the UDO Laboratory for the most common TL materials, but this works shows the importance of selfdose in routine equipments such as Panasonic personal and environmental TLD systems.

Results on measured selfdose rates show slight differences between phosphors but other parameters can be noticeable. The presence of metallic elements (filters, rings) can increase the selfdose rate more than ten times. Variations in batch production could be also appreciated.

Introduction

The measurement of environmental radiation doses implies the ability to detect very low signals. One of the parameters to be considered for the environmental detectors is the self irradiation[1,2]. The estimates[3,4] of the selfdose in the TL phosphors show that the self irradiation from the TL detector itself is negligible for the common phosphors.

However, the TL detector can be affected by the inherent background due to the intrisic radiactivity in the building materials of the detector itself and the surroundings filters, electronics and weatherproof cases.

In order to get accurate estimation of the inherent background or selfdose is convenient to perform these measurements in a laboratory with a low environmental doserate very stable.

The P.T.B. Ultra Low Dose Laboratory (UDO) is an optimal facility for this purpose[5]. Placed at 925 m deep in the Asse salt mine (Germany), the P.T.B. UDO Lab offers a very low dose rate (≈ 0.6 nGy/h) and very stable temperature control.

Since 1990 CIEMAT has been performing selfdose experiments in the UDO Lab for the most commonly employed TL phosphors. These activities were funded by an European Union Project about environmental radiation dosimetry in collaboration with Riso National Laboratory (Denmark) and P.T.B. (Germany).

During 1993, a long term selfdose experiment was performed in the UDO Lab. One of the objectives was to check the selfdose in different TL phosphors and hanger combinations.

Experiment Design

Long term experiments with TLD systems need to consider the possible fading or sensitivity changes and the small differences in energy response from one calibration source to another with the same radionuclide. Thus, the following experiment was designed with the aim to get the maximum information about the intrinsic selfdose but minimising the systematical influences. For each TLD badge four different groups of detectors were defined:

Group N: Detectors annealed at the beginning of the experiment, exposed in UDO Lab during the integration time, then read. This batch only detects the expected background in the UDO Lab **U** and the inherent selfdose rate **S**:

$$N = U + S$$

Group A: Detectors annealed at the beginning of the experiment, exposed in UDO Lab during the integration time, then irradiated and read. The detectors will accumulate the inherent contributions from the Lab (U) and the badge (S), plus the imparted calibration dose **QB** (irradiation

performed in the Asse salt mine before storage):

$$A = U + S + QB$$

Group B: Detectors annealed and irradiated at the beginning of the experiment, exposed in UDO Lab during the integration time, then read. As above, the readout of this batch will include U, S and the imparted calibration dose **QA** (irradiation performed in the Asse salt mine after storage):

$$B = U + S + QA$$

Group C: Control batch annealed, irradiated in the Asse salt mine and read inmediately. This control batch was evaluated at the beginning of the experiment (group CB) and one more time at the end of the practice (group CA). Obviously, these readouts only contain information about the calibration doses imparted before (CB) or after storage (CA).

Data from A, B and C groups were used to calculate the calibration factors and to check the fading or sensitivity changes during the integration time. In order to discriminate the U and S contributions, the value U = 0.7 nGy/h was used[5].

In 1991, a preliminar test was performed installing in the UDO Lab a Panasonic UD-705 manual reader provided by Welhöffer Dosimetry. The detectors were annealed and irradiated inside the mine, and they were kept there for a month storage and then the detectors were read in the UDO lab. With this experiment, it was tried to avoid the transit dose from our TLD lab in Spain and the UDO lab, but the available storage period at that time showed too short and only some indications could be appreciated.

In 1993 a six month exposure period was available in the UDO lab, the earlier experiment was repeated with the same detectors, but it was not possible to get a Panasonic reader to be installed in the UDO lab for such a long time. Then the same experiment was plannified including control dosemeters to assess the transit dose between both laboratories.

Materials and equipments

Panasonic TLD badges were used for the measurements because it is possible to get different combination of plastic and metallic filters in two complementary phosphors such $Li_2B_4O_7$:Cu (tissue equivalent) and $CaSO_4$:Tm (high sensitivity).

Every badge has four detectors consisting in a fine phosphor powder deposited in a plastic tape. This tape is inserted in a case containing the plastic and metallic filters, depending on the type of the badge. The complete configurations of the badge types used are shown in Tables 1, 2 and 3.

The UD-800 badge is used for TLD system calibration purposes and it only includes plastic filters. The filtration is enough to provide secondary electron particle equilibrium for Cs-137 photon radiation.

The UD-802 badge is intended to be used as universal personal dosemeter because it provides a discriminant algorithm able to determine photon, beta and neutron components. Two different fabrication batches were tested in order to determine the influence of this factor.

The UD-814 badge is the Panasonic environmental badge with three redundant Calcium Sulphate elements with a metallic filter for energy compensation response. Two different batches provided by Panasonic representant in Germany (Welhöffer Dosimetry) were tested: Standard batch and Anomalous batch with specially high background.

The dosemeters were annealed and read at CIEMAT in a Panasonic UD-710 Automatic TLD reader based in optical heating. Glow curves were recorded and checked for anomalies. Individual correction factors for each detector were applied. The system was calibrated in terms of kerma in air using the facilities of the Spanish Secondary Standard Laboratory managed by CIEMAT's Metrology Unit.

In order to estimate the contamination in the lead filters, individual counting of some metallic filters were performed in a low level alpha-beta gas flow proportional counter (lower detection limit 20 mBq/g).

Results

The phosphor/filter configuration of each badge and the obtained selfdose rates are showed in the Tables 1, 2 and 3.

Table 1: Results from the Panasonic UD-800 badge

Phosphor	$Li_2B_4O_7$:Cu	$Li_2B_4O_7$:Cu	$CaSO_4$:Tm	$CaSO_4$:Tm
Filtration	Plastic 2 mm	Plastic 2 mm	Plastic 2 mm	Plastic 2 mm
Self Dose Rate (nGy/h)	4.0±0.4	3.4±0.3	1.2±0.2	1.1±0.2

Table 2: Results from the Panasonic UD-802 badge

Phosphor	$Li_2B_4O_7$:Cu	$Li_2B_4O_7$:Cu	$CaSO_4$:Tm	$CaSO_4$:Tm
Filtration	Plastic 0.2 mm	Plastic 2 mm	Plastic 2 mm	Lead 0.7 mm
Self Dose Rate (nGy/h)				
Batch 84/12	3.6±0.4	4.0±0.4	3.0±0.2	3.7±0.3
Batch 91/08	2.4±0.4	4.0±0.4	1.0±0.1	1.9±0.2
Filter Activity (mBq/g)				
Batch 84/12	-	-	-	22
Batch 91/08	-	-	-	<20

Table 3: Results from the Panasonic UD-814 badge

Phosphor	$Li_2B_4O_7$:Cu	$CaSO_4$:Tm	$CaSO_4$:Tm	$CaSO_4$:Tm
Filtration	Plastic 2 mm	Lead 0.7 mm	Lead 0.7 mm	Lead 0.7 mm
Self Dose Rate (nGy/h)				
Batch 87/12 (usual)	3.4±0.3	0.5±0.1	0.5±0.1	0.9±0.1
Batch 84/02 (anomalous)	3.1±0.8	34.0±3.0	30.0±3.0	25.0±2.5
Filter Activity (mBq/g)				
Batch 87/12 (usual)	-	<20	<20	<20
Batch 84/02 (anomalous)	-	215	218	203

Small selfdose rates have been obtained for both phosphors. Slight increase can be apreciated in the fourth element of UD-802 badge because of the lead filter. This is also the reason for the little higher dose rates in this configuration when it is compared with the UD-800 badge (only plastic filters).

Slight dependence on the batch production has been observed for the UD-802 badge, where the selfdose rate is twice but only very weak activity could be measured in the lead filter from the batch 84/12.

Badge UD-814 is intended to environmental monitoring and usually it shows very small selfdose rate, even lower than in absence of lead filters (batch 87/12). However, batch 84/02 clearly shows a very high selfdose rate due to a small contamination in the lead. This fact was confirmed by the independent beta counting measurement performed with the proportional counter.

Conclusions

Selfdose rates below 5 nGy/h (<0.05 mGy per year) have been obtained for both Panasonic phosphors in any badge configuration. However, slight increase is observed when metallic filters are used to correct the energy response. Even slight differences between batches has been appreciated. Anyway, these differences can not disturb the ususal measurements in personal or environmental monitoring.

Although the manufacturers usually perform contamination tests in the metal they use to build the filters for the badges, it is recommended to check the selfdose rate in every new batch of dosemeters. This can be easily done keeping 10-20 dosemeters in a lead shield 5 cm thick for a period 30-90 days, depending on the phosphor sensitivity.

The value for the acceptable selfdose rate is to be discussed. If the value 100 nGy/h is accepted as usual gamma environmental dose rate, it seems reasonable not to accept selfdose rates greater than 10% of this common rate, i.e., 10 nGy/h.

Acknowledgements

We would like to express our gratitude to Dr. Lauterbach and Dr. Peßara (P.T.B.) for their invaluable help, essential for the succesful completion of these experiments.

We are also grateful to Mr. Fiedler (Wellhöfer Dosimetrie) for his important collaboration and technical support.

References

[1] "Performance, Testing and procedural specifications for thermoluminiscence dosimetry (environmental applications". ANSI N545-1975 (1975).

[2] "Thermoluminiscence dosimetry for personal and environmental monitoring". Draft IEC 45B (Central Office) 77-E, IEC (1987).

[3] "Selfdose and fading of $CaSO_4$ (Dy/Tm) and CaF_2 (natural) TL phosphors in environmental radiation monitoring". Nambi K.S.V. Nucl.Instrum.Meth. 197, 453-457 (1982).

[4] "Intrinsic self-irradiation and long term stability of Lif TLD-100 and GR-200 TL detectors". Delagado A., Sáez-Vergara J.C., Romero A.M.. To be published.

[5] "An extreme low level underground Laboratory for dosimetry and spectroscopy (UDO)". Peßara W., Lauterbach U.. Umweltradioaktivität Radioökologie Strahlenwirkungen, Fachverband Stahlenschutz. Verlag TUV Rheinland, 455-460 (1993).

DATE
FILMED
10/21/94

END